Universidade de Lisboa
Faculdade de Farmácia

Novel C11 Amino Derivatives of Cryptolepine

Synthesis and *in vitro* studies with DNA and haeme

João Paulo Martins Ferreira Lavrado

Doutoramento em Farmácia
(Especialidade em Química Farmacêutica e Terapêutica)

2010

Dissertação submetida à Faculdade de Farmácia da Universidade de Lisboa em cumprimento dos requisitos para obtenção do grau de Doutor em Farmácia, especialidade em Química Farmacêutica e Terapêutica

Novel C11 Amino Derivatives of Cryptolepine

Synthesis and *in vitro* studies with DNA and haeme

Orientação:

Professor Rui Ferreira Alves Moreira
Doutora Maria Alexandra da Silva Paulo

João Paulo Martins Ferreira Lavrado

Faculdade de Farmácia
Universidade de Lisboa

Lisboa
2010

Statement

This thesis represents my own work, performed in the Faculdade de Farmácia, Universidade de Lisboa, Portugal, and in the School of Pharmacy and Pharmaceutical Sciences, University of Manchester, U.K., and where work was done in collaboration with other researchers a statement of the fact is made.

No portion of the work referred to in the thesis has been submitted in support of an application for another degree or qualification of this or any other university or other institute of learning. Part of the work here presented has been already published or submitted for publication (see appendix L).

Copyright Statement

The author and the (co-)promoters give the authorization to consult and to copy parts of this thesis for **personal use only** and made **only** in accordance with instructions given by the author and lodged in the library of Faculdade de Farmácia, Universidade de Lisboa This page must form part of any such copies made. Any other use is limited by the Laws of Copyright, specially the obligation to refer the source whenever results from this thesis are cited

Acknowledgments

I would like to express my gratitude to my supervisors **Prof. Rui Moreira** and **Dr. Alexandra Paulo** for their sage advice, insightful criticism, and patient encouragement aided my Ph.D. progress in innumerable ways.

I am also very grateful to **Prof. Kenneth Douglas** and **Dr. Elena Bichenkova**, University of Manchester, for all their help, advice and assistance in the studies with DNA and interpretation of results.

I would like to thanks **Dr. Phil Rosenthal** and **Giri Gut**, University of California, USA, for providing the *in vitro* and *in vivo* antiplasmodial assays necessary to the development of this study.

I would like to thanks **Dr. Maria M. Mota**, **Dr. Miguel Prudêncio** and **Dr. Ghislain Cabal**, Unidade de Malária, Instituto de Medicina Molecular, Universidade de Lisboa, for providing the *in vitro* antiplasmodial and fluorescence microscopy assays imperious to the knowledge of antiplasmodial mode of action of the developed compounds.

I am also very grateful to **Dr. Cecília Díaz**, Departamento de Bioquímica, Escuela de Medicina and Instituto Clodomiro Picado, Universidad de Costa Rica, Costa Rica for the *in vitro* cytotoxicity studies of the developed cryptolepine derivatives.

I would like to thanks **Dr. Virgílio do Rosário** and **Dr. Dinora Lopes**, Centro da Malária e Outras Doenças Tropicais, IHMT, Universidade Nova de Lisboa, for provinding the *in vitro* cytotoxicity assays of the developed quindolone derivatives.

I would also like to express my indebtedness gratitude **to Fundação para a Ciência e Tecnologia** for their financial support (SFRH/BD/29202/2006), to the **Faculdade de Farmácia, Universidade de Lisboa**, Portugal and Scholl of Pharmacy and Pharmaceutical Sciences, University of Manchester, UK by the availability of facilities, material and equipment necessary to the development of this study.

I would like to thanks to **Dr. Rita Guedes** and **Dr. Daniel Santos**, Faculdade de Farmácia, Universidade de Lisboa, for their help in the development of computational studies.

I wish also to thank to all the staff of the Faculdade de Farmácia, Universidade de Lisboa and in particular to **Francisco Carvalho** and **Ana Margarida Madureira** for their help and humor.

I would also like express my deep gratitude to **my family and friends** for their great support during the course of my study.

Last, but not least, I would like to thank to everyone who helped me along this theses in innumerous ways, in particular to all who are and were my laboratory colleagues in Faculdade de Farmácia: **Rita Capela, Tiago Rodrigues, Cátia Ramalhete, Jalmira Mulchande, Maria Santos, Maria Teresa Dias, Patricia Rijo, Ana Newton, Pedro Góis, Paulo Glória, Nuno Candeias, Marta Carrasco, Ana Ressurreição, Susana Lucas, Praveen K. Siripuram, João Rosa, Alexandre Pinto, Pedro Cal, Francesco Montalbano, Nilsa Oliveira, Rudi Oliveira and Sudarshan Reddy. R.**

Autobiography

Ph.D 2006-2010

Faculdade de Farmácia, Universidade de Lisboa, Portugal

Thesis Title: Novel C11 Amino Derivatives of Cryptolepine: Synthesis and *in vitro* studies with DNA and Haeme.

Supervisors: Professor Rui Ferreira Alves Moreira; Doctor Alexandra da Silva Paulo.

M.Sc.in Pharmacy, (specialty Medicinal Chemistry), 2004 – 2006

Faculdade de farmácia, Universidade de Lisboa, Portugal

Thesis Title: Estudo da Síntese de Agentes Quimioterápicos.

Supervisors: Professor Rui Ferreira Alves Moreira

Degree in Chemistry (Licenciatura), 1998 – 2003

Departamento de Química e Bioquímica, Faculdade de Ciências, Universidade de Lisboa, Portugal

Thesis Title: Distribuição e Reactividade de Mercúrio em Sedimentos do Estuário do Tejo

Supervisors: Doctor Ana Paula Paiva; Doctor João Alfredo Vieira Canário.

List of Publications

Books Chapters

1. Lavrado, J.; R., M.; Paulo, A. Synthetic Strategies Towards Bioactive Indolo[3,2-b]quinolines. In **Heterocyclic Targets in Advanced Organic Synthesis**, Carreiras, M.D.; Marco-Contelles, J., Eds. Research Signpost: Kerala, India, ISBN. 978-81-308-0431-6, (**In Press**).

Papers in International Scientific Periodicals with Referees (See Appendix L)

1. Lavrado, J.; Cabal, G.; Prudêncio, M.; Mota, M.M.; Rita C. Guedes, Daniel J.V.A. dos Santos; Gut, J.; Rosenthal, P.J.; Díaz, C.; Bichenkova, E.; Douglas, K.T.; Moreira, R.; Paulo, A. (**Submitted**) Incorporation of Basic Side-Chains into Cryptolepine Scaffold. Structure-Antimalarial Activity Relationships and Mechanistic Studies ***Journal of Medicinal Chemistry***.
2. Lavrado, J.; Reszka, A.P.; Moreira, R.; Neidle, S.; Paulo, A. (**In press**) C-11 diamino cryptolepine derivatives NSC748392, NSC748393 and NSC748394: anticancer profile and G-quadruplex stabilization. ***Bioorganic & Medicinal Chemistry Letters***.
3. Lavrado, J.; Gani, K.; Nobre, P.A.; Santos, S.A.; Lopes, D.; Rosário, V.; Gut, J.; Rosenthal, P.J.; Moreira, R.; Paulo, A. (**2010**) Bis-alkylamine quindolone derivatives as new antimalarial leads. ***Bioorganic & Medicinal Chemistry Letters***, 5634-5637.
4. Lavrado, J.; Moreira, R.; Paulo, A. (**2010**) Indoloquinolines as Scaffolds for Drug Discovery. ***Current Medicinal Chemistry*****,** 17, 2348-2370.
5. Lavrado, J.; Paulo, A.; Gut, J.; Rosenthal, P.J.; Moreira, R. (**2008**) Cryptolepine derivatives containing basic aminoalkyl side chains at C11: synthesis, antiplasmodial activity, and cytotoxicity. ***Bioorganic & Medicinal Chemistry Letters*****,** 18, 1378-81.

Patents

1. Paulo, A.; Lavrado, J.; Moreira, R. **(2010)** Use of 11-Substituted Derivatives of Cryptolepine as Anticancer Agents. Provisional patent application number: 20101000049330, INPI, 2010/06/18.

Meeting Abstracts in Scientific Periodicals with Referees

1. Lavrado, J.; Paulo, A.; Gut, J.; Rosenthal, P.J.; Douglas, K.T.; Bichenkova, E.V.; Moreira, R. (**2008**) C-11 Amino Aanalogues of Cryptolepine: Antiplasmodial Activity, Cytotoxicity and Interactions with a 12 mer DNA oligonucleotide d(GATCCTAGGATC)$_2$. ***Drugs of the Future*****,** 33, Suppl. A., 108.

2. Lavrado, J., Paulo, A., Douglas, K.T., Bichenkova, E.V., Moreira, R., (**2008)**, Antiplasmodial cryptolepine derivatives: Interactions with single and double stranded oligonucleotides. Revista Portuguesa de Farmácia, ISSN 0484-811, X Vol LII (nº3), Supplement, 49.

Oral communications in Scientific Conferences

1. Paulo, A., Lavrado, J., Gut, J., Rosenthal, P.J., Moreira, R., **2009**, From Traditional Medicines to Drug Leads: The Case of Cryptolepine. **A Collaborative Solution for Tropical Diseases: The Luso-American Response – Malaria conference** 2009, July 8-10, Headquarters of the Luso-American Development Foundation, Lisbon, Portugal.

Posters in Scientific Conferences with Referees

1. Lavrado, J., Paulo, A., Guedes, R.C., dos Santos, D.J.V.A., Moreira, R., (**2009)**, Derivatives of bioactive natural alkaloid cryptolepine: molecular docking simulations with a 12-mer double-stranded oligonucleotide. **8th National Meeting on Organic Chemistry**, Portuguese Society of Chemistry, July 1st-3rd, University of Aveiro, Aveiro, Portugal.

2. Lavrado, J., Paulo, A., Gut, J., Rosenthal, P.J., Hansell, E., McKerrow, J.H., Douglas, K.T., Bichenkova, E.V., Moreira, R., (**2009)**, Derivatives of the bioactive alkaloid cryptolepine: improved antiplasmodial and antitrypanosomal activities. **Drug Discovery for Protozoan Parasites**, March 22–26th, Breckenridge, Colorado, Unites States of America.
3. Lavrado, J., Paulo, A., Douglas, K.T., Bichenkova, E.V., Moreira, R., (**2008**), Antiplasmodial cryptolepine derivatives: Interactions with single and double stranded oligonucleotides. **1st National Meeting on Medicinal Chemistry**, November 13-15th, University of Porto, Porto, Portugal.
4. Lavrado, J., Paulo, A., Gut, J., Rosenthal, P.J., Douglas, K.T., Bichenkova, E.V., Moreira, R., (**2008)**, C-11 Amino derivatives of Cryptolepine: Antiplasmodial Activity, Cytotoxicity and interactions with a 12 mer DNA oligonucleotide $(GATCCTAGGATC)_2$. **ISMC XXth International symposium on medicinal chemistry EFMC – ISMC**, 31th August – 4th September, Vienna, Austria
5. Lavrado, J., Paulo, A., Gut, J., Rosenthal, P.J., Moreira, R., (**2007**), C-11 Amino derivatives of Cryptolepine with Improved Antiplasmodial Activity. **ACS-EFMC Frontiers in CNS and Oncology Medicinal Chemistry**, 7-9th October 2007, Siena, Italy.

Abstract

Malaria is one of the most widespread infectious diseases of our time. The global malaria map has been shrinking over the past 60 years, but today more people are at risk of suffering from malaria than any other time in history. In the past few years malaria has once again attracted more attention, partly because it is recognized that malaria spread in sub-Saharan Africa has increased in the recent years, mainly due to the development of drug resistances.

Cryptolepine (**1**), is an indoloquinoline alkaloid, extracted from the West African climbing shrub *Cryptolepis sanguinolenta* (Lindl.) Schltr, a traditional herb used in folk medicine for the treatment of malaria. Several authors hypothesized that the mechanism of action of cryptolepine could be by inhibition of haemozoin formation in the digestive vacuole (DV) of the parasite, however in a microscopic fluorescence study, the indoloquinoline chromophore, was suggested to accumulate into specific parasite structures that could correspond to the parasite nuclei, and thus justifying its activity due to cytotoxic effects on DNA and topoisomerase II activity.

Cryptolepine derivatives (**3**) have been synthesized through the incorporation of basic side-chains in the C-11 position of the 10*H*-indolo[3,2-*b*]quinoline scaffold and evaluated for their antiplasmodial and cytotoxicity properties. The derivative containing a conformationally restricted piperidine side-chain (**3n**) presented IC_{50} values of 23-44 nM against chloroquine resistant strains and a selectivity index value of ca 1400, i.e. a 1000-fold improvement in selectivity when compared with **1**. The introduced side chains are weakly basic, with pK_a values in the terminal amine functionality ranging from 5.2 to 12.5, and are predicted to promote accumulation inside the DV to an extent similar to that of chloroquine. All compounds within this series showed the ability to interact with monomeric haematin (FPIX-OH), with a stoichiometry of 1:1 (**3**:FPIX-OH) and with association constants (K_{ass}) values between 0.062 and 0.41 $\times 10^6$ M^{-1}, comparable to chloroquine ($K_{ass} = 0.085 \times 10^6$ M^{-1}). The complex stabilization is assured by π-π stacking interactions modulated by the aromatic core, and H-bond between the terminal amine side chain and haematin carboxylate anions, thus capable to inhibit haemozoin formation in DV. However, localization studies of compound **3n** inside parasite blood stages suggest an additional mechanism of action, like interactions with DNA, besides inhibition of haemozoin crystal growth. Cryptolepine derivatives (**3**) bind strongly to double-stranded $d(GATCCTAGGATC)_2$ oligonucleotide with association constants ranging from 10^5 M^{-1} to 10^7 M^{-1}. Furthermore, molecular docking simulations showed that, in contrast with **1**, compounds **3** are predicted to not intercalate into DNA double helix, binding essentially to single- and double-stranded DNA, with a stoichiometry of 2:1 (**3**:DNA), through electrostatic and H-bonding interaction involving charged nitrogens.

In order to explore the indolo[3,2-*b*]quinolin-11-one (quindolone) scaffold (**4**), and get new antimalarial chemotypes, we decided to synthesize a series of quindolones derivatives (**5**), targeting malaria parasite digestive vacuole and haeme detoxification pathway, through the introduction of *N,N*-

diethylethanamine in the indolo[3,2-*b*]quinoline aromatic nucleus (N^5,N^{10}-alkylation). This reaction gave *N,O*- (**94**), *N,N*- (**5**) and *O*-(**95**) alkylated products containing two or one basic side-chains, which were evaluated for antiplasmodial activity against chloroquine-resistant *P. falciparum* W2 strain and cytotoxicity for HepG2 A16 hepatic cells. By incorporating alkylamine side chains and chlorine atoms in the quindolone nucleus we transformed the inactive tetracyclic parent quindolones (**4**, **91a** and **91b**) into moderate or highly active and selective compounds to the resistant *P. falciparum* W2 strain, with IC_{50} ranging from 51 to 2638 nM and with selectivity ratios up to 98. All the quindolone derivatives in the series showed the ability to complex FPIX-OH (1:1 stoichiometry) with associations constants (K_{ass}) ranging from 0,074 to 0,14 x10^6 M^{-1}, being the main intermolecular interactions due to π-π stacking interactions and H-bond between derivatives and haematin.

Cryptolepine and the new antimalarial chemotype, quindolone, are suitable scaffolds for the design of active and selective compounds targeting parasite haemozoin detoxification pathway, with potential for development as antimalarial agents.

KEYWORDS: Cryptolepine, indolo[3,2-*b*]quinolines, antiplasmodial, synthesis, Haem, DNA.

Resumo

A malária ou paludismo é uma doença infecciosa provocada por parasitas do género *Plasmodium* e transmitida pela picada do mosquito fêmea do género *Anopheles*. A malária é uma das infecções mais difundida por todo o mundo. Apesar propagação ter diminuído nos últimos 50 anos, nos dias de hoje há mais pessoas em risco de contaminação com malária do que em qualquer outra época da história. Em 2008, a malária era endémica em 108 países, contando com cerca de 247 milhões de casos reportados, 3,3 mil milhões de pessoas em risco. Anualmente, entre 1 a 3 milhões de casos culminam em morte, dos quais, muitos são crianças com idade inferior a 5 anos. A malária é a principal causa de morte infantil em África, sendo que 60 % dos novos casos registados todos os anos ocorrem na África sub-Sahariana, onde ocorrem 90 % dos casos fatais de malária. Para além de ser um grave problema de saúde pública, a malária é também um problema sócio-económico, não só devido ao elevado investimento efectuado na prevenção e tratamento, mas também devido a custos indirectos resultantes da perda de productividade que advêm da elevada morbilidade e mortalidade. No entanto, recentemente a malária voltou a chamar a atenção da comunidade, muito porque foi reconhecido que o número de casos reportados em África tem aumentado nos últimos anos devido ao aumento de fenómenos de resistência nos parasitas aos fármacos utilizados para tratamento da infecção.

Apesar da enorme variedade de compostos com actividade antimalárica, a sua eficácia contínua no entanto a ser reduzida devido aos fenómenos de resistência associados. A cloroquina (**2**) é uma 4-amionoquinolina sintetizada em 1934 e tem sido um dos pilares do tratamento da malária nos últimos 60 anos, sendo de consenso geral, que a sua actividade antimalárica se deva à inibição da formação do cristal de hemozoína no vacúolo digestivo do parasita. No organismo humano, o parasita ingere hemoglobina e digere-a, libertando os amino ácidos necessários para o seu desenvolvimento, e o heme, tóxico para o parasita. Este heme é então biocristalizado pelo parasita a hemozoina, um cristal inerte e não tóxico. A cloroquina, devido às suas propriedades básicas, apresenta a capacidade de se acumular no interior do vacúolo digestivo acídico e formar complexos estáveis cloroquina:heme, através de interacções π-π entre os anéis aromáticos, impedindo assim a formação da hemozoina e originando a morte do parasita. Vários autores referem ainda que a cloroquina apresenta também a capacidade de complexar com as faces em crescimento do cristal de hemozoina, inibindo assim o processo de cristalização.

Nos últimos 30 anos, extractos de uma enorme variedade de espécies de plantas, incluindo muitas utilizadas na medicinal tradicional, têm sido avaliadas *in vitro* quanto à sua actividade antimalárica. O alcalóide criptolepina (**1**), constituinte maioritário da raíz da *Cryptolepis sanguinolenta*, um arbusto trepador africano normalmente utilizado na medicina tradicional para tratamento da malária, demonstrou possuir propriedades antiplasmodicas equivalentes à cloroquina. A criptolepina parece exercer as propriedades antiplasmodicas devido à capacidade de inibir a formação da hemozoina, tal como a cloroquina, ligando-se ao heme e bloqueando assim o mecanismo de destoxificação do parasita. No entanto, a criptolepina é também um agente intercalante de cadeias de ADN ricas em guanina (G) e citosina (C), e tendo preferência por sequências CC não alternadas. Assim, a criptolepina apresenta propriedades citotóxicas devido à inibição da topoisomerase II e da síntese do ADN. Estas propriedades citotóxicas podem também estar na origem da actividade antiplasmódica uma vez que, um estudo de localização intracelular em eritrócitos infectados com *P. falciparum*, revelou que o alcalóide se acumula em estruturas no interior do parasita que poderão corresponder ao núcleo.

Neste trabalho foram sintetizados 25 análogos da criptolepina (**3**) com cadeias laterais diamino-alquílicas, na posição C11 do núcleo aromático da indolo[3,2-*b*]quinolina e avaliados quanto as suas propriedades antiplasmodicas e citotóxicas em linhas celulares de mamífero. O análogo com uma cadeia lateral de piperidina (**3n**), apresentou uma actividade antiplasmódica (IC_{50}) variando entre 23 e 44 nM, contra diferentes estripes resistentes à cloroquina, e um índice de selectividade de aproximadamente 1400, representando um aumento de cerca de 1000 vezes quando comparado com **1**. Os nossos estudos sugerem que a introdução de cadeias laterais com aminas terminais basicas, apresentando valores de pK_a variando entre 5,2 e 12,5, promove a acumulação dos compostos no interior do vacúolo digestivo do parasita, em níveis de concentração semelhantes aos da cloroquina. Todos os análogos da criptolepina sintetizados apresentam a capacidade de formar complexos com o monómero da hematina (FPIX-OH), com constantes de associação (K_{ass}) variando entre 0,062 e 0,41 $\times 10^6$ M^{-1}, semelhante à constante de associação determinada para a cloroquina (K_{ass} = 0,085 $\times 10^6$ M^{-1}). Os complexos são estabilizados maioritariamente através de interacções π-π entre o núcleo aromático da indolo[3,2-*b*]quinolina e o núcleo porfirínico da hematina. Estudos de modelação molecular revelaram também que os azotos protonados nas aminas terminais das cadeias laterais podem formar pontes de hidrogénio com os iões carboxilato da hematina. Estes resultados demonstraram que os novos análogos da criptolepina apresentam a capacidade de complexar com a FPIX-OH e inibir a formação da hemozoina. No entanto, o estudo de localização intracelular realizado por microscopia de fluorescência em eritrócitos infectados com *P. falciparum*, demonstrou que os análogos da criptolepina também apresentam a capacidade de se acumularem no núcleo do parasita e assim, potenciar a actividade antiplasmódica. De modo a avaliar a capacidade de **3** para interagir com estruturas de ADN, foram realizados estudos de interacção com um oligonucleótido de cadeia única d(5'-GCCAAACACAGAATCG-3') e de cadeia dupla $d(GATCCTAGGATC)_2$. Os compostos **3** apresentaram forte capacidade de complexação com ambas as estruturas de DNA e valores de constante de associação (K_{ass}) variando entre 10^5 M^{-1} e 10^7 M^{-1}. Estudos de modelação molecular com estruturas de ADN de hélice duplas semelhante à utilizada no ensaios *in vitro*, demonstraram que os compostos não são agentes intercalantes, tal como verificado para a criptolepina, mas ligam-se à fenda menor/maior, com uma estequiometria 2:1 (análogo da criptolepina:ADN) e interagem preferencialmente com a cadeia de fosfatos através de interacções electrostáticas e pontes de hidrogénio.

Estes resultados demonstraram que a actividade antiplasmódica dos novos análogos da criptolepina parece ser justificada por efeitos sinérgicos ou aditivos à inibição da formação da hemozoina e citotoxicidade associada à interacção com estruturas de ADN.

Com o objectivo de aumentar a diversidade de esqueletos químicos com actividade antimalárica, foram sintetizados novos análogos da indolo[3,2-*b*]quinolin-11-ona (11-quindolona), tendo como propósito aumentar a retenção destes compostos no interior do vacúolo digestivo do parasita. Para tal, foram introduzidas duas cadeias amino-alquílicas (*N,N*-dietiletanoamina) no núcleo aromático da quindolona (alquilação em N^5 e N^{10}). A reacção originou no entanto padrões de alquilação adicionais, *N,O-* (**94**) e *O-* (**95**), que foram também avaliados quanto ao seu potencial antiplasmódico e citotoxicidade em células hepáticas HepG2 A16. Com introdução de uma ou duas cadeias amino-alquílicas e átomos de cloro no núcleo aromático, as quindolonas (**4**, **91a** e **91b**), inicialmente inactivas, deram origem a compostos com actividade moderada a forte contra a estirpe W2 do *P. falciparum* resistente à cloroquina, apresentando valores de IC_{50} entre 51 e 2638 nM, e com maior selectividade para o parasita. Todos os análogos da quindolona sintetizados apresentam também a capacidade de formar complexos com a hematina, com uma estequiometria 1:1 (análogo:FPIX-OH) e constantes de associação (K_{ass}) que variam entre 0,074 e 0,14 $\times 10^6$ M^{-1}. A estabilidade do complexo é assegurada pela formação de interacções π-π entre o núcleo aromático e o anel de porfírina da hematina e estudos de modelação molecular confirmaram a possibilidade de formação de pontes de hidrogénio entre a amina terminal da cadeia lateral e os aniões carboxilato do dimero da hematina. Estes resultados demonstraram que a introdução de cadeias amino-alquílicas no núcleo da quindolona origina compostos com boa actividade antiplasmódica, com aparente capacidade de inibição da formação da hemozoína e possivelmente com maior capacidade de acumulação no vacúolo digestivo do parasita.

As indolo[3,2-*b*]quinolinas demonstraram assim serem bons esqueletos para o desenho e desenvolvimento de compostos para tratamento da malária, obtendo-se compostos mais activos e selectivos para o parasita.

PALAVRAS-CHAVE: Criptolepina, indolo[3,2-*b*]quinolinas, actividade antiplasmódica, síntese, Heme, ADN.

Table of Contents

Statement ... **i**
Copyright Statement ... **i**
Acknowledgments ... **iii**
Autobiography ... **v**
List of Publications ... **vii**
Abstract. ... **ix**
Resumo.. ... **xi**
Table of Contents ... **xv**
List of Figures ... **xix**
List of Tables ... **xxv**
List of Schemes ... **xxvii**
List of Compounds ... **xxix**
List of Equations ... **xxxiii**
Abbreviations and Definitions ... **xxxv**

GENERAL INTRODUCTION ... **1**
RATIONALE AND AIMS OF THIS THESIS ... 1
OUTLINE OF THIS THESIS ... 2

CHAPTER I – MALARIA, FROM DISEASE TO THERAPEUTICS ... **5**
1.1 MALARIA OVERVIEW ... 7
1.1.1 Global Malaria Burden ... 8
1.1.2 Plasmodium Species ... 9
1.1.3 Malaria Chemotherapeutics ... 15
1.1.4 Chloroquine Resistance in Plasmodium sp. ... 21
1.2 INDOLO[3,2-*B*]QUINOLINE, A SCAFFOLD FOR ANTIPLASMODIAL DRUG DEVELOPMENT ... 24
1.2.1 Synthetic Pathways ... 26
1.2.2 Antiplasmodial Activities ... 34
1.2.3 Interactions with DNA and Cytotoxic Activities ... 38
1.2.4 Whole Body Distribution of Cryptolepine in Mice and Toxicity ... 40

CHAPTER II – SYNTHESIS OF INDOLO[3,2-*B*]QUINOLINES ... **43**
2.1 INTRODUCTION ... 45
2.2 SYNTHETIC METHODOLOGIES ... 46
*2.2.1 Synthesis of 5H-Indolo[3,2-b]-quinolin-11(10H)-one (**4** and **91**) and 5-Methyl-11-chloro-10H-indolo[3,2-b]quinolines (**93**) Intermediates ... 46*
*2.2.2 Synthesis of Cryptolepine (**1**) ... 54*
*2.2.3 Synthesis of Cryptolepine Derivatives (**3**) ... 56*
*2.2.4 Synthesis of Quindolone Derivatives (**5**) ... 61*
2.2.5 Synthesis of Alkyldiamines ... 65

CHAPTER III – ACID DISSOCIATION CONSTANTS (p*K*$_a$) ... **69**
3.1 INTRODUCTION ... 71
3.1 DETERMINATION OF ACID DISSOCIATION CONSTANTS BY UV-VISIBLE SPECTROSCOPY ... 73
3.1.1 Cryptolepine ... 73
3.1.2 Cryptolepine derivatives ... 74
3.2 DETERMINATION OF ACID DISSOCIATION CONSTANTS BY ^{1}H-NMR SPECTROSCOPY ... 77
3.2.1 Cryptolepine ... 78
3.2.2 Cryptolepine derivatives ... 79

CHAPTER IV - DNA AND HAEM BINDING PROPERTIES ... **87**
4.1 INTRODUCTION ... 89

4.2 INTERACTIONS OF CRYPTOLEPINE AND DERIVATIVES WITH SINGLE- AND DOUBLE-STRANDED OLIGONUCLEOTIDES 91
4.2.1 Binding Stoichiometry with Double-Stranded Oligonucleotide 91
4.2.2 Thermal Denaturation Studies with Double-Stranded Oligonucleotide 92
4.2.3 Association Constants (K_{ass}) with Oligonucleotides 94
4.3 INTERACTIONS OF CRYPTOLEPINE AND QUINDOLONE DERIVATIVES WITH HAEMATIN 102
4.3.1 Binding stoichiometry 102
4.3.2 Association Constants (K_{ass}) with Haematin 103

CHAPTER V - MOLECULAR MODELING STUDIES 111
5.1 INTRODUCTION 113
5.1.1 Molecular Mechanics 114
5.1.2 Electronic Structure Methods 114
5.1.3 Molecular Docking 115
5.1.4 Molecular Dynamics 117
5.2 DENSITY FUNCTIONAL THEORY (DFT) CALCULATIONS 117
5.3 DOCKING STUDIES WITH DOUBLE-STRANDED OLIGONUCLEOTIDE 119
5.4 DOCKING STUDIES WITH HAEMOZOIN DIMER 126
5.4.1 Cryptolepine and Derivatives 128
5.4.2 Quindolone and Derivatives 132

CHAPTER VI – GENERAL DISCUSSION AND CONCLUSIONS 137
6.1 INTRODUCTION 139
6.2 CHEMISTRY AND STRUCTURAL CHARACTERIZATION 140
6.3 ANTIPLASMODIAL ACTIVITY, CYTOTOXICITY AND MODE OF ACTION 143
6.3.1 Cryptolepine and Derivatives 143
6.3.2 Quindolones and Derivatives 156
6.4 CONCLUSIONS 159

CHAPTER VII - MATERIALS AND METHODS 161
7.1 GENERAL 164
7.1.1 Chemicals 164
7.1.2 Instrumentation 164
7.1.3 Methods 165
7.2 CHEMISTRY 165
*7.2.1 Synthesis of 2-(2-Bromoacetamido)benzoic Acids (**89**) 165*
*7.2.2 Synthesis of 2-[2-(Phenylamino)acetamido]benzoic Acids (**90**) 166*
*7.2.3 Synthesis of 5H-Indolo[3,2-b]quinolin-11(10H)-ones (**4** and **91**) 168*
*7.2.4 Synthesis of 11-Chloro-10H-indolo[3,2-b]quinolines (**92**) 170*
*7.2.5 Synthesis of 5-Methyl-11-chloro-10H-indolo[3,2-b]quinolin-5-ium Chlorides (**93**) 172*
*7.2.6 Synthesis of 10H-Indolo[3,2-b]quinoline (**25**) 174*
*7.2.7 Synthesis of 5-Methyl-10H-indolo[3,2-b]quinolin-5-ium Trifluoromethanosulfonate (**1**) 175*
*7.2.8 Synthesis of Cryptolepine Derivatives (**3**) 175*
*7.2.9 Synthesis of Quindolone Derivatives (**5**) 186*
*7.2.10 Synthesis of N^1,N^1-Dimethylpropane-1,2-diamine (**97**) 189*
*7.2.11 Synthesis of 2-(3-(Piperidin-1-yl)-propyl)isoindoline-1,3-dione (**99**) 189*
*7.2.12 Synthesis of 3-Piperidin-1-yl-propan-1-amine (**100**) 190*
*7.2.13 Synthesis of Tert-butyl-4-(diethylamino)butylcarbamate (**102**) 190*
*7.2.14 Synthesis of N^1,N^1-Diethyl-butane-1,4-diamine (**103**) 190*
*7.2.15 Synthesis of N-(4-((Diethylamino)-methyl)-3-hydroxyphenyl)-acetamido (**105**) 191*
7.3 ACID DISSOCIATION CONSTANTS (pK_A) 191
7.3.1 UV-visible Spectrophotoscopy 191
7.3.2 Nuclear Magnetic Resonance (NMR) 191

7.4 INTERACTION WITH OLIGONUCLEOTIDES 192
7.4.1 Determination of Oligonucleotides Concentration 192
7.4.2 Binding Stoichiometry 192
7.4.3 Association Constants (K_{ass}) 192
7.4.4 Melting Curves 193
7.5 INTERACTIONS WITH HAEM 193
7.5.1 Binding Stoichiometry 193
7.5.2 Association Constants (K_{ass}) 193
7.6 COMPUTATIONAL DETAILS 194
7.6.1 Density Functional Theory Optimizations 194
7.6.2 Double-Stranded DNA Docking Studies 194
7.6.3 Haematin Dimer Docking Studies 195

REFERENCES 197

APPENDICES 225
Appendix A. ^{1}H and ^{13}C NMR chemical shifts (ppm) of cryptolepine (1) and derivatives (3) 229
Appendix B. ^{1}H and ^{13}C NMR chemical shifts (ppm) of quindolones (4 and 91a-c) and their derivatives (5, 94 and 95) 233
Appendix C. Fitting of the UV-visible Vs pH experimental data of the cryptolepine derivatives (3) to the Henderson-Hasselbalch equation 236
Appendix D. Acid dissociation constants (pK_a) of cryptolepine and derivatives (3a-y) as well as of quindolones (4, 91a and 91b) and derivatives (5, 94 and 95) predicted by SPARC software (release W4.2.1405-s4.2.1408) 241
Appendix E. UV-Visible Spectrophotometry Determination of Binding Constants to DNA in buffer solutions containing 0.1 M NaCl 243
Appendix F. Spectrophotofluorimetry Determination of Binding Constants to DNA in buffer solutions containing 0.1 M NaCl 245
Appendix G. Spectrophotometric Determination of Binding to DNA in buffer solutions containing 0.01 M or 1.0 M NaCl 250
Appendix H. UV-Visible Spectrophotometry Determination of Binding Constants to FPIX-OH in pH 5.5 HEPES buffer (40 % DMSO) 252
Appendix I. Docking studies with DNA 259
Appendix J. Docking studies with haemozoin dimer 263
Appendix K. Derivation of vacuolar accumulation ratio equation 266
Appendix L. Relevant Publications 268

List of Figures

Figure 1.1 – Estimated incidence of malaria per 1000 population, 2006 data.(26) 8
Figure 1.2 – Schematic representation of the *Plasmodium* sp. life cycle.(47) 10
Figure 1.3 – Schematic representation of the *Plasmodium* cell structure.(54) 11
Figure 1.4 – Schematic representation of the haemoglobin degradation mechanism in the digestive vacuole of *Plasmodium.(62)* 12
Figure 1.5 – a) Two unit cells of the crystal of *β*-haematin viewed along the [001] direction; b) Packing diagram of the crystal structure of *β*-haematin.(63) 12
Figure 1.6 – Schematic representation of the processes involved in the haemozoin formation.(18) 13
Figure 1.7 – a) Theoretical growth from *β*-haematin viewed: (top) perpendicular to the {100} face, (bottom) along *c*-axis; b) Crystal structure of *β*-haematin, which consists of molecular haem dimers, viewed along the *c*-axis; c) field emission inlens scanning electron microscopy micrographs of haemozoin purified from *P. falciparum*.(77) 14
Figure 1.8 – Schematic representation of the plasmodium life cycle with phases targeted by antimalarial drugs in the human host. 15
Figure 1.9 – Structures of selected key antimalarial compounds. 17
Figure 1.10 – Chloroquine bound to the face {001} ***β***-haematin crystal highlighting energetically favourable interactions. The distances are between highlighted atoms. NH···NC=C 2.4 Å, Cl-H_3C 3.0 Å, NH···O2C 2.7 Å, NH···C**=**C (***π***-cloud) 2.7 Å.(77) 20
Figure 1.11 – Schematic representation of the parasite at equilibrium in the red blood cell. Top) parasite wild-type, sensitive to chloroquine; bottom) parasite resistant to chloroquine with mutation in PfCRT.(166) 22
Figure 1.12 – Structure of the calcium channel blocker verapamil (24) 23
Figure 1.13 – Indoloquinolines from *Cryptolepis sanguinolenta* and synthetic isoneocryptolepine. 25
Figure 1.14 – Cryptolepine (1) acid-base equilibrium. 26
Figure 1.15 – Indolo[3,2-*b*]quinolines evaluated against *Plasmodium falciparum* strains. 37
Figure 1.16 – Indolo[3,2-*b*]quinolines evaluated against *Plasmodium falciparum* strains. 38
Figure 1.17 – Crystal structure of the cryptolepine intercalated into $d(CCTAGG)_2$. 40

Figure 2.1 – Retrosynthetic analysis for the synthesis of the cryptolepine and quindolone derivatives (**3** and **5**). 47
Figure 2.2 – Structure of the 2-(2-Bromoacetamido) benzoic acids (**89**) 48
Figure 2.3 – Assignment of ^{1}H and ^{13}C NMR of **89a**. 48
Figure 2.4 – Structure of the 2-(2-(phenylamino)acetamido)benzoic acids **90**. 49
Figure 2.5 – Assignment of ^{1}H and ^{13}C NMR of **90a**. 49
Figure 2.6 – Structure of the 5*H*-indolo[3,2-*b*]quinolin-11(10*H*)-ones **91**. 50
Figure 2.7 – Assignment of ^{1}H and ^{13}C NMR of **4**. 51
Figure 2.8 – Structure of the 11-chloro-10*H*-indolo[3,2-*b*]quinolines **92**. 52
Figure 2.9 – Assignment of ^{1}H and ^{13}C NMR of **92a**. 53
Figure 2.10 – Stucture of the 5-methyl-11-chloro-10*H*-indolo[3,2-*b*]quinolin-5-ium chlorides 93 53
Figure 2.11 – Assignment of ^{1}H and ^{13}C NMR of **93a**. 54
Figure 2.12 – Assignment of ^{1}H and ^{13}C NMR of **25**. 55
Figure 2.13 – Assignment of ^{1}H and ^{13}C NMR of **1**. 56

Figure 2.14 – Structure of the cryptolepine derivatives **3**. 57
Figure 2.15 – Assignment of ^{1}H and ^{13}C NMR of **3n**. 59
Figure 2.16 – Quindolone tautomeric resonance after deprotonation of N^{5} (red) and N^{10} (blue). 61
Figure 2.17 – Structure of the quindolone derivatives **5**. 62
Figure 2.18 – Structures of 2-(11-(2-(diethylamino)ethoxy)-10*H*-indolo[3,2-*b*]quinolin-10-yl)-*N,N*-diethylethanamine (**94**) and 2-((10*H*-indolo[3,2-*b*]quinolin-11-yl)oxy)-*N,N*-diethylethanamine (**95**). 63
Figure 2.19 – Assignment of ^{1}H and ^{13}C NMR of **94a**. 63
Figure 2.20 – Assignment of ^{1}H and ^{13}C NMR of **5a**. 64
Figure 2.21 – Assignment of ^{1}H and ^{13}C NMR of **95a**. 65

Figure 3.1 – a) UV-visible stacked spectra of cryptolepine (5μM) in the pH range from 3 to 13.7; b) UV-visible relative absorbance values of **1** at different wavelengths as a function of pH at 25 ºC (lines represent the fitting of the experimental data using the Hendersson-Hasselbach modified equation). 73
Figure 3.2 – a) UV-visible stacked spectra of **3b** (5μM) in the pH range 3 to 13.7; b) UV-visible relative absorbance values of **3b** at different wavelengths as a function of pH at 25 ºC (lines represent the fitting of the experimental data using the Hendersson-Hasselbach modified equation). 74
Figure 3.3 – a) UV-visible stacked spectra of **3s** (5μM) in the pH range 3 to 13.7; b) UV-visible relative absorbance values of **3s** at different wavelengths as a function of pH at 25 ºC (lines represent the fitting of the experimental data using the Hendersson-Hasselbach modified equation). 77
Figure 3.4 – a) ^{1}H NMR stacked spectra of cryptolepine in the pH* range from 1.6 to 12 (increasing from the bottom to the top) at 25 ºC; b) ^{1}H NMR chemical shifts (δ_H) of **1** as a function of pH in D_20:DMSO-d_6 (60:40) and 25 ºC (lines represent the fitting of the experimental data using the Hendersson-Hasselbach equation). 78
Figure 3.5 –Deprotonation of the indolic nitrogen atom of cryptolepine induces a strong electronic effect in the *orto* and *para* positions (H^{9} and H^{7}) to C9a. 79

Figure 4.1 - Job plots for a) cryptolepine (**1**) and b) 3-chloro-5-methyl-11-(3-(diethylamino)propylamino)quindolinium chloride (**3v**) complexed with 12-mer ds oligonucleotide at 0.01 M phosphate buffer, 0,1 M NaCl at 25 ºC. The sum of the concentrations of the ligand and oligonucleotide was kept constant at [ds-DNA]+[Ligand]= 12.5 μM (for compound 1) and 2.5 μM (for compound **3v**). For compound **1** absorbance was measured at 368 nm and for compound 3v, fluorescence was measured at 483 nm with an excitation wavelength of 339 nm. The crossover points lie in 0.67 (**1**) and 0.66 (**3v**) consistent with a ligand:oligonucleotide ratio of 2:1. 92
Figure 4.2 – A typical melting curve of double-stranded DNA. 93
Figure 4.3 – Double strand DNA thermal melting monitored by UV absorbance at 260 nm in 0.01 M phosphate buffer containing 0.1 M NaCl, for a) **1** and cryptolepine derivatives b) **3j**, c) **3n** and d) **3v**. Melting curves represent ligand to DNA ratios of 0.5, 1, 2, 4 and 6. 94
Figure 4.4 – Curve resulting from the saturation analysis of complexation between a ligand and a receptor (one-site ligand binding). 95
Figure 4.5 – Curve resulting from the saturation analysis of complexation between a ligand and a receptor (strong binding event followed by a weak binding event). 96

Figure 4.6 – a) UV-visible spectra changes at 25.0 ºC on titration of cryptolepine, **1** (5 µM) with the 12-mer sequence DNA in 0.01 M phosphate buffer at pH 7.40 containing 0.1 M NaCl; b) Plot of the absorbance at 367 nm *vs.* [ds-DNA] and the fits to binding models for one- and two-sites binding. The points are experimental: the lines are best fit to the two-site binding model. The expanded box show details of the data in the region of the 374 nm isosbestic point. The DNA:Ligand ratio increase as follows: 0 (black bold line), 0.2, 0.5, 1.0, 1.6, 2.1, 2.6, 3.1, 4, 5, 6.4, 7.6, 8.8, 10.2, 11.3 and 12.3, sequentially from the top in the region of 367 nm. 96

Figure 4.7 – UV-visible spectra of the titration of **1** with the 16-mer single-stranded oligonucleotide in 0.01 M phosphate buffer containing 0.1 M NaCl at 25 ºC. The concentration of cryptolepine was 5 µM and the DNA:Ligand ratio increase as follows: 0 (black bold line), 0.25, 0.50, 0.75, 1.00, 1.25, 1.50 and 1.75. 97

Figure 4.8 – a) UV-visible spectral changes at 25.0 °C on titration **3n** (5.00 µM) with added aliquots of 12-mer d(GATCCTAGGATC)$_2$ oligonucleotide duplex in 0.01 M phosphate buffer at pH 7.40 containing 0.1 M NaCl; The expanded box shows detail of the data in the region of the 365 nm isosbestic point. The ds-DNA:Ligand ratio increase as follows: 0 (black bold line), 0.3, 0.6, 0.8, 1.1, 1.6, 2.2, 2.7, 3.2 and 3.7, sequentially from the top spectrum in the region around 356 nm. b) Plot of absorbance at 356 nm *vs.* [ds-DNA] and the fits to binding models for 1 and 2 sites. The points are experimental; the lines are best fit to the two-site binding model................98

Figure 4.9 – a) Fluorescence emission spectra of **3n** (5 µM): the DNA:Ligand increased as follows: 0 (black bold line), 0.3, 0.5, 0.8, 1.1, 1.6, 2.1, 2.6 and 3.1 sequentially from the top spectrum into the region of 465 nm (the curve with strongest emission, around 465 nm was ligand 3n in the absence of ds-DNA). b) Plot of emission at 465 nm *vs.* [ds-DNA] and the fits to binding models for 1 and 2 sites. The points are experimental: the lines are best fit to the two-site binding model. 99

Figure 4.10 – Job plots for a) cryptolepine (**1**), b) chloroquine (**2**), c) derivative **3c** and d) **3n** complexed with FPIX-OH in buffered 40 % DMSO, pH 5.5 at 25 ºC. The sum of the concentrations of the ligand and FPIX-OH was kept constant [ligand]+[FPIX-OH]=10 µM. The absorbance changes of the Soret band was measured at 402 nm. y-axes is the corrected absorbance ($y = -\{A-(\varepsilon_{FPIX-OH}[FPIX-OH]+ \varepsilon_{compound}[compound])b\}$), where A is the measured absorbance, $\varepsilon_{FPIX-OH}$ and $\varepsilon_{compound}$ are the molar absorptivities of hematin and **1**, **2**, **3c** and **3n**, and b the optical path length.(342) 103

Figure 4.11 – Job plots for a) quindolone (**4**) and derivatives b) **5a**, c) **94a** and d) **95a** complexed with FPIX-OH in buffered 40 % DMSO, pH 5.5 at 25 ºC. The sum of the concentrations of the ligand and FPIX-OH was kept constant [ligand]+[FPIX-OH]=10 µM. The absorbance changes of the Soret band was measured at 402 nm. y-axes is the corrected absorbance ($y = -\{A-(\varepsilon_{compound}[compound]+ \varepsilon_{FPIX-OH}[FPIX-OH])\}$), where A is the measured absorbance, $\varepsilon_{FPIX-OH}$ and $\varepsilon_{compound}$ are the molar absorptivities of hematin and **4**, **5a**, **94a** and **95a**, and b the optical path length.(342)................104

Figure 4.12 – Models of binding between indolo[3,2-*b*]quinolines and haematin monomers................105

Figure 4.13 – a) UV-visible spectral changes at 25.0 °C on titration of haematin (10 µM) with chloroquine (**2**) in HEPES buffer pH 5.5. The **2**:haematin ratio increase as follows: 0 (black bold line), 0.05, 0.1, 0.15, 0.2, 0.25, 0.3, 0.35, 0.4, 0.5, 0.6, 0.7, 0.8, 0.9, 1.1, 1.5, 2.5, 3, 5 and 7, sequentially from the top spectrum in the region around 402 nm. b) Fitting to 1:1 drug:FPIX-OH complex (model 1) of the absorbance at 402 nm *vs.* [**2**]. The points are experimental: the lines are best fit to binding model for 1:1 drug:FPIX-OH. c) UV-visible spectral changes at 25.0 °C on titration of haematin (10 µM) with cryptolepine (**1**) in HEPES buffer pH 5.5. The **1**:haematin ratio increase as follows: 0 (black bold line), 0.05, 0.1, 0.15, 0.2, 0.25, 0.3, 0.35, 0.4, 0.5, 0.6, 0.7, 0.8, 0.9, 1, 1.2, 1.4, 1.6, 1.8, 2.0, 2.5, 3, sequentially from the top spectrum in the region around 402 nm. d) Fitting to 1:1

drug:FPIX-OH complex (model 1) of the absorbance at 402 nm *vs.* [**1**]. e) UV-visible spectral changes at 25.0 °C on titration of haematin (10 μM) with **3n** in HEPES buffer pH 5.5. The **3n**:haematin ratio increase as follows: 0 (black bold line), 0.05, 0.1, 0.15, 0.2, 0.25, 0.3, 0.35, 0.4, 0.5, 0.6, 0.7, 0.8, 0.9, 1, 1.2, 1.4, 1.6, 1.8, 2.0 , sequentially from the top spectrum in the region around 402 nm. f) Fitting to 1:1 drug:FPIX-OH complex (model 1) of the absorbance at 402 nm *vs.* [**3n**]. The points are experimental: the lines are best fit to binding model for 1:1 drug:FPIX-OH. 106

Figure 4.14 – UV-visible spectrophotometric experimental data of FPIX-OH (5 μM)in pH 5.5 HEPES buffer at 25 ºC titrated with quindolone **4** and derivatives **5a**, **94a** and **95a** fitted to 1:1 drug:FPIX-OH complex (model 1). Absorbance at 402 nm vs. a) [**4**], b) [**5a**], c) [**94a**] and d) [**95a**]. 108

Figure 5.1 – Molecular Electrostatic Potential (MEP, values in e/au^3) maps for cryptolepine and some derivatives. 120

Figure 5.2 – Four different docking orientations investigated for intercalation of 1, corresponding to the rotation of the molecule around two orthogonal axes located in the molecule plan. 121

Figure 5.3 – Stereo view of the projection up the helix axis of a d(GpG)-d(CpC) dinucleotide of the double-stranded d(GATCCTAGGATC)$_2$ oligonucleotide with the ligand **1** sandwiched (dot-grey: H-bond between bases); b) Stereo view of the Van Der Walls interactions map of the ligand **1** intercalated, looking into the major groove (blue: mild polar; red: hydrophobic: yellow: H-bonding), shown intercalation pocket only for clarity, value in Å); c) Interactions map of ligand **1** intercalated into d(GpG)-d(CpC) dinucleotide of the double-stranded d(GATCCTAGGATC)$_2$ oligonucleotide. (blue circle: receptor exposure; pink circle: polar; blue: ligand exposure; dot green π-π interaction; dot purple: proximity contour). 122

Figure 5.4 – Final docking complex of **3n** intercalated in pose 2 into GC-sites of double-stranded oligonucleotide d(GATCCTAGGATC)$_2$. (grey dot-lines:H-bond between bases: dashed-black: H-Bond; dashed-red: ionic binding; dashed-green: π-π interactions; phosphate backbone was removed for clarity) 124

Figure 5.5 – a) Model of **3n** interacting with minor groove and phosphate backbone (blue: weakly polar; red: hydrophobic: yellow: H-bonding; dashed-black: H-Bond; dashed-red: ionic binding); b) Interactions map of **3n** with the minor groove and phosphate backbone of the double-stranded d(GATCCTAGGATC)$_2$ oligonucleotide. (blue circle: receptor exposure; pink circle: polar; blue: ligand exposure; arrow dashed green: H-bonding with chain; dashed red: ionic binding; dashed purple: proximity contour; values are in Å). 125

Figure 5.6 – H-bond interaction of **3x** with the phosphate backbone in the major groove region. 126

Figure 5.7 - Model of chloroquine (**2**) and cryptolepine (**1**) interacting with haemozoin dimer. a) chloroquine top-view; b) chloroquine; c) cryptolepine top-view; d) cryptolepine. (dashed-black. H-bond; solid green: π-π interactions; solid-black: distances; values in Å). 127

Figure 5.8 - Model of cryptolepine derivatives **3g**, **3n** and **3y** interacting with haemozoin dimer. a) **3g** top-view; b) **3g**; c) **3n** top-view; d) **3n**; e) **3y** top-view; f) **3y**. (dashed-black. H-bond; solid green: π-π interactions; dashed-red: ionic binding; solid-black: distance; values in Å). 130

Figure 5.9 – Conformational analysis of the cryptolepine derivatives a) **3f**, b) **3l** and c) **3n**, determined using density functional theory (DFT) with B3LYP. 132

Figure 5.10 – Model of quindolone (**4**) interacting with haemozoin dimer. a) quindolone top-view; b) quindolone. (dashed-black. H-bond; solid green: π-π interactions; solid-black: distances; values in Å). 133

Figure 5.11 – Model of quindolone derivatives **5a**, **94a** and **95a** interacting with haemozoin dimer. a) **5a** top-view; b) **5a**; c) **94a** top-view; d) **94a**; e) **95a** top-view; f) **95a**. (dashed-black. H-bond; solid green: π-π interactions; dashed-red: ionic binding; solid-black: distance; values in Å). 134

Figure 6.1 – Natural bond orbitals (NBO) charges of **1**, **93** and cryptolepine derivatives **3n**. 142

Figure 6.2 – Intracellular localization of **1** and **3n** in *P. falciparum*-infected erythrocytes. 148

Figure 6.3 – a) Fluorescence emission spectrum (λ_{ex} = 339 nm) of 1 μM **3n** in the presence (dashed line) and absence (solid line) of 1μM FPIX-OH. b) Fluorescence emission spectrum (λ_{ex} = 339 nm) of 0.5 μM **3n** in the presence (dashed line) and absence (solid line) of 0.69 μM ds-DNA...................................149

List of Tables

Table 1.1 – IC_{50} values of lead indoloquinolines (IQ) against CQ-R and CQ-S *Plasmodium falciparum* strains. 35

Table 2.1 – ^{1}H NMR chemical shifts (δ_H) of the aliphatic CH_2 in **90** and its reaction yields. 49

Table 2.2 – ^{13}C NMR chemical shift (δ_C) of carbonyl carbon in **4** and **91** and its reaction yields......................................51

Table 2.3 – Yields of the alkylation reaction of quindolones (**4**, **91a** and **91b**), to afford their derivatives **5**, **94** and **95**. 62

Table 3.1 – Acid dissociation constants at 25 ºC for cryptolepine (**1**) and cryptolepine derivatives (**3a-y**), determined by UV-visible spectrophotometry. 76

Table 3.2 – Changes in ^{1}H NMR chemical shift (δ_H) in the studied pH range of protons H^7, H^9 and H^{11} of cryptolepine and protons H^1, H^7 and H^9 of cryptolepine derivatives. 79

Table 3.3 – Non-linear fitting of the ^{1}H NMR chemical shifts to the Henderson-Hasselbalch modified equation of cryptolepine derivatives in the studied pH* range 3 to 13...80

Table 3.4 – Acid dissociation constants (pK_a^*) and observed acid dissociation group constants (pK_a^{Obs}) at 25 ºC for cryptolepine (1) and cryptolepine derivatives (3a-y), determined by nuclear magnetic resonance spectroscopy. 83

Table 4.1 – Melting temperatures (T_m) and their variation (ΔT_m) for d(GATCCTAGGATC)$_2$ (2.83 µM)-ligand (**1**, **3j**,**n**,**w**) complex, monitored at 260 nm in phosphate buffer pH 7.4 containing 0.1 NaCl, for a range of ligand concentrations...93

Table 4.2 – Association constants for complexes between cryptolepine (**1**) and derivatives **3a-y** with ds-DNA at 25 ºC in 0.01 M phosphate buffer pH 7.4 containing 0.1 M NaCl...100

Table 4.3 – Association constants for complexes between cryptolepine (**1**), chloroquine (**2**) and cryptolepine derivatives **3a-y** with haematin monomer at 25 ºC in pH 5.5 HEPES buffer. 107

Table 4.4 – Association constants for complexes between quindolones (**4** and **91**) and quindolone derivatives **5**, **94** and **95** with haematin monomer at 25 ºC in HEPES buffer pH 5.5 109

Table 5.1 – Traditional and hybrid theoretical functionals defined to DFT calculations...115

Table 5.2 – Standard basis set pre-defined in Gaussian software.$^{(376)}$...116

Table 5.3 - Electrical dipole moment, molar volume and partial NBO charges in the nitrogens of cryptolepine (1) and some derivatives (3). 118

Table 5.4 – Calculated energies of complex formation $\Delta E_{bind} = E_{complex} - (E_{DNA} + E_{ligand})$, van der Walls energy ($E_{vdw}$) and electrostatic energy (E_{ele}) obtained for different orientations of 1 intercalated with d(GATCCTAGGATC)$_2$ oligonucleotide in non-alternating CC sites, bound to major and minor groove of cryptolepine derivatives (**3f**, **3i-j**, **3n**, **3q**, **3r-s**, **3v-x**) intercalated and/or bound to major and minor groove of d(GATCCTAGGATC)$_2$ oligonucleotide. 123

Table 5.5 – GoldScore$^{(380)}$ values of the doctking studies of chlorquine (**2**), cryptolepine (**1**) and derivatives **3f-h**, **3j**, **3l**, **3n**, **3s**, **3u-v**, **3x-y** with haematin dimer using GOLD software. 131

Table 5.6 – GoldScore$^{(380)}$ values of the docking studies of quindolones (**4**, **91a** and **91b**), as well as of its derivatives **5**, **94** and **95** with haematin dimer using GOLD software. 135

Table 6.1 – *In vitro* antiplasmodial activity (IC_{50}) against *P. falciparum* W2, V1/S, 3D7 and D6 strains, cytotoxicity activity (IC_{50}) against *Vero* cells, selectivity index (SI), resistance index (RI), association constants (K_{ass}) in pH 5.5 DMSO solutions with haematin at 25 ºC and K_{ass} in phosphate buffer pH 7.4 containing 0.1 M NaCl with ds-DNA at 25 ºC of cryptolepine (**1**), derivatives **3** and chloroquine (**2**). 146

Table 6.2 – Vacuolar accumulation ratios (Acc ratio and α) and normalized antiplasmodial IC_{50} values ($IC_{50} \times \alpha$), calculated from UV-visible pK_{a2}^{Obs} group constant values and pK_{a1} SPARC predicted values, of chloroquine (**2**), cryptolepine (**1**) and derivatives **3**, and vacuolar accumulation ratios (Acc ratio and α) and normalized antiplasmodial IC_{50} values ($IC_{50} \times \alpha$), calculated from NMR pK_{a1}, pK_{a2} and pK_{a3} acid constant values, of cryptolepine (**1**) and its derivatives **3b**, **3e**-**f**, **3i**, **3n**, **3s** and **3y**. 151

Table 6.3 - *In vitro* antiplasmodial activity (IC_{50}) against *P. falciparum* W2 strains, cytotoxicity activity (IC_{50}) against HepG2 A16 and selectivity index (SI) of quindolones **4**, **91a** and **91b** and derivatives **5**, **94** and **95**. 158

List of Schemes

Scheme 1.1 – Synthesis of quindoline-11-carboxilic acid (38) by condensation of indoxyl with isatinic acid. 26
Scheme 1.2 – Görlitzer and Weber total synthesis and derived methodologies. 27
Scheme 1.3 – Joule's method total synthesis 28
Scheme 1.4 – Fan and Ablordeppey total synthesis. 29
Scheme 1.5 – Görlitzer and VentzkeNeu total synthesis..................30
Scheme 1.6 – Rocca total synthesis..................31
Scheme 1.7 – Timári total synthesis..................31
Scheme 1.8 – Rádl total synthesis..................32
Scheme 1.9 – Mohan total synthesis 33
Scheme 1.10 – Ray total synthesis. 34

Scheme 2.1 – Synthetic methodology for the synthesis of the common indolo[3,2-*b*]quinolines intermediates..................47
Scheme 2.2 – Acid-catalyzed cyclization of **90** to afford 5H-indolo[3,2-b]quinolin-11(10H)-ones (**91**, 11-quindolones). 50
Scheme 2.3 - Halogenation mechanism of **91** to give the 11-cloroquindolines (**92**) in a Vilsmeier reaction. 52
Scheme 2.4 – Synthetic methodology for the synthesis of cryptolepine from **92**..................55
Scheme 2.5 – Synthetic methodology for synthesis of the cryptolepine derivatives **3**. 58
Scheme 2.6 – Synthetic methodology for the synthesis of the cryptolepine derivatives **3o-q**..................58
Scheme 2.7 – Reductive amination mechanism of **3n** with aldehyde to afford **3o,p** and **q**..................59
Scheme 2.8 – Synthetic methodology for the synthesis of the quindolone derivatives **5**. 61
Scheme 2.9 – Products of the synthetic methodology used for the synthesis of the quindolone derivatives **5**..................62
Scheme 2.10 – Synthetic methodology for the synthesis of alkyldiamines **97**, **100**, **103** and **105** used in the synthesis of cryptolepine derivatives **3d,j,l** and **t**. 66
Scheme 2.11 - Mannich reaction mechanism of the N-(4-((diethylamino)methyl)-3-hydroxyphenyl)-acetamido (**105**) synthesis. 68

Scheme 3.1 – Proposed macroscopic acid base equilibrium for the cryptolepine derivatives **3a-x**..................72
Scheme 3.2 – Proposed macroscopic acid base equilibrium for the cryptolepine derivatives **3y**. 72
Scheme 3.3 – Proposed microscopic acid base equilibrium for the cryptolepine derivatives **3**..................75

Scheme 6.1 – Synthesis of the cryptolepine derivatives (**3**) and quindolone derivatives (**5**)..................141

List of Compounds

(**1**) Cryptolepine 1
(**2**) Chloroquine 1
(**3**) Cryptolepine derivatives 1
(**3a**) 5-methyl-11-[(2-aminoethyl)amino]-10*H*-indolo[3,2-*b*] quinolin-5-ium chloride 57
(**3b**) 5-methyl-11-{[2-(dimethylamino)ethyl]amino}10*H*-indolo[3,2-*b*] quinolin-5-ium chloride 57
(**3c**) 5-methyl-11-{[2-(diethylamino)ethyl]amino}-10*H*-indolo[3,2-*b*] quinolin-5-ium chloride 57
(**3d**) 5-methyl-11-[1-(diethylamino)propan-2-yl)amino]-10*H*-indolo[3,2-*b*] quinolin-5-ium chloride 57
(**3e**) 5-methyl-11-[(3-aminopropyl)amino]-10*H*-indolo[3,2-*b*] quinolin-5-ium chloride 57
(**3f**) 5-methyl-11-{[3-(dimethylamino)propyl]amino}-10*H*-indolo[3,2-*b*] quinolin-5-ium chloride 57
(**3g**) 5-methyl-11-{[3-(diethylamino)propyl]amino}-10*H*-indolo[3,2-*b*] quinolin-5-ium chloride 57
(**3h**) 5-methyl-11-{[3-(dimethylamino)-2,2-dimethylpropyl] amino}-10*H*-indolo[3,2-*b*]quinolin-5-ium chloride 57
(**3i**) 5-methyl-11-{[3-(isopropylamino)propyl]amino}-10*H*-indolo[3,2-*b*] quinolin-5-ium chloride 57
(**3j**) 5-methyl-11-{[3-(piperidin-1-yl)propyl]amino}-10*H*-indolo[3,2-*b*] quinolin-5-ium chloride 57
(**3k**) 5-methyl-11-[(4-aminobutyl)amino]-10*H*-indolo[3,2-*b*] quinolin-5-ium chloride 57
(**3l**) 5-methyl-11-{[4-(diethylamino)butyl]amino}-10*H*-indolo[3,2-*b*] quinolin-5-ium chloride 57
(**3m**) 5-methyl-11-{[5-(diethylamino)pentan-2-yl]amino}-10*H*-indolo[3,2-*b*] quinolin-5-ium chloride 57
(**3n**) 5-methyl-11-(piperidin-4-ylamino)-10*H*-indolo[3,2-*b*] quinolin-5-ium chloride 57
(**3o**) 5-methyl-11-[(1-isobutylpiperidin-4-yl)amino]-10*H*-indolo[3,2-*b*] quinolin-5-ium chloride 57
(**3p**) 5-methyl-11-[(1-benzylpiperidin-4-yl)amino]-10*H*-indolo[3,2-*b*] quinolin-5-ium chloride 57
(**3q**) 5-methyl-11-{[1-(2-hydroxybenzyl)piperidin-4-yl]amino}-10*H*-indolo[3,2-*b*]quinolin-5-ium chloride 57
(**3r**) 5-methyl-11-(phenylamino)-10*H*-indolo[3,2-*b*]quinolin-5-ium chloride 57
(**3s**) 5-methyl-11-{[4-(piperidin-1-yl)phenyl]amino}-10*H*-indolo[3,2-*b*] quinolin-5-ium chloride 57
(**3t**) 5-methyl-11-{{4-[(diethylamino)methyl]-3-hydroxy-phenyl}amino}-10*H*-indolo[3,2-*b*]quinolin-5-ium chloride 57
(**3u**) 5-methyl-11-(pyridin-3-ylamino)-10*H*-indolo[3,2-*b*] quinolin-5-ium chloride 57
(**3v**) 3-chloro-5-methyl-11-{[3-(diethylamino)propyl]amino}-10*H*-indolo[3,2-*b*] quinolin-5-ium chloride 57
(**3w**) 3-chloro-5-methyl-11-(piperidin-4-ylamino)-10*H*-indolo[3,2-*b*] quinolin-5-ium chloride 57
(**3x**) 3,8-dichloro-5-methyl-11-(piperidin-4-ylamino)-10*H*-indolo[3,2-*b*] quinolin-5-ium chloride 57
(**3y**) 5-methyl-11-(diethylamino)-10*H*-indolo[3,2-*b*]quinolin-5-ium chloride 57
(**4**) Quindolone 4
(**5**) Quindolone derivatives 4
(**6**) Atovaquone 17
(**7**) Proguanil, R = H, ... 17
(**8**) Chloroproguanil, R = Cl 17
(**9**) Pyrimethamine 17
(**10**) Primaquine 17
(**11**) Pamaquine 17
(**12**) Tafenoquine 17
(**13**) Piperaquine 17
(**14**) Amodiaquine 17
(**15**) Pyronaridine 17
(**16**) Quinine 17

(**17**) Mefloquine 17
(**18**) Halofantrine 17
(**19**) Lumefantrine 17
(**20**) Artemisinin 17
(**21**) Arteether, R = OEt 17
(**22**) Artemether, R = OMe 17
(**23**) Dihydroartemisinin 17
(**24**) Verapamil 23
(**25**) Quindoline 25
(**26**) Hydroxycryptolepine, R = OH 25
(**27**) Cryptolepinoic acid, R = COOH 25
(**28**) Methylcryptolepinoate, R = $COOCH_3$ 25
(**29**) Neocryptolepine 25
(**30**) Isocryptolepine 25
(**31**) Cryptospirolepine 25
(**32**) Cryptomisrine 25
(**33**) Bis-cryptolepine 25
(**34**) Cryptoquindoline 25
(**35**) Isoneocryptolepine 25
(**36**) Indoxyl 26
(**37**) Isatinic Acid 26
(**38**) Quindoline-11-carboxilic acid 26
(**39**) methyl 2-aminobenzoate 27
(**40**) N-(2-(2-bromoacetyl)phenyl)-4-methylbenzenesulfonamide 27
(**41**) methyl 2-((2-(2-(4-methyl-phenylsulfonamido)phenyl)-2-oxoethyl)amino)benzoate 27
(**42**) Anthranilic Acids 27
(**43**) 2-(2-bromo-acetamido)benzoic acids 27
(**44**) 2-(2-(phenylamino)-acetamido)benzoic acids 27
(**45**) 1-(pheny-lsulfonyl)-1*H*-indole 28
(**46**) (1-(phenyl-sulfonyl)-1*H*-indol-2-yl)lithium 28
(**47**) 2-nitro-phenyl-(1-(phenylsulfonyl)-1*H*-indol-2-yl)methanol 28
(**48**) 2-aminophenyl-(1-(phenylsulfonyl)-1*H*-indol-2-yl)methanone 28
(**49**) *N*-(2-(1-(phenylsulfon-yl)-1*H*-indole-2-carbonyl)-phenyl)benzamide 28
(**50**) 5-benzoyl-quindolone 28
(**51**) quinolin-3-amine 29
(**52**) *N*-phenylquinolin-3-amine 29
(**53**) diethyl malonate 30
(**54**) 1-(chloromethyl)-2-nitrobenzene 30
(**55**) diethyl 2,2-bis(2-nitrobenzyl)malonate 30
(**56**) 10-hydroxy-10*H*-indolo[3,2-*b*]quinoline 5-oxide 30
(**57**) 10-(2-ethoxy-2-oxoethoxy)-10*H*-indolo[3,2-*b*]quinoline 5-oxide 30
(**58**) 3-fluoro-4-iodoquinoline 31
(**59**) 2-iodo3-fluoro-4-substituted-quinolines 31
(**60**) *N*-(2-(3-fluoroquinolin-2-yl)phenyl)pivalamide 31
(**61**) (2-pivalamidophenyl)boronic acid 31

(62) 2,3-dibromoquinoline ... 31
(63) N-(2-(3-bromoquinolin-2-yl)phenyl)pivalamide ... 31
(64) 2-(3-bromoquinolin-2-yl)aniline ... 31
(65) Ethyl (2-cyanophenyl)-carbamate ... 32
(66) 2-Bromo-1-(2-substituted-phenyl)ethanone ... 32
(67) Ethyl (2-cyanophenyl)(2-(2-substituted-phenyl)-2-oxoethyl)carbamate ... 32
(68) Ethyl 3-amino-2-(2-substituted-benzoyl)-1*H*-indole-1-carboxylate ... 32
(69) 3-Bromoquinoline ... 33
(70) 2-Substituted-anilines ... 33
(71) *N*-(2-substituted-phenyl)quinolin-3-amine ... 33
(72) 7*H*-indolo[2,3-*c*]quinoline ... 33
(73) 1-(2-Nitrophenyl)-ethanone ... 34
(74) (Z)-3-Chloro-3-(2-nitrophenyl)acrylaldehyde ... 34
(75) (E)-4-Substituted-*N*-((Z)-3-((4-substituted-phenyl)amino)-3-(2-nitrophenyl)allylidene)aniline ... 34
(76) 6-Substituted-2-(2-nitrophenyl)quinoline ... 34
(77) 2-Substituted-quindoline ... 34
(78) Ethylcryptolepionate, R = COOEt ... 37
(79) 11-((3-((diethylammonio)methyl)-5-substituted-4-hydroxy-phenyl)amino)-7,10-substituted-10,11a-dihydro-4a*H*-indolo[3,2-*b*]quinolin-5-ium chloride ... 37
(80) 11-substituted Cryptolepine ... 37
(81) 11-substituted quindoline ... 37
(82) 11-substituted Crypt. triflate ... 37
(83) mono, di and tri-subtituted IQ ... 37
(84) mono and di-substituted Crypolepine ... 37
(85) 10,10'-(pentane-1,5-diyl)bis(5-methyl-10H-indolo[3,2-b]quinolin-5-ium) iodide ... 38
(86) 5,5'-(substituted-diyl)bis-(10H-indolo[3,2-b]quinolin-5-ium) ... 38
(87) 10-(5-phenylpentyl)-cryptolepine iodide ... 38
(88) Anthranilic acids ... 47
(89) 2-(2-Bromoacetamido) benzoic acids ... 47
(90) 2-[2-(Phenylamino)-acetamido]benzoic acids ... 47
(90a) 2-(2-(phenylamino)acetamido)benzoic acid ... 49
(90b) 4-chloro-2-[2-(phenylamino)acetamido]benzoic acid ... 49
(90c) 4-chloro-2-{2-[(3-chlorophenyl)amino]acetamido}benzoic acid ... 49
(90d) 4-chloro-2-{2-[(4-chlorophenyl)amino]acetamido}benzoic acid ... 49
(90e) 4-chloro-2-(2-((4-(trifluoromethyl)phenyl)amino)acetamido)-benzoic acid ... 49
(90f) 4-chloro-2-(2-((4-methoxyphenyl)amino)acetamido)benzoic acid ... 49
(90g) 4-chloro-2-(2-((4-methylphenyl)amino)acetamido)benzoic acid ... 49
(91) 5*H*-indolo[3,2-*b*]quinolin-11(10*H*)-ones ... 47
(91a) 3-chloro-5*H*-indolo[3,2-*b*]quinolin-11(10*H*)-one ... 50
(91b) 3,8-dichloro-5*H*-indolo[3,2-*b*]quinolin-11(10*H*)-one ... 50
(91c) 3,7-dichloro-5*H*-indolo[3,2-*b*]quinolin-11(10*H*)-one ... 50
(91d) 3-chloro-7-trifluoromethyl-5*H*-indolo[3,2-*b*]quinolin-11(10*H*)-one ... 50
(91e) 3-chloro-7-methoxy-5*H*-indolo[3,2-*b*]quinolin-11(10*H*)-one ... 50
(91f) 3-chloro-7-methyl-5*H*-indolo[3,2-*b*]quinolin-11(10*H*)-one ... 50
(92) 11-chloro-10*H*-indolo[3,2-*b*]quinolines ... 47

(**92a**) 11-chloro-10*H*-indolo[3,2-*b*]quinoline 52
(**92b**) 3,11-dichloro-10*H*-indolo[3,2-*b*]quinoline 52
(**92c**) 3,8,11-trichloro-10*H*-indolo[3,2-*b*]quinoline 52
(**92d**) 3,7,11-trichloro-10*H*-indolo[3,2-*b*]quinoline 52
(**92e**) 3,11-dichloro-7-trifluoromethyl-10*H*-indolo[3,2-*b*]quinoline 52
(**92f**) 3,11-dichloro-7-methoxy-10*H*-indolo[3,2-*b*]quinoline 52
(**92g**) 3,11-dichloro-7-methyl-10*H*-indolo[3,2-*b*]quinoline 52
(**93**) 5-methyl-11-chloro-10*H*-indolo[3,2-*b*]quinolines 47
(**93a**) 5-methyl-11-chloro-10*H*-indolo[3,2-*b*]quinolin-5-ium chloride 53
(**93b**) 3,11-dichloro-5-methyl-10*H*-indolo[3,2-*b*]quinolin-5-ium chloride 53
(**93c**) 3,8,11-trichloro-5-methyl-10*H*-indolo[3,2-*b*]quinolin-5-ium chloride 53
(**93d**) 3,7,11-trichloro-5-methyl-10*H*-indolo[3,2-*b*]quinolin-5-ium chloride 53
(**93e**) 3,11-dichloro-5-methyl-7-trfifluoromethyl-10*H*-indolo[3,2-*b*] quinolin-5-ium chloride 53
(**93f**) 3,11-dichloro-5-methyl-7-methoxy-10*H*-indolo[3,2-*b*] quinolin-5-ium chloride 53
(**93g**) 3,11-dichloro-5-methyl-7-methyl-10*H*-indolo[3,2-*b*]quinolin-5-ium chloride 53
(**94**) 2-(11-(2-(diethylamino)ethoxy)-10*H*-indolo[3,2-*b*]quinolin-10-yl)-*N,N*-diethylethanamines 62
(**94a**) 2-(11-(2-(diethylamino)ethoxy)-10*H*-indolo[3,2-*b*]quinolin-10-yl)-*N,N*-diethylethanamine 63
(**94b**) 2-((3-chloro-10-(2-(diethylamino)ethyl)-10*H*-indolo[3,2-*b*]quinolin-11-yl)oxy)-*N,N*-diethylethanamine 63
(**94c**) 2-((3,7-dichloro-10-(2-(diethylamino)ethyl)-10*H*-indolo[3,2-*b*]quinolin-11-yl)oxy)-*N,N*-diethylethanamine 63
(**95**) 2-((10*H*-indolo[3,2-b]quinolin-11-yl)oxy)-*N,N*-diethylethanamines 62
(**95a**) 2-((10*H*-indolo[3,2-*b*]quinolin-11-yl)oxy)-*N,N*-diethylethanamine 63
(**95b**) 2-((3-chloro-10*H*-indolo[3,2-*b*]quinolin-11-yl)oxy)-*N,N*-diethylethanamine 63
(**95c**) 2-((3,7-dichloro-10*H*-indolo[3,2-*b*]quinolin-11-yl)oxy)-*N,N*-diethylethanamine 63
(**96**) *N,N*-dimethylamino-propanone 66
(**97**) N^1,N^1-dimethyl- propane-1,2-diamine 66
(**98**) *N*-(3-bromopropyl)-phthalimide 66
(**99**) 2-(3-(piperidin-1-yl)-propyl)isoindoline-1,3-dione 66
(**100**) 3-piperidin-1-yl-propan-1-amine 66
(**101**) *tert*-butyl-4-aminobutylcarbamate 66
(**102**) *tert*-butyl-4-(diethylamino)butylcarbamate 66
(**103**) N^1,N^1-diethyl-butane-1,4-diamine 66
(**104**) *N*-(3-hydroxyphenyl)-acetamide 66
(**105**) *N*-(4-((diethylamino)-methyl)-3-hydroxyphenyl)-acetamide 66

List of Equations

Eq. 3.1 – Modified Henderson-Hasselbalch equation. 73
Eq. 3.2 – pH-meter readings in D_2O solutions and H_2O pK_a correlation equation 77

Eq. 4.1 – Binding constant equation of a complexation process. (L - ligand, R – receptor; C - complex) 94
Eq. 4.2 – Saturated analysis non-linear equation of one-site ligand binding. (y = change in specific physicochemical property)....95
Eq. 4.3 – Scatchard equation of the saturated analysis of one-site ligand binding (n=1), or multiple-site ligand binding (n>1). 95
Eq. 4.4 – Saturated analysis non-linear equation of the two-site ligand binding (strong binding event followed by a weak binding event)....96
Eq. 4.5 - Binding equation between one haematin monomer with one molecule of ligand....105

Eq. 5.1 – Energy of complex formation. 121

Eq. 6.1 - Predicted vacuolar accumulation ratios(123) $[Q]_v/[Q]_e$, assuming indoloquinolines with two acids dissociation constants (digestive vacuole pH = 5.5(123) and an external pH = 7.4) 149
Eq. 6.2 - Predicted vacuolar accumulation ratios $[IQ]_v/[IQ]_e$, assuming indoloquinolines with three acids dissociation constants (digestive vacuole pH = 5.5(123) and an external pH = 7.4). 149

Abbreviations and Definitions

Abs	*Absorbance*
AcOEt	*Ethyl Acetate*
AQ	*Amodiaquine*
ART	*Artemisinins*
ax	*Axial*
a.u.	*Atomic units*
Cal	*Calculated*
CCDC	*Cambridge Crystallographic Data Centre*
cis	*On the same side (from latin)*
^{13}C NMR	*Carbon nuclear magnetic resonance*
COSY	*Proton - proton correlation spectroscopy*
CQ	*Chloroquine*
CQ-R	*Chloroquine-resistant*
CQ-S	*Chloroquine-sensitive*
CRYP	*Cryptolepine*
d	*Doublet*
Da	*Daltons*
dd	*Double-doublet*
DFT	*Density functional theory*
DIPEA	*N,N-diisoproprylethylamine*
DMF	*Dimethylformamide*
ds	*Double stranded*
DV	*Digestive vacuole*
ε	*Molar extinction coefficient*
EA	*Elemental analysis*
eq	*Equivalents, equatorial or equation*
E-state	*Electrotopological state*
EtOAc	*Ethyl Acetate*
EXAFS	*Extended X-ray absorption fine structure*
FPIX	*Ferriprotoporphyrin IX*
FS	*Fluorescence spectroscopy*
H-bond	*Hydrogen-bond*
HD	*Halogen Dance reaction*
HF	Hartree-Fock
HMBC	*Heteronuclear Multiple Bond Correlation spectroscopy*
HMQC	*Heteronuclear Multiple Quantum Correlation spectroscopy*
^{1}H NMR	*Proton nuclear magnetic resonance*
HOMO	*Highest occupied molecular orbital*
HPR-II	*Histidine Rich Protein II*
HZ	*Haemozoin*
IQ	*Indolo[3,2-b]quinoline*
IUPAC	*International Union of Pure and Applied Chemistry*
IV	*Infrared spectroscopy*
K_{ass}	*Association constant*
λ_{em}	*Fluorescence emission wavelength*
λ_{ex}	*Fluorescence excitation wavelength*
Log P	*Octanol - water partition coefficient*
LUMO	*Lowest unoccupied molecular orbital*
MeOH	*Methanol*

m	*Multiplet*
MEP	*Molecular Electrostatic Potential*
mp	*Melting point*
MS	*Mass spectroscopy*
n.d.	*Not determined*
NMR	*Nuclear magnetic resonance spectroscopy*
NOESY	*Nuclear Overhauser Effect Spectroscopy*
NVT	*constant-temperature, constant-volume ensemble*
OTf	*Trifluoromethanesulfonate*
PDB	*Protein database file*
PET	*Polyethylene Terephthalate*
PfCRT	*Plasmodium falciparum Chloroquine Resistance Transporter*
$\mathrm{p}K_\mathrm{a}$	*Acid dissociation constant*
$\mathrm{p}K_\mathrm{a}^*$	*Acid dissociation constant as function of direct pH-meter readings of deuterium solutions*
$\mathrm{p}K_\mathrm{a}^\mathrm{D}$	*Acid dissociation constant in deuterium solutions corrected experimentally*
$\mathrm{p}K_\mathrm{a}^\mathrm{Obs}$	*Observed acid dissociation group constants*
$\mathrm{p}K_\mathrm{a}^{*\mathrm{Obs}}$	*Observed acid dissociation group constants as function of direct pH-meter readings of deuterium solutions*
PPA	*Polyphosphoric acid*
ppm	*parts per million*
q	*Quadruplet*
QSAR	*Quantitative Structure-Activity Relationships*
RBC	*Red blood cells*
δ_c	*Carbon nuclear magnetic resonance chemical shift*
δ_H	*Proton nuclear magnetic resonance chemical shift*
s	*Singlet*
SAR	*Structure-activity relationships*
SN_2	*Nucleophilic reaction of second order*
sp.	*species*
ss	*single stranded*
t	*Triplet*
TEA	*Triethylamine*
TEM	*Transmission electron microscopy*
TLC	*Thin-layer chromatography*
T_m	*Melting temperature*
trans	*On the other side (from latin)*
TSP	*Trimethylsilyl propionic acid*
UV-Vis	*Ultraviolet-visible spectroscopy*
VAR	*Vacuolar accumulation ratio*
vs.	*versus*
WHO	*World Health Organization*
χ	*Molar fraction*

General Introduction

Rationale and Aims of this Thesis

Cryptolepine (**1**) is an indolo[3,2-*b*]quinoline alkaloid, first isolated in 1929 by Clinquart(1) from the roots of *Cryptolepis sanguinolenta* (synonymy of *Cryptolepis triangularis* N.E.Br.), a traditional herb used in the folk medicine for the treatment of malaria. Cryptolepine possesses a broad range of biological activities that include antiplasmodial, antibacterial, antifungal, antihyperglycemic, anti-inflammatory, and antitumor among others reviewed elsewhere.(2-3) The antiplasmodial activity of **1** was first reported in 1991 by Naomesi(4) after extracting it from the roots of *C. sanguinolenta*. They tested cryptolepine for *in vitro* activity against the *P. falciparum* multi-resistant K1 and found to be highly active with an IC_{50} value of 134 nM, comparable with that of chloroquine (**2**, IC_{50} = 230 nM). However **1** also presents cytotoxic properties that precludes its clinical use. These cytotoxic properties are likely to be due to its DNA interactions properties and its ability to intercalate into GC-rich sequences, inhibiting topoisomerase II as well as DNA synthesis.(5-8)

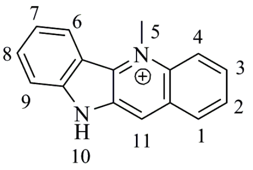

(**1**) Cryptolepine

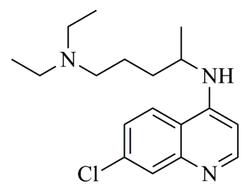

(**2**) Chloroquine

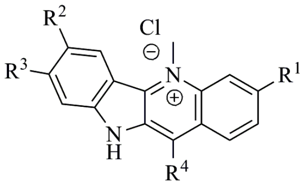

R^1, R^2, R^3 = H, CH_3, CF_3, OCH_3 or Halogen
R^4 = Alkyl, cycloalkyl or aryldiamine

(**3**) Cryptolepine derivatives

Studies on the possible antimalarial mode of action suggest that **1** can also inhibit the haemozoin formation in the parasite digestive vacuole, in a way similar to that of chloroquine and related aminoquinolines. However, no correlation between the antiplasmodial activity and the accumulation in the acid digestive vacuole, determined by a mathematical method, based on the compounds acid dissociation constants (pK_a), was seen, suggesting that the antimalarial activity involves other mechanisms in addition to the inhibition of haemozoin formation.(9-10)

Prompted by these results, the main objective of this project is to synthesise novel derivatives of the antimalarial natural compound cryptolepine as part of a larger project of development of safer and potent antimalarial drugs, at an affordable cost. The proposed approach is to synthesise cryptolepine derivatives (**3**), with an ionisable diamine side chain at position C11 of the alkaloid scaffold, which is expected to improve the antimalarial activity and the selectivity against *Plasmodium* sp., through an increase in the accumulation of compounds inside the acidic digestive vacuole of the intraerythrocytic parasite, where they can target the haem and thus inhibit haemozoin formation.

The specific objectives of this PhD project are:

- to develop robust synthetic methods for the target cryptolepine derivatives (**3**) based on a common synthetic building-block that can be used to prepare a wide range of compounds. These methods can allow the creation of a small library of cryptolepine analogues.
- to use advanced two-dimensional NMR techniques (COSY, HMQC and HMBC) to confirm the chemical structure of all synthesized derivatives;
- to study the binding of compounds to DNA and haeme by a range of methods including melting profiles, UV-visible spectroscopy, fluorescence and molecular modeling simulation;
- to calculate the ratio of compounds concentration inside the parasite food vacuole based on their acid-base equilibrium constants determined by UV-visible and NMR titration;
- based on the antimalarial activity displayed by the target compounds (obtained in Dr. Phil Rosenthal's laboratory, at the University of California), determine structure-activity relationships;
- to use the above mentioned relationships and the in vitro cytotoxicity of compounds (determined at Dr. Cecília Díaz laboratory, at Universidad de Costa Rica) to select compounds for *in vivo* evaluation against *P. berghei* infected mice;

Outline of this Thesis

Chapter 1 gives a short overview of the global malaria spread, the *Plasmodium* life cycle and drugs developed or employed in the malarial therapy, as well as the setbacks of the drug development, like *Plasmodium* resistance. Also the indoloquinolines compounds with antiplasmodial activity are reviewed as well as their synthetic methodologies.

Chapter 2 will discuss the design and synthetic strategies used to obtain the indolo[3,2-*b*]quinolines scaffolds. The cryptolepine derivatives (**3**) synthesis, obtained through the methodology developed by Görlitzer and Weber(11-12) and adapted by Bierer(13-14) will be reported. Characterization of obtained compounds by several methodologies, like NMR, will be discussed, as well as the synthesis and characterization of several intermediates used to achieve these derivatives. In addition, we decided to start a second line of research based on the indolo[3,2-*b*]quinoline chemical structure and engineered, based on the common intermediate indolo[3,2-*b*]quindolin-11-one (**4**, quindolone) a new scaffold for antiplasmodial drug development. The synthesis of new quindolone derivatives with an ionisable alkylamine chain at positions N^5 and N^{10} (**5**) will be described.

In **Chapter 3** the establishment of acid dissociation constants (pK_a) of the synthesized indolo[3,2-*b*]quinoline **3** through the Henderson-Hasselbalch methodology(15-16) will be discussed. The acid-base chemistry is of great importance in biological systems, because it will affect its permeability through biological membranes and interaction with biological targets.

Chapter 4 will present the binding interactions of the cryptolepine derivatives (**3**) with double-stranded DNA structures. Since it is commonly accepted that cryptolepine can exert its cytotoxic properties due to interactions with DNA and topoisomerase II in host cells(8, 17) it is of great importance to understand the type of interaction, the binding affinity as well as the structure-activity relationships of **3**, with double-stranded DNA structures. Also, the study of the binding interactions with haematin, the precursor of the malaria pigment in the detoxification pathway of malaria parasites,(18-21) is essential in the development of novel antiplasmodial drugs. Here, we present the binding type and affinity of the new cryptolepine and quindolone derivatives (**3** and **5**) with haematin monomer, as well as their structures-activity relationships.

Nowadays**,** *in silico* studies can provide information about molecules and binding to biological targets that was very difficult or even impossible to obtain through experimental observation. **Chapter 5** will discuss electronic and charges distribution properties of the cryptolepine derivatives (**3**) obtained through density functional theory (DFT). In addition, docking studies of these derivatives (**3**) with short double-stranded DNA structures will be presented, as well as, docking studies of cryptolepine and quindolones derivatives (**3** and **5**) with haematin dimer will be discussed, allowing to understand their binding interactions.

Chapter 6 will integrate all the studies described in the previous five chapters and provide a global overview of the *in vitro* antiplasmodial properties of the synthesized cryptolepine and quindolone derivatives. Based on the physical and chemical properties of these derivatives, as well as on the DNA and haematin binding properties, the antiplasmodial mode of action of these indolo[3,2-*b*]quinolines will be discussed. Additionally, *in vivo* studies in infected mice infected with *P. berghei*, as well as *in vitro* antiplasmodial activity in human hepatoma cells and intracellular localization of **3n** in *P. falciparum*-infected erythrocytes by fluorescence microscopy will be included in the discussion, aiming to contribute to a better knowledge of their mode of action.

In **Chapter 7** it will be presented all the experimental procedures used to the development of the present study. Synthetic methodologies, physical-chemical properties and *in vitro* binding studies, as well as *in silico* studies will be described.

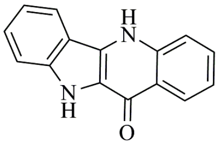

(**4**) Quindolone

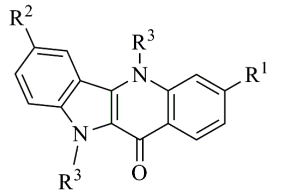

R^1, R^2 = H, Cl

R^3 = Alkyl, cycloalkylamine

(**5**) Quindolone derivatives

I

Chapter I – **Malaria, from Disease to Therapeutics**

> "God not only plays dice, He also sometimes throws the dice where they cannot be seen"
>
> **Stephen Hawking** (1942)
> *British theoretical physicist*

Abstract

Malaria is one of the most prevalent tropical diseases and one of the most wide spread infections of our time. Malaria is caused by protozoal parasites of the genus Plasmodium and the infectious stages of the parasite reside in the salivary glands of female Anopheles mosquitoes that bite humans for a blood meal. During blood extraction the mosquito injects the parasite into the blood stream giving rise to a complex life cycle in human host. Considerable success in gaining control over malaria was achieved in the 1950s and 60s through administration of 4-aminoquinolines, specially chloroquine, the most important antimalarial agent ever. However, the development of resistance by the parasite against antimalarial drugs, has underscored the importance to develop new medicines for the malaria treatment. Natural products remain a rich source of novel molecular scaffolds and cryptolepine, an indolo[3,2-b]quinoline alkaloid extracted from the roots of Cryptolepis sanguinolenta is one example of natural products with antiplasmodial activity. Beside its extraction from natural sources, several synthetic methodologies have been developed and new cryptolepine derivatives with improved antiplasmodial activity have been reported.

List of Contents

1.1 MALARIA OVERVIEW 7
1.1.1 Global Malaria Burden 8
1.1.2 Plasmodium Species 9
1.1.3 Malaria Chemotherapeutics 15
1.1.4 Chloroquine Resistance in Plasmodium sp. 21
1.2 INDOLO[3,2-*B*]QUINOLINE, A SCAFFOLD FOR ANTIPLASMODIAL DRUG DEVELOPMENT 24
1.2.1 Synthetic Pathways 26
1.2.2 Antiplasmodial Activities 34
1.2.3 Interactions with DNA and Cytotoxic Activities 38
1.2.4 Whole Body Distribution of Cryptolepine in Mice and Toxicity 40

1.1 Malaria Overview

Malaria is one of the most widespread infectious diseases of our time. Malaria is a diseases caused by infection with eukaryotic parasites of the genera *Plasmodium.* There are more than 120 species of *Plasmodium*, but only five infect humans; *P. malariae*, *P. ovale*, *P. vivax*, *P. falciparum* and occasionally some human malaria can be caused by *P. Knowlesi*, although it has not been established whether human-mosquito-human transmission can occur. Infections with all these species cause initially similar illness, cyclical fevers, anemia and splenomegaly (enlarged spleen), the classic triad associated with malaria. The benign tertian (*P. vivax and P. ovale*) and quartan malaria (*P. malariae*) very rarely lead to serious illness or life-threatening complications, whereas *P. falciparum* malaria may progress towards severe disease in those not particularly protected by acquired immunity or if not treated promptly.(22)

Malaria is one of the earliest reported infectious diseases in humans and through the years, the development of antimalarial drugs has long been neglected in industrialized countries. The global fight against malaria requires a multiple approach. Nowadays, a wide range of effective tools, which includes insecticides to prevent infection by mosquitoes, and medicines to treat and prevent the infection are available.(23) However, long-term prophylaxis by vaccination has been especially challenging as the parasite has various sophisticated mechanisms to avoid the host immune system.(24) The most effective first generation vaccine in development, GlaxoSmithKline (GSH)'s RTSS, reduces the risk of clinical malaria, delays time to new infection, reduces episodes of severe malaria and it has recently entered Phase III clinical trials.(25) Nevertheless, with all available strategies, several gaps remain in our armory against malaria, and a substantial number of patients will suffer from this disease over the coming decades. To achieve the goal of eradication, antimalarial drug discovery must continue working on the development of new medicines to treat malaria, mainly targeting the asexual blood stages of *Plasmodium* overcoming the emerging drug resistance and also blocking the transmission of the parasite to other persons by the mosquito vector.

1.1.1 Global Malaria Burden

The global malaria map has been shrinking over the past 60 years, but today more people are at risk of suffering from malaria than any other time in history. Malaria is a global health problem with 109 endemic countries in 2008, 247 million cases among 3.3 billion people at risk in 2006 and killing between 1 and 3 million people annually, most of whom are children under 5 years old. Also, pregnant women and their unborn children are particularly vulnerable to the parasites. Malaria is a particularly devastating disease in sub-Saharan Africa, where about 90 % of cases and deaths occur. However, 40 % of the world's population lives in areas where there is risk of transmission. Malaria is found in tropical regions throughout Africa, Southeast Asia, Pacific Islands, India and Central and South America (Figure 1.1). In certain epidemiological circumstances, malaria is a devastating disease with high morbidity and mortality. *Plasmodium falciparum* is the most virulent and deadly of malaria parasites and is responsible for more than 90 % of the cases. In 10-40 % of all cases of severe malaria *P. falciparum* is also lethal, because it can lead to high parasitaemia and additional bind to endothelial cells leading to disruption of organ function.(26)

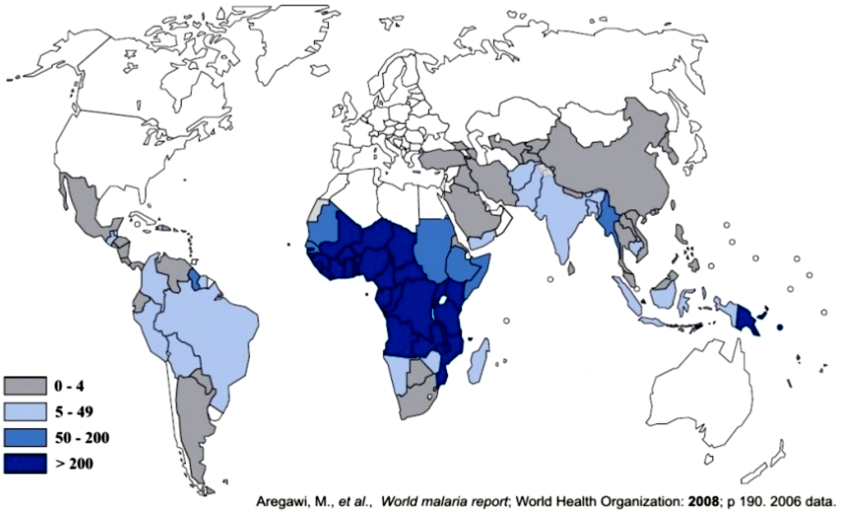

Aregawi, M., *et al.*, *World malaria report*; World Health Organization: **2008**; p 190. 2006 data.

Figure 1.1 – Estimated incidence of malaria per 1000 population, 2006 data.(26)

Malaria can be transmitted by several species of female *Anopheles* mosquitoes that differ in behavior, contributing to the different epidemiological patterns of the disease observed worldwide. After the II World War exhausting efforts were made to eradicate malaria worldwide and were successful over large geographical areas, however in tropical Africa and many parts of Asia were not.

In the past few years malaria has once again attracted more attention. Projects such as *Roll Back Malaria Partnership* (supported by the Word Heath Organization) and the *Bill and Melinda Gates Foundation* malaria eradication program,(27) had contributed to the reinvestment in research, partly because it is recognized that malaria spread in sub-Saharan Africa has increased in the recent years, mainly due to the development of drug resistances. The global climate warming, war and civil conflicts also led to an upsurge of malaria in many parts of Africa where health services are ineffective.(28-31) In addition, malaria and the Human Immunodeficiency Virus (HIV) infection can also interact in several ways, increasing the viral load, increasing malaria fevers and interacting adversely during pregnancy, leading to an increase of the illness and life risk.(32-34)

1.1.2 *Plasmodium* Species

Life Cycle

The malaria parasite is a complex eukaryote with a dynamic pattern of genomic expression, able to constantly change its gene expression to generate a sequence of forms that can subsist in different environments in human and mosquito host.(35) The development of the *Plasmodium* is carried in two hosts, namely mosquito (*Anopheles* sp.) and humans and the events of the plasmodium infection within human bloodstream were extensively reviewed elsewhere.(36)

The infectious stages of the malaria parasite reside in salivary glands of female *Anopheles* mosquitoes that bite humans for a blood meal. During the blood extraction *Anopheles* mosquitoes inject its saliva into the lesion, thereby transferring 15-20 sporozoites into the blood stream (step 1, Figure 1.2). The sporozoites are able to overcome host's immune system and rapidly taken up into the liver, where they pass the Kupffer cells and infect the hepatocytes, developing each one into tissue schizonts containing 10 to 30 thousand merozoites.(37-39) This hepatic development, also called exoerythrocytic, takes a minimum of 6 days after inoculation in *P. falciparum* malaria, 9 days in the benign tertian and about 15 days in quartan malaria. An average incubation of 2 weeks between infection and the onset of the disease might be considered as a rule of thumb in *vivax* and *falciparum* malaria (step 2, Figure 1.2).(40) After the hepatic stage, the developed schizonts rupture the liver cells and release the merozoites into the blood stream, starting the erythrocytic stage of the *Plasmodium* sp. life cycle, the post-hepatic infection (step 3, Figure 1.2).(41) Left untreated, parasites multiply in the red blood cells (RBC) at a rate of about 10-fold increase every two days, leading to high parasitaemia within a few days and associated clinical symptoms and complications, which may lead to death. In the cases of *P. vivax* and *P. ovale*, some sporozoites turn into hypnozoites, a form that can remain dormant in the liver cells, causing relapses months or even years after the initial infection.(42) Inside the erythrocyte, parasite ingests the host-cell hemoglobin to develop synchronously from a ring stage via a trophozoite, into blood schizonts that release new merozoites to the blood stream (step 4, Figure 1.2), leading to the classical cycle of fever that is observed clinically.

Some merozoites infecting the RBC develop into male and female gametocytes (step 5, Figure 1.2). In *P. falciparum*, these are formed in the later stages of infection and by contrast, in *P. vivax*, they are formed at the same time as the asexual stages.(43-45) Gametocytes are taken up into the female mosquito gut during the blood meal (step 6, Figure 1.2) and the male gametocytes are activated to form gametes, which fuse with the female gametes to form diploid ookinetes (step 7, Figure 1.2). These ookinetes migrate to the midgut of the insect, pass through the gut wall and form the oocyst, which after meiotic division originates sporozoites. After migration to the salivary glands of the female mosquito (step 8, Figure 1.2), the sporozoites are ready to renew the cycle again.(46)

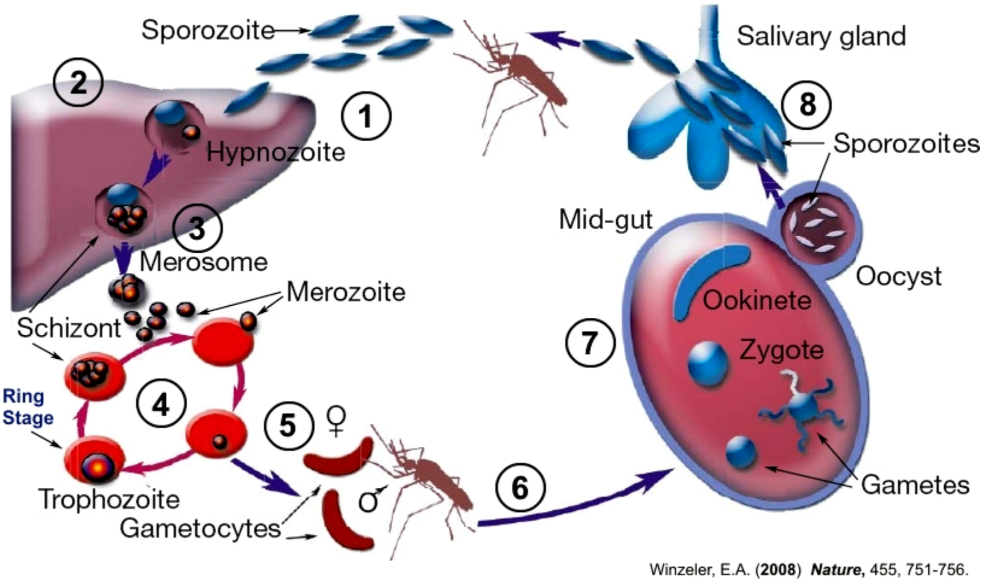

Figure 1.2 – Schematic representation of the *Plasmodium* sp. life cycle.(47)

Step 1 – Mosquito blood meal and sporozoites invasion; **Step 2** - Sporozoites pass the Kupffer cells and infect the hepatocytes, developing each one into tissue schizonts; **Step 3** – The developed schizonts rupture the liver cells and release the merozoites into the blood stream; **Step 4** - Inside the erythrocyte, parasite develops synchronously from a ring stage to new merozoites; **Step 5** - Some merozoites infecting the RBC develop into male and female gametocytes; **Step 6** – Gametocytes are taken up into mosquito during a new blood mead of the infected host; **Step 7** – Male and female gametocytes develops into new sporozoites via oocyst; **Step 8** - Migration of the sporozoites to the salivary glands of the female mosquito to renew the cycle.

Digestive Apparatus of Plasmodium sp.

Malaria parasites in bloodstream reside within host erythrocytes (RBC) where 95 % of the soluble proteins present is haemoglobin.(48) An estimated 75 % of haemoglobin is consumed by *P. falciparum* during its brief intraerythrocytic stay. Thus, haemoglobin degradation in the metabolic active trophozoite stage, is a catabolic and efficient process, in which some enzymes are involved. *Plasmodium* parasites utilize haemoglobin as an amino acid source for protein synthesis and also as energy source. (49)

Plasmodium ingests the haemoglobin and other RBC content, from the host cell through an opening called cytostome (Figure 1.3), which is transported by transport vesicles to the acidic digestive vacuole of the parasite, where the degradation may start before the delivery in the vacuole.(50) In *P. falciparum* double-membrane transport vesicles bud off from the cytostome and migrate toward and fuse with the large digestive vacuole, an specialized acidic (pH ~ 5.5) degradative organelle(51-52) where acidic conditions are maintained primarily by a V-type H^+-ATPase pump.(53)

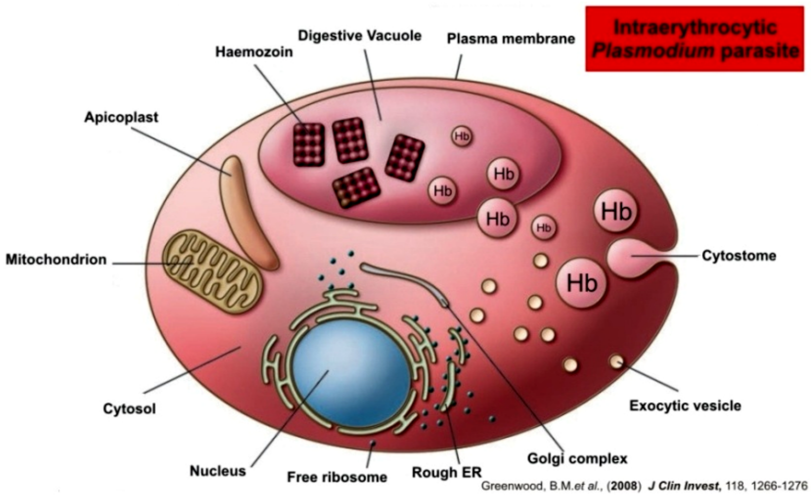

Greenwood, B.M.*et al.*, **(2008)** ***J Clin Invest*****,** 118, 1266-1276

Figure 1.3 – Schematic representation of the *Plasmodium* cell structure.(54)

Host cell cytoplasm is ingested by cytostome and packaged in transport vesicles. Degradation of the haemoglobin (Hb) may start in the transport vesicles and is completed in the digestive vacuole. Haem released from the Hb digestion is converted into a crystalline substance called haemozoin (HZ) or malarial pigment that is harmless to the parasite.

Clearly the digestive vacuole is a major site of haemoglobin degradation and its function has been extensively reviewed. (55-56) In the acidic digestive vacuole, a multitude of processes involved in haemoglobin degradation has been indentified. During digestion, the protein part of haemoglobin is broken down, initially into large peptides and later in small peptides, as a result of a concerted action of several proteins. These include a group of aspartic proteases called plasmepsins, a group of cysteine proteases called falcipains, a metalloprotease called falcilysin, aminopeptidases and at least one dipeptidylpeptidase (Figure 1.4). The degradation pathway taken by the degradative enzymes is a semi-ordered pathway, with plasmepsins making the initial cleavage of the intact haemoglobin, followed by secondary cleavages realized by plasmepsins and falcipains. In later stages falcilysin recognize and degrades short peptides generated by the upstream enzymes and the dipeptidylpeptidase and the aminopeptidases make the final cleavage in the process, with released of the amino acids. (49)

Early in the haemoglobin degradation pathway, haem (Fe^{+2}-ferriprotoporphyrin IX, FPIX (Fe^{+2})) is released and immediately oxidised to haem (Fe^{+3}-ferriprotoporphyrin IX, FPIX (Fe^{+3})), which are toxic to the parasite. These iron products can generate reactive oxygen species, which may lead to parasite death, and as such are detoxified by assembly in a crystalline array called haemozoin (HZ) or malaria pigment that is harmless to the parasite.(18-21)

Haemozoin, the Detoxification Pathway

Haemozoin was assumed to be a haemoprotein until 1987, when Fitch and Kanjananggulpan,(57) showed that it consists only of ferriprotoporphyrin IX (Fe^{+3}), identical to the synthetic product *β*-haematin, described by Hamsik in 1936,(58) that can be crystallized from aqueous solution with acetic acid.(59) Later Slater *et al.* reported several studies of elemental analysis, infrared spectroscopy, extended X-ray absorption fine structure (EXAFS) and X-ray diffraction confirming that haemozoin consists only of FPIX (Fe^{+3}) and is indeed apparently identical to *β*-haematin.(60) They also established that the FPIX (Fe^{+3}) molecules are linked through coordination of haem propionate group of one molecule to the Fe^{+3} centre of its neighbour, making a polymer structure of linked FPIX (Fe^{+3}). Later several studies showed the symmetry of the crystal and were able to determine the unit cell parameters of the well-defined faces.(61)

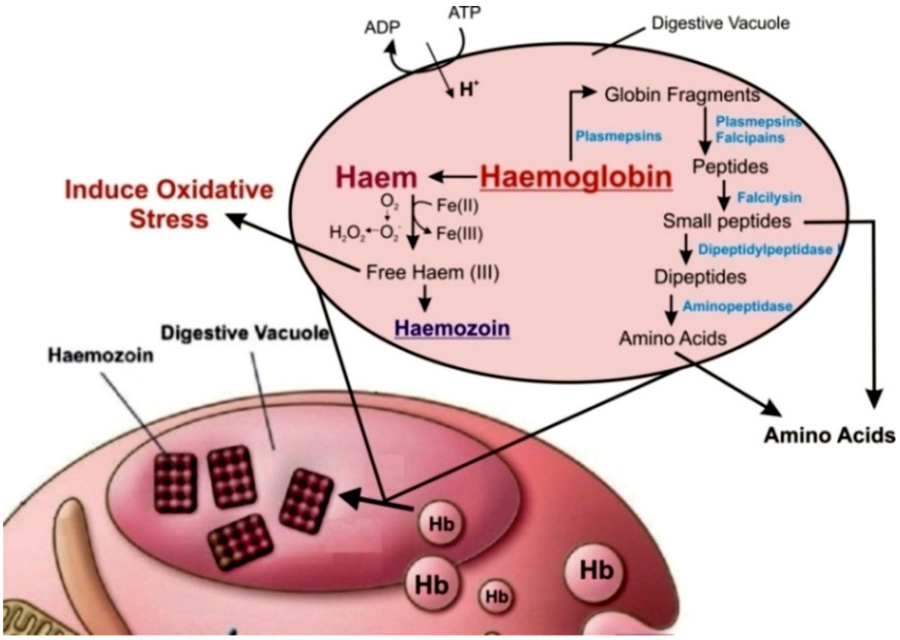
ADP
ATP
H^+
Digestive Vacuole
Globin Fragments
Plasmepsins
Plasmepsins
Falcipains
Peptides
Haem
Haemoglobin
Falcilysin
Small peptides
Induce Oxidative Stress
O_2
Fe(II)
H_2O_2
O_2^-
Fe(III)
Dipeptidylpeptidase I
Free Haem (III)
Dipeptides
Aminopeptidase
Haemozoin
Digestive Vacuole
Haemozoin
Amino Acids
Amino Acids
Hb
Hb
Hb
Hb

Figure 1.4 – Schematic representation of the haemoglobin degradation mechanism in the digestive vacuole of *Plasmodium.*(62)

Ingested haemoglobin is transported into the DV where is degraded to haem and globin. The globin fragments are cleaved by several proteases until amino acids used in the peptide synthesis by *Plasmodium*. Haem fragment, which is toxic to the parasite is oxidised (Fe^{2+} to Fe^{3+}) and crystallized to HZ through several mechanism like, spontaneous formation, biocrystallization and mediated by proteins and lipids.

However, in 2000 in a X-ray powder diffraction study, Pagola *et al.*, showed that *β*-haematin/haemozoin are not in fact polymers but rather a cyclic dimers of FPIX (Fe^{+3}) in which the propionate group of each FPIX (Fe^{+3}) molecule coordinates to the FPIX (Fe^{+3}) centre of its partner, while the dimers are linked through hydrogen bonding of the propionic acid groups (Figure 1.5).(63)

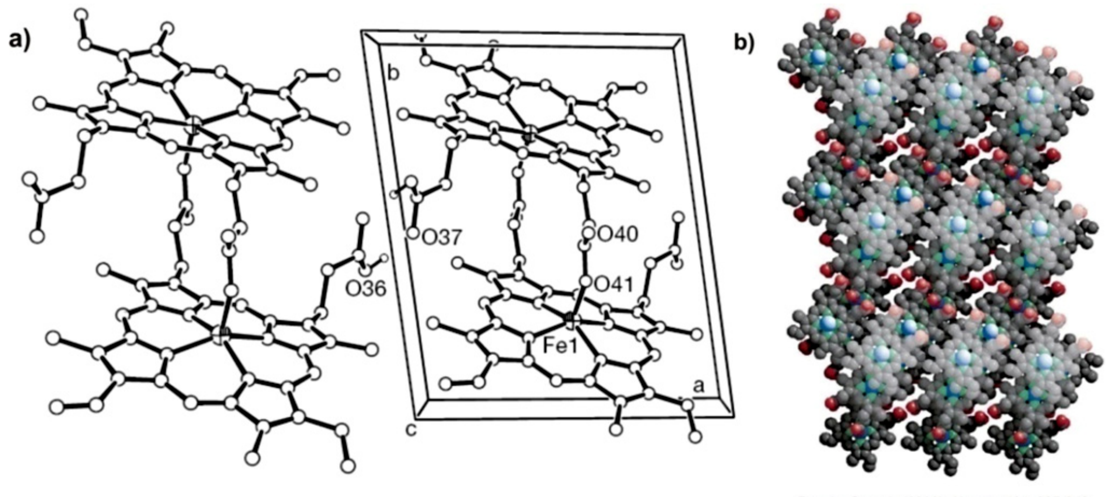
a)
b
O37
O40
O36
O41
Fe1
a
c
b)

Pagola, S *et al.*, (**2000**), ***Nature***, 404, 307-310.

Figure 1.5 – a) Two unit cells of the crystal of *β*-haematin viewed along the [001] direction; b) Packing diagram of the crystal structure of *β*-haematin.(63)

a) Formation of bonds occurs through Fe1-O41 bonds, whereas dimers are linked by hydrogen bonds through O36 and O37. All other hydrogens were removed for clarity, b) Lighter shaded atoms (C, grey; O, red; N, green; Fe, blue; H, not shown) are nearer the viewer. The chains of hydrogen-bonded dimers extend from the left to the right.

The degradation of haemoglobin by *Plasmodium* sp., in addition to goblin, FPIX (Fe^{+2}) and this detoxification pathway has been extensively reviewed elsewhere.(64-66) During the haemoglobin degradation process, all the haem released to the digestive vacuole is oxidised from Fe^{+2} to Fe^{+3} by a mechanism that is not fully understood. However, it is presumed to involve O_2 as oxidant, and indeed, it has been shown that oxyhaemoglobin is rapidly oxidised to methaemoglobin at low pH (step 1,Figure 1.6). In the process vast quantities of superoxide (O_2^-) are generated, which under acid conditions are transformed into O_2 and H_2O_2, and the latest to O_2 and H_2O through catalytic activities, preventing its toxicity.(67)

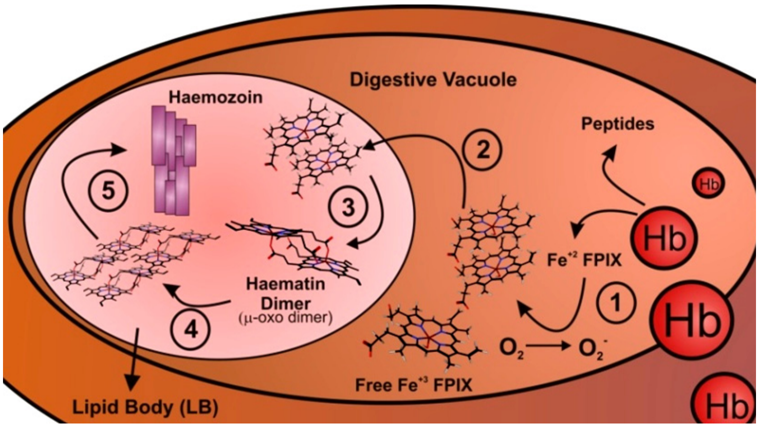

Figure 1.6 – Schematic representation of the processes involved in the haemozoin formation.(18)

Haemoglobin transported to the digestive vacuole is digested and the haem (FPIX(II)) is oxidised presumably by molecular oxygen to haem (FPIX(III))(Step 1). In aqueous solution Fe(III)FPIX dimerises probably to form a π-π dimer which is delivered to a lipid body (LB) dubbed a lipid nanosphere (Step 2). In the lipid nanosphere Fe(III)FPIX forms a "haematin precursor" dimer which converts to haemozoin dimer by displacement of axial water ligands of H_2O-FPIX(III) together with formation of Fe(III)-propionate bonds (step 3). In absence of competing hydrogen bonding to the solvent, these dimers can start to assemble haemozoin nuclei by hydrogen bonding (step 4) to each other and finally assembling the haemozoin crystal (step 5).

The resulting FPIX (Fe^{+3}), presumably presented as H_2O-FPIX (Fe^{+3}), is insoluble at digestive vacuole pH and also toxic to the *Plasmodium* sp., due to its capacities to induce oxidative stress, leading to membrane peroxidation and consequently parasite death.(64, 68-69) Thus, under digestive vacuole conditions the oxidized H_2O-FPIX (Fe^{+3}) spontaneously form π- π complexes, dimerizing in a neutral [H_2O-FPIX (Fe^{+3})]$_2$ in which one propionic acid group on each porphyrin is ionised and the other is not, corroborating what has been long held that dimerization involves formation of a µ-oxo dimer (step 2 and 3, Figure 1.6).(70-71)

The exact mechanism of haemozoin formation is unknown, but many theories have been suggested to explain this mechanism. Spontaneous haemozoin (*β*-haematin) formation, biomineralization or biocrystalazation, haemozoin formation mediated by proteins and mediated by lipids are some of the proposed mechanisms.(18) *Plasmodium falciparum* contains unique histidine rich proteins (HRP), which bind to FPIX (Fe^{+3}) and efficiently promotes the *in vitro* haemozoin formation. Based on these results it was claimed that haemozoin formation in malaria parasites involves the joint action of both HRP and lipids.(72-74) However, recent studies involving genetic and cell biology evidences have begun to point against any involvement of HRP in haemozoin formation. The most convincing argument for this is the formation of haemozoin in parasites clones lacking genes for both HRP-II and HRP-III, which are morphologically indistinguishable.(75) In addition, 97 % of the HPR-II is exported from the parasite to the RBC, while only 3 % is localized in the digestive vacuole where haemozoin formation occurs.(76)

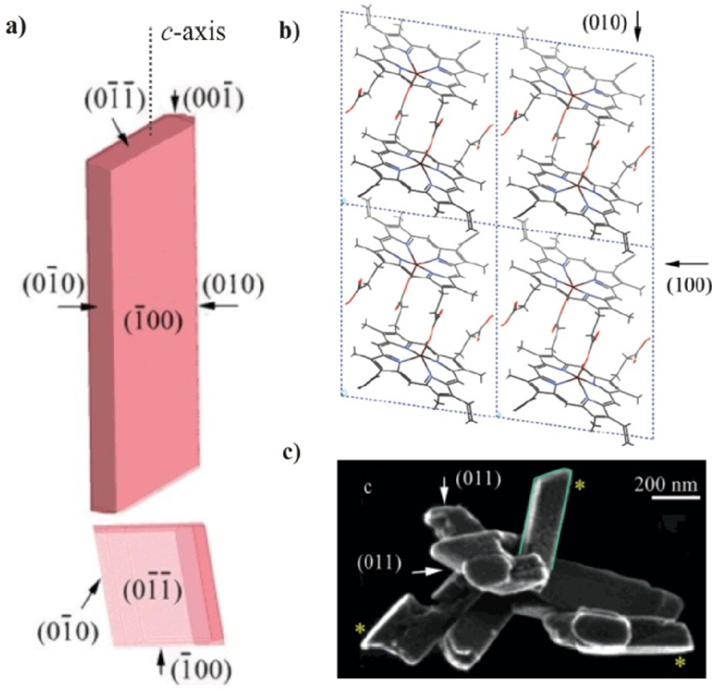

Buller, R., (**2002**) ***Crystal Growth & Design***, 2, 553-562

Figure 1.7 – a) Theoretical growth from β-haematin viewed: (top) perpendicular to the {100} face, (bottom) along *c*-axis; b) Crystal structure of β-haematin, which consists of molecular haem dimers, viewed along the *c*-axis; c) field emission inlens scanning electron microscopy micrographs of haemozoin purified from *P. falciparum*.(77)

In view of the evidence that HRP are not involved in the formation of the haemozoin in malaria parasites, Jackson et al., investigated the neutral lipid bodies in *P. falciparum* and demonstrated the presence of lipid particles associated with the digestive vacuole of the parasite. (78) One year later, in 2005, the publication of an electron micrograph image by Coppens and co-workers, showed for the first time the completely encapsulated haemozoin within a neutral lipid body in the digestive vacuole of *P. falciparum*.(79-80) A recent study developed by Pisciotta and co-workers changed the entire outlook on haemozoin formation, confirming that it forms within lipid bodies inside the digestive vacuole of the parasite.(81) In the study they provide ultrastructural evidence that neutral lipid nanospheres present within the digestive vacuole are the *in vivo* site of haemozoin formation, and it seems that the origin of the lipid bodies is the inner membrane of the endocytotic transport vesicles.(50) Following this evidence, molecular dynamics simulations have provided insight into molecular mechanism of haemozoin formation at lipid-water interface, where interaction of two monomers in vacuum showed rapid formation of the "haemozoin precursor dimer".(82-83)

Finally, inside the lipid body, μ-oxo dimers are linked through hydrogen bonds to form the haemozoin crystal (step 4 and 5, Figure 1.6). However, several mechanisms in the haemozoin formation process remain partially understood, like the mechanism of haemozoin growing. According to the theoretical growth morphology of β-haematin crystals reported by Buller and co-workers the crystals elongated in the c-direction, are delineated by well-developed {100} and {010} side faces and smaller

{011} end faces (Figure 1.7).(77) However some questions remain unanswered: how is delivered FPIX (Fe^{+3}) to the lipid body? Is there any protein or proteins involved in these processes?

1.1.3 Malaria Chemotherapeutics

Malaria chemotherapeutics are traditionally classified according to the stages of the *Plasmodium* life cycle that are targeted by the drug (Figure 1.8). One of the most wide used antimalarial drug was quinine (Figure 1.9), a natural product extracted from the bark of the tree *Cinchona calisaya* and it was the basis to the development of the antimalarial drugs. The drug development can follow several strategies, ranging from minor modifications of existing agents to the design of novel agents that act on new targets. Synthetic derivatives of quinine, such as the 4-aminoquinoline chloroquine (**2**, CQ) can be considered as the first antimalarial drugs developed after the pioneer work of Ehrlich(84) with methylene blue in the end of the eighteenth century. The antimalarial compounds used for the treatment of malaria as been extensively reviewed in the past.(23, 85-88)

Most of the antimalarial drugs used today are blood schizonticides, i.e., act on the asexual intraerythrocytic stages (ring, trophozoite and schizont) of the *Plasmodium* sp.. Tissue schizonticides kill persistent hepatic schizonts, and thus prevent the invasion of the erythrocytes, acting as prophylactic drugs. Hypnozoiticides act on the persistent intrahepatic stages of *P. vivax* and *ovale*, preventing relapses and the gametocytocides drug class destroy the intraerythrocytic sexual forms of the *Plasmodium* sp., and thereby hinder the transmission from human to mosquito hosts.(89)

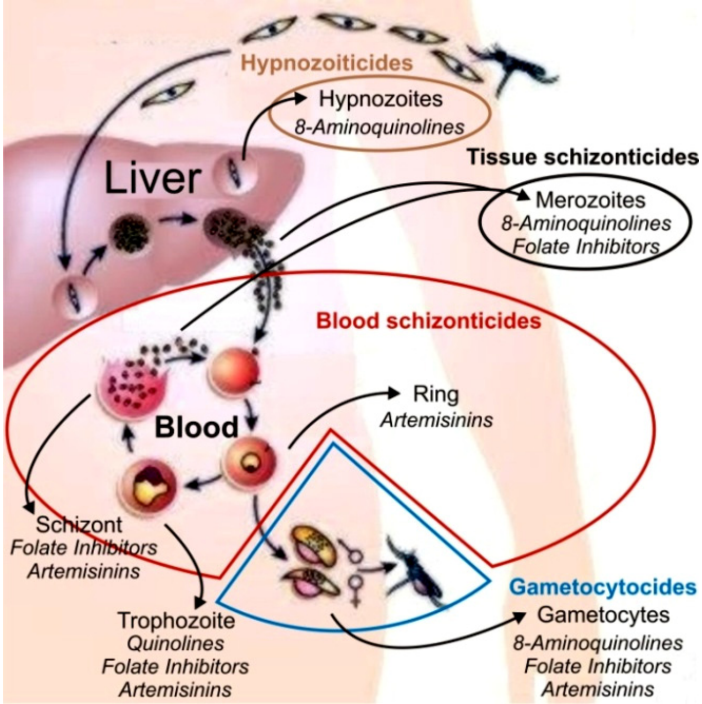
Hypnozoiticides
Hypnozoites
8-Aminoquinolines
Tissue schizonticides
Liver
Merozoites
8-Aminoquinolines
Folate Inhibitors
Blood schizonticides
Ring
Artemisinins
Blood
Schizont
Folate Inhibitors
Artemisinins
Trophozoite
Quinolines
Folate Inhibitors
Artemisinins
Gametocytocides
Gametocytes
8-Aminoquinolines
Folate Inhibitors
Artemisinins

Figure 1.8 – Schematic representation of the plasmodium life cycle with phases targeted by antimalarial drugs in the human host.

Tissue schizonticides act on the primary tissue forms of the plasmodia (merozoites), which after growth within the liver, initiate the erythrocytic stage. By blocking this stage, further development of the infection can be theoretically prevented; **Hypnozoiticides** act on the dormant liver stages of the parasite (hypnozoites) preventing relapses; **Blood schizonticides** act on the erythrocytic stages of the *Plasmodium* sp., ending with the clinical symptoms of malaria; **Gametocytocides** destroys the sexual forms of the parasite in the blood and thereby prevent transmission of the infection to the mosquito.

The tissue schizonticides class comprise drugs from the family of the folate inhibitors and 8-aminoquinolines. The folate inhibitors (Atavaquone **6**, Proguanil **7**, Chloroproguanil **8**, and

Pyrimethamine **9**, Figure 1.9) are some of the most widely used antimalarial drugs, inhibiting the enzymes of the folate pathway, resulting in the decrease of pyrimidine synthesis, hence, reducing the DNA, serine and methionine formation. The activity of these compounds is exerted at all growing stages of the *Plasmodium* sp., being also blood schizonticides and gametocytocides, albeit their role in the malaria is hampered by the rapid emergence of drug resistance.(90)

The 8-aminoquinolines (Primaquine **9**, Pamaquine **10** and Tafenoquine **11**, Figure 1.9) act on the pre-erythrocytic and transmission stages of the parasite life cycle and are the only class of compounds capable of exert its antiplasmodial effect on hypnozoites (hypnozoiticides). The mechanism by which the 8-aminoquinolines exert activity is likely to be due to the disruption of the mitochondrial function, swelling and thickening the mitochondria in the tissue-stage of the parasite.(85, 91)

The blood schizonticides are the major class of antimalarial drugs and include compounds from the family of the folate inhibitors, aminoquinolines, amino-alcohols (Chloroquine **2**, Piperaquine **13**, Amodiaquine **14**, Pyronaridine **15**, Quinine **16**, Mefloquine **17**, Halofantrine **18** and Lumefantrine **19**, Figure 1.9) and artemisinins (Artemisinin **20**, Arteether **21**, Artemether **22** and Dihydroartemisinin *21*, Figure 1.9). The quinoline-containing drugs class includes some of the most common antimalarial compounds. Their primary target is believed to be the *Plasmodium* digestive vacuole, being commonly accepted that these drugs act on haeme detoxification pathway, and for most of them, are only active against those stages of the parasite that actively degrade haemoglobin.(85, 92) Despite widespread resistance to chloroquine and quinine compounds, there is a continued interest in this type of compounds. Their mode of action and mechanism of resistance, although only partially understood, seems to occur independently of each other and due to the complexity of the digestive food vacuole environment and the immutable nature of the haem molecule, quinoline-resistance have probably been delayed for decades in the past.(93)

Furthermore, quinoline drugs target do not exits at such a concentration under physiological conditions in the human host, increasing the selectivity of these compounds to the *Plasmodium* sp., and thus representing a better target in comparison to some parasite enzymes that are derivatives of those in human host (several proteases, farnesyl transferase and enzymes involved in the choline uptake).(94)

The artemisinin-type compounds (Figure 1.9) act on the intraerythrocytic stages and in the sexual forms of the *Plasmodium*, being at the same time blood schizonticides and gametocytocides. The key pharmacophore in artemisinin (**20**) is the 1,2,4-trioxane unit, and in particular the endoperoxide bond is crucial for expression of antiparasitic activity.(95) In current use are either the natural product artemisinin itself and the semi-synthetic derivatives **21-23**. The mechanism of action is not completely understood, but the prevailing hypothesis is the reductive cleavage of the peroxide bridge by the FPIX (Fe^{+2}), generating C-centred radicals, which would alkylate biomolecules, leading to the death of the parasite. These compounds achieve, per cycle, the highest parasitaemia reduction rate when compared to any other drug known to date.(96) However, recently it was identified in Western Cambodia several cases of resistance to artemisinin-type compounds.(97-98)

Folate inhibitors

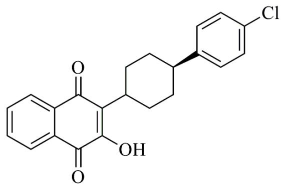

(**6**) Atovaquone

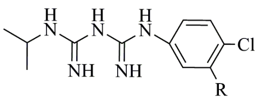

(**7**) Proguanil, R = H,
(**8**) Chloroproguanil, R = Cl

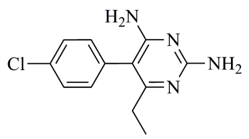

(**9**) Pyrimethamine

8-aminoquinolines

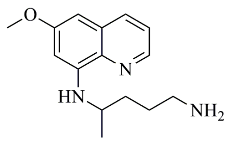

(**10**) Primaquine

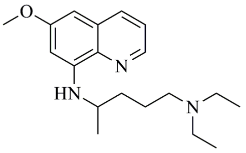

(**11**) Pamaquine

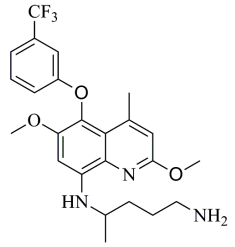

(**12**) Tafenoquine

4-aminoquinolines and amino-alcohols

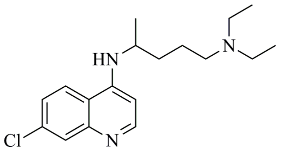

(2) Chloroquine

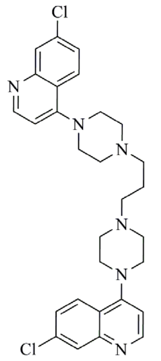

(**13**) Piperaquine

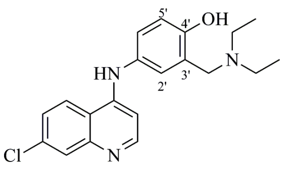

(**14**) Amodiaquine

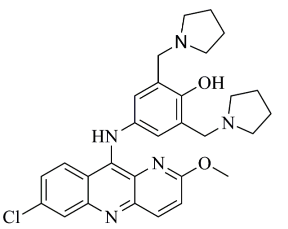

(**15**) Pyronaridine

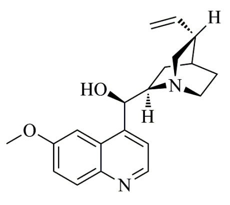

(**16**) Quinine

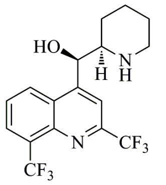

(**17**) Mefloquine

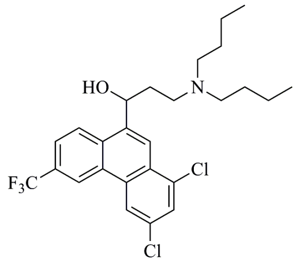

(**18**) Halofantrine

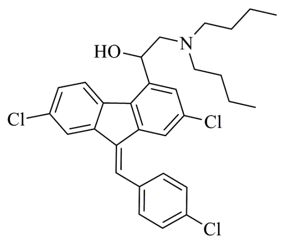

(**19**) Lumefantrine

Artemisinins

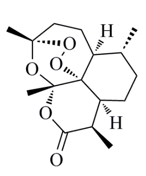

(**20**) Artemisinin

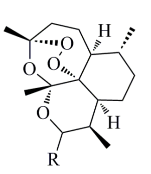

(**21**) Arteether, R = OEt
(**22**) Artemether, R = OMe

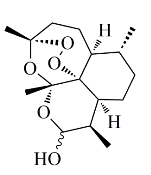

(**23**) Dihydroartemisinin

Figure 1.9 – Structures of selected key antimalarial compounds.

Furthermore, the high neurotoxicity of the dihydroartemisinin, which is believed to be the active metabolite of all artemisinins, is the major concern and the stopper to the wide use of these compounds.(99)

Several other drug targets like proteases involved in haemoglobin digestion (plasmepsins, falcipains, etc.), metabolic pathways, fatty acid biosynthesis, isoprenoid biosynthesis, haem biosynthesis and several membrane, mitochondrial and cytosolic targets, among others, have been identified in *Plasmodium* sp.(100-103) Additionally, drug combination therapies, consisting on combined administration of drugs with different targets, have been formulated to delay the development and spread of drug resistance malaria parasites.(104) Continuous efforts to develop drug candidates to several drug targets, in addition to the development of hybrid molecules (double-drugs), inhibiting two different targets at the same time, to overcome the spread of malaria and associated drug resistance, have been made and extensively reviewed elsewhere.(23, 88, 105-107)

Haem Target Based Chemotherapy, the Quinoline-Containing Drugs

Haemozoin formation is one of the most attractive drugs targets to the development of new antiplasmodial drugs and can be justified by three reasons:

i. haem formation does not seem to be dependent of any specific parasite enzyme, which consequently makes the appearance of resistance to the drugs more difficult. For instance, **2** was extensively used for 20 years before the parasite develop resistance, whereas one year was sufficient to the development of resistance to **11**, an inhibitor of dihydropteroate synthase);(102)
ii. the haem detoxification pathway is not directly involved in the mechanism of quinoline resistance, whereas drug transporters are probably responsible for the alteration of the drug accumulation inside the digestive vacuole of the parasite;(100)
iii. in the haem detoxification pathway the drug target is the free haem that does not exit at such a concentration in the human cells under physiological conditions, increasing the selectivity and thus representing a better target when compared to others that have analogous in human host.

Several types of antiplasmodial drugs, like 4-aminoquinolines, (which we will deepen in this section), acridones, xanthones, azoles, among others are reported to exhibit antiplasmodial activity by π-π stacking interactions, enhancing the free haem toxicity through inhibition of haemozoin formation.(18, 108-110) Also, artemisinins show antiplasmodial activity due to the decomposition of the endoperoxide bond by haem (Fe^{+2}), to produce initially an oxy radical that subsequently rearranges into one or both of two distinctive carbon-centered radical species.(111) The evidence to support that each individual carbon radical species is the responsible for the antimalarial activity remains an area of intense debate, however it has been proposed that the final alkylation, by these reactive species, of biomolecules such as haem, specific proteins and other targets result in the death of the parasite.(112-115)

The quinoline-containing drugs such as chloroquine (**2**), amodiaquine (**14**), quinine (**16**) and mefloquine (**17**) have been mainstays of malaria chemotherapy for much of the past 60 years. The first widely used antimalarial drug was quinine, a natural product extracted from the bark of the tree *Cinchona calisaya* by Pelletier and Caventou in 1820.(85) The structure of quinine was elucidated in 1908 and provided evidence that the quinoline nucleus could be a useful component of an antimalarial drug. In the 1930s, Andersag investigated the activity of the structural related 4-aminoquinoline **2**, which displayed excellent activity. However, after initial trials in Germany, chloroquine was regarded as too toxic for use in humans, but after the II World War, chloroquine was re-evaluated and became the foundation of malaria therapy for the next decades.(116) In 1948, Burckhalter found that a group of heterocyclic α-dialkyl-o-cresols and related group of benzylamines were effective antimalarials. From this, the 4-aminoquinoline **14** was discovered and found to have an excellent activity/toxicity profile.(117) The key to the success of the most important synthetic quinoline, CQ has been the excellent clinical efficacy, limited toxicity, easy of use and simple, cost-effective synthesis.

However, the exact mode of action of chloroquine and related 4-aminoquinolines remains to be elucidated, but most investigators now accept that a critical step of this process is the binding of the drug to the FPIX (Fe^{+3}).(18, 118) Also, the antimalarial activity of CQ stems directly from its highly selective uptake and concentration in malaria infected erythrocytes.(119) This could be due to a proton trapping mechanism. Chloroquine is a weak base ($pK_a^1 = 8.1$, $pK_a^2 = 10.2$)(85) which in its uncharged form diffuses freely into acidic compartments, like the DV of *Plasmodium*, where it protonates and becomes trapped. Chloroquine accumulation is 20-fold higher in malaria parasite than in mammalian cells, due to pH trapping and binding with dimers of FPIX (haematin dimers), and thus, inhibiting haemozoin formation. (120-121)

Since the interaction with haematin appears to be the key to the mechanism of action of 4-aminoquinoline drugs, Vippagunta and co-workers employed isothermal titration calorimetry studies to derive association constants for **2**-FPIX (Fe^{+3}) complex bind at neutral pH.(122) From this work it was shown that **2** binds to haematin μ-oxo dimers in a sandwich arrangement through π-π stacking interactions between quinoline and the porphyrin ring. Also, stoichiometric studies regarding **2** binding to FPIX monomer were recorded to be 1:1, in 40 % DMSO in water to maintain FPIX in monomeric state.(123) Molecular modelling experiments also reinforced the view that enthalpically favourable π-π interactions observed, derived from a positive alignment of the out-of-plan π-electron density in **2** and haematin dimers at the points of intermolecular contact.(121, 124-126)

Other studies have suggested that **2** and related drugs may inhibit haemozoin formation by blocking the growing face of the HZ crystal by a capping effect.(77, 127-128) In 2002, based in the theoretical growth of *β*-haematin, Buller and co-workers proposed a non-covalent binding site for the quinoline drug family at the end of the fast-growing face {001} of *β*-haematin, elucidating the differences in activity of various quinolines.(77) In the model, the quinoline aromatic ring is interleaved between porphyrin rings within a fissure at the {001} surface and attached by a salt bridge between the amine functionality in the side chain and the carboxylate group, as well as various interactions between the quinoline and FPIX that have a strong Coulombic contribution, such as 7-Cl···CH_3 interaction and N···HC=C of the haematin surface (Figure 1.10).

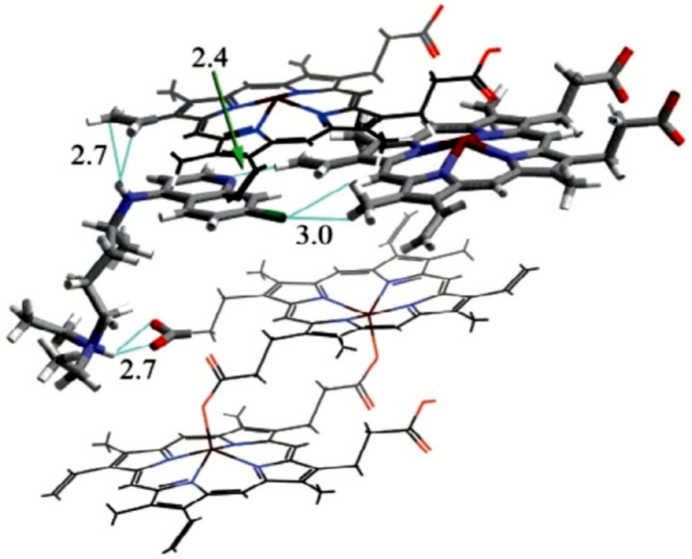

Buller, R., (**2002**) ***Crystal Growth & Design***, 2, 553-562.

Figure 1.10 – Chloroquine bound to the face {001} β-haematin crystal highlighting energetically favourable interactions. The distances are between highlighted atoms. NH···NC=C 2.4 Å, Cl-H_3C 3.0 Å, NH···O_2C 2.7 Å, NH···C=C (π-cloud) 2.7 Å.(77)

The exocyclic amine chain should be sufficiently long and flexible to ensure the optimal bind distance to the host acid moiety and allow the appropriated intercalation of the quinoline. However, in the case of **2** and other 4-aminoquinolines since interactions are primarily with FPIX (Fe^{+3}) monomers, haematin μ-oxo dimers, haemozoin growing crystals or other forms of FPIX (Fe^{+3}) present in the DV the binding interactions are co-facial and would be expected that the interaction energies involved in the complexation may be similar.(129) The haemozoin formation and its role in the antimalarial activity of the 4-aminoquinoline drugs has been excellently reviewed recently by Weissbuch and Leiserowitz.(130)

Nevertheless, the efficacy of the quinoline-based antimalarials has decreased in recent years, mainly as a result of the development and spread of parasite resistance.(131) To overcome the extend of the quinoline-resistance, several studies to develop 4-aminoquinolines and to recognize its structure-activity relationships (SAR) has been done in the last decades. The basic structure of the 4-aminoquinoline used in malaria chemotherapy contains a 7-chloroquinoline substituted ring system with a flexible side chain in position 4 of the quinoline system. The 7-chloro functionality is optimal for the antimalarial efficacy both *in vitro* and *in vivo*, providing moderately strong electron-withdrawn capacity necessary to inhibit haemozoin formation (strong electron-withdrawn capacity diminishes the pK_a of the quinolinic nitrogen and consequently the antiplasmodial efficiency) and strong lipophilicity.(48, 132-133)

In the 4-position of chloroquine and related 4-aminoquinolines, an alkyldiamine side chain is attached and different approaches, including length, lipophilicity and distal nitrogen substituent variations, have been.(23, 129, 134) Variations on the side chain length of chloroquine revealed that side chains of 2-3 and 10-12 carbons length retain the activity against chloroquine-resistant (CQ-R) strains of *Plasmodium*.(135-136) In addition, the introduction of hydrogen-bond acceptors in the substituents in the distal basic nitrogen of the side chain also retain the activity against CQ-R strains.(137) Several other modifications like the introduction of small heterocyclic systems and functional groups, like sulfonamides and thioureas, in the terminal nitrogen of the side chain allowed the antiplasmodial activity/toxicity modulation, showing that this kind of approaches are useful for the development of new antimalarial drugs.(135, 138-141)

The introduction of one aryl ring, in the side chain of the 4-aminoquinolines (increasing lipophilic character of the drug) led to compounds with good activity *in vivo*. Amodiaquine (**14**) differs chemically from **2** in the fact that contains a 4-hydroxyanilino function in its side chain.(117) However, the greatest difference between the structures is the presence of the aryl ring, since chloroquine and amodiaquine both have four carbons between the secondary nitrogen and tertiary nitrogen in the side chain. The presence of the 4-hydroxyanilino reduces the pK_a values of amodiaquine ($pK_a^1 = 7.1$ $pK_a^2 = 8.1$)(134) when compared to **2**, so might be expected to have reduced activity due to diminished accumulation in the DV. Nevertheless, **14** is accumulated more efficiently than **2** and have potent antiplasmodial activity. The mechanism of accumulation cannot be only explained by the weak-base effect and thus additional binding components, settled by structural features of the molecule seems to be involved.(120, 142) However, the therapeutic value of amodiaquine is significantly decreased by the biotransformation of its *p*-aminophenol moiety into a quinonimine, which is susceptible to nucleophilic attacks by thiols groups, resulting in severe hepatotoxicity.(143) In order to avoid this hepatotoxicity, several modifications have been made in amodiaquine chemical structure. The substitution of the 4'-hydroxyl functionality of **14** for fluorine, the isomerisation of the 3'-(diethylamino)methyl-4'-hydroxyl for 3'-hydroxyl-4'-(diethylamino)methyl (isoquine series), the introduction of a 5'-chlorophenyl moiety (tebuquine series) and related isomer isoterbuquine has been made to afford structures with improved antiplasmodial activity against CQ-S and CQ-R strains and reduced associated toxicities.(120, 144-150) Another strategy to overcome the *Plasmodium* sp. resistance has been the dimerization of two quinoline nucleus with linkers of varying length (i.e. piperaquine, **13**). The activity of such bisquinolines against CQ-R strains has been explained by their steric bulk, which prevent them to fitting into the substrate binding site of the several membrane proteins, in addition to the possible increased accumulation efficiency due to their four positive charges. Although the developed bisquinolines showed activity against CQ-R strains, it appears to be a certain degree of cross resistance with chloroquine and some of them have been marred by some cytotoxicity issues.(151-154)

1.1.4 *Chloroquine Resistance in Plasmodium sp.*

During the 1940s and 1950s the 4-aminoquinoline chloroquine proved to be worldwide a safe and cheap antimalarial drug for prophylaxis and therapeutic. However, in the beginning of the 1960s, due to the massive use of the drug, *Plasmodium* sp. have developed resistance to chloroquine, independently of the world regions, with devastating consequences mainly in the poorest countries.(155) Resistance to a drug can arise in several ways. Firstly the drug may be transformed to become less active, secondly the drug target may be altered so the drug cannot exert its activity, thirdly the drug target can be overexpressed thereby reducing the drug action and fourthly the drug may be denied access to its target by either a reduced accumulation or an increase in its efflux out of its site of action. In the blood stages of *P. falciparum* CQ-R strains the concentration of chloroquine within the infected cell is diminished, probably to the efflux currently understood to occur across the membrane of the DV and so the drug does not achieve intravacuolar concentration to inhibit haemozoin formation.(156-158) Also, changes in the pH gradient across the digestive vacuolar membrane were proposed to be associated with certain drug resistance phenotypes, although after some controversy among authors, recent evidence has suggested that there is no difference in the DV pH between CQ-R and CQ-S strains.(159-162) Through the years, the drug resistance mechanism has been the subject of study of several authors and has been extensively reviewed elsewhere.(29, 89, 163-168)

It is generally accepted that changes in the sequence of the vacuolar membrane protein PfCRT (codified by gene p*fcrt* on chromosome 7) are convincingly linked to CQ-R in *P. falciparum*.(169-170) This membrane protein is a 424 amino acid protein called chloroquine resistance transporter (PfCRT), where a polar, positively charged residue (lysine) is replaced by threonine (K76T) which is neutral and hydrophobic, mediating the efflux of the positively charged chloroquine (Figure 1.11).

Other changes in PfCRT, which modify the overall hydrophobicity of the protein, are associated with the CQ-R.(169, 171) As consequence of these protein mutations, CQ concentration descrease inside the DV and three different models to mediate this process have been proposed:

i. CQ efflux out of the DV *via* an energy dependent transporter;
ii. leak of CQ out of the DV down its concentration gradient (not related with energy);
iii. opening of an aqueous pore that permits the passive outward movement of protonated forms of the drug.(168)

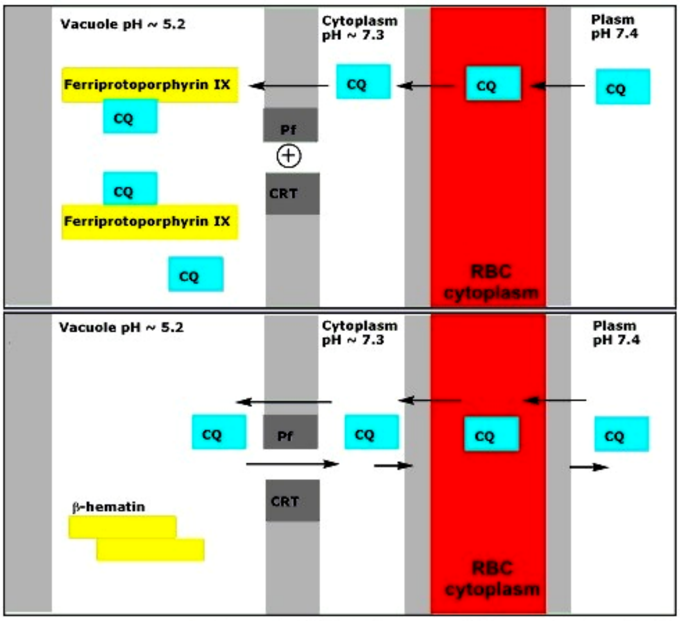

Warhurst, D.C. (**2007**), ***Current Science***, 92, 1556-1560

Figure 1.11 – Schematic representation of the parasite at equilibrium in the red blood cell. Top) parasite wild-type, sensitive to chloroquine; bottom) parasite resistant to chloroquine with mutation in PfCRT.(166)

Top) Weak base chloroquine travels through the RBC membrane, cytoplasm, parasite cytoplasm and become concentrated into the parasite DV under the pH gradient and unable to exit through the positively charged PfCRT, and inhibiting haemozoin formation. Bottom) Chloroquine is shown leaking out through the modified CQ-R PfCRT channel into the cytoplasm, allowing haemozoin formation. (membranes are shown in grey).

The multidrug resistance phenotype was first identified in tumor cells and is associated with over expression of certain transporters of the ABC superfamily (transmembrane proteins that carry out certain biological processes including translocation of various substrates across membranes). Some of these transporters are known as multidrug resistance (MDR) and consist on proteins that are able to maintain the toxic compound's concentration bellow lethal level.(172) As in neoplastic cells it has been identified a gene responsible for the MDR in *P. falciparum*, the *pfmdr1*.(173) It codifies for a protein known as PGH-1, localized in the DV, that are able to transport chloroquine, quinine and other antimalarial drugs.(174) Additionally, different clones of *P. falciparum* containing *pfmdr1* and *pfcrt* alleles have a large susceptibility variation to antimalarial drugs, which may indicate that other genes play a role in parasite resistance.(175)

It is recognized that 4-aminoquinolines more hydrophobic than **2**, such as amodiaquine, retain activity against some CQ-R strains and this is believed to be due to their interactions with the hydrophobic lining of CQ-R PfCRT.(176) Additionally, CQ derivatives with shortened and lengthened aminoalkyl side chains have been shown to exhibit undiminished activity against CQ-R parasites.(136) These data suggests that the side chain is a primary recognition motif for CQ-R, although there is some evidence that the 4-amino-7-chloroquinoline ring itself may be weakly correlated with cross-resistance with CQ.(138, 177)

Another well documented property of chloroquine-resistance is the ability that 'reversor' agents have to increase the sensitivity to CQ to levels associated with CQ-S strains, like in MDR in cancer cells. Verapamil (**24**), a monoprotic weak base that is known to block the calcium channels, was the first drug to be demonstrated to reverse CQ-R.(178-179) Verapamil as the ability to enhance the action of chloroquine in CQ-R strains but has no effect on CQ-S strains. The sensitivity of *P. falciparum* parasites to **24** has been linked to mutations in *pfmdr1* and *pfcrt*.(180-181)

After the discovery of the chemosensitizing potential of **24**, a wide range of structural and functionally diverse agents, like others calcium channel blockers, tricyclic antidepressants, antihistamines among others, have been described to reverse CQ-R.(182) However, despite the wide chemical diversity among the compounds able to reverse CQ-R, all of them share several common characteristics: a cationic charge at digestive vacuole pH, two planar rings, significant lipophilicity and a nitrogen atom, often tertiary.(183) In 2002, in a 3D QSAR study, Bhattacharjee and co-workers revealed a common pharmacophore to CQ-R reversal agents.(184) The basic features are two hydrophobic aromatic rings and a hydrogen bond acceptor, preferably nitrogen, being optimal for tertiary or secondary amines. Using a molecular modelling approach Aliber *et al.*, defined an interaction site to this nitrogen atom, in which there is hydrogen bonding to a hydroxyl of a

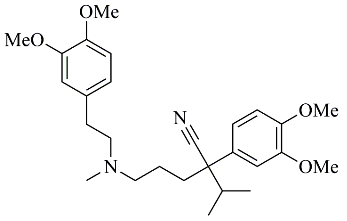

(**24**) Verapamil

Figure 1.12 – Structure of the calcium channel blocker verapamil (**24**).

serine residue and a salt bridge formed between the same positively charged N and an aspartate residue, consistent with pfCRT in CQ-R parasites.(185) Thus, CQ-R reversal may involve direct competition of the resistance reverser for the CQ binding site in PfCRT.

While the safety, efficacy and cost-effectiveness of CQ was undeniable in the past, maintaining these advantageous, while reactivating its antiplasmodial activity in combination with resistance reversers could be a great challenge. In the meantime, the search for new compounds with improved efficacy to CQ-R and CQ-S *Plasmodium* sp. should be stimulated to increase the armory in the fight against malaria and to keep the ancient plague in check.

1.2 Indolo[3,2-*b*]quinoline, a Scaffold for Antiplasmodial Drug Development

Nature has been a wide source of antimalarial compounds and alkaloids from traditional herbal medicines have contributed greatly over the centuries not only to the discovery of new antimalarial and therapeutic agents but also to the elucidation of biochemical pathways allowing the development of modern pharmaceutical industry.(186-189) Indoloquinolines are unique natural alkaloids, characterized by an indole and a quinoline fused rings, found almost exclusively in the West African climbing shrub *Cryptolepis sanguinolenta* (Lindl.) Schltr. The roots' aqueous extracts of this plant have been used for centuries by African traditional healers mainly for the treatment of fevers including malaria, hepatitis and bacterial infections, although others uses, such as antirheumatic, spasmolytic and as a tonic have also been reported (190-192). The chemical composition of the roots of *C. sanguinolenta* (synonymy of *C. triangularis* N.E.Br.)(193) was first studied in 1929 by Clinquart (1) and an alkaloid named cryptolepine was isolated from a sample collected in Zaire. Later, Delvaux (194), working with a root sample from Nigeria, established the molecular formula of cryptolepine as $C_{16}H_{12}N_2$, but it was only in 1951 that Gellért *et al.* (195) identified the correct structure of cryptolepine as 5-methyl-5*H*-indolo[3,2-*b*]quinoline (**1**).

In 1978, Dwuma-Badu *et al.* (196) reported the isolation of another minor alkaloid from the roots of *C. sanguinolenta*, the simplest indolo[3,2-*b*]quinoline, named quindoline (**25**), but it was only between 1993 and 2000, with the development of modern spectroscopic methodologies allowing the complete structural identification of a compound with few milligrams or even micrograms, that several other minor indoloquinoline alkaloids were isolated from *C. sanguinolenta* and their structures identified (Figure 1.13). Most of them show the indolo[3,2-*b*]quinoline nucleus as hydroxycryptolepine (**26**) (197), cryptolepinoic acid (**27**), methylcryptolepinoate (**28**) (198) and quindolone (**4**)(199). However, other regioisomers such as the 5-methyl-5*H*-indolo[2,3-*b*]quinoline (**29**) named by different groups as neocryptolepine (200) or cryptotackieine (201) and the 5-methyl-5*H*-indolo[3,2-*c*]quinoline (**30**) named isocryptolepine (202) or cryptosanguinolentine (201) were also identified in this botanical species, together with dimeric alkaloids: cryptospirolepine (**31**) (203), cryptomisrine (**32**) (204), bis-cryptolepine (**33**) (200) and cryptoquindoline (**34**) (197). Cryptolepine was also identified in some *Sida* species (Malvaceae) and in *Microphilis guianensis* (Sapotaceae).(205-206) Although the synthesis of **25** was first reported in 1906

(207), before its isolation from *C. sanguinolenta*. For indoloquinoline alkaloid cryptolepine (**1**) as well as for its isomers, neocryptolepine (**7**), isocryptolepine (**8**) and the synthetic isoneocryptolepine (**35**, 5-methyl-5*H*-indolo[2,3-*c*]quinoline) several methodologies for its synthesis have been reported(12, 14, 208-234) and reviewed elsewhere for the indolo[3,2-*b*]quinolines.(2)

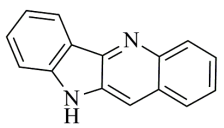

(**25**) Quindoline

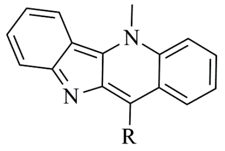

(1) **Cryptolepine**, R = H

(**26**) Hydroxycryptolepine, R = OH

(**27**) Cryptolepinoic acid, R = COOH

(**28**) Methylcryptolepinoate, R = $COOCH_3$

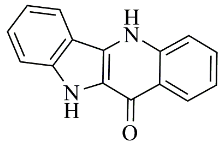

(**4**) Quindolone

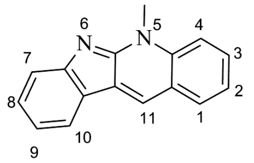

(**29**) Neocryptolepine

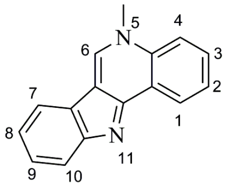

(**30**) Isocryptolepine

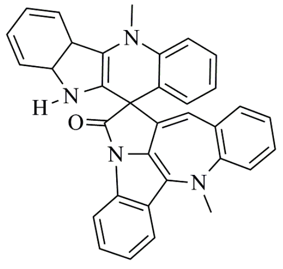

(**31**) Cryptospirolepine

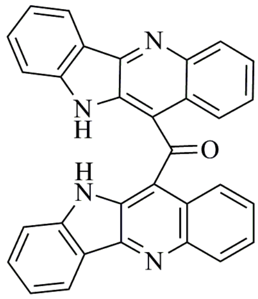

(**32**) Cryptomisrine

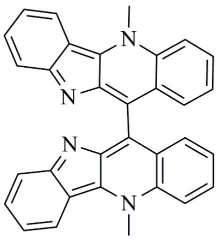

(**33**) Bis-cryptolepine

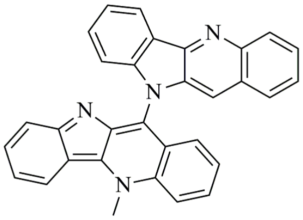

(**34**) Cryptoquindoline

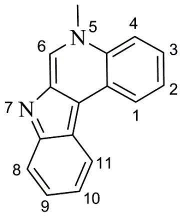

(**35**) Isoneocryptolepine

Figure 1.13 – Indoloquinolines from *Cryptolepis sanguinolenta* and synthetic isoneocryptolepine.

Cryptolepine (**1**) is by far the most studied indoloquinoline. It has two nitrogens but only one (N^{10}) is acid, with a pK$_a$ of 11.8 and under acidic conditions, cryptolepine exists has a salt (Figure 1.14).(235) Several authors make reference to **1** in the salt and basic form as two different compounds, showing different biological results for each form. However, in this review we will consider the structure of **1** as either of the two forms since, as it is an equilibrium, both forms can co-exist depending the concentration of each one on the pH of the medium.

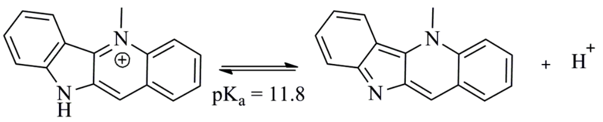

Figure 1.14 – Cryptolepine (**1**) acid-base equilibrium.

1.2.1 Synthetic Pathways

The synthesis of quindoline, the simplest member of the indolo[3,2-*b*]quinoline alkaloids, was accomplished by Fichter and Boehringer in 1906.(207) Since then, ten others synthetic strategies have been proposed, seeking not only to be faster and more efficient but also to use available starting materials. The earliest synthetic approach to the synthesis of indolo[3,2-*b*]quinolines (Ray's method) involves a condensation reaction of two building blocks. However, besides the good yields, these types of reactions take long time to be accomplished. In the beginning of the 80's, Görlitzer and Weber methodology evolved to the first total synthesis of indolo[3,2-*b*]quinolines with commercially available starting materials and without coupling of two building blocks. This synthetic approach has, however the disadvantage of involving 5-9 steps. To overcome this weakness Fan and Ablordeppey developed in 1997 a synthesis of quindoline, which involves only a two step reaction and is completed in one day, but affording also the regioisomer 7*H*-indolo[2,3-*c*]quinoline. In the last decades several methodologies involving different approaches and type of reactions have been reported in the literature and will be reviewed in this section. The newest methodologies simplify the design and synthesis of new indolo[3,2-*b*]quinolines, making the overall process faster, with higher efficiency and with increased versatility. Continuing efforts towards new synthetic methodologies should make synthesis of indolo[3,2-*b*]quinolines pharmaceutical leads simpler and more flexible.

Armit and Robinson method

In 1922, Armit and Robinson(208) prepared the quindoline-11-carboxylic acid by condensation of isatinic acid with an alkaline solution of indoxyl (shown in Scheme 1.1) and in 1947, Holt and Petrow (209) synthesized the same compound, with good yields (~70 %) using *O,N*-diacetylindoxyl and *N*-acetylindoxyl, which have the advantage of being very much less oxidized than the parent indoxyl. Quindoline was then prepared from quindoline-11-carboxylic acid by reduction with zinc in alkali, or with sodium amalgam, followed by oxidation with air. The Holt and Petrow's methodology has been applied during decades to synthesize C11 carboxylic acid quindolines with different substituents in aromatic nucleus.(13-14, 206, 210, 235-238)

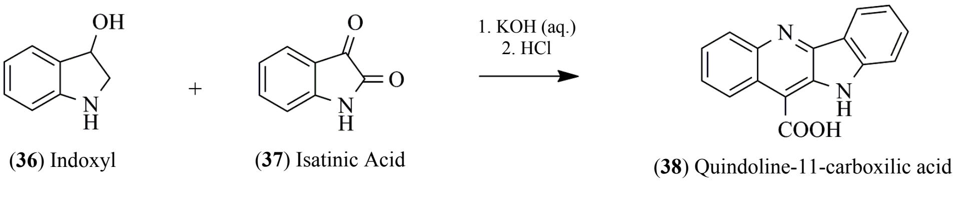

Scheme 1.1 – Synthesis of quindoline-11-carboxilic acid (**38**) by condensation of indoxyl with isatinic acid.

However, these methods of synthesis require a difficult condensation reaction, which involve long time to be completed (10 days in Holt and Petrow methodology) and with starting materials of reduced availability. In the last three decades, several others synthetic strategies towards indolo[3,2-*b*]quinolines and derivatives have been reported.

Görlitzer and Weber's method

In 1981, Görlitzer and Weber (11) synthesized the indolo[3,2-*b*]quinoline nucleus. Their synthesis uses a nucleophilic substitution of second order to couple two building blocks, methyl anthranilate (**39**) and N-(2-(2-bromoacetyl)phenyl)-4-methylbenzenesulfonamide (**40**) to give the intermediate **41** (Scheme 1.2).

After deprotection of the amine group with sodium methanolate, the intermediate **41** undergoes double intramolecular thermal cyclization in strong acid medium to afford quindolone (**4**). Quindoline is subsequently obtained after chlorination of C11 in **4** with phosphorus oxide trichloride(12) followed by hydrogenation on Pd/C to remove the chloride.(239) Cryptolepine can then be obtained after reaction of quindoline with methylating agents, which undergoes through selective N-alkylation.(240)

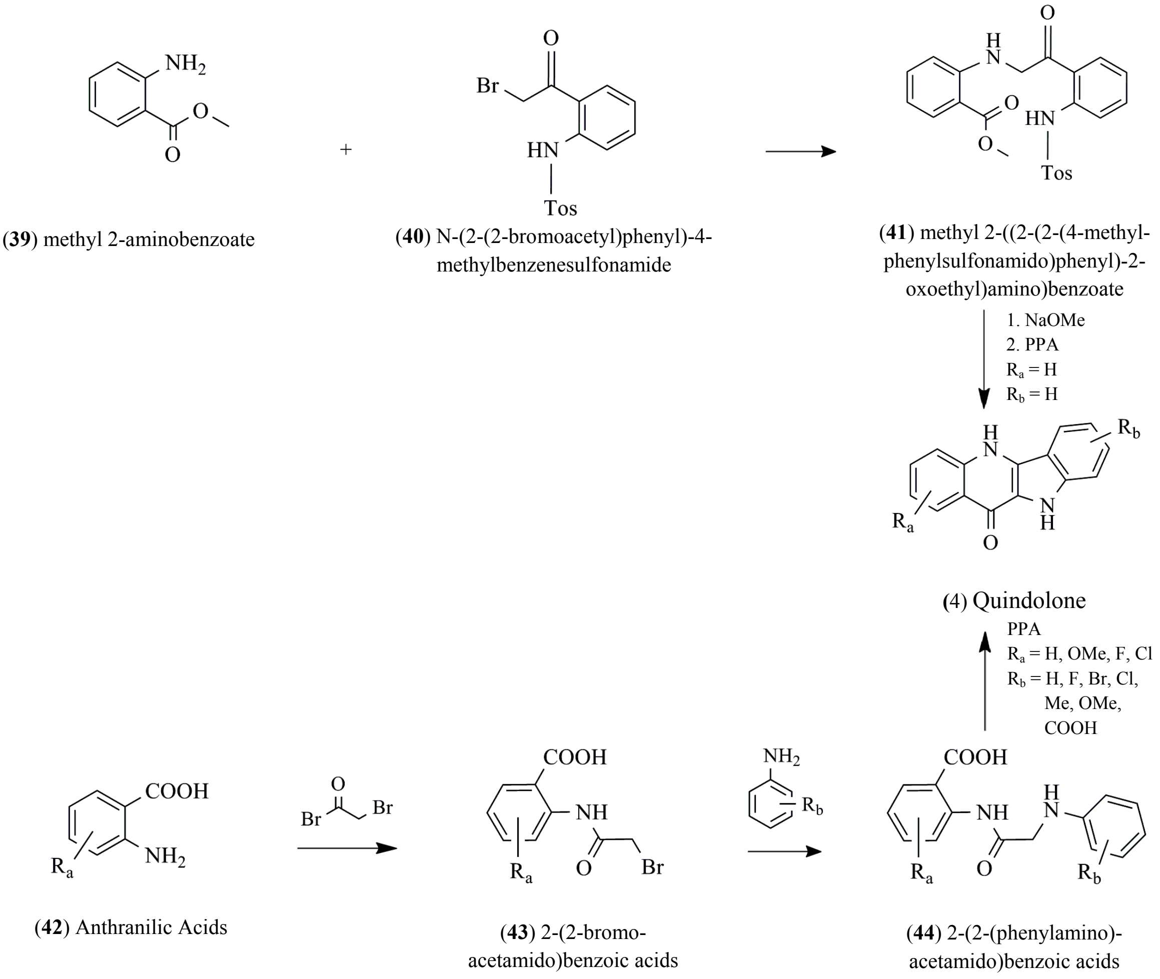
(39) methyl 2-aminobenzoate
(40) N-(2-(2-bromoacetyl)phenyl)-4-methylbenzenesulfonamide
(41) methyl 2-((2-(2-(4-methylphenylsulfonamido)phenyl)-2-oxoethyl)amino)benzoate
1. NaOMe
2. PPA
Ra = H
Rb = H
(4) Quindolone
PPA
Ra = H, OMe, F, Cl
Rb = H, F, Br, Cl, Me, OMe, COOH
(42) Anthranilic Acids
(43) 2-(2-bromo-acetamido)benzoic acids
(44) 2-(2-(phenylamino)-acetamido)benzoic acids
NH2
O
Br
HN
Tos
COOH
NH
Ra
Rb

Scheme 1.2 – Görlitzer and Weber total synthesis and derived methodologies.

Görlitzer and Weber total synthesis experienced some adaptations to afford different quindoline derivatives.(13, 239, 241-249) A substituted anthranilic acid (**42**) is treated with haloacetyl halogen (bromoacetyl bromide in Scheme 1.2) to afford the haloacetyl derivate **43**, and subsequent reaction with substituted aniline provides the derivative **44**. Condensation of **43** with aniline is strongly influenced by the substituents in the aniline. In anilines with strong electron withdrawing groups conversion is too low to obtain the desired compound **44** with good yields. Acid-promoted intramolecular cyclization of **44** gives quindolone (**4**), which can undergo an incompletely conversion, and an 18 member ring trioligomer is formed.(248) This polyphosphorous catalyzed cyclization is the key step to obtain the indolo[3,2-*b*]quinolines and the presence of electron withdrawing groups can reduce significantly the yield, if the optimal experimental conditions are not assured.

Joule's method

In 1996, Joule's group synthesized the indolo[3,2-*b*]quinolines, cryptolepine, hydroxycryptolepine and quindoline based on the intramolecular β-nucleophilic substitution of a 1-phenylsulfonyl-2-acylindole (**48**, shown in Scheme 1.3).(211)

In the overall process the acylindole undergoes intramolecular nucleophilic substitution at indole β-position and the *N*-susbtituent is expelled as phenylsulfinate.(250) (2-Aminophenyl)(1-(phenylsulfonyl)-1*H*-indol-2-yl)methanone (**48**) is achieved by condensation of 2-lithiated 1-phenylsulfonylindole **(46)** with 2-nitrobenzaldehyde to afford **47** and consequent oxidation with manganese dioxide followed by catalytic reduction of the nitro group to amine.

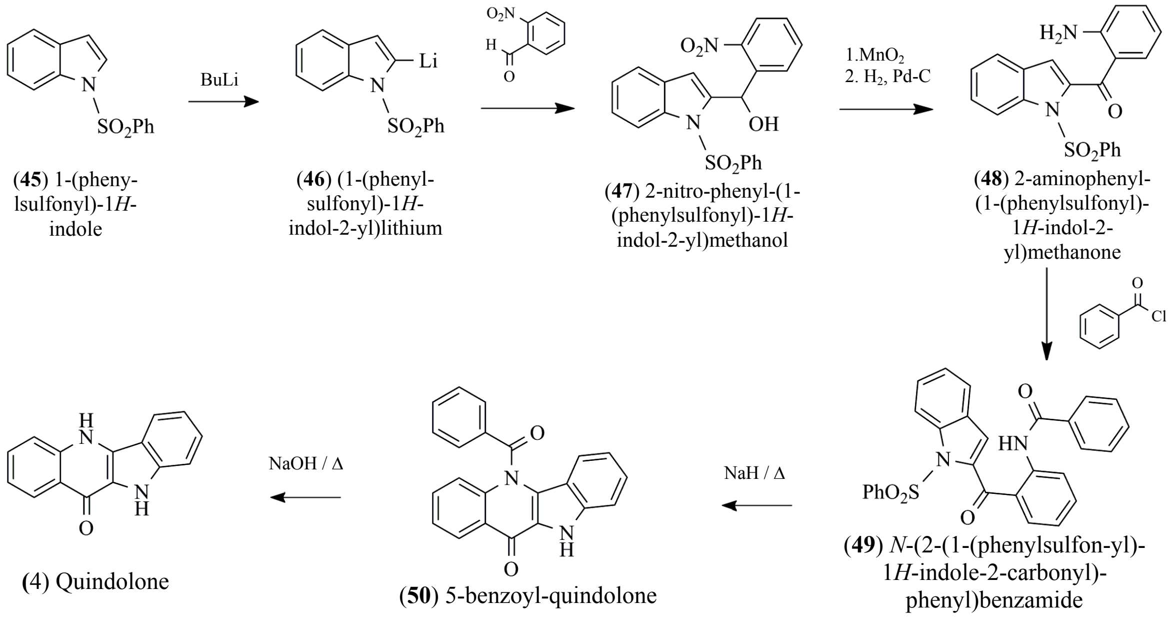
SO2Ph
BuLi
Li
SO2Ph
O2N
H
O
O2N
OH
SO2Ph
1.MnO2
2. H2, Pd-C
H2N
O
SO2Ph
(45) 1-(pheny-lsulfonyl)-1H-indole
(46) (1-(phenyl-sulfonyl)-1H-indol-2-yl)lithium
(47) 2-nitro-phenyl-(1-(phenylsulfonyl)-1H-indol-2-yl)methanol
(48) 2-aminophenyl-(1-(phenylsulfonyl)-1H-indol-2-yl)methanone
O
Cl
O
HN
N
PhO2S
O
(49) N-(2-(1-(phenylsulfon-yl)-1H-indole-2-carbonyl)-phenyl)benzamide
NaH / Δ
O
N
N
H
O
(50) 5-benzoyl-quindolone
NaOH / Δ
H
N
N
H
O
(4) Quindolone

Scheme 1.3 – Joule's method total synthesis

N-Benzoylation of **48** through nucleophilic acyl substitution gave **49** and *N*-deprotonation using sodium hydride allowed the ring closure through intramolecular indole-β-nucleophilic substitution of the acylindole giving in the indolo[3,2-*b*]quinoline **50**. Hydrolysis of N^5-benzoyl-quindolone (**50**) produced quindolone (**4**).(211) Quindoline and cryptolepine can be achieved from **4** through the process already described in Görlitzer and Weber total synthesis section.

Fan and Ablordeppey's method

In 1997, Fan and Ablordeppey synthesized the indolo[3,2-*b*]quinoline nucleus from the 3-aminoquinoline (**51**, shown in Scheme 1.4).(236, 240) Compound **51** undergoes through arylation with triphenylbismuth diacetate to form the intermediate 3-anilinoquinoline **52**. Subsequent oxidative cyclization of **52** with palladium (II) acetate in triflouracetic acid produces the desired quindoline **25**. This new methodology involves only a two steps reaction, completed in one day, and so represents an advantage when compared with the synthetic routes described so far. However, the formation of the regioisomer resulting from cyclization at 4-position of the quinoline reduces the yield of **25**.

To improve the efficiency of the cyclization step, the authors made some modifications in the methodology, changing the acid medium and the oxidant, but it was verified a reduction in the yield of the reactions, and in some cases, an increase of the side products. Blocking the 4-position of quinoline, in order to avoid cyclization in that position, was another strategy attempted by Fan and Ablordeppey, but this increased the reaction steps and reduced the advantage of this method over the others, i.e. a shorter reaction time with comparable yields.

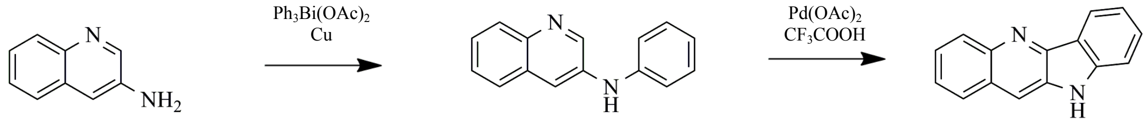

(**51**) quinolin-3-amine

(**52**) *N*-phenylquinolin-3-amine

(**25**) Quindoline

Scheme 1.4 – Fan and Ablordeppey total synthesis.

In 2008, Ablordeppey's group using this approach with some modifications synthesized substituted 10*H*-indolo[3,2-*b*]quinolines and 7*H*-indolo[2,3-*c*]quinolines with good yields.(251)

Görlitzer and VentzkeNeu's method

In the same year as Fan and Ablordeppey, 1997, Görlitzer and VentzkeNeu(212) also succeeded in a total synthesis of quindoline (Scheme 1.5), driven by the commercial availability of the starting materials.

The four steps reaction starts with the treatment of diethyl malonate (**53**) with 1-chloromethyl-2-nitrobenzene (**54**), in presence of a base, to afford **55** through nucleophilic aromatic substitution at the alpha carbon of **53**. Cyclization of **55**, under basic conditions yields compound **56**, which after nucleophilic substitution with 2-ethoxyacetyl bromide affords the intermediate **57**. Quindoline (**25**) was accomplished after reaction with phosphorus trichloride acting as electrophile.

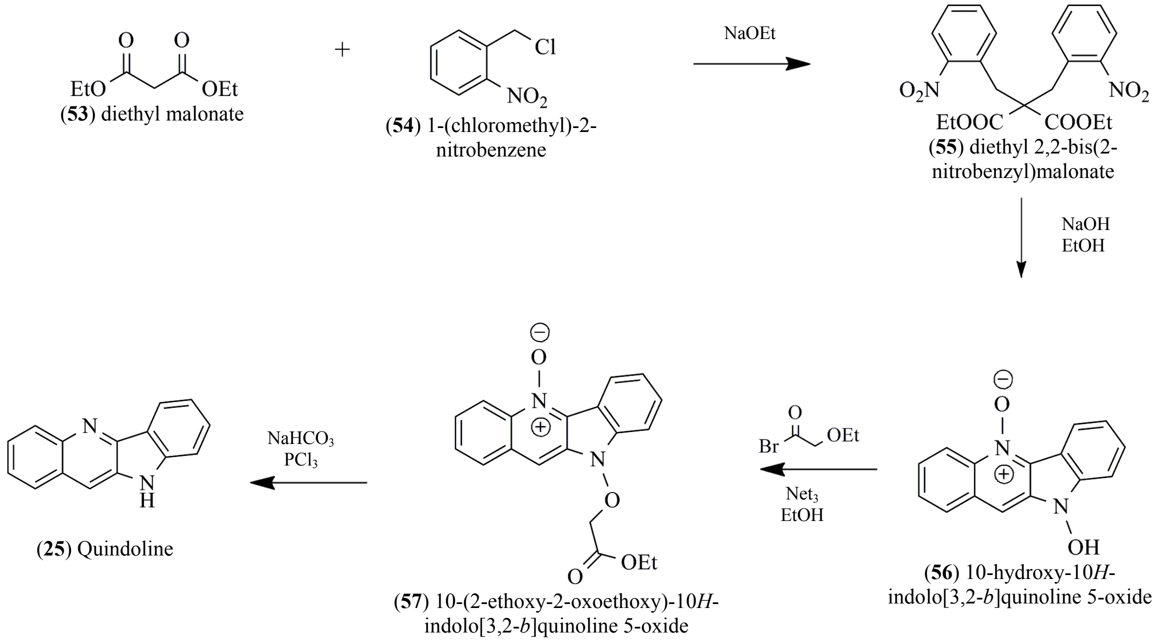
(53) diethyl malonate
(54) 1-(chloromethyl)-2-nitrobenzene
NaOEt
(55) diethyl 2,2-bis(2-nitrobenzyl)malonate
NaOH
EtOH
(56) 10-hydroxy-10H-indolo[3,2-b]quinoline 5-oxide
Net3
EtOH
(57) 10-(2-ethoxy-2-oxoethoxy)-10H-indolo[3,2-b]quinoline 5-oxide
NaHCO3
PCl3
(25) Quindoline

Scheme 1.5 – Görlitzer and VentzkeNeu total synthesis

Rocca’s method

The first Halogen-Dance reaction (HD) in quinoline series, as well as a new three steps synthesis was accomplished in 1998 by the Rocca group (Scheme 1.6).(213) The HD represents a base induced reaction of a haloaromatic compound in which the position of the halogen atom in the product **59**, differs from its position in the starting material **58**.(252) The mechanism consists in a sequence of deprotonation and metal-halogen exchange reactions, which in the end, lead to the most stable organometal species. These processes allow the introduction of an external electrophile at the former position of the halogen by concomitant establishment of a new reactive center at the new position of the halogen.(253)

Treatment of **58** with LDA led to substituted quinoline **59**, where fast isomerization to the more stable 4-lithioquinoline occurs, quenched with several electrophiles. Palladium-catalyzed cross-coupling reaction, under Suzuki conditions (254), between **59** and boronic acid derivative gave **60**, which undergoes cyclization to quindoline **25**, by a nucleophilic aromatic substitution (213). One year later, the same group described the total synthesis of cryptomisrine, a bis-quindoline linked by a keto group in position 11 of the indolo[3,2-*b*]quinoline nucleus, with the same HD methodology (214). As a extension of this methodology in 2001 Rocca’s group synthesized C11 substituted cryptolepines (255). Cross-coupling palladium-catalyzed reactions of functionalized boronic acids with iodoquinolines produced the desired biaryls, which was then readily functionalized in the quinoline nucleus by metalation with n-BuLi at low temperatures, followed by quenching with various electrophiles. The C11 substituted cryptolepines were achieved after cyclization of the prepared phenylquinolines and methylation of the prepared quindolines through a methodology already described in Görlitzer and Weber total synthesis section.(13)

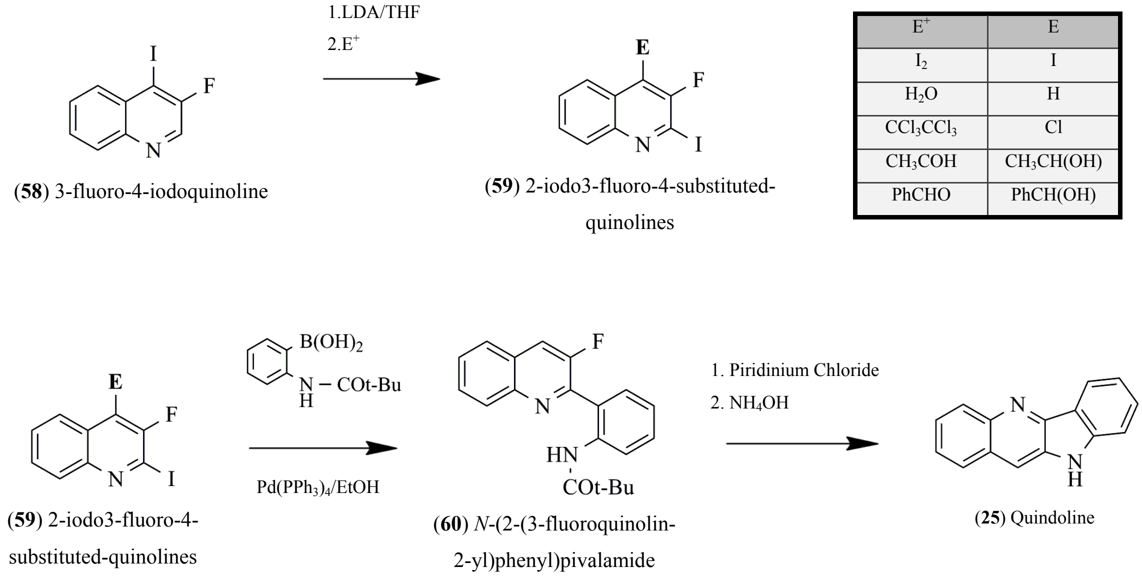

(**58**) 3-fluoro-4-iodoquinoline

(**59**) 2-iodo3-fluoro-4-substituted-quinolines

E^+	E
I_2	I
H_2O	H
CCl_3CCl_3	Cl
CH_3COH	$CH_3CH(OH)$
PhCHO	PhCH(OH)

(**59**) 2-iodo3-fluoro-4-substituted-quinolines

(**60**) *N*-(2-(3-fluoroquinolin-2-yl)phenyl)pivalamide

(**25**) Quindoline

Scheme 1.6 – Rocca total synthesis

Timári method

In 1999 Timári's group synthesized in a three step reaction the alkaloid quindoline (**25**, Scheme 1.7), using the palladium-catalyzed cross-coupling reaction, under Suzuki conditions,(254) like Rocca total synthesis, between (2-pivalamidophenyl)boronic acid (**61**) and halogen substituted quinolines. (256)

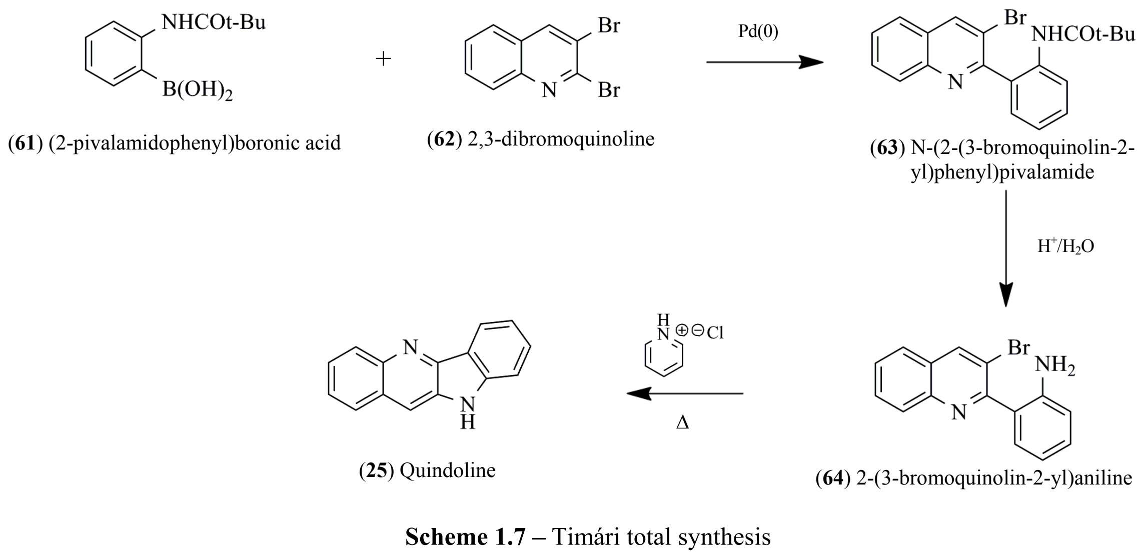

(**61**) (2-pivalamidophenyl)boronic acid

(**62**) 2,3-dibromoquinoline

(**63**) N-(2-(3-bromoquinolin-2-yl)phenyl)pivalamide

(**64**) 2-(3-bromoquinolin-2-yl)aniline

(**25**) Quindoline

Scheme 1.7 – Timári total synthesis

This strategy was accomplished by a regioselective coupling reaction of 2,3-dibromoquinoline (**62**) with **61**, taking in consideration the fact that the α-heteroaryl halogen atom is more reactive in such coupling reactions.(257) After the cross-coupling reaction, the intermediate **63** was deprotected affording the appropriate substituted 2-aryl-quinoline **64**. The intermediate64 undergoes in a substitution reaction using pyridinium hydrochloride, both as reagent and solvent, to afford the quindoline (**25**).

Rádl's method

Rádl's group developed in 2000 a total synthesis for the indolo[3,2-*b*]quinoline, quindolone (**4**, Scheme 1.8) and subsequently for quindoline and cryptolepine (216). The new methodology undergoes through second order nucleophilic reactions of benzonitriles with highly reactive α-bromoketones having suitable functionalized groups (R).

Reaction of the ethyl 2-(cyanophenyl)carbamate (**65**) with 2-bromo-1-(2-fluorophenyl)ethanone or 2-bromo-1-(2-nitrophenyl)ethanone (**66**) provided the corresponding compound **68**. The uncyclized intermediate **67** was not isolated and the reactions undergoes through addition of the enolate from **67**, to the cyano group. Cyclization of derivative **68** through nucleophilic aromatic substitution in the presence of sodium hydride provided the required tetracyclic N-unsubstituted quindolone **4**. This new approach to the synthesis of indolo[3,2-*b*]quinolines may be useful for the preparation of substituted derivatives. A large number of salicylonitriles and anthrainlonitriles are commercially available for use as starting materials.(216)

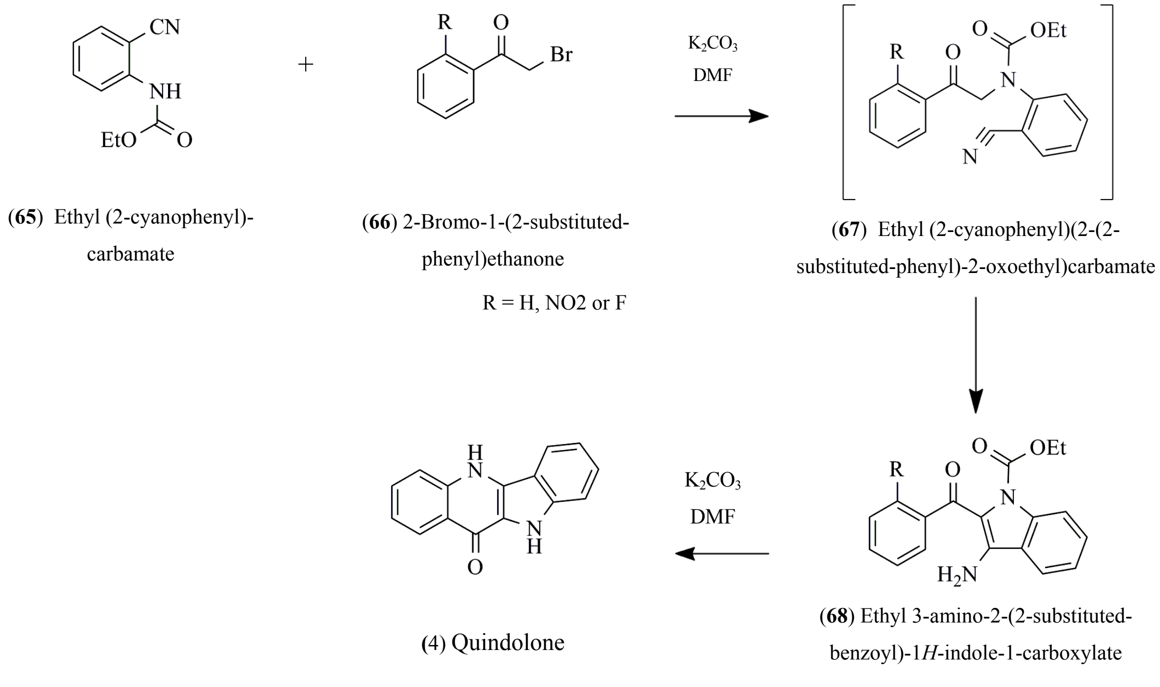

(**65**) Ethyl (2-cyanophenyl)-carbamate

(**66**) 2-Bromo-1-(2-substituted-phenyl)ethanone

R = H, NO2 or F

(**67**) Ethyl (2-cyanophenyl)(2-(2-substituted-phenyl)-2-oxoethyl)carbamate

(**68**) Ethyl 3-amino-2-(2-substituted-benzoyl)-1*H*-indole-1-carboxylate

(4) Quindolone

Scheme 1.8 – Rádl total synthesis

Mohan's method

A three step synthesis of indolo[3,2-*b*]quinoline alkaloids was reported in 2006 by Mohan's group. (217) This methodology involves the heteroatom directed photocyclization of anilinoquinolines in the presence of protic solvents (Scheme 1.9).

The term heteroatom-directed photoarylation describes electrocyclic reactions initiated photochemically and originated from the arrangements of an available electron pair in a heteroatom (in this case a nitrogen) and those from at least one aromatic π-bond. (258) This class of reactions has high regiospecificity of the aromatic substitution *ortho* to the heteroatom, with elimination of smaller molecules like H_2O, H_2, HCl and MeOH. The haloquinoline **69** condenses with aniline **70** at temperatures ranging from 100 to 200 ºC affording the intermediate **71**. The photochemical irradiation of **71**, in acidic solvent, yields both the linearly- and angularly fused products of photocyclization. The presence of suitable leaving groups X is an important requirement for photocyclization. In the absence of protic acidic solvents, indolo[3,2-*b*]quinoline was not produced when X = OH and high yields were found when X = Cl, H and OMe. The developed methodology is an attractive synthetic route to the synthesis of indolo[3,2-*b*]quinolines, both linear (**25**) and angularly-fused (**72**) due to the easy availability of the starting materials.(217)

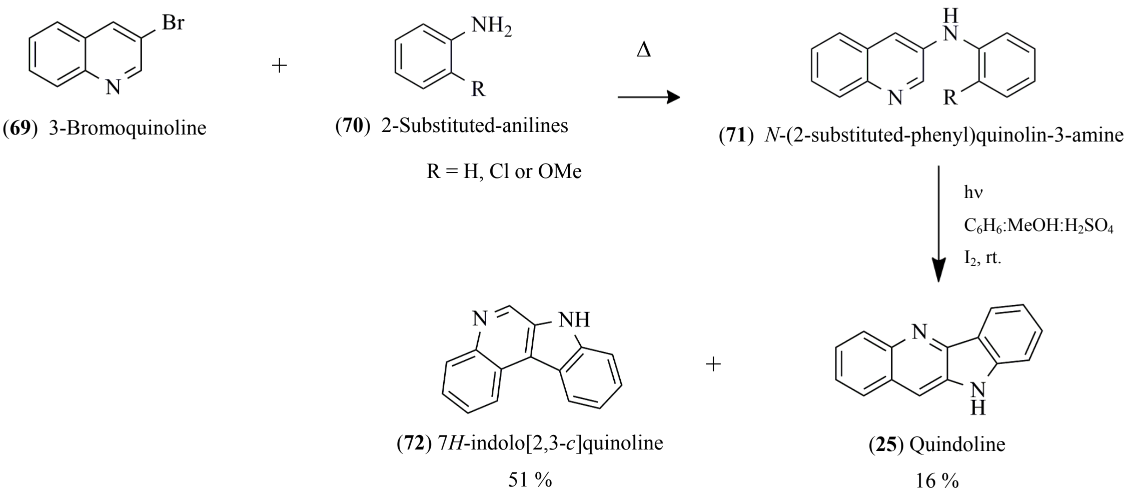

Scheme 1.9 – Mohan total synthesis

Ray's method

In the same year as Mohan's group, Ray's group developed the total synthesis of indolo[3,2-*b*]quinolines starting from 1-(2-nitrophenyl)-ethanone (**73**, Scheme 1.10).(259) The synthesis involved two important steps, regioselective thermal cyclization and generation of a nitrene intermediate followed by insertion into a sp^2 C-H bond.

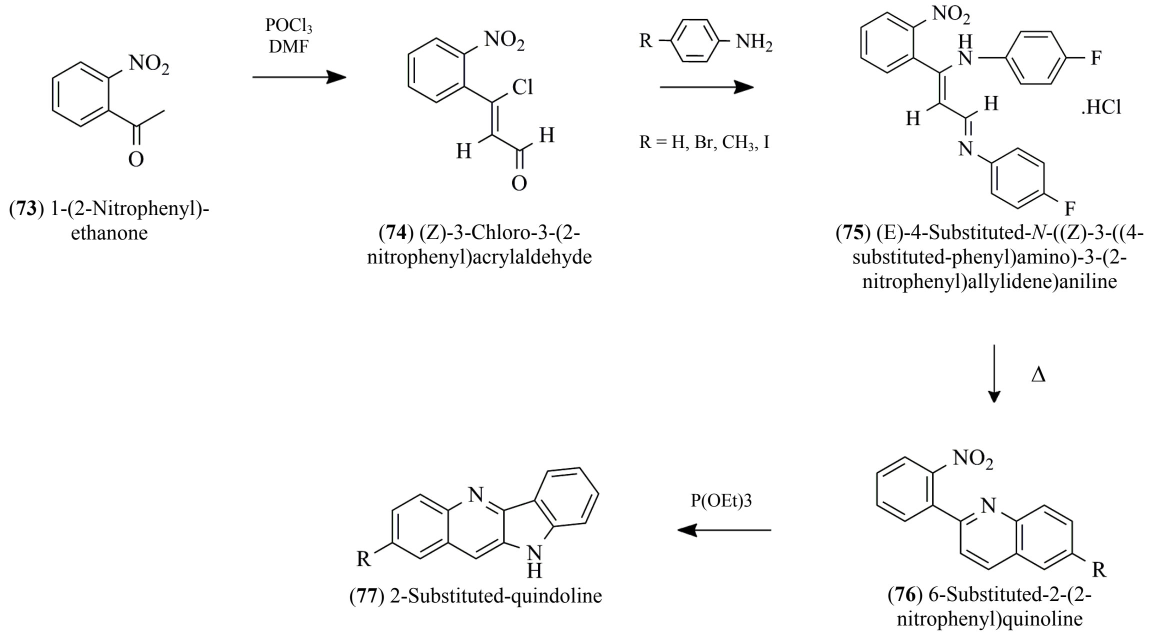
POCl3
DMF
R = H, Br, CH3, I
Δ
P(OEt)3
.HCl
(73) 1-(2-Nitrophenyl)-ethanone
(74) (Z)-3-Chloro-3-(2-nitrophenyl)acrylaldehyde
(75) (E)-4-Substituted-N-((Z)-3-((4-substituted-phenyl)amino)-3-(2-nitrophenyl)allylidene)aniline
(76) 6-Substituted-2-(2-nitrophenyl)quinoline
(77) 2-Substituted-quindoline

Scheme 1.10 – Ray total synthesis.

The reaction starts with the treatment of 1-(2-nitrophenyl)-ethanone (**73**) with phosphorus oxide trichloride in a Vilsmeier-Haack reaction to afford the β-chlorocinnamaldehyde (**74**), with the nitro group remaining intact. The intermediate **74** undergoes through double nucleophilic reaction with aniline and the corresponding enaminoimine hydrochloride **75** was produced. Thermal cyclization of the enaminoimine **75** generated the 2-(2-nitrophenyl)quinoline **76**, and after reaction with triethyl phosphite, which involves intramolecular annulations through nitrene intermediate, produced the 2-susbtituted-quindoline **77**. Ray's group developed a simple methodology for the synthesis of 2-substituted quindolines in a four steps reaction starting from accessible materials.(259-260)

1.2.2 Antiplasmodial Activities

The pharmacological activities of extracts of *C. sanguinolenta* and its major indoloquinoline alkaloid cryptolepine (**1**) as well as its isomers, neocryptolepine (**7**), isocryptolepine (**8**) and the synthetic isoneocryptolepine (**35**, 5-methyl-5*H*-indolo[2,3-*c*]quinoline) have been extensively studied. Since 1937 and in the last 30 years, several publications have demonstrated that indoloquinolines have a variety of biological activities including antibacterial, antifungal, antiprotozoal, antitumoral, antihyperglycemic, anti-inflammatory, hypotensive, antithrombotic and vasodilation. Due to its rigid structure and scope of derivatization, the indolo[3,2-b]quinolines, quindoline and specially cryptolepine, have been intensively investigated for finding of new derivatives with improved biological properties.(261)

Cryptolepine (**1**) is by far the most studied indoloquinoline with activity against malaria parasite (Table 1.1) being the subject of a recent review.(262) The antiplasmodial activity of **1** was first reported in 1991 by Noamesi *et al.*(4) after extracting it from the roots of *C. sanguinolenta*. The authors tested cryptolepine for *in vitro* antimalarial activity against the multi-resistant (K1) strain of *P. falciparum* and found the compound to be highly active with an IC_{50} value of 134 nM, comparable with that of chloroquine (IC_{50} = 230 nM). Cryptolepine also showed i*n vivo* significant activity against *P. berghei yoelii* and *P. berghei berghei* when administrated orally to infected mice, but showed no significant efficacy when administered subcutaneously to infected mice with *P. berghei* strain NK65 at non toxic doses.(263-264) In order to explain the high *in vitro* antiplasmodial activity of **1**, which was not supported by the *in vivo* experiments, Kirby *et al.* demonstrated by a spectrophotometric method that **1** was able to intercalate into DNA and related this with its antiplasmodial mechanism of action.(264)

In the following years several authors reported isolation from the roots of *C. sanguinolenta* and the antimalarial activity of not only cryptolepine, but also of neocryptolepine and isocryptolepine against chloroquine resistant and sensitive strains of *P. falciparum* (Table 1.1). *Cryptolepis sanguinolenta* has been investigated since 1929 for its chemical composition and several indolo[3,2-*b*]quinolines, beside cryptolepine, were isolated and their antiplasmodial activity evaluated. (198, 265-266) In Figure 1.15 one can see that **1** is the most active of all natural indolo[3,2-*b*]quinolines (**25-28**) and methylation of N^5 is required for antiplasmodial activity, since **25** is inactive against both resistant and sensitive *P. falciparum* strains. It was also observed that introduction of acidic groups at C11 (**26**, **27**) abolishes the activity but esterification of the carboxylic group (**78**) leads to partial recovery of activity. Based on these observations the authors suggested that weak basic properties were necessary for antiplasmodial activity of indolo[3,2-*b*]quinolines.(198) Corroborating this conclusion is the improved antiplasmodial activity shown by 10*H*-indolo[3,2-*b*]quinolin-11-yl-amines **79**. Compound **79a** which contains a *para*-aminophenol amine in C11 like amodiaquine was the most active of the series when tested against the *P. falciparum* resistant strain K1, with an IC_{50} around 30 nM .(243)

Table 1.1 – IC_{50} values of lead indoloquinolines (IQ) against CQ-R and CQ-S *Plasmodium falciparum* strains.

IQ	**IC_{50} (nM)**					
	P. Falciparum CQ-R strains			*P Falciparum* CQ-S strains		
	W2 (Ref)	K1 (Ref)	FcB1 (Ref)	D6 (Ref)	T996 (Ref)	F32 (Ref)
Cryptolepine (**1**)	177-194 (263) 2000 (267) 755 (268)	134 (4) 142-231(263) 134 (264) 330 (255) 440 (210) 120 (269) 440 (235) 755 (249) 230 (198) 120 (270)	430-560 (266)	180 (271) 116-153 (263)	14 (198)	190-300 (266)
Neocryptolepine (**29**)	280 (263) 14000 (267) 14000 (272)	220 (263) 2610 (269)	--	150 (263)	--	--
Isocryptolepine (**30**)	--	780 (269)	300 (266)	--	--	--
Isoneocryptolepine (**35**)	--	230 (269)	--	--	--	--

The influence of the structural modifications at N^5 and C11 of the indolo[3,2-*b*]quinoline nucleus was also evaluated *in vitro* against the *Plasmodium falciparum* by Arzel and co-workers.(255) They confirmed that methylation on N^5 increases the antiparasitic activities, since **2** was about 100 times less active against both parasites than **1** and the alkylation at C11 in absence of 5-methyl substitution (**81**), does not affect significantly the antiplasmodial activity. With the 5-methyl substituent, alkyl groups at C11 (**80** and **82**) decrease the activity against both parasites, with exception of **82a** which was about 5 times more active against *P. falciparum* than cryptolepine.

The search for indolo[3,2-*b*]quinolines with improved antiplasmodial activities led Wright and co-workers to synthesize new cryptolepine derivatives substituted in the aromatic nucleus (**83**).(210) The monosubstitued compounds 2-Br (**83a**) and 7-Br (**83b**) showed improved antiplasmodial activity when compared with **1** and the disubstitued compound **83c** (2,7-diBr) was about 10 times more potent against *P. falciparum* K1 strain. In this study it was also shown that compounds **1, 83a-c,e,g** share the ability to inhibit *β*-haematin formation, in a cell-free system, like chloroquine.(210) Compound 2,7-dibromo (**83c**) was also evaluated *in vivo* at several doses and a dose-dependent suppression of parasitemia was seen with an ED_{90} of 21.6 $mg.kg^{-1}.day^{-1}$. This structure-activity study was completed later with a series of 16 new cryptolepine derivatives (**84**).(235)

The IC_{50} of these compounds (**84a**,**k-m**,**o**) against *P. falciparum* K1 strain were <100 nM, 5-10 fold lower than that of **1** but their cytotoxicities were only 2-4 times lower than that of **1**. In infected mice with *P. berghei*, the 2-chloro-7-bromo (**84k**) suppressed parasitemia by 90% at doses of 25 $mg.kg^{-1}.day^{-1}$, with no apparent toxicity to the mice.

Like previously, the authors hypothesized that the mechanism of action of these compounds could be by inhibition of hemozoin formation in the food vacuole, however, no correlation between antiplasmodial activity and accumulation in the acid food vacuole, determined by a mathematical method on the bases of compounds pK_a, was seen, suggesting that the antimalarial activity involves other mechanisms in addition to the inhibition of hemozoin formation.(10, 235)

Arzel and co-workers, taking advantage of the fluorescence of the indoloquinoline chromophore, had previously shown that in *P. falciparum*-infected erythrocytes cryptolepine accumulates into specific parasite structures that could correspond to the parasite nuclei.(255) The antiprotozoal activities of dimeric indoloquinolines were also evaluated (269). Both dimeric alkaloids **33** and **34** were equally or less active than cryptolepine against *P. falciparum* CQ-R strain K1 (Figure 1.16), demonstrating that dimerization does not have a positive effect on the antiprotozoal activity. On the other hand, bis-indoloquinolines **85** and **86a-b** showed *in vitro* antiplasmodial activity against *P. falciparum* D6 and W2 strains with IC_{50} of 157 and 115 nM for the most active compound **86b (**Figure 1.16**)**.(271)

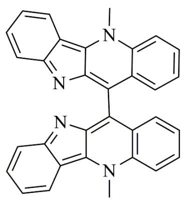

IC$_{50}$ (nM)	K1
(**33**) Bis-cryptolepine	270

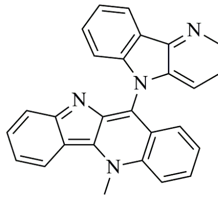

IC$_{50}$ (nM)	K1
(**34**) Cryptoquindoline	>10000

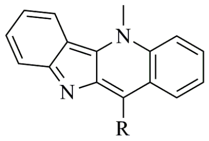

IC$_{50}$ (nM)	K1
(**26**) Hydroxycryptolepine, R = OH	120000
(**27**) Cryptolepinoic acid, R = COOH	>181000
(**78**) Ethylcryptolepionate, R = COOEt	3760
(**80**) 11-substituted Cryptolepine	
a: R = Me	101
b: R = Et	1100
c: R = *i*Pr	2200
D R = C$_6$H$_6$	1100

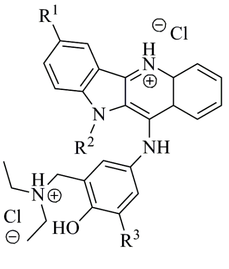

	EC$_{50}$ (nM) K1
(**79**) 11-((3-((diethylammonio)methyl)-5-substituted-4-hydroxy-phenyl)amino)-7,10-substituted-10,11a-dihydro-4a*H*-indolo[3,2-*b*]quinolin-5-ium chloride	
a: R^1 = H, R^2 = H, R^3 = H	30.9
b: R^1 = H, R^2 = CH$_3$, R^3 = H	
c: R^1 = Cl, R^2 = CH$_3$, R^3 = H	
d: R^1 = H, R^2 = H, R^3 = CH$_2$HN$^+$(CH$_2$CH$_3$)$_2$	
e: R^1 = H, R^2 = CH$_3$, R^3 = CH$_2$HN$^+$(CH$_2$CH$_3$)$_2$	
f: R^1 = Cl, R^2 = CH$_3$, R^3 = CH$_2$HN$^+$(CH$_2$CH$_3$)$_2$	

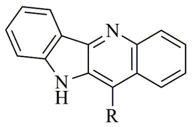

IC$_{50}$ (nM)	K1
(**25**) Quindoline	36200
(**81**) 11-substituted quindoline	
a: R = Me	74600
b: R = Et	30900
c: R = C$_6$H$_6$	74600

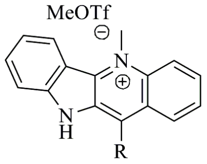

IC$_{50}$ (nM)	K1
	330
(1) Cryptolepine, R = H	
(**82**) 11-substituted Crypt. triflate	
a: R = Me	62
b: R = Et	480
c: R = *i*Pr	1300
d: C$_6$H$_6$	1100

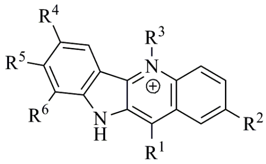

IC$_{50}$ (nM)	K1	HB3
(**83**) mono, di and tri-subtituted IQ		
a: R^2 = Br, R^3 = CH$_3$	260	450
b: R^3 = CH$_3$, R^4 = Br	260	190
c: R^2 = Br, R^3 = CH$_3$, R^4 = Br	49	26
d: R^1 = CONH^2, R^3 = H	>100000	- -
e: R^3 = CH$_3$, R^4 = NO$_2$	650	140
f: R^3 = CH$_3$, R^6 = NO$_2$	6920	4140
g: R^3 = CH$_3$, R^4 = NO$_2$, R^6 = NO$_2$	650	450
h: R^3 = CH$_3$, R^4 =NHAc	520	470
i: R^1 = Cl, R^3 = CH$_3$	240	1670
j: R^1 = Cl, R^2 =Br, R^3 = CH$_3$	4650	- -
k: R^1 = Cl, R^3 = CH$_3$, R^5 = Br	7180	- -
l: R^1 = Cl, R^3 = CH$_3$, R^4 = Cl	7620	- -
m: R^1 = Cl, R^3 = CH$_3$, R^5 = Cl	27000	- -

In absence of **R** default is hydrogen

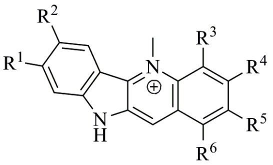

IC$_{50}$ (nM)	K1
	440
(1) Cryptolepine	
(**84**) mono and di-substituted Crypolepine	
a: R^5 = Cl, R^6 = Cl	88
b: R^5 = Cl	166
c: R^4 = Cl, R^5 = Cl	356
d: R^4 = Cl	448
e: R^3 = Cl	4690
f: R^1 = Cl	>10000
g: R^5 = F	1210
h: R^5 = CH$_3$	410
i: R^5 = OCH$_3$	950
j: R^4 = CH$_3$	149
k: R^2 = Br, R^5 = Cl	30
l: R^2 = Br, R^5 =F	63
m: R^2 = Br, R^4 = Cl	37
n: R^2 = Br, R^5 = CH$_3$	260
o: R^1 = Cl	45

In absence of **R** default is hydrogen

Figure 1.15 – Indolo[3,2-*b*]quinolines evaluated against *Plasmodium falciparum* strains.

Alkylation of N^{10} with ω-phenylpentyl group (compound **87**, Figure 1.16) was shown to improve antiplasmodial activity against both sensitive *P. falciparum* D6 strain (IC$_{50}$ = 122 nM) and resistant W2 strain (55 nM) .(271) However, isosteric replacement of N^{10} by sulfur or oxygen resulted in compounds with moderate activities against *P. falciparum* D6 (IC_{50} = 755-4241 nM) and W2 (IC_{50} = 755-5302 nM) strains (271).

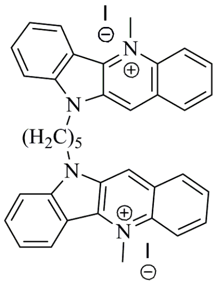

IC_{50} (nM)	D6	W2
(**85**) 10,10'-(pentane-1,5-diyl)bis(5-methyl-10H-indolo[3,2-b]quinolin-5-ium) iodide	33	177

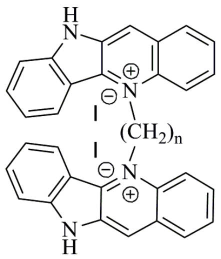

IC_{50} (nM)	D6	W2
(**86**) 5,5'-(substituted-diyl)bis-(10H-indolo[3,2-b]quinolin-5-ium)		
a: n = 4	> 707	- -
b: n = 5	157	115

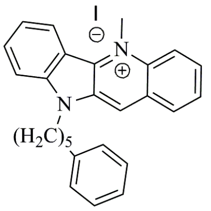

IC_{50} (nM)	D6	W2
(**87**) 10-(5-phenylpentyl)-cryptolepine iodide	122	55

Figure 1.16 – Indolo[3,2-*b*]quinolines evaluated against *Plasmodium falciparum* strains.

1.2.3 Interactions with DNA and Cytotoxic Activities

Due to the apparent structural similarity between the indolo[3,2-*b*]quinoline cryptolepine (**1**) and 9-aminoacridine, which intercalates into DNA (273), Kirby *et al.* performed titrations of **1** with DNA and observed a hypochromic effect upon addition of DNA.(264) In the same study, molecular simulations suggested that stabilization of intercalation complex is made through π-π charge transfer complexes between nitrogens of purine-pyrimidine bases and **1**. Corroborating these results, Bonjean *et al.* reported that **1** competes with the triphenylmethane dye for binding to DNA with the same efficiency as the well known intercalating drug doxorubicin.(274) In 1998 the same author studied the binding of **1** to DNA, the inhibition of topoisomerase II and the cytotoxicity towards mouse B16 melanoma cells. Association constants to calf thymus DNA ($K_1 = 3x10^6$ and $K_2 = 4x10^4$ M^{-1}) were consistent with those determined to intercalating agents and it was observed a noticeable preference for GC-rich sequences. Cryptolepine was also shown to be a potent topoisomerase II inhibitor, stabilizing the topoisomerase II-DNA complex, stimulating the cut of DNA at a subset preexisting topoisomerase II cleavage sites and inhibiting preferentially the DNA synthesis rather than RNA and protein synthesis. This indoloquinoline easily crosses the cell membranes and accumulates selectively into the nuclei rather than in the cytoplasm of B16 melanoma cells, blocking the cell cycle in G_2/M phase and being 4-5 times more cytotoxic than ellipticine.(17) The alkaloid altered the B16 melanoma cell cycle distribution without signs of drug-induced apoptosis, pointing to a cell death via necrosis.(7) However in 2000 Dassonneville *et al.* extended the study of cytotoxic effects of cryptolepine at the cellular level and showed that **1** provokes a massive accumulation of P388 murine leukemia cells in the G_2/M phase but in HL-60 human leukemia cells **1** leads to the appearance of a hypo-diploid DNA, characteristic of the apoptotic cell population, with mitochondria and caspases playing a central role in the activation of the cryptolepine induced apoptosis. They also observed cross-resistance patterns with cryptolepine comparable with those reported for anticancer drugs that are weak inhibitors of topoisomerase II, concluding that topoisomerase inhibition would play a relatively minor role in cryptolepine's cytotoxicity. (275)

The genotoxicity of **1** was studied by Ansah & Gooderham on V79 cells, a Chinese hamster lung fibroblast. (8) Cryptolepine induced accumulation of cells in the sub-G_1 phase of the cell cycle, indicative of apoptotic cell death, but was not mutagenic (*hprt* gene) in a concentration range from 0.5 to 5 μM. However, after 24 hours of treatment, cryptolepine induced a dose-dependent increase in micronuclei, a signal that it can lead to DNA damage and carry some genotoxic risk. Nevertheless, the poor genotoxicity of cryptolepine coupled with the potent cytotoxic action could support their anticancer potential.(8, 276) In 2002 Lisgarten *et al.* reported the crystal structure of cryptolepine intercalated with the DNA fragment $d(CCTAGG)_2$.(277) Cryptolepine was found to bind to DNA in GC-rich sequences and to interact with those DNA sites in a base-stacking intercalation mode (Figure 1.17). The asymmetry of the alkaloid induces a perfect stacking with the asymmetry of the site, allowing the stability of the complex in the absence of hydrogen bonding interaction.(5)

Cryptolepine also interacts with triplexes and quadruplexes DNA structures. In a dialysis competition assay Guittat *et al.* demonstrated that cryptolepine is not a good substrate for DNA or RNA single strands, but displays good affinity for triplexes (ΔT_m = 10 ºC) rather than for G-quadruplexes (ΔT_m = 3 ºC). Additionally, cryptolepine showed weak telomerase inhibition activity, with an IC_{50} of 9.4 μM and a moderated PCR inhibition at ~5 μM, before telomerase elongation was observed, probably reflecting the preference of cryptolepine for a duplex than a G-quadruplex structure.(278)

In 2007 a study with murine macrophage cell line RAW 264.7 showed that cryptolepine inhibits NF-κB (nuclear factor kappa-light-chain-enhancer of activated B cells) mediated gene expression, directly acting on the DNA binding step of activated NF-κB and thus impairing the initiation of transcription of not only inflammatory proteins, but also regulators of the NF-κB pathway. It was also suggested that cryptolepine might alkylate one of the crucial cysteine residues of the p65/p50 gene and thereby impair DNA binding of the nuclear factor.(279) Interestingly, a recent report emphasis the importance of the NF-κB pathway for the pathogenesis of malaria and the antimalarial activity of cryptolepine may be based on its inhibitory effect on NF-κB.(280)

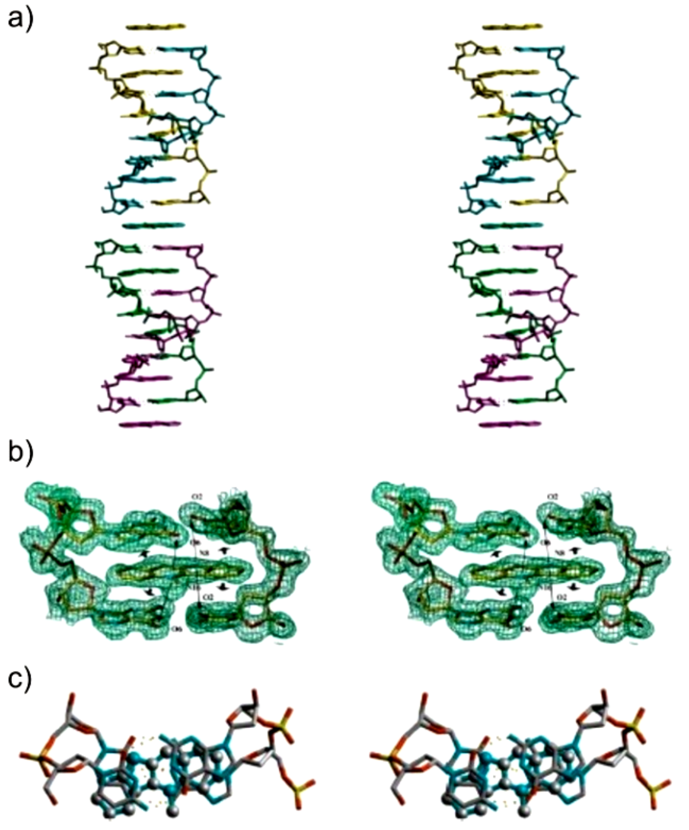

Lisgarten, J.N., *et al.*, (**2002**), ***Nature Structural Biology***, 9, 57-60.

Figure 1.17 – Crystal structure of the cryptolepine intercalated into d(CCTAGG)$_2$.

a) Stereo view of two bis-intercalated d(CCTAGG)$_2$ hexanucleotides in the ab-plane, with the end-stacked ligand bound between then. Four asymmetric units are represented in different colours. b) Stereo view of the 2F$_o$-F$_c$ electron density map at the area of the intercalated ligand, looking into the major groove. The map was contoured at the 1.2 σ level. Stacking (large arrows) and electrostatic (small arrows) interactions are shown. c) Stereo view of the projection down the helix axis of a d(CpC)-d(GpG) dinucleotide with the sandwiched ligand.

More recently Matsui *et al.* showed that the treatment of human osteosarcoma MG63 cells with cryptolepine (1-4 μM) induces p21$^{WAF1/C1P1}$ mRNA and protein expression, resulting in G$_2$/M phase arrest of the cell cycle in a p53-independent manner.(281) Although the indolo[3,2-*b*]quinoline **1** presents good cytotoxicity activity in cancer cell lines, the simplest 10*H*-indolo[3,2-*b*]quinoline **25** shows only moderate activity with IC$_{50}$ ranging from 15.5 to 66 μM.(282) Due to the cytotoxic and antitumoral activity of natural indolo[3,2-*b*]quinolines **1** and **25**, several derivatives with improved properties have been synthesized in the last 20 years.(238-239, 241, 244-245, 283-291)

1.2.4 Whole Body Distribution of Cryptolepine in Mice and Toxicity

The distribution of ^{3}H-cryptolepine salt in pigmented and albino mice and in pregnant mice on day 16 of gestation was studied by whole-body distribution autoradiography, after a single intravenous injection of 0.5 mg.kg^{-1} which is about 10% of the theraupeutic dose.(292) It was reported that 5 minutes after injection most of ^{3}H-cryptolepine left the blood and was localized in several tissues like, muscles, liver, gastrointestinal mucosa, adrenal medulla, thyroid, thymus, spleen, lymph glands and eye but not in central nervous system (brain and spinal cord). In most tissues a pronounced decrease of concentration occurred between 1 and 4 hours pos-injection. In the liver an initially high level of radiolabeled compound was gradually followed by a long tail of low concentrations which could be discerned even after 8 days. This fact and the observed radioactivity in the gall bladder and intestinal lumen indicated biliary secretion and an enterohepatic circulation, although it is not known if the radioactivity referred to cryptolepine or to its possible metabolites. The kidney level of radioactivity increased after 20 minutes of injection and decreased rapidly from 1 hour and onwards. Organs with a rapid cell proliferation (spleen, thymus and gastrointestinal mucosa) showed a relatively high and prolonged retention. For instances, in thymus and spleen a slight activity was still retained after 4 days.

The most notable and prolonged retention was found in the adrenal medulla and in the melanin-contained tissues of the eyes in which the radioactivity could be found 8 days after administration. Following this observation, the authors suggested that this marked localization of cryptolepine in the adrenal medulla could explain the hypotensive activity of the alkaloid which would act by decreasing the catecholamine turnover. The overall distribution of ^{3}H-cryptolepine in female mice was not significantly different from that of male mice. In fetal tissues the radioactivity was found to be much lower than in maternal tissue and this suggests a low influence of cryptolepine on the fetus if the compound is being used during pregnancy.(292)

The studies of acute toxicity revealed that the intraperitoneal injection of 120 mg.kg^{-1} of cryptolepine is lethal for guinea-pigs after 12 hours.(293) In other studies the dose of **1** that killed 50 % of the mice over a 24 hours period after intraperitoneal administration was calculated as being 146 mg.kg^{-1}.(294) Studies on the subacute toxicity showed that chronic administration by subcutaneous injection of 30 or 60 mg.kg^{-1} of **1** to mice after 2 weeks caused no damage in liver cells and only moderate necrosis in the kidney. However, after 6 weeks of administration both doses caused foci congestion of liver chronic inflammatory cells and the higher dose caused widespread cortical necrosis with hyperemia in the kidney.(294)

II

Chapter II – **Synthesis of Indolo[3,2-*b*]quinolines**

"Problems are only opportunities with thorns on them"

Hugh Miller (1802 – 1856)
Scottish geologist and writer

Abstract

*Indolo[3,2-b]quinolines represent a important scaffold to the development of new antimalarial drugs with improved activity against malaria parasites. Introduction of one alkyldiamine side chains in the cryptolepine (**1**) nucleus is expected to increase its antiplasmodial activity, by improving its accumulation in the parasite DV. The indolo[3,2-b]quinoline nucleus have been synthesized through already described synthetic methodology, that allowed us to prepare a small library of compounds from a common intermediate. In this study, a series of cryptolepine derivatives (**3**) has been synthesized through the incorporation of short basic side-chains in position C-11 of the 10H-indolo[3,2-b]quinoline skeleton. In order to explore the indoloquinoline scaffold and create new antimalarial chemotypes, we decided to synthesize also novel indolo[3,2-b]quinolin-11-one (**4**, **91a** and **91b**) derivatives by alkylating positions* N^5 *and* N^{10} *(**5**) of the aromatic nucleus. However, reaction with 2-chloro-N,N-diethylethanamide gave also different alkylation patterns, N,O- (**94**) and O- (**95**).*

List of Contents

2.1 INTRODUCTION....45
2.2 SYNTHETIC METHODOLOGIES....46
*2.2.1 Synthesis of 5H-Indolo[3,2-b]-quinolin-11(10H)-one (**4** and **91**) and 5-Methyl-11-chloro-10H-indolo[3,2-b]quinolines (**93**) Intermediates....46*
*2.2.2 Synthesis of Cryptolepine (**1**)....54*
*2.2.3 Synthesis of Cryptolepine Derivatives (**3**)....56*
*2.2.4 Synthesis of Quindolone Derivatives (**5**)....61*
2.2.5 Synthesis of Alkyldiamines....65

2.1 Introduction

Malaria is a global health problem and one of the most widespread infections of our time. Due to the development of the drugs-resistance by the different *Plasmodium* sp. the development of safer, potent and affordable antimalarial drugs to increase our armory in the fight against malaria is needed.(26, 167) The indolo[3,2-*b*]quinolines are a novel scaffold in the antimalarial armamentarium and cryptolepine (**1**) is by far the most studied one. Despite of cryptolepine be as active as chloroquine against the *Plasmodium* falciparum., its cytotoxicity precludes its clinical use.(8) However, previous studies on the possible antimalarial mode of action of cryptolepine and related natural indoloquinolines led to the conclusion that this class of compounds is able to inhibit haemozoin formation, through π-π stacking interactions between the aromatic core and the FPIX, like chloroquine and related 4-aminoquinolines.(210) Also, previous studies on the possible structure-activity relationships of these compounds showed that the introduction of halogens as substituents in the aromatic nucleus of the 5-methyl-indolo[3,2-*b*]quinolines increase the antiplasmodial activity, as well as the introduction of acidic groups in position C11 abolish the activity against the *Plasmodium* sp.(9, 198) In view of what is already known on the mode of action of cryptolepine (and related indoloquinolines), we synthesized new indoloquinolines capable of targeting the haemozoin formation in the digestive food vacuole of the *Plasmodium* sp. in the erythrocytic stage. The development of compounds targeting haemozoin formation need to cover the design of compounds capable of forming strong interactions with the propionic acid and carboxylate-iron moieties on the haemozoin fast growing faces {001} and {011}, able to interact with haematin through π-π stacking interactions and an ionisable function to promote the accumulation inside the parasite DV.

The new cryptolepine derivatives (**3**) were synthesized with an alkyl- or aryldiamine side chain in position C11 of the indoloquinoline nucleus, while the new quindolone derivatives (**5**) were synthesized with an alkylamine side chain in positions N^5 and N^{10} of the indoloquinoline core. Since cryptolepine already possess antiplasmodial activity, it is reasonable to think that introduction of alkyl- or aryldiamine groups in position C11 (**3**) will contribute to the accumulation of these compounds in the acidic DV, promote the interactions between the drug and the propionic acid and carboxylate-iron moieties of haematin, increasing consequently the specificity and antiplasmodial activity through inhibition of haemozoin formation. Also, based on the quindolone scaffold (**4**), which do not show antiplasmodial activity by itself, we introduced alkylamine side chains in positions N^5 and N^{10}, aiming to achieve potent antiplasmodial activity through the inhibition of haemozoin formation in DV. The introduction of the two alkylamine side chains is expected to contribute to the accumulation in the DV through the ionisable amine functionality (weak base, pK_a between 8 and 10) and to promote the electrostatic interactions with the propionic acid and carboxylate-iron moieties in the fast growing faces of haemozoin. Also, additional H-bond acceptors, like the carbonyl group in C11 and the substituents in the aromatic nucleus are expected to increase the interaction with haematin, together with the aromatic core of the quindolone scaffold, which would be able to interact with the haematin through π-π stacking interactions.

One of the requirements of any synthetic strategy for drug development is that the synthetic pathway must be amenable to provide chemical diversity in order to obtain a large number of structural motifs. The synthesis of the new library of cryptolepine derivatives (**3**) with an alkyldiamine side chain at C11, and quindolone derivatives (**5**) with alkylamine side chains attached to nitrogens N^5 and N^{10} was attained through a common intermediate. This strategy, also allowed us to appraise the effect of the amine side chain length, flexibility, electron-density and corresponding substituent on terminal amine, as well as the effect of the substitutions in the cryptolepine aromatic nucleus on the antiplasmodial activity.

Cryptolepine and its derivatives were synthesized from a common intermediate, 11-quindolone (**91**), according to the retrosynthetic analysis represented in Figure 2.1 The key intermediates **91**, were synthesized according to the procedure developed by Görlitzer and Weber (section 0)(11-12) and adapted by Bierer.(13-14) From **91** the quindolone derivatives (**5**) were synthesized through nucleophilic reaction with the appropriated haloalkylamine and the cryptolepine derivatives (**3**) were synthesized after chlorination of position C11, methylation of N^5 and finally nucleophilic substitution of the chloride atom at position C11 by the appropriate alkyl- or aryldiamine. This synthetic strategy allowed us to introduce a large variety of alky- or aryldiamines, alkylamines and different substitution patterns in the aromatic core of the cryptolepine and quindolone derivatives (**3** and **5**).

2.2 Synthetic Methodologies

2.2.1 Synthesis of 5*H*-Indolo[3,2-*b*]-quinolin-11(10*H*)-one (**4** and **91**) and 5-Methyl-11-chloro-10*H*-indolo[3,2-*b*]quinolines (**93**) Intermediates

Several methodologies have been already described for the synthesis of the indoloquinoline scaffold (Section 1.2.1). However, not all of them allow the straightforward synthesis of the quindolone (**91**) with the desired substitution pattern in the aromatic nucleus. Due to the simplicity, efficiency and relatively low price of the reagents, the cryptolepine derivatives (**3**) and the quindolone derivatives (**5**) were synthesized through the methodology developed by Görlitzer and Weber$^{(11-12)}$ and adapted by Bierer.$^{(13-14)}$

Cryptolepine derivatives (3)

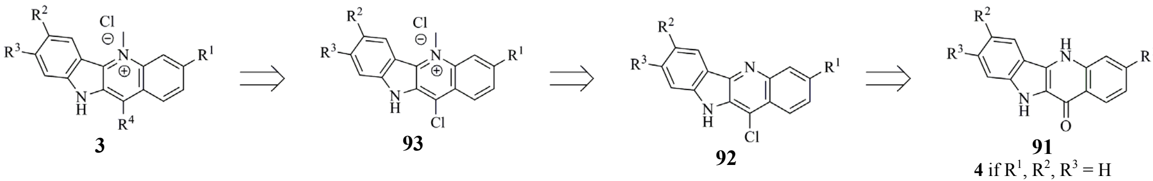
R2
R3
Cl
N
R1
H
R4
3
93
92
91
4 if R1, R2, R3 = H

R^1, R^2, R^3 = H, CH_3, CF_3, OCH_3 or Halogen
R^4 = Alkyl, cyclo or aryldiamine

Quindolone derivatives (5)

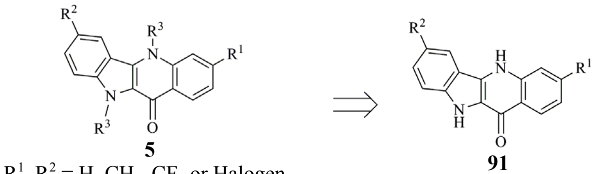
R2
R3
N
R1
O
5
H
91
4 if R1, R2 = H

R^1, R^2 = H, CH_3, CF_3 or Halogen
R^3 = Alkylamine

Figure 2.1 – Retrosynthetic analysis for the synthesis of the cryptolepine and quindolone derivatives (**3** and **5**).

This methodology allowed us to synthesize the common indoloquinoline 5*H*-indolo[3,2-*b*]-quinolin-11(10*H*)-one (**91**, 11-quindolones), used for the synthesis of cryptolepine, its derivatives and of the quindolone derivatives **5**, as described in Scheme 2.1. The quindolone derivatives were synthesized directly from the intermediates **91** and the cryptolepine derivatives **3** were synthesized from the common intermediates 5-methyl-11-chloro-10*H*-indolo[3,2-*b*]quinolines (**93**), using the methodology described by Bierer and co-workers, which undergoes through a chlorination to give the 11-chloro-10*H*-indolo[3,2-*b*]quinolines (**92**) and a methylation into N^5 to afford **93**, as represented in Scheme 2.1.$^{(13-14)}$

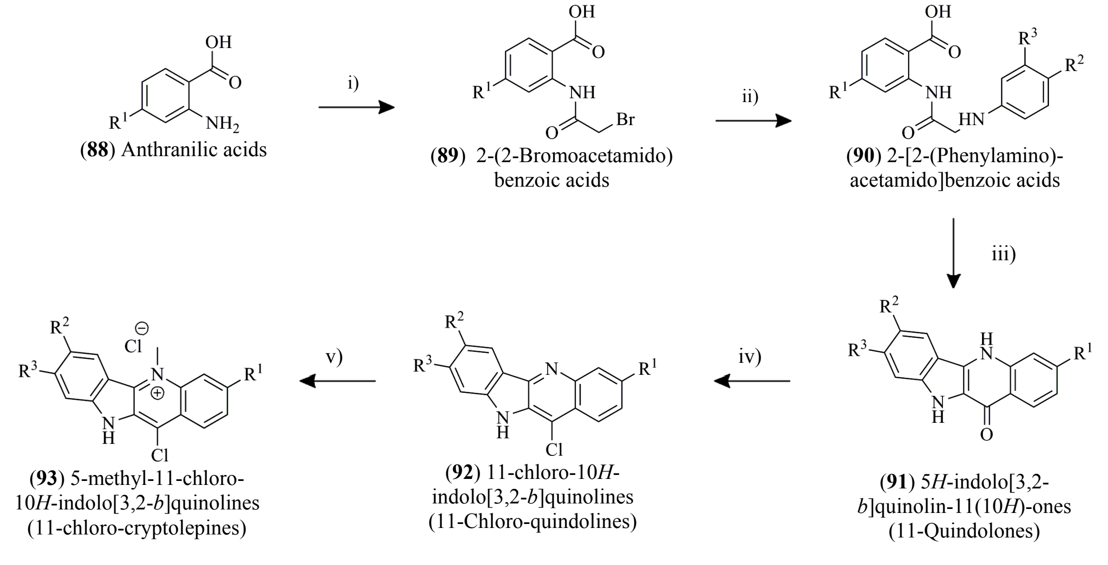
OH
O
R1
NH2
(88) Anthranilic acids
i)
NH
Br
(89) 2-(2-Bromoacetamido) benzoic acids
ii)
R3
R2
HN
(90) 2-[2-(Phenylamino)-acetamido]benzoic acids
iii)
(91) 5H-indolo[3,2-b]quinolin-11(10H)-ones (11-Quindolones)
iv)
Cl
(92) 11-chloro-10H-indolo[3,2-b]quinolines (11-Chloro-quindolines)
v)
(93) 5-methyl-11-chloro-10H-indolo[3,2-b]quinolines (11-chloro-cryptolepines)

Scheme 2.1 – Synthetic methodology for the synthesis of the common indolo[3,2-*b*]quinolines intermediates.
i) Bromoacetyl bromide, DMF:1,4-Dioxane (1:1), overnight, r.t.; ii) Aniline, DMF, 120 ºC, 18 to 96 h; iii) PPA; 130 ºC, 2 hours; iv) $POCl_3$, reflux, 2 hours; v) MeOTf, Toluene, r.t., 24 hours.

The synthetic pathway starts with reaction of the appropriate anthranilic acid (R^1 = H or Cl), with an excess of bromoacetyl bromide in DMF/1,4-dioxane (1:1). The nucleophilic substitution occurs after attack of the anthranilic acid amino group to the carbonyl of the bromoacetyl bromide with release of bromide, giving **89a** and **89b** in 96 % and 99 % yield, respectively.

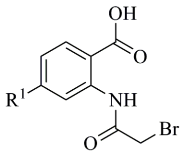

R^1		Section
H	(**89a**) 2-(2-bromoacetamido)benzoic acid	7.2.1.1
Cl	(**89b**) 2-(2-bromoacetamido)-4-chlorobenzoic acid	7.2.1.2

Figure 2.2 – Structure of the 2-(2-Bromoacetamido) benzoic acids (**89**)

The products of the reaction were characterized by ^{1}H-NMR, ^{13}C-NMR, bidimensional COSY, HMQC and HMBC nuclear magnetic resonance techniques, and melting point determination (Section 7.2.1). The results are in agreement with the chemical structure of the compounds and with the literature.(13, 199)

The attribution of the NMR signals (shown for **89a** in Figure 2.3) allows to verify the presence of the acetamide carbonyl carbons in ^{13}C-NMR with ^{13}C chemical shifts (δ_c) of 165.04 and 165.92 ppm for **89a** and **89b**, respectively and the presence of one singlet at ^{1}H chemical shift (δ_H) of 3.87 and 4.28 ppm (**89a** and **89b**, respectively), corresponding to 2 protons of the acetyl aliphatic CH_2, confirming the formation of the desired product.

The ^{1}H NMR coupling pattern showed two doublets (*d*) in aromatic region, H^3 and H^6 coupling with positions *ortho* H^4 and H^5, respectively, and also two double-doublets (*dd*) corresponding to H^4 and H^5 coupling with *ortho* positions (i.e. H^4 with H^3 and H^5), as shown in figure Figure 2.3. All the other signals in ^{1}H NMR appears as singlets (*s*).

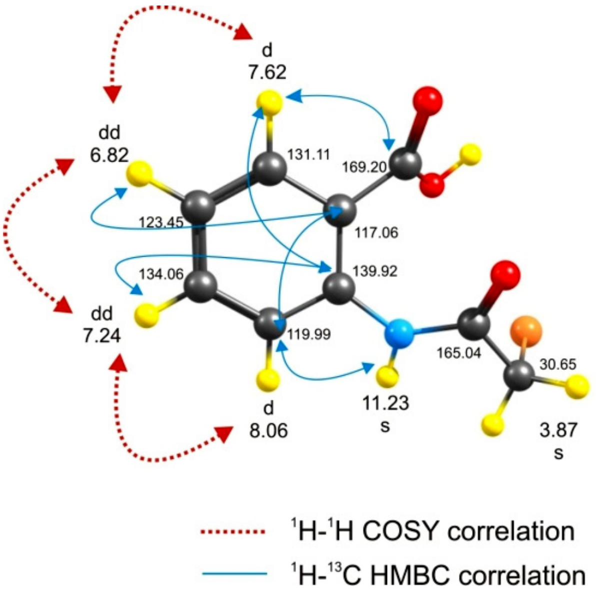

Figure 2.3 – Assignment of ^{1}H and ^{13}C NMR of **89a**.
Colour codes: H-yellow, C-grey, N-blue, O-red, Br-orange.
Wireframe representation

The synthesis of the 2-[2-(phenylamino)-acetamido]benzoic acid derivatives (**90**) was accomplished after reaction of **89a** or **89b**, with the appropriated aniline to give the required substitution pattern in the aromatic nucleus of the required indoloquinolines. The nucleophilic reaction of second order (SN_2) occurs in DMF at 90 ºC with the attack of the aniline amino group to the electrophilic carbon α (aliphatic CH_2) of the starting material with release of bromide.

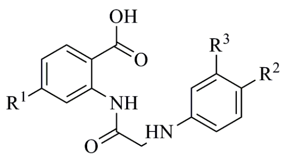

R^1	R^2	R^3		Section
H	H	H	(**90a**) 2-(2-(phenylamino)acetamido)benzoic acid	7.2.2.1
Cl	H	H	(**90b**) 4-chloro-2-[2-(phenylamino)acetamido]benzoic acid	7.2.2.2
Cl	H	Cl	(**90c**) 4-chloro-2-{2-[(3-chlorophenyl)amino]acetamido}benzoic acid	7.2.2.3
Cl	Cl	H	(**90d**) 4-chloro-2-{2-[(4-chlorophenyl)amino]acetamido}benzoic acid	7.2.2.4
Cl	CF_3	H	(**90e**) 4-chloro-2-(2-((4-(trifluoromethyl)phenyl)amino)acetamido)-benzoic acid	7.2.2.5
Cl	OCH_3	H	(**90f**) 4-chloro-2-(2-((4-methoxyphenyl)amino)acetamido)benzoic acid	7.2.2.6
Cl	CH_3	H	(**90g**) 4-chloro-2-(2-((4-methylphenyl)amino)acetamido)benzoic acid	7.2.2.7

Figure 2.4 – Structure of the 2-(2-(phenylamino)acetamido)benzoic acids **90**.

The products of the reaction were obtained in good yields (Table 2.1) and characterized by NMR techniques, and melting point determination. The attribution of the ^1H and ^{13}C NMR of **90a** is shown in Figure 2.5. The results are in concordance with the chemical structure of the compounds and in agreement with the literature.(13, 199) The analysis of the NMR spectra (Section 7.2.2) confirms the formation of the desired products through the presence of the aromatics protons, from the introduced aniline and the singlet corresponding to 2 protons from the acetamide group in **90** (Table 2.1). The ^1H NMR coupling pattern of **90a** was similar to that of **89a**, showing two *d* and two *dd* corresponding to the signals of H^3, H^6 and H^4, H^5 respectively, two *s* corresponding to the signals of the NH and CH_2 of the acetamide, in addition to one singlet corresponding to the NH of the introduced aniline, two *d* and one *dd*, corresponding to $H^{2'}$, $H^{4'}$ and $H^{3'}$ respectively, in case of **90a**, due to *ortho* coupling in the aromatic ring, as shown in Figure 2.5.

Table 2.1 – ^1H NMR chemical shifts (δ_H) of the aliphatic CH_2 in **90** and its reaction yields.

Compound	δ_H (ppm)	Yield (%)
(**90a**)	3.73	70
(**90b**)	3.86	96
(**90c**)	3.92	84
(**90d**)	3.88	70
(**90e**)	3.98	64
(**90f**)	3.79	72
(**90g**)	3.81	83

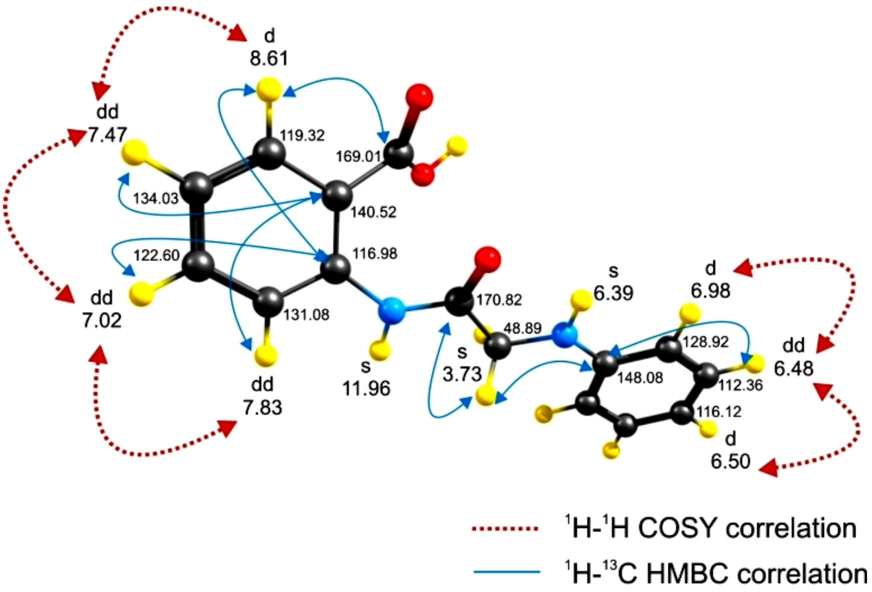

Figure 2.5 – Assignment of ^1H and ^{13}C NMR of **90a**.
Colour codes: H-yellow, C-grey, N-blue, O-red. Wireframe representation

The 5*H*-indolo[3,2-*b*]quinolin-11(10*H*)-ones (**91**, 11-quindolones), the third intermediate in the synthetic pathway for the synthesis of the cryptolepine derivatives **3** and the final common intermediate for the synthesis of the quindolone derivatives **5**, were achieved after cyclization of **90** in acid medium. The reaction is catalysed by polyphosphoric acid (PPA) and the mechanistic pathway is represented in Scheme 2.2. Polyphosphoric acid is recognized as a cyclising agent and it has been extensively used in a wide variety of reactions catalyzed by acids, due to its unique combination of properties: good solvent for organic compounds, a proton donor which improves condensation reactions and a cyclodehydrating agent which ensure slow intramolecular cyclization over a wide range of temperatures.(295)

The acid-catalyzed mechanism of cyclization stars with the formation of an enolate equilibrium between the α-carbon and the carbonyl from the acetyl group. The enolate attacks the carbonilic carbon of the acid functionality with formation of a 6-member ring and release of water.

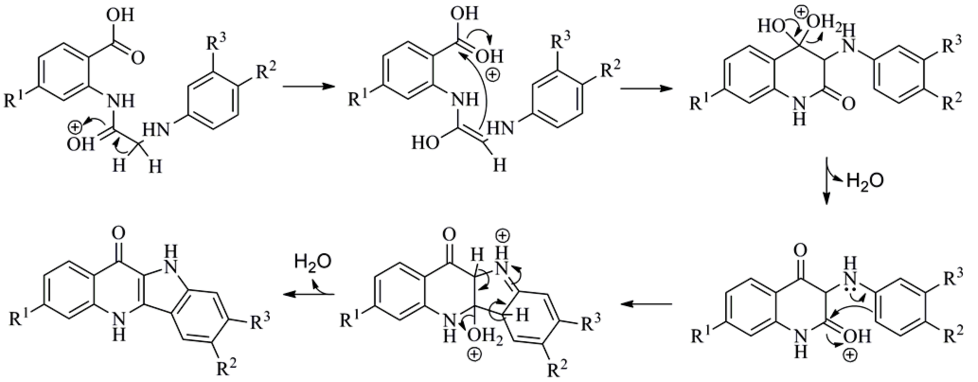

Scheme 2.2 – Acid-catalyzed cyclization of **90** to afford 5H-indolo[3,2-b]quinolin-11(10H)-ones (**91**, 11-quindolones).

The next step is the nucleophilic attack of the electrons in the aromatic ring of the aniline function to the carbonilic carbon in position 2 of the formed quinoline ring, closing the 5-member ring of the indole. After the ring closures the aromaticity is reestablished with release of a water molecule.

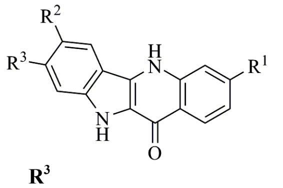

R^1	R^2	R^3		Section
H	H	H	(**4**) 5*H*-indolo[3,2-*b*]quinolin-11(10*H*)-one	7.2.3.1
Cl	H	H	(**91a**) 3-chloro-5*H*-indolo[3,2-*b*]quinolin-11(10*H*)-one	7.2.3.2
Cl	H	Cl	(**91b**) 3,8-dichloro-5*H*-indolo[3,2-*b*]quinolin-11(10*H*)-one	7.2.3.3
Cl	Cl	H	(**91c**) 3,7-dichloro-5*H*-indolo[3,2-*b*]quinolin-11(10*H*)-one	7.2.3.4
Cl	CF_3	H	(**91d**) 3-chloro-7-trifluoromethyl-5*H*-indolo[3,2-*b*]quinolin-11(10*H*)-one	7.2.3.5
Cl	OCH_3	H	(**91e**) 3-chloro-7-methoxy-5*H*-indolo[3,2-*b*]quinolin-11(10*H*)-one	7.2.3.6
Cl	CH_3	H	(**91f**) 3-chloro-7-methyl-5*H*-indolo[3,2-*b*]quinolin-11(10*H*)-one	7.2.3.7

Figure 2.6 – Structure of the 5*H*-indolo[3,2-*b*]quinolin-11(10*H*)-ones **91**.

The products of the reaction (**4** and **91**) were obtained with yields ranging from 15 to 67 % (Table 2.2) and were characterized with NMR techniques, infrared spectra and melting point determination (Section 7.2.3). For instance, the assignment of the ^{1}H and ^{13}C NMR spectra of **4** is illustrated in Figure 2.7.

Table 2.2 – ^{13}C NMR chemical shift (δ_C) of carbonyl carbon in **4** and **91** and its reaction yields.

Compound	δc (ppm)	Yield (%)
(**4**)	167.77	67
(**91a**)	167.30	36
(**91b**)	167.49	15
(**91c**)	167.54	40
(**91d**)	168.11	33
(**91e**)	167.35	27
(**91f**)	167.23	52

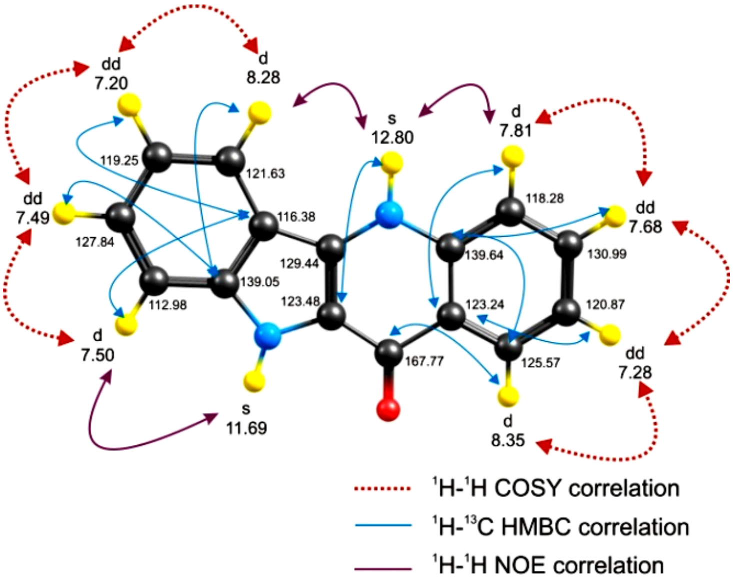

Figure 2.7 – Assignment of ^{1}H and ^{13}C NMR of **4**.
Colour codes: H-yellow, C-grey, N-blue, O-red. Wireframe representation

The ^{1}H NMR coupling pattern showed the presence of four *dd* corresponding to the proton H^{2}, H^{3}, H^{7} and H^{8}, and four *d* corresponding to protons H^{1}, H^{4}, H^{6} and H^{9} due to the *ortho* couplings (as shown in Figure 2.7). The NMR analysis reveal also the presence in the ^{13}C NMR spectra of the carbonilic carbon (Table 2.2) in addition to a infrared band at 1625 cm^{-1}, belonging to the stretching of C=O, corroborating the formation of the 11-quindolones **91a**. The NMR data for all compounds are in concordance with the chemical structure of the compounds and with those described elsewhere.$^{(13, 199)}$

The introduction of chloride in the position 11 of the quindoline nucleus gave the 11-chloroquindolines (**92**). The reaction occurs between the intermediates **4** or **91** and phosphorus oxychloride in a Vilsmeier halogenation reaction, with formation of the iminium ion as intermediate (Scheme 2.3). The mechanistic pathway begins with the nucleophilic attack of the electrons in the carbonilic oxygen to the phosphorous atom of the phosphorous oxychloride reagent, with release of chloride and formation of the iminium ion, which after the attack of the chloride to position C11, release phosphorodichloridic acid with formation of the 11-cloroquindolines (**92**).

The products of the reaction were obtained with yield ranging from 49 to 78 % and characterized with NMR techniques, infrared spectra and melting point determination (Section 7.2.4). The NMR data are in good agreement with the chemical structure of the compounds and with those described elsewhere. $^{(13, 199)}$ The NMR analysis reveals the absence in the ^{13}C-NMR spectra of the carbonilic carbon from the previous intermediate, corroborating the introduction of the chloride in position C11, giving **92**.

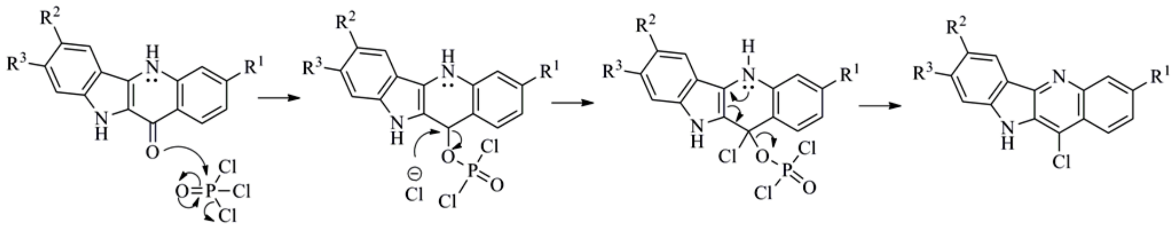

Scheme 2.3 - Halogenation mechanism of **91** to give the 11-cloroquindolines (**92**) in a Vilsmeier reaction.

Figure 2.9 shows the assignment of the ^{1}H and ^{13}C NMR spectra of **92a**. The analysis of the spectra reveals a downfield shift in the δ_C of the carbons 4a and 5a signals, when compared with the parent compound **4**. Carbons 4a and 5a in **4** showed and δ_C of 139.64 and 129.44 ppm, respectively, which in **92a** showed a δ_C of 144.28 and 146.52 ppm.

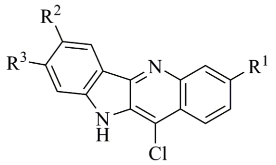

R^1	R^2	R^3		Section
H	H	H	**(92a)** 11-chloro-10*H*-indolo[3,2-*b*]quinoline	7.2.4.1
Cl	H	H	**(92b)** 3,11-dichloro-10*H*-indolo[3,2-*b*]quinoline	7.2.4.2
Cl	H	Cl	**(92c)** 3,8,11-trichloro-10*H*-indolo[3,2-*b*]quinoline	7.2.4.3
Cl	Cl	H	**(92d)** 3,7,11-trichloro-10*H*-indolo[3,2-*b*]quinoline	7.2.4.4
Cl	CF_3	H	**(92e)** 3,11-dichloro-7-trifluoromethyl-10*H*-indolo[3,2-*b*]quinoline	7.2.4.5
Cl	OCH_3	H	**(92f)** 3,11-dichloro-7-methoxy-10*H*-indolo[3,2-*b*]quinoline	7.2.4.6
Cl	CH_3	H	**(92g)** 3,11-dichloro-7-methyl-10*H*-indolo[3,2-*b*]quinoline	7.2.4.7

Figure 2.8 – Structure of the 11-chloro-10*H*-indolo[3,2-*b*]quinolines **92**.

Also, the introduction of the chlorine in position C11 originated changes in the δ_H of the ^{1}H NMR spectra. The most significant changes occur in H^4, which in **4** showed a δ_H of 7.81 ppm, and due to an upfield shift verified in **92a** showed δ_H of 7.29 ppm (Figure 2.9). The analysis of the infrared spectroscopy spectra also reveals the disappearance of the band in the near-infrared region (≈1670 cm^{-1}) corresponding to the stretching of carbonyl, reinforcing the successful introduction of the chlorine in position C11.

The key intermediate for the synthesis of cryptolepine derivatives was obtained from **92a-c** after reaction with methyl trifluoromethanesulfonate (methyl triflate) in anhydrous toluene. The reaction gave 5-methyl-11-chloro-10*H*-indolo[3,2-*b*]quinolin-5-ium trifluoromethanosulfonate (**93a-c**) which in order to avoid the mixture of triflate and chloride anions (resulting from the reaction of introduction of alkyldiamine) in the final product (**3**), was treated with a basic solution of Na_2CO_3 5% to forming its basic specie and then precipitated with HCl to achieve 5-methyl-11-chloro-10*H*-indolo[3,2-*b*]quinolin-5-ium chloride (**93a-c**) as an orange solid, yielding 46 to 90 %.

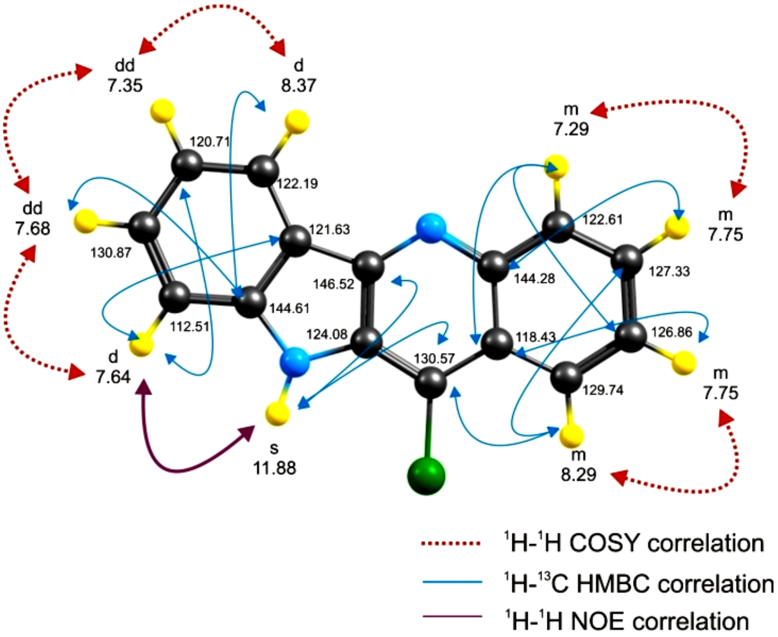
dd
7.35
d
8.37
m
7.29
dd
7.68
m
7.75
d
7.64
s
11.88
m
8.29
m
7.75
120.71
122.19
121.63
130.87
146.52
144.61
112.51
124.08
130.57
144.28
122.61
127.33
118.43
126.86
129.74
^{1}H-^{1}H COSY correlation
^{1}H-^{13}C HMBC correlation
^{1}H-^{1}H NOE correlation

Figure 2.9 – Assignment of ^{1}H and ^{13}C NMR of **92a.**
Colour codes: H-yellow, C-grey, N-blue, Cl-green. Wireframe representation.

The characterization of **93a-c** was done through NMR techniques and melting point determinations (Section 7.2.5). The assignment of the ^{1}H and ^{13}C NMR chemical shifts of **93a** is shown in Figure 2.11. The data for compounds **93a-c** are in agreement with the chemical structure of the compound and with the data already described in the literature.(13)

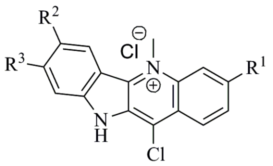
R2
R3
Cl
N
R1
N
H
Cl

R¹	**R²**	**R³**		**Section**
H	H	H	(**93a**) 5-methyl-11-chloro-10*H*-indolo[3,2-*b*]quinolin-5-ium chloride	7.2.5.1
Cl	H	H	(**93b**) 3,11-dichloro-5-methyl-10*H*-indolo[3,2-*b*]quinolin-5-ium chloride	7.2.5.2
Cl	H	Cl	(**93c**) 3,8,11-trichloro-5-methyl-10*H*-indolo[3,2-*b*]quinolin-5-ium chloride	7.2.5.3
Cl	Cl	H	(**93d**) 3,7,11-trichloro-5-methyl-10*H*-indolo[3,2-*b*]quinolin-5-ium chloride	7.2.5.4
Cl	CF_3	H	(**93e**) 3,11-dichloro-5-methyl-7-trfifluoromethyl-10*H*-indolo[3,2-*b*] quinolin-5-ium chloride	7.2.5.4
Cl	OCH_3	H	(**93f**) 3,11-dichloro-5-methyl-7-methoxy-10*H*-indolo[3,2-*b*] quinolin-5-ium chloride	7.2.5.4
Cl	CH_3	H	(**93g**) 3,11-dichloro-5-methyl-7-methyl-10*H*-indolo[3,2-*b*]quinolin-5-ium chloride	7.2.5.4

Figure 2.10 – Stucture of the 5-methyl-11-chloro-10*H*-indolo[3,2-*b*]quinolin-5-ium chlorides **93**

NMR spectra of compound **93a** revealed the introduction of the N^5-CH_3, since and additional ^{1}H chemical shift (δ_H) at 5.04 ppm, integrating to three protons, and a ^{13}C chemical shift (δ_C) of 40.97 ppm. This ^{1}H signal showed Nuclear Overhauser Effect (NOE) with the proton H^4 (δ_H = 8.88 ppm) of the aromatic nucleus (Figure 2.11). The introduction of the methyl group in N^5 leads to a downfield in the protons in the aromatic nucleus, especially in protons H^1 to H^4 and in the indolic proton (11.88 in **92a** to 13.39). Also, it was verified an upfield on the ^{13}C chemical shifts of carbons C4a and C5a (144.28 ppm in **92a** to 136.15 ppm and 146.52 ppm in **92a** to 139.03 ppm, respectively).

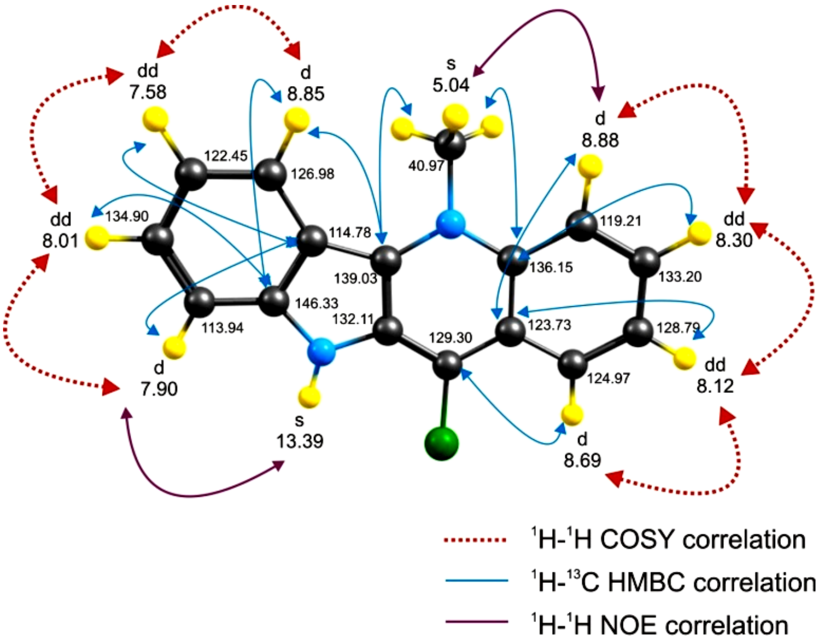

Figure 2.11 – Assignment of ^{1}H and ^{13}C NMR of **93a**.
Colour codes: H-yellow, C-grey, N-blue, Cl-green. Wireframe representation.

The synthesis of compounds **93d-g** were also tried with reaction of **92d-g** with methyl triflate as described above for **93a-c** (Section 7.2.5.1). However, the NMR characterization of the reaction products revealed that the desired product was not formed or very small amounts (5-10% of product, from inspection of ^{1}H NMR). Since the product of the reaction is a salt very slightly soluble in most organic solvents, its purification processes, like chromatography, are not very efficient, being the recristalization form chloroform or ethyl acetate/methanol mixtures with diethyl ether the most successful one. However, due to the limited amount of reaction product, it was not possible to recrystallized **93d-g** from the mixtures with **92d-g**.

In order to achieve the cryptolepine derivatives intermediates **93d-g** we tried different synthetic methodologies (Section 7.2.5.4), aiming to increase the amount of product. Changes of solvent from toluene to anhydrous dichloromethane, acetone or dimethylformamide, inert atmosphere (N_2), heating at given temperature or until reflux, as well as, extending the reaction time until 96 hours and increasing the equivalents of alkylating agent were attempted, however without success. Changing the alkylating agent was also tried. Reaction of **92d-g** with trimethyloxonium tetrafluoroborate (Meerwein's reagent),(296-298) which is a strong alkylating agent, in dimethylformamide at 80ºC for 120 hours revealed no improvement in the product formation. As such, it was not possible to synthesize the compounds **93d-g**.

2.2.2 Synthesis of Cryptolepine (**1**)

The synthesis of cryptolepine from the intermediate (**92**) was achieved through the synthetic methodology described in Scheme 2.4. The 11-chloroquindoline (**92**) undergoes through an hydrogenation reaction to give quindoline (**25**), which after alkylation gives cryptolepine.

The hydrogenation of **92a** was achived using the methodology adapted by Ablordeppey and co-workers(237) (method 1, Section 7.2.6.1.1) , in which the reaction occurs in a high pressure vassel, containing H_2 and catalazed by palladium. In addition, a methodology developed by Mandal and McMurray(299) with *in situ* generation of H_2 (method 2, Section 7.2.6.1.2) and palladium catalyzed, was also used.

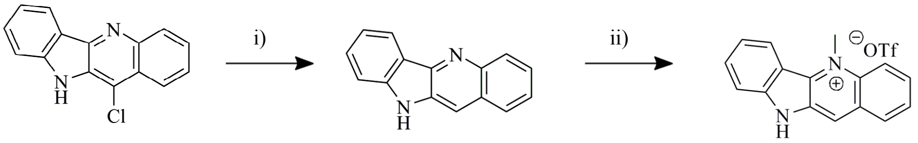
N
H
Cl
i)
N
H
ii)
N
OTf
N
H

92

(**25**) 10*H*-indolo[3,2-*b*]
quinoline (Quindoline)

(**1**) 5-methyl-10*H*-indolo
[3,2-*b*]quinolin-5-ium
trifluoromethanesulfonate
(Cryptolepine)

Scheme 2.4 – Synthetic methodology for the synthesis of cryptolepine from **92**.
i) H_2 Pd-C 10% NaOAc, AcOH, 60 psi, 2h or EtSiH, 10% Pd-C, MeOH, 20 min.; ii) methyl triflate, toluene, r.t., 24h.

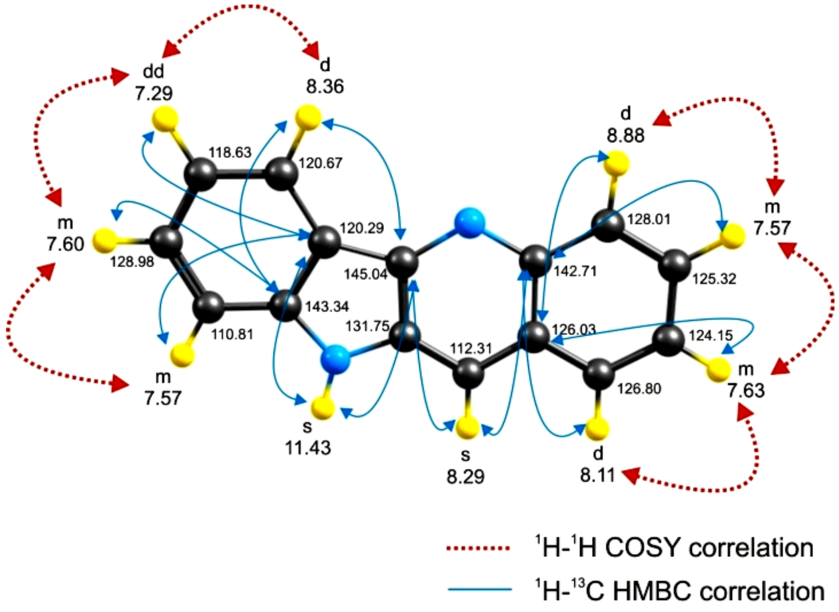
dd
7.29
d
8.36
d
8.88
m
7.60
m
7.57
m
7.57
m
7.63
s
11.43
s
8.29
d
8.11
118.63
120.67
120.29
128.98
145.04
143.34
110.81
131.75
112.31
128.01
142.71
125.32
126.03
124.15
126.80
^{1}H-^{1}H COSY correlation
^{1}H-^{13}C HMBC correlation

Figure 2.12 – Assignment of ^{1}H and ^{13}C NMR of **25**.
Colour codes: H-yellow, C-grey, N-blue. Wireframe representation

Hydrogenation reaction in absence of metal catalyst only takes place at very high temperatures. The use of palladium catalist allowed us to react hydrogen and the substrate at lower temperatures with good yields. Palladium binds both H_2 and the substrate, transfering the hydrongen catalyticaly to the substrate.(300-301) The quindoline **25** was synthsized with good yields with both methodologies (85 % and 78 % for method 1 and 2, respectivily).

However, reaction with tetraethylsilane as an hydrogen donor (Mandal and McMurray, methd 2), revealed to be more advantageus due to the simplicity of the experimental procedure. The reaction was carried out at room temperature, atmosferic pressure and in a short period of time (20 minutes), using excess of tetraethylsilane and 15 % Pd-C (by weight). The products of both reactions were caracterized by NMR spectroscopy and melting point (Section 7.2.6) being the results in good agreement with the literature.(302) The assignment of the NMR spectra reveals the introduction of the hydrongen in position 11 of the indoloquinoline nucleus (Figure 2.12). The proton appears as a singlet with a δ_H of 8.29 ppm and the ^{13}C chemical shift of C11 suffers and upfield shift from 130.57 ppm in **92a** to 112.31 ppm in **25**. In addition, carbons 10a and 11a suffer and downfiled shift when compared with the parent compound **92a** (124.08 and 118,42 ppm in **92a** to 131.75 and 126.03 ppm in **25**, respectively).

Cryptolepine (**1**) was achieved after reaction of the intermediate **25** with methyl trifluoromethanosulfonate. Like already described for compounds **93**, it is a nucleophilic reaction between N^5 and the methyl group of the alkylating agent.

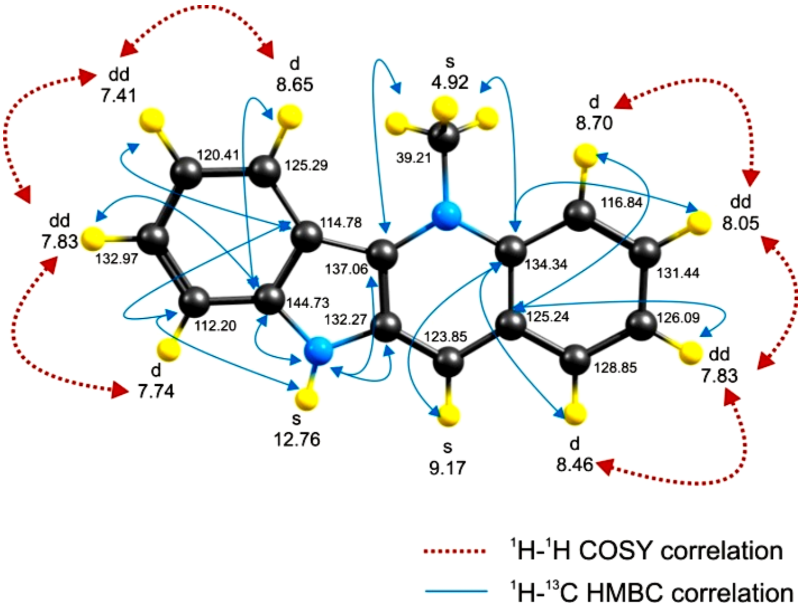

Figure 2.13 – Assignment of ^{1}H and ^{13}C NMR of **1**.
Colour codes: H-yellow, C-grey, N-blue. Wireframe representation

The product of the reaction was characterized by NMR spectroscopy, melting point and elemental analysis, being the results in agreement with the literature (Section 7.2.7).(303) The assignment of the NMR spectra reveals the presence of a singlet with a chemical shift of 4.92 ppm, corresponding to three protons and a ^{13}C signal with a δ_C of 39.21 ppm, corroborating the introduction of the methyl in N^5 (Figure 2.13). As demonstrated with compounds **92**, a downfield shift on the δ_H of the aromatic protons and, as well as in the proton of the indolic nitrogen (N^{10}) was verified. Also, an upfield on the ^{13}C chemical shifts of carbons 4a and 5a (145.04 in **92a** to 137.06 and 142.71 in **92a** to 134.34, respectively) was verified.

2.2.3 Synthesis of Cryptolepine Derivatives (3)

The cryptolepine derivatives with alkyldiamine side chains (**3a-n,r-y**), in position C11 of the quindoline nucleus were synthesized after reaction of the key intermediate **93**, with the required alkyldiamine, through a nucleophilic substitution reaction with release of chloride (Scheme 2.5). All alkyldiamine were used as received from the commercial supplier, except for those which the syntheses are described in Section 2.2.5. Thus, the cryptolepine derivatives **3d,j,l** and **t** were obtained after reaction of the key intermediate **93** with the synthesized alkyldiamine **97**, **100**, **103**, and **105**, respectively.

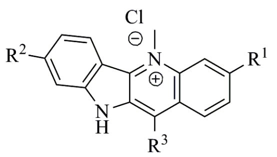

R^1	R^2	R^3		Section
H	H	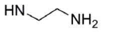	**(3a)** 5-methyl-11-[(2-aminoethyl)amino]-10*H*-indolo[3,2-*b*] quinolin-5-ium chloride	7.2.8.1
H	H	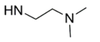	**(3b)** 5-methyl-11-{[2-(dimethylamino)ethyl]amino}10*H*-indolo[3,2-*b*] quinolin-5-ium chloride	7.2.8.2
H	H	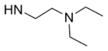	**(3c)** 5-methyl-11-{[2-(diethylamino)ethyl]amino}-10*H*-indolo[3,2-*b*] quinolin-5-ium chloride	7.2.8.3
H	H	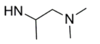	**(3d)** 5-methyl-11-[1-(diethylamino)propan-2-yl)amino]-10*H*-indolo[3,2-*b*] quinolin-5-ium chloride	7.2.8.4
H	H	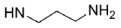	**(3e)** 5-methyl-11-[(3-aminopropyl)amino]-10*H*-indolo[3,2-*b*] quinolin-5-ium chloride	7.2.8.5
H	H	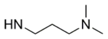	**(3f)** 5-methyl-11-{[3-(dimethylamino)propyl]amino}-10*H*-indolo[3,2-*b*] quinolin-5-ium chloride	7.2.8.6
H	H	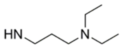	**(3g)** 5-methyl-11-{[3-(diethylamino)propyl]amino}-10*H*-indolo[3,2-*b*] quinolin-5-ium chloride	7.2.8.7
H	H	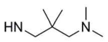	**(3h)** 5-methyl-11-{[3-(dimethylamino)-2,2-dimethylpropyl] amino}-10*H*-indolo[3,2-*b*]quinolin-5-ium chloride	7.2.8.8
H	H	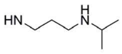	**(3i)** 5-methyl-11-{[3-(isopropylamino)propyl]amino}-10*H*-indolo[3,2-*b*] quinolin-5-ium chloride	7.2.8.9
H	H	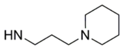	**(3j)** 5-methyl-11-{[3-(piperidin-1-yl)propyl]amino}-10*H*-indolo[3,2-*b*] quinolin-5-ium chloride	7.2.8.10
H	H	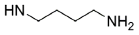	**(3k)** 5-methyl-11-[(4-aminobutyl)amino]-10*H*-indolo[3,2-*b*] quinolin-5-ium chloride	7.2.8.11
H	H	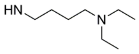	**(3l)** 5-methyl-11-{[4-(diethylamino)butyl]amino}-10*H*-indolo[3,2-*b*] quinolin-5-ium chloride	7.2.8.12
H	H	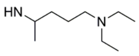	**(3m)** 5-methyl-11-{[5-(diethylamino)pentan-2-yl]amino}-10*H*-indolo[3,2-*b*] quinolin-5-ium chloride	7.2.8.13
H	H	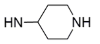	**(3n)** 5-methyl-11-(piperidin-4-ylamino)-10*H*-indolo[3,2-*b*] quinolin-5-ium chloride	7.2.8.14
H	H	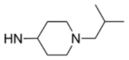	**(3o)** 5-methyl-11-[(1-isobutylpiperidin-4-yl)amino]-10*H*-indolo[3,2-*b*] quinolin-5-ium chloride	7.2.8.15
H	H	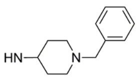	**(3p)** 5-methyl-11-[(1-benzylpiperidin-4-yl)amino]-10*H*-indolo[3,2-*b*] quinolin-5-ium chloride	7.2.8.16
H	H	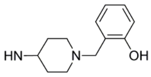	**(3q)** 5-methyl-11-{[1-(2-hydroxybenzyl)piperidin-4-yl]amino}-10*H*-indolo[3,2-*b*]quinolin-5-ium chloride	7.2.8.17
H	H	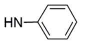	**(3r)** 5-methyl-11-(phenylamino)-10*H*-indolo[3,2-*b*]quinolin-5-ium chloride	7.2.8.18
H	H	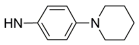	**(3s)** 5-methyl-11-{[4-(piperidin-1-yl)phenyl]amino}-10*H*-indolo[3,2-*b*] quinolin-5-ium chloride	7.2.8.19
H	H	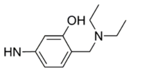	**(3t)** 5-methyl-11-{{4-[(diethylamino)methyl]-3-hydroxy-phenyl}amino}-10*H*-indolo[3,2-*b*]quinolin-5-ium chloride	7.2.8.20
H	H	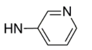	**(3u)** 5-methyl-11-(pyridin-3-ylamino)-10*H*-indolo[3,2-*b*] quinolin-5-ium chloride	7.2.8.21
Cl	H	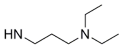	**(3v)** 3-chloro-5-methyl-11-{[3-(diethylamino)propyl]amino}-10*H*-indolo[3,2-*b*] quinolin-5-ium chloride	7.2.8.22
Cl	H	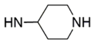	**(3w)** 3-chloro-5-methyl-11-(piperidin-4-ylamino)-10*H*-indolo[3,2-*b*] quinolin-5-ium chloride	7.2.8.23
Cl	Cl	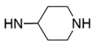	**(3x)** 3,8-dichloro-5-methyl-11-(piperidin-4-ylamino)-10*H*-indolo[3,2-*b*] quinolin-5-ium chloride	7.2.8.24
H	H	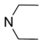	**(3y)** 5-methyl-11-(diethylamino)-10*H*-indolo[3,2-*b*]quinolin-5-ium chloride	7.2.8.25

Figure 2.14 – Structure of the cryptolepine derivatives **3**.

The reaction was performed in ethyl acetate, where **93** proved to be quite insoluble. However, the addition of the amine deprotonates the indolic nitrogen (N^{10}) and the indoloquinolines become soluble. With the progress of the reaction, the concentration of H^+ increase in the solution, the indole nitrogen protonates and the product of the reaction precipitates in the reaction medium. The precipitated cryptolepine derivatives **3a-n, r-y** were then purified by recristalization techniques, yielding from 29 to 82 %.

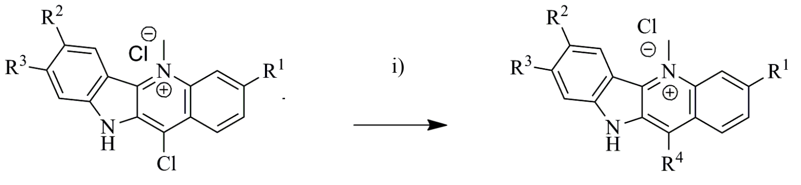

93 **3**

Scheme 2.5 – Synthetic methodology for synthesis of the cryptolepine derivatives **3**.
i) Alkyl- cycloalkyl- or aryldiamine, AcOEt, reflux, 24h.

The cryptolepine derivatives **3o-q** were synthesized after reaction of the derivative **3n** with isobutyraldehyde, salicyladehyde and benzaldehyde, respectively (Scheme 2.6). The reaction undergoes through a reductive amination, in which occurs the nucleophilic attack of the secondary amine of **3n** to the carbonyl group of the aldehyde with formation of an imine intermediate and release of water. In a second step the imine is reduced to give the tertiary amine and the new cryptolepine derivative (Scheme 2.7). These reactions occur in dry MeOH, yielding 59 %, 30 % and 66 %, respectively.

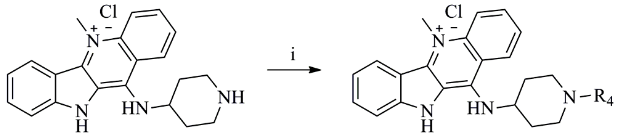

3n

3o: R4 = isobutyl
p: R4 = benzyl
q: R4 = 2-hydroxybenzyl

Scheme 2.6 – Synthetic methodology for the synthesis of the cryptolepine derivatives **3o-q.**
i) Aldehyde, anhydrous Na_2SO_4, $NaBH_3CN$, dry MeOH, ***r.t.***, 24 h.

All the cryptolepine derivatives were characterized by NMR techniques, elemental analysis and melting point determinations (Section 7.2.8 and Appendix A). The results are in good agreement with the chemical structure of the compounds. For instance, the attribution of ^1H and ^{13}C NMR chemical shifts for **3n** are shown in Figure 2.15. The ^1H NMR spectra reveal two distinct areas of chemical shifts: the first one, between 2.05 ppm and 4.80 ppm corresponding to the aliphatic protons of the piperidine side chain (Figure 2.15) and including the methyl group at N^5 and a second area between 7.44 ppm and 8.66 ppm, corresponding to the eight aromatic and showing coupling constants ($^3J_{HH}$) between 7.4 and 9.0 Hz, typical *ortho* coupling constants for aromatic protons.

The introduction of the alkyldiamine side chain in position C11 of the cryptolepine nucleus of **3n** was confirmed with NOE difference experiments in which the protons of the introduced side chain interact with the doublet (δ_H 8.29 ppm) of proton C1 and with the singlet (δ_H 12.16 ppm) attributed to the indolic proton, as shown in Figure 2.15.

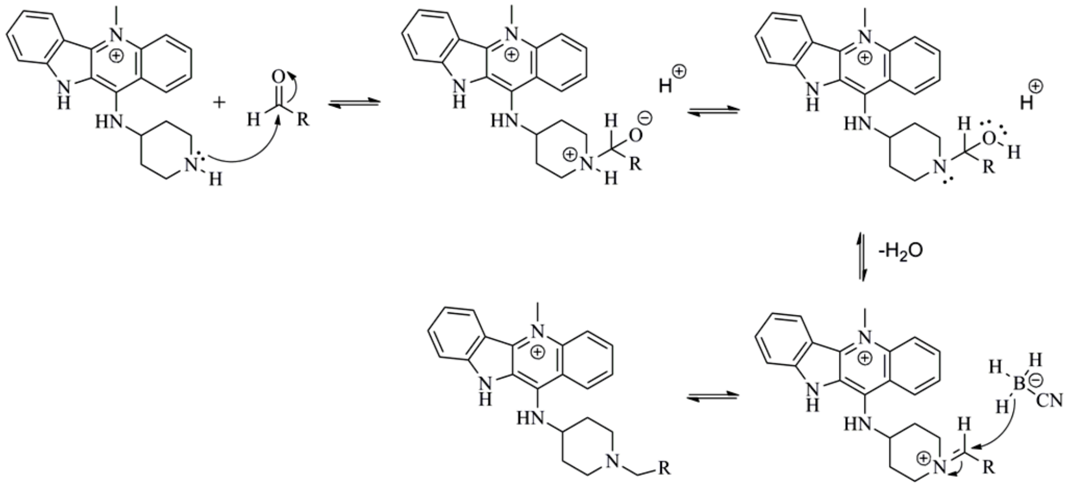
-H2O
HN
H
R
O
N
H3B CN

Scheme 2.7 – Reductive amination mechanism of **3n** with aldehyde to afford **3o**,**p** and **q**.

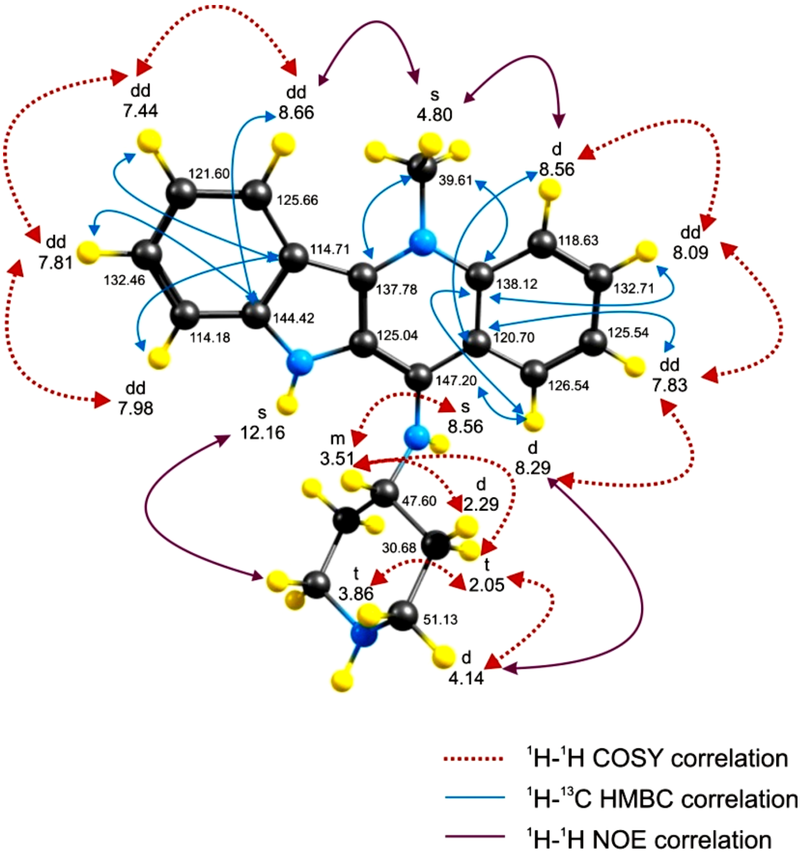
dd 7.44
dd 8.66
s 4.80
d 8.56
dd 8.09
dd 7.81
dd 7.98
dd 7.83
s 12.16
s 8.56
m 3.51
d 8.29
d 2.29
t 3.86
t 2.05
d 4.14
121.60
125.66
39.61
114.71
118.63
132.46
137.78
138.12
132.71
144.42
114.18
125.04
120.70
125.54
147.20
126.54
47.60
30.68
51.13
¹H-¹H COSY correlation
¹H-¹³C HMBC correlation
¹H-¹H NOE correlation

Figure 2.15 – Assignment of ^{1}H and ^{13}C NMR of **3n**.
Colour codes: H-yellow, C-grey, N-blue. Wireframe representation

The side chain induced a shielding effect on the chemical shift of N^{5} -CH_3 ($\Delta\delta_H$ = 0.24 ppm) when compared with **93a**. Also the ^{13}C chemical shifts of C10a and C11a showed and upfield shift, when compared to **93a**, of 7 and 2 ppm, respectively, whereas the ^{13}C NMR chemical shift of C11 showed a downfield shift of almost 18 ppm, when compared with the parent compound **93a**, and of approximately 24 ppm when compared to **1**. Since the CH_2 pairs on the piperidine side chain of **3n** are diastereotopic, easily discerned as one of the hydrogens in the pair will be *cis* to the NH group attached to C11, while the other will be *trans* to it, these protons showed different chemical shifts, in consequence of its different chemical environments. In addition, the equatorial protons in a rigid six-member ring are deshielded due to anisotropic effects of the σ electrons in the C-C bond (deshielding cone have the same axis than the C-C bond), like verified in circulating aromatic π electrons, although with lower intensity.(304) The assignment of the chemical shifts on the aliphatic region of the ^{1}H NMR spectra (Figure 2.15), reveals a triplet integrating for two protons and attributed to $H^{3'}{}_{(ax)}$ and $H^{5'}{}_{(ax)}$, with a δ_H value of 2.05 ppm, a geminal coupling constant ($^2J_{HH}$) of 11.5 Hz and a vicinal coupling constant ($^3J_{HH}$) of 11.0 Hz. Protons $H^{3'}{}_{(eq)}$ and $H^{5'}{}_{(eq)}$ showed a δ_H value of 2.29 ppm and a coupling constant $^2J_{HH}$ of 11.5 Hz. At δ_H 3.51 ppm , appears a broad multiplet, almost superimposed with the water singlet, which correspond to the proton $H^{4'}$ of 4-aminopiperidine ring. Protons $H^{2'}{}_{(ax)}$ and $H^{6'}{}_{(ax)}$ of piperidine appears at 3.86 ppm with coupling constant values of 12.6 and 11.0 Hz for $^2J_{HH}$ and $^3J_{HH,}$ respectively. Lastly, at lower field (4.14 ppm) appears protons $H^{2'}{}_{(eq)}$ and $H^{6'}{}_{(eq)}$ of the piperidine ring, showing a geminal coupling constant ($^2J_{HH}$) value of 12.6 Hz. In the 2D NMR correlation spectroscopy (COSY) it is possible to verify the strong correlation between protons $H^{3'}{}_{(ax)}$ and $H^{5'}{}_{(ax)}$ with $H^{2'}{}_{(ax)}$ and $H^{6}{}_{(ax)}$, as expected for *ortho* axial protons and between $H^{3'}{}_{(ax)}$ and $H^{5'}{}_{(ax)}$ with proton $H^{4'}$. This results, seems to point out that proton $H^{4'}$ is in axial position and the bond with the NH-C11 is in the equatorial position of C4 of the piperidine ring.

The attribution of the NMR spectra of the cryptolepine derivatives **3** showed similar results to those described for compound **3n**. Also **3h** showed NOE correlation between the proton in the carbon adjacent to C11-NH in the side chain (δ_H = 4.21 ppm) with the proton in the indole nitrogen (δ_H = 10.75 ppm). The introduction of the side chain in C11 of cryptolepine nucleus, generally induced a shielding effect on the chemical shift of N^5-CH_3, ranging between 0.1 to 0.45 ppm when compared with **93**. Also the ^{13}C chemical shifts of C10a and C11a showed an upfield shift in the order of 10 ppm and for N^5-CH_3 of 3 ppm when compared to **1** and **93**, whereas the chemical shift of C11 showed a deshielding effect of 10 to 15 ppm when compared with the parent compounds **1** and **93**.

In addition to the NMR spectroscopy, all the cryptolepine derivatives **3** were also characterized through elemental analysis (C,N,H) and melting point determination to evaluate their degree of purity. For all the compounds the experimental elemental analysis results showed shifts of at least or low than 0.4 %, showing ≥ 95 % purity, and the melting point determination showed for all the compounds a melting range (ΔT) lower than 3 ºC, revealing the high degree of purity of the synthesized compounds.

The synthetic methodology employed for the synthesis of the cryptolepine derivatives **3**, with the 11-chloro-5-methyl-*10H*-indolo[3,2-*b*]quinolines **93** as common intermediate, proved to be efficient, giving the desired compounds in good yields and with high degree of purity.

2.2.4 Synthesis of Quindolone Derivatives (**5**)

The quindolone derivatives with alkylamine side chains in positions N^5 and N^{10} (**5**, Figure 2.17) were synthesized after reaction of **91** with 2-chloro-*N,N*-diethylethanamine in presence of base, through a nucleophilic substitution reaction with release of chlorine (Scheme 2.8). The alkylamine was used as received from the commercial supplier. The reaction was attempted with several different bases, like K_2CO_3, NaH, triethylamine (TEA) and *N,N*-diisoproprylethylamine (DIPEA) in dry acetone or tetrahrydrofuran (THF). However, the best results were achieved using as base K_2CO_3 in dry acetone.

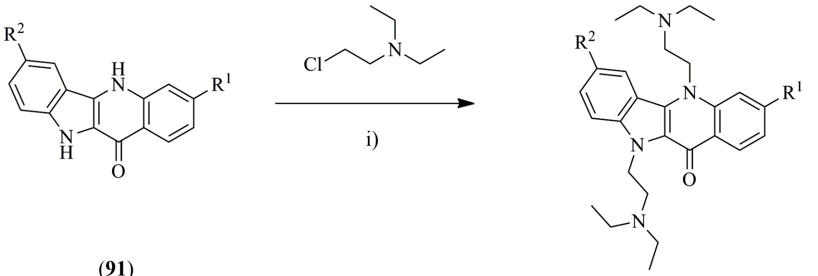

(**91**)
4 if R^1 and R^2 = H

(**5**) 5,10-bis(2-(diethylamino)ethyl)-5H-indolo[3,2-b]quinolin-11(10H)-ones

Scheme 2.8 – Synthetic methodology for the synthesis of the quindolone derivatives **5**.
i) K_2CO_3, NaI, dry acetone, overnight, reflux.

The presence of base in the reaction medium, deprotonates the nitrogens and give rise to the tautomeric resonance in the aromatic nucleus of the quindolone, as shown in Figure 2.16. This tautomeric resonance activate the carbonylic oxygen, giving nucleophilic oxygen species, which can attack the 2-chloro-*N,N*-diethylethanamine and lead to the formation of O-alkylated products in the reaction. In fact, it was possible to verify the formation of three different products with the described synthetic methodology (Scheme 2.9). The three products of the reaction were characterized through NMR spectroscopy, elemental analysis and melting point determination. The assignment of the NMR spectra of the three reaction products revealed that the major product was the (*N,O*) dialkylated species (**94**), yielding between 34 and 55 % (depending on the starting quindolone) as shown in Table 2.3.

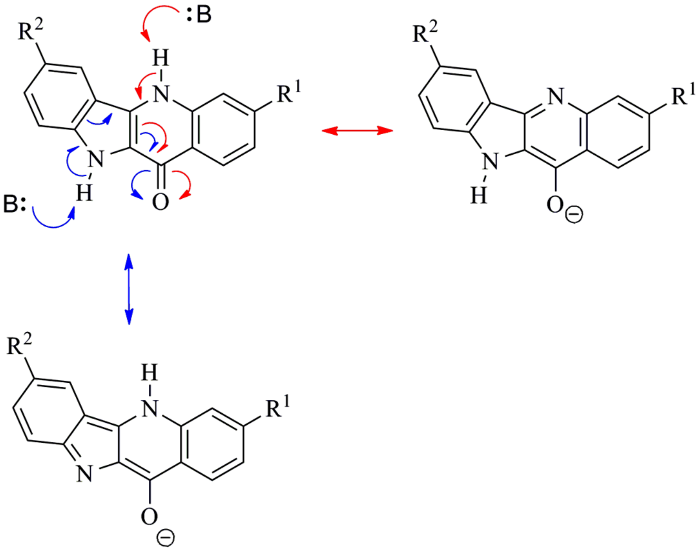

Figure 2.16 – Quindolone tautomeric resonance after deprotonation of $\mathbf{N^5}$ (red) and $\mathbf{N^{10}}$ (blue).

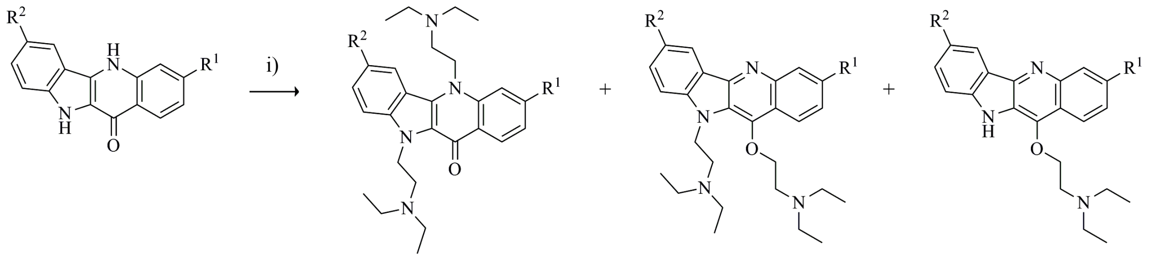

(**91**)
4 if R^1 and R^2 = H

(**5**) 5,10-bis(2-(diethylamino)ethyl)-5*H*-indolo[3,2-*b*]quinolin-11(10*H*)-ones

(**94**) 2-(11-(2-(diethylamino)ethoxy)-10*H*-indolo[3,2-*b*]quinolin-10-yl)-*N,N*-diethylethanamines

(**95**) 2-((10*H*-indolo[3,2-b]quinolin-11-yl)oxy)-*N,N*-diethylethanamines

Scheme 2.9 – Products of the synthetic methodology used for the synthesis of the quindolone derivatives **5**. i) K_2CO_3, 2-chloro-*N,N*-diethylethanamine, NaI, dry acetone, overnight, reflux.

The ^{1}H NMR spectra of the major product of the reaction (**94a**) displayed the signals corresponding to the introduction of two alkylamine side chains in the quindolone nucleus. The spectra showed two sets of two triplets at δ_H 4.73 and 2.79 ppm and δ_H 4.32 and 3.10 ppm, corresponding to 2 protons each one, and three bond correlation between them (^{1}H-^{1}H Correlation Spectroscopy, COSY).

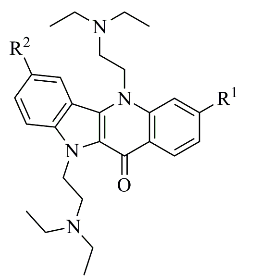

R^1	R^2		Section
H	H	(**5a**) 5,10-bis(2-(diethylamino)ethyl)-5H-indolo[3,2-b]quinolin-11(10H)-one	7.2.9.1
Cl	H	(**5b**) 3-chloro-5,10-bis(2-(diethylamino)ethyl)-5H-indolo[3,2-b]quinolin-11(10H)-one	7.2.9.2
Cl	Cl	(**5c**) 3,7-dichloro-5,10-bis(2-(diethylamino)ethyl)-5H-indolo[3,2-b]quinolin-11(10H)-one	7.2.9.3

Figure 2.17 – Structure of the quindolone derivatives **5**.

Table 2.3 – Yields of the alkylation reaction of quindolones (**4**, **91a** and **91b**), to afford their derivatives **5**, **94** and **95**.

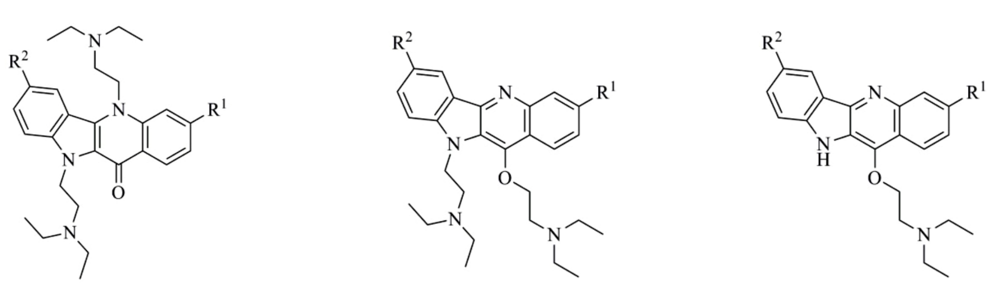

	5				**94**				**95**		
	R^1	**R^2**	Yield (%)		**R^1**	**R^2**	Yield (%)		**R^1**	**R^2**	Yield (%)
5a	H	H	23	**94a**	H	H	55	**95a**	H	H	17
5b	Cl	H	21	**94b**	Cl	H	33	**95b**	Cl	H	7
5c	Cl	Cl	29	**94c**	Cl	Cl	34	**95c**	Cl	Cl	5

In addition, the spectra showed two sets of one quadruplet and one triple at δ_H 2.70 and 1.13 ppm and δ_H 2.62 and 1.00 ppm, respectively, integrating to 4 and 6 protons and with ^{1}H-^{1}H COSY interactions, as shown in Figure 2.19 for **94a**. The ^{13}C NMR showed the signals corroborating the introduction of two side chains and the disappearance of the carbonilic carbon of the starting quindolone. Further experiments revealed the attendance of nuclear Overhauser effect (NOE) between the ^{1}H NMR triplet signals of the CH$_2$ in the side chains with the aromatic protons H^1 and H^9.

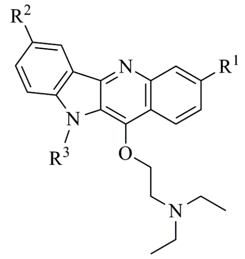
R2
R1
N
N
R3
O
N

R^1	R^2	R^3		Section
H	H	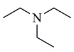	(**94a**) 2-(11-(2-(diethylamino)ethoxy)-10*H*-indolo[3,2-*b*]quinolin-10-yl)-*N,N*-diethylethanamine	7.2.9.1
Cl	H	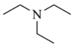	(**94b**) 2-((3-chloro-10-(2-(diethylamino)ethyl)-10*H*-indolo[3,2-*b*]quinolin-11-yl)oxy)-*N,N*-diethylethanamine	7.2.9.2
Cl	Cl	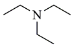	(**94c**) 2-((3,7-dichloro-10-(2-(diethylamino)ethyl)-10*H*-indolo[3,2-*b*]quinolin-11-yl)oxy)-*N,N*-diethylethanamine	7.2.9.3
H	H	H	(**95a**) 2-((10*H*-indolo[3,2-*b*]quinolin-11-yl)oxy)-*N,N*-diethylethanamine	7.2.9.1
Cl	H	H	(**95b**) 2-((3-chloro-10*H*-indolo[3,2-*b*]quinolin-11-yl)oxy)-*N,N*-diethylethanamine	7.2.9.2
Cl	Cl	H	(**95c**) 2-((3,7-dichloro-10*H*-indolo[3,2-*b*]quinolin-11-yl)oxy)-*N,N*-diethylethanamine	7.2.9.3

Figure 2.18 – Structures of 2-(11-(2-(diethylamino)ethoxy)-10*H*-indolo[3,2-*b*]quinolin-10-yl)-*N,N*-diethylethanamine (**94**) and 2-((10*H*-indolo[3,2-*b*]quinolin-11-yl)oxy)-*N,N*-diethylethanamine (**95**).

As illustrated in Figure 2.19 for compound **94a**, the triplet at δ_H 4.32 ppm, integrating for two protons, showed NOE with the doublet at δ_H 8.40 ppm, corresponding to H^1 and the triplet at δ_H 2.79 ppm, integrating for 2 protons, showed NOE coupling with the doublet at δ_H 7.52 ppm, corresponding to H^9.

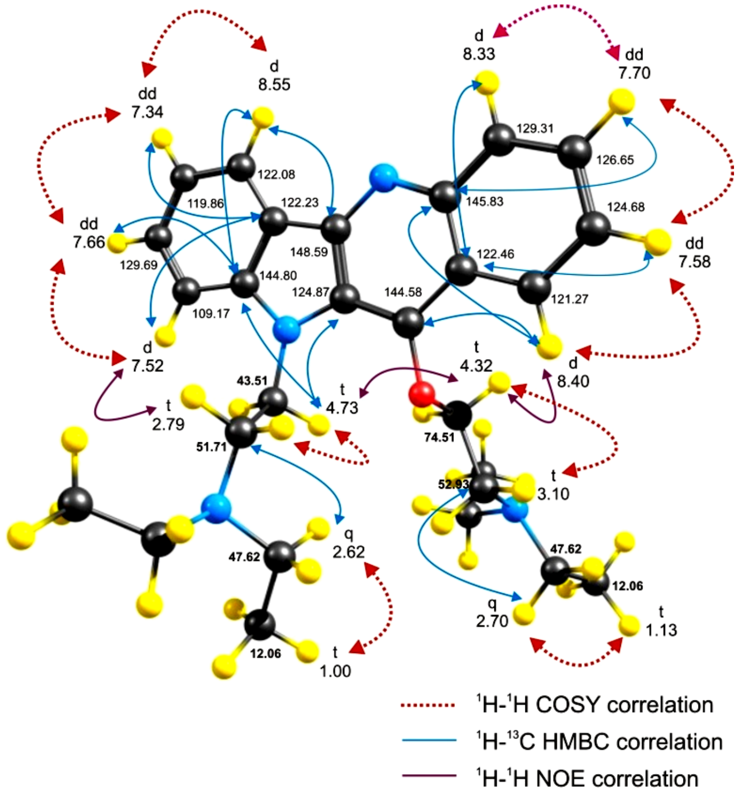
dd
7.34
d
8.55
d
8.33
dd
7.70
122.08
119.86
122.23
129.31
126.65
145.83
124.68
dd
7.66
129.69
148.59
144.80
124.87
144.58
122.46
dd
7.58
121.27
109.17
d
7.52
t
4.32
d
8.40
43.51
t
4.73
t
2.79
51.71
74.51
52.93
t
3.10
47.62
q
2.62
47.62
12.06
q
2.70
t
1.13
12.06
t
1.00
¹H-¹H COSY correlation
¹H-¹³C HMBC correlation
¹H-¹H NOE correlation

Figure 2.19 – Assignment of ^{1}H and ^{13}C NMR of **94a**.
Colour codes: H-yellow, C-grey, N-blue, O-red. Wireframe representation

In addition, it was also verified a deshielding effect in the δ_C of carbons in positions 4a and 5a, from 139.64 and 129.44 to 145.53 and 148.59, respectively, when compared with the parent compound **4**.

The second major product of the reaction was the species dialkylated in both nitrogens, N^5 and N^{10} (**5**), yielding from 19 to 23 % (Table 2.3). The assignment of the NMR spectra of **5a** is shown in Figure 2.20. The ^{1}H NMR spectra of the **5a** showed the same pattern as described to **94a** and their analysis reveal the introduction of two *N,N*-diethylamine-ethyl side chains in the quindolone nucleus.

The ^{13}C NMR spectra showed the presence of the signals corresponding to two ethyl-*N,N*-diethylamine side chains and one carbon at δ_C 169.13 ppm, characteristic of the carbonilic carbon in the quindolone nucleus, demonstrating that no alkylation occurred in the oxygen. Furthermore, the triplet at δ_H 4.84 ppm showed NOE coupling with the aromatic protons H^4 and H^6 at δ_H 7.70 and 8.25 ppm, respectively and the triplet at δ_H 5.00 ppm with the proton H^9 at δ_H 7.59 ppm, corroborating the alkylation of the N^5 and N^{10} positions.

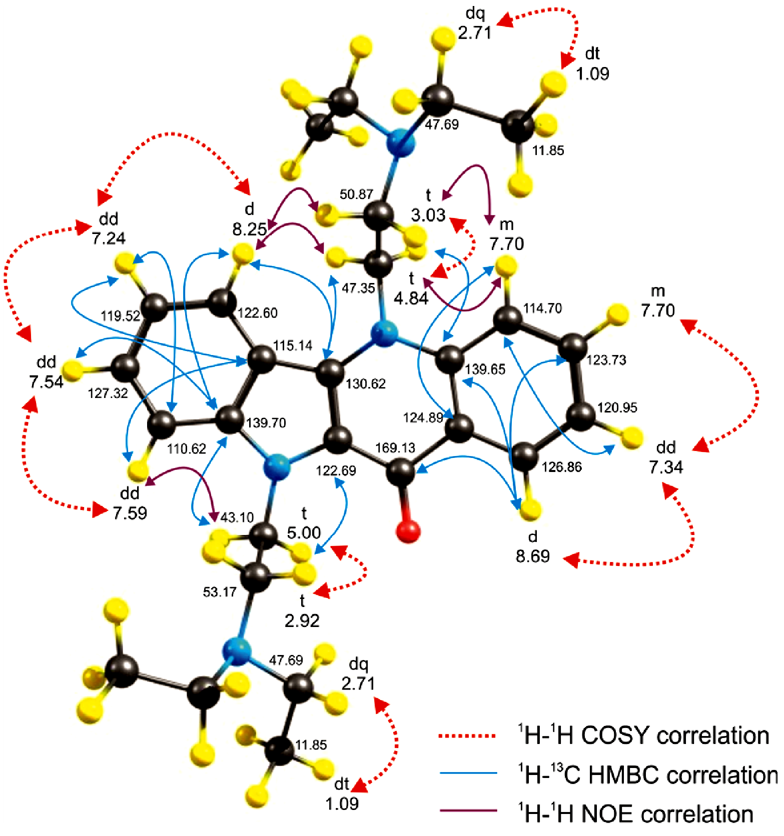
dq
2.71
dt
1.09
47.69
11.85
50.87
t
3.03
m
7.70
d
8.25
dd
7.24
47.35
t
4.84
114.70
m
7.70
119.52
122.60
115.14
139.65
123.73
dd
7.54
127.32
130.62
124.89
120.95
139.70
169.13
dd
7.34
110.62
126.86
122.69
dd
7.59
43.10
t
5.00
d
8.69
53.17
t
2.92
47.69
dq
2.71
11.85
dt
1.09
^{1}H-^{1}H COSY correlation
^{1}H-^{13}C HMBC correlation
^{1}H-^{1}H NOE correlation

Figure 2.20 – Assignment of ^{1}H and ^{13}C NMR of **5a**. Colour codes: H-yellow, C-grey, N-blue, O-red. Wireframe representation.

The third and last product isolated from the crude mixture was the species alkylated in the oxygen (**95**), yielding between 5 and 17 %. NMR assignments for compound **95a** is shown in Figure 2.21. The ^{1}H NMR spectra showed two triplets at δ_H 4.58 and 3.07 ppm, integrating for two protons which one and with ^{1}H-^{1}H COSY interactions between them, in addition to one quadruplet and one triplet integrating to 4 and 6 protons, respectively and with ^{1}H-^{1}H COSY coupling. The described NMR pattern is in good agreement with the presence of one side chain in the chemical structure of the final product. Furthermore, in the ^{13}C NMR it was not recognized the predictable signal of the carbonilic carbon, around δ_C 170 ppm, indicative of the alkylation of the carbonyl functionality with the ethyl-*N,N*-diethylamine side chain (**95**), as well as the presence of the a ^{13}C NMR δ_C at 73.99 ppm typical of the ether function.

The developed synthetic methodology used for the synthesis of the quindolone derivatives (**5**), allowed the attainment of the compounds with high degree of purity. However, the alkylation reaction did not show any selectivity, since the tautometic effect between the nitrogens and oxygen gave rise to the appearance of side products (**94** and **95**).

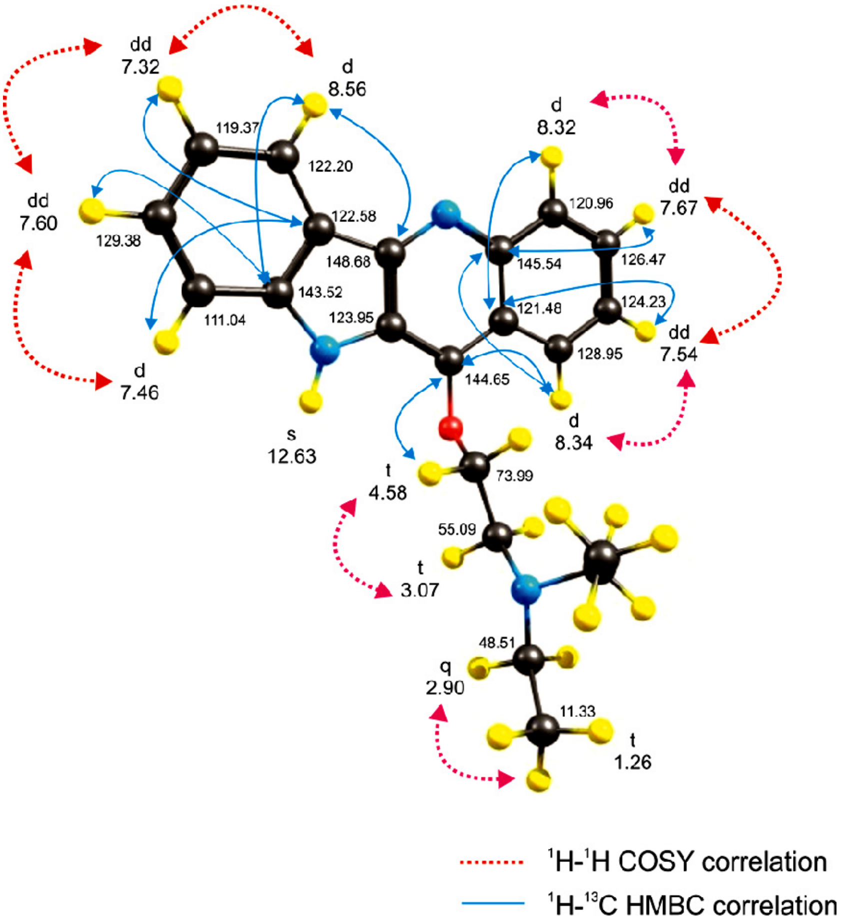
dd
7.32
d
8.56
dd
7.60
119.37
122.20
122.58
129.38
148.68
143.52
111.04
123.95
d
7.46
s
12.63
d
8.32
120.96
dd
7.67
145.54
126.47
121.48
124.23
dd
7.54
128.95
144.65
d
8.34
t
4.58
73.99
55.09
t
3.07
48.51
q
2.90
11.33
t
1.26
^{1}H-^{1}H COSY correlation
^{1}H-^{13}C HMBC correlation

Figure 2.21 – Assignment of ^{1}H and ^{13}C NMR of **95a**.
Colour codes: H-yellow, C-grey, N-blue. Wireframe representation

2.2.5 Synthesis of Alkyldiamines

The *N^1,N^1*-dimethylpropane-1,2-diamine **(97)**, used for the synthesis of **3d**, was prepared all in one pot, by reductive amination of *N,N*-dimethylaminopropanone (**96**), with ammonium acetate and $NaBH_3CN$, according to the route depicted in Scheme 2.10. The ammonium acetate reacts with the carbonyl group of the ketone, to form an imine accompanied by the loss of one molecule of water. This imine intermediate is then reduced with cyanoborohydride to form the amine **97** in 24 % yield. The reaction product was characterised by ^{1}H and ^{13}C NMR, confirming the chemical structure **97** (Section 7.2.10). For instance, the analysis of the NMR spectra revealed the disappearance of the carbonilic carbon on the ^{13}C NMR spectra and a shielding effect on the δ_H of the protons attached to C3 from 2.07 ppm in **96** to 1.01 ppm in **97**.

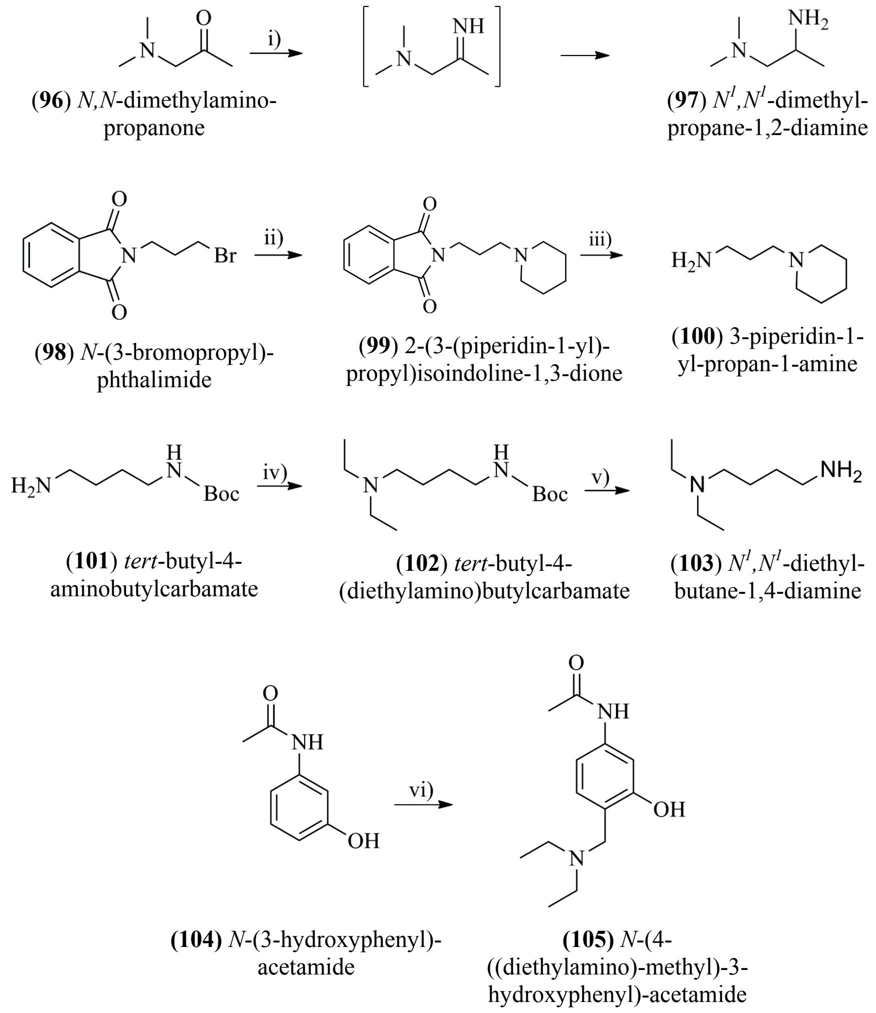
(**96**) *N,N*-dimethylamino-propanone

(**97**) N^1,N^1-dimethyl-propane-1,2-diamine

(**98**) *N*-(3-bromopropyl)-phthalimide

(**99**) 2-(3-(piperidin-1-yl)-propyl)isoindoline-1,3-dione

(**100**) 3-piperidin-1-yl-propan-1-amine

(**101**) *tert*-butyl-4-aminobutylcarbamate

(**102**) *tert*-butyl-4-(diethylamino)butylcarbamate

(**103**) N^1,N^1-diethyl-butane-1,4-diamine

(104) *N*-(3-hydroxyphenyl)-acetamide

(105) *N*-(4-((diethylamino)-methyl)-3-hydroxyphenyl)-acetamide

Scheme 2.10 – Synthetic methodology for the synthesis of alkyldiamines **97**, **100**, **103** and **105** used in the synthesis of cryptolepine derivatives **3d,j,l** and **t**.
i) NH_4OAc, $NaBH_3CN$, anhydrous $MgSO_4$, dry MeOH, reflux, 20h.; ii) piperidine, TEA, CH_2Cl_2, reflux, 30h.; iii) hydrazine, EtOH, reflux,3h.; iv) Acetaldehyde, anhydrous $MgSO_4$, $NaBH_3CN$, dry MeOH, 0 ºC, 2h.; v) CH_2Cl_2:TFA (1:1), r.t., 1 h.; vi) formaldehyde, diethylamine, EtOH, reflux, 96 h.

The synthesis of compound **3j** required the synthesis of 3-piperidin-1-ylpropan-1-amine (**100**). The alkyldiamine was synthesized according to the route in Scheme 2.10. The intermediate 2-(3-(piperidin-1-yl)propyl)isoindoline-1,3-dione (**99**) was obtained after reaction of N-(3-bromopropyl)phthalimide (**98**) with piperidine in the presence of TEA, yielding 51 %. It is a nucleophilic substitution of second order, in which occurs the nucleophilic attack of the piperidine nitrogen to the saturated carbon adjacent to the halogen of **98**, with release of bromide. The product of the reaction was characterized by NMR techniques and the data are in agreement with the chemical structure of the compound (Section 7.2.11). In the sequence of the synthetic route represented in Scheme 2.10, the next step is the synthesis of the final alkyldiamine 3-(piperidin-1yl)propan-1-amine (**100**). The reaction occurs between the intermediate **99** and hydrazine in EtOH, yielding 71 %. It is a nucleophilic substitution at the carbonyl groups of the intermediate **99**. The nucleophilic nitrogens of the diamine hydrazine attack the carbonyl groups with formation of 2,3-dihydrophthalazine-1,4-dione and release of the 3-(piperidin-1yl)propan-1-amine (**100**). The product of the reaction was characterized NMR techniques and the results are in agreement wit the chemical structure of the alkyldiamine **100** (Section 7.2.12).

In Scheme 2.10 is also described the synthetic methodology used for the synthesis of N^1,N^1-diethyl-butane-1,4-diamine (**103**) required for the synthesis of the cryptolepine derivative **3l**. The alkyldiamine **103** was synthesized from the *tert*-butyl-4-aminobutylcarbamate (**101**) through reductive amination with acetaldehyde in dry MeOH, following a mechanism similar to that outlined in Scheme 2.7, to achieve the intermediate *tert*-butyl-4-(diethylamino)butylcarbamate (**102**) with 94 % yield. The product of the reaction was characterized by NMR techniques (Section 7.2.13) and it was possible to notice the introduction of the diethyl groups with δ_H at 2.48 ppm integrating to 4 protons and with δ_H at 0.97 ppm integrating to 6 protons, corroborating the synthesis of **102**. In order to complete the synthetic route described in Scheme 2.10, the protecting group tert-butyl carbamate was cleaved under acidic conditions with trifluoroacetic acid, with release of carbon dioxide, tert-butanol and N^1,N^1-diethyl-butane-1,4-diamine (**103**), yielding 63 %. The product of the reaction was characterized through NMR techniques and the results are in agreement with the chemical structure of the compound, revealing the disappearance of the tert-Butyl ^{1}H NMR signals and a singlet at 3.94 ppm, integrating to 2 protons and corresponding to the primary amine hydrogens (Section 7.2.14).

The synthesis of the *N*-{4-[(diethylamino)-methyl]-3-hydroxyphenyl}acetamide (**105**), required to the synthesis of the cryptolepine derivative **3t**, was accomplished after reaction of *N*-(3-hydroxyphenyl)-acetamide as described in Scheme 2.10. The mechanistic pathway starts with a Mannich reaction type, in which, nucleophilic addition of diethylamine to the acetaldehyde, followed by a dehydration gave an imine intermediate (Schiff base), as depicted in Scheme 2.11. This electrophile (Schiff base) reacts in a second step with the electron-rich aromatic ring of *N*-(3-hydroxyphenyl)-acetamide (**104**), through an electrophile aromatic substitution with formation of the final aryldiamine **105**, yielding 55 %.

The product of the reaction was characterized through NMR techniques and the results are in agreement with the chemical structure of the compound (Section 7.2.15). The product of the reaction showed in the ^{1}H NMR spectra a singlet at 3.71 ppm, integrating for two protons and corresponding to the protons of the CH_2 attached at position 4 of the aromatic nucleus. In addition the singlet showed a Heteronuclear Multiple Bond Coherence (HMBC) effect with C3 (δ_C = 158.08 ppm) and with C5 (δ_C = 128.25 ppm). Also, it was noticed the presence of one quadruplet (δ_H = 2.60 ppm) and one triplet (δ_H =

1.09 ppm) integrating to four and six protons, respectively, thus corresponding to the *N,N*-diethylamine group.

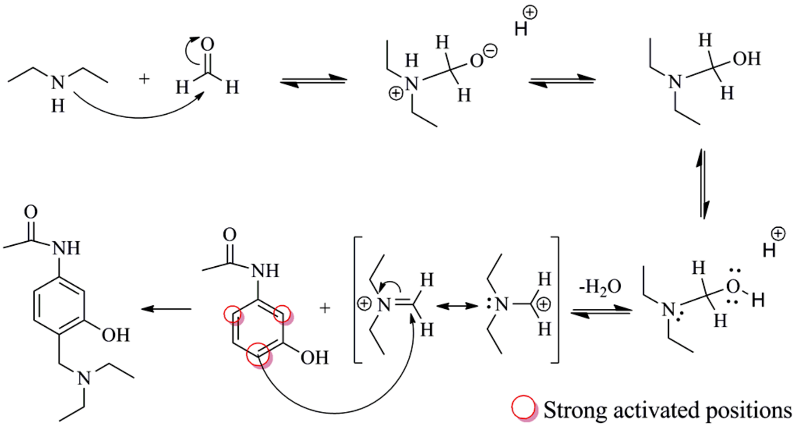
-H$_2$O
Strong activated positions

Scheme 2.11 - Mannich reaction mechanism of the N-(4-((diethylamino)methyl)-3-hydroxyphenyl)-acetamido (**105**) synthesis.

III

Chapter III – **Acid Dissociation Constants (pK_a)**

“The important thing is to know how to take all things quietly”

Michael Faraday (1791-1876)
English chemist and physicis

Abstract

*Acid-base chemistry of antiparasitic drugs plays a key role in their biological properties. In this study are reported the acid dissociation constants (*pK_a*) of several C-11 diamine-substituted cryptolepine derivatives with established antiplasmodial activities. The assignment of the* pK_a *values was accomplished by spectroscopic techniques and analyzed through the Hendersson-Hasselbach methodology. A structural dependence of the* pK_a *values is observed, namely the proximity of the terminal amine side-chain to the indolo[3,2-b]quinoline aromatic nucleus, the substitution pattern, as well as electron density distribution.*

List of Contents

3.1 INTRODUCTION 71
3.1 DETERMINATION OF ACID DISSOCIATION CONSTANTS BY UV-VISIBLE SPECTROSCOPY 73
  3.1.1 Cryptolepine 73
  3.1.2 Cryptolepine derivatives 74
3.2 DETERMINATION OF ACID DISSOCIATION CONSTANTS BY ^{1}H-NMR SPECTROSCOPY 77
  3.2.1 Cryptolepine 78
  3.2.2 Cryptolepine derivatives 79

3.1 Introduction

Antimalarial mode of action of aminoquinoline antimalarials, such as chloroquine, is at least in part due to the inhibition of haemozoin formation, a process that takes place in the DV of the parasite. In order to be active, these drugs have to accumulate in the DV and therefore the molecule must contain a basic functionality, protonable at DV acidic pH, in order to accumulate by a pH trapping mechanism. Therefore, physical and chemical properties of organic compounds, like acid dissociation constants (pK_a), play a pivotal role in the development of new antiplasmodial compounds targeting the DV and the knowledge of cryptolepine and analogues acid dissociation constants is crucial to a better understanding of their mode of action. These equilibrium constants are normally used to characterize the acid-base chemistry of a compound that has either a single protonatable site or multiple sites with well separated (>3 pH units) pK_as, and are often referred as the macroscopic equilibrium constants.(305) In a molecule with overlapping acid-base equilibrium constants, these constants characterize the system as a whole, but fail to provide information on specific protonatable sites. A compound with *n* protonatable sites can potentially exists in 2^n protonation states, called micro-species, and as consequence, the equilibrium constants called microscopic equilibrium constants.(305)

Cryptolepine has two nitrogen atoms but only one ionizable site at the indole nitrogen (pK_a = 11.0 by NMR spectroscopy and pK_a = 11.8 by UV-visible spectroscopy). Under acid conditions, cryptolepine exists as a salt (Figure 1.14). In basic conditions, the indole nitrogen atom loses its indolic proton, the electrons of the aromatic nucleus are redistributed and the alkaloid exists as neutral organic base. Although, synthesized cryptolepine derivatives (**3a-x**) possess three ionizable functions. Thus, the pK_{a1} values correspond to the deprotonation of the terminal nitrogen in the side chain, expected to be between 7 and 10 for alkylamines or lower for arylamines.(306) The indolic nitrogen of cryptolepine has a pK_a value around 11(9, 307) and as such, the pK_{a2} correspond to its ionization in cryptolepine analogues, while the pK_{a3} value correspond to the ionization of the NH attached to C11, which is expected to be also around 11, or higher, since the pK_a of the acidic nitrogen in position 4 of the 4-anilinoquinoline SKI-606 was calculated as 11.2.(308) The acid base equilibrium for cryptolepine analogues are schematized in Scheme 3.1.

However, the cryptolepine derivative **3y** do not have basic nitrogen attached to C11, due to the possible conjugation of lone pair of electrons in the nitrogen atom with the aromatic system. Thus, we considered only one acid base equilibrium in the cryptolepine derivative **3y**, pK_{a1}, corresponding to the deprotonation of the indole nitrogen atom in the aromatic nucleus of the indolo[3,2-*b*]quinoline (Scheme 3.2).

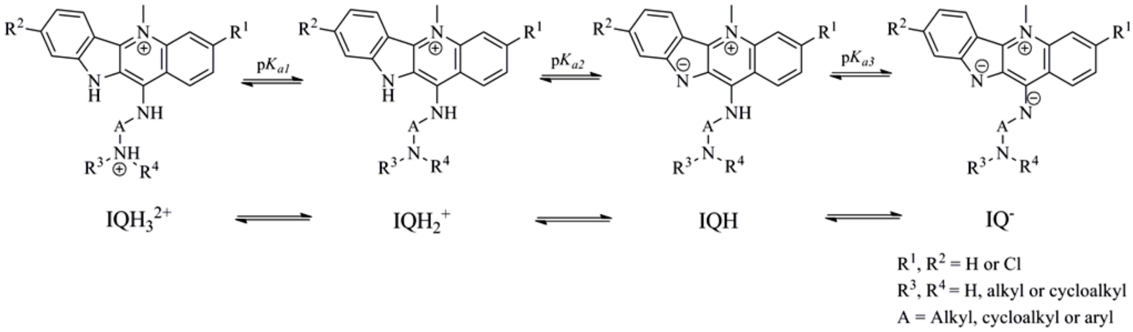

Scheme 3.1 – Proposed macroscopic acid base equilibrium for the cryptolepine derivatives **3a-x**.

Several methodologies can be used to determine acid dissociation constants (pK_a) values and are reviewed elsewhere.(309) Changes in physical or chemical properties can be determined at several different pH values.

Potentiometric pH titrations are the usual method for determination of acid dissociation constants in aqueous solutions with good reproducible results for compounds with pK_a values between 2.5 and 10.5. Outside this range potentiometric titrations suffer from limitations of interference due to the titration of the water solvent.(310-311)

UV-spectroscopic titrations have been used as an alternative method to measure pK_a values of compounds with high absorption coefficients and with a chromophore close enough to the site of the acid base function, allowing the usage of low concentrations, such as 1 µM.(312)

Also, nuclear magnetic resonance (NMR) spectroscopy through the dependence of the ^{1}H chemical shift (δ_H), allows the determination of acid dissociation constants from the direct observation of the magnetic environment of a particular nucleus and can identify the exact site of protonation.(305, 313-314)

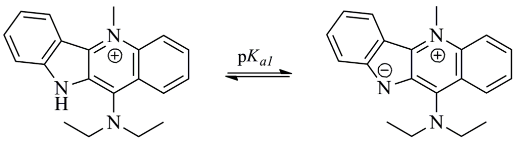

Scheme 3.2 – Proposed macroscopic acid base equilibrium for the cryptolepine derivatives **3y**.

In addition to the methodologies used for pK_a determination, several *in silico* methodologies to estimate these properties have been developed. The computer program SPARC (SPARC Performs Automated Reasoning in Chemistry, http://ibmlc2.chem.uga.edu/sparc), developed in University of

Georgia, United States of America, has been used to predict ionization states of drugs. (315-317) SPARC analyze the chemical structure relative to a specific reactivity query and quantifies several descriptors commonly used in organic chemistry such as resonance, field effects, sigma induction, intramolecular hydrogen bonding and steric effects, among others and uses them to the final pK_a prediction.(316-317) SPARC predicted values of acid dissociation constants for **1** and **3** are shown in Appendix D.

3.1 Determination of Acid Dissociation Constants by UV-visible spectroscopy

The acid dissociation constants of cryptolepine and derivatives from UV-visible spectrophotometry titrations were obtained with working concentrations of 5.0 µM and in pH range 3 to 13.7. The spectroscopic behaviour at acid, neutral and basic pH followed the Beer-Lambert law. The acid dissociation constants of **1** and **3a-y** were determined by nonlinear regression to the modified Hendersson-Hasselbach (Eq. 3.1) equation of the absorbance data at different pH values and at different wavelengths (Appendix C). However, the analysis of the UV-visible spectra only allows the determination of the acid dissociation constants of the ionizable function close to a chromophore. In cryptolepine and the majority of its derivatives (except compounds **3p-u**) the only chromophore is indolo[3,2-*b*]quinoline skeleton, so that it is only possible to identify the pK_a corresponding to the ionization of the indolic nitrogen and of the nitrogen attached to C11.

$$X = \frac{X_{max} + X_{min} \times 10^{(pH-pK_a)}}{10^{(pH-pK_a)} + 1}$$

Eq. 3.1 – Modified Henderson-Hasselbalch equation.
(X equal to absorbance or ^{1}H NMR chemical shift)

3.1.1 Cryptolepine

Cryptolepine UV-visible spectra showed three main absorption bands at acid pH (λ = 280, 368 and 430 nm), and as the pH increases (pH >11) a bathochromic shift (red shift) of approximately 10 nm is observed in all bands, in addition to hypochromic effects. For instance, the band at 280 nm verified and hypochromic effect at pH 11 followed by a 10 nm red shift at higher pH's (Figure 3.1a). The UV-visible spectra also exhibit three isosbestic points at λ = 285, 373 and 394 nm, respectively.

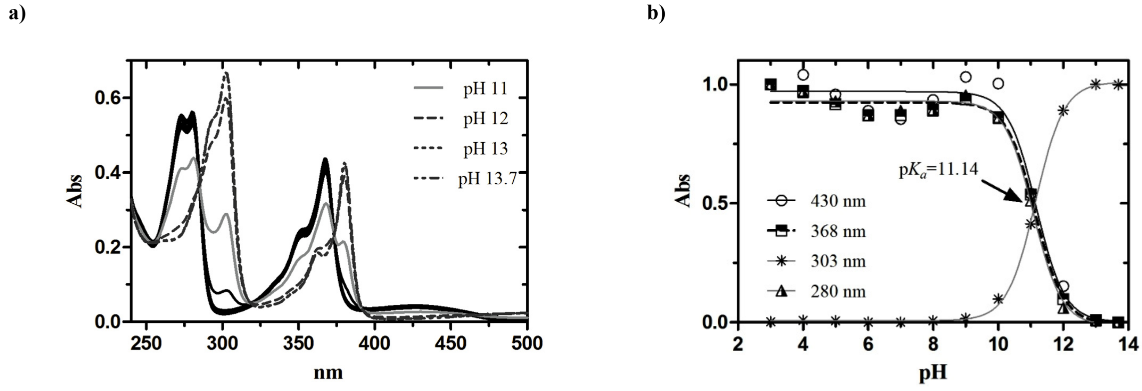

Figure 3.1 – a) UV-visible stacked spectra of cryptolepine (5µM) in the pH range from 3 to 13.7; b) UV-visible relative absorbance values of **1** at different wavelengths as a function of pH at 25 ºC (lines represent the fitting of the experimental data using the Hendersson-Hasselbach modified equation).

The analysis of the experimental data for **1** fitted to the modified Hendersson-Hasselbach equation (Eq. 3.1) reveals the presence of one protonatable site over the studied pH range with a pK_a value of 11.14 (Figure 3.1b), attributed to the ionization process (NH to N$^-$), occurring in the indolic nitrogen of the indoloquinoline ring system. The described results are in good agreement with published data.(9, 307)

3.1.2 Cryptolepine derivatives

To a better knowledge of the acid base chemistry of cryptolepine derivatives, their acid dissociation constants were also studied by UV-visible. For instance, the UV-visible stacked spectra of **3b** in the studied pH range (3 to 13.7), as well as the fitting of the experimental data to the modified Henderson-Hasselbalch equation (Eq. 3.1) are given in Figure 3.2.

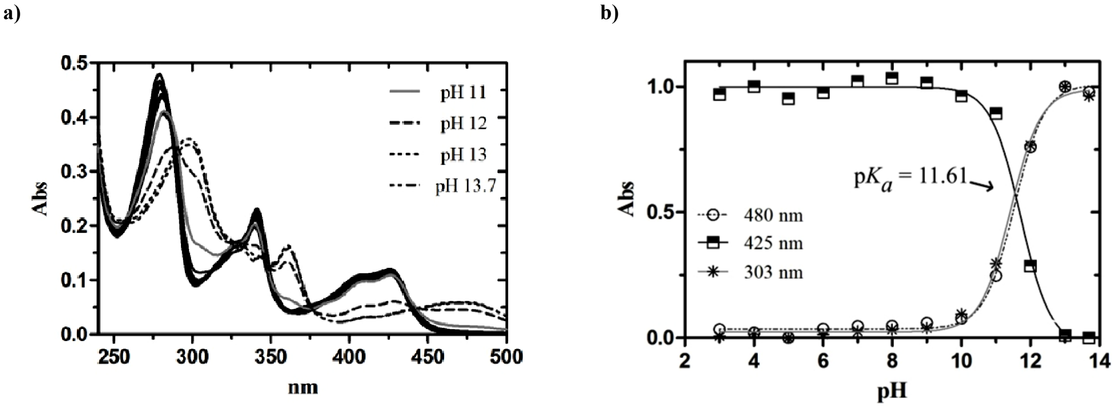

Figure 3.2 – a) UV-visible stacked spectra of **3b** (5μM) in the pH range 3 to 13.7; b) UV-visible relative absorbance values of **3b** at different wavelengths as a function of pH at 25 ºC (lines represent the fitting of the experimental data using the Hendersson-Hasselbach modified equation).

As cryptolepine, derivative **3b** also showed three major absorption bands (λ = 272, 342 and 425 nm) at acid pH and up to pH 11. With increasing basicity (pH>11) hypochromic effects and a bathochromic shifts of approximately 15-20 nm were observed for the 272 and 342 nm bands, while a more pronounced hypochromic effect was observed in the 425 nm band. The analysis of the **3b** UV-visible experimental data fitted to Eq. 3.1 (Figure 3.2b) reveals the presence of one inflection point in the best fitting curve, giving a pK_a value of 11.61±0.02.

Since the cryptolepine derivatives show two ionizable sites close to the chromophore (indole NH and C^{11}-NH), it was expected to observe two inflection points in the non-linear fitting to the Hendersson-Hasselbach modified equation. This observation can have two interpretations:

i. ionization of NH at C11 of compounds **3** occurs at pH higher than 13.7;
ii. ionization of indole nitrogen and nitrogen attached to C11 take place at overlapping pH intervals.

The C11 nitrogen atom is attached to an sp^2 carbon, and on losing its hydrogen, the negative charge becomes stabilized by conjugation with the aromatic nucleus of the indoloquinoline. It is known that electron withdrawing groups in the vicinity of a basic function decrease its basicity. In fact the pK_a of the acidic nitrogen in position 4 of a 4-anilinoquinoline was calculated as 11.2 by potentiometri, UV-visible spectroscopy and ^{1}H NMR.(308) Due to the chemical similarity between the nitrogen atom in position 4 of 4-anilinoquinoline and the nitrogen at C11 of the indolo[3,2-*b*]quinoline nucleus, its acid dissociation constant (pK_{a3}) will probably be very close to the described acid dissociation constant in the indolic nitrogen (p$K_{a2} \approx 11$)(9, 307) of cryptolepine. Thus, cryptolepine derivatives **3** will probably have two overlapping acid dissociation constants (pK_{a2} and pK_{a3}). Therefore, the acid base equilibrium of the indolo[3,2-*b*]quinoline nucleus of derivatives can be described in terms of microconstants k_1, k_2, k_3, and k_4, as depicted in Scheme 3.3.

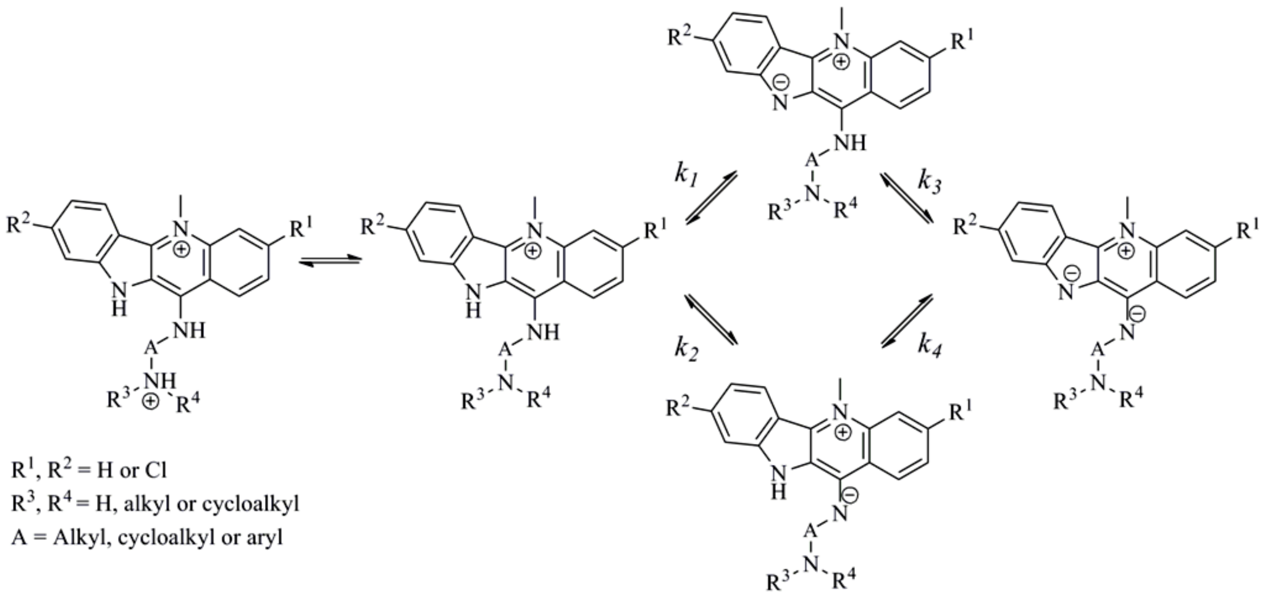
R1, R2 = H or Cl
R3, R4 = H, alkyl or cycloalkyl
A = Alkyl, cycloalkyl or aryl
k1
k2
k3
k4

Scheme 3.3 – Proposed microscopic acid base equilibrium for the cryptolepine derivatives **3**.

The macroscopic acid base constant pK_{a2}, assigned to acid base equilibrium in the indole nitrogen atom (Scheme 3.1), will be a combination of two site specific or "microscopic" dissociation reactions, k_1 and k_4, while the macroscopic acid base constant pK_{a3}, assigned to the dissociation in the nitrogen atom attached to C11, will be a combination of the two site specific dissociation reactions with equilibrium constants k_2 and k_3. Hence, and due to the overlapping of the acid base reactions (pK_{a2} and pK_{a3} are probably separated by less than 3 pK_a units), the value ascribed from the fitting of the UV-visible data to the Hendersson-Hasselbach modified equation, do not correspond to a macroscopic acid dissociation constant, but probably, to a group constant that embrace all the microconstants (pk_1 – pk_4) and which we designated of observed acid dissociation group constant (pK_{a2}^{Obs}).

From the fitting of the UV-visible data to the Hendersson-Hasselbach modified equation it was attributed a pK_{a2}^{Obs} value of 11.61±0.02 for cryptolepine derivative **3b**. Table 3.1 shows the observed acid dissociation group constants (pK_{a2}^{Obs}) for the cryptolepine analogues **3**, obtained in a similar way as described for **3b**.

Table 3.1 – Acid dissociation constants at 25 ºC for cryptolepine (**1**) and cryptolepine derivatives (**3a-y**), determined by UV-visible spectrophotometry.

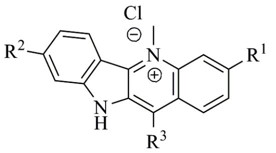

	R^1	R^2	R^3	pK_{a1}	pK_{a2}^{Obs}		R^1	R^2	R^3	pK_{a1}	pK_{a2}^{Obs}
1	H	H	H	11.14 ± 0.06	--	**3m**	H	H	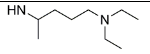	--	11.45±0.04
3a	H	H	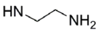		11.1±0.1	**3n**	H	H	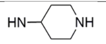	--	11.6±0.1
3b	H	H	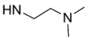	--	11.61±0.02	**3o**	H	H	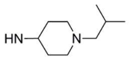	--	11.6±0.1
3c	H	H	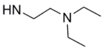	--	11.6±0.2	**3p**	H	H	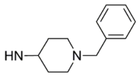	--	11.5±0.2
3d	H	H	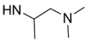	--	11.6±0.2	**3q**	H	H	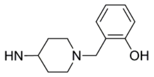	--	11.6±0.2
3e	H	H	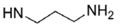	--	11.5±0.1	**3r**	H	H	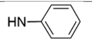	--	10.6±0.3
3f	H	H	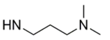	--	11.9±0.1	**3s**	H	H	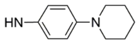	5.42±0.02	10.0±0.2
3g	H	H	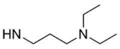	--	11.6±0.1	**3t**	H	H	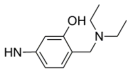	--	10.8±0.1
3h	H	H	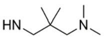	--	11.7±0.1	**3u**	H	H	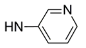	4.5±0.2	10.3±0.2
3i	H	H	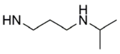	--	11.49±0.02	**3v**	Cl	H	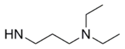	--	11.2±0.2
3j	H	H	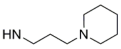	--	11.7±0.1	**3w**	Cl	H	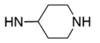	--	11.1±0.2
3k	H	H	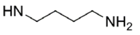	--	11.18±0.06	**3x**	Cl	Cl	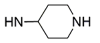	--	10.3±0.1
3l	H	H	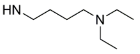	--	11.77±0.02	**3y**	H	H		11.74±0.03	--

pK_{a1} – Acid dissociation constant of the indole nitrogen atom of **1** and acid dissociation constant of terminal nitrogen atom of the side chain of **3**; pK_{a2}^{Obs} – Observed acid dissociation group constant of the ionization processes occurring in the indolo[3,2-*b*]quinoline chromophore of **3.**

Cryptolepine analogues **3s** and **3u** present an aromatic side chain attached at C11 with an ionizable function close to a chromophore. For instance, the UV-visible spectra of **3s** showed three main absorption bands at acid pH (λ = 287, 356 and 447 nm) and as the pH increase hypochromic effects were verified in all bands (40, 70 and 30 %, respectively), together with a hypsochromic shift (blue shift) of ≈ 5 nm in the 447 nm absorption band. Additionally, an hyperchromic effect of approximately 80 % was verified at 303 nm and an isosbestic point at 337 nm (Figure 3.3a). The analysis of the experimental data fitted to the Hendersson-Hasselbach modified equation reveals the presence of two protonable sites over the pH studied (3 – 13.7) with acid dissociation constant values of 5.42±0.02 and 10.0±0.2 (Table 3.1), corresponding to the acid dissociation constant in the nitrogen atom in the side chain (pK_{a1}) and to the observed acid dissociation group constant (pK_{a2}^{Obs}) of the ionization processes occurring in the indolic nitrogen atom and in the nitrogen attached at C11.

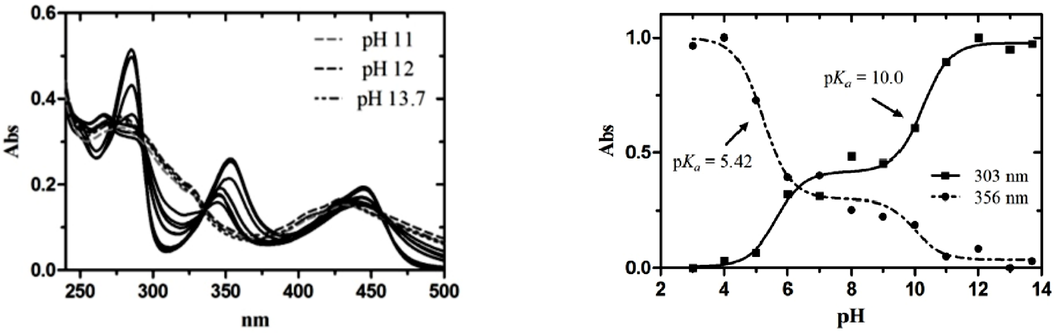

Figure 3.3 – a) UV-visible stacked spectra of **3s** (5μM) in the pH range 3 to 13.7; b) UV-visible relative absorbance values of **3s** at different wavelengths as a function of pH at 25 ºC (lines represent the fitting of the experimental data using the Hendersson-Hasselbach modified equation).

3.2 Determination of Acid Dissociation Constants by ^{1}H-NMR spectroscopy

Since the analysis of the acid base chemistry of cryptolepine derivatives through UV-visible spectroscopy suffer from some limitations, the analysis by nuclear magnetic resonance (NMR) spectroscopy through the dependence of the ^{1}H chemical shift (δ_H), is expected to overcome some of those restrictions. NMR spectroscopy allows the determination of acid dissociation constants from the direct observation of the magnetic environment of a particular nucleus.(305, 313-314) Assuming that changes in protons' chemical shift of a set of protons are only due to ionization of the adjacent ionizable groups, the determination of microscopic equilibrium constants of the several micro-species of a multiple protonatable molecule is possible. Although NMR spectroscopy requires the use of deuterated solvents and pK_a values in D_2O can be corrected into the H_2O equivalent system. The measurement of pD in D_2O solutions can be made by glass electrodes using standard buffer solutions, where recommended values for buffers were published by the International Union of Pure and Applied Chemistry (IUPAC).(318) However, in practice, a related quantity is used, the so called pH*, which is a direct read of the pD in the D_2O solution, with a H_2O-calibrated pH-meter. The conversion of pH* into pD is than accomplished experimentally, measuring the pH and the pH* of solutions with known concentration of H^+ and D^+ and adding a experimental correction constant. However, this experimental correction is electrode dependent (generally around +0.4 pH units), and should be determined for each step, if accurate pD values are needed. Recently, Krężel and Bal, through a linear correlation between pH-meter readings in equivalent D_2O and H_2O solutions, determine experimentally a novel equation (Eq. 3.2) to correlate the pK_a^* values measured in D_2O into a H_2O equivalent system.(319) Unfortunately, neither the acid dissociation constants obtained from pH* values (pK_a^*) nor acid dissociation constants obtained from corrected pD values (pK_a^D) are not straightforward comparable with pK_a

$$pK_a = 0.929pK_a^* + 0.42$$

Eq. 3.2 – pH-meter readings in D_2O solutions and H_2O pK_a correlation equation values in water. As such, in this chapter, only uncorrected pH* values are used and reported. Similarly, pK_a^* values obtained from the pH-meter direct readings are used for acid dissociation constants values, without isotope correction, to avoid the introduction of errors resulting from empirical equation.

The pK_a assignment of cryptolepine and derivatives **3** from NMR titrations were conducted by assigning the signals of each proton in ^{1}H NMR spectra, through the two dimensional NMR spectroscopy technique COSY (^{1}H-^{1}H correlation spectroscopy) at different pH values. As cryptolepine and its derivatives are insoluble in water, dimethylsulfoxide was added to improve solubility without affecting the pK_a values. In fact, pK_a values in aqueous dimethylsulfoxide (up to 27 vol %) are consistently slightly higher than in pure water, but differ by less than 0.2 pK_a units from pK_as in 100% water.(320) Working concentrations of approximately 50 mM in mixtures D_2O:DMSO-d_6 (60:40) with 3-(trimethylsilyl)propionic acid (TSP) as reference signal (δ_H 0.00 ppm) were used and the solutions titrated with DCl (0.2 M) or NaOD (0.2 M). All the spectra were recorded at 25 ºC. Water and dimethylsulfoxide do give very large peaks ($\delta_H \approx 4.5$ and ≈ 2.5 ppm, respectively), which do not interfere with the aromatic protons of the aromatic nucleus (in contrast to the N^5 -CH_3 singlet and some side chain protons of **3**), the key signals for pK_a determination. For each experiment the chemical shifts changes were followed with the pH changes.

3.2.1 Cryptolepine

The acid dissociation constant of cryptolepine was also calculated by fitting the ^{1}H NMR chemical shift (δ_H, ppm) to Eq. 3.1 as a function of pH*. The ^{1}H NMR stacked spectra of cryptolepine in the pH* range 1.6 to 12 and the non-linear regression fit of the chemical shifts versus pH* to the modified Henderson-Hasselbalch modified(307) equation are showed in Figure 3.4.

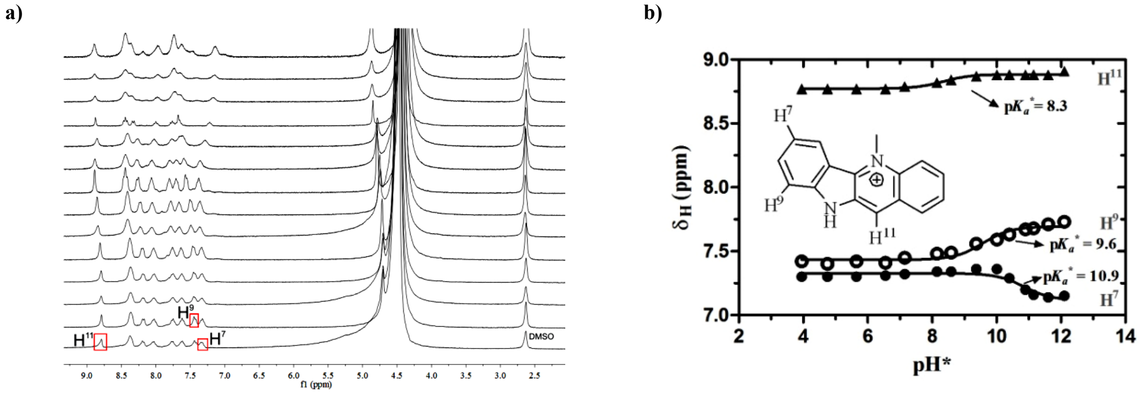

Figure 3.4 – a) ^{1}H NMR stacked spectra of cryptolepine in the pH* range from 1.6 to 12 (increasing from the bottom to the top) at 25 ºC; b) ^{1}H NMR chemical shifts (δ_H) of **1** as a function of pH in D_20:DMSO-d_6 (60:40) and 25 ºC (lines represent the fitting of the experimental data using the Hendersson-Hasselbach equation).

For cryptolepine, the chemical shifts of protons H^7, H^9 and H^{11} (Figure 3.4) showed significant shifts in δ_H with pH and as such, are the best probes to monitor the deprotonation of the indolic nitrogen. The analysis of the ^{1}H NMR spectra of cryptolepine at different pH* values showed a significant decrease in the chemical shift of the H^7 proton and an increase in the chemical shifts of protons H^9 and H^{11}. Taking into account the resonance structure of cryptolepine resulting from the ionization process, protons H^7 and H^9 showed the highest changes in chemical shift ($\Delta\delta_H$ = 0.15 and 0.33 ppm, respectively) because they are in *para* and *ortho* positions, relative to the carbon undergoing the biggest change in electron distribution (C9a), as shown in Figure 3.5.

Table 3.2 – Changes in ^{1}H NMR chemical shift (δ_H) in the studied pH range of protons H^7, H^9 and H^{11} of cryptolepine and protons H^1, H^7 and H^9 of cryptolepine derivatives.

	$\Delta\delta_H$ (ppm)			
	H^1	**H^7**	**H^9**	**H^{11}**
1	--	0.15	0.33	0.14
3b	0.36	0.33	0.26	--
3e	0.09	0.29	0.03	--
3f	0.30	0.33	0.19	--
3i	0.29	0.34	0.21	--
3n	0.16	0.35	0.21	--
3s	0.81	0.25	n.d.	--
3y	0.03	0.21	0.10	--

n.d. – not determined due to no attribution in the 1H NMR spectra.

Thus, protons H^7 and H^9 seem to be excellent probes for monitoring the deprotonation of N^{10} and became the focus of this pK_a assignment study for cryptolepine and its derivatives. To attain consistency with the cryptolepine analogues **3**, the chemical shifts of H^7 were used as reference to determine the pK_a values for the indole nitrogen, since it is the proton with more consistent deviation of it δ_H upon increasing pH (Table 3.2). The analysis of the NMR titration data for **1** fitted to the modified Hendersson-Hasselbach equation (Eq 3.1) reveals the presence of one inflection in the region of pH 11, corresponding to one protonatable site over the studied pH* range with a p$K_{a1}{}^*$ value of 10.9±0.2 (Table 3.4) and attributed to the ionization of the indolic nitrogen, corroborating the results from UV-visible spectrophotometry titrations.

3.2.2 Cryptolepine derivatives

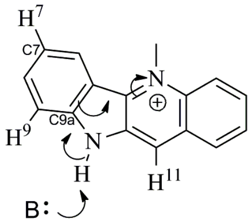

Figure 3.5 –Deprotonation of the indolic nitrogen atom of cryptolepine induces a strong electronic effect in the *orto* and *para* positions (H^9 and H^7) to C9a.

To realize acid base chemistry of the cryptolepine derivatives, titrations of some of these compounds (**3b**, **e-f**, **i**, **n**, **s** and **y**) with deuterated solutions were performed and analysed through NMR spectroscopy. The non-linear regression analysis of the chemical shifts versus pH* to the Henderson-Hasselbalch modified equation of the cryptolepine derivatives are showed in Table 3.3. For instance, to understand the acid base chemistry of compound **3b** and determine its acid dissociation constants the δ_H vs. pH* (Table 3.3) were considered. Two ionizable functions are located in the side chain of **3b** (pk_{a1} and pk_{a3}, according to Scheme 3.1) and monitoring its protons' chemical shifts (H^A, H^B and H^C) allows the determination of the acid dissociation constant values. Also, monitoring the protons' chemical shifts in the aromatic nucleus allows the determination of the acid dissociation constants of the indole nitrogen atom (pk_{a2}).

Due to this close proximity to the terminal nitrogen in the side chain, protons H^B and H^C are the best probes and showed only one inflection point in the pH* range 7-9, with a significant decrease of chemical shifts ($\Delta\delta_H$ between 0.65 and 0.9 ppm, respectively) on increasing pH*.

Table 3.3 – Non-linear fitting of the ^{1}H NMR chemical shifts to the Henderson-Hasselbalch modified equation of cryptolepine derivatives in the studied pH* range 3 to 13.

3b	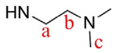	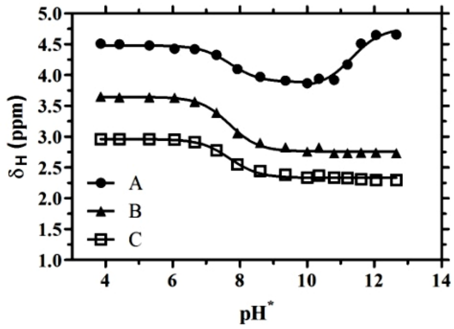	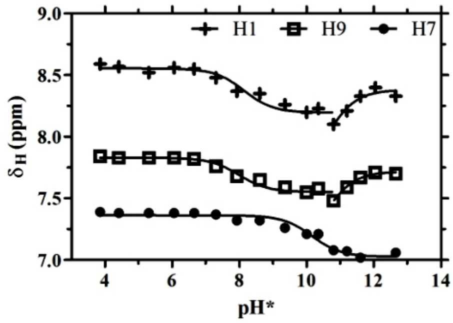
3e	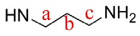	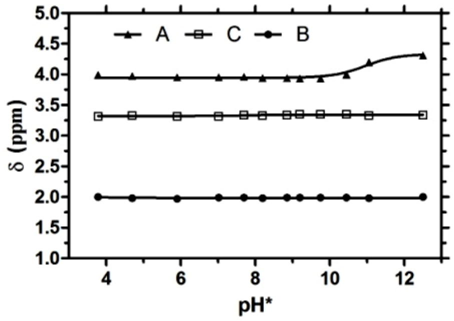	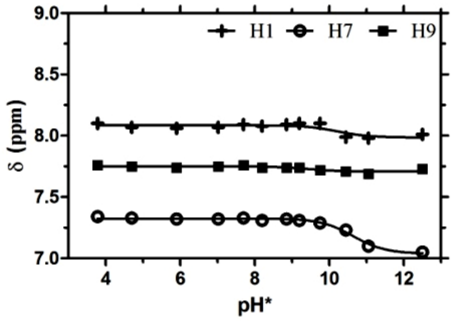
3f	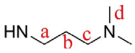	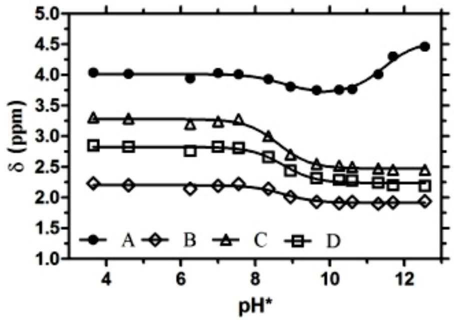	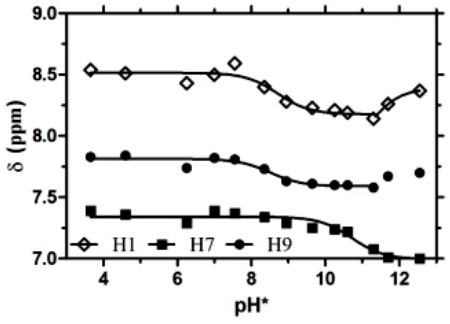
3i	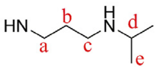	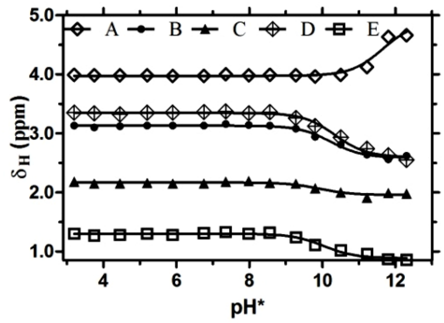	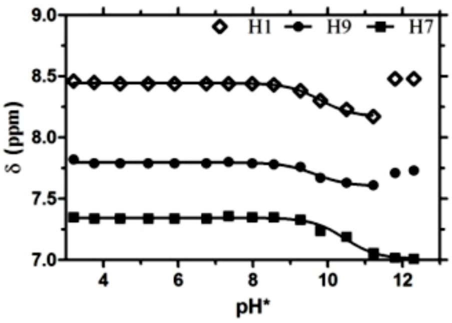

Table 3.3 (Cont.) – Non-linear fitting of the ^{1}H NMR chemical shifts to the Henderson-Hasselbalch modified equation of cryptolepine derivatives in the studied pH* range 3 to 13.

3n	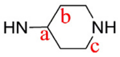	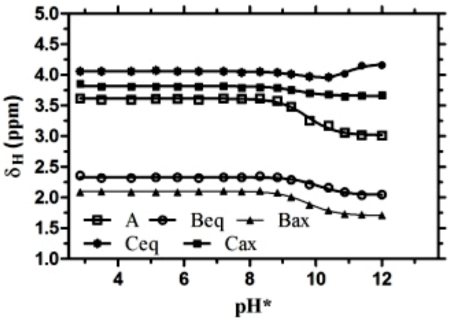	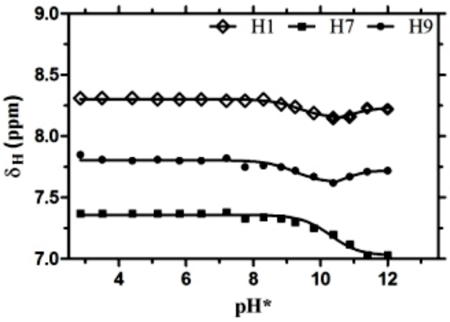
3s	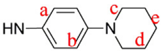	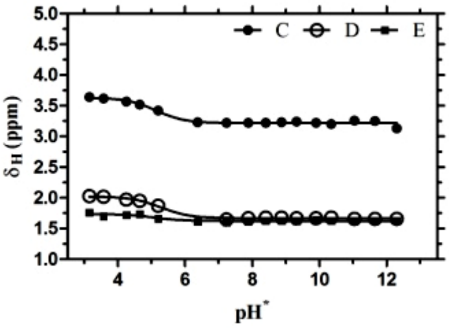	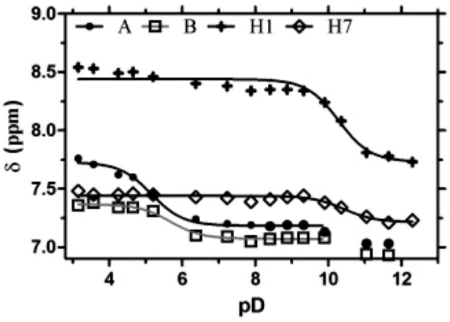
3y	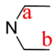	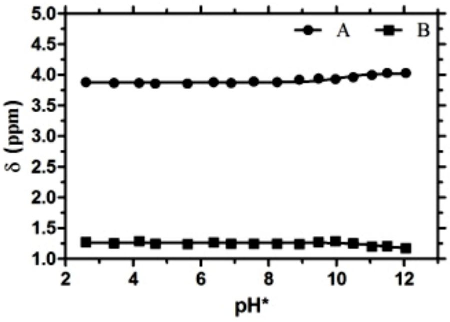	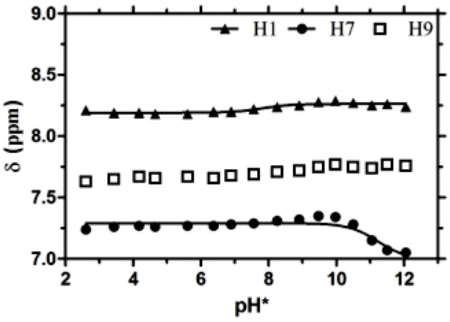

These changes clearly reflect the deprotonation extent of the terminal nitrogen atom in the side chain, with the chemical shift undergoing to upfield values. Taking into account H^C, which showed the highest $\Delta\delta_H$, and fitting the NMR data to the modified Henderson-Hasselbalch equation, the best fitting curve showed one inflection corresponding to a pK_{a1}^* value of 7.70±0.05.

In order to establish the pK_{a2} (Scheme 3.1) value of **3b** the experimental δ_H values of H^7 and H^9 were taken into account. However, H^7 seems to be the only proton which does not suffer influences from ionization processes in the side chain besides the ionization of the indole nitrogen (Table 3.3). ^{1}H NMR spectroscopy δ_H of H^7 fitted to Eq. 3.1 showed an inflection in the best-fitting curve corresponding to a pK_a^* value of 10.2±0.1. Although, since the macroscopic acid base equilibrium constant pK_{a2} is described in terms of the microconstants pk_1 and pk_4 (Scheme 3.3) the obtained value do not correspond to a macroscopic acid dissociation constant, but probably to an observed acid dissociation group constant (pK_{a2}^{*Obs}) that reflects the different contribution of the micro species to the acid base equilibrium.

The titration curve of H^A of **3b** (Table 3.3) shows a small upfield inflection ($\Delta\delta_H$ = 0.56 ppm) in the region of pH* 7-8, probably reflecting the three-bond distance from the protonable terminal amine, and a major downfield inflection ($\Delta\delta_H$ = 0.79 ppm) in the region of 10-12. This deshielding upon pH* increase could correspond to the deprotonation extent of the close nitrogen atom attached to C11. Thus, monitoring the chemical shift of H^A gave a pK_a^* value of 11.3±0.2. Analogously to the described to the ionization of the indole nitrogen atom, the macroscopic acid dissociation constant pK_{a3} (Scheme 3.1) is described in terms of the micro species characterized though the micro equilibrium constants pk_2 and pk_3. Thus, the determined value could probably correspond to an observed acid dissociation group constant, pK_{a3}^{*Obs} reflecting the different contributions of the acid base micro species.

However, as the pK_{a3} function overlaps the pK_{a2} of the indole nitrogen, the chemical shift of proton H^A can also be influenced by the ionization process occurring in the indole nitrogen (pK_{a2}). To investigate this hypothesis, analysis of the protons' chemical shifts of cryptolepine derivative **3y**, which do not have a basic nitrogen atom attached C11 will allow to understand the possible influences of the ionization in the indolo nitrogen atom in the protons of the side chain adjacent to the nitrogen attached to C11 (proton H^A). Thus possible changes in the chemical shifts occurring in the protons of the side chain of **3y** would reflect the ionizations occurring in the indolo[3,2-*b*]quinoline nucleus.

The analysis of the δ_H of H^1, H^9, H^A and H^B fitted to Eq. 3.1 (Table 3.3) did not allow the determination of any acid dissociation constant, at this pH* range, due to the lack of significant variations in the chemical shifts of these protons. Therefore, it can be deduced that the chemical shifts of H^A in the side chain of **3y** and in general, of the cryptolepine derivatives, do not suffer significant influence from the ionization process occurring in the indole nitrogen. The analysis of the ^{1}H NMR δ_H of H^7 fitted to the Hendersson-Hasselbach modified equation allow to notice one inflection point in the studied pH* range, corresponding to the acid dissociation constant of the indole nitrogen atom, with a pK_{a1}^* value of 11.2±0.3.

The attribution of the acid dissociation constants to the other cryptolepine derivatives (**3e-f**, **i**, **n** and **s**) followed the reported methodology for cryptolepine derivative **3b** and are reported in Table 3.4. The terminal side chain amine functionality of cryptolepine derivatives **3a-q** and **3s-x** are neutral nitrogen bases, due to the availability of the lone pair of electrons for protonation. Any substituent that increases the electron density (electron donating groups) on the nitrogen atom therefore raises the energy of the lone pair of electrons thus making it more available for protonation and increasing the basicity of the amine (larger pK_a). The acid dissociation constants for the terminal nitrogen atom in the side chain (pK_{a1}), for cryptolepine derivatives **3b**,**e-f**,**i**,**n** and **s**, established through NMR spectroscopy, range between 5.1 and 10.43, excluding **3e** for which it was not possible to establish any value in the studied pH* range (3.7-12.5).

Table 3.4 – Acid dissociation constants (pK_a^*) and observed acid dissociation group constants (pK_a^{Obs}) at 25 ºC for cryptolepine (**1**) and cryptolepine derivatives (**3a-y**), determined by nuclear magnetic resonance spectroscopy.

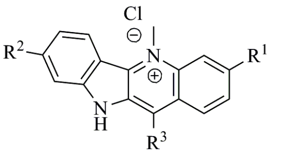

	R^1	**R^2**	**R^3**	**pK_{a1}^***	**pK_{a2}^{*Obs}**	**pK_{a3}^{*Obs}**
1	H	H	H	10.9±0.2	--	--
3b	H	H	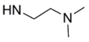	7.70±0.05	10.2±0.1	11.3±0.2
3e	H	H	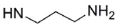	>12.5	10.64±0.07	10.9±0.1
3f	H	H	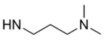	8.75±0.09	10.7±0.2	11.5±0.1
3i	H	H	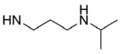	10.43±0.08	10.45±0.08	11.7±0.2
3n	H	H	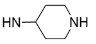	9.4±0.1	10.3±0.1	9.75±0.06
3s	H	H	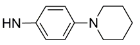	5.1±0.3	10.4±0.2	9.9±0.6
3y	H	H		11.2±0.3	--	--

pK_{a1} – Acid dissociation constant of the terminal nitrogen in the side chain of **3,** except for **3y** that correspond to the ionization of the indole nitrogen atom.; pK_{a2}^{Obs} – Observed acid dissociation group constant in the indolic nitrogen atom (N^{10}) of **3**; pK_{a3}^{Obs} – Observed acid dissociation group constant in the nitrogen atom attached to C11 (C^{11}-N) of **3**.

The lowest pK_{a1} value (5.1±0.3) was established for cryptolepine derivative **3s** , with the terminal amine functionality of the side chain close to an aromatic ring. Corroborating this result, analysis by UV-Visible spectroscopy also established a pK_{a1} value of 5.42±0.02 obtained from data fitted to the Henderson-Hasselbalch modified equation (Table 3.1). The proximity of the ionizable functionality to the aromatic ring, in which the nitrogen is directly attached to a sp^2 carbon with the possibility of electron resonance of the lone pair of electrons with the aromatic ring, makes it less available for protonation (decreased basicity).

The derivative with a short side chain (**3b**) showed the lowest pK_{a1} value (7.70±0.05), when compared with its counterparts with tertiary amines of longer linear side chains 8.75±0.09 (**3f**). As expected, these results showed the contribution of the aromatic electron density of the cryptolepine nucleus to the acid dissociation constant of the terminal amine side chain. The closer proximity to the aromatic nucleus decreased the basicity due to inductive effects that fall off rapidly with distance and consequently increasing the pK_a values of derivatives with longer side chains.

Also the substitution on the terminal amine functionality seems to strongly influence the pK_{a1} values of this functionality. The substitution of the terminal nitrogen with alkyl groups (electron donating groups) would increase the amine basicity (RNH_2 < R_2NH < R_3N). The solvent have also contributions to the charge stabilization. Every hydrogen atom attached to the nitrogen will be hydrogen bonded with solvent, helping to stabilize the charge. Thus, the charge stabilization must be due to a combination of effects:$^{(321\text{-}322)}$

1. the increased availability of the lone pair and the stabilization of the charge due to the replacement of the hydrogen atom by alkyl groups;
2. the stabilization due to solvation, an important part of which is due to hydrogen bonding, an effect that decreases with the increasing number of alkyl groups.

The base strengths of primary, secondary and tertiary terminal amines of side chains (**3e-f** and **3i**, respectively) were studied by NMR spectroscopy, which showed that the basicity reduces with the substitution of the amine functionality (NH_2 > NH-*i*-Propyl > $N(CH_3)_2$, **3e**, **3i** and **3f**, respectively). Therefore, due to substitution on the terminal nitrogen, the pK_{a1}^* values decrease with the introduction alkyl groups. It seems that the solvent effects play an important role in the basicity of the studied cryptolepine derivatives, increasing the basicity of the terminal primary and secondary amines (**3e** and **3f**, respectively). In fact, it is well known that a marked base strengthening effect, due to hydration of N^+H groups, occurs in the following order; primary amines > secondary amines > tertiary amines.$^{(321\text{-}323)}$

The acid dissociation constants of the indole nitrogen and amine function attached to C11 were also established through UV-visible and NMR spectroscopy. However, due to the overlapping values of pK_{a2} and pK_{a3} the values achieved by means of UV-visible titration spectroscopy, represent an observed acid dissociation group constant (pK_{a2}^{Obs}) comprising all the contributions to the acid base equilibrium of the micro species (k_1-k_4). These observed acid dissociation group constant of cryptolepine derivatives **3a-y** ranges between 10.0 and 11.9 (Table 3.1). No significant differences in pK_{a2}^{Obs} values were found between derivatives with aliphatic side chains with different lengths or with cyclic aliphatic side chains. However, significant differences were found between the pK_{a2}^{Obs} aliphatic and aromatic side chains, as well as between derivatives with additional withdrawing groups. Lower values were found for derivatives with an aromatic side chain attached to C11, namely 10.6, 10.0, 10.8 and 10.3 (for **3r-u**, respectively).

Also, in derivatives substituted in the aromatic ring with chlorine (**3v-x**) a reduction on the pK_{a2}^{Obs} values (11.2, 11.1, 10.3, respectively) was verified, when compared with counterparts (**3g** and **3n**, pK_{a2}^{Obs} = 11.6 and 11.6, respectively). The introduction of electron-withdrawing substituents (phenyl group and halogens) in the cryptolepine' nucleus would be expected to decrease the pK_{a2}^{Obs} value, making the indole nitrogen and the nitrogen atom attached to C11 less basic. The inductive effects of the electron-withdrawing groups facilitate the stabilization of the negative charge on the nitrogens atoms, and this effect is clearly visible when comparing pK_{a2}^{Obs} values of compounds **3w** (11.1) and **3x** (10.3) with one and two chlorine substitutions, respectively. The introduction of one additional chlorine atom in position C8 of the indoloquinoline nucleus (**3x**), when compared with **3w**, clearly increases the stabilization of the negative charge on the indolic nitrogen and amine nitrogen attached to C11, making the compound more acidic.

The observed acid dissociation group constants of the indole nitrogen (pK_{a2}^{*Obs}) determined through NMR spectroscopy for cryptolepine derivatives **3b**, **3e-f**, **3i**, **3n**, **3s**, and **3y** and corresponding to the sum of the different contributions of the micro species involved in the acid base equilibrium, range from 10.2 to 10.7. The results show that the introduction of the side chain at position C11 did not induces significant changes in the acid base equilibrium in the indole nitrogen atom, when compared to its counterpart cryptolepine (pK_{a1}^{*} = 10.9).

Additionally, the values corresponding to the ionization process occurring in the nitrogen directly attached to the C11 (pK_{a3}^{*Obs}) determined by NMR spectroscopy for **3b**, **3e-f**, **3i**, **3n**, **3s**, and **3y** and corresponding to the contribution of the equilibrium described by the microconstants pk_2 and pk_3, range between 9.75 and 11.7. Like the indolic nitrogen, the nitrogen attached to C11 shows weak acid properties. The nitrogen atom is directly attached to an sp^2 carbon and because the nitrogen atom can become aromatic (by losing the hydrogen atom), with the lone pair of electrons fully conjugated with the aromatic system in a p orbital, the ionized negative charge would be stabilized in sp^2 hybridization. The lowest value (pK_{a3}^{*Obs} = 9.75) was found for cryptolepine derivatives **3s**, and can be justified by the close proximity to an electron-withdrawing side chain, which increases the capability of the ionizable functionality to donate the proton, while no significant differences was found in cryptolepine derivatives with alkyl side-chains (**3b**, **3e-f**, **3i** and **3n**).

Overall, the used methodologies allowed to better understand the acid base chemistry of cryptolepine and of its derivatives with a basic amino side chain at position C11 of the indolo[3,2-*b*]quinoline nucleus.

IV

Chapter IV - **DNA and Haem Binding Properties**

"A man's errors are his portals of discovery"

James Joyce (1882-1941)
Irish writer and poet

Abstract

*Cryptolepine (**1**) shows DNA binding properties, being a strong intercalating agent with preference for GC rich structures containing non-alternated CC sites. These binding properties are responsible for cytotoxic properties that can probably explain the antiplasmodial activity and the low selectivity. Additionally, it is also recognized that cryptolepine can exert is antimalarial mode of action through inhibition of haemozoin formation, due to complexation with haematin. In this study we now report the DNA binding properties of **3** and the haem binding properties of the novel cryptolepine and quindolone derivatives in order to contribute to a better knowledge of their antimalarial mechanism of action. These cryptolepine derivatives **3** bind very strongly to double-stranded d(GATCCTAGGATC)$_2$ and single-stranded d(GCCAAACACAGAATCG) oligonucleotides with association constants, K_{ass}, ranging from 10^5 M^{-1} to 10^7 M^{-1}. Analysis of structure-binding affinity relationships revealed that linear alkyldiamine side chains markedly increase the binding affinity to double-stranded oligonucleotide when compared to the parent compound **1**. Incorporation of a chlorine atom at C-3 of the indoloquinoline moiety further increases binding affinity of **3**. All compounds **3** within this series showed the ability to interact with strictly monomeric haematin (FPIX-OH), as well as all the quindolone derivatives (**5**, **94** and **95**) The association constants (K_{ass}) range between 0.062 and 0.41 x10^6 M^{-1} for the novel cryptolepine derivatives **3** and between 0.074 and 0.14 x10^6 M^{-1} for the quindolone derivatives, comparable to chloroquine.*

List of Contents

4.1 INTRODUCTION 89
4.2 INTERACTIONS OF CRYPTOLEPINE AND DERIVATIVES WITH SINGLE- AND DOUBLE-STRANDED OLIGONUCLEOTIDES 91
  4.2.1 Binding Stoichiometry with Double-Stranded Oligonucleotide 91
  4.2.2 Thermal Denaturation Studies with Double-Stranded Oligonucleotide 92
  4.2.3 Association Constants (K_{ass}) with Oligonucleotides 94
4.3 INTERACTIONS OF CRYPTOLEPINE AND QUINDOLONE DERIVATIVES WITH HAEMATIN 102
  4.3.1 Binding stoichiometry 102
  4.3.2 Association Constants (K_{ass}) with Haematin 103

4.1 Introduction

Non-covalent intramolecular associations are ubiquitous in chemical and biological systems. The association or binding constant (K_{ass}) of ligand (L)-receptor (R) complexation process provide a fundamental measure of the affinity and stability of the complex, and consequently, an important feature to describe and understand molecular interactions. The non-covalent interactions between ligands and receptors can be classified generally as either specific or non-specific, depending whether the ligand bind with selectivity to a particular region of the receptor. However, specific binding ligands can also bind to non-specific regions with lower affinity.(324) The binding of ionic ligands to receptors, and specially to nucleic acids, is particularly sensitive to the ionic strength of the environment in solution. This is due to the polyelectrolyte nature of nucleic acids, which results in a local accumulation to high concentration of cations (e.g. K^+, Na^+, Mg^{2+}) in the vicinity of the oligonucleotide structures, hindering the complex stability.(325) Binding interactions can also be classified according to the cooperativity of ligand binding. Cooperativity is a thermodynamic factor that reflects the influence of one bound ligand on the binding of a second ligand, and can contribute either positively or negatively (second binding is enhanced or reduced with respect to the affinity of the first ligand). True cooperativity reflects changes in the intrinsic binding parameters.(326)

Important binding parameters are the association constants, which are a special case of the equilibrium constants, where the equilibrium state is the molecular binding. Many methods for determining these binding constants have been described in the literature in the last decades. They can be grouped in two separated categories: (327-333)

i. *Separated based methodologies* separate the free solute and the bound solute and evaluate their concentrations.
ii. *Non-separation based methods* monitors the change in specific physicochemical properties of the solute or ligand upon complexation.

Chief among these methodologies are methods based on spectroscopic changes, particular those based on absorption, fluorescence or nuclear magnetic resonance properties of receptors and ligands.(334-

337) Equilibrium binding titration is a technique that allows the determination of dissociation constants (K_{diss}) of complexation between a ligand and a receptor through saturation analysis.(338) Essentially, a solution of receptor at fixed concentration is monitored by a spectroscopic technique on addition of serial aliquots of ligand (e.g. DNA or oligonucleotide) and analyzed only for the ligand component in terms of free ligand and the resulting complex.

The binding equilibrium is described by intrinsic equilibrium association constants that normally reflect the binding of only one form of the ligand to yield the complex. Therefore, if multiple forms of the ligand exist in equilibrium (e.g. equilibrium between monomer, dimer and tetramer forms), then a separate intrinsic binding constant is required to describe the interaction. Similarly, if a ligand can bind to the receptor in a number of different modes, then the binding of each mode is described by separate intrinsic binding constant.

The natural occurring indolo[2,3-*b*]quinoline alkaloid cryptolepine (**1**) bind to DNA structures and several lines of evidence suggest that these interactions can contribute to its broad spectrum of biological activities.(3) In 2002, Lisgarten and co-workers(5) showed that cryptolepine could bind to DNA through intercalation with CG-rich sequences containing non-alternating CC sites. This interaction with DNA is probably responsible for the cytotoxic effects of cryptolepine through inhibition of DNA synthesis and interfering with topoisomerase II activity in the cells.(8, 17) Bonjean et al., investigated the strength and the binding mode of cryptolepine to DNA using calf thymus DNA and double-stranded polymers.(17) Cryptolepine acted as a typical intercalating agent, with tight and geometrically homogeneous binding. The affinity constant of the drug for double-stranded DNA (ds-DNA) was comparable to the values of others intercalating agents and there was a noticeable preference for GC-rich sequences. Cryptolepine also stabilizes topoisomerase II-DNA covalent complexes and stimulates the cutting of DNA at a subset of preexisting topoisomerase II cleavage sites, being cytotoxic to B16 melanoma cells.(7, 17)

An X-ray diffraction study of cryptolepine bound to d(CCATGG)$_2$ showed intercalated cryptolepine molecules (Figure 1.17). In the reported crystal structure, two d(CCATGG)2 duplexes were located end to end as contiguous duplexes with cryptolepine molecules stacked between them, as well as at each extremity of the double-hexamer duplex and intercalated in two CC-GG sites. Cryptolepine interacts with the CC-GG sites through base-stacking intercalation, enhanced by the asymmetry of the drug, fitting the target with different stacking on both sides (CC and GG).(5, 277) Most recent studies further reveal that cryptolepine is capable of interacting with unusual DNA structures like triplexes and quadruplexes. Dialysis competition assay confirmed that cryptolepine preferentially binds to poly d(GC) rather than poly d(AT) rich duplex sequences, recognizes triplex and quadruplex structures, and that DNA or RNA single strands are not good substrates for cryptolepine.(278)

Also, cryptolepine could elicit its antiplasmodial activity due to its interaction properties with haem,(210) inhibiting haemozoin formation, the detoxification process of malaria parasites.(18-21) In 2001, Wright and co-workers in is search for indolo[3,2-*b*]quinolines with improved antiplasmodial activity showed that cryptolepine inhibit *β*-haematin formation in a cell-free system, like chloroquine and related 4-aminoquinolines, demonstrating that the antiplasmodial mode of action could be due to the inhibition of haemozoin formation.(210)

Thus the knowledge of the binding properties of the synthesized indoloquinolines to potential targets, as DNA and haem, is crucial to better understand their biological properties. Here we describe binding affinity and stoichiometry of cryptolepine (**1**) and its derivatives (**3**) to a short self-complementary 12-mer double-stranded oligonucleotide d(GATCCTAGGATC)$_2$, to a single-stranded oligonucleotide d(5'-GCCAAACACAGAATCG-3') and to haematin monomer, as well as the binding affinity of quinolones (**4**, **91a** and **91b**) and its derivatives (**5**, **94** and **95**) to haematin monomer.

4.2 Interactions of Cryptolepine and Derivatives with Single- and Double-Stranded Oligonucleotides

Binding stoichiometry of the indolo[3,2-*b*]quinolines were obtained with the Job's methodology(339-342) through fluorescence and UV-visible spectrophotometric experiments. In addition, the binding properties of **1** and developed derivatives **3** to single- (ss) and double-stranded (ds) oligonucleotides were obtained by means of the described spectroscopic techniques.

4.2.1 Binding Stoichiometry with Double-Stranded Oligonucleotide

Job's method of continuous variations is a commonly used procedure for determining the composition of complexes in solution. Despite the principle of continuous variation has been employed by several authors, this method is normally associated with the name of Job, who in 1928(339) published a detailed application of the method to study a wide range of coordination compounds. The method is based on plotting measured spectroscopic properties against mole fractions of the two constituents of a complex. Thus, a series of solutions are prepared by mixing different volumes of equimolar solutions of the two components and diluting to a constant volume, to give solutions having identical total molar concentrations. If a single stable complex is formed, a plot of absorvance *vs.* molar fraction of reactant gives a characteristic triangular plot, where the resulting curves, called Job's plot, yields a maximum (or a minimum) indicating the molar fraction value of the stoichiometric composition of the complex. However, a number of requirements must be satisfied in order for Job's method to be applicable. These requirements are:

i. the system must obey the Lambert-Beer's law;(343)
ii. complexation must predominate under the conditions of the experiment;(344)
iii. the total concentration of ligand and receptor must be maintained constant;
iv. pH and ionic strength must be maintained constant.(343)

Job plots (Figure 4.1) were determined for cryptolepine (**1**) and derivative **3v** complexing with the d(GATCCTAGGATC)$_2$ duplex in 0.01 M phosphate buffer at pH 7.4 containing 0.1 M NaCl. The sum of the concentrations of the ligand and oligonucleotide was kept constant at [oligonucleotide]+[Ligand]= 12.5 μM for **1** (UV-visible spectroscopy) or 2.5 μM for **3v** (fluorescence spectroscopy). For **1** the absorbance was measured at 368 nm, and for compound **3v,** fluorescence was measured at 483 nm (with an excitation wavelength of 339 nm). The crossover points were at ligand mole fractions of 0.67 (**1**) and 0.66 (**3v**) consistent with a ligand:oligonucleotide ratio of 2:1 for both complexes.

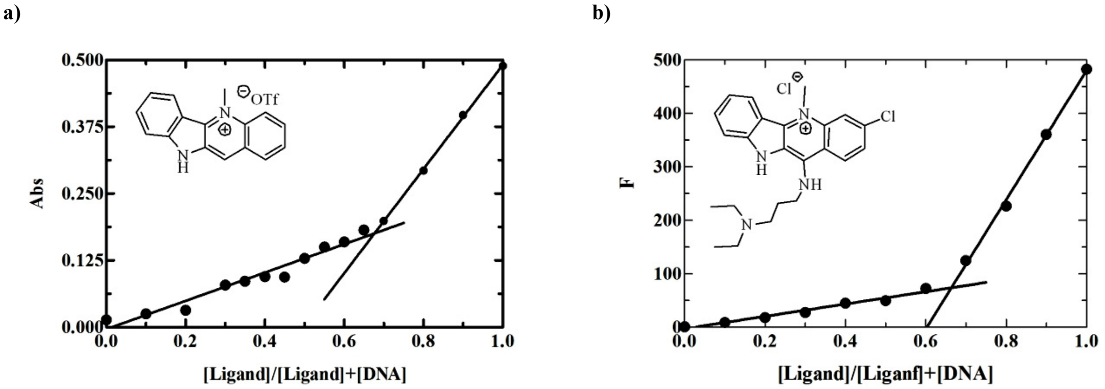

Figure 4.1 - Job plots for a) cryptolepine (**1**) and b) 3-chloro-5-methyl-11-(3-(diethylamino)propylamino)quindolinium chloride (**3v**) complexed with 12-mer ds oligonucleotide at 0.01 M phosphate buffer, 0,1 M NaCl at 25 ºC. The sum of the concentrations of the ligand and oligonucleotide was kept constant at [ds-DNA]+[Ligand]= 12.5 μM (for compound **1**) and 2.5 μM (for compound **3v**). For compound **1** absorbance was measured at 368 nm and for compound **3v**, fluorescence was measured at 483 nm with an excitation wavelength of 339 nm. The crossover points lie in 0.67 (**1**) and 0.66 (**3v**) consistent with a ligand:oligonucleotide ratio of 2:1.

The obtained experimental results confirm the anticipated binding stoichiometry to the double-stranded oligonucleotide that would be a 2:1 (ligand:DNA) complex with intercalation, if it were to take place, occurring preferentially in the two CC sites, according to the already published results for indolo[3,2-*b*]quinoline **1**.

4.2.2 Thermal Denaturation Studies with Double-Stranded Oligonucleotide

Due to the electronic absorption properties of a B-DNA(345) solution, the particular case of complexation between a drug and double-stranded nucleic acids, as well as its base content, can be characterized by melting temperature studies.(346-348) A typical UV-visible spectra for a DNA nucleotide has an absorption maximum at 260 nm with a molar extinction coefficient (ε) around 6000 $M^{-1}cm^{-1}$, as long as it is in B-DNA conformation. When the duplex is separated into single strands of DNA, such by heating or some other means, the absorption intensity at 260 nm is greatly increased, due to the large increase of ε at 260 nm in any single strand nucleotide. The reduced ε of double-stranded DNA resulted from the interactions of the π electrons between the aromatic residues when they are stacked vertically (hypochromism). Following the changes in the intensity measurement at 260 nm, during the heat denaturation, it is possible to monitor the extend of drug binding (particularly intercalation), because the base stacking should decrease as the event proceed. The resulting curve is called a "*melting curve*" of the DNA, as it refers to the dissociation of the duplex and the temperature at midpoint of the transition is called *melting temperature* (T_m), as shown in Figure 4.2, and varies according to base composition and the salt concentration in the solution.(349)

Since thermal denaturation studies investigate the ability of a compound to stabilize double-stranded DNA on heating, studies with cryptolepine (**1**) and derivatives (**3j, n** and **v**) with the 12-mer oligonucleotide sequence d(GATCCTAGGAT)$_2$ show that the compounds bind to the DNA. The ability of the ligands to stabilize the ds-DNA were monitored at 260 nm for a series of ligand/DNA ratios (0.5, 1, 2, 4 and 6) in 0.01 M phosphate buffer containing 0.1 M NaCl (Figure 4.3).

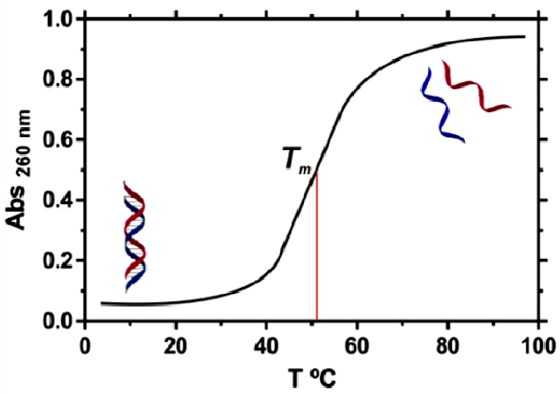

Figure 4.2 – A typical melting curve of double-stranded DNA

The values of T_m and ΔT_m for the ligand:ds-DNA complexes are collected in Table 4.1. The results show that all the compounds bind to the ds-DNA. In all cases, 2-state melting curves were observed and the transition remained sharp even through the T_m changes. Cryptolepine binds to the oligonucleotide sequence with moderate affinity (ΔT_m of 5-6 ºC), decreasing the thermal denaturation temperature, which indicates that cryptolepine destabilizes the DNA double strand, with no significant difference in binding on increasing the ligand to DNA ratio.

Table 4.1 – Melting temperatures (T_m) and their variation (ΔT_m) for d(GATCCTAGGATC)$_2$ (2.83 µM)-ligand (**1**, **3j**,**n**,**w**) complex, monitored at 260 nm in phosphate buffer pH 7.4 containing 0.1 NaCl, for a range of ligand concentrations.

Compound	R^1	R^2	R^3	T_m DNA alone	T_m / °C ΔT_m / °C		
					5.66 µM^a 2^b	11.31 µM^a 4^b	16.98 µM^a 6^b
No ligand	--	--	--	53 (±2)	--	--	--
1	H	H	H	--	48 (±2) 5	47 (±2) 6	48 (±2) 5
3j	H	H	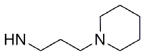	--	58 (±3) 5	61 (±2) 8	62 (±2) 9
3n	H	H	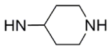	--	54 (±2) 1	55.4 (±0.6) 2.4	57 (±3) 4
3v	Cl	H	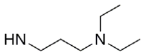	--	62 (±4) 9	64 (±2) 11	65 (±1) 12

$^{a)}$ Ligand concentration $^{b)}$ Ligand/DNA ratio

These results are not in agreement with previously reported for the binding of cryptolepine to calf thymus DNA and polyoligonucleotides,(17, 278) but can be explained by the small size and structural homogeneity of the oligonucleotide used in our experiments. On the other hand, compounds **3j**, **3n** and **3v**, increased the thermal denaturation temperature. This stabilizing effect is more pronounced for **3j** and **3v**, which show ΔT_m values ranging from 5 to 12 ºC. Overall, these results are in line with previous thermodynamic stability studies performed with N^5 methylated indoloquinolines (including **3b**, **3c**, **3f** and **3g**)$^{(291)}$ and others indoloquinolines,$^{(289)}$ which showed that both types of compounds are able to stabilise G-quadruplex DNA structures on heating.

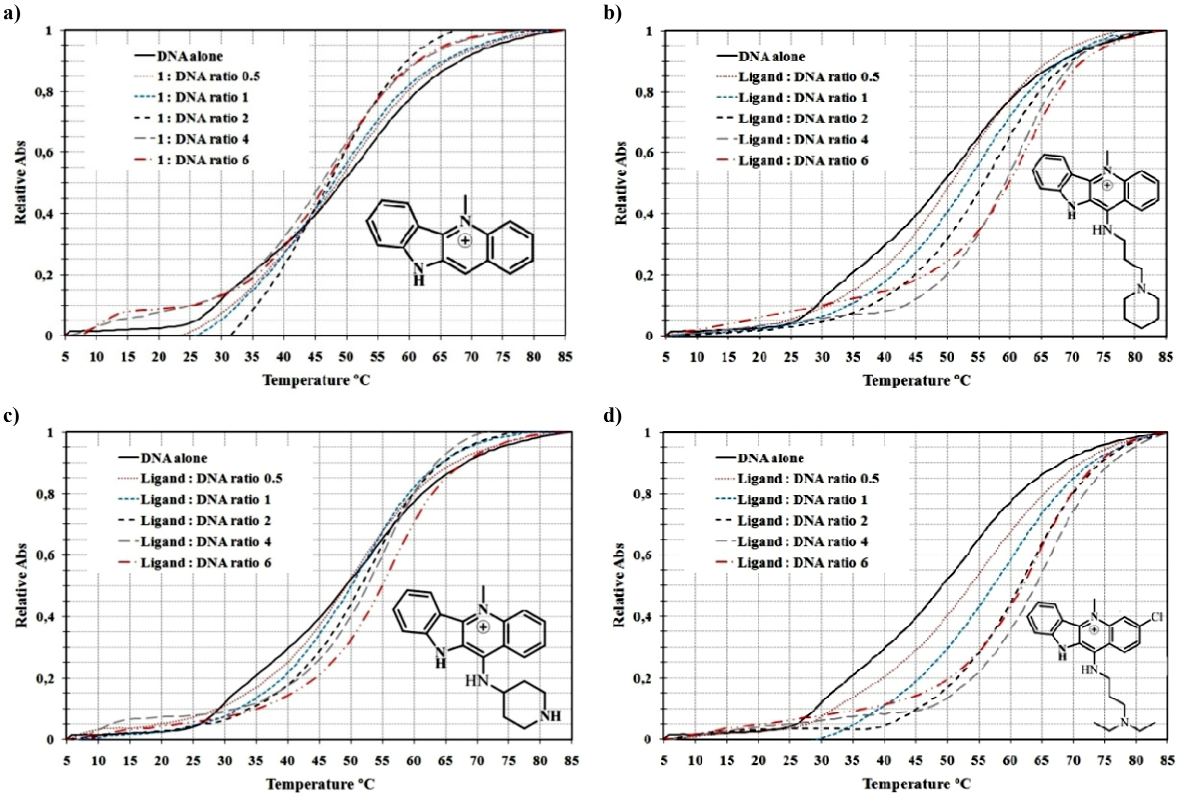

Figure 4.3 – Double strand DNA thermal melting monitored by UV absorbance at 260 nm in 0.01 M phosphate buffer containing 0.1 M NaCl, for a) **1** and cryptolepine derivatives b) **3j**, c) **3n** and d) **3v**. Melting curves represent ligand to DNA ratios of 0.5, 1, 2, 4 and 6.

4.2.3 Association Constants (K_{ass}) with Oligonucleotides

Association constants of cryptolepine and analogues with the studied oligonucleotides were obtained through a saturation analysis methodology, performed with spectroscopic binding titration technique.

$$K_{ass} = \frac{[C]}{[L][R]} \qquad L + R \underset{K_{diss}}{\overset{K_{ass}}{\rightleftharpoons}} C$$

Eq. 4.1 – Binding constant equation of a complexation process. (L - ligand, R – receptor; C - complex)

At the simplest scenario of binding equilibrium, the bimolecular association (one-site ligand binding), the equilibrium is described by Eq. 4.1 and when [L] = K_{diss} = 1/K_{ass}, then [L][R] = [R_t]/2, being the R_t the total receptor concentration. In other words, if the free concentration of L reaches the value of K_{diss} the receptor-binding sites will be half-saturated with ligand. The value of K_{diss} is one-half of the maximal binding (B_{max}). The free ligand concentration at 50% receptor saturation is a measure of K_{diss} (or 1/K_{ass}), determined in the saturation analysis (Figure 4.4), by non-linear regression analysis with Eq. 4.2.$^{(350)}$ Additionally, Eq. 4.2 can be formally analyzed by the Scatchard analysis that is summarized in the

Scatchard Plot, which in the case of a bimolecular interaction (one-site ligand binding), this should lead to a straight line with a negative slope.(351) In the Scatchard analysis the amount of bound ligand divided by the amount of free ligand in solution (*y*-axis) is plotted against the amount of bound ligand (*x*-axis), as represented in Eq. 4.3. The intercept point with *x*-axis represents the B_{max} value and the absolute value of slope represents the K_{diss} value.

Additionally, if a ligand can bind to the receptor in a number of different modes, then the binding of each mode is described by separate intrinsic binding constant. If L, R and C are involved in equilibrium in addition to what is defined by Eq. 4.1 and other possible equilibrium are not explicitly considered in the analysis of the interaction, then only an "apparent" dissociation constant (K_{obs}) will be obtained from the analysis of the binding interaction. This "apparent" dissociation constant will be a composite parameter reflecting all the multiple equilibriums.(350)

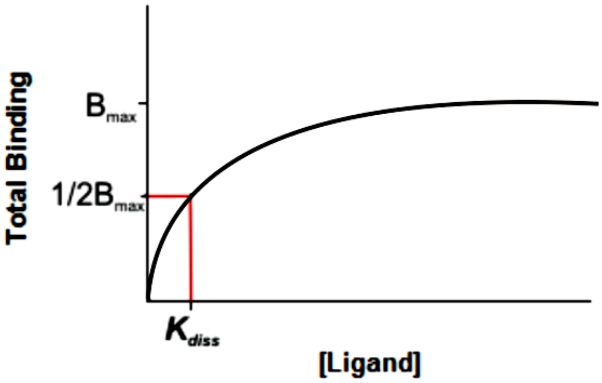

Figure 4.4 – Curve resulting from the saturation analysis of complexation between a ligand and a receptor (one-site ligand binding).

$$y = \frac{B_{max}[L]}{K_{diss} + [L]}$$

Eq. 4.2 – Saturated analysis non-linear equation of one-site ligand binding. (y = change in specific physicochemical property)

$$\frac{y}{[L]} = \frac{n}{K_{diss}} - \frac{y}{K_{diss}}$$

Eq. 4.3 – Scatchard equation of the saturated analysis of one-site ligand binding (n=1), or multiple-site ligand binding (n>1).

To determine if whether such multiples equilibriums exist, it is generally examined the ligand-receptor interactions over a range of ligand and receptor concentrations. If L and R are involved only in the equilibrium defined in Eq. 4.1, then the value of K_{obs} will be independent of L and R concentration. Otherwise, the "apparent" dissociation constant will be a function of the L and/or R and therefore will not represent the intrinsic association constant for the reaction in Eq. 4.1.(352) In addition, the experimental data can also be fitted to non-linear regression equations that describe another binding process than bimolecular association.

The two-site binding event describes one strong binding event, followed by a second weak binding event. Since the second binding event dissociation constant is much higher than the ligand concentration, this K^{2}_{diss} can be neglected, as a constant (the second term of Eq. 4.4 describe the linear drift of the two-site binding equation), allowing the achievement of K^{1}_{diss}, as deducted to Eq. 4.4.

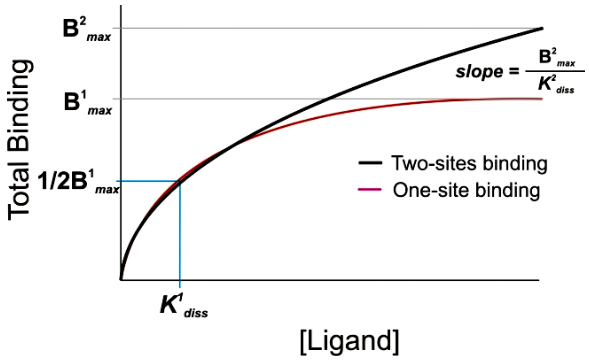

Figure 4.5 – Curve resulting from the saturation analysis of complexation between a ligand and a receptor (strong binding event followed by a weak binding event).

$$y = \frac{B^1_{max}[L]}{K^1_{diss} + [L]} + \frac{B^2_{max}[L]}{K^2_{diss} + [L]} \qquad \text{if } K^2_{diss} >> [L]$$

$$y = \frac{B^1_{max}[L]}{K^1_{diss} + [L]} + \frac{B^2_{max}[L]}{K^2_{diss}} \qquad \frac{B^2_{max}}{K^2_{diss}} = C$$

$$y = \frac{B^1_{max}[L]}{K^1_{diss} + [L]} + C[L]$$

Eq. 4.4 – Saturated analysis non-linear equation of the two-site ligand binding (strong binding event followed by a weak binding event).

Cryptolepine

Double-stranded oligonucleotide

The absorbance titration spectra of **1** in phosphate buffer pH 7.4 at 25 ºC and containing 0.1 M of NaCl (Figure 4.6) was used to determine its association constant (K_{ass}) to ds-DNA. Bathochromic and hypochromic shifts were observed on addition of oligonucleotide to **1**.

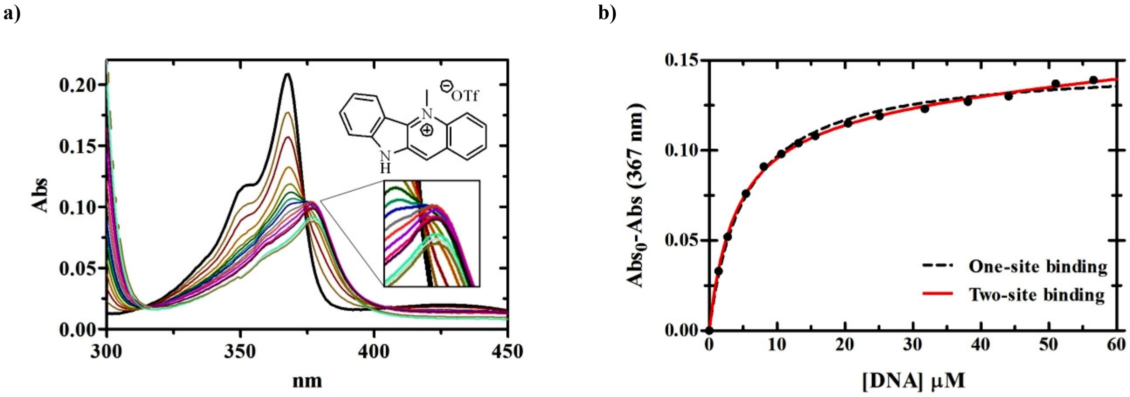

Figure 4.6 – a) UV-visible spectra changes at 25.0 ºC on titration of cryptolepine, **1** (5 µM) with the 12-mer sequence DNA in 0.01 M phosphate buffer at pH 7.40 containing 0.1 M NaCl; b) Plot of the absorbance at 367 nm *vs.* [ds-DNA] and the fits to binding models for one- and two-sites binding. The points are experimental: the lines are best fit to the two-site binding model. The expanded box show details of the data in the region of the 374 nm isosbestic point. The DNA:Ligand ratio increase as follows: 0 (black bold line), 0.2, 0.5, 1.0, 1.6, 2.1, 2.6, 3.1, 4, 5, 6.4, 7.6, 8.8, 10.2, 11.3 and 12.3, sequentially from the top in the region of 367 nm.

A shift from 367 to 377 nm and about 60 % hypochromicity was determined for the 367 nm peak at high DNA:ligand ratios. Sharp isosbestic points were present at 374, 405 and 460 nm for DNA:Ligand ratios from 0 to 2.6, which represents a region of relatively strong binding of the ligand to the DNA. Further increases of DNA in solution caused the isosbestic point shift, indicating a second weak binding process at higher DNA concentrations, seen as a linear drift in the Abs at 367 nm values plotted in Figure 4.6b. Thus, binding of **1** to d(GATCCTAGGATC)$_2$ has at least two types of binding sites evident from the two regions (strong binding + linear drift).

The data at 367 nm, the maximum absorbance wavelength, fitted to two-sites binding model gave an association constant of 0.25±0.01 $x10^6$ M^{-1} for the stronger binding process. The data at 377 nm, the appearance of the new peak, also fit to the binding equation but with a K_{ass} of 0.21±0.03 $x10^6$ M^{-1} and as ds-DNA concentration increases (>20 μM), the absorbance decreases showing additional classes of weak binding site.

The absorbance data at 374 nm (isosbestic point) for concentration larger than 20 μM (DNA:ligand ratios higher than 4.0) does not fit to any binding equation, hindering the determination of the second association constant for the weaker binding process.

These results suggest two independent and non-cooperative types of binding as previously reported.(6) Although, the K_{ass} determined for the strongest binding process to the 12-mer ds-DNA is 10-fold weaker (0.25±0.01 $x10^6$ M^{-1}) than the K_{ass} reported for cryptolepine binding to calf thymus DNA (3 $x10^6$ M^{-1})(6), although still in the range of a typical association constant for intercalating agents, 10^3 - 10^6.(7, 353) The spectrofluorometric assay failed with **1** because no quenching was observed with increasing concentrations of the oligonucleotide.

The K_{ass} of **1** with 12-mer double-stranded $d(GATCCTAGGATC)_2$ oligonucleotide in phosphate buffer pH 7.4 containing 1 M of NaCl was also determined. Cryptolepine maintains its binding capabilities to ds-DNA at high ionic strength solutions (1 M NaCl), showing a 40 % hypochromicity in absorbance at 367 nm and no shift in λ_{max} (Appendix G), with an association constant of 0.10±0.01 $x10^6$ M^{-1}.

Single-stranded oligonucleotide

UV-visible spectrophotometric titration analysis of **1** with 16-mer single-stranded d(5'-GCCAAACACAGAATCG-3') oligonucleotide in phosphate buffer pH 7.4 containing 0.1 and 1 M of NaCl were also determined. However, no bind to single-stranded oligonucleotides was verified in solutions containing 0.1 M of NaCl (Figure 4.7) or in solutions containing 1 M NaCl. These results show that cryptolepine was not able to bind to single-stranded oligonucleotide and interact with DNA structures mainly through intercalation. Moreover, intercalation binding mode is reinforced since binding of cryptolepine to double-stranded was not destroyed at high ionic strength solutions, showing that electrostatic interaction do not play a major rule in complex stability.(325) These results are in good agreement with what is already known,

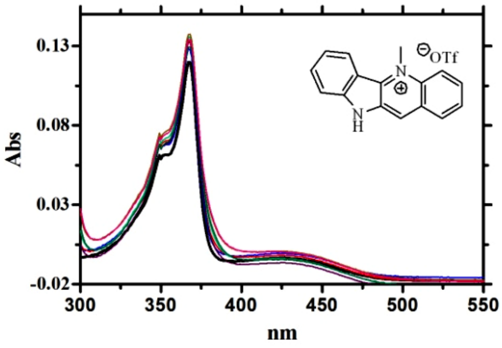

Figure 4.7 – UV-visible spectra of the titration of **1** with the 16-mer single-stranded oligonucleotide in 0.01 M phosphate buffer containing 0.1 M NaCl at 25 ºC. The concentration of cryptolepine was 5 μM and the DNA:Ligand ratio increase as follows: 0 (black bold line), 0.25, 0.50, 0.75, 1.00, 1.25, 1.50 and 1.75.

since cryptolepine bind to DNA structures mainly through π-π stacking interactions and in absence of hydrogen bonding interactions.(5)

Cryptolepine derivatives

Double-stranded oligonucleotide

The association constants for cryptolepine derivatives with the 12-mer ds-DNA were assessed by spectrophotometry or by spectrofluorometry titrations. All titration spectra were recorded at an excitation wavelength of 339 nm. Emission of compounds **3** in aqueous solutions was proportional to their concentrations up to 20 μM, indicating that there is no significant intermolecular stacking which would give rise to a quenching effect. The fluorescence titration spectra of compounds **3** with d(GATCCTAGGATC)$_2$ showed in general a 4-10 nm shifts on addition of DNA and 50-65 % quenching. The best fit of emission data from compounds **3a-y** to one- or two-site binding models gave the association constant, K_{ass}, values presented in Table 4.2.

For instance, Figure 4.8a shows the absorbance titration spectra of **3n** on sequential addition of d(GATCCTAGGATC)$_2$. Bathochromic (5 nm) and hypochromic (≈ 50 %) shifts were observed at higher DNA/ligand ratios for the maximum absorption band at 356 nm. Two isosbestic points at 365 and 458 nm were observed for the ds-DNA concentration range of 0 to 4.18 μM. Shifts at higher concentrations indicate a second weaker type of binding.

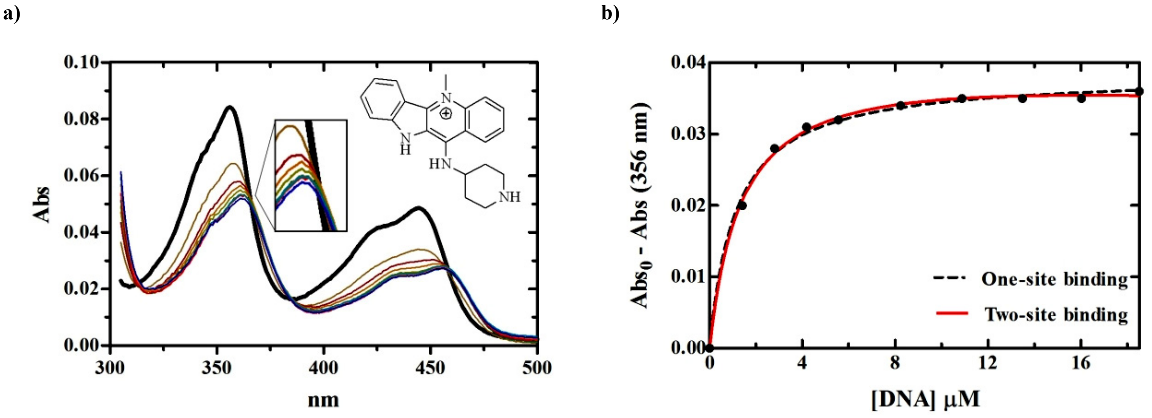

Figure 4.8 – a) UV-visible spectral changes at 25.0 °C on titration **3n** (5.00 μM) with added aliquots of 12-mer d(GATCCTAGGATC)$_2$ oligonucleotide duplex in 0.01 M phosphate buffer at pH 7.40 containing 0.1 M NaCl; The expanded box shows detail of the data in the region of the 365 nm isosbestic point. The ds-DNA:Ligand ratio increase as follows: 0 (black bold line), 0.3, 0.6, 0.8, 1.1, 1.6, 2.2, 2.7, 3.2 and 3.7, sequentially from the top spectrum in the region around 356 nm. b) Plot of absorbance at 356 nm *vs.* [ds-DNA] and the fits to binding models for 1 and 2 sites. The points are experimental; the lines are best fit to the two-site binding model.

The plot of absorbance maximum at 356 nm *vs.* [ds-DNA] appears equally well fit to two-site model (R^2 = 0.9982) when compared with the one-site binding model (R^2 = 0.9966), giving an association constants for the stronger binding process of 0.72 x10^6 M^{-1} with two-site model and an association constant of 0.87 x10^6 M^{-1} with one-site model. In order to make an accurate comparison between both methods an F-test were performed with GraphPad software. The F test compares the fit of two equations, where the more complicated equation (two-site binding) fits better (has a smaller sum-of-squares) than the simple equation.(354) The analysis gave an F value of 6.327 which means that the two-site binding mode is the preferred, when compared with one-site binding model (one-site model would be preferred if F value is around 1).To obtain the second association constant, the data at 365 nm (isosbestic point) for ds-DNA concentrations higher than 5 µM (after disappearance of the isosbestic point) was analysed. However, the experimental data does not fit to any binding equation, hindering the determination of the second dissociation constant, for the weaker binding process.

To demonstrate equivalence between the UV-visible and fluorescence spectroscopic methods, compound **3n** was also titrated by spectrofluorometry. The spectrofluorometric titration of **3n** with ds-DNA at 0.01 M phosphate buffer at 25 ºC and containing 0.1 M NaCl is presented in Figure 4.9. The fluorescence titration spectra of **3n** (Figure 4.9a) with ds-DNA shows an 4 nm shift on addition of DNA and about 60 % quenching, due to complex formation. The fitting of the fluorescence experimental data of **3n** to the binding equations (Eq. 4.2 and Eq. 4.4) showed a slightly higher goodness of fit (R^2) to the two-site binding equation ($R^2 = 0.9996$) than to the one-site binding equation ($R^2 = 0.9993$) and F value of 5.151. Thus, an association constant (K_{ass}) for the stronger binding process of 0.74 x10^6 M^{-1} was established with the two-site binding model (Figure 4.9b). These results are in good agreement with those obtained using spectrofluorometric titrations, showing that the methods are equivalent.

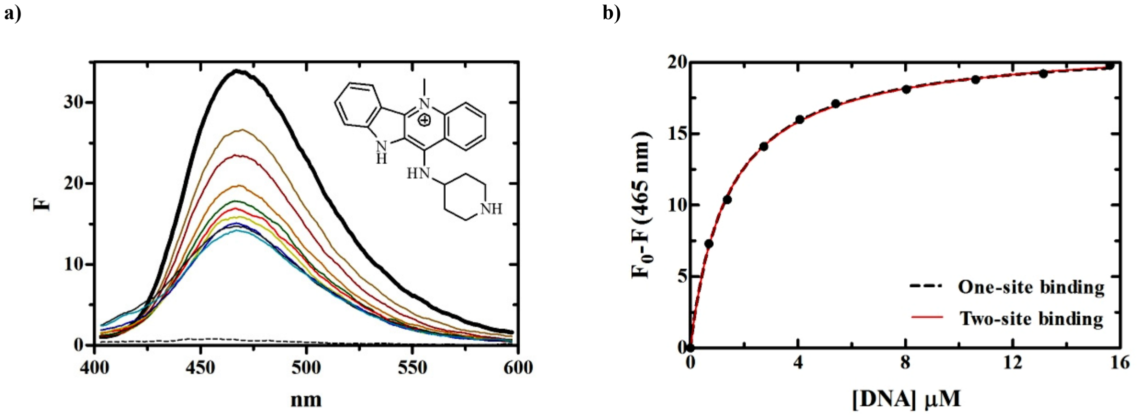

Figure 4.9 – a) Fluorescence emission spectra of **3n** (5 µM): the DNA:Ligand increased as follows: 0 (black bold line), 0.3, 0.5, 0.8, 1.1, 1.6, 2.1, 2.6 and 3.1 sequentially from the top spectrum into the region of 465 nm (the curve with strongest emission, around 465 nm was ligand **3n** in the absence of ds-DNA). b) Plot of emission at 465 nm *vs.* [ds-DNA] and the fits to binding models for 1 and 2 sites. The points are experimental: the lines are best fit to the two-site binding model.

Association constants for **3c** and **3t** with the duplex were also determined in 0.01 M phosphate buffer pH 7.4, but with different concentrations of NaCl. For **3c**, 0.01 M NaCl was used, and for **3t**, 1M NaCl. The binding affinity of **3c** to ds-DNA increase (K_{ass} = 2.0±0.4 x10^6 M^{-1}) when compared to those in 0.1 M NaCl (K_{ass} = 1.14±0.05 x10^6 M^{-1}). On the other hand, ds-DNA binding was destroyed at 1 M NaCl for **3t** as there was no change in emission fluorescence spectra at 460 nm with increase in oligonucleotide concentration up to 1 µM. Thus, it seems that ionic strength of the solution strongly influences the binding of the cryptolepine derivatives to double-stranded oligonucleotides, showing that electrostatic interactions do play a major rule in complex stability.

Single-stranded oligonucleotide

The K_{ass} for **3n** with the 16-mer single strand oligonucleotide d(GCCAAACACAGAATCG) in 0.01 M phosphate buffer (pH 7.4) containing 0.1 M NaCl at 25 ºC was calculated by UV-visible spectrophotometry titration (Appendix G). The UV-visible spectrophotometry titration with 16-mer oligonucleotide showed 40 % of hypochromicity in the absorbance at 358 nm with a shift of 5 nm. Sharp isosbestic points were present at 366, 388 and 459 nm representing a relatively strong binding of the ligand to the DNA.

Table 4.2 – Association constants for complexes between cryptolepine (**1**) and derivatives **3a-y** with ds-DNA at 25 ºC in 0.01 M phosphate buffer pH 7.4 containing 0.1 M NaCl.

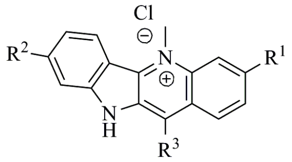

	R^1	R^2	R^3	K_{ass} (ds-DNA) (x10^{6} M^{-1})		R^1	R^2	R^3	K_{ass} (ds-DNA) (x10^{6} M^{-1})
1	H	H	H	0.25±0.01 [b,c]	**3m**	H	H	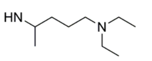	4.3±0.2 [b,d]
3a	H	H	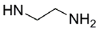	0.85±0.01 [a,c]	**3n**	H	H	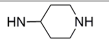	0.74±0.03 [b,d]
3b	H	H	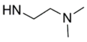	3.1±0.7 [a,d]	**3o**	H	H	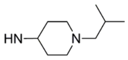	0.74±0.07 [a,d]
3c	H	H	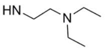	1.14±0.05 [a,d]	**3p**	H	H	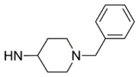	0.68±0.09 [a,d]
3d	H	H	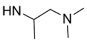	1.9±0.1 [a,d]	**3q**	H	H	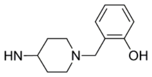	0.6±0.3 [b,d]
3e	H	H	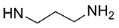	0.25±0.01 [a,c]	**3r**	H	H	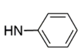	0.51±0.06 [a,c]
3f	H	H	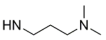	3.0±0.2 [a,d]	**3s**	H	H	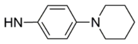	3.4±0.6 [b,d]
3g	H	H	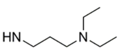	9.1±0.6 [a,d]	**3t**	H	H	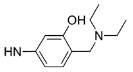	0.8±0.3 [b,d]
3h	H	H	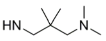	2.6±0.4 [a,d]	**3u**	H	H	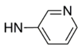	1.0±0.1 [a,d]
3i	H	H	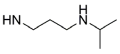	5.0±0.8 [a,d]	**3v**	Cl	H	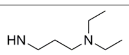	17±1 [a,d]
3j	H	H	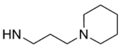	5.3±0.3 [b,d]	**3w**	Cl	H	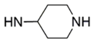	4.5±0.4 [a,d]
3k	H	H	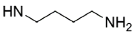	1.4±0.1 [a,c]	**3x**	Cl	Cl	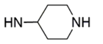	1.6±0.4 [b,d]
3l	H	H	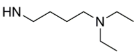	9±1 [a,d]	**3y**	H	H	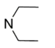	0.47±0.06 [a,c]

a) One-site binding model; **b)** Two-site binding model; **c)** Determined by UV-Visible spectrophotometry; **d)** Determined by spectrophotofluorimetry with excitation wavelength of 339 nm.

The fitting of the UV-visible data to the two-sites binding model gave an K_{ass} of 0.370 ± 0.001 x10^{6} M^{-1} for the stronger binding process. Thus, cryptolepine derivative **3n** and probably all the cryptolepine derivatives, maintain its binding capabilities to single-stranded oligonucleotides, like in double-stranded oligonucleotides. This results point out that intercalation binding mode is not probably, the main driving interaction in complex stabilization with double-stranded oligonucleotides.

SAR with double-stranded oligonucleotides

All the tested cryptolepine derivatives (**3a-y**), reveal stronger affinity for the 12-mer DNA oligonucleotide d(GATCCTAGGATC)$_2$ than the lead compound **1**. The analysis of the structure-activity relationship in cryptolepine derivatives, **3a-y** complex formation with 12-mer DNA oligonucleotide revealed:

Side chain length: no consistent variation between association constants of derivatives with two (**3a-d**) tree (**3e-j**) and four (**3k-m**) carbon side chains at position C11 of the cryptolepine nucleus was verified.

Terminal nitrogen substitution: substitution on terminal nitrogen does not modulate the binding affinity to DNA, nor the type of substituents (alkyl or cycloalkyl) neither if it is a secondary or tertiary amine.

Branched side chains: introduction of ramifications in the side chain (**3d,h,m**) slightly decrease the association constants for complex formation when compared with those of counterparts **3c,f,l**, respectively.

Alkyl, cycloalkyl and aromatic side chains: compounds with less flexible alkyl side chains such as piperidine (**3n-q**) showed lower binding affinity with 12-mer oligonucleotide and the changing of terminal nitrogen from a secondary amine (**3n**) to a tertiary amine (**3o-q**) do not introduces significant differences in the association constants. Additionally, aromatic side chains showed K_{ass} to double-stranded oligonucleotides comparable with those of cycloalkyl compounds with exception of **3s**.

Halogen substitution in the aromatic nucleus: introduction of one halogen on the aromatic nucleus of the cryptolepine derivatives at position 3 (**3v-w**), dramatically increases the association constants and the introduction of a second halogen in position 8 (**3x**) decreases the K_{ass} to values almost equivalent to the counterpart with no halogens substitution.

Side chains without basic nitrogen: side chains without a terminal amine moiety (**3r** and **3y**) gave K_{ass} comparable to those with piperidine side chains. However, the lowest K_{ass} of this type of compounds (**3r**, 0.51 x10^6 M^{-1}) was found for a compound without terminal nitrogen in the side chain, reducing probably, the electrostatic interactions with the DNA backbone.

In general, compounds with linear side chains show higher binding affinities than the ones with cycloalkyl or aromatic chains. These can probably be explained by the higher flexibility of the side chain, interacting more effectively with the phosphate backbone and/or bases pairs of the DNA sequence, increasing the electrostatic interactions. Rigid side chains are probably unable to permit the desired favourable interactions with DNA due to their reduced degree of freedom.(355) Taken together, cryptolepine derivatives **3** bind strongly to 12-mer ds-DNA as well as to ss-DNA and these bindings were destroyed at high ionic strength solutions. These observations, together with the binding stoichiometry, indicate that complexation of compounds **3** to DNA involves the simultaneous a non-intercalative binding of two equivalents of ligand per equivalent of oligonucleotide and would suggests a strong influence of ionic and hydrogen bonding interactions, in particular with the phosphate backbone, due to the polyelectrolyte nature of DNA.

4.3 Interactions of Cryptolepine and Quindolone Derivatives with Haematin

Binding stoichiometry of the indolo[3,2-*b*]quinolines were obtained with the Job's methodology of continuous variations(339-342) by means of UV-visible spectrophotometric experiments. The binding properties of **1** and developed derivatives **3**, as well as quindolones **4**, **91** and its derivatives **5**, **94** and **95** to haematin monomer (FIPX-OH) were obtained through the described spectroscopy technique. However, the experimental data obtained from the Job's method of continuous variation did not give a direct Job's plot, being necessary to correct the absorbance according to the equation $y = -\{A-(\varepsilon FPIX\text{-}OH[FPIX\text{-}OH]+ \varepsilon_{compound}[compound])b\}$, where A is the measured absorbance, εFPIX-OH and $\varepsilon_{compound}$ are the molar absorptivities of hematin and indolo[3,2-*b*]quinolines, and b the optical path length.**(342)** All the UV-visible experiments were monitored in the Soret region of the haematin spectrum at the wavelength of 402 nm.(356) The Soret band is very strong absorption band in the blue region of optical absorption spectrum of a porphyrin.(357)

4.3.1 Binding stoichiometry

Cryptolepine and derivatives

Job's methodology of continuous variation of cryptolepine (**1**), chloroquine (**2**) and cryptolepine derivatives **3c** and **3n** complexed with haematin in HEPES buffer pH 5.5 containing 40 % DMSO, in order to minimize porphyrin aggregation and μ-oxo dimer formation, were performed using UV-visible spectroscopy.(122, 145-146, 358-359) Job's plots were obtained after correction of the measured absorbance (Figure 4.10).(342)

The sum of the concentrations of the FPIX-OH and ligand was kept constant at [FPIX-OH]+[Ligand]= 10 μM. The absorbance was monitorized at the Soret band of FPIX-OH (λ = 402 nm).(356) The cross points were at FPIX-OH mole fractions of 0.52 (**1**), 0.51 (**2**), 0.49 (**3c**) and 0.60 (**3n**), consistent with a FPIX-OH:ligand ratio of 1:1 for the complexes.

However, for chloroquine, some authors reported, based in mathematical expressions, the stoichiometry of complexation between FPIX-OH and chloroquine to be 1:2 (**2**:FPIX-OH).(146) Nevertheless, Egan and co-workers(360) reported that this stoichiometry only occur at lower ratios of **2** to

FPIX-OH, while at higher ratios, the 1:1 complex would be expected to predominate, as found in our Job's methodology assay.

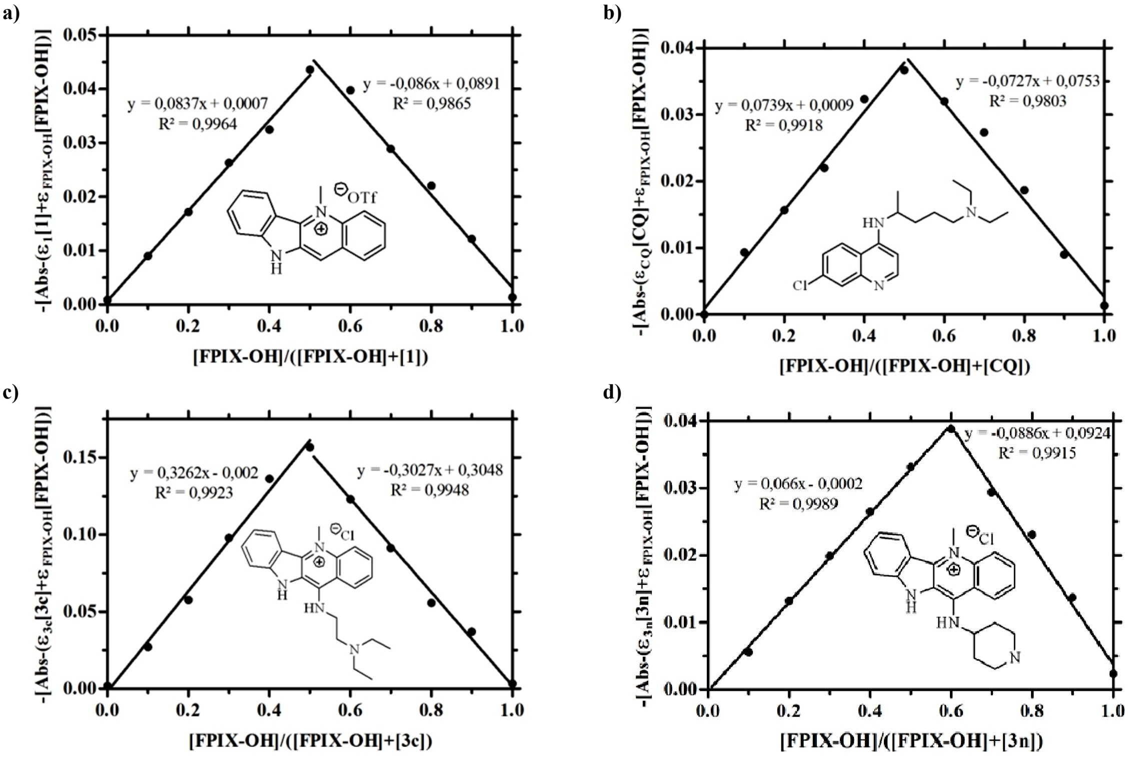

Figure 4.10 – Job plots for a) cryptolepine (**1**), b) chloroquine (**2**), c) derivative **3c** and d) **3n** complexed with FPIX-OH in buffered 40 % DMSO, pH 5.5 at 25 ºC. The sum of the concentrations of the ligand and FPIX-OH was kept constant [ligand]+[FPIX-OH]=10 μM. The absorbance changes of the Soret band was measured at 402 nm. y-axes is the corrected absorbance ($y = -\{A-(\varepsilon_{FPIX\text{-}OH}[FPIX\text{-}OH]+\varepsilon_{compound}[compound])b\}$), where A is the measured absorbance, $\varepsilon_{FPIX\text{-}OH}$ and $\varepsilon_{compound}$ are the molar absorptivities of hematin and **1**, **2**, **3c** and **3n**, and b the optical path length.(342)

Quindolones and derivatives

Job's plots of quindolone (**4**), and derivatives (**5a**, **94a** and **95a**) complexed with haematin monomer in the same experimental conditions described for cryptolepine and derivatives were used to determine the complexation stoichiometry (Figure 4.11). Also, the sum of the concentrations of the FPIX-OH and ligand was kept constant at [FPIX-OH]+[Ligand]= 10 μM. The cross points were at FPIX-OH mole fractions of 0.49 (**4**), 0.52 (**5a**), 0.58 (**94a**) and 0.52 (**95a**) consistent with a FPIX-OH:ligand ratio of 1:1 for the complexes.

4.3.2 Association Constants (K_{ass}) with Haematin

Association constants of the indolo[3,2-*b*]quinolines with haematin monomer, in pH 5.5 HEPES buffer (40% DMSO) were obtained through a saturation analysis methodology and employed to establish the binding affinity of cryptolepine, quindolones and derivatives to haematin. Additionally, and for comparison purposes, the association constant of chloroquine was also established with the same methodology. In the used concentration range, FPIX-OH solutions obey the Beer-Lambert law, indicating that further haeme aggregation and/or precipitations do not occur under the experimental conditions. Like performed for DNA (4.2.3), the absorbance was plotted as a function of drug concentration.

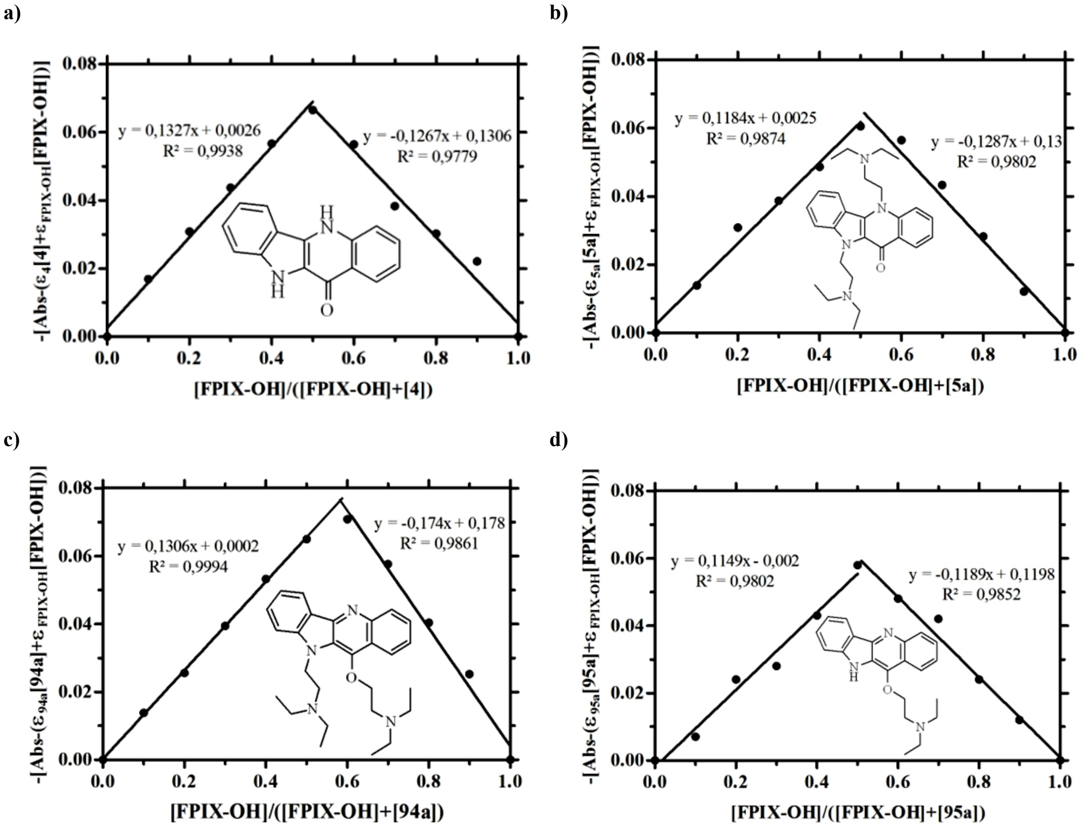

Figure 4.11 – Job plots for a) quindolone (**4**) and derivatives b) **5a**, c) **94a** and d) **95a** complexed with FPIX-OH in buffered 40 % DMSO, pH 5.5 at 25 ºC. The sum of the concentrations of the ligand and FPIX-OH was kept constant [ligand]+[FPIX-OH]=10 μM. The absorbance changes of the Soret band was measured at 402 nm. y-axes is the corrected absorbance ($y = -\{A-(\varepsilon_{compound}[compound]+\varepsilon_{FPIX-OH}[FPIX-OH])\}$), where A is the measured absorbance, $\varepsilon_{FPIX-OH}$ and $\varepsilon_{compound}$ are the molar absorptivities of hematin and **4**, **5a**, **94a** and **95a**, and b the optical path length.(342)

The binding affinity of indolo[3,2-*b*]quinolines to haematin were investigated using a 1:1 stoichiometric complexation model, as previously reported for xanthones(361), quinolines(360) and other drugs(362) (Figure 4.12). The UV-visible experimental data was fitted to the binding equation (Eq. 4.5)(20) describing a 1:1 stoichiometry complexation, in order to attain the association constants (K_{ass}) with FPIX-OH.

Chloroquine

UV-visible titrations of FPIX-OH with **2** clearly cause hypochromic shifts (≈ 50%) on the Soret band of FPIX-OH, as shown in Figure 4.13a. Two possible processes can be envisaged which would lead to this effect:

1. addiction of the quinoline induces aggregation of FPIX-OH;
2. changes reflect quinoline association with FPIX-OH.

However, Shelnutt⁽³⁶³⁾ has shown that association of methyl viologen di-cation with Fe(III)uroporphyrin cause ca. 75% of hypochromicity on the Soret band without aggregation, giving the evidence for π-π stacking interactions.

The UV-visible titration experimental absorbances at 402 nm (Soret band) were analyzed and fitted to Eq. 4.5, as shown in Figure 4.13b. Chloroquine gave excellent fitting results with a goodness of fit (R^2) of 0.997 and association constant of 0.085±0.005 x10^6 M^{-1}, comparable to the values already reported in the literature (K_{ass} = 0.039 x10^6 M^{-1}(146) or 0.32 x10^6 M^{-1}(364)).

$$\text{FPIX-OH} + \text{IQ} \xrightleftharpoons{K_{ass}} \text{FPIX-OH-IQ}$$

Figure 4.12 – Models of binding between indolo[3,2-*b*]quinolines and haematin monomers.

$$A = \frac{A_0 + A_\infty K_{ass}[L]}{1 + K_{ass}[L]}$$

Eq. 4.5 - Binding equation between one haematin monomer with one molecule of ligand. (A=absorbance, A_0 = Absorbance without ligand, A_∞ = absorbance for haem complex, K_{ass} = association constant, L = concentration of ligand).

Cryptolepine

The UV-visible spectra obtained after titration of FPIX-OH with cryptolepine also caused hypochromic shifts (≈ 20%) on the Soret band, as shown in Figure 4.13c. The UV-visible experimental absorbances at 402 nm (Soret band) were analyzed and fitted to Eq. 4.5 as shown in Figure 4.13d. As chloroquine, cryptolepine gave excellent fitting results to the binding equation, with a goodness of fit (R^2) of 0.997 and it was established an association constant (K_{ass}) with haematin monomer, in pH 5.5 phosphate buffer containing 40 % DMSO, of 0.045±0.003 x10^6 M^{-1}.

Cryptolepine derivatives

UV-visible titration spectral data of FPIX-OH with cryptolepine derivative **3n** is shown in Figure 4.13e. Addition of **3n** to FPIX-OH solution clearly cause hypochromic shifts (≈ 30%) and the data fitted to Eq. 4.5 gave an association constant of 0.154±0.006 x10^6 M^{-1}.

FPIX-OH titration data with cryptolepine derivatives (**3**) was also investigated. The data for all the cryptolepine derivatives, forms closely to the model were one ligand associates with one FPIX-OH, with a goodness of fit (R^2) varying from 0.993 to 0.999, in agreement with a 1:1 complexation found in the continuous variation technique (Section 4.3.1). Association constants of **3** with haematin monomer are shown in Table 4.3. Comparison of the results with other well known polycyclic drugs that complex with haematin, like acridines(365-366) and quinolines,(123, 126, 360, 367) suggests that the main interaction of the porphyrin ring system with the indolo[3,2-*b*]quinolines could be π-π stacking interactions as well as electrostatic.

Cryptolepine and its derivatives share with chloroquine the capability to interact with FPIX-OH monomer through π-π stacking interactions.(363) The K_{ass} of cryptolepine derivatives (**3**) with haematin showed that **3** have enhanced binding ability of five- to ten-fold when compared with the parent compound **1**, with K_{ass} values ranging from 0.062 to 0.41 x10^{6} M^{-1}.

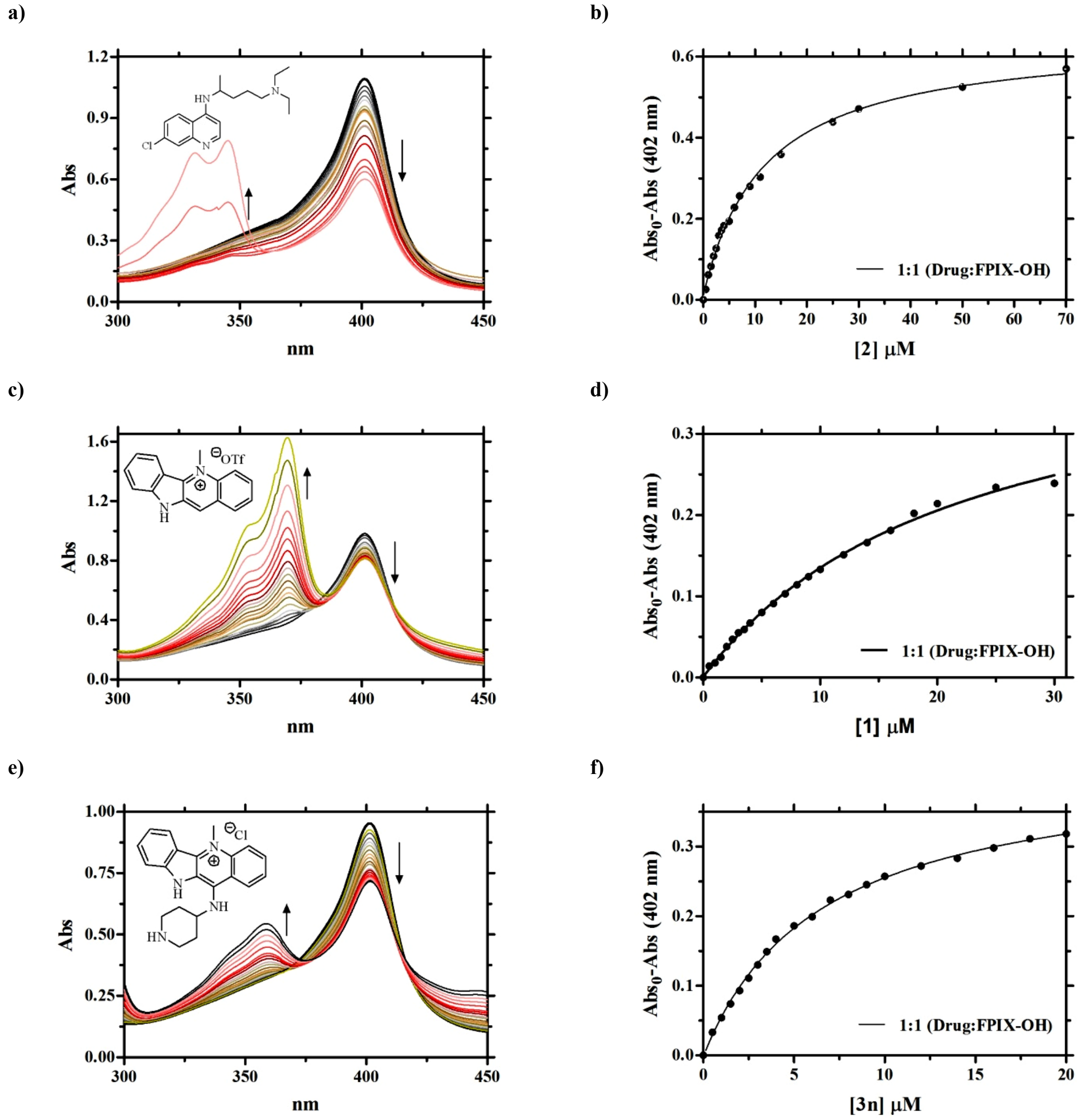

Figure 4.13 – **a)** UV-visible spectral changes at 25.0 °C on titration of haematin (10 µM) with chloroquine (**2**) in HEPES buffer pH 5.5. The **2**:haematin ratio increase as follows: 0 (black bold line), 0.05, 0.1, 0.15, 0.2, 0.25, 0.3, 0.35, 0.4, 0.5, 0.6, 0.7, 0.8, 0.9, 1.1, 1.5, 2.5, 3, 5 and 7, sequentially from the top spectrum in the region around 402 nm. **b)** Fitting to 1:1 drug:FPIX-OH complex (model 1) of the absorbance at 402 nm *vs.* [2]. The points are experimental: the lines are best fit to binding model for 1:1 drug:FPIX-OH. **c)** UV-visible spectral changes at 25.0 °C on titration of haematin (10 µM) with cryptolepine (**1**) in HEPES buffer pH 5.5. The **1**:haematin ratio increase as follows: 0 (black bold line), 0.05, 0.1, 0.15, 0.2, 0.25, 0.3, 0.35, 0.4, 0.5, 0.6, 0.7, 0.8, 0.9, 1, 1.2, 1.4, 1.6, 1.8, 2.0, 2.5, 3, sequentially from the top spectrum in the region around 402 nm. **d)** Fitting to 1:1 drug:FPIX-OH complex (model 1) of the absorbance at 402 nm *vs.* [**1**]. **e)** UV-visible spectral changes at 25.0 °C on titration of haematin (10 µM) with **3n** in HEPES buffer pH 5.5. The **3n**:haematin ratio increase as follows: 0 (black bold line), 0.05, 0.1, 0.15, 0.2, 0.25, 0.3, 0.35, 0.4, 0.5, 0.6, 0.7, 0.8, 0.9, 1, 1.2, 1.4, 1.6, 1.8, 2.0 , sequentially from the top spectrum in the region around 402 nm. **f)** Fitting to 1:1 drug:FPIX-OH complex (model 1) of the absorbance at 402 nm *vs.* [**3n**]. The points are experimental: the lines are best fit to binding model for 1:1 drug:FPIX-OH.

SAR with haematin monomer

The introduction of an alkylamine side chain in position C11 of the indolo[3,2-*b*]quinoline aromatic nucleus increases the binding potency, however no significant structure-activities relationships can be drawn from the results.

Side chain length: there is no consistent variation in K_{ass} when alkyl side chain length is changed from two to four carbons, to cycloalkyl or aryl. These results are in line with a study developed by Egan and co-works(132)with 4-aminoquinolines in which, it was shown that the side chains length or substitution do not play a major rule in the 4-aminoquinoline:FPIX complex formation and suggesting that in most of the cases do not interact strongly with FPIX.

Table 4.3 – Association constants for complexes between cryptolepine (**1**), chloroquine (**2**) and cryptolepine derivatives **3a-y** with haematin monomer at 25 ºC in pH 5.5 HEPES buffer.

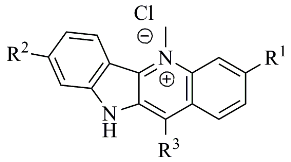

	R1	R2	R3	Haematin binding K_{ass}[a] (x10^6 M^{-1})		R1	R2	R3	Haematin binding K_{ass}[a] (x10^6 M^{-1})
2	--	--	--	0.085±0.005					
1	H	H	H	0.045±0.003	**3m**	H	H	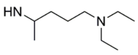	0.062±0.07
3a	H	H	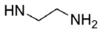	0.127±0.007	**3n**	H	H	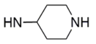	0.154±0.006
3b	H	H	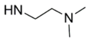	0.120±0.005	**3o**	H	H	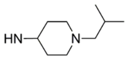	0.227±0.008
3c	H	H	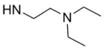	0.41±0.03	**3p**	H	H	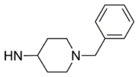	0.125±0.007
3d	H	H	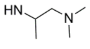	0.148±0.008	**3q**	H	H	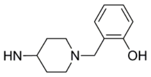	0.108±0.005
3e	H	H	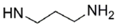	0.18±0.02	**3r**	H	H	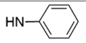	0.155±0.008
3f	H	H	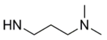	0.066±0.005	**3s**	H	H	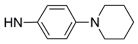	0.21±0.02
3g	H	H	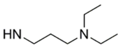	0.127±0.007	**3t**	H	H	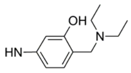	0.075±0.009
3h	H	H	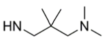	0.069±0.007	**3u**	H	H	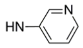	0.17±0.01
3i	H	H	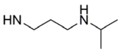	0.20±0.01	**3v**	Cl	H	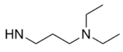	0.11±0.01
3j	H	H	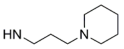	0.161±0.008	**3w**	Cl	H	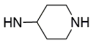	0.18±0.01
3k	H	H	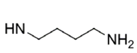	0.147±0.006	**3x**	Cl	Cl	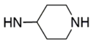	0.12±0.01
3l	H	H	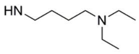	0.15±0.01	**3y**	H	H	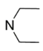	0.19±0.01

[a] 1:1 drug:FPIX-OH complex model

Side chains without basic nitrogen: it seems that the positively charged terminal nitrogen on the side chain by itself do not play a major role in the binding interactions, since the derivative **3y**, which do not have a basic nitrogen in the side chain, have association potency comparable to the other cryptolepine derivatives. However, several studies with 4-aminoquinolines indicate that interaction of the tertiary amino group in the side chain is essential for complexation with FPIX-OH via intramolecular hydrogen bonding to haeme carboxylate groups.(77, 108, 121) Nevertheless, both carboxylate anions in FPIX-OH are far away from the chromophore aromatic nucleus and any interaction with these anions will not interfere with π-electrons. Thus, in our opinion, no significant changes in the Soret band of haematin monomer would probably be observed if any interaction between the carboxylate and the terminal amine functionality in the side chain exits.

Halogen substitution in the aromatic nucleus: substitution with chloride atoms in the aromatic nucleus of cryptolepine derivatives seems to not interfere with the haem binding affinity. Cryptolepine derivatives with one chlorine atom at C3 (**3v** and **3w**) showed K_{ass} values of 0.11 and 0.18 x10^6 M^{-1}, respectively while non-substituted derivatives (**3g** and **3n**) showed K_{ass} values of 0.127 and 0.154 x10^6 M^{-1}, respectively. These results do not corroborate a recent *in silico* study, in which, it was shown that organic chlorine atoms are favorably involved in a wide variety of non-covalent binding interactions, like in aromatic π–systems.(368-369)

Quindolones and Derivatives

Titration of FPIX-OH in pH 5.5 HEPES buffer in 40 % DMSO, with increasing amounts of quindolone (**4**, **91a** and **91b**), as well as with quindolone derivatives **5**, **94** and **95**, were performed to evaluate the binding affinity of these indolo[3,2-*b*]quinolines to haemozoin (Appendix H).

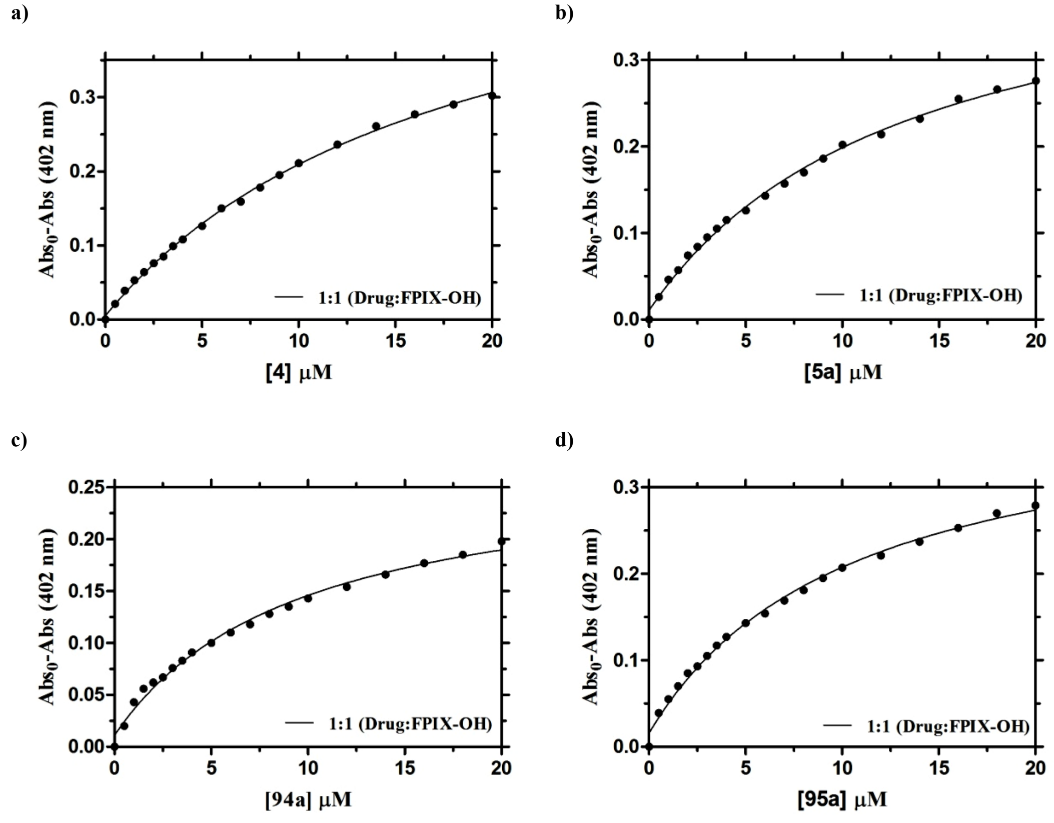

Figure 4.14 – UV-visible spectrophotometric experimental data of FPIX-OH (5 μM)in pH 5.5 HEPES buffer at 25 ºC titrated with quindolone **4** and derivatives **5a**, **94a** and **95a** fitted to 1:1 drug:FPIX-OH complex (model 1). Absorbance at 402 nm vs. a) [**4**], b) [**5a**], c) [**94a**] and d) [**95a**].

Hypochromic shifts on the Soret band of the FPIX-OH UV-visible spectra, were verified upon addition of quindolone and derivatives due to its association with FPIX-OH, giving the evidence for π-π stacking interactions between both aromatic nucleus. All experimental data were plotted as a function of drug concentration according to Eq. 4.5. Figure 4.14 shows **4, 5a, 94a** and **95a** UV-visible experimental data fitted to 1:1 binding equation and closely correlated with Eq. 4.5, with R^2 ranging from 0.989 to 0.999, corroborating the 1:1 binding stoichiometry verified in Job's methodology (Section 4.2.1). Quindolones **4**, **91a** and **91b** showed association constants (K_{ass}) ranging from 0.055 and 0.10 x10^6 M^{-1}, while quindolone derivatives **5**, **94** and **95** range from 0.074 to 0.14 x10^6 M^{-1} (Table 4.4).

Table 4.4 – Association constants for complexes between quindolones (**4** and **91**) and quindolone derivatives **5**, **94** and **95** with haematin monomer at 25 ºC in HEPES buffer pH 5.5

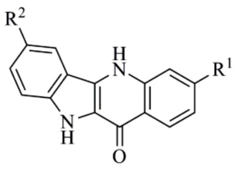

4 or **91**

	R¹	**R²**	Haematin binding K_{ass} (M^{-1})
4	H	H	0.055±0.003
91a	Cl	H	0.10±0.02
91b	Cl	Cl	0.076±0.008

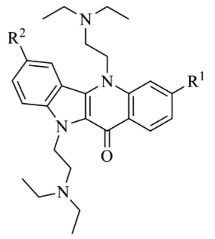

5

	R¹	**R²**	Haematin binding K_{ass} (M^{-1})
5a	H	H	0.074±0.006
5b	Cl	H	0.076±0.006
5c	Cl	Cl	0.115±0.008

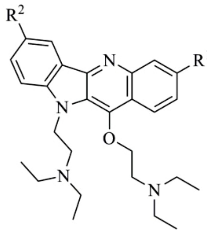

94

	R¹	**R²**	Haematin binding K_{ass} (M^{-1})
94a	H	H	0.08±0.01
94b	Cl	H	0.079±0.005
94c	Cl	Cl	0.14±0.02

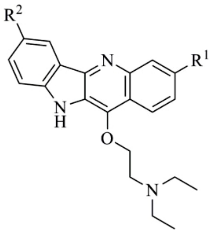

95

	R¹	**R²**	Haematin binding K_{ass} (M^{-1})
95a	H	H	0.096±0.009
95b	Cl	H	0.12±0.02
95c	Cl	Cl	n.d.

n.d. – Not determined.

The introduction of ionizable side chains seems to not interfere with the haem binding affinity, as no significant differences were verified between non-alkylated (**4**, **91a** and **91b**) and alkylated (**5**, **94** and **95**) compounds (Table 4.4)

Additionally, it seems that the introduction of chlorine atoms in the aromatic nucleus of the indolo[3,2-*b*]quinolin-11-one do not affect the binding affinity of the compounds to haem. Changes in the association constants between chlorine substituted and non-substituted compounds do not clearly affect the π-π interactions between the porphyrin and the quindolone derivatives aromatic nucleus.

V

Chapter V - **Molecular Modeling Studies**

“God used beautiful mathematics in creating the world”

Paul A.M. Dirac (1902-1984)
British theoretical physicist

Abstract

Physical-chemical properties of molecules and simulation procedures to predict the binding interactions between ligand and receptors are important features to understand a compound mode of action. In order to understand how the molecular properties of the cryptolepine derivatives could modulate the affinity of these compounds to molecular targets, here we report a DFT study with 10 representative cryptolepine derivatives ***3*** *and their predicted binding properties to DNA structures. Additionally, the cryptolepine and quindolone derivatives binding mode to haemozoin dimer is also described. Introduction of alkyldiamine side chain in the cryptolepine aromatic nucleus originate high polarized derivatives with increased molar volume. Molecular docking simulations showed that, in contrast with parent compound cryptolepine, compounds* ***3*** *are predicted to not intercalate into DNA double helix, but bind to major/minor groove bases and to phosphate backbone of the oligonucleotides, mainly through electrostatic and H-bonding interactions. Also molecular docking simulations showed that both cryptolepine and quindolone derivatives bind to haemozoin dimer through π-π stacking interactions between the aromatic nucleus, and through H-bond between the protonated terminal nitrogen in the side chain with the carboxylate anion (Fe-COO$^-$) of haemozoin dimer.*

List of Contents

5.1 INTRODUCTION 113
5.1.1 Molecular Mechanics 114
5.1.2 Electronic Structure Methods 114
5.1.3 Molecular Docking 115
5.1.4 Molecular Dynamics 117
5.2 DENSITY FUNCTIONAL THEORY (DFT) CALCULATIONS 117
5.3 DOCKING STUDIES WITH DOUBLE-STRANDED OLIGONUCLEOTIDE 119
5.4 DOCKING STUDIES WITH HAEMOZOIN DIMER 126
5.4.1 Cryptolepine and Derivatives 128
5.4.2 Quindolone and Derivatives 132

5.1 Introduction

Physical and chemical and structural properties of molecules are important features to understand concepts such as reactivity of a molecule in a given environment or the affinity to a given molecular target. Models have been used by chemists both to predict and to help to understand these molecular properties. Plastic models and drawing programs are a useful tool to beginning chemistry students and experienced researchers. In a similar way, computational chemistry simulates chemical structures and reactions numerically, based in a full or in part on the fundamental laws of physics. It allows chemists to study chemical phenomena by running calculations on computers rather than examining reactions and compounds experimentally. In this way, it can be provided information about molecules and reactions which is very difficult or even impossible to obtain through observation. There are two broad areas within computational chemistry devoted to the structure of molecules and their reactivity: *molecular mechanics* and *electronic structure theory*.(370-371)

Computational chemistry methods also allow the simulation procedures to predict the conformation of a receptor-ligand complex, where the receptor is usually a protein or nucleic acid (DNA or RNA) and the ligand is either a small molecule or other protein, and is called *molecular modeling*. Molecular docking simulations may be used to reproduce and understand experimental data through docking validation algorithms, where complex conformations obtained *in silico* are compared to structures obtained from x-ray crystallography or NMR. This technique is one of the main tools for virtual screening procedures, where a library of several compounds is ”docked” against one drug target and returns the best hit.(372-373) Furthermore, another molecular modeling useful technique to understand the movements of a molecule and its flexibility is the molecular dynamics. It is also frequently used in NMR structure determination as means of molding an initial structure into one that is experimentally realistic. Also, molecular docking can be combined with molecular dynamics simulations to more accurately dock small molecules into receptors.(373)

5.1.1 Molecular Mechanics

Molecular mechanics simulations predict the structures and properties of molecules, without treat the electrons in a molecular system. Instead, they perform computations based upon the interactions among the nuclei, using a single classical expression for the energy of the compound, for instance the harmonic oscillator, while the electronic effects are implicitly included in force fields (a set of parameters that characterize the energies variation, the atom types and its characteristics and define force constants). Therefore, molecular mechanics allows the calculation with large systems containing many thousands of atoms, but also carries several limitations related with the force fields (limited to those molecules for which is parameterized) and unable to solve problems where electronic effects predominate (neglect of electrons do not permit describe several processes, like bond formation and breaking).(370)

5.1.2 Electronic Structure Methods

Electronic structure methods use laws of quantum mechanics rather than classical physics as the basis for their computations. Quantum mechanics states that the energy and other related properties of a molecule may be obtained by solving the Schrödinger equation.

However, the exact solutions of the Schrödinger equation are not computationally practical and electronic structure methods are characterized by their various mathematical approaches to its solutions. Several models can be used in electronic structure methods, ranging from highly accurate to very approximate, being the highly accurate methods only feasible to small systems. *Ab initio* quantum chemistry methods are based on quantum chemistry and describe with high accuracy a given system, while the so-called empirical or semi-empirical methods employ experimental results from acceptable related models to approximate some elements of the underlying theory.(370) The *ab initio* methods uses quantum mechanical calculations to solve the molecular Schrödinger equation associated with the molecular Hamiltonian (Hamiltonian representing the energy of the electrons and nuclei in a molecule). The simplest model used determine the ground-sate wave function and ground-state energy of a quantum body system as an extension of the molecular orbital theory, and is called Hartree-Fock (HF) or in the old literature self-consistent field method (SCF).(374)

A third class of electronic structure methods have been developed: *density functional methods* (DFT). These methods are similar to the *ab initio* HF methods, determining the molecular electronic structure, even though many of the most common functionals use parameters derived from empirical date, or from more complex calculations. In DFT, the total energy is expressed in a total one-electron density rather than a wave function, and is more attractive because it includes the effects of electron correlation (the fact that electrons in a system react to one another’s motion and attempt to keep out of one another’s way), while HF calculations consider this fact only in a average sense (i.e. each electron reacts to an average electron density). This approximation made in HF methodologies results to be less accurate for some types of systems. DFT methods can be very accurate for little computational cost. Some methods combine Hartree–Fock exchange term with DFT exchange, along with the DFT correlation and are known as hybrid functional methods.

In this work, all the theoretical calculations using DFT were performed in Gaussian 03 software.(375) The theoretical models in Gaussian software have been subjected to testing procedures and it is recommended for general use with any system for which they are computationally feasible. In Gaussian software the chemistry models are characterized by the combination of theoretical procedure and a basis set. The theoretical functionals are hierarchized according to the different approximation methods (commonly referred to as different levels of theory) and are functions of the electron density (Table 5.1).

Table 5.1 – Traditional and hybrid theoretical functionals defined to DFT calculations.

Functional Type		**Description**
Traditional functionals	**Local exchange and correlation functionals**	Involve only the values of the electron spin densities. Slater and $X\alpha$ are well known functionals and the local spin density treatment of Vosko, Wilk and Nusair (VWN) is a widely used local correlation functional.
	Gradient-corrected correlation functional (non-local functionals)	Involve both the values of electron spin density and their gradients. A popular gradient-corrected exchange functional is one proposed by Becke (B) and the gradient-corrected correlation functional proposed by Lee, Yang and Parr (LYP) and the combination of both forms the B-LYP method.
Hybrid Functionals .		Define exchange functional as linear combination of HF, local and gradient corrected exchange terms. The best known hybrid functional is Becke's three-parameter formulation (B3LYP). Becke-style functional have been proven to be superior to the traditional functionals.

The basis set is a mathematical representation of the molecular orbitals within a molecule, confining each electron to a particular region of space. Larger basis sets impose fewer constraints on electrons and more accurately molecular orbitals are obtained.(376) Gaussian software uses a wide range of pre-defined basis sets, which are classified according with the number and basis functions that they contain. Table 5.2 summaries some of the standard basis sets pre-defined in Gaussian software.

5.1.3 Molecular Docking

Molecular docking procedures aim to identify correct poses of ligands in the binding site of a given receptor. In other words, molecular docking describes a process by which two molecules fit one in each other.(377) The docking methodology can be separated into a number of steps: preparation of the ligand, preparation of the target, definition of the target binding site, exploration of ligand flexibility, exploration of the ligand orientation in the binding site and scoring the final poses.(372) However, the success of the docking procedure depends on two components: the search algorithm and the scoring function.(373)

Table 5.2 – Standard basis set pre-defined in Gaussian software.(376)

Basis set type	Description
Minimal basis sets	Contain the minimal basis functions needed for describe fixed-size atomic-type orbitals of each atom (H: 1s; C: 1s, 2s, $2p_x$, $2p_y$, $2p_z$). *Ex: STO-3G (Slater-type orbitals)*
Split valence basis set	Allow the orbitals to change size. Have two, or more sizes of basis function for each orbital (H: 1s, 1s'; C: 1s, 1s', 2s, 2s' $2p_x$, $2p_y$, $2p_z$, $2p'_x$, $2p'_y$, $2p'_z$). *Ex. 3-21G, 6-31G* *6-311G (triple split valence basis set)*
Polarized basis sets	Allow the orbitals to change shape (add orbitals with angular momentum), in addition to the size changing allowed by the split valence basis set. Polarized basis set add **d** functions to carbon atoms, **f** functions to transition metals and some of them **p** functions to hydrogens. *Ex: 6-31G(d) also known as 6-31G** *6-31G(d,p) also known as 6-31G***
Diffuse basis	Are large-size versions of s and p type functions that allow orbitals to occupy a larger region of space. For instance, basis sets with diffuse functions are important for systems where electrons are relatively far from the nucleus, molecules with done pairs, anions and other system with significant negative charge, systems with low ionization potentials. *Ex: 6-31+G(d) is the 6-31G basis set with diffuse functions added to heavy atoms.*
High angular momentum basis set	Is a even larger basis set the add multiple polarization functions per atom. *Ex: 6-31G(2d) add to d functions per heavy atom* *6-311++G(3df,3pd) basis set contain three sets of valence, diffuse functions on both heavy and hydrogens, and multiple polarization functions: 3d and 1f function on heavy atoms and 3p and 1d function on hydrogen atoms.*

Docking applications can be classified by their search algorithm which is defined by a set of parameters applied to predict the conformations. There are several docking programs, such as DOCK,(378) AUTODOCK,(379) GOLD,(380) MOE(381) and others. Each docking application is based on a specific search algorithm such as Monte Carlo and Incremental Construction.(382) The search algorithms perform a selection of the best fit between two or more molecules taking into account several parameters obtained from the input coordinates, like structure flexibility, interatomic interactions, van der Waals radius and charge, among others. At the end of the selection algorithm, the docking software returns the predicted orientations (poses) of a ligand in the receptor binding site. After the selection, the predicted orientations are classified according with the scoring functions. These functions are able to evaluate intermolecular binding, affinity or binding free energy, allowing optimization, ordering and ranking the results obtained after the docking procedure. There are three general classes of scoring functions: *molecular mechanics force field*, *empirical* and *knowledge-based* scoring functions. In molecular mechanics force fields the affinities are estimated by assuming the strength of bonded terms that relate to atoms that are linked by covalent bonds, and non-bonded (non-covalent) terms that describe the long-range electrostatic and van der Waals forces.(383) Empirical scoring functions are based on counting the number of various types of interactions between the two binding molecules. For instance, these interaction terms of the function may include hydrophobic contacts (favorable), hydrophilic contacts (unfavorable), hydrophilic contacts, among others. The coefficients of the scoring functions are usually fit using multiple regression analysis methods. (384) Lastly the knowledge based scoring functions were introduced in 2000 and are based on statistical observations of intermolecular contacts in 3D database. These scoring functions are founded in the fact that certain types of atoms which interact more frequently are likely to be more energetically favorable than atoms which would expect to interact in a random distribution manner and therefore contribute favorably to binding affinity.(373, 385)

5.1.4 Molecular Dynamics

Molecular modeling can also be used to simulate the movement of a molecule by a process called molecular dynamics. This is done by subjecting the initial molecular structure to a process called *simulated annealing*, which is very similar to a melting curve analysis.(386) The kinetic energy of the atoms in the model structure is increased, such as by raising the temperature (often to 400 – 600 K), and then, after a short period of time, it is slowly lowered back to 275 K, where it is allowed to equilibrate for further period of time. This kinetic energy increase allows the molecule to explore more conformations by allowing bond vibrations and rotations to move more freely. As it “cools back down” the potential energy surface of the molecule guides it toward a realistic structure with a relatively lower total energy. The structure is then subjected to an energy minimization procedure, based on a force field, to remove any additional structural anomalies and produce a lowest-energy structure.(352, 387-389)

5.2 Density Functional Theory (DFT) Calculations

In order to understand how the molecular properties of the cryptolepine derivatives, such electron density, atomic charges and molar volume could modulate the affinity of these compounds to molecular targets we performed a DFT study with 10 representative derivatives, including derivatives with linear alkyl side chain (**3f**,**i-j**), cycloalkyl side chains (**3n**,**q**), aromatic side chains (**3r-s**) and aromatic chlorine derivatives (**3v-x**). Cryptolepine properties were also determined and compared with those of the derivatives. In the theoretical we treated the terminal amine functionality of the side chain of cryptolepine derivatives as protonated (except for **3s**) as it should be at physiological and *Plasmodium* digestive vacuole pH, according to the calculated and predicted pK_a values showed in Table 3.4 and Appendix D. The proposed geometry of cryptolepine and derivatives were optimized, after a conformational search using DFT with the B3LYP(390-392) functionality and the 6-31G+(d,p)(393) basis set, which is known to produce accurate geometries, in Gaussian03 software package.(375) The vibrational frequency calculations were performed at the same level of theory to check that all structures represented global minima of the potential energy surface (lack of negative vibrational frequencies) and to correct the computed energies to zero-point energies. For all calculations the value considered for the spin multiplicity was 1, but the charge value was +1 for **1** and derivative **3s** (not protonated in the terminal amine functionality side chain) and +2 for the derivatives with protonated side chain at C11.

The electrical dipole moment, molar volume and natural bond orbital (NBO) charges(394) of the nitrogens in cryptolepine and derivatives were also calculated and shown in Table 5.3. The introduction of the side chain in the cryptolepine nucleus highly increases the electrical dipole moment from 0.75 Debye in **1** to 20.37 Debye in **3x**, except for those derivatives that have aromatic rings in the side chain (**3q-s**). The molar volume of the cryptolepine derivatives also increases when compared with **1**. The values range from 2125 in **1** to 3561 bohr^3.mol^{-1} in **3v** being the derivatives with chlorine substitutions the compounds with the highest values. The N^5 NBO charge (Table 5.3) do not differ too much in cryptolepine and derivatives ranging from -0.312 in **1** to -0.344 in **3r**. For all the cryptolepine derivatives the introduction of the alkyldiamine side chain, contributes with a small increase in the N^5 charge, being more pronounced in derivatives with aryl side chain (**3r-s**). The charges in N^{10} ranging from -0.558 in **3s** to -0.597 in **3n** also slightly increase with the introduction of a non-aromatic side chain at C11, when compared to cryptolepine.

Table 5.3 - Electrical dipole moment, molar volume and partial NBO charges in the nitrogens of cryptolepine (**1**) and some derivatives (**3**).

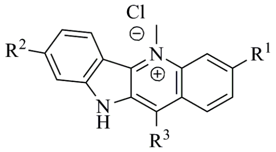

	R^1	R^2	R^3	Electrical dipole Moment$^{a)}$	Molar Volume$^{b)}$	q(N^5)$^{c)}$	q(N^{10})$^{c)}$	q(N-C^{11})$^{c)}$	q(N^{ter})$^{c)}$
1	H	H	H	0.748	2125	-0.312	-0.563	--	--
3f	H	H	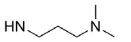	16.748	2562	-0.325	-0.586	-0.661	-0.476
3i	H	H	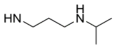	16.439	2596	-0.336	-0.593	-0.623	-0.637
3j	H	H	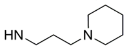	11.744	3363	-0.326	-0.590	-0.476	-0.647
3n	H	H	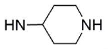	15.708	2742	-0.325	-0.597	-0.643	-0.642
3q	H	H	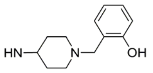	3.059	3290	-0.329	-0.594	-0.631	-0.477
3r	H	H	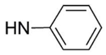	1.948	2177	-0.344	-0.561	-0.589	--
3s	H	H	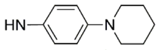	5.321	3321	-0.351	-0.558	-0.580	-0.486
3v	Cl	H	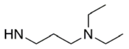	17.280	3561	-0.335	-0.576	-0.636	-0.474
3w	Cl	H	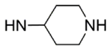	19.242	3274	-0.327	-0.596	-0.634	-0.642
3x	Cl	Cl	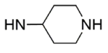	20.366	3491	-0.327	-0.596	-0.634	-0.642

$^{a)}$ Electrical Dipole moment in Debye $^{B)}$ Molar volume in Bohr^3.mol^{-1} $^{c)}$ Atomic charges in atomic units.

The additional charges introduced with the nitrogens present in the side chain vary from -0.476 in **3j** to -0.661 in **3f** for the nitrogen directly connected to C11 (N^{11}) and from -0.474 in **3v** to -0.647 in **3j** for the terminal nitrogen (N^{ter}) of the side chain.

The three-dimensional Molecular Electrostatic Potential (MEP) maps were generated for better understanding of the short-range interactions between molecules. At each point of the map, the electrostatic potential expresses the value of the electrostatic energy of interaction with a unitary positive charge. This type of MEP isosurfaces can account for the interpretation of how interactions between two molecules can occur.(395)

Three-dimensional MEP maps, ranging from -0.4 to 1.0 e/au^3, for cryptolepine and derivatives are represented in Figure 5.1. The MEP map of **1** shows a positive region extending from the area of C-1 to C-6, making a diagonal over the middle of ring system. The most negative areas of cryptolepine are in the opposite extreme of the molecular structure, over the area of C4 and C9. However, the three distinct potential areas described, do not represent a large variation in the electrostatic potential of the molecule.

The introduction of the alkyldiamine side chain at C11 of the cryptolepine nucleus represents a substantial variation on the distribution of the electrostatic potential in the molecule. In general, the introduction of the alkyldiamine side chain creates a large positive area in the region of C1/C11a, except for those who have an aromatic side chain (**3r** and **3s**). The cryptolepine derivatives **3w** and **3x** with chloride atoms in C3 and C3, C7 of the indolo[3,2-*b*]quinoline nucleus respectively, are the compounds with higher polarization. In these compounds, a large positive region appears in the quinolinic ring system, when compared to **1**.

From the DFT studies are possible to conclude that the cryptolepine derivatives (**3**) become more polarized molecules capable of interact with molecular targets through electrostatic interactions (dipole-dipole interactions or London forces that arise from transitory dipoles). Compounds with chlorine substitutions in the aromatic nucleus may have specially propensity to interact with targets presenting negative electrostatic potential due to the presence of a large positive electrostatic potential centred over the indolo[3,2-*b*]quinoline nucleus. Additionally, the introduction of more two nitrogens in the side chain with electronegative potential charges ($q(N^{11})$ and $q(N^{ter})$ in table Table 5.3) can lead to the formation of hydrogen bonds and/or ionic bonds (π-cation bond) with molecular targets, increasing greatly the binding affinity of a given indolo[3,2-*b*]quinoline:receptor complex.

5.3 Docking Studies with Double-Stranded Oligonucleotide

In order to understand how cryptolepine derivatives interact with double-stranded oligonucleotides, docking simulations with a short 12-mer double-stranded $d(GATCCTAGGATC)_2$ oligonucleotide were performed with MOE (Molecular Operating Environment) software.(381, 396) The duplex DNA (B-helix)(345) was constructed with MOE software and minimized with Amber99(397-398) force field and born solvation(399-401) scheme. After minimization, the structure was subjected to molecular dynamics (MD) with simulation annealing conditions(386) to obtain the most favorable conformational structure and relax the system to a minimal energy. After MD and subsequent energy minimization the DNA structure was used in the docking study.

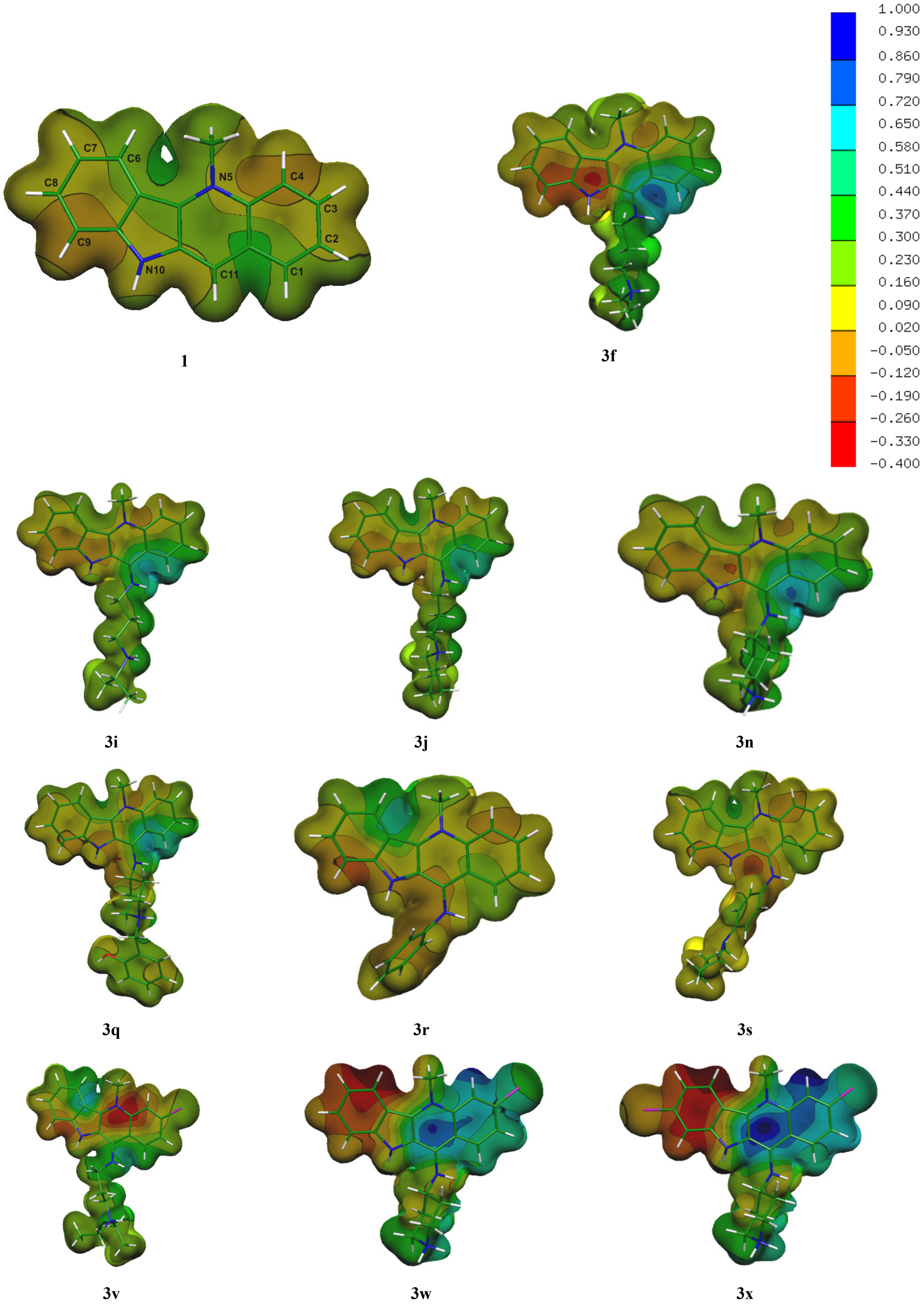
1.000
0.930
0.860
0.790
0.720
0.650
0.580
0.510
0.440
0.370
0.300
0.230
0.160
0.090
0.020
-0.050
-0.120
-0.190
-0.260
-0.330
-0.400
C7
C6
N5
C4
C8
C3
C2
C9
N10
C11
C1

1 **3f**

3i **3j** **3n**

3q **3r** **3s**

3v **3w** **3x**

Figure 5.1 – Molecular Electrostatic Potential (MEP, values in e/au^3) maps for cryptolepine and some derivatives.

It is known that cryptolepine intercalates into DNA, binding to CG-rich sequences containing non-alternating CC sites in a base-stacking intercalation mode in absence of hydrogen bond interactions.$^{(5)}$ In order to get information on the solidity of our model we docked cryptolepine with the ds d(GATCCTAGGATC)$_2$ oligonucleotide. Due to the asymmetry of our molecule, different orientation analyses were required. We considered four different orientations for intercalation, as shown in Figure 5.2.

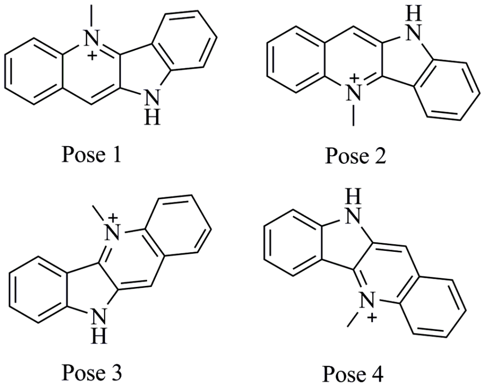
Pose 1
Pose 2
Pose 3
Pose 4

Figure 5.2 – Four different docking orientations investigated for intercalation of **1**, corresponding to the rotation of the molecule around two orthogonal axes located in the molecule plan.

$$\Delta E_{bind} = E_{complex} - \left(E_{DNA} + E_{ligand}\right)$$

Eq. 5.1 – Energy of complex formation.

The complexes stability were evaluated according to the energy of complex formation (ΔE_{bind}). This energy was determined according to Eq. 5.1, where $E_{complex}$ is the energy of the oligonucleotide:**1** complex, E_{DNA} is the energy of the free oligonucleotide and E_{ligand} is the energy of the free ligand. The most favorable energy of complex formation for intercalation of **1** into non-alternating CC sites of d(GATCCTAGGATC)$_2$ oligonucleotide was obtained for pose 2 (E_{cf} = -577 kJ.mol^{-1}) as shown in Table 5.4. The docked structure is in excellent agreement with the results already described for the intercalation of cryptolepine into DNA structures containing non-alternated CC sites.(5) In the intercalation cavity, the bases are separated by 6.9 Å while in the others the base separation is only 3-4 Å. Compound **1** intercalates alongside to the major axis of the base pairing, maximizing the occupation of the intercalation cavity. The double-six ring portion of the molecules stacks between the two guanines (G8-G9), the positively charged nitrogen (N^5) is placed between the two oxygens of the consecutive guanines of the major groove and the indole nitrogen (N^{10}) is placed between the oxigens of consecutive cytosines (C4-C5) of the minor groove, enhanced the stability of the complex as shown in Figure 5.3a. The interactions of **1** with the DNA structure are mainly of van der Walls type with absence of H-bonding. Figure 5.3b shows a van der Walls interaction map of the ligand with the DNA residues in the intercalation cavity.

The complex stability is enhanced by mild-polar and hydrophobic interactions, where hydrophobic interactions predominate in the plans directly above and below of the four-ring fused plan and the mild-polar interactions in the regions of the aromatic hydrogens (equatorial), positioning the center of mass of **1** where both hydrophobic and electrostatic interactions are maximized. The absence of H-bonding interactions indicates that the stacking forces provide alone the stability of the complex, like the π-π stacking interactions between the 6-member aromatic ring of the double-six ring portion and the aromatic rings of the guanines (G8-G9) consecutives bases, as shown in Figure 5.3c.

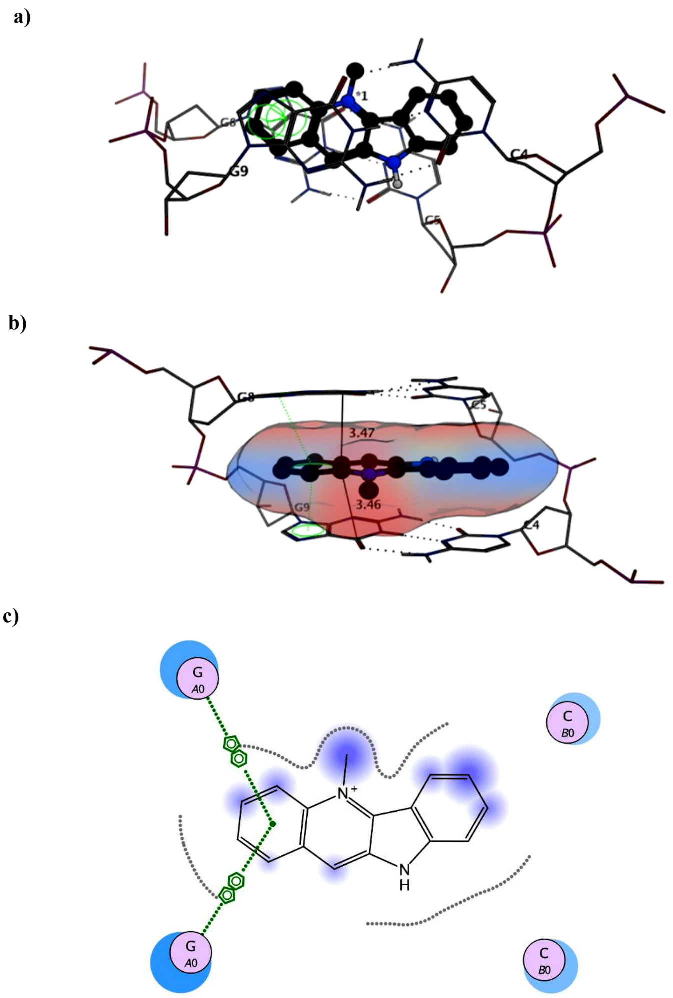

Figure 5.3 – Stereo view of the projection up the helix axis of a d(GpG)-d(CpC) dinucleotide of the double-stranded d(GATCCTAGGATC)$_2$ oligonucleotide with the ligand **1** sandwiched (dot-grey: H-bond between bases); b) Stereo view of the Van Der Walls interactions map of the ligand **1** intercalated, looking into the major groove (blue: mild polar; red: hydrophobic: yellow: H-bonding), shown intercalation pocket only for clarity, value in Å); c) Interactions map of ligand **1** intercalated into d(GpG)-d(CpC) dinucleotide of the double-stranded d(GATCCTAGGATC)$_2$ oligonucleotide. (blue circle: receptor exposure; pink circle: polar; blue: ligand exposure; dot green π-π interaction; dot purple: proximity contour).

The docking studies of cryptolepine derivatives (**3f 3i-j**, **3n**, **3q-s** and **3v-x**) with the double-stranded d(GATCCTAGGATC)$_2$ oligonucleotide reveal a different binding mode when compared with parent compound **1**. The intercalation docking studies in non-alternated CC sites of compound **3n**, in pose 2 which is the most favourable orientation according to the results obtained for **1**, showed high ΔE_{bind} (537 KJ.mol^{-1}), destroying the Watson and Crick base pairing and consequently the B-like conformation helix, as shown in Figure 5.4. The quinolinic double ring portion of the four ring system stacks under the G8 base and over the G9 base, which are separated from each other by 8.7 Å, while C4 and C5 bases are separated by 8.5 Å. The base paring between C4-G9 and C5-G8 is destroyed, where the nitrogenns of the six ring portion of G8 interact with the phosphate backbone through H-bonding and G9 interact with T3 through H-bonding between the NH and the carbonyl oxygen's of the bases, due to the downshift of G9 orientation.

Table 5.4 – Calculated energies of complex formation $\Delta E_{bind} = E_{complex} - (E_{DNA} + E_{ligand})$, van der Walls energy ($E_{vdw}$) and electrostatic energy (E_{ele}) obtained for different orientations of 1 intercalated with d(GATCCTAGGATC)$_2$ oligonucleotide in non-alternating CC sites, bound to major and minor groove of cryptolepine derivatives (**3f**, **3i-j**, **3n**, **3q**, **3r-s**, **3v-x**) intercalated and/or bound to major and minor groove of d(GATCCTAGGATC)$_2$ oligonucleotide.

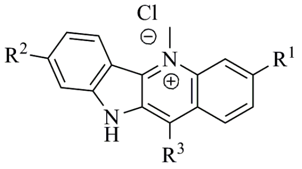

	R^1	R^2	R^3	Docking Mode	ΔE_{bind} $^{a)}$	E_{vdw} $^{a)}$	E_{ele} $^{a)}$
1	H	H	H	Intercal. 1$^{b)}$	-542	-977	-15798
				Intercal. 2$^{b)}$	-577	-1214	-16056
				Intercal. 3$^{b)}$	-566	-1193	-16437
				Intercal. 4$^{b)}$	-574	-1197	-16249
				Major gro.	-307	-1230	-16820
				Minor gro.	-331	-1234	-16676
3f	H	H	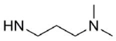	Major gro.	-348	-1265	-16652
				Minor gro.	-452	-1265	-17389
3i	H	H	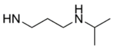	Major gro.	-546	-1255	-17613
				Minor gro.	-606	-1279	-17633
3j	H	H	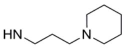	Major gro.	-382	-1249	-17517
				Minor gro.	-516	-1299	-17723
3n	H	H	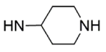	Major gro.	-482	-1265	-17092
				Minor gro.	-534	-1318	-17243
3q	H	H	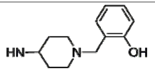	Major gro.	-493	-1242	-17517
				Minor gro.	-564	-1299	-17723
3r	H	H	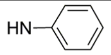	Major gro.	-334	-1252	-16837
				Minor gro.	-377	-1276	-16882
3s	H	H	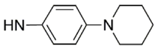	Major gro.	-364	-1244	-16474
				Minor gro.	-408	-1232	-16883
3v	Cl	H	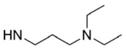	Major gro.	-478	-1293	-17386
				Minor gro.	-310	-1284	-17756
3w	Cl	H	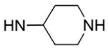	Major gro.	-491	-1261	-17169
				Minor gro.	-500	-1302	-17802
3x	Cl	Cl	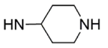	Major gro.	-574	-1266	-17517
				Minor gro.	-552	-1287	-17524

$^{a)}$ Energy in kJ.mol^{-1} $^{b)}$ Docking orientation pose

The major interactions contribution to the complex stabilization are the π-π stacking and the π-cation between **3n** and G8 and the H-bonding between the nitrogens of the side chain and the indole NH with the phosphate backbone of the DNA helix. The intercalation studies for the other cryptolepine derivatives reveal similar results. These mean that the final docking mode for these compounds is not the intercalation of the ligand, due to its expulsion from intercalation cavity, after energy minimization of the complex. A possible explanation for this change in DNA binding mode when a diamine side chain is introduced at C11 of cryptolepine nucleus, is the observed increased molar volume of the derivatives **3** when compared to **1** (Table 5.3), leading to the separation of the bases in the intercalation cavity, so breaking H-bonding between base pairs, prompting a structural rearrangement of the DNA helix.

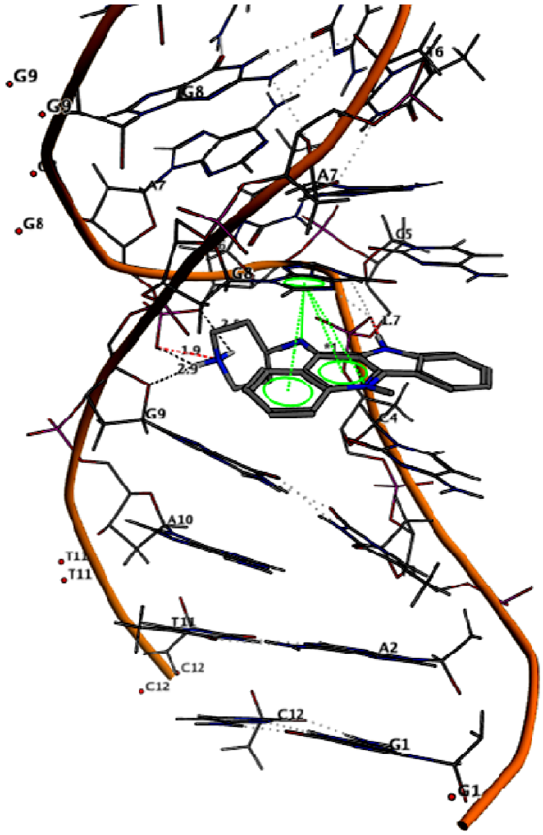

Figure 5.4 – Final docking complex of **3n** intercalated in pose 2 into GC-sites of double-stranded oligonucleotide d(GATCCTAGGATC)$_2$. (grey dot-lines:H-bond between bases: dashed-black: H-Bond; dashed-red: ionic binding; dashed-green: π-π interactions; phosphate backbone was removed for clarity)

Subsequent docking experiments showed that interaction of the cryptolepine derivatives with ds-DNA occurs preferentially with the minor or major grooves. For instance, molecular docking simulations of cryptolepine derivative **3n** with such DNA models, showed that interactions for minor groove binding turned out to be more favorable (ΔE_{bind} = -534 kJ.mol^{-1}), than for major groove binding (ΔE_{bind} = -482 kJ.mol^{-1}), maximizing the interactions between the ligand and the DNA. Compound **2n** interacts with the DNA bases and phosphate backbone (Figure 5.5a), in which the two phosphate chains of the interaction cavity are separated by 9 Å, the same distance as in the absence of ligand. Binding occurs with the ligand four-ring aromatic system plane positioned in the minor groove axis. The charged nitrogen (N^5) is located on the outside of the DNA helix, interacting with DNA phosphate groups of T6 and T11 nucleotides through ionic interactions (Figure 5.5a and b). The indole nitrogen (N^{10}) and the alkyldiamine side chain are turned directly to the DNA helix core, enhancing the stability of the complex due to formation of hydrogen bonds (Figure 5.5b). H-bonding interactions of ligand **3n** to the DNA helix are mainly through the terminal amine functionality on the alkyldiamine side chain with the carbonyl oxygen of T3 and the indole NH with the aromatic nitrogen of A10, representing an important contribution (1.89 Å of bound length) to the complex stability. The hydrophobic interactions above and below the four-ring fused plane and on the aliphatic ring of the side chain with the phosphate backbone (red in Figure 5.5a), also contribute to the stability of the complex. The weakly polar interactions (blue in Figure 5.5a) occur between the aromatic hydrogens of **3n** with the bases and phosphate backbone of the DNA.

For the other compounds studied (except **3v** and **3x**), the binding interactions energies are more favourable for the minor groove binding (Table 5.4). Similarly to **3n**, these cryptolepine derivatives bind to DNA aligning with the minor groove curvature, perpendicularly to the DNA major axis, and with the four-fused ring system surface interacting with the phosphate backbone through hydrophobic, weakly polar and ionic forces (Appendix I). However, we cannot find any specificity in the binding orientation of these cryptolepine derivatives. The indole nitrogen of **3j**, and **3q-s** faces the helix core, while for **3f**, **3i** and **3w** it is in the opposite direction. The binding to the DNA minor groove is also through H-bonding involving the side chain terminal amine and the indole group (N^{10}) and through hydrophobic and weakly-polar interactions involving the aromatic system. The H-bonding is mainly established with the phosphate backbone although in some cases (**3j**, **3n** and **3v**) it is with the bases of the DNA helix.

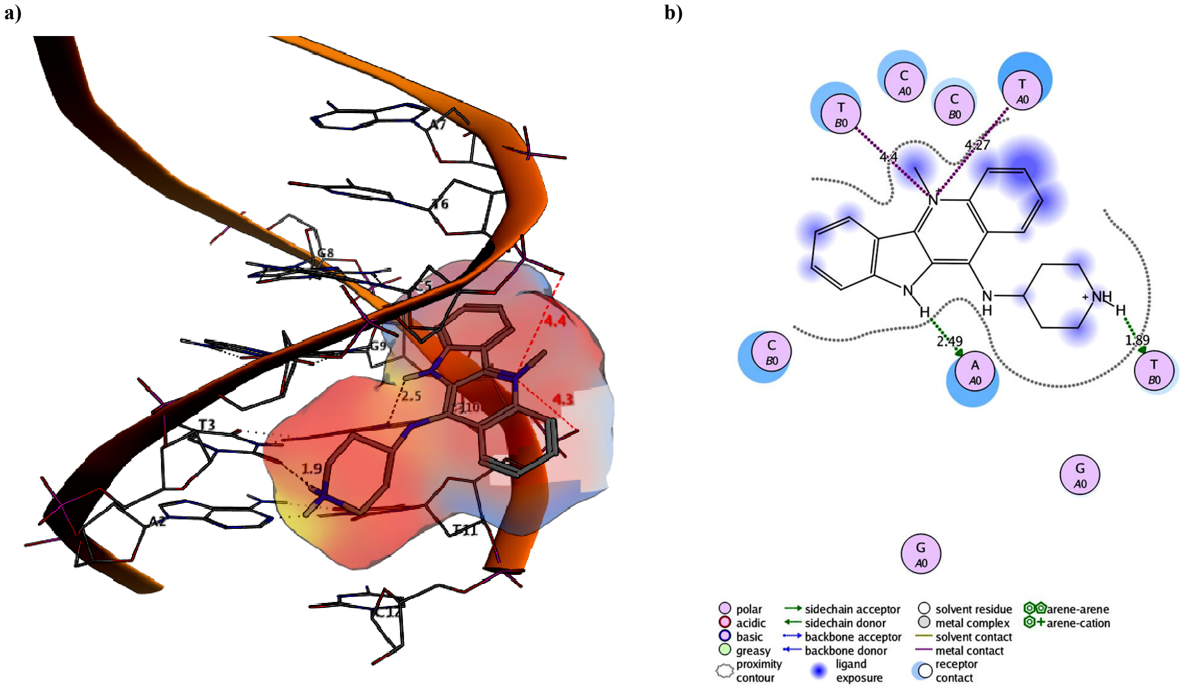
a)
b)
A7
T6
G8
C5
G9
2.5
4.4
4.3
C10
T3
1.9
A2
T11
C12
T B0
C A0
C B0
T A0
4.4
4.27
N
N
H
N
H
+NH
H
2.49
1.89
C B0
A A0
T B0
G A0
G A0
polar
acidic
basic
greasy
proximity contour
sidechain acceptor
sidechain donor
backbone acceptor
backbone donor
ligand exposure
solvent residue
metal complex
solvent contact
metal contact
receptor contact
arene-arene
arene-cation

Figure 5.5 – a) Model of **3n** interacting with minor groove and phosphate backbone (blue: weakly polar; red: hydrophobic: yellow: H-bonding; dashed-black: H-Bond; dashed-red: ionic binding); b) Interactions map of **3n** with the minor groove and phosphate backbone of the double-stranded d(GATCCTAGGATC)$_2$ oligonucleotide. (blue circle: receptor exposure; pink circle: polar; blue: ligand exposure; arrow dashed green: H-bonding with chain; dashed red: ionic binding; dashed purple: proximity contour; values are in Å).

The cryptolepine derivatives **3v** and **3x** bind preferentially to the major groove of the DNA helix (Table 5.4). The binding occurs with the four-ring fused plane aligned parallel to the DNA phosphate backbone plane. Compound **3v** shows H-bonding and π-cation interactions between the terminal amine function of the side chain or the C11 amine group and the DNA bases (Appendix I). Compound **3x** binds also to the major groove, but only with H-bonding between the ligand and the DNA phosphate chain. For instance, the terminal amine functionality of the side chain and the N^{10} of **3x**, make H-bonding interactions with the phosphate groups of T6 and A7 of the major groove (Figure 5.6). The hydrophobic interactions between the four ring-fused plane and the DNA helix occur in the region of G8 and A7, with the DNA phosphate chains and bases.

These docking experiments showed that interaction of the cryptolepine derivatives with ds-DNA occurs preferentially with the minor or major grooves, mainly through H-bonding as well as hydrophobic interactions of the aromatic four-fused rings system with the phosphate backbone and bases.

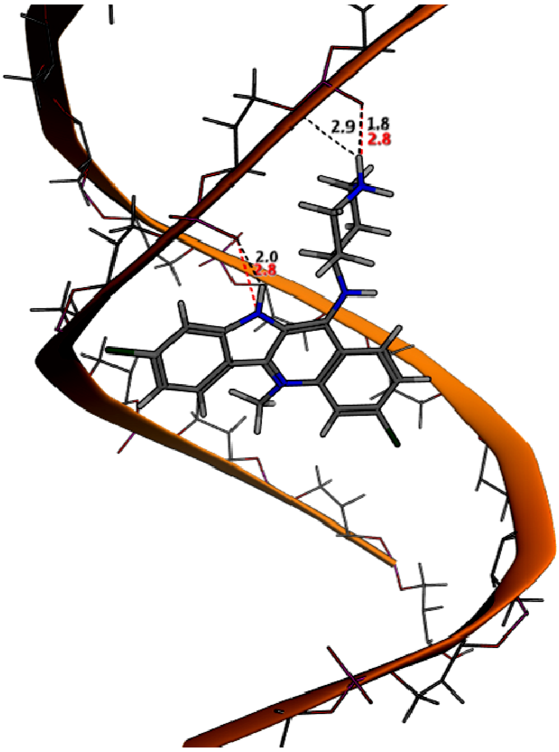

Figure 5.6 – H-bond interaction of **3x** with the phosphate backbone in the major groove region.
(DNA bases removed for clarity, dashed black: H-bond; dashed red: ionic binding; Value in Å.)

Additionally, our results are consistent with previously reported molecular modeling studies on interactions between C11-alkyldiamine-quindoline derivatives and guanine-quadruplex structures that show that this type of compounds are not that intercalative and nitrogen atoms in the alkyl side chain are able to form H-bonds with the phosphate diester backbone of DNA structures, hence contributing to the stabilization of the ligand:DNA complex.(289) Most of the cryptolepine derivatives studied are predicted to bind preferentially to the minor groove, as shown by the decreasing energies for complex formation (Table 5.4), except for **3v** and **3x** which bind preferentially to the major groove. Once again, these differences can probably be explained by the increased molar volume of these two compounds (Table 5.3), meaning that compounds bind to the DNA region where their size allow a good fit to the DNA structure, and consequently interactions between the ligand and the DNA are maximized.

5.4 Docking Studies with Haemozoin Dimer

In the light of the finding that derivatives **3**, **5**, **94** and **95** have affinity to FPIX-OH monomer, as chloroquine, cryptolepine and their counterparts indoloquinolines **1**, **4**, **91a** and **91b** (Section 4.3), we decided to evaluate *in silico* their binding properties in order to gain an understanding of the SAR of this family of compounds, as well as their main interaction with drug receptors.

A molecular docking simulation with several cryptolepine and quindolone derivatives should be performed with three-dimensional structure of haematin monomer, for further comparison with *in vitro* results. However, this structure was not available and had to be modelled. Thus, we performed the docking experiments with the haemozoin dimer, obtained from the *Cambridge Crystallographic Data Centre (CCDC)*,(63) in order to obtain structural motifs of these compounds interacting with the target haemozoin. The docking simulations were performed with Genetic Optimisation for Ligand Docking (GOLD) algorithm(380) which performs a stochastic search for preferred orientation and conformation of the ligand in relation to the receptor.(402) As receptor was used the structure of haemozoin (PDB file obtained from CCDC), and chosen as active site one of the iron atoms, in the centre of the porphyrin ring, and including all the atoms within a radius of 12 Å. The results presented here correspond to the best-scored solutions of 2500 docking runs for each structure. Table 5.5 shows the GoldScore values of the best docking solutions between haemozoin dimer and chloroquine, cryptolepine and its derivatives **3f-h**, **3j**, **3l**, **3n**, **3s**, **3u-v, 3x-y**.

Chloroquine

The algorithm was validated by docking chloroquine with the structure of the haemozoin dimer. The proposed geometry of chloroquine was optimized after a conformational search using DFT with the B3LYP(390-392) functionality and the 6-31G+(d,p)(393) basis set in Gaussian03 software package.(375) The calculations were performed on the receptor with chloroquine in the diprotonated form as it should be at pH 5.5 (pK_{a1} = 8.55 and pk_{a2} = 9.81),(403) in the *Plasmodium* sp. digestive vacuole.(51-52) Docking results of chloroquine, performed for comparison purposes, showed binding of **2** to haemozoin dimer through π-π stacking interactions and H-bonding, in good agreement with already described molecular modeling(121) and nuclear magnetic resonance(118, 124) results with haem. The docking results are shown in Figure 5.7a and Figure 5.7b.

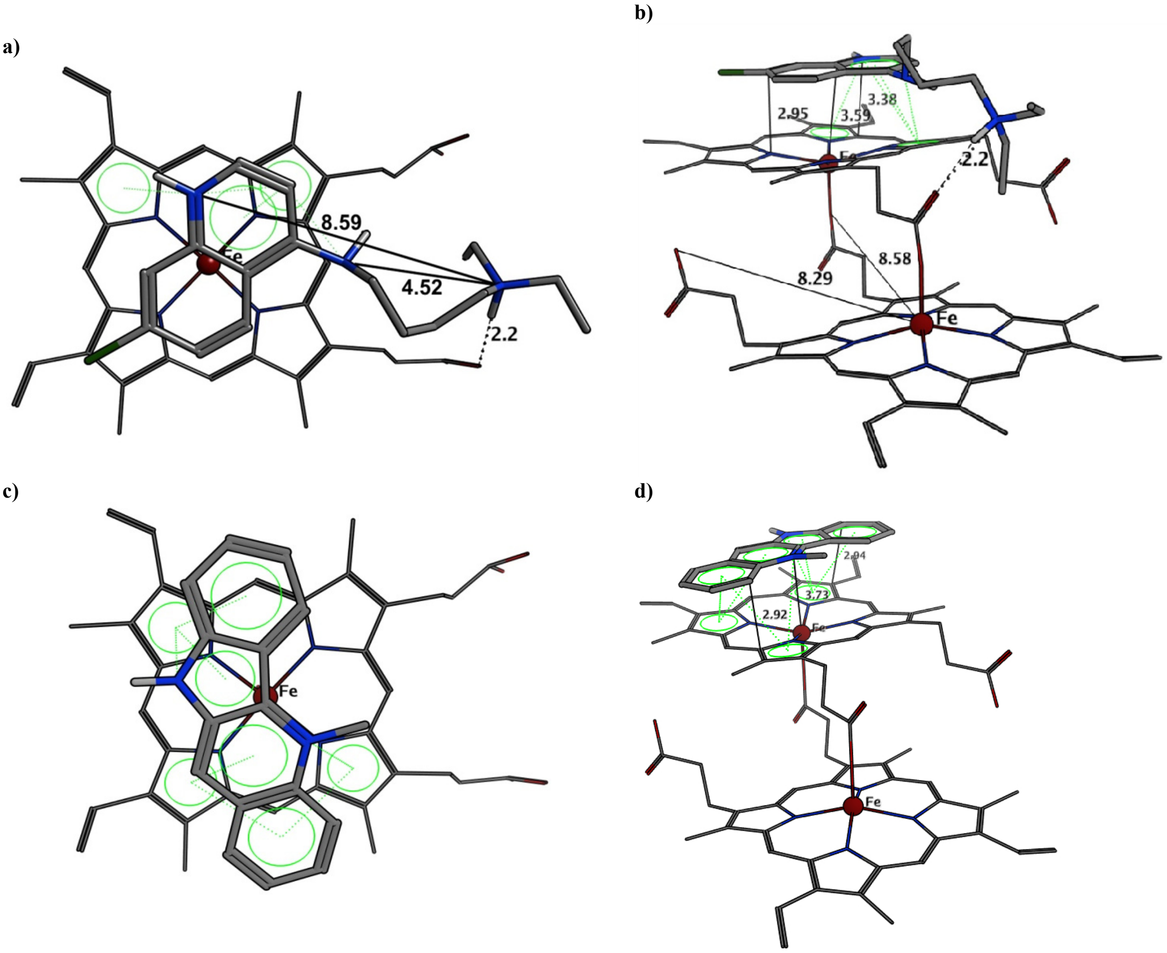

Figure 5.7 - Model of chloroquine (**2**) and cryptolepine (**1**) interacting with haemozoin dimer. a) chloroquine top-view; b) chloroquine; c) cryptolepine top-view; d) cryptolepine. (dashed-black. H-bond; solid green: π-π interactions; solid-black: distances; values in Å).

The quinoline ring stacks over of the center porphyrin ring of haemozoin dimer, which has a planar flat region of approximately 35 Å^2. Chloroquine interact mainly through π-π stacking interactions, with an intermolecular distance between ligand and aromatic receptor nucleus of about 3 Å and of about 3.6 Å of the iron atom (iron atom is above the aromatic ring). The charged nitrogen of the aminoquinolines side chain interacts with the carboxylate oxygens (Fe-COO$^-$), mainly through H-bond with a distance between the oxygen and the proton in the charged nitrogen of 2.2 Å. Furthermore, the docking results showed that the interatomic distances between the hydrogen donators in the ligand (N^{quin} - $N^{diethyl}$ = 8.59 Å) and the interatomic distances between the acceptors in the in the receptor (Fe – COO$^-$ of c.a 8.3 – 8.6 Å) are essential the same (Figure 5.7). These results seem to indicate that a two-point interaction may be the major role for haemozoin-drug complexation. However, it was expected to see binding interactions between the central acceptor in the porphyrin ring and the quinolinic nitrogen, but no binding interactions were verified between these two moieties.

5.4.1 Cryptolepine and Derivatives

Cryptolepine (**1**) and some of its C11 alkyldiamine derivatives (**3f-h**, **3j**, **3l**, **3n**, **3s**, **3u-v, 3x-y**) were docked with haemozoin dimer. The calculations were performed on the receptor with the cryptolepine derivatives in an ionization state according to their pK_a values (Table 3.4 and Appendix D). The proposed geometry of cryptolepine and derivatives was optimized, after a conformational search using DFT with the B3LYP(390-392) functionality and the 6-31G+(d,p)(393) basis set in Gaussian03 software package.(375) For all the cryptolepine derivatives, with exception of **3s** and **3u**, the ionization state was +2, due to the protonation of the terminal nitrogen of the side chain as it should be at pH 5.5. Calculation with derivatives **3s** and **3u** were conducted with a ionization state of +1, with the terminal nitrogen on the side chain in the neutral form.

Cryptolepine

Docking results of cryptolepine with haemozoin dimer are shown in Figure 5.7c and Figure 5.7d. Like chloroquine, cryptolepine stacks over the center of porphyrin ring, interacting exclusively by π-π stacking interactions, in which the lone pair of electrons of the nitrogens of N^{10} seems to be involved. The complex stability is assured with cryptolepine aromatic nucleus staying at ca. 3.0 Å of the porphyrin ring, and with the N^5 of the indoloquinoline staying at 3.7 Å of the iron atom. Chloroquine showed a GoldScore value of 32.89 while cryptolepine showed a value of 40.32. From the analysis of the scoring results it seems that the increased π-π stacking interactions, due to the higher aromatic region of cryptolepine when compared with chloroquine, contribute greatly to the complex stabilization.

Cryptolepine derivatives

Also cryptolepine derivatives **3f-h**, **3j**, **3l**, **3n**, **3s**, **3u-v, 3x-y** interact with porphyrin ring through π-π stacking interactions, like cryptolepine. However, most of them showed also the ability to interact with carboxylate ions through H-bonding between the protonated terminal nitrogen of the side chain and the oxygen atom. Cryptolepine derivatives without protonated terminal nitrogen (**3s**, **3u** and **3y**) are an exception. In these cases the complex stability is enhanced only by π-π stacking interactions. In addition to the π-π stacking and H-bonding interactions, some derivatives (**3n**, **3f**, **3h**, **3j**, and **3x**) also showed ionic interactions with the haemozoin dimer. The proximity of the positively charged nitrogen in side chain to the negatively charged carboxylate oxygen (COO^-), attracts each other, with formation of the ionic interactions.

For example, cryptolepine derivative **3g**, stacks over the center of the porphyrin ring (Figure 5.8a,b) and like chloroquine and cryptolepine with a distance of approximately 3 Å, separating the porphyrin ring and the indolo[3,2-*b*]quinoline nucleus. However, the inserted alkyldiamine side chain of 3 carbons length, introduces a hydrogen donor with the necessary distance (approximately 8.2 Å) to interact with the carboxylate group of the haemozoin dimer. Thus, the complex stability is enhanced by π-π stacking interactions between the aromatic moieties of the ligand and receptor and by H-bond between the protonated terminal nitrogen in the side chain and with the oxygen of the carboxylate linked to the iron atom in the porphyrin ring (bond length of 2.0 Å).

Docking of cryptolepine derivative with a piperidine side chain **3n** (Figure 5.8c,d), showed that the complex stability is also enhanced by π-π interactions, but due to the reduced side chain length, the aromatic nucleus of the indolo[3,2-*b*]quinoline lies on the edge of the porphyrin ring, allowing the formation of H-bonding between the protonated nitrogen in the side chain and the carboxylate group (Fe-COO). Additionally, the rigid character of the piperidine side-chain introduces some steric hindrance. The optimal distance between the two aromatic nucleus seems to be around 3 Å, and to be centre in the porphyrin ring, the indolo[3,2-*b*]quinoline nucleus of **3n**, would probably be at a distance exceeding this value, and thus reducing the complex stability. In Figure 5.8e,f is showed the docking results for the cryptolepine derivative **3y**. The complex stability is only achieved by π-π interaction, due to the absence of a basic side chain and like for **3n**, the steric hindrance introduced by the diethylamine group in C11, put away the indolo[3,2-*b*]quinoline nucleus from the center of the porphyrin ring. Docking results of the cryptolepine derivative not described above are shown in Appendix J.

The cryptolepine derivatives showed GoldScore values ranging between 29.79 and 49.54, being most of them very close to the cryptolepine GoldScore value (40.32). These results show that the main driving forces for the complex stability are the π-π stacking interactions, but being dependent of the side chain structure. The analysis of the scored docking results (Table 5.5) allows us to deduce some structure-activity relationships (SAR) for the binding of these compounds to haematin dimer.

SAR with haemozoin dimer

Terminal nitrogen substitution and branched side chains: GoldScore results for the cryptolepine derivatives with a side chain of three carbons length (**3f-h** and **3j**) showed that bulky substituents on the terminal nitrogen (**3g** and **3j**) have higher binding affinities than derivatives with smaller substituents (**3f**) and the introduction of branched side chains (**3h**) reduce the complex stability when compared with linear ones (**3f**).

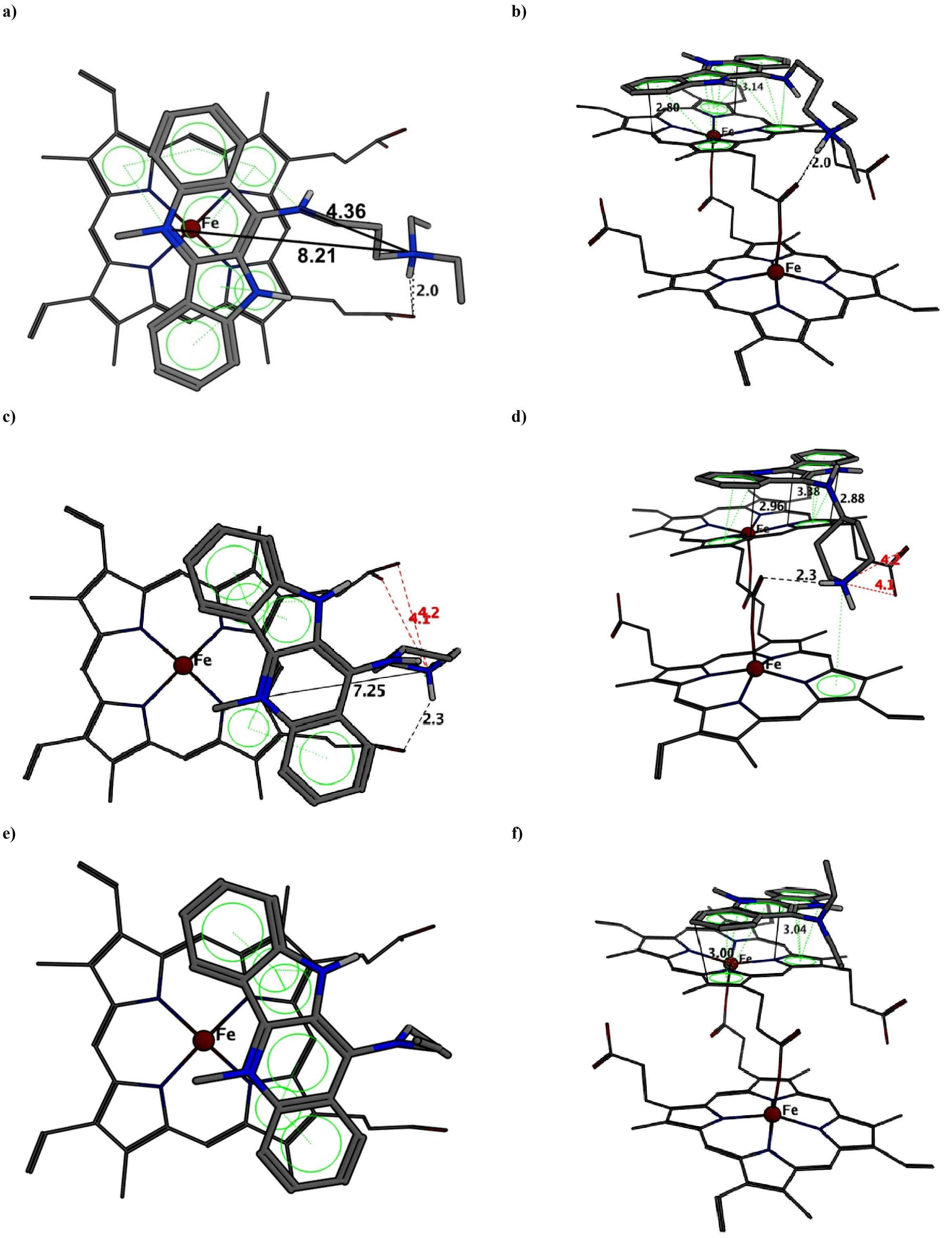
a)
b)
c)
d)
e)
f)
Fe
4.36
8.21
2.0
2.80
3.14
7.25
2.3
4.2
4.1
2.96
3.38
2.88
3.00
3.04

Figure 5.8 - Model of cryptolepine derivatives **3g**, **3n** and **3y** interacting with haemozoin dimer. a) **3g** top-view; b) **3g**; c) **3n** top-view; d) **3n**; e) **3y** top-view; f) **3y.** (dashed-black. H-bond; solid green: π-π interactions; dashed-red: ionic binding; solid-black: distance; values in Å).

Table 5.5 – GoldScore(380) values of the doctking studies of chlorquine (**2**), cryptolepine (**1**) and derivatives **3f-h**, **3j**, **3l**, **3n**, **3s**, **3u-v**, **3x-y** with haematin dimer using GOLD software.

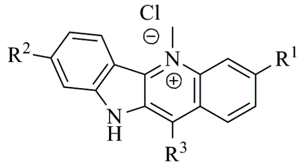

	R^1	R^2	R^3	GoldScore
2	--	--	--	32.89
1	H	H	--	40.32
3f			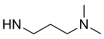	40.44
3g	H	H	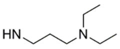	46.06
3h	H	H	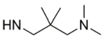	31.93
3j	H	H	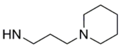	49.54
3l	H	H	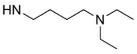	46.60
3n	H	H	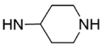	39.58
3s	H	H	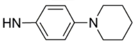	29.79
3u	H	H	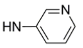	44.52
3v	Cl	H	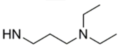	47.50
3x	Cl	Cl	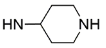	39.00
3y	H	H		33.98

Halogen substitution in the aromatic nucleus: The introduction of one chlorine atom (**3v**) and two chlorine atoms (**3x**) did not affect significantly the binding affinity of these derivatives to haemozoin dimer when compared with its counterparts **3g** and **3n**, respectively.

Additionally, a conformational analysis of the cryptolepine derivatives **3f**, **3l** and **3n** showed that these derivatives share some structural features with some common antimalarials (Figure 5.9). Geometry optimizations calculations were determined using density functional theory (DFT) with B3LYP(390-392) parameterization of the density functional and the 6-31+G(d,p) basis set,(393) using the Gaussian03 software package.(375) The vibrational frequency calculations were accomplished at the same level of theory. The results showed that the cryptolepine derivatives with side chains of three or four carbons have similar bioactive conformation as chloroquine and amodiaquine. Cryptolepine derivatives showed distances between the quinolinic nitrogen (N^5) and the terminal nitrogen atom in the side chain ranging from 8.037 and 9.795 Å, while chloroquine and amodiaquine have values of 8.38 and 8.30 Å, respectively.(134)

Overall, the results suggest that the cryptolepine derivatives are able to complex with haemozoin through π-π stacking interactions between the two aromatic nucleus. Additionally, the terminal amine side chain is also able to form H-bond with the carboxylate groups (Fe-COO). The side chain length and its substitution pattern seems to strong influence the interactions with the haemozoin dimer.

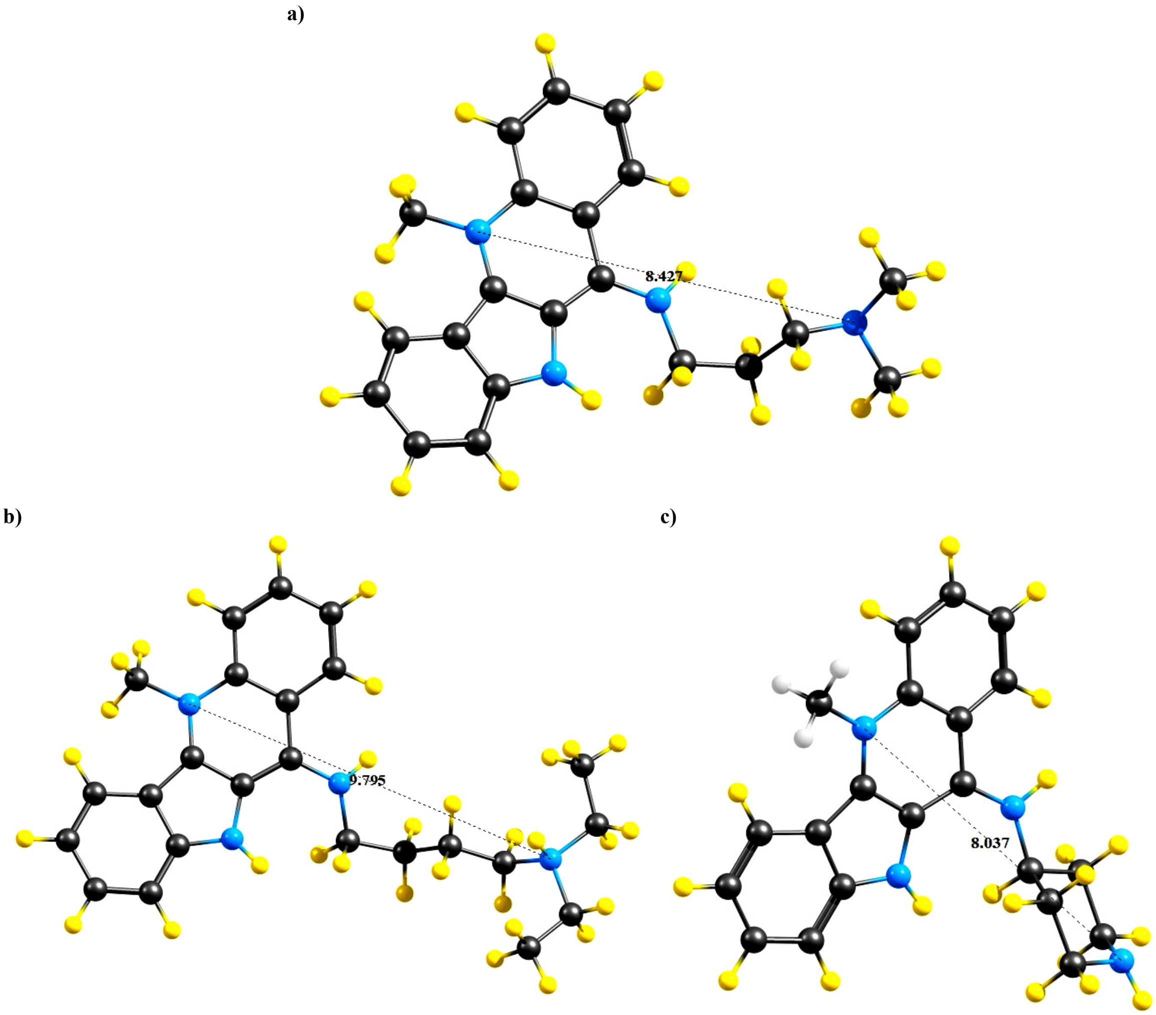

Figure 5.9 – Conformational analysis of the cryptolepine derivatives a) **3f**, b) **3l** and c) **3n**, determined using density functional theory (DFT) with B3LYP.

5.4.2 Quindolone and Derivatives

Quindolones (**4**, **91a** and **91b**) and their derivatives **5**, **94** and **95** were also docked against the haemozoin dimer. Also, the proposed geometries were optimized, after a computational search with DFT, using the B3LYP(390-392) functionality and the 6-31G+(d,p)(393) basis set in Gaussian03 software package.(375) The calculations were performed with the compounds in the ionization state according to the SPARC predicted pK_a values shown in Appendix D. Thus, the geometries optimizations of **4**, **91a** and **91b** were performed with the ionization state value of zero, **5** with the ionization state of +2, **94** with the ionization state of +2 and **95** with the ionization state of +1.

Quindolones

Docking results of **4** with haemozoin dimer are shown in Figure 5.10. Like chloroquine, cryptolepine and derivatives, also quindolone **4** stacks over the porphyrin aromatic ring, with an intermolecular distance of ca. 3 Å. The main interactions seem to be due to π-π stacking interactions between the aromatic nucleus, in which the lone pair of electrons of both nitrogens seems to be involved. Docking with quindolones **91a** and **91b** showed similar results to those of **4** and the docking fitness values are shown in Table 5.6. Quindolone **4** showed a GlodScore of 42.65, while **91a** and **91b** showed values of 44.17 and 45.26, respectively. The results seem to point out that the introduction of chlorine atoms stabilizes the complex formation, thus corroborating the *in silico* studies showing that organic chlorine atoms are constructively involved in a wide variety of non-covalent binding interactions with aromatic π-systems.(368-369)

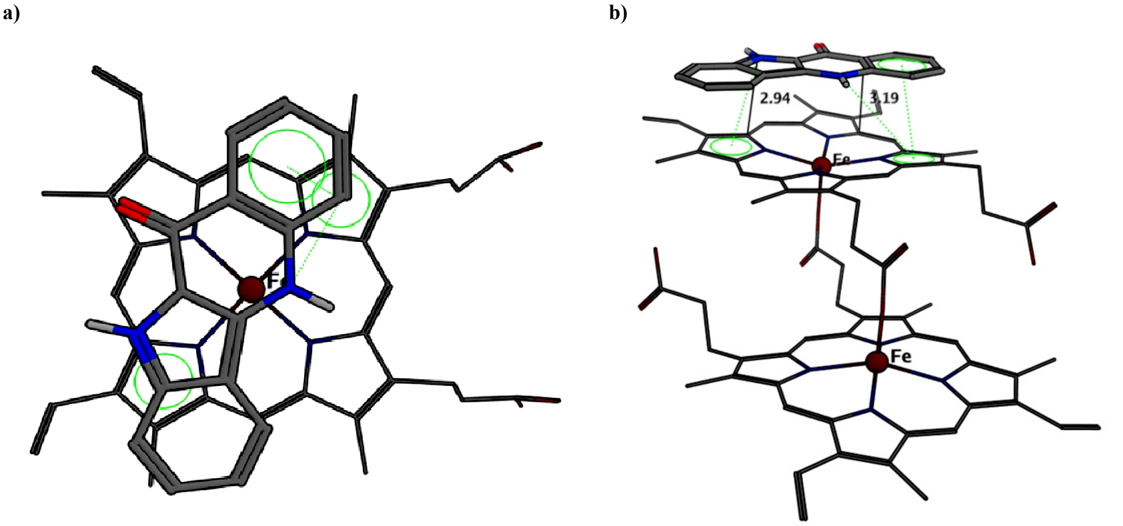

Figure 5.10 – Model of quindolone (**4**) interacting with haemozoin dimer. a) quindolone top-view; b) quindolone. (dashed-black. H-bond; solid green: π-π interactions; solid-black: distances; values in Å).

Quindolone derivatives

Quindolone derivatives **5**, **94** and **95** were also docked against haemozoin dimer. The results for **5a**, **94a** and **95a** are shown in Figure 5.11. Quindolone **5a** stacks over the porphyrin ring with an intermolecular distance of ca. 3 Å. Like to the other indolo[3,2-*b*]quinolines the complex stabilization is achieved due to the π-π stacking interactions between both aromatic rings. The distance between the terminal nitrogen in the side chain linked into N^{10} is approximately 7 Å, which due to its H-bond with carboxylate groups, in addition to the sterical hindrance induced by the orientation of the side chain, obligates the indolo[3,2-*b*]quinoline ring to stay on the edge of the porphyrin ring. The side chain linked to N^5 stays above the plan of the indolo[3,2-*b*]quinoline ring with the terminal nitrogen interacting with the porphyrin ring through π-stacking interactions.

The quindolone derivatives **5b** and **5c** showed similar results to those described for **5a**. Also quindolone derivatives **94a** and **94b** docked with haemozoin stack over the porphyrin aromatic ring with a intermolecular distance of ca. 3 Å. Complex stability with **94a** is also achieved due to π-π stacking interactions between both aromatic nucleus and due to the H-bond between the protonated terminal amine side chain and the carboxylate anions of haemozoin dimer. However, for **95a** the stability of the complex is only enhanced by π-π stacking interactions in absence of H-bond involving terminal amine side chain.

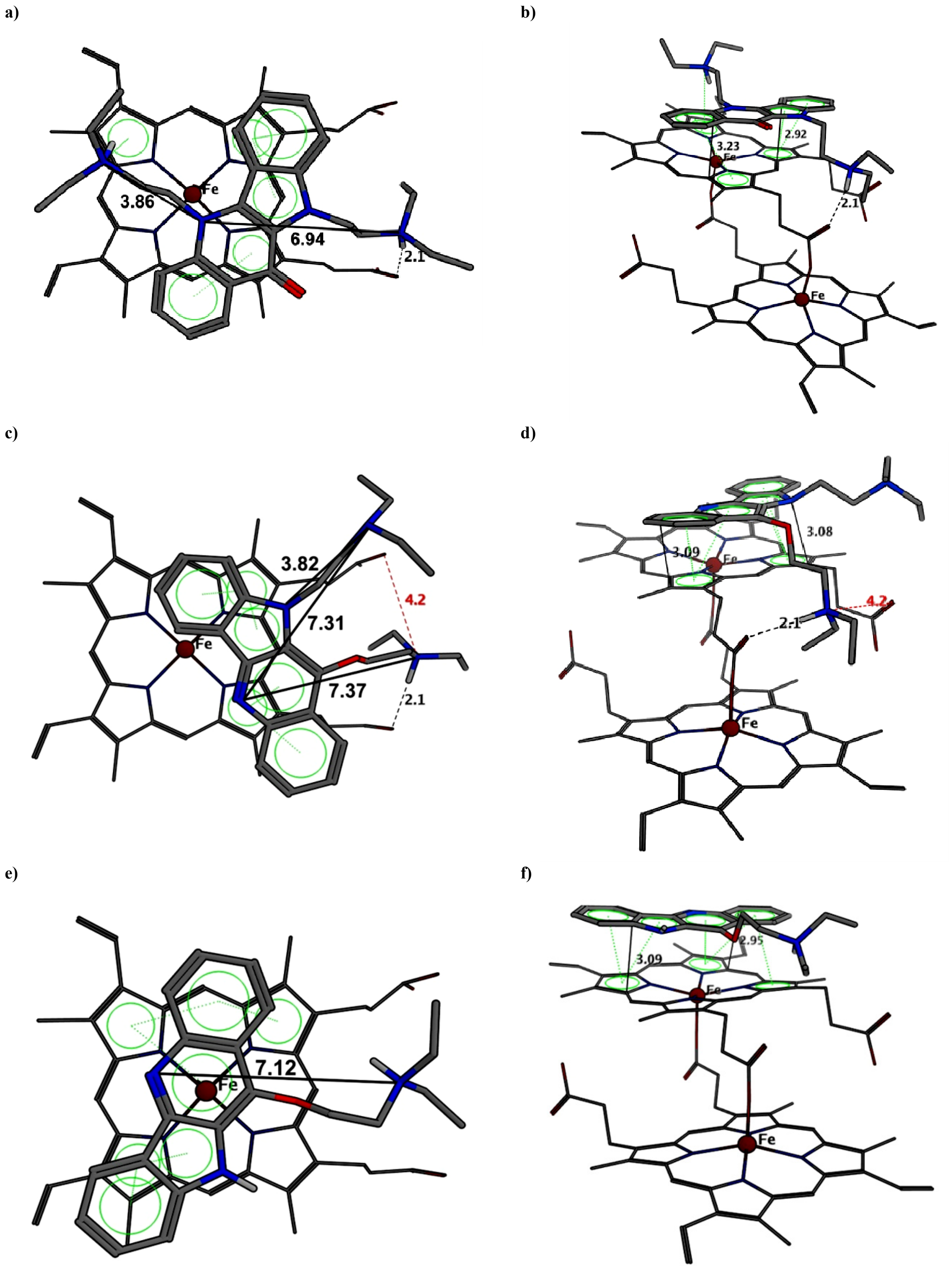
a)
Fe
3.86
6.94
2.1
b)
3.23
2.92
Fe
2.1
Fe
c)
3.82
4.2
7.31
Fe
7.37
2.1
d)
3.08
3.09
Fe
4.2
2.1
Fe
e)
7.12
Fe
f)
2.95
3.09
Fe
Fe

Figure 5.11 – Model of quindolone derivatives **5a**, **94a** and **95a** interacting with haemozoin dimer. a) **5a** top-view; b) **5a**; c) **94a** top-view; d) **94a**; e) **95a** top-view; f) **95a.** (dashed-black. H-bond; solid green: π-π interactions; dashed-red: ionic binding; solid-black: distance; values in Å).

For derivative **94a**, the side chain attached to N^{10} is positioned above the plane of the indolo[3,2-*b*]quinoline ring an unable to interact with the haemozoin dimer. As described for quindolone derivative **5a**, the formation of H-bond between the terminal amine of the side chain and the sterical hindrance induced by the side chain orientation, force the indoloquinoline aromatic nucleus to stack on the edge of the porphyrin ring system.

Table 5.6 – GoldScore(380) values of the docking studies of quindolones (**4**, **91a** and **91b**), as well as of its derivatives **5**, **94** and **95** with haematin dimer using GOLD software.

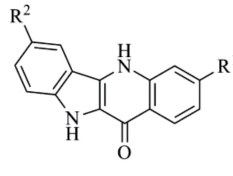

4 or **91**

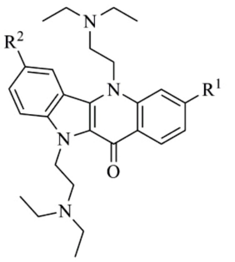

5

	R^1	R^2	GoldScore
4	H	H	42.65
91a	Cl	H	44.17
91b	Cl	Cl	45.26

	R^1	R^2	GoldScore
5a	H	H	37.50
5b	Cl	H	37.21
5c	Cl	Cl	37.83

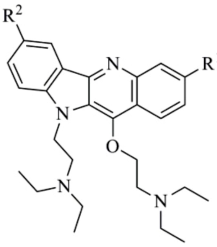

94

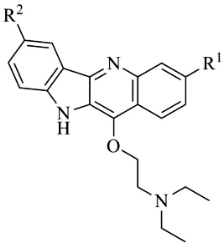

95

	R^1	R^2	GoldScore
94a	H	H	44.17
94b	Cl	H	44.35
94c	Cl	Cl	46.04

	R^1	R^2	GoldScore
95a	H	H	47.13
95b	Cl	H	48.34
95c	Cl	Cl	49.19

The docking fitness values for the quindolone derivatives **5**, **94** and **95** presented in Table 5.6 showed that derivatives **95** have the highest GoldScore values, ranging between 47.13 and 49.19, pointing out that these derivatives have higher degree of fitting with the haemozoin dimer than **5** and **94**. The lowest values was found to derivatives **5**, ranging between 37.50 and 37.83, and probably reflect the orientation of the side chain that stays above the plan of indolo[3,2-*b*]quinoline, away from possible interactions with the porphyrin ring. Nevertheless, derivatives **94** also have a side chain out of the plane and the GoldScore values are substantially higher than those of **5**, ranging from 44.17 to 46.04. As already verified to the quindolones themselves, the introduction of chlorine in the indolo[3,2-*b*]quinoline aromatic nucleus seems to point out to an increase of the binding affinity with the haemozoin dimmer.

Overall, the docking results suggest that quindolone derivatives **5**, **94** and **95** are able to stack over the porphyrin ring of haemozoin due to the formation of π-π stacking interactions. Also the terminal amine side chain can form H-bonding between one of the protonated terminal amine side chains with the carboxylate groups of the porphyrin ring.

VI

Chapter VI – **General Discussion and Conclusions**

> "A man should look for what is, and not for what he thinks should be..."
>
> **Albert Einstein** (1879-1955)
> *German-born Swiss-American theoretical physicist*

Abstract

Cryptolepine and quindolone derivatives have been synthesized through the incorporation of basic side-chains in the 10H-indolo[3,2-b]quinoline scaffold and evaluated for their antiplasmodial and cytotoxicity properties. Cryptolepine derivatives ***3*** *with propyl, butyl and cycloalkyl diamine side-chains significantly increased antiplasmodial activity against both chloroquine-resistant and chloroquine-sensitive P. falciparum strains when compared with the parent compound, while cytotoxicity was in general lower than that of cryptolepine. The derivative containing a conformationally restricted piperidine side-chain presented* IC_{50} *values of 23-44 nM against chloroquine-resistant strains and a selectivity index value of ca 1400, i.e. a 1000-fold improvement in selectivity when compared with the parent compound. Introduction of a basic terminal amine promotes accumulation inside the acid digestive vacuole to an extent similar to that of chloroquine. However, Localization studies inside parasite blood stages suggest a dual mechanism of action, oscillating between inhibition of haemozoin formation and cytotoxicity induced by DNA interactions. The quindolone derivatives with one or two basic side chains (****5****,* ***94*** *and* ***95****) were evaluated for antiplasmodial activity against chloroquine-resistant P. falciparum W2 strain and cytotoxicity for HepG2 A16 hepatic cells. By incorporating alkylamine side chains and chlorine atoms in the quindolone nucleus we transformed the inactive tetracyclic parent quindolones into moderate or highly active and selective compounds to the resistant P. falciparum W2 strain. The most active and selective compound,* ***5c****, showed an* IC_{50} *= 51 nM for P. falciparum and a selectivity ratio of 98. However, the aantiplasmodial activity of bis-alkylamine quindolone derivatives cannot be entirely justified by their affinity to haematin monomer.*

List of Contents

6.1 INTRODUCTION 139
6.2 CHEMISTRY AND STRUCTURAL CHARACTERIZATION 140
6.3 ANTIPLASMODIAL ACTIVITY, CYTOTOXICITY AND MODE OF ACTION 143
6.3.1 Cryptolepine and Derivatives 143
6.3.2 Quindolones and Derivatives 156
6.4 CONCLUSIONS 159

6.1 Introduction

The emergence and spread of chloroquine-resistance *Plasmodium falciparum* parasites has been a major global health problem and contributes to the continued high prevalence of malaria.(104, 404) Thus, new and safe drugs active against multi-resistant *P. falciparum* strains are needed. Over the centuries, medicinal plants have been used for treating parasitic diseases, including malaria, and since the beginning of the last century constitute an important source of molecules for new lead compounds.(129, 188-189, 405)

Cryptolepine, **1** is an indolo[3,2-*b*]quinoline alkaloid first isolated in 1929(1) from the roots of *Cryptolepis sanguinolenta*, a traditional herb used in traditional medicine for the treatment of malaria in Central and West Africa.(4, 198) The antimalarial mode of action it is not yet clarified, but it was shown that the activity is due, at least in part, to a chloroquine-like action, i.e, inhibition of haemozoin formation (the haem detoxification path way of the malaria parasite) in the parasite digestive vacuole, via π-π stacking interactions with the porphyrin moiety.(77, 119, 134, 160, 210) However, cryptolepine possess cytotoxic properties which precluded its clinical used. These cytotoxic properties are likely to be due to its DNA interactions properties and its ability to intercalate into GC-rich sequences, inhibit topoisomerase II as well as DNA synthesis.(5-8) In addition, a cellular localization study by Arzel and co-workers showed that cryptolepine accumulates into specific structures of the parasite that could correspond to the parasite nucleus, showing that its antiplasmodial activity could also be due to the interactions with the DNA.(255) This suggests that the affinity of **1** for haeme may not be sufficient to drive its accumulation on the digestive vacuole in the absence of a pH-dependent trapping mechanism, as proposed for chloroquine.(406)

Additionally, a previous study developed in our research unit, showed that cryptolepine natural derivatives substituted in position C11 with acidic groups had no *in vitro* antiplasmodial activity.(198) Thus, we decided to introduce in this position a basic amino side chain, which is the major requirement for chloroquine accumulation inside the parasite digestive vacuole.(407) The basic amino side chain would increase the accumulation inside the acid digestive vacuole of the parasite, as well as, bind to the propionate group of haeme, through ionic and/or hydrogen bond, increasing the drug:haem complex stability and thus inhibiting the growth of haemozoin crystal.(77) In addition, we also decided to initiate a second line of research, based on the indolo[3,2-*b*]quinoline scaffold. Based on quindolone structure

(**4** and **91**) we decided to introduce a basic amino side chain in position N^5 and N^{10} of the aromatic nucleus. As for the cryptolepine derivatives **3** an ionisable side chain is expected to promote the accumulation of compounds in the parasite acidic digestive vacuole and target haemozoin crystal growing faces.

6.2 Chemistry and Structural Characterization

Cryptolepine and quindolones derivatives were synthesized through a common synthetic methodology that allowed us to achieve key indolo[3,2-*b*]quinolones (**4** and **91**) intermediates. Cryptolepine derivatives **3** and quindolone derivatives **5** were synthesized according to the route depicted in Scheme 6.1, based on the procedure developed by Görlitzer and Weber(11-12) and adapted by Bierer,(13-14) via intermediate **93** for derivatives **3** and intermediate **4** or **91** for derivatives **5**.

Anthranilic acids, **88**, were treated with bromoacetyl bromide to afford the corresponding bromoacetyl derivatives **89**, which were then reacted with the appropriate aniline to give compounds **90**. Acid-catalyzed cyclization of **90** with polyphosphoric acid (PPA) gave the indolo[3,2-*b*]quinolin-11-ones (quindolones) **4** or **91**, which, by reaction with $POCl_3$, gave the corresponding substituted 11-chloro-indolo[3,2-*b*]quinolines (11-chloroquindolines) **92**. Hydrogenation of **92a** with 10 % Pd-C at 60 psi, provided the indolo[3,2-*b*]quinoline **(**quindoline) **25**. N^5 methylation of **25** and **92** was achieved by reaction with methyl triflate and the 5-methyl-indolo[3,2-*b*]quinoline derivatives were then treated with hydrochloric acid to afford the corresponding cryptolepine chlorides, **93**. Finally, cryptolepine derivatives **3a-n** and **3r-y** were obtained generally in good yields (30-82%) by aromatic nucleophilic substitution on **93** with excess of appropriate amine. Compounds **3o-q** were synthesized by reaction of **3n** with isobutyraldehyde, benzylaldehyde and salicyladehyde, and subsequent reduction with $NaBH_3CN$, in 59, 66 and 30 % yields, respectively (Scheme 6.1).

For derivatives **3d**, **3j**, **3l**, and **3t**, it was necessary to synthesize the corresponding diamines required for the substitution reaction with **93**. Thus, N^1,N^1-dimethylpropane-1,2-diamine, **97**, used for the synthesis of **3d**, was prepared by reductive amination of *N*,*N*-dimethylaminopropanone, **96**, with ammonium acetate and $NaBH_3CN$ (Scheme 2.10). 3-(Piperidin-1-yl)propan-1-amine, **100**, required for the synthesis of **3j**, was prepared via Gabriel synthesis, using phthalimide **98** as starting material (Scheme 2.10). N^1,N^1-Diethylbutane-1,4-diamine, **103**, required for the synthesis of **3l**, was prepared by reductive alkylation of **101** with acetaldehyde and $NaBH_3CN$, followed by removal of the Boc protecting group with triflouroacetic acid (Scheme 2.10). Compound **3t** was synthesized by reaction of **93a** with acetamide, **105**, which was obtained by Mannich reaction of phenol **104** with formaldehyde and diethylamine (Scheme 2.10).

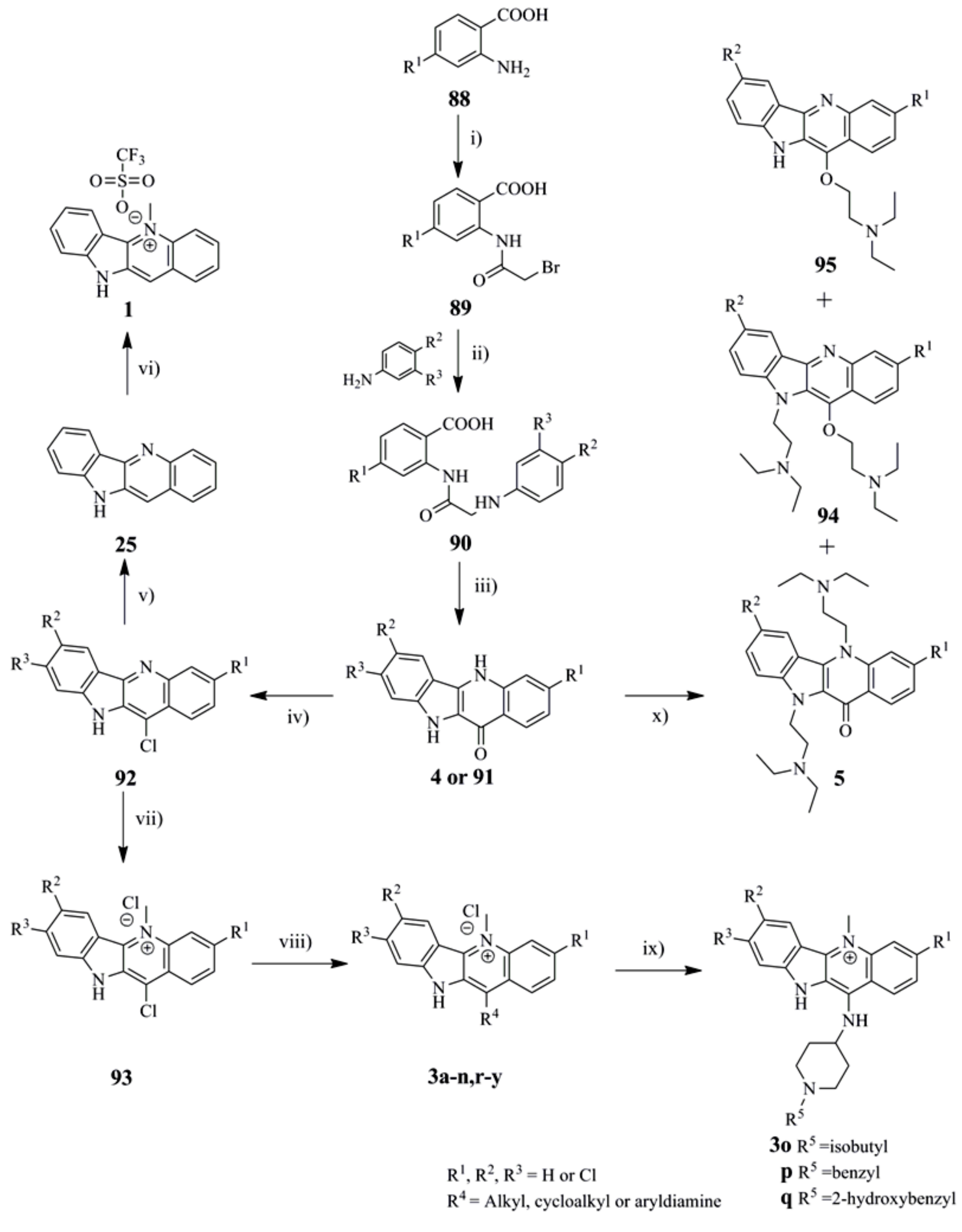
88
i)
89
ii)
90
iii)
4 or 91
iv)
92
v)
25
vi)
1
vii)
93
viii)
3a-n,r-y
ix)
x)
5
94
95
3o R⁵ =isobutyl
p R⁵ =benzyl
q R⁵ =2-hydroxybenzyl
R¹, R², R³ = H or Cl
R⁴ = Alkyl, cycloalkyl or aryldiamine

Scheme 6.1 – Synthesis of the cryptolepine derivatives (**3**) and quindolone derivatives (**5**).

i) Bromoacetyl bromide, DMF/1,4-dioxane (1:1), r.t., overnight; ii) DMF, 120 ºC, 18 to 96h: iii) PPA, 130 ºC, 2h; iv) $POCl_3$, reflux, 2h; v) H_2, Pd-C 10% NaOAc, AcOH, 60 psi, 2h or EtSiH, 10% Pd-C, MeOH, 20 min; vi) MeOTf, toluene, r.t., 24h.; vii) MeOTf, toluene, r.t., 24h.; viii) AcOEt, diamine, reflux, 24h; ix) **3n**, aldehyde, anhydrous Na_2SO_4, $NaBH_3CN$, dry MeOH, ***r.t.***, 24 h x) 2-chloro-*N,N*-diethylethanamine, dry acetone, K_2CO_3, NaI, reflux, overnight.

Structures of all key intermediates and final compounds were established on the basis of NMR ^1H-^1H homonuclear correlation spectroscopy (COSY and NOESY) and ^1H-^{13}C heterocorrelation experiments (HMQC and HMBC). Position of the side chain at C11 was confirmed by NOE difference experiments (Section 2.2.3). Both, cryptolepine and quindolone derivatives were also characterized with

C, N, H elemental analysis, showing that the purity of all compounds submitted for biological testing were in all cases ≥ 95%.

Cryptolepine derivatives **3** showed a shield effect on ^{1}H chemical shifts of N^5-CH_3 of 0.1 to 0.45 ppm when compared with **93**. Additionally, the ^{13}C chemical shifts of C10a and C11a showed an upfield shift in the order of 10 ppm and for N^5-CH_3 of 3 ppm when compared to **1** and **93**, whereas the chemical shift of C11 showed a deshielding effect of ca. 10 to 15 ppm when compared with the parent compounds **1** and **93**.

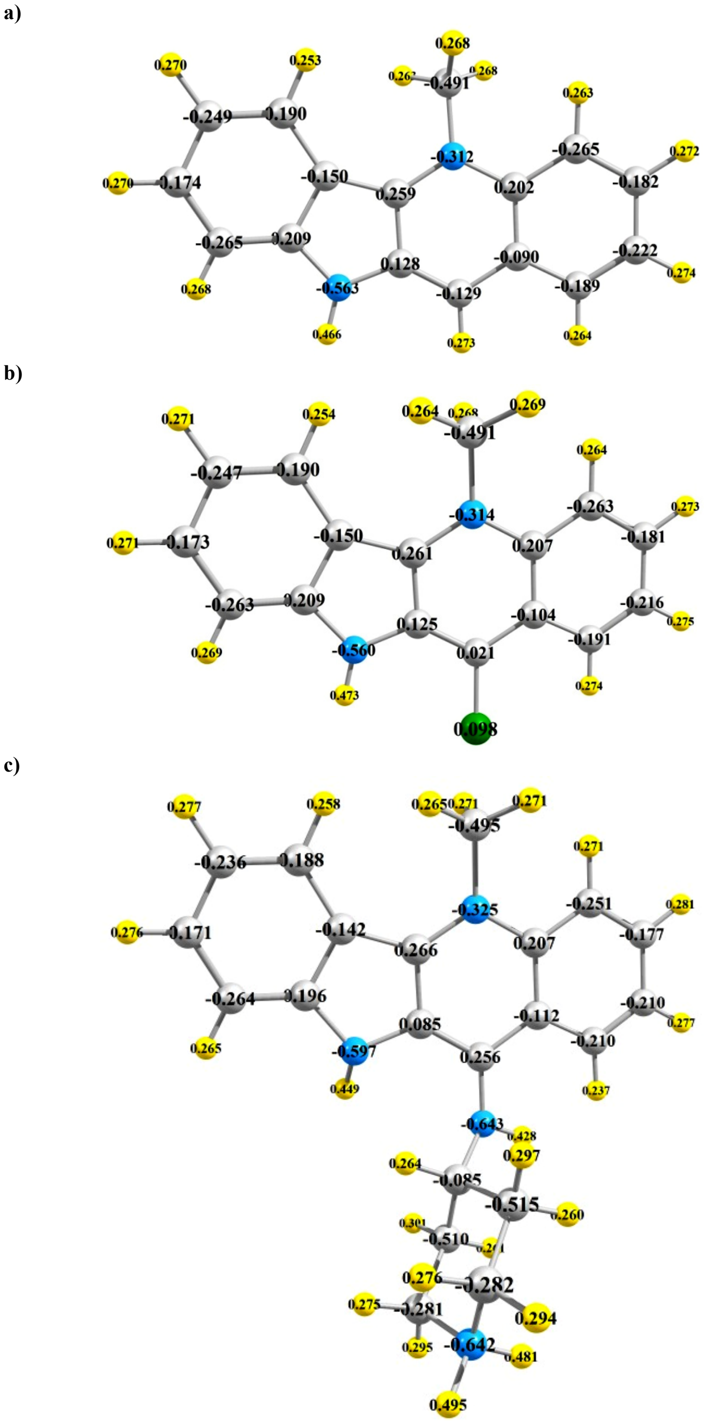
a)
0.268
0.270
0.253
0.262
-0.491
0.268
0.263
-0.249
0.190
-0.312
-0.265
0.272
-0.150
0.259
0.202
-0.182
0.270
-0.174
-0.265
0.209
0.128
-0.090
-0.222
0.274
-0.563
-0.129
-0.189
0.268
0.466
0.273
0.264
b)
0.271
0.254
0.264
0.268
0.269
-0.491
0.264
-0.247
0.190
-0.314
-0.263
0.273
0.271
0.173
-0.150
0.261
0.207
-0.181
-0.263
0.209
-0.104
-0.216
0.275
0.125
-0.191
0.269
-0.560
0.021
0.473
0.274
0.098
c)
0.277
0.258
0.265
0.271
0.271
-0.495
0.271
-0.236
0.188
-0.325
-0.251
0.281
0.276
0.171
-0.142
0.266
0.207
-0.177
-0.264
0.196
0.085
-0.112
-0.210
0.277
0.265
-0.597
0.256
-0.210
0.449
0.237
-0.643
0.428
0.297
0.264
-0.085
-0.515
0.260
0.301
-0.510
0.271
0.276
-0.282
0.275
-0.281
0.294
0.295
-0.642
0.481
0.495

Figure 6.1 – Natural bond orbitals (NBO) charges of **1**, **93** and cryptolepine derivatives **3n**. (Atomic charges in atomic units, a.u.)

Analysis of the Natural Bond Orbitals (NBO) charges of the cryptolepine derivatives **3** in comparison with the parent compounds **1** and **93** allow us to understand their nuclear magnetic resonance behaviour. Figure 6.1 shows the NBO charges of **1**, **93** and derivative **3n**. The introduction of the side chain in position C11 of the indolo[2,3-*b*]quinoline nucleus induce a reduction of NBO charge in the carbon attached to N^5 (N^5-CH_3) of 4 atomic units for **3n** (increased electron density), when compared with **1** and **93**, justifying the shielding effect verified on the ^{13}C NMR chemical shifts of CH_3-N^5. Although, NBO charges do not explain the upfield shift of N^5-CH_3 protons on the ^1H NMR spectra, since in the charge analysis it is observed and increase of charge (≈ 3 a.u.) in these protons, prefiguring a decrease on electron density on the hydrogens. Additionally, the verified upfield ^{13}C NMR shift of C10a and C11a could be justified by the increased electron density in these atoms, due to the introduction of the side chain. The predicted NBO charges, which showed a reduction of the charge ca. 40 and 20 a.u. for C10a and C11a, respectively, when compared with **1** and **93**, justifying the verified upfield shift. The introduction of the side chain in C11 decreases the electron density in this atom as verified with the increasing of ca. 300 a.u. in the NBO charge, which is also verified in ^{13}C NMR with a downfield shift of ca. 10 to 15 ppm when compared to the parent compounds **93** and **1**, respectively.

Quindolone derivatives **5** were synthesized from the common intermediate **4** or **91** after reaction with 2-chloro-*N,N*-diethylethanamine in presence of base, yielding from 19 to 23 %. Although, due to the tautomeric resonance in the quindolone aromatic ring (Figure 2.16) in presence of base, the oxygen nucleophilic species are more reactive than the N^5 nucleophilic species, and thus synthetic methodology gave two more products besides **5**, the 10-(2-(diethylamino)ethyl)-*10H*-indolo[3,2-*b*]quinolin-11-yl)oxy)-*N,N*-diethylethanamines **94** and the *10H*-indolo[3,2-*b*]quinolin-11-yl)oxy)-*N,N*-diethylethanamines **95** (Figure 2.18). The major products of the reactions were compounds **94**, yielding between 34 and 55% (Table 2.3.).

The synthetic methodology adapted by Bierer,(13-14) was applied to the synthesis of the indolo[3,2-*b*]quinolines and proved to be efficient, allowing the synthesis of cryptolepine derivatives. Derivatives **3** were obtained from the intermediate **93**, with large chemical diversity, good yields and high degree of purity. Also, this synthetic methodology showed to be efficient for the synthesis of quindolone derivatives from the common intermediate **4** or **91**, allowing the possible exploration of the chemical diversity and substitution on the aromatic nucleus, giving compounds in good yields and with high degree of purity.

6.3 Antiplasmodial Activity, Cytotoxicity and Mode of Action

6.3.1 Cryptolepine and Derivatives

In vitro **Antiplasmodial Activity in human red blood cells and cytotoxicity**

The synthesized cryptolepine derivatives **3** were evaluated *in vitro* for their antiplasmodial activity in Human red blood cells infected with 1% ring stage *P. falciparum*(408-409) strains with different drug resistance phenotypes (Dr. Phil Rosenthal laboratory): W2 (chloroquine-resistant), 3D7 (chloroquine-sensitive), V1/S (chloroquine- and pyrimethamine-resistant) and D6 (chloroquine-sensitive, mefloquine-resistant). The *in vitro* cytotoxicity of compounds **3** and cryptolepine was evaluated using mammalian *Vero* cells (Dr. Cecília Díaz laboratory). Table 6.1 shows the *in vitro* antiplasmodial activity (IC_{50}) and cytotoxic activities (IC_{50}) against *Vero* cells of **3** together with their selectivity index ($IC_{50}^{Vero}/IC_{50}^{W2}$) and resistance index (RI), as expressed by the ratio $IC_{50}^{W2}/IC_{50}^{3D7}$. The IC_{50} values are calculated from experiments carried out in triplicate and compared with CQ. The cryptolepine derivative (**3n**) was also evaluated against liver stages of the rodent malaria parasite *P. berghei*.

The *in vitro* antiplasmodial activity data (IC_{50}) showed that these cryptolepine derivatives showed good antimalarial activity (IC_{50} ranging from 21 to 1252 nM against W2 strain) and low RI (ranging from 0.2 to 3.5), suggesting that the introduction of the diamine side chains is very well tolerated and a promising approach to the development of indolo[3,2-*b*]quinoline based antimalarials. Also, a comparison of SI results, reveals that compounds **3** were significantly more selective than the parent compound **1**,with **3a**, **3k** and **3n** being 60- to 85-fold less cytotoxic than cryptolepine.

Cryptolepine was found to be 2- to 3.5-fold more active against the CQ-S strains than to CQ-R strains with RI value of 2.9, similar to that published in previous reports, while chloroquine showed a RI value of 25.(4, 9, 198, 210, 410) The introduction of an alkyldiamine side chain at C11 (**3a-y**) improved significantly the antiplasmodial activity against *P. falciparum* chloroquine-resistant strains W2 and V1/S (IC_{50} values range from 20 to 455 and from 20 to 536 nM, respectively) and against *P. falciparum* chloroquine-sensitive strains 3D7 and D6 (IC_{50} values ranging from 15 to 422 and from 24 to 287 nM, respectively). Also, the introduction of the diamine side chain reduced notably the resistance index, in almost cases, when compared with **1** (RI values range from 0.2 to 3.5). The introduction of a tertiary amine at C11 of the cryptolepine nucleus without terminal basic nitrogen (**3y**), reduced appreciably the antiplasmodial activity against all studied strains (IC_{50} values range from 1252 to 2205 nM). These results clearly indicate that an alkyldiamine side chain with weak basic properties is a requirement for the antiplasmodial activity of the new cryptolepine derivatives. The exception seems to be derivatives **3** containing a terminal primary amine, as these compounds displayed reduced activity, particularly against CQ-S strains 3D7 and D6, when compared with compounds with secondary (**3e** vs. **3i**) or tertiary terminal amines (e.g. **3a** vs. **3c**, **3e** vs. **3g** and **3k** vs. **3l**). The reason for these differences in activity is not obvious and an extended evaluation of terminal amines will be necessary to further understand the loss of potency in compounds **3** with a terminal primary amine. Also, these compounds (**3a**, **3e** and **3k**) showed to be significantly more selective (higher SI) than the parent compound. Compound **3e** showed the highest acid dissociation constant in the terminal nitrogen of the side chain ($pK_{a1}^{*} > 12.5$, Table 3.4) of all the evaluated derivatives, and it is predicted to be fully protonated at physiological pH. Thus, this protonation state, may difficult the passage through biological membranes and induce lower cytotoxic effects when compared with the others derivatives **3**.

In vitro antiplasmodial activity SAR

The variations in the antiplasmodial IC_{50} values of **3** can be attributed to several factors and some structure activity relationships can be drawn:

Side chain length: side chains with three (**3e-j**) and four carbons (**3k-m**) present better antiplasmodial activity than compounds with side chains with two carbons(**3a-d**) and in general side chains with four carbons presents lower RI (**3k-m**). For instance, the *N,N*-diethylaminopropyl and *N,N*-diethylaminobutyl derivatives, **3g** and **3l**, are about 2.5 times more potent that their ethyl counterpart, **3c**, against the CQ-resistant W2 strain. These results are largely consistent with reports that 4-aminoquinoline derivatives with shortened side chains retain activity against CQ-resistant strains.(411-412)

Branched side chains: the introduction of branched side chains produce compounds with reduced antiplasmodial activity, independently of the side chain length, when compared with their counterparts (two carbons: **3d** vs. **3a-c**, three carbons: **3h** vs. **3e-g,i-j**, four carbons: **3m** vs. **3k-l**). Furthermore, compound **3m**, containing a side chain identical to that of chloroquine, displayed reduced activity against both CQ-resistant and CQ-sensitive *P. falciparum* strains (IC_{50} ranging from 120 to 275 nM), being 2- to 6-fold less potent than its linear butyl counterpart **3l**. These results are in line with the observation that 4-aminoquinolines containing the chloroquine side chain give consistently lower potency than those with a propyl side chain against both 3D7 and W2.(138)

Cycloalkyl side chains: Compounds with less flexible piperidine side chain (**3n**) was highly active against both CQ-resistant and CQ-sensitive strains, suggesting that a conformational constraint between the distal basic center and the indolo[3,2-*b*]quinoline scaffold may improve potency. Appending a sterically demanding iso-butyl or benzyl group to the nitrogen atom of the piperidine moiety (**3o** and **3p**, respectively) did not significantly alter antiplasmodial activity. To our surprise, the derivative containing a 2-hydroxybenzyl group, **3q**, was 2- to 10-fold less active than its benzyl counterpart, **3p**, since it is recognized that introduction of H-bond acceptors increase the antiplasmodial activity.(137)

Aromatic side chains: side chains with higher electron density (**3r-s, u**) reduced significantly the antiplasmodial activity of these cryptolepine derivatives, when compared to derivatives with aliphatic side chains. In contrast, compound **3t**, which contains a 2-diethylaminomethylphenol moiety, exhibited IC_{50} values of about 20 nM and 54 nM against the CQ-sensitive and CQ-resistant strains, respectively. The 2-diethylaminomethylphenol and related α-aminocresol motifs are commonly found in potent antimalarials such as amodiaquine (**14**) and its isomer isoquine,(144-145, 406) and it has been postulated that intramolecular hydrogen bonding between the protonated amine (H-bond donor) and the hydroxyl (H-bond acceptor) may be an important feature for activity against CQ-resistant *P. falciparum* strains.(137) Although, incorporation of isoquine's α-aminocresol motif at C11 (i.e. **3t**), resulted in a cytotoxicity level comparable to that of cryptolepine, despite the improvement in SI.

Table 6.1 – *In vitro* antiplasmodial activity (IC_{50}) against *P. falciparum* W2, V1/S, 3D7 and D6 strains, cytotoxicity activity (IC_{50}) against *Vero* cells, selectivity index (SI), resistance index (RI), association constants (K_{ass}) in pH 5.5 DMSO solutions with haematin at 25 ºC and K_{ass} in phosphate buffer pH 7.4 containing 0.1 M NaCl with ds-DNA at 25 ºC of cryptolepine (**1**), derivatives **3** and chloroquine (**2**).

	R^1	R^2	R^3	*In vitro* antiplasmodial activity IC_{50}[a] (nM)				IC_{50} *Vero* cells (µM)	SI[b]	RI[c]	Haeme binding K_{ass} ($10^6 M^{-1}$)	ds-DNA binding K_{ass} ($10^6 M^{-1}$)
				W2	V1/S	3D7	D6					
2	–	–	–	138±16	89±31	5.5±0.3	14.2±0.3	-	–	25	0.085±0.005	–
1	H	H	H	755±1	424±78	259±29	222±5	1.05±0.03	1.4	2.9	0.045±0.003	0.25±0.01
3a	H	H	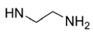	89±8	115±68	156±40	107±10	60±20	678	0.6	0.127±0.007	0.85±0.01
3b	H	H	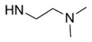	50±8	62±3	85±26	66±8	5.5±0.5	111	0.8	0.120±0.005	3.1±0.7
3c	H	H	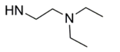	82±23	130±18	72±1	70±5	2.8±0.5	34	1.2	0.41±0.03	1.14±0.05
3d	H	H	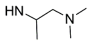	142±2	202±47	165±25	78±5	3±1	23	0.9	0.148±0.008	1.9±0.1
3e	H	H	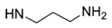	26±5	54±16	133±3	71±10	10±4	371	0.2	0.18±0.02	0.25±0.01
3f	H	H	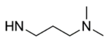	20±1	24±2	51±1	46±5	2.2±0.04	109	0.4	0.066±0.005	3.0±0.2
3g	H	H	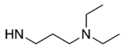	32±5	20±8	29±3	32±2	2.5±0.3	78	1.1	0.127±0.007	9.1±0.6
3h	H	H	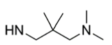	184±21	146±22	144±6	250±25	3±1	18	1.3	0.069±0.007	2.6±0.4
3i	H	H	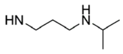	22±2	26.1±0.6	28±1	34±1	3±1	125	0.8	0.20±0.01	5.0±0.8
3j	H	H	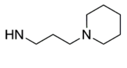	36±2	23±9	28±7	34±5	2.0±0.3	56	1.3	0.161±0.008	5.3±0.3
3k	H	H	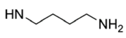	65±1	190±59	422±15	245±71	>85	1307	0.2	0.147±0.006	1.4±0.1
3l	H	H	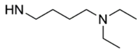	29±2	22.3±0.4	66±7	71±2	10±3	358	0.4	0.15±0.01	9±1
3m	H	H	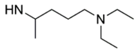	122±3	145±5	274±25	161±9	13±5	103	0.4	0.062±0.07	4.3±0.2
3n	H	H	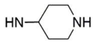	44±1	23±5	60±12	59±1	62±9	1408	0.7	0.154±0.006	0.74±0.03
3o	H	H	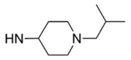	70±1	70±34	76±1	86±25	5±1	70	0.9	0.227±0.008	0.74±0.07
3p	H	H	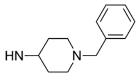	108±19	56±16	59±2	86±15	2.2±0.1	21	1.8	0.125±0.007	0.68±0.09
3q	H	H	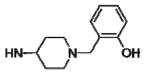	276±31	536±7	418±76	185±29	2.6±0.7	10	0.7	0.108±0.005	0.6±0.3
3r	H	H	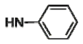	265±70	291±241	128±2	154±29	0.6±0.2	2	0.2	0.155±0.008	0.51±0.06
3s	H	H	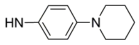	455±18	375±56	176±17	287±67	4.83±0.07	11	2.6	0.21±0.02	3.4±0.6
3t	H	H	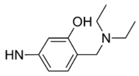	52±1	56±22	15±2	24±1	0.8±0.3	17	3.5	0.075±0.009	0.8±0.3
3u	H	H	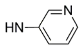	180±14	247±34	279±71	166±2	2.6±0.6	14	0.6	0.17±0.01	1.0±0.1
3v	Cl	H	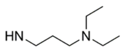	21±1	34±15	40±12	70±9	1.3±0.4	60	0.5	0.11±0.01	17±1
3w	Cl	H	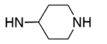	45(±1)	65±4	52±4	70±16	4.4±0.2	98	0.9	0.18±0.01	4.5±0.4
3x	Cl	Cl	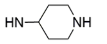	48±6	31±12	35±4	30±2	0.8±0.3	16	1.4	0.12±0.01	1.6±0.4
3y	H	H	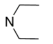	1252±98	2205±689	1773±70	1289±69	3±2	2	0.7	0.19±0.01	0.47±0.06

[a]The IC_{50} values are calculated from experiments carried out in triplicate and compared with CQ, [b]Selectivity index expressed by the ratio $IC_{50}^{Vero}/IC_{50}^{W2}$, [c]Resistance index expressed by the ratio $IC_{50}^{W2}/IC_{50}^{3D7}$

Halogen substitution in the aromatic nucleus: the introduction of substituents in the aromatic nucleus of cryptolepine does not affect significantly the antiplasmodial activity or the RI. The 3-chloro and 3,8-dichloro derivatives, **3w** and **3x**, respectively, were equipotent ($IC_{50} \approx 45$ nM) with their unsubstituted counterpart, **3n**, against the panel of CQ-sensitive and CQ-resistant strains, suggesting that introduction of electron-withdrawing substituents in the indolo[3,2-*b*]quinoline moiety does not significantly affect antiplasmodial activity when a diaminoalkane side chain is present at C11. Interestingly, it has been reported that 3-chlorocryptolepine is equipotent to cryptolepine against the *P. falciparum* K1 strain, while its 8-chloro counterpart is inactive.(9) In contrast 2,8-dichlorocryptolepine was found to be 10-fold more potent than cryptolepine, in the same screen. However, adding chlorine atoms to the indolo[3,2-*b*]quinoline with piperidine side chain (**3w** and **3x**) led to an increase in cytotoxicity, when compared to the unsubstituted counterpart, **3n**.

Basic distal amine functionally: the importance of a basic distal amine for antiplasmodial activity comes from the observation that compound **3y** which lacks a distal basic amine group is poorly active, with IC_{50} values of 1299 to 2200 nM against CQ-sensitive and CQ- resistant strains.

***In vitro* antiplasmodial activity in human hepatoma cells**

Cryptolepine and derivative **3n** were also assayed against liver stages of the rodent malaria parasite *P. berghei* up to a concentration of 5 μM, using a recently described fluorescence activated cell sorting (FACS)-based method (Dr. Maria M. Mota laboratory).(413) This method is based on the measurement of the fluorescence of Huh-7 cells, a human hepatoma cell line, following infection with GFP-expressing *P. berghei* sporozoites. Both compounds were inactive in this assay, a result that points toward the selectivity of **1** and derivatives **3** for erythrocytic stage malaria parasites.

***In vivo* antiplasmodial activity in Swiss Webster female mice**

Prompted by the great improvement in the *in vitro* antiplasmodial activity and selectivity of **3**, we evaluated compound **3n** and in an *in vivo* drug screening against *P. berghei* in Swiss Webster female mice (Dr. Phil Rosenthal laboratory).(408) However, administration of cryptolepine derivative **3n** 50 mg/kg twice per day via intraperitoneal route, led to the death of the animals at day 2.

Probing the site of action at cellular level

It is well known that cryptolepine may exert its antiplasmodial mode of action due to interactions with FPIX-OH (Fe^{3+}), inhibiting haemozoin formation in a mechanism similar to that of chloroquine and related aminoquinolines.(210) However, it is also known that cryptolepine exert its cytotoxic properties due to its DNA intercalating properties and can accumulate in parasite DNA-containing structures,(255) which led to the conclusion that cryptolepine interferes with the parasite's replication due to its DNA intercalating ability.(255)

In order to investigate if compounds **3** retain the ability to accumulate inside the blood stages of the parasite, the intracellular distribution of **3n** in blood stages of *P. falciparum* was studied by fluorescence microscopy (Dr. Maria M. Mota Laboratory). Figure 6.2 shows the contrast phase and fluorescence images of *P. falciparum*-infected erythrocytes after incubation of *P. falciparum* cultures with the compounds.

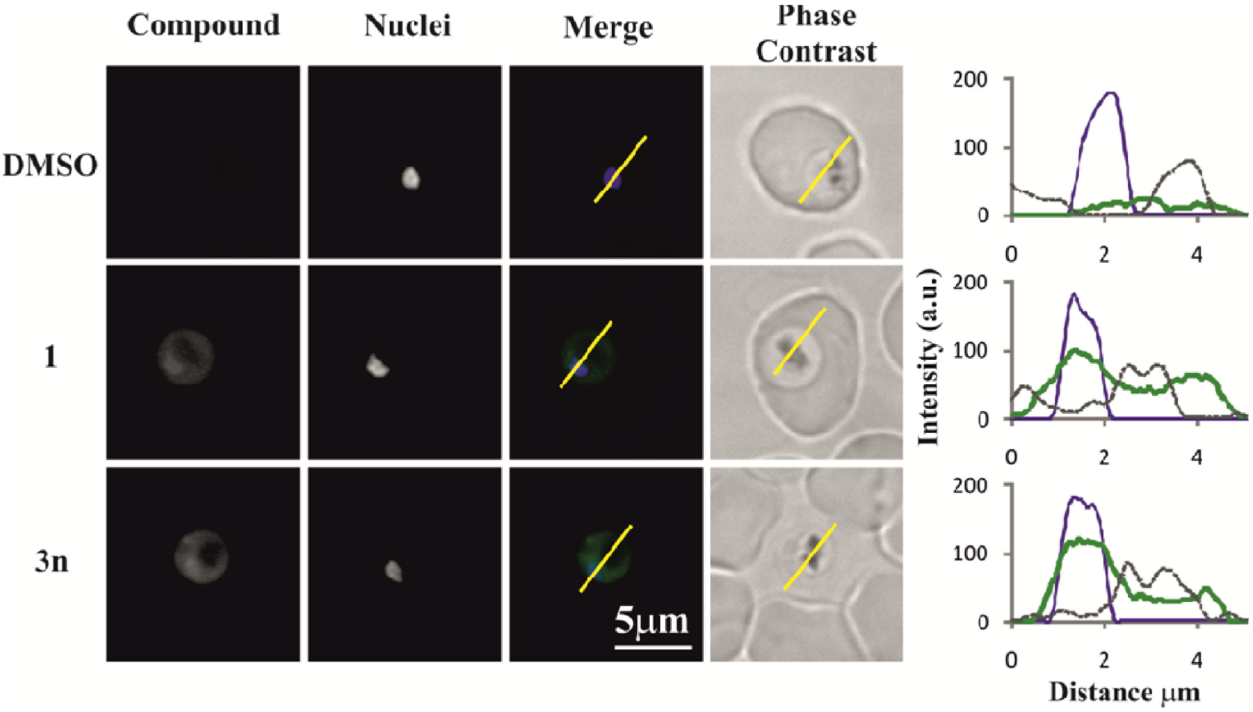

Figure 6.2 – Intracellular localization of **1** and **3n** in *P. falciparum*-infected erythrocytes.

Cells were incubated for 3 hours at room temperature, in the dark, with 5 μM of cryptolepine and its derivative **3n** and immediately observed after washed with PBS using a fluorescence microscope. The yellow lines indicate the regions corresponding to the plot profiles on the right. Green – compounds **1** or **3n**; blue – nuclei; gray line – gray scale intensity of phase contrast image.

Our data show that **1** and its derivative **3n** accumulate inside erythrocytic ring-stage parasites and the observed intensity of fluorescence indicates that nucleus and food vacuole are parasite organelles targeted by both compounds. It should be noted that hematin quenches very efficiently the fluorescence of cryptolepine derivative **3n**, around 60% for a 1:1 ligand:hematin concentration (**Erro! A origem da referência não foi encontrada.**a), a problem also reported for the fluorescence of acridine conjugates(414), but DNA only quenches 20% the fluorescence of **3n** (**Erro! A origem da referência não foi encontrada.**b). This result suggests that quenching of **3n** in the food vacuole may occur as a result of the presence of hematin, thus underestimating the vacuolar signal when compared with the nonvacuolar signal arising from accumulation in the nucleus.

Thus, cryptolepine and its derivatives **3** do not seem to show any specific preference for a parasite organelle and are able to accumulate also inside digestive vacuole.

Antiplasmodial potential targets - Haem

Localization of **3n** inside blood stages of parasite suggests that haemozoin crystal growing can be a mechanism of action for these compounds and our results showed that the presence of a distal basic nitrogen atom is important for potency, thus suggesting that accumulation in the acid digestive vacuole, where haemozoin formation occurs, is a requirement for biological activity of compounds **3**.

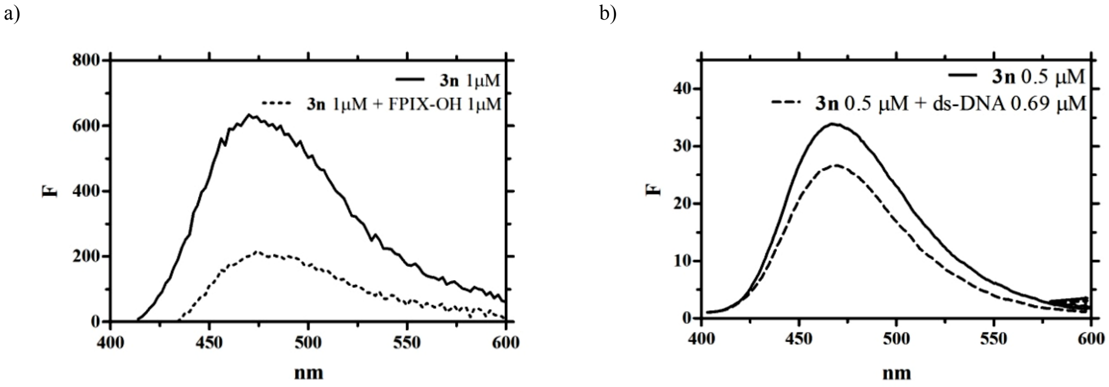

Figure 6.3 – a) Fluorescence emission spectrum (λ_{ex} = 339 nm) of 1 μM **3n** in the presence (dashed line) and absence (solid line) of 1μM FPIX-OH. b) Fluorescence emission spectrum (λ_{ex} = 339 nm) of 0.5 μM **3n** in the presence (dashed line) and absence (solid line) of 0.69 μM ds-DNA.

To predict the extent of their accumulation into the acidic parasite digestive vacuole, the pK_a values for cryptolepine (**1**) and derivatives **3b**, **3e**, **3f**, **3i**, **3n**, **3s** and **3y** were determined using a spectrophotometric and nuclear magnetic resonance methods, in addition to the pK_a values for the remain cryptolepine derivatives determined with spectrophotometric methods and predicted using the SPARC v3.2 on-line calculator (Appendix D).

A. Predicted accumulation in digestive vacuole of parasites

According to Kaschula and co-workers,$^{(123)}$ the extent of pH trapping of quinolines (vacuolar accumulation ratios, VAR), into the parasite digestive vacuole can be estimated from the corresponding pK_a values according to Eq. 6.1 where $[Q]_v$ and $[Q]_e$ represent the vacuolar and external concentrations of the compound, respectively, and $[H^+]_v$ and $[H^+]_e$ represent the vacuolar and external hydrogen ion concentrations. The calculation presupposes that equilibrium is achieved and assumes that the cellular membranes are completely impervious to the ionized aminoquinoline species.

$$\frac{[\mathrm{Q}]_v}{[\mathrm{Q}]_e} = \frac{\left\{1 + \frac{[\mathrm{H}^+]_v}{K_{a2}} + \frac{[\mathrm{H}^+]_v^2}{K_{a1}K_{a2}}\right\}}{\left\{1 + \frac{[\mathrm{H}^+]_e}{K_{a2}} + \frac{[\mathrm{H}^+]_e^2}{K_{a1}K_{a2}}\right\}}$$

Eq. 6.1 - Predicted vacuolar accumulation ratios$^{(123)}$ $[Q]_v/[Q]_e$, assuming indoloquinolines with two acids dissociation constants (digestive vacuole pH = 5.5$^{(123)}$ and an external pH = 7.4)

$$\frac{[\mathrm{IQ}]_v}{[\mathrm{IQ}]_e} = \frac{\left\{1 + \frac{[H^+]_v^2}{K_{a1}K_{a2}} + \frac{[H^+]_v}{K_{a2}} + \frac{K_{a3}}{[H^+]_v}\right\}}{\left\{1 + \frac{[H^+]_e^2}{K_{a1}K_{a2}} + \frac{[H^+]_e}{K_{a2}} + \frac{K_{a3}}{[H^+]_e}\right\}}$$

Eq. 6.2 - Predicted vacuolar accumulation ratios $[IQ]_v/[IQ]_e$, assuming indoloquinolines with three acids dissociation constants (digestive vacuole pH = 5.5$^{(123)}$ and an external pH = 7.4).

According with these assumptions, the extent of pH trapping of the cryptolepine derivatives **3**, can be estimated using Eq. 6.1. This vacuolar accumulation was estimated using de observed acid dissociation group constants pK_{a2}^{Obs} (Table 3.1), determined by UV-visible spectroscopy, which comprise the different contributions of the micro species in the acid base equilibrium occurring in the indole nitrogen and in the nitrogen atom attached to C11, in addition to the pK_{a1} values for the terminal amine in the side chain, predicted by SPARK (Appendix D).

The predicted vacuolar accumulation ratios, $[Q]_v/[Q]_e$, assuming a digestive vacuole pH value of 5.5(123) and an external pH value of 7.4, are presented in Table 6.2. Also included in Table 6.2 are the accumulation ratios relative to chloroquine, α, and the normalized IC_{50} values, i.e., the IC_{50} values theoretically expected if the compounds accumulated in the vacuole to the same extent as chloroquine.

Nevertheless, since the cryptolepine derivatives present three possible acid base equilibriums, we derived Eq. 6.2 (Appendix K) to calculate the extent of its pH trapping into the parasite digestive vacuole and to validate the predicted VAR obtained with Eq. 6.1 (presuppose only two acid dissociation constants). The predicted VAR, $[Q]_v/[Q]_e$, for cryptolepine and derivatives (**3b**, **3e-f**, **3i**, **3n**, **3s** and **3y**), assuming a digestive vacuole pH value of 5.5,(123) external pH value of 7.4 and the acid dissociation constants (pK_{a1}^{*}, pK_{a2}^{*Obs}, pK_{a3}^{*Obs}) determined by NMR spectroscopy (Table 3.4), are presented in Table 6.2. Also included in Table 6.2 are the accumulation ratios relative to chloroquine, α, and the normalized IC_{50} obtained from the calculated VAR. The analysis of the results (Table 6.2) allows us to verify that both approaches used to calculate VAR, gave similar results, being Eq. 6.1 and Eq. 6.2 in good agreement.

As shown in Table 6.2, the concentration of the majority of the cryptolepine derivatives **3** in the acidic digestive vacuole of the parasite is predicted to be close to that of chloroquine, i.e. ≈ 6000-fold higher than that in the extracellular fluid and the normalized IC_{50} values are almost identical to their experimental antiplasmodial IC_{50} values (W2 strain). In contrast, the predicted accumulations (α), relative to chloroquine, of **1** and some of its derivatives, like **3r**, **3s**, **3u** and **3y**, range between 0.013 and 0.015, so their normalized IC_{50} values are smaller than the corresponding experimental values.

However, these large differences in VAR arise because compounds **1**, **3r**, **3s**, **3u** and **3y** do not have an additional side chain with a weak basic nitrogen, and these large differences are not consistent with an antiplasmodial potency comparable to chloroquine, suggesting that additional mechanism of action may be involved.

In Table 6.2 it can also be seen that the two fold decrease in antiplasmodial activity of ethyl derivative **3b** when compared to the propyl counterpart **3f** is likely due to decreased basicity of the distal amine group with a consequent two fold decrease in the vacuolar accumulation ratio. However, the extent of pH trapping inside the parasite digestive vacuole does not explain the decrease of antiplasmodial activity observed for compounds with branched alkyl side chains (**3d**, **3h** and **3m**).

Table 6.2 – Vacuolar accumulation ratios (Acc ratio and α) and normalized antiplasmodial IC$_{50}$ values (IC$_{50}$ × α), calculated from UV-visible pK_{a2}^{Obs} group constant values and pK_{a1} SPARC predicted values, of chloroquine (**2**), cryptolepine (**1**) and derivatives **3**, and vacuolar accumulation ratios (Acc ratio and α) and normalized antiplasmodial IC$_{50}$ values (IC$_{50}$ × α), calculated from NMR pK_{a1}, pK_{a2} and pK_{a3} acid constant values, of cryptolepine (**1**) and its derivatives **3b**, **3e-f**, **3i**, **3n**, **3s** and **3y**.

	R^1	**R^2**	**R^3**	**Two p*Ka* values** (UV-visible and SPARC prediction pK_a)			**Three p*Ka* values** (NMR spectroscopy pK_a^*)		
				Acc ratio[a]	**α** [b]	**IC$_{50}$ (nM)× α** [c]	**Acc ratio**[d]	**α** [a]	**IC$_{50}$ (nM)× α** [b]
2	--	--	--	5896,2[e]	1,000	138	--	--	--
1	H	H	H	79.4	0,013	10.2	79.4[f]	0.013	10.2
3a	H	H	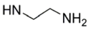	3515	0,596	53.1	--	--	--
3b	H	H	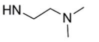	3086	0,524	26.2	4227	0,791	35.8
3c	H	H	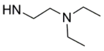	3086	0,524	42.9	--	--	--
3d	H	H	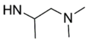	5612	0,952	135.2	--	--	--
3e	H	H	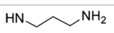	5915	1,003	26.1	6306	1.070	27.8
3f	H	H	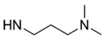	5612	0,952	19.0	6043	1.025	20.5
3g	H	H	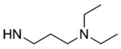	5612	0,952	30.5	--	--	--
3h	H	H	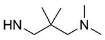	5612	0,952	175.2	--	--	--
3i	H	H	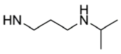	6086	1,032	22.7	6304	1.069	23.5
3j	H	H	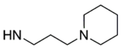	5731	0,972	35.0	--	--	--
3k	H	H	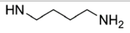	6266	1,063	69.1	--	--	--
3l	H	H	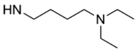	6238	1,058	30.7	--	--	--
3m	H	H	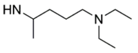	6247	1,060	129.3	--	--	--
3n	H	H	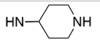	6222	1,055	46.4	6248	1.060	46.6
3o	H	H	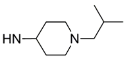	5851	0,992	69.5	--	--	--
3p	H	H	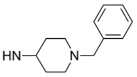	3933	0,667	72.0	--	--	--
3q	H	H	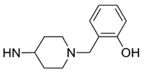	6100	1,035	285.6	--	--	--
3r	H	H	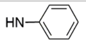	79.4	0,013	3.6	--	--	--
3s	H	H	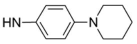	86.4	0,015	6.7	110.16	0.019	8.5
3t	H	H	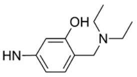	6304	1,069	55.6	--	--	--
3u	H	H	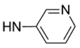	87.2	0,015	2.7	--	--	--
3v	Cl	H	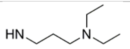	5766	0,978	20.5	--	--	--
3w	Cl	H	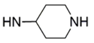	6218	1,055	47.5	--	--	--
3x	Cl	Cl	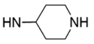	6218	1,055	50.6	--	--	--
3y	H	H		79.4	0,013	16.9	79.4 [f]	0.013	16.9

[a]Vacuolar accumulation ratio calculated using Eq. 6.1; [b] Accumulation ratio relative to chloroquine; [c]Normalized IC$_{50}$ (IC$_{50}$ × α); [d] Vacuolar accumulation ratio calculated Using Eq. 6.2; [e] Accumulation ratio calculated using Eq. 6.1 and assuming pK_a values of 8.55 and 9.81;(9, 403) [f] Accumulation ratio calculated using Eq. 6.1.

A. In vitro binding to haematin monomer

Since the cryptolepine derivatives are predicted to improve ability to accumulate inside the parasite DV, when compared to cryptolepine, and in order to gain some insight into its possible mechanism of action, the corresponding equilibrium binding constants (K_{ass}) with haematin monomer (FPIX-OH) were determined through UV-visible titration (Section 4.3.2).(145-146)

Cryptolepine and its derivatives share with chloroquine the capability to interact with FPIX-OH monomer and the introduction of the side-chain at C11 of the cryptolepine aromatic nucleus slightly increase the interactions when compared with the parent compound **1**. These haem binding properties by themselves could justify the antiplasmodial activity of cryptolepine and some of its derivatives with lower VAR (**3r**, **3s**, **3u** and **3y**). Association of cryptolepine derivatives with haematin by itself could probably lead to an accumulation of the drug inside the digestive vacuole, independently of the pH-trapping mechanism. However, studies with chloroquine have shown that the association with haematin, in the IC_{50} range of concentrations, is negligible in the absence of pH-trapping, because the affinity for haematin is too weak.(123)

From the UV-visible spectroscopic titrations data of FPIX-OH with cryptolepine derivatives (Section 4.3.2), no significant structure-activities relationships could be drawn. The differences in K_{ass} between the various cryptolepine derivatives are very small, nevertheless some interesting generalizations can be made on the strength of the data. It seems that the positively charged terminal nitrogen on the side chain by it self do not represent a crucial feature for haematin monomer binding, like reported to several 4-aminoquinolines with different side chain lengths,(132) since **3y**, which do not have basic nitrogen in the side chain, has comparable FPIX-OH binding potency to the other cryptolepine derivatives. Additionally, the changes on side chain length do not induce obvious relationships in the FPIX-OH binding affinity. Several authors(77, 108, 121) suggest that the interactions of the charged terminal nitrogen in the side chain with the propionate groups of haematin, via intermolecular hydrogen bonding, are essential for complex formation. However, if such interactions exist, they occur in a region distant from the chromophore aromatic centre, and probably not detectable through UV-visible spectroscopic titrations.

No correlation between the antiplasmodial activity (IC_{50}) and the abilities of these compounds to complex with FPIX-OH was found. This data suggests that cryptolepine derivatives may exert their antiplasmodial activity by an additional mechanism than interaction with haematin monomer. The association constants to FPIX-OH were measured with the monomeric form (40 % DMSO) and the biological relevant dimer for haemozoin crystallization is the tethered head-to-tail dimer (Figure 1.5). The associations with this dimer are likely to be similar to that with monomeric form, which are governed by π-π and van der Walls interactions as described.(415-416) Also, binding to one or more haemozoin growing crystal faces needs to be taken in account, when considering these compounds, being probably responsible for their antiplasmodial activity, and those interactions can not be measured in FPIX-OH 40% DMSO binding assay. The titration of haematin monomer with indoloquinolines clearly cause hypochromic shifts on the FPIX-OH Soret band, which in comparison with other well known polycyclic drugs that complex with haematin, like acridines(365-366) and quinolines,(123, 126) suggests that the main interaction between the porphyrin ring system and the cryptolepine derivatives could be π-π stacking interactions.

B. Docking studies with haemozoin

To a better knowledge of the possible interactions between cryptolepine and derivatives with FPIX-OH, we performed a molecular docking simulation with the haemozoin dimer to predict how the these indolo[3,2-*b*]quinolines would bind to haematin receptor (Section 5.4.1). The three-dimensional structure of FPIX-OH was not available and had to be modelled. Thus, we decide to used the three-dimensional structure of haemozoin, obtained from the Cambridge Crystallographic Database.(63) The docking results obtained with chloroquine, performed for comparison purposes, are analogous to the results obtained by nuclear resonance spectroscopy.(118, 124)

The docking results of cryptolepine and derivatives with haemozoin dimer are coherent with the concept of electrostatic potential complementary.(126) Haemozoin dimer denotes the presence of negative values of potential in the central region of coordination with iron(III)(125) and in the regions of carboxylate groups in the propionic chains.(126) Cryptolepine derivatives are highly polarized molecules with vast regions of positive potential (Figure 5.1) and denote to positive regions in the quinolinic nitrogen atom (N^5) and in the terminal nitrogen atom of the side, complementary to haemozoin negative regions. The interactions occur mainly between the aromatic nucleus of cryptolepine and derivatives **3** with the porphyrin through π-π stacking interactions (Figure 5.7 and Figure 5.8). The complex stability is assured with cryptolepine aromatic nucleus staying at ca. 3.0 Å of the porphyrin ring. The protonated terminal amine side chain docked with the area of negative potential over the carbonyl group of the carboxylate group (Fe-COO), interacting with oxygens through H-bonding. In fact, contrary to what was verified in the binding titration assays with FPIX-OH, the terminal amine side chain seems to contribute to the stability of the complex between the cryptolepine derivatives and haemozoin. The best docking score was found for derivatives with three of four carbon side chain (**3g**, **3l**, **3j** and **3v**) and bulky groups as substituents in the terminal amine.

Side chain length seems to be an important factors contributing to the complex stability. In the three-dimensional crystal structure of haemozoin dimer, the carboxylate groups are separated from the iron atom about 8.5 Å (Figure 5.7). Like chloroquine, docked cryptolepine derivatives with three (**3g**) and four carbons (**3l**) side chains have a separation between the quinoline nitrogen (N^5) and the terminal nitrogen in the side chain (N^{ter}) of c.a 8.4 and 9.7 Å, respectively (Figure 5.9), allowing an exact fit between the indoloquinoline aromatic nucleus with the porphyrin ring and the terminal nitrogen with the carboxylate (Fe-COO). Additionally, branched side chains (**3h**) showed reduced docking fitness value when compared with non-branched derivative **3f** (**Table 5.5**). The sterical hindrance induced by the branched side chains, seems to reduce the contact area between the indolo[3,2-*b*]quinoline nucleus and the porphyrin ring (Appendix J), forcing the aromatic nucleus to stack on the edge of porphyrin. Thus, these reduced interactions could probably reduce the haematin complex stability and consequently explain the reduced antiplasmodial activity of derivatives with branched side chains (Table 6.1), since their extent of pH trapping is quite close to the other derivatives with weak basic properties (Table 6.2). However, this hypothesis is not corroborated by our results as we could not find any correlation between the GoldScore values and the antiplasmodial activity.

Overall, these results suggest that although pH trapping may contribute significantly to the antiplasmodial potency of **3**, the activity of these cryptolepine derivatives does not result entirely from their association with haematin monomer, as already noticed for chloroquine derivatives.(417) Chloroquine can also inhibit haemozoin crystal growth by binding to its crystal faces.(77) According to this haemozoin crystal growth model, the flat and well exposed face of the crystal shows series of propionic acid groups separated by 8.0 Å which may be the target of positively charged groups.(130) Remarkably, we found that the distances between the positively charged N^5 nitrogen atom and the distal amine groups of piperidine (**3n**), propyl (**3f**) and butyl (**3l**) derivatives are ≈ 8.5 Å (Figure 5.7), which is consistent with binding to the haemozoin crystal flat face {100}. Additionally, co-facial binding and the implicated interaction energies involved in the complexation with FPIX-OH, haematin μ-oxo dimer and haemozoin growing crystals surfaces are reported to be similar.(129)

Antiplasmodial potential targets - DNA

Localization of **3n** inside *P. falciparum*-infected erythrocytes, through fluorescence microscopy (Figure 6.2) also suggest that parasite DNA could also be a target for the cryptolepine derivatives **3**, has already reported for cryptolepine.(255) In view of this, the mode and strength of binding of C11 diamine cryptolepine derivatives to DNA is of crucial importance for a better knowledge of its antiplasmodial mode of action.

A. In vitro binding to single- and double-stranded oligonucleotides

Cryptolepine showed an association constant (K_{ass}) value of 0.25x10^{-6}, 10-fold weaker than K_{ass} reported for cryptolepine binding to calf thymus DNA (K_{ass} = 3.2x10^{-6} M^{-1}),(17) while the cryptolepine derivatives showed K_{ass} values ranging from 0.25 to 17 x10^{-6} M^{-1}.

Cryptolepine did not show binding affinity to single-stranded oligonucleotide, being consistent with an intercalating mode of binding, as well as the maintenance of binding to ds-DNA at high ionic concentrations, revealing a binding mode where ionic and H-bond interactions contribute little to the stability of the complex compared with hydrophobic forces.

In contrast with **1**, cryptolepine derivatives **3** bound to ss-DNA and the binding to ds- and ss-oligonucleotides were destroyed at high ionic strength solutions. These observations indicate that compounds **3** do not intercalate into DNA and suggest a strong influence of ionic and H-bonding interactions, especially with the phosphate backbone, stabilizing the complex formation with single- and double-stranded oligonucleotides. Thermal denaturation studies with three selected cryptolepine derivatives (**3j**, **3n** and **3v**) showed that these compounds stabilise the ds-DNA structure (Table 4.1). This stabilizing effect is more pronounced for **3j** and **3v**, which show ΔT_m values ranging from 5 to 12 ºC. Also, the observed magnitudes of ΔTm are consistent with association constants determined by spectroscopic titration, since both studies show that compound **3n** has lower binding affinity to ds-DNA than **3j** and **3v** (Table 4.1 and Table 4.2).

B. Docking studies with double-stranded oligonucleotide

Molecular docking simulations indicated that **1** intercalates into 12-mer ds-DNA at nonalternated (CC)-(GG)-sites, being the complex stabilized mainly by π-π stacking interactions between the aromatic ring of the quinoline moiety of the cryptolepine and the aromatic rings of the consecutive guanine bases, in complete agreement with the X-ray diffraction studies.(277)

The docking simulation studies of cryptolepine derivatives **3** (Section 5.3) with the double-stranded d(GATCCTAGGATC)$_2$ oligonucleotide showed that these compounds do not intercalate into DNA structures, in the manner of parent compound **1**, confirming the conclusions from the *in vitro* binding studies. A possible explanation for this change in DNA binding mode when a diamine side-chain is introduced at C11 of cryptolepine nucleus, is the observed increased molar volume of the derivatives when compared to **1** (Table 5.3), leading to the separation of the bases in the intercalation cavity, so breaking H-bonding between base pairs, prompting a structural rearrangement of the DNA helix (Appendix I). Most of the cryptolepine derivatives studied are predicted to bind preferentially to the minor groove, except for **3v** and **3x** which bind preferentially to the major groove. However, the binding stoichiometry of the cryptolepine derivative **3v**:DNA complex from the Job plot was determined as 2:1 (Figure 4.1), indicating that cryptolepine derivatives can bind to the major and to the minor grooves of the same molecule of DNA, although only small differences in preference for minor or major grooves is evidenced by the complex formation energies (Table 5.4).

In an attempt to understand these observed structure-binding relationships, molecular properties of ten selected cryptolepine derivatives (**3f**, **3i-j**, **3n**, **3q-s** and **3v-x**) were studied by DFT (Table 5.3). However, we must conclude that DFT studies alone were not able to consistently explain the differences in binding affinities observed in titration experiments of the compounds series presented in this work. Incorporation of basic side-chain into the indoloquinoline scaffold shifts the binding mode from intercalation, as for cryptolepine, to interaction via electrostatic interactions, most likely to the phosphate backbone. Another major finding is that the novel cryptolepine derivatives also bind more strongly to double and single-stranded DNA than cryptolepine itself. Analysis of structure-binding affinity relationships revealed that linear alkyldiamine side-chains and a chlorine atom at position 3 of the indoloquinoline moiety markedly increase the binding affinity to the double-stranded oligonucleotide. However, no correlation with antiplasmodial activity or cytotoxicity was found.

Overall, cryptolepine derivatives seems to accumulate inside the digestive vacuole of parasites and are able to complex with FPIX-OH at the same extent as chloroquine, which means that they can inhibit haemozoin formation. Additionally, cryptolepine derivatives are also able to complex with DNA structures, which could justify its antiplasmodial activity due to induced cytotoxicity. As such, these results suggest that the cryptolepine derivatives mode of action could probably be a combination of effects due to inhibition of haemozoin inside the digestive vacuole and cytotoxicity induced by interaction with DNA structure in the parasite nucleus.

6.3.2 Quindolones and Derivatives

In vitro Antiplasmodial Activity in human red blood cells and cytotoxicity

The synthesized quindolones (**4**, **91a** and **91b**) and derivatives derivatives **5**, **94** and **95** were evaluated *in vitro* for their antiplasmodial activity in Human red blood cells infected with 1% *P. falciparum*$^{(408-409)}$ strains with the chloroquine resistance phenotype W2. Also, The *in vitro* cytotoxicity of quindolone **4** and of quindolone derivatives **5**, **94** and **95a** was evaluated using human hepatoma cell line HepG2 A16 (Dr. Virgílio do Rosário laboratory). Table 6.3 shows the *in vitro* antiplasmodial activity (IC_{50}) and cytotoxic activities (IC_{50}) against HepG2 A16 cells of **4** and derivatives, together with their selectivity index (cytotoxicity/antiplasmodial ratio).

From the data in Table 6.3 it can be concluded that introduction of an alkylamine side chain (**95**) is essential for antiplasmodial activity as unsubstituted quindolones **4**, **91a** and **91b** are inactive (IC_{50} ranging from 8 to >10 μM). The introduction of a second alkylamine side chain further increased antiplasmodial activity, with derivatives **5** and **94** showing IC_{50} values between 51 and 539 nM. Analyzing the influence of chlorine substitution on antiplasmodial activity of *bis*-alkylated derivatives **5** and **94**, it can be clearly seen that halogenation increases antiplasmodial activity of *N,O*- derivatives **94**, whereas mono or di-halogenation of *N,N*- derivatives **5** has no effect on antiplasmodial activity. Improved antiplasmodial activity with introduction of chlorine atoms in quinolines have been referred but the reason to justify that observation was never clearly found.$^{(412)}$ As a consequence of the structure-activity relationships discussed above, the dihalogenated and bis-alkylated quindolone derivative **94c** emerges as the more active compound of the series with an IC_{50} of 51 nM, more active than chloroquine (Table 6.1) Also, monoalkylated derivatives **95a-c** are weakly (IC_{50} of 2.6-1.3 μM) or moderated active (IC_{50} of 0.55 μM). Chlorine atoms in both aromatic rings also improved antiplasmodial activity, being the monohalogenated derivative **95b** two-times more active than **95a** and the dihalogenated derivative **95c** even more active than **95b**. Cytotoxicity was determined for the hepatic cell line HepG2 A16 and IC_{50} values of quindolone **4** and derivatives **5**, **94** and **95a** range from 4.3 to 20 μM (Table 6.3). Introduction of alkylamine side chains slightly increased cytotoxicity but no structure-cytotoxicity pattern was observed for quindolone derivatives. The low cytotoxicity of alkylamine-quindolone derivatives indicates selectivity for erythrocytic stages of malaria parasite, as shown by the selective index (SI, Table 6.3), determined as the cytotocity IC_{50}/antiplasmodial IC_{50} ratio, higher than 10 for all bis-alkylated quindolone derivatives **5** and **94**. The most active compound **94c** is also the most selective one, being 100-folds more toxic to the parasite than to the human hepatic cells HepG2.

Probing the site of action at cellular level

Investigation of the proposed mechanism of antiplasmodial activity of quindolone derivatives was performed by determining equilibrium binding constants (K_{ass}) with hematin monomer (FPIX-OH), by UV-visible titration carried out in pH 5.5,(146, 361-362, 418) and by docking studies with haematin dimer.

Antiplasmodial potential targets - Haem

A. In vitro binding to haematin monomer

Association constants shown in Table 4.4 were determined from the fitting of the experimental data to a binding model with stoichiometry of one quindolone molecule to one FPIX-OH, according to the binding stoichiometry determined with Job's methodology (Section 4.3.1). K_{ass} values for quindolones **4**, **91a** and **91b** and derivatives **5**, **94** and **95** ranges from 0.074 and 0.14 x10^6 M^{-1}, comparable to K_{ass} value determined in our assay for chloroquine (Table 4.3). From this experiment it can also be concluded that binding affinity of quindolone derivatives (**5**, **94** and **95**) to FPIX-OH monomer is only due to their aromatic tetracyclic structure as their K_{ass} are not significantly different from those of parent quindolones **4**. Additionally, chlorine atoms in the aromatic structure of quindolone seems to not affect the π-π interactions with porphyrin, since no significant differences was found between K_{ass}.

B. Docking studies with double-stranded oligonucleotide

In fact, the docking studies with haemozoin showed that the formation of H-bond between the protonated terminal nitrogen and the oxygen of the carboxylate group (Fe-COO) occurs. The formation of the hydrogen bond can modulate the fitting of both aromatic nucleus. The two carbon side chain length, has a distance between the terminal amine in the side chain and the quinolinic nitrogen (N^5) of 6.94 and 7.37 Å in derivative **5** and **94**, respectively, which is small compared with the ca. 8.5 Å of distance between the center of the porphyrin rin (Fe^{3+}) and the oxygen of the carboxylate. These differences obligate the aromatic ring of the quindolone derivatives to stacks on the edge of the porphyrin (Figure 5.11 and Appendix J), when compared with its counterparts **4**, **91a** and **91b** (Figure 5.10 and Appendix J).

Withal, the molecular docking simulations with haemozoin dimer also showed improved ligand binding (GoldScore, Table 5.6) with the introduction of chlorines in the aromatic nucleus. As already showed with 4-aminoquinolines, the presence of organic chlorine atoms can probably favour the formation Coulombic interaction with the porphyrin ring, such as Cl···CH_3, and thus stabilize the complex with haemozoin.(77)

Taken together, and even though no correlation was found between the antiplasmodial activity with binding constants (K_{ass}) and docking fitness values (GoldScore), the results suggest that alkylamine quindolone derivatives **5**, **94** and **95** may share with chloroquine the same antiplasmodial mechanism of action, i.e., by inhibition of haemozoin formation, as far as they reach the target inside digestive vacuole. In fact, the increased antiplasmodial activity when compared with their counterparts **4**, **91a** and **91b** is probably due to the increased accumulation in the parasite digestive vacuole, (18, 130) since derivatives with two side chains **5** and **94**, would probably accumulate more efficiently in the DV than **95** (one side chain) and are around c.a ten-fold more active against the *P. falciparum* W2 strain. Furthermore, the experimental result with FPIX-OH and docking studies with haemozoin dimer suggest that the antiplasmodial activity does not results entirely from association with haematin, but can also be due to the inhibition of haemozoin crystal growth by a capping effect on the crystal surface.(77, 127-128, 419)

Table 6.3 - *In vitro* antiplasmodial activity (IC_{50}) against *P. falciparum* W2 strains, cytotoxicity activity (IC_{50}) against HepG2 A16 and selectivity index (SI) of quindolones **4**, **91a** and **91b** and derivatives **5**, **94** and **95**.

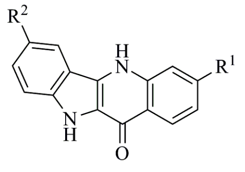

4 or **91**

	R^1	R^2	IC_{50} [a] *P. falciparum* W2 (nM)	IC_{50} Cytotoxicity HepG2 A16 (µM)	SI[b]
4	H	H	> 10 000	21±2	< 2
91a	Cl	H	8424±26	--	--
91b	Cl	Cl	> 10 000	--	--

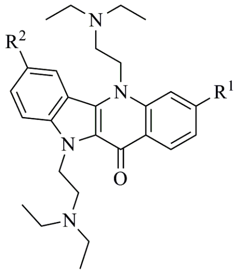

5

	R^1	R^2	IC_{50} [a] *P. falciparum* W2 (nM)	IC_{50} Cytotoxicity HepG2 A16 (µM)	SI[b]
5a	H	H	267±30	4.33±0.02	16
5b	Cl	H	202±8	7±1	33
5c	Cl	Cl	334±14	11±2	31

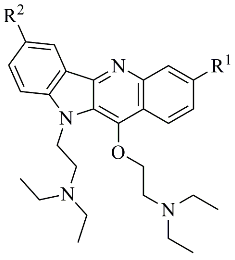

94

	R^1	R^2	IC_{50} [a] *P. falciparum* W2 (nM)	IC_{50} Cytotoxicity HepG2 A16 (µM)	SI[b]
94a	H	H	539±87	7±1	12
94b	Cl	H	186±3	8±2	44
94c	Cl	Cl	51±5	5.0±0.9	98

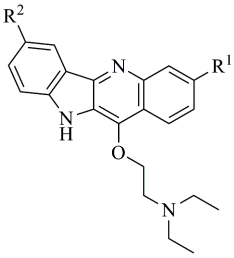

95

	R^1	R^2	IC_{50} [a] *P. falciparum* W2 (nM)	IC_{50} Cytotoxicity HepG2 A16 (µM)	SI[b]
95a	H	H	2638±22	9±1	3.6
95b	Cl	H	1332±20	--	--
95c	Cl	Cl	550±40	--	--

[a] The IC_{50} values are calculated from experiments carried out in triplicate and compared with CQ, [b] Selectivity Index ($IC_{50}^{HepG2\ A16}/IC_{50}^{W2}$).

6.4 Conclusions

The main objective of this project was to synthesise novel derivatives of the antimalarial natural compound cryptolepine as part of a larger project of development of safer and potent antimalarial drugs, at an affordable cost. The proposed approach was to synthesise new cryptolepine derivatives (**3**) with an ionisable diamine side chain at position C11 of the alkaloid scaffold, which was expected to improve the antimalarial activity and the selectivity against *Plasmodium* through an increase in the concentration of the compounds inside the acidic vacuole of the intraerythrocytic parasite. Additionally, we decided to start a second line of research based on the indolo[3,2-*b*]quinoline chemical structure **4** Derivatives **5** were designed based on the same rationale.

Cryptolepine and quindolones derivatives were synthesized from a common synthetic methodology that allowed us to achieve the indolo[3,2-*b*]quinolones intermediates (**4** and **91**) for their synthesis.(13-14) Introduction of alkyldiamine and alkylamine side chains in cryptolepine and quindolone aromatic nucleus was achieved in general with good yields and with high degree of purity (≥ 95 %).

Cryptolepine derivatives **3** showed strong antiplasmodial activity against both CQ-resistant and CQ-sensitive *P. falciparum* strains when compared with the parent compound, and those with IC_{50} values below 100 nM share the following features:

i. they all contain basic amine side chains;
ii. they all form complexes with FPIX-OH;
iii. they all are predicted to accumulate in digestive vacuole in the same extend as chloroquine;
iv. they all form strong complexes with double-stranded oligonucleotides.

Maximum potency, against *Plasmodium* sp. was achieved with propyl and butyl side-chains, while branched linkers seem to be poorly tolerated. Introduction of the basic terminal amine are predicted to increase accumulation inside the acid digestive vacuole of the parasite, improving the antiplasmodial activity. However, the antiplasmodial activity of these cryptolepine derivatives does not result entirely from their association with haematin and binding to the haemozoin crystal cannot be excluded. The cytotoxicity profile was also improved, with compound containing the conformationally restricted piperidine side-chain, **3n**, presenting a selectivity index value of ca 1400, i.e. a 1000-fold increase when compared with the parent compound **1**. This study revealed also that these cryptolepine derivatives are active against the blood-stages, but not to the liver-stages, of the parasite. Localization of **3n** inside blood stages of parasite suggests that the mechanism of action for these compounds besides inhibition of haemozoin crystal growth can also be due to interaction with DNA structures.

In the indolo[3,2-*b*]quindolin-11-one skeleton the introduction of two alkylamine side chains generally improves antiplasmodial activity, probably by increasing accumulation in acidic digestive vacuole. On the other hand, substitution by chlorine atoms at positions 3 and 7 of quindolone skeleton improves antiplasmodial activity for *N,O*- bis-alkylamine derivatives but not for *N,N*-di-substitued ones, what is an interesting finding that deserves further investigation. Additionally, antiplasmodial activity of bis-alkylamine quindolone derivatives cannot be entirely justified by their affinity to haematin monomer. Taken together, these results indicate that the quindolone nucleus is a suitable scaffold for the design of active and selective compounds targeting parasite haem detoxification pathway and bis-alkylamine quindolones are a novel chemotype with potential for development as antimalarial agents.

Overall, cryptolepine and quindolone derivatives containing basic side-chains have been confirmed as promising lead compounds for the development of new agents active against the blood stages of *P. falciparum* malaria with improved activity and increased selectivity for the *Plasmodium* sp.

VII

Chapter VII - **Materials and methods**

An expert is a man who has made all the mistakes which can be made, in a narrow field

Niels Bohr (1885-1962)
Danish physicist

List of Contents

7.1 GENERAL 164

7.1.1 Chemicals 164

7.1.2 Instrumentation 164

7.1.3 Methods 165

7.2 CHEMISTRY 165

*7.2.1 Synthesis of 2-(2-Bromoacetamido)benzoic Acids (**89**) 165*

*7.2.2 Synthesis of 2-[2-(Phenylamino)acetamido]benzoic Acids (**90**) 166*

*7.2.3 Synthesis of 5H-Indolo[3,2-b]quinolin-11(10H)-ones (**4** and **91**) 168*

*7.2.4 Synthesis of 11-Chloro-10H-indolo[3,2-b]quinolines (**92**) 170*

*7.2.5 Synthesis of 5-Methyl-11-chloro-10H-indolo[3,2-b]quinolin-5-ium Chlorides (**93**) 172*

*7.2.6 Synthesis of 10H-Indolo[3,2-b]quinoline (**25**) 174*

*7.2.7 Synthesis of 5-Methyl-10H-indolo[3,2-b]quinolin-5-ium Trifluoromethanosulfonate (**1**) 175*

*7.2.8 Synthesis of Cryptolepine Derivatives (**3**) 175*

*7.2.9 Synthesis of Quindolone Derivatives (**5**) 186*

*7.2.10 Synthesis of N^1,N^1-Dimethylpropane-1,2-diamine (**97**) 189*

*7.2.11 Synthesis of 2-(3-(Piperidin-1-yl)-propyl)isoindoline-1,3-dione (**99**) 189*

*7.2.12 Synthesis of 3-Piperidin-1-yl-propan-1-amine (**100**) 190*

*7.2.13 Synthesis of Tert-butyl-4-(diethylamino)butylcarbamate (**102**) 190*

*7.2.14 Synthesis of N^1,N^1-Diethyl-butane-1,4-diamine (**103**) 190*

*7.2.15 Synthesis of N-(4-((Diethylamino)-methyl)-3-hydroxyphenyl)-acetamido (**105**) 191*

7.3 ACID DISSOCIATION CONSTANTS (pK_A) 191

7.3.1 UV-visible Spectrophotoscopy 191

7.3.2 Nuclear Magnetic Resonance (NMR) 191

7.4 INTERACTION WITH OLIGONUCLEOTIDES 192

7.4.1 Determination of Oligonucleotides Concentration 192

7.4.2 Binding Stoichiometry 192

7.4.3 Association Constants (K_{ass}) 192

7.4.4 Melting Curves 193

7.5 INTERACTIONS WITH HAEM 193

7.5.1 Binding Stoichiometry 193

7.5.2 Association Constants (K_{ass}) 193

7.6 COMPUTATIONAL DETAILS 194

7.6.1 Density Functional Theory Optimizations 194

7.6.2 Double-Stranded DNA Docking Studies 194

7.6.3 Haematin Dimer Docking Studies 195

7.1 General

7.1.1 Chemicals

Reagents and solvents were purchased from **Aldrich Chemical Company LTd.,** (Spain) and used without further purification.

Water and buffers: all water used was distilled and purified by ion exchange and charcoal using a MilliQ system (Millipore Ltd.). All buffers were prepared from analytical reagent grade material according to standard procedures.(420)

7.1.2 Instrumentation

Nuclear Magnetic Resonance (NMR): NMR spectra were record in a Bruker ultrashield 400 MHz (9.4 T) spectrometer equipped with a 5 mm Quad Nuclear Probe (QNP), operating at 400.1 MHz for ^{1}H NMR and 100.6 MHz for ^{13}C NMR (Faculty of Science, University of Lisbon) or recorded in a Bruker ultrashield 300 MHz (7.05 T) spectrometer (Avance-300) equipped with a 5 mm single-axis Z-gradient quattro nucleus probe, operating at 300.1 MHz for ^{1}H NMR and 75.5 MHz for ^{13}C NMR (School of Pharmacy and Pharmaceutical Sciences, University of Manchester, UK). Chemical Shifts (δ) are reported in parts per million (ppm), using solvent as internal reference, tetramethylsilane (TMS) or 2,2,3,3-tetradeutero-3-trimethylsilylpropionic acid (TSP). Coupling constants (J) are in Hz. Data are reported using the following convention: splitting patterns are abbreviated as: s (singlet), d (doublet), t (triplet), q (quartet) and m (multiplet).

UV-visible spectrophotometry (UV-Vis): UV-Visible spectra were record in 1 cm pathlength quartz cuvettes at 25 ºC using a Shimadzu UV-1603 UV-visible spectrometer with a temperature-controlled (25 ºC) cell holder or using a Varian Cary-4000 UV-visible spectrophotometer (Varian Ltd. Mulgrave Victoria, Australia) connected to a Cary Peltier-thermostatted cuvette holder (School of Pharmacy and Pharmaceutical Sciences, University of Manchester, UK).

Florescence spectroscopy (FS): Fluorescence emission and excitation spectra were record in 4-sided quartz cuvettes using a Cary-Eclipse fluorescence spectrophotometer equipped with a Cary Peltier-thermostatted cuvette holder (School of Pharmacy and Pharmaceutical Sciences, University of Manchester, UK).

Infrared spectroscopy (IV): Infrared spectra were record in a Nicolet Impact 400 FTIR Spectrophotometer in KBr homogenized powder samples and pressurized into a thin pellet.

Mass spectrometry (MS): Mass spectra were recorded using a Micromass Autospec spectrometer with electronic impact as ionization method and high resolution mass spectra (accurate mass) were record on a Bruker Microtof spectrometer with ESI-TOF as ionization method (Unit of Mass spectrometry, University of Santiago de Compostela, Spain).

Elemental analysis (EA): C, H and N analyses were carried out by the Unit Elemental Analysis, University of Santiago de Compostela, Spain, on a LECO model CHNS-932 elemental analyzer.

Melting points: Melting points were determined using an Bock-Monoscop M melting apparatus (temperature range 0-330 ºC) and are uncorrected.

Determination of pH: Values of pH and pH* (measurement in D_2O solutions) were measured using a HI 9321 microprocessor pH metter from Hanna Instruments, calibrated with standard buffers (4.00±0.01, 7.00±0.01 and 10.00±0.01, Sigma-Aldrich at 20 ºC).

7.1.3 Methods

Thin-layer chromatography (TLC): Reactions were followed by thin-layer chromatography using coated silica gel plates (Merck, aluminum sheets, silica gel 60 F_{254}, 200 μm layer-thickness, 25 μm particle size) or in aluminium oxide matrix (60 Å medium pore diameter and 200 μm layer-thickness) with fluorescent indicator in PET support.

Preparative thin-layer chromatography (P-TLC): P-TLC were performed in coated silica-gel plates (Merk, silica gel 60 GF_{254}, 750 μm layer-thickness) capable of separating around 10-50 mg, depending on separation efficiency.

Column chromatography: Purification of compound by column chromatography was performed using silica-gel (Sigma-Aldrich, silica-gel 220-240 mesh, 35-70 μm pore size, flash cromatography) or in aluminum oxide (Sigma-Aldrich,50-150 μm of pore size and Brockmann activity I) as stationary phase.

7.2 Chemistry

7.2.1 Synthesis of 2-(2-Bromoacetamido)benzoic Acids (**89**)

7.2.1.1 General procedure A: synthesis of 2-(2-Bromoacetamido)benzoic acid (89a)

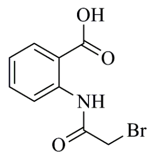

A solution of 2-amino-benzoic acid (10.0 g, 72.9 mmol) in DMF (30 mL) and dioxane (30 mL) was cooled to 0 ºC. Bromoacetyl bromide (8.0 mL, 91.7 mmol, 1.25 eq.) was added dropwise over a 20 min period, keeping the internal temperature between 0 and 5 ºC. After the addition was complete, the ice bath was removed and stirring was continued overnight at room temperature. The reaction mixture was added to water (300 mL), and the light yellow precipitate which formed was filtered, washed with water until neutral pH, and then dried to give 18.1 g (96%) of **89a** as a white solid, mp 162-165 ºC. ^{1}H NMR (400 MHz, DMSO) δ_H (ppm) 11.23 (s, NH), 8.06 (d, *J* = 8.4 Hz, 1H), 7.62 (dd, *J* = 7.9, 1.4 Hz, 1H), 7.24 (dd, *J* = 8.4, 7.3 Hz, 1H), 6.82 (dd, *J* = 7.9, 7.3 Hz, 1H), 3.87 (s, 2H). ^{13}C NMR (101 MHz, DMSO) δ_C (ppm) 169.20, 165.04, 139.92, 134.06, 131.11, 123.45, 119.99, 117.06, 30.65.

7.2.1.2 *Synthesis of 2-(2-Bromoacetamido)-4-chlorobenzoic acid (89b)*

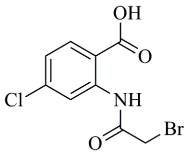

Reaction of 2-amino-4-chloro benzoic acid (10 g, 58.2 mmol) and bromoacetyl bromide (14.7 g, 6.3 mL, 72.8 mmol, 1.25 eq.) according to general procedure A, gave 17.1 g (99 %) of **89b** as a light yellow solid. mp 166-168 ºC. ^{1}H NMR (400 MHz, DMSO) δ_H (ppm) 11.73 (s, NH), 8.54 (d, *J* = 2.1 Hz, 1H), 7.98 (d, *J* = 8.6 Hz, 1H), 7.24 (dd, *J* = 8.6, 2.1 Hz, 1H), 4.28 (s, 2H). ^{13}C NMR (101 MHz, DMSO) δ_C (ppm) 169.03, 165.92, 141.54, 138.95, 133.26, 123.73, 119.61, 115.91, 30.98.

7.2.2 Synthesis of 2-[2-(Phenylamino)acetamido]benzoic Acids (**90**)

7.2.2.1 *General procedure B: synthesis of 2-(2-(phenylamino)acetamido)benzoic acid (90a)*

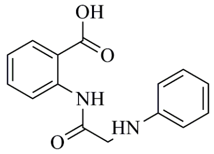

A solution of **89a** (15.0 g, 58.1 mmol) and aniline (19.0 mL, 208.3 mmol, 3.5 eq.) in DMF (30 mL) was heated at 120 ºC for 18 hours. After cooling the reaction mixture was poured into ice-water (500 mL), aqueous 5 % KOH was added to solubilize the solid product and adjust the pH to 10-11. Then the mixture was extracted with dichloromethane (3x300 mL). The combined dichloromethane extracts were set aside and aqueous layer was acidified to pH 3 with a solution of 5 % HBr. The precipitate which formed was collected, washed with water and then dried, yielding 11.0 g (70 %) of **90a** as a white solid, mp 194-197 ºC. ^{1}H NMR (400 MHz, DMSO) δ_H (ppm) 11.96 (s, NH), 8.61 (d, *J* = 8.7 Hz, 1H), 7.83 (d, *J* = 7.9 Hz, 1H), 7.47 (dd, *J* = 8.7, 8.0 Hz, 1H), 7.02 (dd, *J* = 8.0, 7.9 Hz, 1H), 6.98 (d, *J* = 7.3 Hz, 2H), 6.50 (d, *J* = 7.7 Hz, 1H), 6.48 (dd, *J* = 7.7, 7.3 Hz, 2H), 6.39 (s, NH), 3.73 (s, 2H). ^{13}C NMR (101 MHz, CD3OD) δ_C (ppm): 170.82, 169.01, 148.08, 140.52, 134.03, 131.08, 128.92, 122.60, 119.32, 116.98, 116.12, 112.36, 48.89.

7.2.2.2 *Synthesis of 4-chloro-2-[2-(phenylamino)acetamido]benzoic acid (90b)*

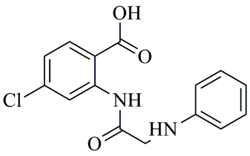

Reaction of **89b** (15g, 51.3 mmol) with aniline (16.7g, 16.3 mL, 179.6 mmol, 3.5 eq) according to general procedure B gave 11.8 g of **90b** (76 %) as a white solid, mp 217-220 ºC. ^{1}H NMR (400 MHz, DMSO) δ_H (ppm) 12.13 (s, NH), 8.83 (d, *J* = 2.2 Hz, 1H), 7.94 (d, *J* = 8.6 Hz, 1H), 7.21 (dd, *J* = 8.6, 2.2 Hz, 1H), 7.10 (dd, *J* = 8.0, 7.4 Hz, 2H), 6.63 (d, *J* = 7.4 Hz, 1H), 6.59 (d, *J* = 8.0 Hz, 2H), 3.86 (s, 2H). ^{13}C NMR (101 MHz, DMSO) δ_C (ppm) 171.96, 168.80, 148.46, 141.99, 139.03, 133.33, 129.45, 123.08, 119.16, 117.63, 115.16, 112.90, 49.36.

7.2.2.3 *Synthesis of 4-chloro-2-{2-[(3-chlorophenyl)amino]acetamido}benzoic acid (90c)*

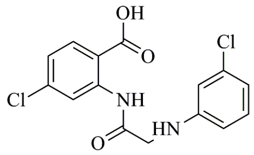

A solution of **89b** (3.0 g, 10.2 mmol) and *3*-chloroaniline (4.04 g, 3.34 mL, 31.7 mmol, 3 eq.) in DMF (10 mL) was heated at 120 ºC for 72 hours and treated according to general procedure B to gave 3.0 g of **90c** (84 %) as a white solid, mp 223-226 ºC. ^{1}H NMR (400 MHz, DMSO) δ_H (ppm) 12.10 (s, NH), 8.80 (d, *J* = 2.2 Hz, 1H), 7.95 (d, *J* = 8.6 Hz, 1H), 7.20 (dd, *J* = 8.6, 2.2 Hz, 1H), 7.11 (dd, *J* = 8.0 Hz, 1H), 6.84 (s, NH), 6.55 (m, 2H), 6.54 (dd, *J* = 8.2, 1.4 Hz, 1H), 3.92 (d, *J* = 5.5 Hz, 2H). ^{13}C NMR (101 MHz, DMSO) δ_C (ppm) 171.29, 168.95, 149.99, 141.93, 139.03, 134.00, 133.34, 131.02, 123.13, 119.16, 117.04, 115.24, 112.41, 111.32, 48.80.

7.2.2.4 *Synthesis of 4-chloro-2-{2-[(4-chlorophenyl)amino]acetamido}benzoic acid (90d)*

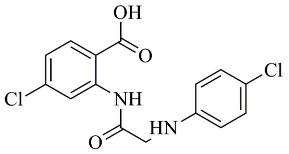

Reaction of **89b** (3.0 g, 10.2 mmol) and *4*-chloroaniline (4.04 g, 3.34 mL, 31.7 mmol, 3 eq.) in DMF (10 mL) was heated at 120 ºC for 48 hours and than treated according to general procedure B to give 2.47 g (70 %) of **90d** as a white solid, mp 194-197 ºC. ^{1}H NMR (400 MHz, DMSO) δ_H (ppm) 12.07 (s, 1H), 8.81 (s, 1H), 7.95 (d, J = 8.6 Hz, 1H), 7.22 (dd, J = 8.6, 2.2 Hz, 1H), 7.13 (d, J = 8.8 Hz, 2H), 6.73 (s, 1H), 6.60 (d, J = 8.9 Hz, 2H), 3.88 (d, J = 4.9 Hz, 2H). ^{13}C NMR (101 MHz, DMSO) δ_C (ppm) 171.48, 168.87, 147.39, 141.94, 139.05, 133.35, 129.17, 123.15, 120.91, 119.17, 115.15, 114.31, 49.13.

7.2.2.5 *Synthesis of 4-chloro-2-{2-[(4-(trifluoromethyl)phenyl)amino]acetamide} benzoic acid (90e)*

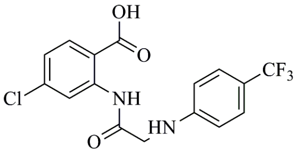

A solution of **89b** (4.0 g, 13.6 mmol) and 4-trifluoromethyl-aniline (4.39 g, 3.39 mL, 27.3 mmol, 2 eq.) in DMF (15 mL) was heated at 120 ºC for 72 hours and treated according to general procedure B, to give 3,23 g (64 %) of **90e** as a white solid, mp 201-203 ºC. ^{1}H NMR (400 MHz, DMSO) δ_H (ppm) 12.04 (s, NH), 8.80 (s, 1H), 7.94 (d, *J* = 8.5 Hz, 1H), 7.43 (d, *J* = 8.5 Hz, 2H), 7.20 (m, 2H), 6.73 (d, *J* = 8.5 Hz, 2H), 3.98 (s, 2H). ^{13}C NMR (101 MHz, DMSO) δ_C (ppm) 170.97, 169.00, 151.55, 141.93, 139.09, 133.34, 129.46, 126.78, 124.26, 123.19, 119.19, 115.11, 112.47, 48.52.

7.2.2.6 *Synthesis of 4-chloro-2-(2-((4-methoxyphenyl)amino)acetamido)benzoic acid (90f)*

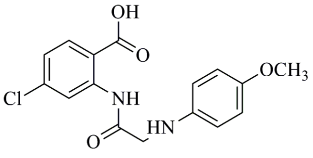

Reaction of **89b** (3.0 g, 10.25 mmol) and 4-methoxy-aniline (3.79 g, 30.75 mmol, 3 eq.), in DMF (10 mL) was heated at 120 ºC for 96 hours and treated according to general procedure B, gave 2.52 g (72 %) of **90f** as a light brown solid, mp 191-193 ºC. ^{1}H NMR (400 MHz, DMSO) δ_H (ppm) 12.16 (s, NH), 8.84 (d, *J* = 2.2 Hz, 1H), 7.94 (d, *J* = 8.5 Hz, 1H), 7.21 (dd, *J* = 8.5, 2.2 Hz, 1H), 6.73 (d, *J* = 8.9 Hz, 2H), 6.54 (d, *J* = 8.9 Hz, 2H), 3.79 (s, 2H), 3.62 (s, 3H). ^{13}C NMR (101 MHz, DMSO) δ_C (ppm) 172.25, 168.70, 152.03, 142.52, 141.99, 138.99, 133.32, 123.02, 119.15, 115.22, 115.02, 113.90, 55.63, 50.16.

7.2.2.7 Synthesis of 4-chloro-2-(2-((4-methylphenyl)amino)acetamido)benzoic acid (90g)

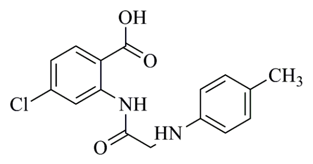

A solution of **89b** (4.0 g, 13.6 mmol) and 4-methyl-aniline (2.93 g, 27.3 mmol, 2 eq.) in DMF (15 mL) was heated at 120 ºC for 48 hours and treated according to general procedure B, to give 3.68 g (83 %) of **90g** as a light yellow solid, mp 187-189 ºC. ^{1}H NMR (400 MHz, DMSO) δ_H (ppm) 12.13 (s, 1H), 8.83 (d, *J* = 2.0 Hz, 1H), 7.94 (d, *J* = 8.5 Hz, 1H), 7.21 (dd, *J* = 8.5, 2.0 Hz, 1H), 6.91 (d, *J* = 8.3 Hz, 2H), 6.49 (d, *J* = 8.3 Hz, 2H), 3.81 (s, 2H), 2.14 (s, 3H). ^{13}C NMR (101 MHz, DMSO) δ_C (ppm) 172.15, 168.74, 146.19, 142.00, 139.02, 133.32, 129.88, 126.05, 123.04, 119.14, 115.14, 112.96, 49.67, 20.53.

7.2.3 Synthesis of 5*H*-Indolo[3,2-*b*]quinolin-11(10*H*)-ones (**4** and **91**)

7.2.3.1 General procedure C: Synthesis of 5H-indolo[3,2-b]quinolin-11(10H)-one (4)

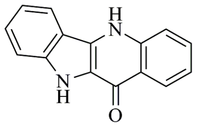

A mixture **90a** (6.0 g, 21.5 mmol) and polyphosphoric acid (PPA, 160 g) was heated with mechanical stirring at 130 ºC for 2 hours. The reaction mixture was poured into-ice water (500 mL), neutralized with saturated KOH solution, and then extracted with EtOAc (3x500 mL). The extract was washed with water and brine, dried (anhydrous Na_2SO_4), and then concentrated. The product was recrystallized from AcOEt with diethyl ether:hexane (9:1) to give 3.47 g (67 %) of **4** as a light green solid, mp > 300 ºC. ^{1}H NMR (400 MHz, DMSO) δ_H (ppm) 12.81 (s, 1H), 11.69 (s, 1H), 8.35 (d, *J* = 8.0 Hz, 1H), 8.28 (d, *J* = 8.0 Hz, 1H), 7.81 (d, *J* = 8.4 Hz, 1H), 7.68 (dd, *J* = 8.4, 7.5 Hz, 1H), 7.50 (d, *J* = 8.2, 1H), 7.49 (dd, *J* = 8.2, 7.4 Hz, 1H), 7.28 (dd, *J* = 8.0, 7.5 Hz, 1H), 7.20 (dd, *J* = 8.0, 7.4 Hz, 1H). ^{13}C NMR (101 MHz, DMSO) δ_C (ppm) 167.77, 139.54, 139.05, 130.99, 129.44, 127.84, 125.57, 123.48, 123.24, 121.63, 120.87, 119.25, 118.28, 116.38, 112.98. Infrared (KBr, cm^{-1}): 3350 (NH); 3169 ($CH_{aromatic}$); 1625 (CO). Anal. (C, H, N) Cal. for $C_{15}H_{10}N_2O{\cdot}4H_2O$: C, 58.82, H, 5.92, N, 9.15, found: C, 58.53, H, 5.70, N, 9.43.

7.2.3.2 Synthesis of 3-chloro-5H-indolo[3,2-b]quinolin-11(10H)-one (91a)

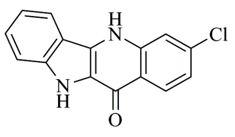

A mixture of **90b** (2.0 g, 6.6 mmol) and PPA (60 g) was treated according general procedure C, giving 0.630 g (36 %) of **91a** as a light green solid, mp > 300 ºC. ^{1}H NMR (400 MHz, DMSO) δ_H (ppm) 12.56 (NH, 1H), 11.81 (NH, 1H), 8.35 (d, *J* = 8.7 Hz, 1H), 8.15 (d, *J* = 8.1 Hz, 1H), 7.73 (d, *J* = 1.8 Hz, 1H), 7.51 (d, *J* = 6.2 Hz, 1H), 7.49 (dd, *J* = 7.3, 6.2 Hz 1H), 7.30 (dd, *J* = 8.7, 1.8 Hz, 1H), 7.23 (dd, *J* = 8.1, 7.3 Hz, 1H). ^{13}C NMR (101 MHz, DMSO) δ_C (ppm) 167.30, 140.02, 139.08, 135.65, 129.40, 128.10, 127.94, 123.64, 121.96, 121.31, 121.15, 119.62, 117.13, 116.14, 113.17. Infrared (KBr, cm^{-1}): 3421 (NH); 3190

($CH_{aromatic}$); 1631 (CO). Anal. (C, H, N) Cal. For $C_{15}H_9ClN_2O\cdot2.3H_2O$: C, 58.09, H, 4.42, N, 9.03, found: C, 58.35, H, 4.77, N, 9.13.

*7.2.3.3 **Synthesis of 3,8-dichloro-5H-indolo[3,2-b]quinolin-11(10H)-one (91b)***

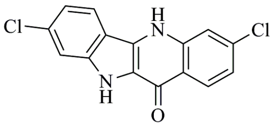

Compound **90c** (2.0g, 5.90 mmol) was reacted with PPA (60 g) according to general procedure C. After extraction, the solvent was removed at reduced pressure and the residue purified by flash chromatography (silica gel 230-400 mesh, 40-63 µm, AcOEt:hexane 6:4) to give 0.271 g (15 %) of **91c** as light green solid, mp > 300 ºC. ^{1}H NMR (400 MHz, DMSO) δ_H (ppm) 12.27 (s, NH), 11.33 (s, NH), 8.36 (d, *J* = 2.0 Hz, 1H), 8.34 (d, *J* = 8.8 Hz, 1H), 7.49 (d, *J* = 0.9 Hz, 1H), 7.46 (d, *J* = 7.1 Hz, 1H), 7.33 (dd, *J* = 8.8, 2.0 Hz, 1H), 7.24 (dd, *J* = 7.1, 0.9 Hz, 1H). ^{13}C NMR (101 MHz, DMSO) δ_c (ppm) 167.49, 140.50, 139.88, 135.94, 128.69, 127.60, 127.45, 126.41, 124.33, 121.87, 121.73, 119.76, 118.64, 113.84, 112.24. Infrared (KBr, cm^{-1}): 3432 (NH); 3156 ($CH_{aromatic}$); 1635 (CO).

*7.2.3.4 **Synthesis of 3,7-dichloro-5H-indolo[3,2-b]quinolin-11(10H)-one (91c)***

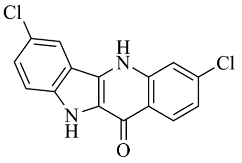

Reaction of **90d** (2.0 g, 5.9 mmol) with PPA (60 g) according to general procedure C, gave 0.725 g (40%) of **91c**, as a light green solid, mp > 300 ºC. ^{1}H NMR (400 MHz, DMSO) δ_H (ppm) 12.57 (s, NH), 12.02 (s, NH), 8.33 (d, *J* = 8.7 Hz, 1H), 8.20 (d, *J* = 1.7 Hz, 1H), 7.69 (d, *J* = 1.8 Hz, 1H), 7.54 (d, *J* = 8.8 Hz, 1H), 7.49 (dd, *J* = 8.8, 1.7 Hz, 1H), 7.31 (dd, *J* = 8.7, 1.8 Hz, 1H). ^{13}C NMR (101 MHz, DMSO) δ_c (ppm) 167.54, 140.08, 137.34, 136.04, 128.52, 128.03, 127.97, 124.51, 123.73, 121.91, 121.55, 120.41, 117.15, 117.03, 114.91. Infrared (KBr, cm^{-1}): 3417 (NH); 3173 ($CH_{aromatic}$); 1628 (CO). Anal. (C, H, N) Cal. for $C_{15}H_8Cl_2N_2O\cdot0.4H_2O$: C, 48.02, H, 4.30, N, 7.47, found: C, 48.36, H, 4.52, N, 7.03.

*7.2.3.5 **Synthesis of 3-chloro-7-trifluoromethyl-5H-indolo[3,2-b]quinolin-11(10H)-one (91d)***

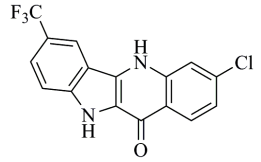

Reaction of **90e** (1.5 g, 4.4 mmol) with PPA (45 g) according to general procedure C, gave 0.457 g (33 %) of **91d**, as a light green solid, mp >300 ºC. ^{1}H NMR (400 MHz, DMSO) δ_H (ppm) 12.93 (s, NH), 12.22 (s, NH), 8.97 (s, 1H), 8.34 (d, *J* = 8.7 Hz, 1H), 8.05 (d, *J* = 8.8 Hz, 1H), 7.76 (d, *J* = 1.7 Hz, 1H), 7.56 (d, *J* = 8.7 Hz, 1H), 7.32 (dd, *J* = 8.8, 1.7 Hz, 1H). ^{13}C NMR (101 MHz, DMSO) δ_c (ppm) 168.11, 141.03, 140.17, 135.94, 130.19, 128.72, 127.92, 124.57, 124.33, 122.18, 122.02, 121.66, 117.31, 116.04, 15.63. Infrared (KBr, cm^{-1}): 3456 (NH); 3123 ($CH_{aromatic}$); 1632 (CO). Anal. (C, H, N) Cal. for $C_{16}H8ClF_3N_2O\cdot2.3H_2O$: C, 52.77, H, 4.04, N, 7.69, found: C, 52.92, H, 4.29, N, 7.59.

*7.2.3.6 **Synthesis of 3-chloro-7-methoxy-5H-indolo[3,2-b]quinolin-11(10H)-one (91e)***

Reaction of **90f** (1.0 g, 3.0 mmol) with PPA (30 g) according to general procedure C, gave 0.242 g (27 %) of **91e**, as a light green solid, mp >300 ºC. ^{1}H NMR (400 MHz, DMSO) δ_H (ppm) 12.50 (s, NH), 11.63 (s, NH), 8.33 (d, *J* = 8.7 Hz, 1H), 7.70 (d, *J* = 1.7 Hz, 1H), 7.61 (d, *J* = 2.2 Hz, 1H), 7.44 (d, *J* =

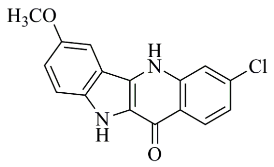

9.0 Hz, 1H), 7.28 (dd, *J* = 8.7, 1.7 Hz, 1H), 7.15 (dd, *J* = 9.0, 2.2 Hz, 1H), 3.87 (s, 3H). ^{13}C NMR (101 MHz, DMSO) δ_c (ppm) 167.35, 153.49, 139.99, 135.63, 134.47, 129.17, 127.98, 124.30, 121.75, 121.13, 119.19, 117.00, 115.93, 114.27, 101.51, 55.86. Infrared (KBr, cm^{-1}): 3482 (NH); 3143 ($CH_{aromatic}$); 1625 (CO). Anal. (C, H, N) Cal. for $C_{16}H_{11}ClN_2O_2\cdot 0.5H_2O$: C, 62.45, H, 3.93, N, 9.10, found: C, 62.76, H, 3.92, N, 9.08.

7.2.3.7 *Synthesis of 3-chloro-7-methyl-5H-indolo[3,2-b]quinolin-11(10H)-one (91f)*

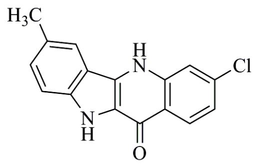

Reaction of **90g** (1.5 g, 4.7 mmol) with PPA (45 g) according to general procedure C, gave 0.697 g (52 %) of **91f**, as a light green solid, mp >300 ºC. ^{1}H NMR (400 MHz, DMSO) δ_H (ppm) 12.53 (s, NH), 11.67 (s, NH), 8.33 (d, *J* = 8.7 Hz, 1H), 7.92 (s, 1H), 7.72 (d, *J* = 1.7 Hz, 1H), 7.42 (d, *J* = 8.5 Hz, 1H), 7.32 (d, *J* = 8.5 Hz, 1H), 7.28 (dd, *J* = 8.7, 1.7 Hz, 1H), 2.47 (s, 3H). ^{13}C NMR (101 MHz, DMSO) δ_c (ppm) 167.23, 139.98, 137.57, 135.55, 129.89, 129.05, 128.31, 127.92, 123.86, 121.88, 121.19, 120.33, 117.07, 116.24, 112.95, 21.61. Infrared (KBr, cm^{-1}): 3432 (NH); 3179 ($CH_{aromatic}$); 1627 (CO). Anal. (C, H, N) Cal. for $C_{16}H_{11}ClN_2O\cdot H_2O$: C, 63.90, H, 4.36, N, 9.31, found: C, 64.16, H, 4.38, N, 9.14.

7.2.4 Synthesis of 11-Chloro-10*H*-indolo[3,2-*b*]quinolines (**92**)

7.2.4.1 *General procedure D: Synthesis of 11-chloro-10*H*-indolo[3,2-*b*]quinoline (92a)*

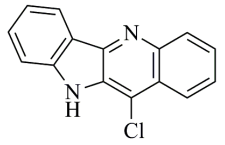

A solution of **4** (1.5 g, 6.58 mmol) in $POCl_3$ (20 mL) was refluxed for 2 hours. The reaction mixture was cooled, poured into ice, neutralized with a cold saturated solution of KOH while keeping the internal temperature below 45 ºC. The aqueous solutions was then extracted with EtOAc (3x200 mL), and then the combined organic extracts was washed with water and brine, dried (anhydrous Na_2SO_4), and the solvent redmoved at reduced pressure to give 0.95 g (60 %) **92a**, as a strong yellow solid, mp 180-185 ºC. ^{1}H NMR (400 MHz, DMSO) δ_H (ppm) 11.88 (s, 1H), 8.37 (d, *J* = 7.7 Hz, 1H), 8.29 (m, 2H), 7.75 (m, 2H), 7.68 (dd, *J* = 6.9, 8.0 Hz, 1H), 7.64 (d, *J* = 8.0 Hz, 1H), 7.35 (dd, *J* = 7.3, 7.7 Hz, 1H). ^{13}C NMR (101 MHz, DMSO) δ_C (ppm) 146.52, 144.61, 144.28, 130.87, 130.57, 129.74, 127.33, 126.86, 124.08, 122.61, 122.19, 121.63, 120.71, 118.43, 112.51. Infrared (KBr, cm^{-1}): 3271 (NH); 3031 ($CH_{aromatic}$).

7.2.4.2 *Synthesis of 3,11-dichloro-10*H*-indolo[3,2-*b*]quinoline (92b)*

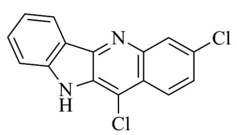

According with general procedure D, **91a** (1.5 g, 4.42 mmol) was reacted with $POCl_3$ (20 mL) to give 1.0 g of **92b** (66%) as a light orange solid, mp 171-176 ºC. ^{1}H NMR (400 MHz, DMSO) δ_H (ppm) 11.98 (s, NH), 8.33 (d, *J* = 7.8, 1H), 8.29 (d, *J* = 2.1, 1H), 8.28 (d, *J* = 9.2, 1H), 7.73 (m, 1H), 7.68 (dd, *J* = 7.0, 1.1, 1H), 7.63 (d, *J* = 8.1, 1H), 7.35 (dd, *J* = 7.8, 7.0, 1H). ^{13}C NMR (101 MHz, DMSO) δ_C (ppm) 147.43, 144.85, 144.34, 131.76, 131.27, 130.69, 128.07, 127.20, 124.66, 122.74, 122.35, 121.31, 120.89, 118.68, 112.64. Infrared (KBr, cm^{-1}): 3254 (NH); 3093 (CH$_{aromatic}$).

*7.2.4.3 Synthesis of 3,8,11-trichloro-10*H*-indolo[3,2-*b*]quinoline (92c)*

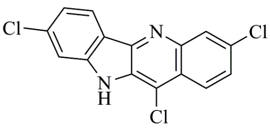

Reaction of **91b** (0.25 g, 1.6 mmol) with $POCl_3$ (10 mL) according with general procedure D gave 0.13 g of **92c** (49 %) as a strong orange solid, mp 167-170 ºC. ^{1}H NMR (400 MHz, DMSO) δ_H (ppm) 12.14 (s, NH), 8.34 (d, *J* = 8.4, 1H), 8.31 (d, *J* = 1.9, 1H), 8.30 (d, *J* = 4.9, 1H), 7.77 (dd, *J* = 9.1, 2.0, 1H), 7.62 (s, 1H), 7.37 (dd, *J* = 8.3, 1.7, 1H). ^{13}C NMR (101 MHz, DMSO) δ_C (ppm) 146.48, 145.34, 144.56, 135.68, 132.23, 130.99, 128.04, 127.57, 124.82, 123.84, 122.82, 121.28, 120.19, 119.36, 112.29. Infrared (KBr, cm^{-1}): 3298 (NH); 3134 (CH$_{aromatic}$).

*7.2.4.4 Synthesis of 3,7,11-trichloro-10*H*-indolo[3,2-b]quinoline (92d)*

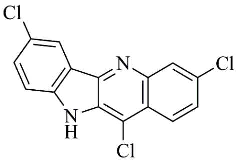

A solution of impure **91c** (0. 725 g, 2.4 mmol) in $POCl_3$ (5 mL) was reacted according to general procedure D, giving 0.58 g (75 %) of **92d** as a strong yellow solid, mp 163-166 ºC. ^{1}H NMR (400 MHz, DMSO) δ_H (ppm) 12.36 (s, NH), 8.34 (d, *J* = 1.8 Hz, 1H), 8.29 (d, *J* = 2.1 Hz, 1H), 8.28 (d, *J* = 9.1 Hz, 1H), 7.76 (dd, *J* = 9.1, 2.1 Hz, 1H), 7.71 (dd, *J* = 8.7, 1.8 Hz, 1H), 7.65 (d, *J* = 8.7 Hz, 1H). ^{13}C NMR (101 MHz, DMSO) δ_C (ppm) 145.00, 143.31, 132.66, 131.40, 131.26, 127.79, 127.04, 125.22, 124.93, 122.85, 121.84, 121.79, 121.65, 114.44, 113.47. Infrared (KBr, cm^{-1}): 3345 (NH); 3079 (CH$_{aromatic}$).

*7.2.4.5 Synthesis of 3,11-dichloro-7-trifluoromethyl-10*H*-indolo[3,2-*b*]quinoline (92e)*

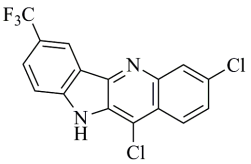

A solution of **91d** (0.5 g, 1.5 mmol) in $POCl_3$ (10 mL) was reacted according to general procedure D to give 0.21 g (53 %) of **92e**, as a light brown solid, mp 176-179ºC. ^{1}H NMR (400 MHz, DMSO) δ_H (ppm) 12.54 (s, NH), 8.87 (s, 1H), 8.32 (d, *J* = 2.0 Hz, 1H), 8.30 (d, *J* = 9.1 Hz, 1H), 8.25 (dd, *J* = 8.6, 1.5 Hz, 1H), 7.77 (dd, *J* = 9.1, 2.1 Hz, 1H), 7.72 (d, *J* = 8.6 Hz, 1H). ^{13}C NMR (101 MHz, DMSO) δC (ppm) 167.74, 147.35, 147.11, 144.70, 132.28, 132.15, 131.28, 128.25, 127.63, 124.88, 124.01, 123.29, 122.98, 121.16, 119.59, 112.58. Infrared (KBr, cm^{-1}): 3295 (NH); 3045 (CH$_{aromatic}$).

*7.2.4.6 Synthesis of 3,11-dichloro-7-methoxy-10*H*-indolo[3,2-*b*]quinoline (92f)*

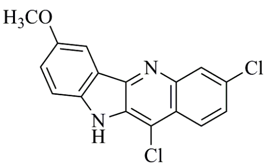

A solution of **91e** (0.4 g, 1.3 mmol,) in $POCl_3$ (10 mL) was reacted according to general procedure D to give 0.33 g (78 %) of **92f**, as a light brown solid, mp 161-164 ºC.^{1}H NMR (400 MHz, DMSO): δ_H (ppm) 11.89 (s, NH), 8.28 (d, *J* = 9.1, 1H), 8.25 (d, *J* = 2.2, 1H), 7.77 (d, *J* = 2.1, 1H), 7.74 (dd, *J* = 9.1, 2.1, 1H), 7.55 (d, *J* = 8.8, 1H), 7.34 (dd, *J* = 8.8, 2.2, 1H), 3.91 (s, 3H). ^{13}C NMR (101 MHz, DMSO) δ_C (ppm) 154.53, 146.00, 142.90, 139.82, 132.27, 131.32, 127.34, 126.92, 124.85, 122.50, 121.60, 120.67, 119.92, 113.77, 103.70, 56.09. Infrared (KBr, cm^{-1}): 3346 (NH); 3115 (CH$_{aromatic}$).

7.2.4.7 *Synthesis of 3,11-dichloro-7-methyl-10*H*-indolo[3,2-*b*]quinoline (92g)*

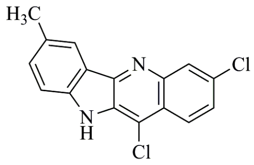

A solution of **91f** (0.5 g, 1.8 mmol,) in $POCl_3$ (10 mL) was reacted according to general procedure D to give 0.34 g (64 %) of **92g**, as a strong yellow solid, mp 173-175 ºC. ^{1}H NMR (400 MHz, DMSO): δ_H (ppm) 11.82 (s, NH), 8.26 (d, *J* = 4.6 Hz, 1H), 8.25 (d, *J* = 2.2 Hz, 1H), 8.12 (s, 1H), 7.71 (dd, *J* = 9.1, 2.1 Hz, 1H), 7.51 (s, 2H), 2.51 (s, 3H). ^{13}C NMR (101 MHz, DMSO) δ_C (ppm) 147.32, 144.22, 143.10, 132.57, 131.60, 130.90, 129.90, 128.02, 127.08, 124.62, 122.67, 121.96, 121.41, 118.44, 112.34, 21.34. Infrared (KBr, cm^{-1}): 3345 (NH); 3040 ($CH_{aromatic}$).

7.2.5 Synthesis of 5-Methyl-11-chloro-10*H*-indolo[3,2-*b*]quinolin-5-ium Chlorides (**93**)

7.2.5.1 *General procedure E: Synthesis of 5-methyl-11-chloro-10H-indolo[3,2-b]quinolin-5-ium chloride (93a)*

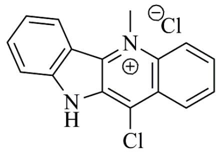

To a suspension of **92a** (2.0 g, 7.91 mmol) in anhydrous toluene (50 mL) was added methyl triflate (3.82 g, 23.7 mmol, 2.55 mL, 3 eq.) and the mixture was stirred at room temperature for 24 hours. The formed solid was filtered, suspended in sodium carbonate 5 % (400 mL) and extracted with chloroform (3x400 mL). The purple base chloroform extracts were washed with water and brine, dried (anhydrous Na_2SO_4), and then concentrated to a small volume. The solution was acidified with HCl in diethyl ether, to a orange end point, to give after filtration and drying, 2.15 g (90 %) of pure **93a**, as an orange solid, mp 269-272 ºC. ^{1}H NMR (400 MHz, DMSO) δ_H (ppm) 13.39 (s, NH), 8.88 (d, *J* = 9.4 Hz, 1H), 8.85 (d, *J* = 8.9 Hz, 1H), 8.69 (d, *J* = 8.3 Hz, 1H), 8.30 (dd, *J* = 9.4, 7.7 Hz, 1H), 8.12 dd, *J* = 8.3, 7.7 Hz, 1H), 8.01 (dd, *J* = 8.4, 7.7 Hz, 1H), 7.90 (d, *J* = 8.4 Hz, 1H), 7.58 (dd, *J* = 8.9, 7.7 Hz, 1H), 5.04 (s, 3H).^{13}C NMR (101 MHz, DMSO) δ_C (ppm) 146.33, 139.03, 136.15, 134.90, 133.20, 132.11, 129.30, 128.79, 126.98, 124.97, 123.73, 122.45, 119.21, 114.78, 113.94, 40.97. Anal. (C, H, N) Cal for $C_{16}H_{12}Cl_2N_2.HCl.H_2O$: C: 53.73, H: 4.23, N: 7.83, found: C, 54.00, H, 4.28, N, 7.82.

7.2.5.2 *Synthesis of 3,11-dichloro-5-methyl-10H-indolo[3,2-b]quinolin-5-ium chloride (93b)*

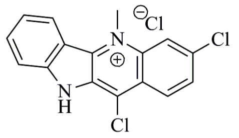

A suspension of **92b** (0.15 g, 0,52 mmol) was treated with methyl triflate (0.169g, 1.04 mmol, 114 µL, 2 eq.) according to general procedure E, giving 0.139 g of **93b** (79 %) as an orange solid, mp 234-237 ºC. ^{1}H NMR (400 MHz, DMSO) δ_H (ppm) 13.63 (NH, 1H), 9.00 (d, *J* = 1.7 Hz, 1H), 8.80 (d, *J* = 8.5 Hz, 1H), 8.60 (d, *J* = 9.1, 1H), 8.09 (dd, *J* = 9.1, 1.7 Hz, 1H), 7.96 (dd, *J* = 8.5, 7.4 Hz, 1H), 7.87 (d, *J* = 8.5 Hz, 1H), 7.53 (dd, *J* = 8.5, 7.4 Hz, 1H), 4.98 (s, 3H). ^{13}C NMR (101 MHz, DMSO) δ_C (ppm)146.60, 139.54, 138.36, 136.52, 135.29, 132.30, 129.40, 129.34, 127.10, 126.98, 122.67, 122.52, 118.68, 114.73, 114.06, 41.27.

7.2.5.3 Synthesis of 3,8,11-trichloro-5-methyl-10H-indolo[3,2-b]quinolin-5-ium chloride (93c)

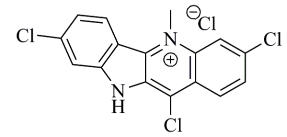

A suspension of **92c** (50 mg, 0.16 mmol) was treated with methyl triflate (52.0 mg, 0.32 mmol, 35 µL, 2 eq.) according to general procedure E, giving 26.1 mg of **93c** (46%) as an orange solid, mp 229-233 ºC. ^{1}H NMR (400 MHz, DMSO) δ_H (ppm) 13.47 (s, NH), 9.00 (s, 1H), 8.82 (d, J = 9.0, 1H), 8.62 (d, J = 9.1, 1H), 8.12 (d, J = 9.1, 1H), 7.81 (d, J = 1.5, 1H), 7.57 (dd, J = 9.0, 1.5, 1H), 4.95 (s, 3H). ^{13}C NMR (101 MHz, DMSO) δ_C (ppm) 146.69, 140.11, 139.05, 138.83, 136.77, 132.64, 129.97, 129.63, 128.70, 127.06, 123.19, 122.77, 118.73, 113.73, 113.41, 41.26.

7.2.5.4 Synthesis of 3,11-dichloro-5-methyl-7-substituted-10H-indolo[3,2-b]quinolin-5-ium chlorides (93d-g)

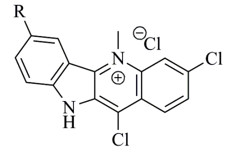

R= Cl, CF_3, OCH_3, CH_3

Since the synthesis of the compounds 3,11-dichloro-5-methyl-7-susbtituted-10*H*-indolo[3,2-*b*]quinolin-5-ium chlorides (**93d-g**) with the procedure E did not work, different methodologies were attempted to alkylate these compounds. Methylating agents such as methyl triflate or trimethyloxonium tetrafluoroborate with different reaction conditions were performed as described below, however without success.

7.2.5.4.1 Method 1

To a solution of **92d-g** in dry dichloromethane and inert atmosphere was added methyl triflate (4 eq.), and the mixture was allowed to react at room temperature. After 48 hours there was no formation of products of the reaction and the mixture was refluxed for more 48 hours. The solvent was removed at reduced pressure and the crude mixture suspended in sodium carbonate 5 % (400 mL). The aqueous solution was extracted with chloroform (3x400 mL). The chloroform extracts were washed with water and brine, dried (anhydrous Na_2SO_4), and then concentrated to a small volume. The solution was acidified with HCl in diethyl ether and the precipitate filtered, washed with Et_2O and then dried

7.2.5.4.2 Method 2

To a solution of **92d-g** in dry acetone and inert atmosphere was added methyl triflate (6 eq.) and refluxed for 48 hours. The solvent was removed at reduced pressure and the crude mixture suspended in sodium carbonate 5 % (400 mL). The aqueous solution was extracted with chloroform (3x400 mL). The chloroform extracts were washed with water and brine, dried (anhydrous Na_2SO_4), and then concentrated to a small volume. The solution was acidified with HCl in diethyl ether and the precipitate filtered, washed with Et_2O and then dried.

7.2.5.4.3 Method 3

To a solution of **92d-g** in anhydrous DMF and inert atmosphere was added methyl triflate (4 eq.). The mixture was reacted at 80 ºC during 24 hours. After this period was added methyl triflate (4 eq.) and the mixture allowed to react at 80 ºC for more 72 hours. The solvent was removed at reduced pressure and the crude mixture suspended in sodium carbonate 5 % (400 mL). The aqueous solution was extracted with chloroform (3x400 mL). The chloroform extracts were washed with water and brine, dried (anhydrous Na_2SO_4), and then concentrated to a small volume. The solution was acidified with HCl in diethyl ether. The precipitate was filtered and washed with Et_2O and dried.

7.2.5.4.4 Method 4

To a solution of **92d-g** in anhydrous DMF and inert atmosphere was added trimethyloxonium tetrafluoroborate (4 eq.). The mixture was reacted at 80 ºC during 48 hours. After this period was added trimethyloxonium tetrafluoroborate (4 eq.) and the mixture allowed to react at 80 ºC for more 72 hours. The solvent was removed at reduced pressure and the crude mixture suspended in sodium carbonate 5 % (400 mL). The aqueous solution was extracted with chloroform (3x400 mL). The chloroform extracts were washed with water and brine, dried (anhydrous Na_2SO_4), and then concentrated to a small volume. The solution was acidified with HCl in diethyl ether. The precipitate was filtered and washed with Et_2O and dried.

7.2.6 Synthesis of 10*H*-Indolo[3,2-*b*]quinoline (**25**)

7.2.6.1.1 Method 1

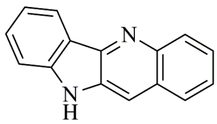

To a portion of **8a** (0.27 g, 1.07 mmol), sodium acetate (1.1 g, 13.4 mmol) and 10 % Pd/C catalyser in acetic acid (25 mL) was hydrogenated at 60 psi for 2 hours. The reaction mixture was filtered to remove Pd/C catalyst, the solvent concentrated to a small volume, basified with ice-cold saturated solution of $NaHCO_3$ and then extracted with EtOAc (3x25 mL). The combined organic extracts was washed with water and brine, dried (anhydrous Na_2SO_4), and the solvent was removed under reduced pressure to give 0.199 g of pure **25** (85%), as a yellow solid.

7.2.6.1.2 Method 2

To a solution of **8a** (0.2 g, 0,79 mmol) in dry methanol, 10 % Pd/C catalyst (15 % w/w of **8a**) was added dropwise triethylsilane (1.37g, 1.89 mL, 11.8 mmol, 15 eq.). The reaction mixture was allowed to react at room temperature and closed atmosphere for 20 minutes. The reaction mixture was filtered with Celite® 501 and the solvent removed at reduced pressure. The crude mixture was purified by column chromatography using as eluent dichloromethane:hexane (8:2), giving 0.134 g of pure **25** (78 %), as a yellow solid.

mp 200-203 ºC. ^{1}H NMR (400 MHz, DMSO) δ_H (ppm) 11.43 (s, NH), 8.36 (d, J = 7.7 Hz, 1H), 8.29 (s, 1H), 8.20 (d, J = 8.5 Hz, 1H), 8.11 (d, J = 8.1 Hz, 1H), 7.63 (m, 1H), 7.60 (m, 1H), 7.57 (m, 2H), 7.29 (dd, J = 7.8, 7.0 Hz, 1H). ^{13}C NMR (101 MHz, DMSO) δ_C (ppm) 145.04, 143.34, 142.71, 131.75, 128.98, 128.01, 126.80, 126.03, 125.32, 124.15, 120.67, 120.29, 118.63, 112.31, 110.81.

7.2.7 Synthesis of 5-Methyl-10*H*-indolo[3,2-*b*]quinolin-5-ium Trifluoromethanosulfonate (**1**)

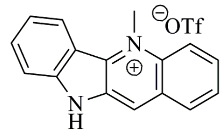

A suspension of **25** (0.085 mg, 0.38 mmol) in anhydrous toluene (2 mL) was treated with methyl triflate (0.104 g, 0.638 mmol, 70 µL, 1.7 eq.) and the mixture was stirred at room temperature for 24 hours. After this period diethyl ether was added (5 mL) and the orange precipitate which formed was filtered, washed with diethyl ether and then dried to give 0.092 g (62 %) of pure **1**, mp > 300 ºC. ^{1}H NMR (400 MHz, DMSO) δ_H (ppm) 12.76 (s, 1H), 9.17 (s, 1H), 8.70 (d, *J* = 7.7 Hz, 1H), 8.65 (d, *J* = 8.5 Hz, 1H), 8.46 (d, *J* = 7.4 Hz, 1H), 8.05 (dd, *J* = 8.5, 6.4 Hz, 1H), 7.83 (dd, *J* = 8.5 6.4 Hz, 2H), 7.74 (d, *J* = 8.0 Hz, 1H), 7.41 (dd, *J* = 8.2, 7.7 Hz, 1H), 4.92 (s, 3H). ^{13}C NMR (101 MHz, DMSO) δ_C (ppm) 144.73, 137.06, 134.34, 132.97, 132.27, 131.44, 128.85, 126.09, 125.29, 125.24, 123.85, 120.41, 116.84, 112.86, 112.20, 39.21. Anal. (C, H, N) Cal. for $C_{17}H_{13}F_3N_2O_3S.H_2O$: C, 51.00, H, 3.78, N, 7.00, found: C, 50.86, H, 3.80, N, 6.74.

7.2.8 Synthesis of Cryptolepine Derivatives (**3**)

7.2.8.1 ***General procedure F: Synthesis of 5-methyl-11-[(2-aminoethyl)amino]-10H-indolo[3,2-b]quinolin-5-ium chloride (3a)***

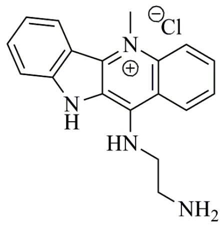

To a suspension of **93a** (40 mg, 0.132 mmol) in EtOAc (5 mL) was added ethane-1,2-diamine (15.8 mg, 0.263 mmol, 17.7 µL, 2 eq.). The reaction mixture was refluxed for 24 hours and the resulting precipitate was collected, washed with dry diethyl ether and dried. The solid was suspended in 5 % sodium carbonate (20 mL) and extracted with chloroform (3x20 mL). The combined organic extracts were washed with water, dried with brine (20 mL) and anhydrous Na_2SO_4 and dried under reduced pressure. Recrystallization from chloroform with HCl in diethyl ether gave 61 % (26.3 mg) of pure **3a**, as a light yellow solid, mp 293-295 ºC. ^{1}H NMR (400 MHz, DMSO) δ ppm 12.29 (s, NH) 9.24 (s, NH), 8.84 (d, *J* = 8.2 Hz, 1H), 8.51 (d, *J* = 8.4 Hz, 1H), 8.44 (s, NH_2), 8.31 (d, *J* = 8.8 Hz, 1H), 8.01 (d, *J* = 8.3 Hz, 1H), 7.97 (dd, *J* = 8.8, 7.4 Hz, 1H), 7.68 (dd, *J* = 8.3, 7.6 Hz, 1H), 7.64 (dd, *J* = 8.2, 7.4 Hz, 1H), 7.32 (d, *J* = 8.4, 7.6 Hz, 1H), 4.58 (s, 3H), 4.44 (m, 2H), 3,32 (m, 2H). ^{13}C NMR (101 MHz, DMSO) δ ppm 143.46, 142.90, 137.02, 135.65, 132.27, 130.52, 124.63, 124.29, 123.88, 120.75, 117.24, 115.95, 115.31, 114.32, 113.72, 42.41, 38,85, 38.08. Anal. (C, H, N) Cal. for $C_{18}H_{19}ClN_4.HCl.0.8H_2O$: C, 57.24, H, 5.76, N, 14.83, found: C, 57.30, H, 5.39, N, 14.54.

7.2.8.2 ***Synthesis of 5-methyl-11-{[2-(dimethylamino)ethyl]amino}-10H-indolo[3,2-b] quinolin-5-ium chloride (3b)***

To a suspension of **93a** (40.0 mg, 0.132 mmol, 1 eq.) in EtOAc (5 mL) was added commercial N^1,N^1-dimethylethane-1,2-diamine (23.3 mg, 0.264 mmol, 29 µL, 2 eq.). The reaction mixture was refluxed

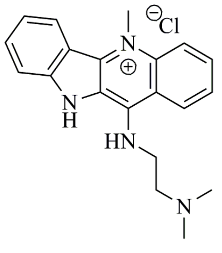

for 24 h and the resulting precipitate was collected, washed with diethyl ether and dried. The product was recrystallized from methanol-EtOAc to give 62 % (29.2 mg) yield of pure **3b**, as a dark yellow solid, mp 260-262 ºC. ^{1}H NMR (400 MHz, CD_3OD) δ_H (ppm) 8.71 (d, J = 8.4 Hz, 1H), 8.48 (d, J = 8.2 Hz, 1H), 8.28 (d, J = 8.1 Hz, 1H), 8.03 (dd, J = 8.1, 7.6 Hz, 1H), 7.91 (d, J = 8.2 Hz, 1H), 7.73 (dd, J = 8.4, 7.6 Hz, 1H), 7.69 (dd, J = 8.2, 7.5 Hz, 1H), 7.40 (dd, J = 8.2, 7.5 Hz, 1H), 4.64 (s, 3H), 4.61 (t, J = 6.2 Hz, 2H), 3.72 (t, J = 6.2 Hz, 2H), 3.05 (s, 6H).^{13}C NMR (101 MHz, CD_3OD) δ_C (ppm) 143.73, 143.16, 137.37, 136.93, 132.41, 131.06, 124.51, 123.78, 123.65, 121.19, 116.85, 116.74, 115.78, 114.67, 113.35, 56.55, 42.68, 40.51, 37.51. Anal. (C, H, N) Cal. for $C_{20}H_{23}ClN_4{\cdot}2HCl{\cdot}0.4H_2O$: C, 55.22, H, 5.98, N, 12.88, found: C, 55.60, H, 6.24, N, 12.68.

7.2.8.3 ***Synthesis of 5-methyl-11-{[2-(diethylamino)ethyl]amino}-10H-indolo[3,2-b] quinolin-5-ium chloride (3c)***

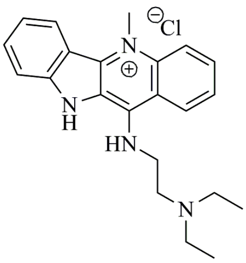

After recrystallization from methanol with ethyl acetate the compound **3c** was obtained in 35 % yield (18.4 mg) as a dark yellow solid, mp >330 ºC, from **93a** (40.0 mg, 0.132 mmol) and commercially available *N^1,N^1*-diethylethane-1,2-diamine (30.7 mg, 0.264 mmol, 37.1 µL, 2 eq.) according to general procedure F. ^{1}H NMR (400 MHz, CD_3OD) δ_H (ppm) 8.82 (d, J = 8.4 Hz, 1H), 8.53 (d, J = 8.1 Hz, 1H), 8.30 (d, J = 8.2 Hz, 1H), 7.98 (dd, J = 8.2, 7.7 Hz, 1H), 7.77 (d, J = 8.6 Hz, 1H), 7.70 (dd, J = 8.6, 7.2 Hz, 1H), 7.66 (dd, J = 8.2, 7.7 Hz, 1H), 7.34 (dd, J = 8.1, 7.2 Hz, 1H), 4.57 (s, 3H), 4.14 (broad s, 2H), 2.98 (broad s, 2H), 2.71 (q, J = 7.0 Hz, 4H), 0.95 (t, J = 7.0 Hz, 6H). ^{13}C NMR (101 MHz, CD_3OD) δ_C (ppm) 144.50, 143.39, 137.53, 135.48, 132.52, 130.71, 124.74, 124.51, 124.19, 120.83, 118.07, 117.68, 115.60, 115.55, 114.01, 53.41, 47.66, 44.62, 38.24, 11.27. Anal. (C, H, N) Cal. for $C_{22}H_{27}ClN_4{\cdot}HCl{\cdot}0.5H_2O$: C, 61.68, H, 6.82, N, 13.08, found: C, 61.61, H, 6.81, N, 13.05.

7.2.8.4 ***Synthesis of 5-methyl-11-[1-(diethylamino)propan-2-yl)amino]-10H-indolo[3,2-b] quinolin-5-ium chloride (3d)***

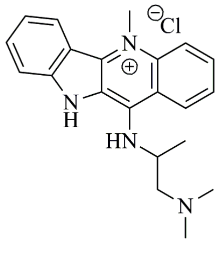

The title compound was obtained in 28 % yield (13.9 mg) as an orange solid, mp 272-276 ºC, by reaction of **93a** (40.0 mg, 0.132 mmol) and *N^1,N^1*-dimethylpropane-1,2-diamine (26.6 mg, 0.264 mmol, 2 eq.) according to general procedure F, and recrystallized from $CHCl_3$:MeOH (1:1) with EtOAc:Et_2O (3:2). ^{1}H NMR (400 MHz, DMSO+D_2O) δ_H (ppm) 8.69 (d, J = 8.5 Hz, 1H), 8.53 (d, J = 8.4 Hz, 1H), 8.30 (d, J = 8.9 Hz, 1H), 8.04 (dd, J = 7.1, 8.9 1H), 7.86 (d, J = 8.5 Hz, 1H), 7.77 (dd, J = 7.4, 8.5 Hz, 1H), 7.73 (d, J = 7.1, 8.5 Hz, 1H), 7.42 (dd, J = 7.4, 8.4 Hz 1H), 5.11 (m, 1H), 4.62 (s, 3H), 3.81 (t, J = 11.7 Hz, 1H), 3.45 (d, J = 11.9 Hz, 1H), 2.88 (s broad, 6H), 1.44 (d, J = 6.3 Hz, 3H). ^{13}C NMR (101 MHz, DMSO+D_2O) δ_C (ppm) 143.73, 143.11, 137.49, 135.73, 133.30, 132.04, 130.69, 125.17, 125.04, 124.82, 122.02, 117.76, 116.30, 115.01, 114.07, 60.90, 47.64, 44.03, 38.47, 20.56. Anal. (C, H, N): Cal. for $C_{21}H_{25}ClN_4{\cdot}HCl{\cdot}3.7H_2O$: C, 53.44, H, 7.13, N, 11.87, found: C, 53.49, H, 7.04, N, 13.80. EI/MS (m/z): Cal. for $C_{21}H_{25}N_4^+$: 333.21 found: 333.204910 (26.9 %), 332.201430 (100%).

7.2.8.5 ***Synthesis of 5-methyl-11-[(3-aminopropyl)amino]-10H-indolo[3,2-b]quinolin-5-ium chloride (3e)***

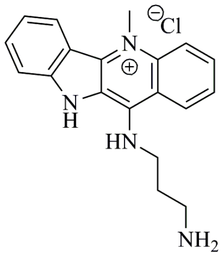

To a suspension of **93a** (40.0 mg, 0.132 mmol) was added commercial propane-1,3-diamine (19.5 mg, 0.264 mmol, 22.0 µL, 2 eq.) according to general procedure F. The product was recrystallized from CH_2Cl_2:MeOH (8:2) with Et_2O to give 24.3 mg (54 %) of **3e** as an yellow solid, mp 243-245 ºC. ^{1}H NMR (400 MHz, DMSO) δ_H 12.28 (s, NH), 9.27 (s, NH), 8.90 (d, *J* = 8.6 Hz, 1H), 8.56 (d, *J* = 8.5 Hz, 1H), 8.36 (d, *J* = 8.9 Hz, 1H), 8.20 (s, NH_2), 8.03 (d, *J* = 8.0 Hz, 1H), 8.01 (dd, *J* = 8.9, 8.1 Hz, 1H), 7.73 (dd, *J* = 8.0, 7.6 Hz, 1H), 7.68 (dd, *J* = 8.6, 8.0 Hz,1H), 7.37 (dd, *J* = 8.5, 7.6 Hz, 1H), 4.61 (s, 3H), 4.32 (d, *J* = 6.0 Hz, 2H), 3.01 (d, *J* = 5.7 Hz, 2H), 2.17 (dd, *J* = 6.0, 5.7 Hz, 2H). ^{13}C NMR (101 MHz, DMSO) δ_C 144.01, 143.21, 137.65, 135.83, 132.76, 130.88, 124.89, 124.74, 124.39, 121.17, 117.83, 116.59, 115.68, 114.75, 114.18, 42.86, 38.51, 36.75, 28.05. Anal. (C, H, N): Cal. for $C_{19}H_{21}ClN_4.HCl.H_2O$: C, 57.73, H 6.12, N, 14.17, found: C, 57.43, H, 5.88, N, 14.52.

7.2.8.6 ***Synthesis of 5-methyl-11-{[3-(dimethylamino)propyl]amino}-10H-indolo[3,2-b] quinolin-5-ium chloride (3f)***

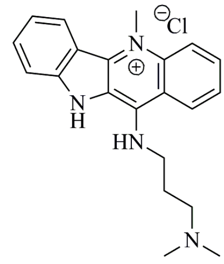

After recrystallization from methanol-ethyl acetate **3f** was obtained in 34 % yield (16.3 mg) as a dark yellow solid, mp 277-280 ºC, from **93a** (40.0 mg, 0.132 mmol) and commercial *N^1,N^1*-dimethylpropane-1,3-diamine (26.9 mg, 0.264 mmol, 33.2 µL, 2 eq.), according to general procedure F. ^{1}H NMR (400 MHz, CD_3OD) δ_H (ppm) 8.65 (d, *J* = 8.4 Hz, 1H), 8.53 (d, *J* = 8.1 Hz, 1H), 8.30 (d, *J* = 8.1 Hz, 1H), 8.05 (dd, *J* = 8.1, 7.0 Hz, 1H), 7.92 (d, *J* = 8.1 Hz, 1H), 7.77 (dd, *J* = 8.1, 7.1 Hz, 1H), 7.73 (dd, *J* = 8.4, 7.0 Hz, 1H), 7.44 (dd, *J* = 8.1, 7.1 Hz, 1H), 4.67 (s, 3H), 4.32 (t, *J* = 6.9 Hz, 2H), 3.37 (t, *J* = 7.9 Hz, 2H), 2.39 (quintet, *J* = 7.5 Hz, 2H), 2.92 (s, 6H). ^{13}C NMR (101 MHz, CD_3OD) δ_C (ppm) 143.63, 143.34, 137.46, 136.45, 134.47, 132.22, 130.71, 124.22, 123.62, 123.23, 120.93, 116.63, 115.51, 114.63, 113.13, 54.79, 42.50, 42.08, 37.22, 25.09. Anal. (C, H, N): Cal. for $C_{21}H_{25}ClN_4{\cdot}2HCl{\cdot}H_2O$: C, 54.85, H, 6.36, N, 12.18, found: C, 54.86, H, 6.33, N, 13.74. EI/MS (m/z): Cal. for $C_{21}H_{25}N_4^+$: 333,21, found: 333.202807 (24.7 %), 332.199995 (100%).

7.2.8.7 ***Synthesis of 5-methyl-11-{[3-(diethylamino)propyl]amino}-10H-indolo[3,2-b] quinolin-5-ium chloride (3g)***

The title compound was obtained in 82 % yield (43.1 mg) as a dark yellow solid, mp 274-277 ºC, by reaction of **93a** (40.0 mg, 0.132 mmol) and commercially available *N^1,N^1*-diethylpropane-1,3-diamine (34.4 mg, 0.264 mmol, 41.6 µL, 2 eq.), according to general procedure F. ^{1}H NMR (400 MHz, CD_3OD) δ_H (ppm) 8.62 (d, *J* = 8.5 Hz, 1H), 8.47 (d, *J* = 8.1 Hz, 1H), 8.25 (d, *J* = 8.5 Hz, 1H), 8.04 (dd, *J* = 8.5,

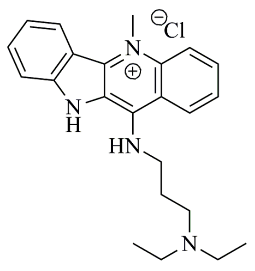

7.4 Hz, 1H), 7.91 (d, *J* = 8.4 Hz, 1H), 7.74-7.70 (m, 2H), 7.41 (dd, *J* = 8.1, 7.7 Hz, 1H), 4.59 (s, 3H), 4.29 (t, *J* = 7.0 Hz, 2H), 3.38 (t, *J* = 7.8 Hz, 2H), 3.26 (q, *J* = 7.2 Hz, 4H), 2.36 (quintet, *J* = 7.5 Hz, 2H), 1.34 (t, *J* = 7.2 Hz, 6H).^{13}C NMR (101 MHz, CD$_3$OD) δ_C (ppm) 143.57, 143.36, 137.46, 136.35, 132.37, 130.81, 124.35, 123.68, 123.39, 121.08, 116.70, 116.53, 115.52, 114.63, 113.27, 49.08, 47.27, 42.84, 37.33, 24.65, 7.87. Anal. (C, H, N): Cal. for $C_{23}H_{29}ClN_4 \cdot 2HCl \cdot 0.5H_2O$: C, 57.69, H, 6.74, N, 11.70, found: C, 57.27, H, 6.93, N, 12.97. EI/MS (m/z): Cal. for $C_{23}H_{29}N_4^+$: 361,24, found: 361.234997 (29.5%), 360.231795 (100%).

7.2.8.8 ***Synthesis of 5-methyl-11-{[3-(dimethylamino)-2,2-dimethylpropyl]amino}-10H-indolo[3,2-b]quinolin-5-ium chloride (3h)***

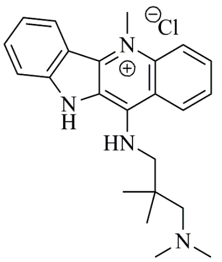

Reaction of **93a** (51.2 mg, 0.164 mmol) and commercial *N^1,N^1*-2,2-tetramethylpropane-1,3-diamine (21.3 mg, 1.64 mmol, 0.26 mL, 10 eq.) according to general procedure F, gave **3h** in 78 % yield (52.6 mg), as an orange solid, mp 171-173 ºC. ^{1}H NMR (400 MHz, DMSO) δ_H (ppm) 10.75 (s, NH), 8.51 (d, *J* = 8.1 Hz, 1H), 8.33 (d, *J* = 8.5 Hz, 1H), 8.20 (d, *J* = 7.9 Hz, 1H), 8.00 (dd, *J* = 8.5, 7.5 Hz, 1H), 7.93 (d, *J* = 8.1 Hz, 1H), 7.75 (dd, *J* = 7.9, 7.5 Hz, 1H), 7.67 (dd, *J* = 8.1, 7.6 Hz, 1H), 7.32 (dd, *J* = 8.1, 7.6 Hz, 1H), 4.56 (s, 3H), 4.21 (s, 2H), 2.59 (s, 2H), 2.44 (s, 6H), 1.13 (s, 6H). ^{13}C NMR (101 MHz, DMSO) δ_C (ppm) 144.59, 143.08, 137.67, 135.60, 132.62, 130.61, 124.83, 124.56, 123.11, 120.99, 118.02, 116.63, 115.58, 114.88, 114.18, 70.03, 57.33, 48.18, 38.31, 35.51, 25.38. Anal. (C, H, N): Cal. for $C_{23}H_{29}ClN_4 \cdot H_2O$: C, 66.57, H, 7.53, N, 13.50, found: C, 66.09, H, 7.13, N, 13.18.

7.2.8.9 ***Synthesis of 5-methyl-11-{[3-(isopropylamino)propyl]amino}-10H-indolo[3,2-b] quinolin-5-ium chloride (3i)***

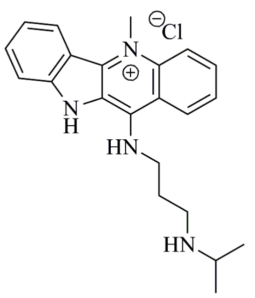

After recristallization from methanol-ethyl acetate, **3i** was obtained in 56 % yield (28.7 mg) as a yellow solid, mp >330 ºC, from **93a** (40.0 mg, 0.132 mmol) and commercial *N^1*-isopropylpropane-1,3-diamine (30.6 mg, 0.264 mmol, 36.9 µL, 2 eq.), according to general procedure F. ^{1}H NMR (400 MHz, CD$_3$OD) δ_H (ppm) 8.67 (d, *J* = 8.3 Hz, 1H), 8.54 (d, *J* = 8.2 Hz, 1H), 8.30 (d, *J* = 8.4 Hz, 1H), 8.05 (dd, *J* = 8.4, 7.3 Hz, 1H), 7.93 (d, *J* = 8.1 Hz, 1H), 7.75 (dd, *J* = 8.1, 7.2 Hz, 1H), 7.73 (dd, *J* = 8.3, 7.3 Hz, 1H), 7.44 (dd, *J* = 8.2, 7.2 Hz, 1H), 4.68 (s, 3H), 4.34 (t, *J* = 7.0 Hz, 2H), 3.42 (quintet, *J* = 6.5 Hz, 1H), 3.27 (t, *J* = 7.6 Hz, 2H), 2.43 (quintet, *J* = 7.3 Hz, 2H), 1.37 (d, *J* = 6.5 Hz, 6H). ^{13}C NMR (101 MHz, CD$_3$OD) δ_C (ppm) 143.86, 143.76, 137.68, 135.73, 132.43, 130.92, 124.43, 123.82, 123.43, 121.16, 116.85, 115.72, 114.79, 113.30, 50.86, 42.65, 42.22, 37.43, 26.93, 17.91. Anal. (C, H, N): Cal. for $C_{22}H_{27}ClN_4 \cdot HCl \cdot 0.5H_2O$: C, 61.68, H, 6.82, N, 13.08, found: C, 61.86, H, 6.55, N, 12.97.

7.2.8.10 *Synthesis of 5-methyl-11-{[3-(piperidin-1-yl)propyl]amino}-10H-indolo[3,2-b] quinolin-5-ium chloride (3j)*

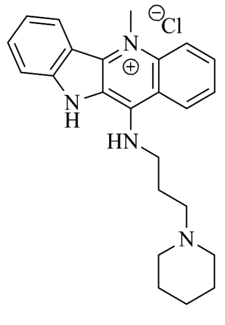

The title compound was obtained in 71 % yield (38.3 mg) as a light orange solid, mp 289-293 ºC, after reaction of **93a** (40.0 mg. 0.132 mmol) with 3-piperidine-1yl-propan-1-amine (37.5 mg, 0.264 mmol, 2 eq.) according to general procedure F, and recrystallization from $CHCl_3$:MeOH (5:1) with EtOAc:Et_2O (8:1). ^1H NMR (400 MHz, DMSO) δ_H (ppm) 12.31 (s, NH), 9.21 (s, NH), 8.87 (d, *J* = 8.1 Hz, 1H), 8.55 (d, *J* = 8.1 Hz, 1H), 8.34 (d, *J* = 8.9 Hz, 1H), 8.01 (m, 2H), 7.71 (dd, *J* =7.5, 6.5 Hz, 1H), 7.68 (dd, *J* =8.1, 4.9 Hz, 1H), 7.36 (dd, *J* = 8.1, 6.5 Hz, 1H), 4.60 (s, 3H), 4.31 (m, *J* = 5.5 Hz, 2H), 3.43 (m, 2H), 3.23 (m, 2H), 2,86 (m, 2H), 2.30 (m, 2H), 1.78 (m, 4H), 1.69 (m, 1H), 1.38 (m, 1H). ^{13}C NMR (101 MHz, DMSO) δ_C (ppm) 143.41, 142.61, 137.02, 135.16, 132.12, 130.20, 124.44, 124.09, 123.70, 120.52, 117.15, 116.06, 115.02, 114.17, 113.58, 53.24, 51.81, 42.93, 37.89, 23.86, 22.12, 21.28. Anal. (C, H, N): Cal. for $C_{24}H_{29}ClN_4{\cdot}2HCl{\cdot}1.7H_2O$: C, 56.24, H, 6.77, N, 10.93, found: C, 56.28, H, 6.64, N, 10.91.

7.2.8.11 *Synthesis of 5-methyl-11-[(4-aminobutyl)amino]-10H-indolo[3,2-b]quinolin-5-ium chloride (3k)*

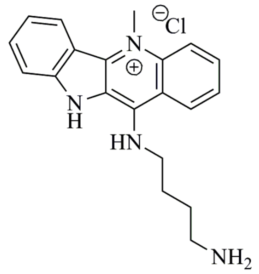

To a suspension of **93a** (40.0 mg, 0.132 mmol) was added commercial butane-1,4-diamine (23.2 mg, 0.264 mmol, 26.6 µL, 2 eq.) according to general procedure F. The product was recrystallized from CH_2Cl_2:MeOH (7:3) with Et_2O to give 21.2 mg (45 %) of **3k** as an yellow solid, mp 263-265 ºC. ^1H NMR (400 MHz, DMSO) δH (ppm) 8.89 (d, *J* = 8.5 Hz, 1H), 8.55 (d, *J* = 8.2 Hz, 1H), 8.34 (d, *J* = 8.5 Hz, 1H), 8.00 (dd, *J* = 8.3, 7.3 Hz, 1H), 7.95 (d, *J* = 8.3 Hz, 1H), 7.71 (dd, *J* = 7.8, 7.3 Hz, 1H), 7.67 (dd, *J* = 8.3, 7.3 Hz, 1H), 7.36 (dd, *J* = 8.2, 7.3 Hz, 1H), 4.60 (s, 3H), 4.22 (t, *J* = 6.6 Hz, 2H), 2.85 (t, *J* = 7.4 Hz, 2H), 1.89 (m, 2H), 1.75 (m, 2H). ^{13}C NMR (101 MHz, DMSO) δ_C (ppm) 144.20, 143.13, 143.08, 137.77, 137.73, 132.70, 130.77, 125.01, 124.69, 124.26, 121.12, 117.78, 115.67, 114.93, 114.18, 45.18, 38.78, 38.45, 27.12, 24.75. Anal. (C, H, N): Cal. for $C_{20}H_{23}ClN_4{\cdot}2HCl$: C, 56.15 H, 5.89 N, 13.10, found: C, 56.33, H, 5.52, N, 12.74.

7.2.8.12 *Synthesis of 5-methyl-11-{[4-(diethylamino)butyl]amino}-10H-indolo[3,2-b] quinolin-5-ium chloride (3l)*

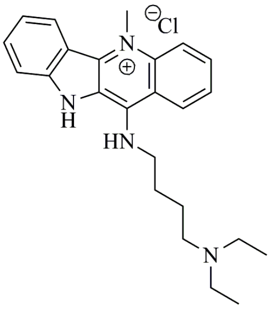

The title compound was obtained in 70 % yield (44.9 mg) as an orange solid, mp 268-272 ºC by reaction of **93a** (47.0 mg, 0.155 mmol) with *N*^{1},*N*^{1}-diethylbutane-1,4-diamine **103** (44.8 mg, 0.31 mmol, 2 eq.) according to general procedure F, and recrystallization from MeOH with EtOAc:Et_2O (2:3). ^1H NMR (400 MHz, DMSO) δ_H (ppm) 12.36 (s, NH), 9.24 (d, *J* = 1.3 Hz, NH), 8.89 (d, *J* = 8.1 Hz, 1H), 8.55 (d, *J* = 8.1 Hz, 1H), 8.33 (d, *J* = 8.6 Hz, 1H), 8.01 (dd, *J* = 8.6, 7.6 Hz, 1H), 7.98 (d, *J* = 8.1 Hz, 1H), 7.72 (dd, *J*

= 8.1, 7.6 Hz, 1H), 7.68 (dd, *J* = 8.1, 7.6 Hz, 1H), 7.38 (dd, *J* = 8.1, 7.6 Hz, 1H), 4.60 (s, 3H), 4.23(q broad, 2H), 3,10 (m, 6H), 1.89 (m, 4H), 1.21 (t, *J* = 7.1 Hz, 6H). ^{13}C NMR (101 MHz, DMSO) δ_C (ppm) 143.75, 142.58, 137.38, 135.13, 132.78, 132.23, 130.28, 124.58, 124.18, 123.76, 120.63, 117.26, 115.16, 114.40, 113.67, 50.27, 45.97, 44.76, 37.95, 26.82, 20.51, 8.34. Anal. (C, H, N): Cal. for $C_{24}H_{31}ClN_4{\cdot}2HCl{\cdot}0.5H_2O$: C, 58.48, H, 6.95, N, 11.37, found: C, 58.01, H, 7.16, N, 11.47.

7.2.8.13 Synthesis of 5-methyl-11-{[5-(diethylamino)pentan-2-yl]amino}-10H-indolo[3,2-b] quinolin-5-ium chloride (3m)

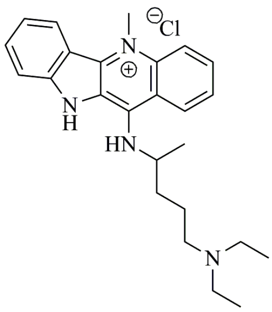

Reaction of **93a** (40.0 mg, 0.132 mmol) *N^1,N^1*-diethylpentane-1,4-diamine (41.7 mg, 0.264 mmol, 51 µL, 2 eq.), according to general procedure F and recrystallization from MeOH with EtOAc:Et$_2$O (1:1), gave **3m** in 30 % yield (17.2 mg), as an orange solid, mp 240-243 ºC. ^{1}H NMR (400 MHz, DMSO) δ_H (ppm) 8.85 (d, *J* = 8.6 Hz, 1H), 8.58 (d, *J* = 8.1 Hz, 1H), 8.58 (d, *J* = 8.1 Hz, NH), 8.37 (d, *J* = 8.5 Hz, 1H), 8.04 (dd, *J* = 8.5, 7.8 Hz, 1H), 7.96 (d, *J* = 8.5 Hz, 1H), 7.76 (dd, *J* = 8.5, 7.7 Hz, 1H), 7.71(dd, d, *J* = 8.6, 7.8 Hz, 1H), 7.39 (dd, *J* = 8.1, 7.7 Hz, 1H), 4.92 (m, 1H), 4.64 (s, 3H), 3.13-2.93 (m, 6H), 2.14-1.98 (m, 2H), 1.91-1.81 (m, 2H), 1.47 (d, *J* = 6.2 Hz, 3H), 1.14 (t, *J* = 7.1 Hz, 6H). ^{13}C NMR (101 MHz, DMSO) δ_C (ppm) 144.24, 143.36, 140.38, 138.04, 136.08, 132.93, 131.09, 125.73, 124.98, 124.46, 121.39, 118.04, 116.04, 115.25, 114.41, 51.01, 46.88, 46.69, 38.87, 34.15, 22.55, 20.75, 9.01. Anal. (C, H, N): Cal. for $C_{25}H_{33}ClN_4{\cdot}HCl{\cdot}2.7H_2O$: C, 58.86, H, 7.79, N, 10.98, Found: C, 58.96, H, 8.08, N, 11.40.

7.2.8.14 Synthesis of 5-methyl-11-(piperidin-4-ylamino)-10H-indolo[3,2-b]quinolin-5-ium chloride (3n)

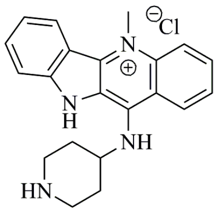

Reaction of **93a** (50.0 mg, 0.165 mmol) and piperidin-4-amine (29.7 mg, 0.296 mmol, 31.1 µL, 1.8 eq.), according to general procedure F, gave **3n** in 66 % yield (40.3 mg) , as an orange solid, mp 325-327 ºC. ^{1}H NMR (400 MHz, DMSO) δ_H (ppm) 12.16 (s, NH), 8.66 (d, *J* = 8.5 Hz, 1H), 8.56 (d, *J* = 9.0 Hz, 1H), 8.51 (s, NH), 8.29 (d, *J* = 8.3 Hz, 1H), 8.09 (dd, *J* = 9.0, 7.4 Hz, 1H), 7.98 (d, *J* = 8.4 Hz, 1H), 7.83 (dd, *J* = 8.3, 7.4 Hz, 1H), 7.81 (dd, *J* = 8.4, 7.7 Hz, 1H), 7.44 (dd, *J* = 8.5, 7.7 Hz, 1H), 4.80 (s, 3H), 4.14 (d, *J* = 12.6 Hz, 2H), 3.86 (dd, *J* = 12.6, 11.0 Hz, 2H), 3.50 (m, 1H), 2.29 (d, *J* = 11.5 Hz, 2H), 2.05 (dd *J* = 11.5, 11.0 Hz, 2H). ^{13}C NMR (101 MHz, DMSO) δ_C (ppm) 147.20, 144.42, 138.12, 137.78, 132.71, 132.46, 126.54, 125.66, 125.54, 125.04, 121.60, 120.70, 118.63, 114.71, 114.18, 51.13, 47.60, 39.61, 30.68. Anal. (C, H, N): Cal. for $C_{21}H_{23}ClN_4{\cdot}2HCl{\cdot}0.4H_2O$: C, 56.42, H, 5.82, N, 12.53, found: C, 56.52, H, 6.01, N, 13.80. ESI-TOF/MS (m/z): Cal. for $C_{21}H_{23}N_4^+$: 331,19, Found: 331.1917.

7.2.8.15 *Synthesis of 5-methyl-11-[(1-isobutylpiperidin-4-yl)amino]-10H-indolo[3,2-b] quinolin-5-ium chloride (3o)*

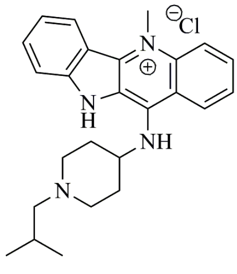

To a solution of **3n** (40.0 mg, 0.108 mmol), anhydrous Na_2SO_4 (2g) and isobutyraldehyde (24.8 mg, 0.432 mmol, 31.2 µL, 4 eq.) in dry MeOH (5 mL) was added $NaBH_3CN$ (33.9 mg, 0.54 mmol, 5 eq.) and the reaction allowed to proceed at room temperature, for 24 h. The anhydrous Na_2SO_4 was filtered off and solvent removed under reduced pressure. The resulting residue was dissolved in water (5 mL) and basified with aqueous KOH 2M to pH=12. The aqueous solution was then extracted with CH_2Cl_2 (3x20 mL) and the combined organic extracts washed with water and brine, dried (anhydrous Na_2SO_4) and concentrated to a small volume under reduce pressure. HCl in Et_2O was added and the precipitate which formed was collected, washed with Et_2O and then dried, yielding 27.3 mg (59 %) of **3o** as a orange solid, mp 270-274 ºC. ^1H NMR (400 MHz, CD_3OD) δ_H (ppm) 8.64 (d, J = 8.2 Hz, 1H), 8.51 (d, J = 8.3 Hz, 1H), 8.46 (d, J = 8.2 Hz, 1H), 8.13 (dd, J = 8.3, 7.6 Hz, 1H), 7.94 (d, J = 8.4 Hz, 1H), 7.88 (dd, J = 8.2, 7.6 Hz, 1H), 7.84 (dd, J = 8.4, 7.3 Hz, 1H), 7.50 (dd, J = 8.2, 7.3 Hz, 1H), 4.90 (s, 3H), 4.27 (d, J = 12.6 Hz, 2H), 3.92 (t, J = 12.2 Hz, 2H), 3.70 (m, 1H), 3.09 (d, J = 7.2 Hz, 2H), 2.52 (d J = 11.2 Hz, 2H), 2.26 (qd, J = 12.1, 3.6 Hz, 2H), 2.16 (m, 1H), 1.16 (d, J = 6.7 Hz, 6H). ^{13}C NMR (101 MHz, CD_3OD) δ_C (ppm) 148.15, 146.06, 139.80, 139.53, 133.83, 133.81, 127.47, 126.81, 126.74, 126.07, 122.92, 122.55, 118.88, 115.94, 114.71, 56.97, 53.37, 52.21, 39.89, 30.22, 27.66, 20.52. Anal. (C, H, N): Cal. for $C_{25}H_{31}ClN_4{\cdot}2HCl{\cdot}0.5H_2O$: C, 59.47, H, 6.79, N, 11.10, found: C, 59.09, H, 6.99, N, 12.05. ESI-TOF/MS (m/z): Cal. for $C_{25}H_{31}N_4^+$: 387.25, Found: 387.2543.

7.2.8.16 *Synthesis of 5-methyl-11-[(1-benzylpiperidin-4-yl)amino]-10H-indolo[3,2-b] quinolin-5-ium chloride (3p)*

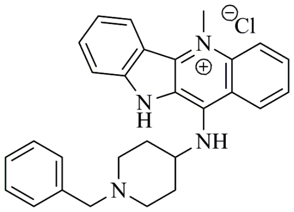

To a solution of **3n** (40.0 mg, 0.108 mmol) and anhydrous Na_2SO_4 (2g) in dry MeOH (5 mL) was added benzaldehyde (45.8 mg, 43.6 µL, 0.432 mmol, 4 eq.) and the mixture stirred for 1 hour. $NaBH_3CN$ (33.9 mg, 0.54 mmol, 5 eq.) was added and the mixture left to react for a further 20 h. The anhydrous Na_2SO_4 was filtered off and the solvent removed under reduced pressure. The residue was dissolved in H_2O (5 mL) and the pH adjusted to 12 with 2M KOH. The aqueous solution was extracted with CH_2Cl_2 (3x20 mL) and the combined extracts washed with water, brine and dried with anhydrous Na_2SO_4. After concentration under reduced pressure HCl in Et_2O was added to precipitate the product as a salt, which was filtered and recrystallized with MeOH:AcOEt (2:5) and Et_2O to give **3p** as a deep yellow solid, mp 275-277 ºC, in 66 % yield. ^1H NMR (400 MHz, DMSO) δ_H (ppm) 8.63 (d, J = 8.2 Hz, 1H), 8.50 (d, J = 8.5 Hz, 1H), 8.47 (d, J = 8.2 Hz, 1H), 8.12 (dd, J = 8.5, 7.6 Hz, 1H), 7.93 (d, J = 8.1 Hz, 1H), 7.87 (dd, J = 8.2, 7.6 Hz, 1H), 7.83 (dd, J = 8.1, 7.6 Hz, 1H), 7.66 (d, J = 5.9 Hz, 2H), 7.56 (d, J = 6.7 Hz, 1H), 7.52 (dd, J = 6.7, 5.9 Hz, 2H), 7.48 (dd, J = 8.2, 7.6 Hz, 1H), 4.88 (s, 3H), 4.44 (s, 2H), 4.27 (d, J = 12.5 Hz, 2H), 3.92 (t, J = 12.5 Hz, 2H), 3.77 (t, J = 10.3 Hz, 1H), 2.58 (d, *J* = 11.6 Hz, 2H), 2.28 (q, *J* = 11.6 Hz, 2H). ^{13}C NMR (101 MHz, DMSO) δ_C (ppm) 146.67, 144.61, 138.35, 138.06, 135.98, 132.38, 132.35, 131.28, 129.71, 129.37, 129.01, 126.03, 125.32, 124.61, 121.46, 121.12, 117.42, 114.47, 113.27, 54.92, 50.73, 48.32, 38.46, 28.93. Anal. (C, H, N): Cal. for $C_{28}H_{29}ClN_4{\cdot}1.5H_2O{\cdot}2HCl$: C, 60.38, H, 6.15, N, 10.06, found: C, 60.68, H, 5.76, N, 10.00.

7.2.8.17 *Synthesis of 5-methyl-11-{[1-(2-hydroxybenzyl)piperidin-4-yl]amino}-10H-indolo[3,2-b]quinolin-5-ium chloride (3q)*

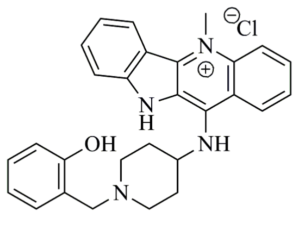

Reaction of **3n** (40.0 mg, 0.108 mmol) with salicylaldehyde (52.7 mg, 0.432 mmol, 45 µL, 4 eq.) according to the procedure described for **3o**, gave **3q**, in 30 % yield (15.8mg), as an orange solid, mp 277-280 ºC. ^{1}H NMR (400 MHz, DMSO) δ_H (ppm) 12.18 (s, NH), 9.47 (d, *J* = 1.2 Hz, NH), 8.67 (d, *J* = 8.1 Hz, 1H), 8.58 (d, *J* = 8.8 Hz, 1H), 8.30 (d, *J* = 8.3 Hz, 1H), 8.10 (dd, *J* = 8.8, 7.1 Hz, 1H), 7.99 (d, *J* = 8.6 Hz, 1H), 7.86 (dd, *J* = 8.3, 7.1 Hz, 1H), 7.82 (dd, *J* = 8.6, 7.3 Hz, 1H), 7.56 (d, *J* = 7.2 Hz, 1H), 7.46 (dd, *J* = 8.1, 7.3 Hz, 1H), 7.28 (dd, *J* = 7.8, 6.9 Hz, 1H), 7.04 (d, *J* = 7.8 Hz, 1H), 6.89 (dd, *J* = 7.2, 6.9 Hz, 1H), 4.82 (s, 3H), 4.23 (s, 2H), 4.17 (d, *J* = 12.2 Hz, 2H), 3.85 (t, *J* = 11.5 Hz, 2H), 3.53 (m, 1H), 2.46 (d broad, 2H), 2.23 (q, *J* = 5.8 Hz, 2H). ^{13}C NMR (101 MHz, DMSO) δ_C (ppm) 155.99, 146.54, 143.94, 137.56, 137.28, 132.21, 132.19, 131.95, 131.63, 130.34, 125.97, 125.04, 124.60, 121.15, 121.07, 119.04, 118.24, 118.13, 115.44, 114.19, 113.67, 53.78, 50.74, 42.04, 39.27, 28.39. Anal. (C, H, N): Cal. for $C_{28}H_{29}ClN_4O{\cdot}2HCl{\cdot}0.5H_2O$: C, 60.60, H, 5.81, N, 10.10, found: C, 60.55, H, 5.89, N, 10.79.

7.2.8.18 *Synthesis of 5-methyl-11-(phenylamino)-10H-indolo[3,2-b]quinolin-5-ium chloride (3r)*

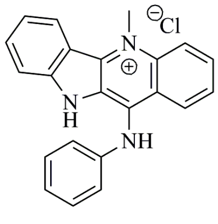

Following general procedure F, a suspension of **93a** (40.0 mg, 0.132 mmol) was allowed to react with aniline (22.1 mg, 21.7 µL, 0.24 mmol, 1.8 eq.) to give **3r** (75 %), mp 269-271 ºC, after recristalization with MeOH:AcOEt (1:2) and Et_2O. ^{1}H NMR (400 MHz, DMSO) δ_H (ppm) 8.49 (d, *J* = 8.6 Hz, 1H), 8.44 (d, *J* = 8.5 Hz, 1H), 8.34 (d, *J* = 8.7 Hz, 1H), 8.03 (dd, *J* = 8.7, 7.6 Hz, 1H), 7.69 (dd, *J* = 8.6, 7.6 Hz, 1H), 7.65 (dd, *J* = 8.2, 7.6 Hz, 1H), 7.53 (d, *J* = 8.2 Hz, 1H), 7.41 (dd, *J* = 7.8, 7.5 Hz, 2H), 7.35 (dd, *J* = 8.5, 7.6 Hz, 1H), 7.28 (d, *J* = 7.5 Hz, 1H), 7.18 (d, *J* = 7.8 Hz, 2H), 4.65 (s, 3H). ^{13}C NMR (101 MHz, DMSO) δ_C (ppm) 143.26, 139.75, 138.78, 137.94, 137.48, 133.65, 132.87, 130.98, 130.51, 126.69, 126.09, 125.34, 125.04, 122.76, 122.32, 118.39, 118.18, 115.27, 114.22, 38.83. Anal. (C, H, N): Cal. for $C_{22}H_{18}ClN_3{\cdot}0.5H_2O$: C, 71.64, H, 5.19, N, 11.39, found: C, 71.13, H, 4.58, N, 11.29.

7.2.8.19 ***Synthesis of 5-methyl-11-{[4-(piperidin-1-yl)phenyl]amino}-10H-indolo[3,2-b] quinolin-5-ium chloride (3s)***

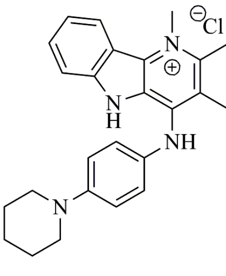

Reaction of 4-(piperidin-1-yl)benzenamine (41.6 mg, 0.236 mmol, 1.8 eq.) with **93a** (40 mg, 0.132 mmol) according to general procedure F, gave **3s** as a yellow solid, mp 311-312 ºC in 66 % yield, after recrystallization using MeOH:AcOEt (1:3) and Et_2O. ^1H NMR (400 MHz, DMSO) δ_H (ppm) 8.65 (d, *J* = 8.1 Hz, 1H), 8.57 (d, *J* = 8.1 Hz, 1H), 8.42 (d, *J* = 8.1 Hz, 1H), 8.10 (dd, *J* = 8.1, 7.7 Hz, 1H), 7.76 (dd, *J* = 8.1, 7.7 Hz, 1H), 7.71 (dd, *J* = 8.0, 7.6 Hz, 1H), 7.60 (d, *J* = 8.0 Hz, 1H), 7.43 (dd, *J* = 8.1, 7.6 Hz, 1H), 7.31 (d, *J* = 8.1 Hz, 2H), 7.16 (d, *J* = 8.1 Hz, 2H), 4.81 (s, 3H), 3.37 (s broad, 4H), 1.80 (s broad, 4H), 1.69 (d, *J* = 4.6 Hz, 2H). ^{13}C NMR (101 MHz, DMSO) δ_C (ppm) 152.10, 143.89, 141.13, 139.22, 137.94, 136.79, 132.58, 132.35, 129.48, 125.95, 125.87, 125.31, 125.21, 122.48, 118.32, 118.25, 116.21, 114.45, 113.30, 51.89, 39.01, 26.85, 25.23. Anal. (C, H, N): Cal. for $C_{27}H_{27}ClN_4 \cdot 1.5H_2O$: C, 69.00, H, 6.43, N, 11.92, found: C, 69.24, H, 6.01, N, 11.93.

7.2.8.20 ***Synthesis of 5-methyl-11-{{4-[(diethylamino)methyl]-3-hydroxyphenyl}-amino}-10H-indolo[3,2-b]quinolin-5-ium chloride (3t)***

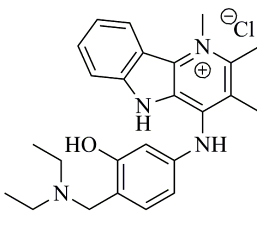

A solution of **105** (47.2 mg, 0.199 mmol, 1.5 eq.) and **93a** (40 mg, 0.132 mmol) in HCl 6M (10 mL) was refluxed for 20 hours. After this period the solution was concentrated under reduced pressure and the residue dissolved in Na_2CO_3 5 % (25 mL). The aqueous solution was extracted with CH_2Cl_2 (3x20 mL) and the combined fractions washed with water and then dried with NaCl (sat.) and with anhydrous Na_2SO_4. After concentration under reduced pressure, HCl in Et_2O was added and the precipitate formed filtered off and dried in a vacuum line, to give **3t** as a orange solid, mp 228-231 ºC, in 31 % yield. ^1H NMR (400 MHz, DMSO) δ_H (ppm) 11.84 (s, NH), 10.98 (s, OH), 10.63 (s, NH), 8.67 (d, *J* = 8.9 Hz, 1H), 8.60 (d, *J* = 8.5 Hz, 1H), 8.58 (d, *J* = 8.5 Hz, 1H), 8.09 (dd, *J* = 8.5, 7.0 Hz, 1H), 7.78 (dd, *J* = 8.2, 6.2 Hz, 1H), 7.76 (d, *J* = 8.2 Hz, 1H), 7.74 (dd, *J* = 8.5, 7.0 Hz, 1H), 7.46 (d, *J* = 8.3 Hz, 1H), 7.43 (dd, *J* = 8.9, 6.2 Hz, 1H), 6.95 (d, *J* = 2.0 Hz, 1H), 6.67 (dd, *J* = 8.3, 2.0 Hz, 1H), 4.83 (s, 3H), 4.20 (d, *J* = 4.8 Hz, 2H), 3.13 (m, 4H), 1.29 (t, *J* = 7.1 Hz, 6H). ^{13}C NMR (101 MHz, DMSO) δ_C (ppm) 157.28, 144.25, 142.71, 142.22, 137.68, 136.58, 136.19, 133.43, 132.91, 132.32, 125.61, 125.22, 124.93, 120.99, 118.48, 117.94, 114.94, 113.60, 113.36, 111.83, 107.90, 49.49, 46.05, 39.32, 8.50. Anal. (C, H, N): Cal. for $C_{27}H_{29}ClN_4O \cdot H_2O \cdot 2HCl$: C, 58.75, H, 6.03, N, 10.15, found: C, 58.16, H, 5.45, N, 9.71.

7.2.8.21 Synthesis of 5-methyl-11-(pyridin-3-ylamino)-10H-indolo[3,2-b]quinolin-5-ium chloride (3u)

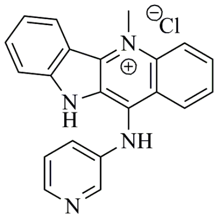

To a solution of **93a** (40.0 mg, 0.132 mmol) in DMF (5 mL) was added pyridin-3-amine (37.2 mg, 0.396 mmol, 3 eq.), and the mixture heated at 100 ºC for 48 h. Solvent was removed under reduced pressure. The remaining crude mixture was dissolved in Na_2CO_3 5 % (20 mL) and extracted with CH_2Cl_2 (3x30 mL). The combined organic extracts were washed with water and brine and dried with anhydrous Na_2SO_4. After concentration under reduced pressure HCl in Et_2O was added and the formed precipitate was filtered, washed with Et_2O and dried in a vacuum line, to give **3u** as a brown solid (22.6 mg), mp 157-159 ºC , in 48 % yield. ^1H NMR (400 MHz, DMSO) δ_H (ppm) 11.64 (s, NH), 8.79 (d, *J* = 8.4 Hz, 1H), 8.69 (d, *J* = 8.4 Hz, 1H), 8.64 (s, 1H), 8.63 (d, *J* = 7.2 Hz, 1H), 8.46 (d, *J* = 8.2 Hz, 1H), 8.13 (dd, *J* = 8.2, 7.2 Hz, 1H), 7.82 (dd, *J* = 8.4, 7.2 Hz, 1H), 7.79 (dd, *J* = 7.8, 7.5 Hz, 1H), 7.67 (d, *J* = 7.8 Hz, 1H), 7.63 (d, *J* = 5.7 Hz, 1H), 7.51 (dd, *J* = 8.2, 5.7 Hz, 1H), 7.44 (dd, *J* = 8.4, 7.2 Hz, 1H), 4.86 (s, 3H). ^{13}C NMR (101 MHz, DMSO) δ_C (ppm) 143.65, 143.62, 141.60, 137.89, 137.44, 137.42, 132.83, 132.58, 128.32, 125.62, 125.53, 125.37, 124.77, 124.55, 121.95, 118.69, 118.49, 115.16, 113.88, 49.05. Anal. (C, H, N): Cal. for $C_{21}H_{17}ClN_4 \cdot 2H_2O$: C, 63.55, H, 5.33, N, 14.12, found: C, 63.12, H, 5.59, N, 13.94.

7.2.8.22 Synthesis of 3-chloro-5-methyl-11-{[3-(diethylamino)propyl]amino}-10H-indolo[3,2-b] quinolin-5-ium chloride (3v)

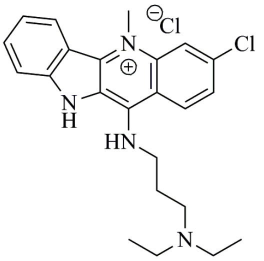

To a suspension of **93b** (40.0 mg, 0.118 mmol) in EtOAc (5 mL) was added commercial *N^1,N^1*-diethylpropane-1,3-diamine (21.2 mg, 0.212 mmol, 21.4 µL, 1.8 eq.), according to general procedure F, giving 25.1 mg (53 %) of **3v**, as dark yellow solid, mp 231-234 ºC. ^1H NMR (400 MHz, DMSO): δ_H (ppm) 12.49 (s, NH), 9.41 (s, NH), 8.91 (d, *J* = 9.1 Hz, 1H), 8.55 (d, *J* = 8.4 Hz, 1H), 8.46 (s, 1H), 8.00 (d, *J* = 8.2 Hz, 1H), 7.73 (d, *J* = 8.0 Hz, 1H), 7.72 (dd *J* = 9.1, 7.4 Hz, 1H), 7.37 (dd, *J* = 8.4, 7.4 Hz, 1H), 4.59 (s, 3H), 4.32 (s broad, 2H), 3.30 (s broad, 3H), 3.11 (q broad, 2H), 2.26 (s broad, 2H), 1.22 (t, *J* = 6.7 Hz, 6H). ^{13}C NMR (101 MHz, DMSO) δ_C (ppm) 144.12, 143.29, 138.45, 137.87, 135.95, 131.01, 127.17, 124.71, 124.56, 121.35, 117.52, 117.24, 116.94, 114.79, 114.41, 48.56, 46.49, 43.60, 38.83, 24.39, 8.87. Anal. (C, H, N): Cal. for $C_{21}H_{28}Cl_2N_4 \cdot 2HCl \cdot 0.5H_2O$: C, 53.81, H, 6.09, N, 10.91, found: C, 53.56, H, 5.87, N, 10.74.

7.2.8.23 Synthesis of 3-chloro-5-methyl-11-(piperidin-4-ylamino)-10H-indolo[3,2-b] quinolin-5-ium chloride (3w)

To a suspension of **93b** (30.0 mg, 0.088 mmol) in EtOAc (5 mL) was added piperidin-4-amine (17.7 mg, 0.177 mmol, 18.6 µL, 2 eq.), according to general procedure F, giving 18.8 mg (53 %) of **3w**, as dark yellow solid, mp 320-322 ºC. ^1H NMR (400 MHz, DMSO): δ_H (ppm) 12.37 (s, NH), 8.71 (s, 1H), 8.66 (d, *J* = 8.2 Hz, 1H), 8.63 (s, NH), 8.28 (d, *J* = 9.1 Hz, 1H), 8.03 (d, *J* = 8.0 Hz, 1H), 7.88 (d, *J* = 9.1 Hz, 1H), 7.82 (dd, *J* = 8.0, 7.7 Hz, 1H), 7.44 (dd, *J* = 8.2, 7.7 Hz, 1H), 4.79 (s, 3H), 4.18 (d, *J* = 11.6 Hz, 2H), 3.92 (t, *J* = 10.7 Hz, 2H), 3.54 (m, 1H), 2.33 (d, *J* = 11.6 Hz, 2H), 2.07 (q, *J* = 10.7 Hz, 2H). ^{13}C NMR (101 MHz, DMSO) δ_C (ppm) 147.35, 144.48, 138.78, 137.90, 137.69, 132.52, 128.75, 125.82, 125.59, 124.90, 121.76, 119.25, 118.00, 114.63, 114.33, 51.38, 47.54, 39.49, 30.72. Anal. (C, H, N): Cal. for $C_{21}H_{22}Cl_2N_4{\cdot}2HCl{\cdot}1.5H_2O$: C, 50.32, H, 5.43, N, 11.18, found: C, 50.03, H, 5.06, N, 11.33.

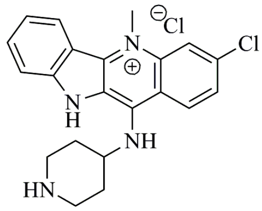

7.2.8.24 ***Synthesis of 3,8-dichloro-5-methyl-11-(piperidin-4-ylamino)-10H-indolo[3,2-b] quinolin-5-ium chloride (3x)***

To a suspension of **93c** (21.7 mg, 0.058 mmol) in EtOAc (5 mL) was added piperidin-4-amine (10.8 mg, 0.116 mmol, 11.3 µL, 1.8 eq.), according to general procedure F, giving 7.7 mg (30 %) of **3x**, as a orange solid, mp 315-317 ºC. ^{1}H NMR (400 MHz, MeOD): δ_H (ppm) 8.55 (d, *J* = 8.9 Hz, 1H), 8.53 (s, 1H), 8.35 (d, *J* = 9.1 Hz, 1H), 7.90 (s, 1H), 7.80 (d, *J* = 9.1 Hz, 1H), 7.41 (d, *J* = 8.9 Hz, 1H), 4.75 (s, 3H), 4.23 (d, *J* = 12.1 Hz, 2H), 3.91 (t, *J* = 12.1 Hz, 2H), 3.64 (s broad, 1H), 2.38 (d, *J* = 11.4 Hz, 2H), 2.15 (d, *J* = 11.4 Hz, 2H). ^{13}C NMR (101 MHz, DMSO) δ_C (ppm) 148.61, 145.94, 140.28, 140.16, 139.76, 139.18, 129.34, 127.27, 126.67, 124.91, 123.55, 120.84, 118.38, 114.47, 114.23, 52.29, 49.22, 39.93, 31.62. Anal. (C, H, N): Cal. for $C_{21}H_{21}Cl_3N_4{\cdot}2HCl$: C, 49.58, H, 4.56, N, 11.01, found: C, 49.76, H, 4.94, N, 11.06.

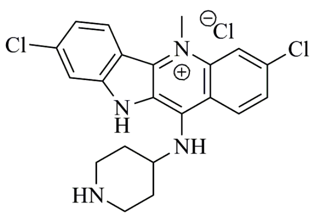

7.2.8.25 ***Synthesis of 5-methyl-11-(diethylamino)-10H-indolo[3,2-b]quinolin-5-ium chloride (3y)***

To a solution of **93a** (40 mg, 0.132 mmol) in DMF (10 mL) was added diethylamine (38.6 mg, 54.8 µL, 0.528 mmol, 4 eq.) and allowed to react overnight at room temperature. The solvent was removed at reduced pressure, the solid suspended in 5 % sodium carbonate (20 mL) and extracted with chloroform (3x20 mL). The combined organic extracts were washed with water, dried with brine (20 mL) and anhydrous Na_2SO_4 and solvent removed under reduced pressure. Recristalization from chloroform with HCl in diethyl ether gave 65% (29.3 mg) of pure **3y**, as a light yellow solid, mp 251-254 ºC. ^{1}H NMR (400 MHz, MeOD) δ_H (ppm) 8.54 (d, *J* = 8.5 Hz, 1H), 8.45 (d, *J* = 8.5 Hz, 1H), 8.41 (d, *J* = 9.0 Hz, 1H), 8.02 (dd, *J* = 9.0 8.4 Hz, 1H), 7.81 (d, *J* = 8.4 Hz, 1H), 7.75 (dd, *J* = 8.5, 8.4 Hz, 1H), 7.71 (dd, *J* = 8.4, 7.7 Hz, 1H), 7.39 (dd, *J* = 8.5, 7.7 Hz, 1H), 4.80 (s, 3H), 4.00 (q, *J* = 7.1 Hz, 4H), 1.30 (t, *J* = 7.1 Hz, 6H). ^{13}C NMR (101 MHz, MeOD) δ_C (ppm) 145.73, 142.53, 136.62, 135.73, 130.64, 130.41, 125.44, 125.35, 123.26, 122.90, 120.89, 119.68, 115.68, 113.10, 111.49, 45.78, 36.73, 11.27. Anal. (C, H, N): Cal. for $C_{20}H_{22}ClN_3{\cdot}HCl{\cdot}0.3H_2O$: C, 62.93, H, 6.23, N, 11.01, found: C, 62.92, H, 6.30, N, 10.74.

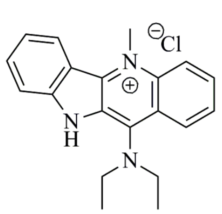

7.2.9 Synthesis of Quindolone Derivatives (**5**)

*7.2.9.1 **General procedure G: Synthesis of 5,10-bis[2-(diethylamino)ethy])-5H-indolo[3,2-b]quinolin-11(10H)-one (5a)***

To a solution of **4** (40 mg, 0.17 mmol), K_2CO_3 (352.4 mg, 2.55 mmol, 15 eq.), NaI (101.9 mg, 0.68 mmol, 4 eq.) in dried acetone (15 mL) was added 2-chloro-N^1,N^1-diethylethanaminium chloride (117.0 mg, 0.68 mmol, 4 eq.) and refluxed overnight. At the end of time, solvent was removed at reduced presure and the remain solid suspended in H_2O (30 mL). The aqueous solution was extracted with CH_2Cl_2 (3x30 mL) and the combined organic extracts, washed with water, dried with brine and anhydrous Na_2SO_4 and reduced to small volume. The crude mixture was purified by preparative thin layer chromatography (P-TLC) using as eluent CH_2Cl:MeOH (9:1) to afford the compounds: 5,10-bis[2-(diethylamino)ethyl]-5H-indolo[3,2-b]quinolin-11(10H)-one (**5a**, 16.9 mg, 23 %, R_f 0.43), 2-{11-[2-(diethylamino)ethoxy]-10*H*-indolo[3,2-*b*]quinolin-10-yl}-*N,N*-diethylethanamine (**94a**, 40.8 mg, 55 %, R_f 0.56) and 2-[(10*H*-indolo[3,2-*b*]quinolin-11-yl)oxy]-*N,N*-diethylethanamine (**95a**, 9.6 mg, 17 %, R_f 0.75) as light yellow solids. Compounds were precipitated as hydrochlorides with HCl in Et_2O.

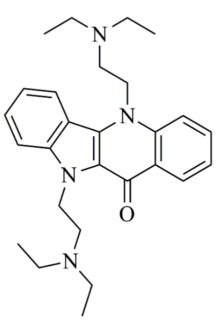

5,10-bis[2-(diethylamino)ethyl]-5H-indolo[3,2-b]quinolin-11(10H)-one (**5a**): mp 228-231 ºC; ^{1}H NMR (400 MHz, $CDCl_3$) δ_H (ppm) 8.69 (d, *J* = 8.3 Hz, 1H), 8.25 (d, *J* = 8.4 Hz, 1H), 7.70 (m, 2H), 7.59 (d, *J* = 8.3 Hz, 1H), 7.54 (dd, *J* = 8.3, 7.6 Hz, 1H), 7.34 (dd, *J* = 8,3, 7.5 Hz, 1H), 7.24 (dd, *J* = 8.4, 7.6 Hz, 1H), 5.00 (t, *J* = 8.0 Hz, 2H), 4.84 (t, *J* = 7.8 Hz, 2H), 3.03 (t, *J* = 8.0 Hz, 2H), 2.92 (t, *J* = 7.8 Hz, 2H), 2.71 (q, *J* = 15.4, 7.1 Hz, 8H), 1.09 (t, *J* = 15.4, 7.1 Hz, 12H). ^{13}C NMR (101 MHz, $CDCl_3$) δ_C (ppm) 169.13, 139.70, 139.65, 131.38, 130.62, 127.32, 126.86, 124.89, 122.69, 122.60, 120.95, 119.52, 115.14, 114.11, 110.63, 53.17, 50.87, 47.69, 47.35, 43.10, 11.85. Anal. (C, H, N): Cal. for $C_{27}H_{36}N_4O\cdot0.4HCl$: C, 72.52 , H, 8.20, N, 12.53, found: C, 72.26, H, 8.33, N, 12.27.

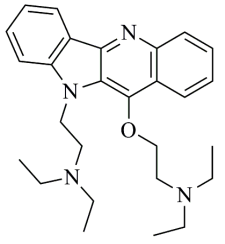

2-{11-[2-(diethylamino)ethoxy]-10*H*-indolo[3,2-*b*]quinolin-10-yl}-*N,N*-diethylethanamine (**94a**): mp 144-146 ºC; ^{1}H NMR (400 MHz, $CDCl_3$) δ_H (ppm) 8.55 (d, *J* = 7.7 Hz, 1H), 8.40 (d, *J* = 8.2 Hz, 1H), 8.33 (d, *J* = 8.5 Hz, 1H), 7.70 (dd, *J* = 8.5, 6.8 Hz, 1H), 7.66 (dd, *J* = 8.2, 7.4 Hz, 1H), 7.58 (dd, *J* = 8.2, 6.80 Hz, 1H), 7.52 (d, *J* = 8.2 Hz, 1H), 7.35 (dd, *J* = 7.7, 7.4 Hz, 1H), 4.73 (t, *J* = 7.70 Hz, 2H), 4.32 (t, *J* = 6.3 Hz, 2H), 3.10 (t, *J* = 6.3 Hz, 2H), 2.79 (t, *J* = 7.70 Hz, 2H), 2.70 (q, *J* = 7.1 Hz, 4H), 2.62 (q, *J* = 7.1 Hz, 4H), 1.13 (t, *J* = 7.1 Hz, 6H), 1.00 (t, *J* = 7.1 Hz, 6H). ^{13}C NMR (101 MHz, $CDCl_3$) δ_C (ppm) 148.59, 145.83, 144.80, 144.58, 129.69, 129.31, 126.65, 124.87, 124.68, 122.46, 122.23, 122.08, 121.27, 119.86, 109.17, 74.51, 52.93, 51.71, 47.69, 47.62, 43.51, 12.06. Anal. (C, H, N): Cal. for $C_{27}H_{38}N_4O{\cdot}4HCl$: C, 55.87, H, 7.29, N, 9.65, found: C, 55.43, H, 7.39, N, 9.24.

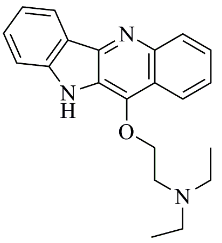

2-[(10*H*-indolo[3,2-*b*]quinolin-11-yl)oxy]-*N,N*-diethylethanamine (**95a**): mp 193-195 ºC; ^{1}H NMR (400 MHz, $CDCl_3$) δ_H (ppm) 12.63 (s, NH), 8.56 (d, *J* = 7.8 Hz, 1H), 8.34 (d, *J* = 8.3 Hz, 1H), 8.32 (d, *J* = 8.6 Hz, 1H), 7.67 (dd, *J* = 8.6, 7.0 Hz, 1H), 7.60 (dd, *J* = 9.1, 7.1 Hz, 1H), 7.54 (dd, *J* = 8.3, 7.0 Hz, 1H), 7.46 (d, *J* = 8.1 Hz, 1H), 7.32 (dd, *J* = 7.8, 7.1 Hz, 1H), 4.58 (t, *J* = 7.5 Hz, 2H), 3.07 (t, *J* = 7.5 Hz, 2H), 2.90 (q, *J* = 7.2 Hz, 4H), 1.26 (t, *J* = 7.2 Hz, 6H). ^{13}C NMR (101 MHz, $CDCl_3$) δ 148.68, 145.54, 144.65, 143.52, 129.38, 128.95, 126.47, 124.23, 123.95, 122.58, 122.20, 121.48, 120.96, 119.37, 111.04, 73.99, 55.09, 48.51, 11.33. Anal. (C, H, N): Cal. for $C_{21}H_{23}N_3O{\cdot}2.8HCl$: C, 57.91, H, 5.97, N, 9.65, found: C, 57.56, H, 5.82, N, 9.83.

7.2.9.2 Synthesis of 3-chloro-5,10-bis[2-(diethylamino)ethyl]-5H-indolo[3,2-b]quinolin-11(10H)-one (5b)

According to general procedure G, **91a** (40 mg, 0.118 mmol) was reacted with 2-chloro-*N^1,N^1*-diethylethanaminium chloride (64.5 mg, 0.472 mmol, 4 eq.). After purification by preparative thin layer chromatography (P-TLC) using as eluent CH_2Cl_2:MeOH (9:1) the compounds were isolated: 3-chloro-5,10-bis[2-(diethylamino)ethyl]-*5H*-indolo[3,2-*b*]quinolin-11(10*H*)-one (**5b**, 11.6 mg, 21 %, R_f 0.22), 2-{[3-chloro-10-(2-(diethylamino)ethyl)-*10H*-indolo[3,2-*b*]quinolin-11-yl]oxy}-*N,N*-diethylethanamine (**94b**, 18.3 mg, 33 %, R_f 0.38) and 2-[(3-chloro-*10H*-indolo[3,2-*b*]quinolin-11-yl)oxy]-*N,N*-diethylethanamine (**95b**, 3.0 mg, 7 %, R_f 0.70) as light yellow solids. .

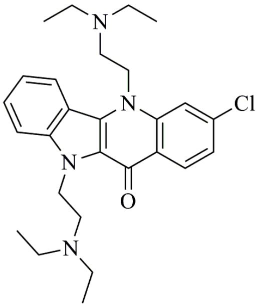

3-chloro-5,10-bis[2-(diethylamino)ethyl]-*5H*-indolo[3,2-*b*]quinolin-11(10H)-one (**5b**): mp 223-225 ºC; ^{1}H NMR (400 MHz, $CDCl_3$) δ_H (ppm) 8.57 (d, *J* = 8.7 Hz, 1H), 8.18 (d, *J* = 8.4 Hz, 1H), 7.72 (d, *J* = 1.6 Hz, 1H), 7.59 (d, *J* = 8.4 Hz, 1H), 7.54 (dd, *J* = 8.4 Hz, 1H), 7.27 (dd, *J* = 8.7, 1.6 Hz, 1H), 7.23 (d, *J* = 8.8 Hz, 1H), 4.97 (t *J* = 7.3 Hz, 2H), 4.77 (t, *J* = 7.4 Hz, 2H), 3.02 (d, *J* = 7.4 Hz, 2H), 2.90 (t, *J* = 7.3 Hz, 2H), 2.69 (q, *J* = 7.1 Hz, 8H), 1.07 (t, *J* = 7.1 Hz, 6H), 1.06 (t, *J* = 7.2 Hz, 6H). ^{13}C NMR (101 MHz, $CDCl_3$) δ_C (ppm) 168.61, 140.36, 139.72, 137.70, 130.62, 128.43, 127.56, 123.26, 122.78, 122.46, 121.66, 119.84, 115.05, 114.33, 110.77, 53.12, 51.10, 47.73, 47.67, 47.57, 43.08, 12.03. Anal. (C, H, N): Cal. for $C_{27}H_{35}ClN_4O{\cdot}3.8HCl$: C, 53.55, H, 6.46, N, 9.25, found: C, 53.22, H, 6.36, N, 9.09.

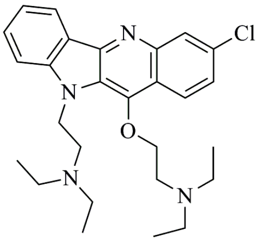

2-{[3-chloro-10-(2-(diethylamino)ethyl)-*10H*-indolo[3,2-*b*]quinolin-11-yl] oxy}-*N,N*-diethylethanamine (**94b**): mp 153-156 ºC; ^{1}H NMR (400 MHz, $CDCl_3$) δ_H (ppm) 8.51 (d, *J* = 7.7 Hz, 1H), 8.39 (d, *J* = 9.0 Hz, 1H), 8.32 (d, *J* = 1.9 Hz, 1H), 7.67 (dd, *J* = 7.3 Hz, 1H), 7.51 (m, 2H), 7.35 (dd, *J* = 7.7, 7.3 Hz, 1H), 4.69 (t, *J* = 7.5 Hz, 2H), 4.28 (t, *J* = 6.1 Hz, 2H), 3.06 (t, *J* = 6.1 Hz, 2H), 2.80 (t, *J* = 7.5 Hz, 2H), 2.69 (q, *J* = 7.1 Hz, 4H), 2.60 (q, *J* = 7.1 Hz, 4H), 1.12 (t,

J = 7.1 Hz, 6H), 0.98 (t, J = 7.1 Hz, 6H). ^{13}C NMR (101 MHz, CDCl$_3$) δ_C (ppm) 149.45, 146.03, 144.92, 144.70, 132.34, 130.02, 128.00, 125.54, 124.95, 122.86, 122.23, 122.18, 120.68, 120.05, 109.29, 74.92, 53.04, 51.76, 47.71, 47.63, 43.60, 12.10, 11.91. Anal. (C, H, N): Cal. for $C_{27}H_{37}ClN_4O \cdot 4.8HCl$: C, 50.35, H, 6.54, N, 8.70, found: C, 50.09, H, 6.87, N, 8.98.

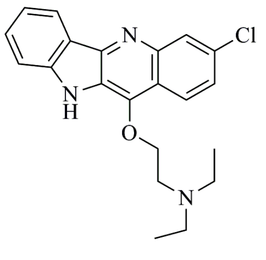

2-[(3-chloro-*10H*-indolo[3,2-*b*]quinolin-11-yl)oxy]-*N,N*-diethylethanamine (**95b**): mp 199-202 ºC; ^{1}H NMR (400 MHz, CDCl$_3$) δ_H (ppm) 8.51 (d, J = 7.8 Hz, 1H), 8.31 (d, J = 1.9 Hz, 1H), 8.25 (d, J = 9.0 Hz, 1H), 7.61 (dd, J = 8.6, 7.8 Hz 1H), 7.49 (d, J = 8.6 Hz, 1H), 7.47 (dd, J = 9.0, 1.9 Hz, 1H), 7.32 (dd, J = 7.8, 7.8 Hz, 1H), 4.62 (t, J = 4.3 Hz, 2H), 3.14 (t, J = 4.3 Hz, 2H), 2.97 (q, J = 7.01Hz, 4H), 1.29 (t, J = 7.1 Hz, 6H). ^{13}C NMR (101 MHz, CDCl$_3$) δ_C (ppm) 148.60, 145.66, 143.71, 132.16, 129.78, 127.69, 125.52, 125.15, 123.75, 122.33, 122.23, 119.73, 119.62, 111.26, 54.90, 48.70, 11.06. Anal. (C, H, N): Cal. for $C_{21}H_{22}ClN_3O \cdot 1.9HCl$: C, 57.70, H, 5.51, N, 9.61, found: C, 57.51, H, 5.82, N, 9.36.

7.2.9.3 Synthesis of 3,7-dichloro-5,10-bis[2-(diethylamino)ethyl]-5H-indolo[3,2-b]quinolin-11(10H)-one (5c)

According to General procedure G, **92c** (40 mg, 0.13 mmol) was reacted with 2-chloro-N^1,N^1-diethylethanaminium chloride (72.1 mg, 5.28 mmol, 4 eq.). After purification by preparative thin layer chromatography (P-TLC) using as eluent CH$_2$Cl$_2$:MeOH (9:1) the following compounds were isolated: 3,7-dichloro-5,10-bis[2-(diethylamino)ethyl]-*5H*-indolo[3,2-*b*]quinolin-11(*10H*)-one (**5c**, 12.6 mg, 19 %, R$_f$ 0.39), 2-{[3,7-dichloro-10-(2-(diethylamino)ethyl)-*10H*-indolo[3,2-*b*]quinolin-11-yl]oxy}-*N,N*-diethylethanamine (**94c**, 22.5 mg, 34 %, R$_f$ 0.56) and 2-[(3,7-dichloro-*10H*-indolo[3,2-*b*]quinolin-11-yl)oxy]-*N,N*-diethylethanamine (**95c**, 2.65 mg, 5 %, R$_f$ 0.80) as light yellow solids.

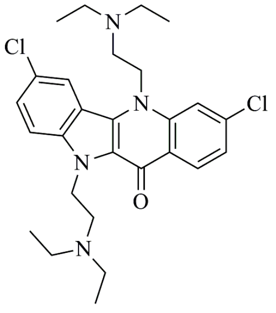

3,7-dichloro-5,10-bis[2-(diethylamino)ethyl]-*5H*-indolo[3,2-*b*]quinolin-11(*10H*)-one (**5c**): mp 230-233 ºC; ^{1}H NMR (400 MHz, CDCl$_3$) δ_H (ppm) 8.57 (d, J = 8.7 Hz, 1H), 8.27 (d, J = 1.6 Hz, 1H), 7.72 (d, J = 1.6 Hz, 1H), 7.57 (t, J = 10.5 Hz, 1H), 7.51 (dd, J = 9.0, 1.7 Hz, 1H), 7.30 (d, J = 8.7 Hz, 1H), 4.96 (t, J = 7.4 Hz, 2H), 4.72 (t, J = 7.8 Hz, 2H), 3.04 (t, J = 7.8 Hz, 2H), 2.92 (t, J = 7.4 Hz, 2H), 2.71 (q, J = 7.1 Hz, 8H), 1.13 (t, J = 7.1 Hz, 6H), 1.05 (t, J = 7.1 Hz, 6H). ^{13}C NMR (101 MHz, CDCl$_3$) δ_C (ppm) 168.73, 140.44, 138.04, 137.96, 129.74, 128.43, 127.82, 125.38, 123.32, 123.18, 121.84, 121.76, 115.68, 114.30, 111.96, 53.22, 50.91, 47.78, 47.53, 43.35, 11.93. Anal. (C, H, N): Cal. for $C_{27}H_{34}Cl_2N_4O \cdot 3.7HCl$: C, 50.96, H, 5.97, N, 8.80, found: C, 50.79, H, 5.76, N, 8.83.

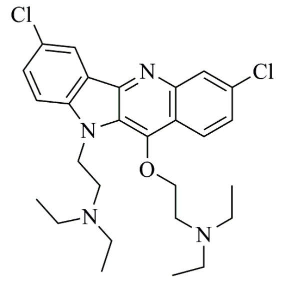

2-{[3,7-dichloro-10-(2-(diethylamino)ethyl)-*10H*-indolo[3,2-*b*]quinolin-11-yl]oxy}-*N*,*N*-diethylethanamine (**94c**) : mp 145-148 ºC; ^{1}H NMR (400 MHz, $CDCl_3$) δ_H (ppm) 8.45 (d, *J* = 2.0 Hz, 1H), 8.37 (d, *J* = 9.0 Hz, 1H), 8.26 (d, *J* = 2.0 Hz, 1H), 7.59 (dd, *J* = 8.7, 2.0 Hz, 1H), 7.50 (dd, *J* = 9.0, 2.0 Hz, 1H), 7.42 (d, *J* = 8.7 Hz, 1H), 4.69 (t, *J* = 7.3 Hz, 2H), 4.27 (t, *J* = 6.0 Hz, 2H), 3.05 (t, *J* = 6.0 Hz, 2H), 2.77 (t, *J* = 7.3 Hz, 2H), 2.69 (q, *J* = 7.1 Hz, 4H), 2.56 (q, *J* = 7.1 Hz, 4H), 1.12 (t, *J* = 7.1 Hz, 6H), 0.93 (t, *J* = 7.1 Hz, 6H). ^{13}C NMR (101 MHz, $CDCl_3$) δ_C (ppm) 148.10, 146.15, 145.09, 143.16, 132.65, 129.86, 128.04, 125.87, 125.56, 125.36, 123.33, 122.91, 121.72, 120.80, 110.48, 75.06, 53.07, 51.88, 47.69, 47.58, 43.88, 12.07, 11.89. Anal. (C, H, N): Cal. for $C_{27}H_{36}Cl_2N_4O{\cdot}4HCl$: C, 49.94, H, 6.21, N, 8.63, found: C, 49.58, H, 6.28, N, 8.30.

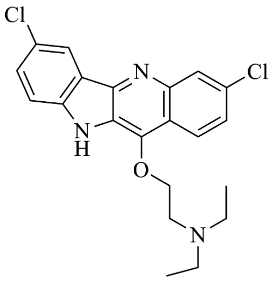

2-[(3,7-dichloro-*10H*-indolo[3,2-*b*]quinolin-11-yl)oxy]-*N*,*N*-diethylethanamine (**95c**): mp 190-194 ºC; ^{1}H NMR (400 MHz, $CDCl_3$) δ_H (ppm) 12.69 (s, NH), 8.48 (d, *J* = 1.9 Hz, 1H), 8.28 (d, *J* = 1.8 Hz, 1H), 8.24 (d, *J* = 9.0 Hz, 1H), 7.54 (dd, *J* = 8.6, 1.9 Hz, 1H), 7.47 (dd, *J* = 9.0, 1.8 Hz, 1H), 7.39 (d, *J* = 8.6 Hz, 1H), 4.63 (t, *J* = 4.4 Hz, 2H), 3.15 (t, *J* = 4.4 Hz, 2H), 2.97 (q, *J* = 7.3 Hz, 4H), 1.28 (t, *J* = 7.3 Hz, 6H). ^{13}C NMR (101 MHz, $CDCl_3$) δ_C via HMQC (ppm) 129.63, 127.55, 125.36, 122.30, 121.63, 112.07, 73.19, 54.58, 48.27, 10.74. Anal. (C, H, N): Cal. for $C_{21}H_{21}Cl_2N_3O{\cdot}3HCl$: C, 49.29, H, 4.73, N, 8.21, found: C, 49.42, H, 4.98, N, 8.25.

7.2.10 Synthesis of *N^1,N^1*-Dimethylpropane-1,2-diamine (**97**)

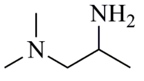

To a solution of NH_4OAc (5.26 g, 68.2 mmol, 8 eq.), $NaBH_3CN$ (0.634 g, 10 mmol, 1.2 eq.), anhydrous $MgSO_4$ (8 g) in dry MeOH was added 1-(dimethylamino)propan-2-one (0.863 g, 8.5 mmol, 1 mL). The reaction mixture was refluxed for 20 hours. After this period the $MgSO_4$ was removed and the reaction mixture acidified with concentrated HCl until pH=2. The solvent was removed at reduced pressure and the crude product dissolved in water (50 mL). The aqueous solution was washed with Et_2O (3x20 mL), basified with NaOH 10 % until pH=10 and extracted with CH_2Cl_2 (3x20 mL). The organic extracts were washed with water and brine, dried (anhydrous Na_2SO_4) and the solvent removed at reduced pressure to give **97**, 24 % (204.2 mg), as a light brown oil. ^{1}H NMR (400 MHz, $CDCl_3$) δ_H (ppm) 3.00 (m, 1H), 2.18 (s, 6H), 2.12 (d, *J* = 10.1 Hz, 1H), 2.04 (dd, *J*= 4.2, 4.1 Hz, 1H), 1.01 (d, *J* = 6.89 Hz, 3H). ^{13}C NMR (101 MHz, $CDCl_3$) δ_C (ppm) 68.20, 45.82, 44.14, 21.07.

7.2.11 Synthesis of 2-(3-(Piperidin-1-yl)-propyl)isoindoline-1,3-dione (**99**)

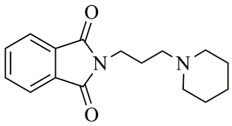

To a solution of N-(3-bromopropyl)phthalimide (2.71 g, 10.1 mmol), TEA (1.22 g, 24.2 mmol, 1.67 mL, 2.4 eq.) in CH_2Cl_2 (40 mL) was added piperidine (0.86 g, 10.1 mmol, 1 mL, 1 eq.). Reaction mixture was refluxed 30 hours and after this period, the solvent was removed at reduce pressure. The crude residue was purified by column chromatography (CH_2Cl_2 and CH_2Cl_2:MeOH (9:1)) to afford **99**, 1.45 g (51 %) as a white solid, mp 266-267 ºC. ^{1}H NMR (400 MHz, $CDCl_3$) δ_H (ppm) 7.83 (dd, J = 5.2, 3.1 Hz, 2H), 7.73 (dd, J = 5.2, 3.1 Hz, 2H), 3.78 (t, J = 6.57 Hz, 2H), 3.06-2.66 (m, 6H), 2.23 (quintet, J = 7.2 Hz, 2H), 1.90 (m, 4H), 1.57 (m, 2H). ^{13}C NMR (101 MHz, $CDCl_3$) δ_C (ppm) 168.18, 134.08, 131.81, 123.28, 55.63, 53.64, 35.66, 23.93, 23.38, 22.58.

7.2.12 Synthesis of 3-Piperidin-1-yl-propan-1-amine (**100**)

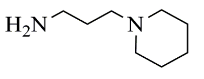

To a solution of **99** (0.5 g, 1.83 mmol) in EtOH (30 mL) was added hydrazine (0.568 g, 4.38 mmol, 0.552 mL, 2.4 eq.). The reaction mixture was refluxed 3 hours. The white precipitate which formed was collected and the solvent removed at reduced pressure. The crude product was dissolved in CH_2Cl_2, the precipitate was again collected and the solvent evaporated at reduce pressure to give **100**, 71 % yield (178 mg), as a light brown oil. ^{1}H NMR (400 MHz, $CDCl_3$) δ_H (ppm) 2.98 (s, 1H), 2.75 (t, J = 6.3 Hz, 2H), 2.39 (m, 6H), 1.63 (quintet, J = 6.9 Hz, 2H), 1.54 (m, 4H), 1.38 (m, 2H). ^{13}C NMR (101 MHz, $CDCl_3$) δ_C (ppm) 57.19, 54.34, 40.69, 28.86, 25.62, 24.07.

7.2.13 Synthesis of *Tert*-butyl-4-(diethylamino)butylcarbamate (**102**)

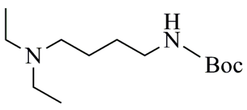

A solution of *tert*-butyl 4-aminobutylcarbamate **101** (98.4 mg, 0.52 mmol, 0.1 mL), anhydrous $MgSO_4$ (2 g) and $NaBH_3CN$ (70.4 mg, 1.25 mmol, 2.4 eq.) in dry MeOH (5 mL) was cooled to 0 ºC. Acetaldehyde (1 mL) was added and reaction continued for 2 hours at in a ice bath. After this period the anhydrous $MgSO_4$ was collect by filtration and the solvent removed at reduced pressure. The crude product was then dissolved in water (5 mL), basified with aqueous solution of KOH 5% until pH=10 and extracted with CH_2Cl_2 (3x20 mL). The combined organic extracts was washed with water and brine, dried (anhydrous Na_2SO_4) and evaporated at reduced pressure to give **102**, 94 % yield (119.9 mg), as a yellow oil. ^{1}H NMR (400 MHz, $CDCl_3$) δ_H (ppm) 5.42 (s, NH), 2.95 (d, J = 5.3 Hz, 2H), 2.43 (q, J = 7.1, Hz 4H), 2.32 (t, J = 6.5 Hz, 2H), 1.36 (s broad, 4H), 1.27 (s, 9H), 0.90 (t, J = 7.1 Hz, 6H). ^{13}C NMR (101 MHz, $CDCl_3$) δ_C (ppm) 155.77, 78.21, 51.96, 46.09, 39.89, 27.99, 27.65, 23.55, 10.55.

7.2.14 Synthesis of N^1,N^1-Diethyl-butane-1,4-diamine (**103**)

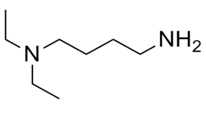

A solution of **102** (119.9 mg, 0.49 mmol) in CH_2Cl_2:TFA (1:1, 2 mL) was stirred at room temperature for 1 hour. After this period the solvent was removed at reduced pressure, and the crude residue neutralized with aqueous solution of KOH (2 M). The aqueous solution was then extracted with CH_2Cl_2 (3x10 mL). The combined organic extracts were washed with water and brine, dried (anhydrous Na_2SO_4) and evaporated at reduced pressure, to give **103**, 63 % yield (44.8 mg), as a yellow oil. ^{1}H NMR (400 MHz, $CDCl_3$) δ_H (ppm) 4.02 (s, NH_2), 2.70 (t, J = 6.2 Hz, 2H), 2.50 (q, J = 7.1 Hz, 4H), 2.39 (t, J = 6.7 Hz, 2H), 1.50 (m, 4H), 0.97 (t, J = 7.1 Hz, 6H). ^{13}C NMR (101 MHz, $CDCl_3$) δ_C (ppm) 52.14, 45.98, 40.92, 30.01, 24.12, 10.60.

7.2.15 Synthesis of *N*-(4-((Diethylamino)-methyl)-3-hydroxyphenyl)-acetamido (**105**)

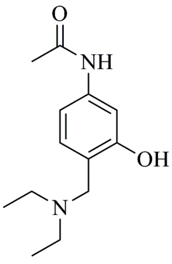

To a solution of N-(3-hydroxyphenyl)acetamide **104** (2 g, 13.2 mmol), formaldehyde (0.792 g, 0.73 mL, 26.4 mmol, 2 eq.) in EtOH (20 mL) was added diethylamine (1.93 g, 2.74 mL, 26.4 mmol, 2 eq.). The mixture was refluxed for 96 h and after this period the solvent was removed at reduced pressure. The remains residue was dissolved in CH_2Cl_2 (20 mL) and extracted with HCl 0.1 M (4x50 mL). The combined aqueous extracts were basified to achieve pH 10 with KOH 5 % and extracted with CH_2Cl_2 (3x 20 mL). The organic extracts were washed with H_2O and dried with NaCl (sat.) and anhydrous Na_2SO_4. Evaporation of the solvent gave **105**, as yellow oil, yielding 55 %. ^{1}H NMR (400 MHz, CDCl3) δ_H (ppm) 8.08 (s, OH), 7.05 (d, *J* = 7.9 Hz, 1H), 6.90 (s, 1H), 6.88 (d, *J* = 7.9 Hz, 1H), 3.71 (s, 2H), 2.60 (q, *J* = 6.7 Hz, 4H), 2.11 (s, 3H), 1.08 (t, *J* = 6.7 Hz, 6H). ^{13}C NMR (101 MHz, $CDCl_3$) δ_C ppm 168.46, 158.08, 138.12, 128.25, 117.41, 110.34, 107.19, 55.86, 45.70, 24.01, 10.63.

7.3 Acid Dissociation Constants (p*K*$_a$)

7.3.1 UV-visible Spectrophotoscopy

Solutions of cryptolepine, quindolone and derivatives (5 μM) were prepared in HCl or NaOH aqueous solutions, ranging from pH 3 to 13.7. All spectra were record at 25 ºC. The acid dissociation constants were obtained after nonlinear regression fitting of the absorbance data at fixed wavelengths and at different pH values to the modified Henderson-Hasselbalch equation {single pK$_a$, $Y=[U+L*(10^{(pH-pKa)})/(10^{(pH-pKa)}+1)]$; two pK$_a$, $Y=[M+L*(10^{(pH-pKa1)})/(10^{(pH-pKa1)}+1)]-$ $[U-M*(10^{(pH-pKa2)})/(10^{(pH-pKa2)}+1)]$} were U is the upper limit of absorbance, M is medium value and L is the lower limit) with GraphPad Prism computer program (GraphPad software, Version 5.00, San Diego, CA).

7.3.2 Nuclear Magnetic Resonance (NMR)

The determination of the acid dissociation constants (pK$_a$) by nuclear magnetic resonance for cryptolepine (**1**) and for some cryptolepine derivatives were obtained after nonlinear regression fitting of the chemical shifts in the ^{1}H-NMR spectra, of selected protons, at different pH* values to the Henderson-Hasselbalch equation {single pK$_a$, $Y=[U+L*(10^{(pH-pKa)})/(10^{(pH-pKa)}+1)]$; two pK$_a$, $Y=[M+L*(10^{(pH-pKa1)})/(10^{(pH-pKa1)}+1)]-$ $[U-L*(10^{(pH-pKa2)})/(10^{(pH-pKa2)}+1)]$} were U is the upper limit, and L is the lower limit) with GraphPad Prism computer program (GraphPad software, Version 5.00, San Diego, CA). The NMR spectra were record in DMSO-d$_6$/D_2O (40:60), at 25 ºC and with the 3-(trimethylsilyl)propionic acid (TSP-d$_4$) as internal reference.

7.4 Interaction with Oligonucleotides

7.4.1 Determination of Oligonucleotides Concentration

Single and double-stranded oligonucleotides were purchased from **ATDBio Ltd., Southampton** (UK). From received oligonucleotide aqueous solution was taken an aliquot (1-2 µL) and the volume made up to 1 mL with water. UV-visible absorption spectrum was then record at 25 ºC with base line correction to water. The concentrations of the samples were determined from the absorbance at 260 nm and the molar extinction coefficients (ε) of the oligonucleotides according to the Beer-Lambert law.

7.4.2 Binding Stoichiometry

Binding stoichiometries for cryptolepine and derivatives with 12-mer double-stranded oligonucleotide were monitored by spectrophotofluorimetry or UV-Visible spectrophotometry using the Job method of continuous variation.(352) The total concentration of DNA and cryptolepine ligand in the solutions was kept constant, and the changes in fluorescence or absorbance intensity monitored as a function of the mole fraction of cryptolepine ligand. The intercept of the two best-fit lines obtained by least squares linear regression analysis, performed with Graph Pad Prism computer program (GraphPad software, Version 5.00, San Diego, CA), indicated the binding stoichiometry of the complex.

7.4.3 Association Constants (K_{ass})

Titrations were carried out using spectrophotofluorimetry or UV-visible spectrophotometry in a 1 cm quartz cuvettes by adding aliquots of a stock solution (0.027 mM or 0.27 mM) of 12-mer oligonucleotide duplex to a solution (0.5 µM, 1 µM or 5 µM) of the ligand in 0.01 M phosphate buffer (pH 7.4) containing 0.1 M NaCl. All the spectrophotofluorimetric titration spectra were recorded at an excitation wavelength of 339 nm and an emission wavelength between 450 and 500 nm. Dissociation constants of cryptolepine analogs in complex with the 12-mer ds-DNA oligonucleotide ($d(GATCCTAGGATC)_2$) were determined by fitting the experimental data to the appropriate equation using least squares nonlinear regression analysis. In some cases the best model was a single binding site model (obeying the equation, $F = F_{max}.[DNA]/(K_d + [DNA])$, where F is the observed value of the experimental parameter followed, F_{max}, its limiting value at high values of [DNA] and K_d the dissociation constant). In other cases, the required equation was that for two binding sites sequestering ligand independently of each other and with relatively weak binding in the second binding equilibrium detectable at higher values of [DNA] (described by parameters, F'_{max} and K'_d. Two independently acting binding sites would fit the equation, $F = \{F_{max}.[DNA]/(K_d + [DNA])\} + \{ F'_{max}.[DNA]/(K'_d + [DNA]\}$. If $K'_d >> [DNA]$, this reduces to $F = (\{F_{max}.[DNA]/(K_d + [DNA]\} + F'_{max}.[DNA]/K'_d)$. Data were fit to the equations supplied with GraphPad Prism computer program (GraphPad software, Version 5.00, San Diego, CA) or to appropriate variants written into that program. Best models were evaluated by analysis of the F-test between one- and two-site binding models, performed by the GraphPad Prism software.(354) Association constants were calculated from dissociation constants and its standard deviations from those associated to the dissociation constants through propagation of uncertainties as described elsewhere.(421)

7.4.4 Melting Curves

DNA thermal melting was monitored by UV absorbance at 260 nm using a Cary 4000 spectrophotometer. Different amounts of cryptolepine analogs were mixed with 2.83 μM 12-mer oligonucleotide duplex in 0.01 M phosphate buffer (pH 7.4) containing 0.1 M NaCl. The sample temperature was typically varied from 5 to 85 ºC with a ramp rate of 0.5 ºC/min. Melting temperatures (T_m) were determined from the cooling profile and values reported are based on the 1st derivative method of the absorbance-temperature curve. Standard deviations for T_m values were calculated from three independent measurements, using standard statistical methods.

7.5 Interactions with Haem

7.5.1 Binding Stoichiometry

Binding stoichiometries for *compounds:haematin complexes* were monitored by UV-Visible spectrophotometry using the Job method of continuous variation.(352) The total concentration of DNA and cryptolepine ligand in the solutions was kept constant (10 μM), and the changes in absorbance intensity monitored as a function of the mole fraction of ligand. The intercept of the two best-fit lines obtained by least squares linear regression analysis, performed with Graph Pad Prism computer program (GraphPad software, Version 5.00, San Diego, CA), indicated the binding stoichiometry of the complex. Job's plot were obtained after correction of the absorbance according to the equation: y-axes is the corrected absorbance ($y = -\{A-(\varepsilon_{FPIX\text{-}OH}[FPIX\text{-}OH]+ \varepsilon_{compound}[compound])b\}$), where A is the measured absorbance, $\varepsilon_{FPIX\text{-}OH}$ and $\varepsilon_{compound}$ are the molar absorptivities of hematin and 1, 2, 3c and 3n, and b the optical path length.(342)

7.5.2 Association Constants (K_{ass})

Titration of haematin in buffered 40% DMSO (pH 5.5) with chloroquine, cryptolepine and derivatives were made according to the procedure: Stocks solutions of haematin, chloroquine, cryptolepine and derivatives (ligands) were obtained by dissolving accurately weighed haematin, chloroquine, cryptolepine and derivatives in UV-spectroscopy grade DMSO to a concentration of 1 mM, and stored in the dark. Buffered 40 % DMSO solution was usually prepared in 250 mL volumetric flasks using DMSO (100 mL), aqueous HEPES (1M, 5ml) and making up to the mark with distilled deionised water. Aqueous buffered DMSO solutions (40 % v/v) of the haematin, chloroquine, cryptolepine and derivatives were prepared daily by mixing an accurately measured sample of the stock solution 100 μL (*via* microsyringe) and making up to 1 mL with buffered 40% DMSO solution. Haematin solutions of 10 μM were prepared with buffered 40 % DMSO solution and transferred to a cuvette and also used as reference cell. Solutions of chloroquine, cryptolepine and derivatives (100 μM) were initially added to the cuvette in amounts as small as 2 μL (gradually increasing the volume in subsequent additions) until final concentrations higher than that of haematin concentration. After each addition the cuvette was stirred for one minute before the absorbance was measured. UV-Visible titrations were performed using a Shimadzu UV-visible spectrophotometer fitted with a thermostated (20 ºC) cell holder. Scans were run between 230 nm and 500 nm to incorporate the Soret band of the porphyrin. The UV-Visible spectra obtained after each titrated addition was analyzed and stacked against the corresponding absorbances. Dissociation constants of chloroquine, cryptolepine and derivatives complexed with the FPIX-OH were determined by fitting the experimental data to the appropriate equation models(360-361) using least squares nonlinear regression analysis with Graph Pad Prism computer program (GraphPad software, Version 5.00, San Diego, CA). Association constants were calculated from dissociation constants and its standard deviations from those associated to the dissociation constants through propagation of uncertainties as described elsewhere.(421)

7.6 Computational Details

7.6.1 Density Functional Theory Optimizations

Geometry optimizations and energy calculations for cryptolepine and derivatives were determined using density functional theory (DFT) with B3LYP(390-392) parameterization of the density functional and the 6-31+G(d,p) basis set,(393) using the Gaussian03 software package.(375) The vibrational frequency calculations were accomplished at the same level of theory. Subsequently, the charges of cryptolepine and derivatives were calculated by the natural bond orbital (NBO) analysis methods,(394, 422-423) at the B3LYP/6-31G+(d,p) level.

7.6.2 Double-Stranded DNA Docking Studies

The duplex DNA was constructed with the Molecular Operating Environment (MOE) software(396) and minimized with a gradient of 0.00001 $\text{Kcal.mol}^{-1}.\text{Å}^{-1}$ using the Amber99(397-398) force field and Born solvation scheme.(399-401) After minimization, the model was subjected to molecular dynamics (MD) simulation annealing (MD conditions: durantion: 100 ps, final temperature: 300 K, heat time: 10 ps, initial temperature: 150 K, time step: 0.001 ps, temperature relaxation: 0.1 ps, pressure relaxation: 0.1 ps) using a Nosé*–Poincaré–Andersen* algorithm(424) to sample, a constant-temperature, constant-volume ensemble (NVT) and the Amber99 force field. The molecular dynamics procedure followed closely a previous protocol to study allopsoralen-DNA binding modes.(425) After the MD simulation, a final energy minimization was performed. The resulting DNA-model was used in the docking. All docking studies were performed using MOE, with the simulated annealing docking algorithm.(426-427) After docking, a final energy minimization was performed with Amber99 force field and Born solvation scheme. The interaction energies between the ligand and ds-DNA, were calculated from the final complex energy, subtracting the sum of the energies of the separated moieties ($\Delta E_{\text{bind}} = E_{\text{complex}} - (E_{\text{DNA}}+E_{\text{ligand}})$).

7.6.3 Haematin Dimer Docking Studies

The molecular modeling simulations were performed using the docking algorithm GOLD 2.1 software (Cambridge Crystallographic Data Centre, CCDC, Cambridge, UK).(380) and the GOLD energy score.(380, 428) A generic algorithm-based software were employed using chloroquine and indoloquinolines structures and the three-dimensional structure of the haemozoin dimer, obtained from the CCDC.(63) The active site midpoint was on Fe1, in the centre of the porphyrin ring, and included all atoms within a radius of 12 Å. Top positions for each compound were scored and ranked with GOLD energy score,(380) after 5000 runs, keeping at the final the best 25 scored solutions. The docking results visualization and all images were carried out using MOE.(429)

R

References

(1) Clinquart, E. (**1929**) Sur la Compesition Chimnique de "Cryptolepis triangularis" plante congolaise. *Bull. Acad. R. Med. Belg.***,** 12, 627-635.

(2) Kumar, E.; Etukala, J.R.; Ablordeppey, S.Y. (**2008**) Indolo[3,2-b] quinolines: Synthesis, biological evaluation and structure activity-relationships. *Mini Rev. Med. Chem.***,** 8, 538-554.

(3) Lavrado, J.; Moreira, R.; Paulo, A. (**2010**) Indoloquinolines as Scaffolds for Drug Discovery. *Curr. Med. Chem.***,** 17, 2348-2370.

(4) Noamesi, B.K.; Paine, A.; Kurb, G.C.; Warhurs, D.C.; Phillipson, J.D. In vitro antimalarial activity of cryptolepine, an indoloquinoline. In *Laboratory Meeting, London School of Hygiene and Tropical Medicine*, Transactions of the Royal Society of Tropical Medicine and Hygiene: 1991; Vol. 85, pp 310-318.

(5) Lisgarten, J.N.; Coll, M.; Portugal, J.; Wright, C.W.; Aymami, J. (**2002**) The antimalarial and cytotoxic drug cryptolepine intercalates into DNA at cytosine-cytosine sites. *Nat. Struct. Biol.***,** 9, 57-60.

(6) Bonjean, K.; De Pauw-Gillet, M.C.; Defresne, M.P.; Colson, P.; Houssier, C.; Dassonneville, L.; Bailly, C.; Greimers, R.; Wright, C.; Quetin-Leclercq, J.; Tits, M.; Angenot, L. (**1998**) The DNA intercalating alkaloid cryptolepine interferes with topoisomerase II and inhibits primarily DNA synthesis in B16 melanoma cells. *Biochemistry***,** 37, 5136-46.

(7) Dassonneville, L.; Bonjean, K.; De Pauw-Gillet, M.C.; Colson, P.; Houssier, C.; Quetin-Leclercq, J.; Angenot, L.; Bailly, C. (**1999**) Stimulation of topoisomerase II-mediated DNA cleavage by three DNA-intercalating plant alkaloids: cryptolepine, matadine, and serpentine. *Biochemistry***,** 38, 7719-7726.

(8) Ansah, C.; Gooderham, N.J. (**2002**) The Popular Herbal Antimalarial, Extract of *Cryptolepis sanguinolenta*, Is Potently Cytotoxic. *Toxicol. Sci.***,** 70, 245-251.

(9) Onyeibor, O.; Croft, S.L.; Dodson, H.I.; Feiz-Haddad, M.; Kendrick, H.; Millington, N.J.; Parapini, S.; Phillips, R.M.; Seville, S.; Shnyder, S.D.; Taramelli, D.; Wright, C.W. (**2005**) Synthesis of some cryptolepine analogues, assessment of their antimalarial and cytotoxic activities, and consideration of their antimalarial mode of action. *J. Med. Chem.***,** 48, 2701-9.

(10) Oluwafemi, A.J.; Okanla, E.O.; Camps, P.; Munoz-Torrero, D.; Mackey, Z.B.; Chiang, P.K.; Seville, S.; Wright, C.W. (**2009**) Evaluation of cryptolepine and huperzine derivatives as lead compounds towards new agents for the treatment of human african trypanosomiasis. *Nat. Prod. Commun.***,** 4, 193-198.

(11) Gorlitzer, K.; Weber, J. (**1981**) Fused Quinolines 5. 10-Hydroxy-10*H*-Indolo[3,2-*b*]Quinoline 5-Oxide (Dioxyquindoline). *Arc. Der Pharm.***,** 314, 850-852.

(12) Gorlitzer, K.; Weber, J. (**1981**) Fused Quinolines 6. 10*H*-Indolo[3,2-*b*]Quinolines. *Arc. Der Pharm.***,** 314, 852-861.

(13) Bierer, D.E.; Dubenko, L.G.; Zhang, P.S.; Lu, Q.; Imbach, P.A.; Garofalo, A.W.; Phuan, P.W.; Fort, D.M.; Litvak, J.; Gerber, R.E.; Sloan, B.; Luo, J.; Cooper, R.; Reaven, G.M. (**1998**) Antihyperglycemic activities of cryptolepine analogues: An ethnobotanical lead structure isolated from Cryptolepis sanguinolenta. *J. Med. Chem.***,** 41, 2754-2764.

(14) Bierer, D.E.; Fort, D.M.; Mendez, C.D.; Luo, J.; Imbach, P.A.; Dubenko, L.G.; Jolad, S.D.; Gerber, R.E.; Litvak, J.; Lu, Q.; Zhang, P.S.; Reed, M.J.; Waldeck, N.; Bruening, R.C.; Noamesi, B.K.; Hector, R.F.; Carlson, T.J.; King, S.R. (**1998**) Ethnobotanical-directed discovery of the antihyperglycemic properties of cryptolepine: Its isolation from Cryptolepis sanguinolenta, synthesis, and in vitro and in vivo activities. *J. Med. Chem.***,** 41, 894-901.

(15) Henderson, L.J. (**1908**) Concerning the relationship between the strength of acids and their capacity to preserve neutrality. *Am J Physiol***,** 21, 173-179.

(16) Hasselbalch, K.A. (**1917**) The calculation of the hydrogen content in blood from free and combined carbonic acid, and the oxygen compound of the blood as the function of the hydrogen content. *Biochem Z*, 78, 112-144.

(17) Bonjean, K.; De Pauw-Gillet, M.C.; Defresne, M.P.; Colson, P.; Houssier, C.; Dassonneville, L.; Bailly, C.; Greimers, R.; Wright, C.; Quetin-Leclercq, J.; Tits, M.; Angenot, L. (**1998**) The DNA intercalating alkaloid cryptolepine interferes with topoisomerase II and inhibits primarily DNA synthesis in B16 melanoma cells. *Biochemistry*, 37, 5136-5146.

(18) Kumar, S.; Guha, M.; Choubey, V.; Maity, P.; Bandyopadhyay, U. (**2007**) Antimalarial drugs inhibiting hemozoin (beta-hematin) formation: A mechanistic update. *Life Sci.*, 80, 813-828.

(19) Rosenthal, P.J.; Meshnick, S.R. (**1996**) Hemoglobin catabolism and iron utilization by malaria parasites. *Mol. Biochem. Parasit.*, 83, 131-139.

(20) Egan, T.J.; Combrinck, J.M.; Egan, J.; Hearne, G.R.; Marques, H.M.; Ntenteni, S.; Sewell, B.T.; Smith, P.J.; Taylor, D.; van Schalkwyk, D.A.; Walden, J.C. (**2002**) Fate of haem iron in the malaria parasite *Plasmodium falciparum*. *Biochem. J.*, 365, 343-347.

(21) Kumar, S.; Bandyopadhyay, U. (**2005**) Free heme toxicity and its detoxification systems in human. *Toxicology Letters*, 157, 175-188.

(22) White, N.J. (**1992**) The Pathophysiology of Malaria. *Advances in Parasitology*, 31, 83-173.

(23) Schlitzer, M. (**2007**) Malaria chemotherapeutics part 1: History of antimalarial drug development, currently used therapeutics, and drugs in clinical development. *Chemmedchem*, 2, 944-986.

(24) Chauhan, V.S. (**2007**) Vaccines for malaria - prospects and promise. *Curr. Sci.*, 92, 1525-1534.

(25) Sacarlal, J.; Aide, P.; Aponte, J.J.; Renom, M.; Leach, A.; Mandomando, I.; Lievens, M.; Bassat, Q.; Lafuente, S.; Macete, E.; Vekemans, J.; Guinovart, C.; Sigauque, B.; Sillman, M.; Milman, J.; Dubois, M.C.; Demoitie, M.A.; Thonnard, J.; Menendez, C.; Ballou, W.R.; Cohen, J.; Alonso, P.L. (**2009**) Long-Term Safety and Efficacy of the RTS,S/AS02A Malaria Vaccine in Mozambican Children. *J. Infec. Disea,*, 200, 329-336.

(26) Aregawi, M.; Cibulskis, R.; Otten, M.; Williams, R.; Dye, C. *World malaria report*; World Health Organization: **2008**; p 190.

(27) Roberts, L.; Enserink, M. (**2007**) Malaria - Did they really say ... eradication? *Science*, 318, 1544-1545.

(28) Plowe, C.V. Antimalarial drug resistance in Africa: Strategies for monitoring and deterrence. In ***Malaria: Drugs, Disease and Post-Genomic Biology***, **2005**; Vol. 295, pp 55-79.

(29) Uhlemann, A.C.; Krishna, S. Antimalarial multi-drug resistance in Asia: Mechanisms and assessment. In ***Malaria: Drugs, Disease and Post-Genomic Biology***, **2005**; Vol. 295, pp 39-53.

(30) Tanser, F.C.; Sharp, B.; le Sueur, D. (**2003**) Potential effect of climate change on malaria transmission in Africa. *Lancet*, 362, 1792-1798.

(31) Saugeon, C.; Baldet, T.; Akogbeto, M.; Henry, M.C. (**2009**) Will climate and demography have a major impact on malaria in sub-Saharan Africa in the next 20 years? *Médecine tropicale*, 69, 203-7.

(32) Whitworth, J.; Morgen, D.; Quigley, M.; Smith, A.; Mayanja, S.; Eotu, H.; Omoding, N.; Okongo, M.; Malamba, S.; Ojwiya, A. (**2000**) Effect of HIV-1 and increasing immunosuppression on malaria parasitaemia and clinical episodes in adults in rural Uganda: a cohort study. *Lancet*, 356, 1051-1056.

(33) French, N.; Nakiyingi, J.; Lugada, E.; Watera, C.; Whitworth, J.A.G.; Gilks, C.F. (**2001**) Increasing rates of malarial fever with deteriorating immune status in HIV-1-infected Ugandan adults. *Aids*, 15, 899-906.

(34) Mount, A.M.; Mwapasa, V.; Elliott, S.R.; Beeson, J.G.; Tadesse, E.; Lema, V.M.; Molyneux, M.E.; Meshnick, S.R.; Rogerson, S.J. (**2004**) Impairment of humoral immunity to *Plasmodium falciparum* malaria in pregnancy by HIV infection. *Lancet***,** 363, 1860-1867.

(35) Nogueira, P.A.; Wunderlich, G.; Pereira da Silva, L.H. (**2001**) Variant antigens of Plasmodium falciparum encoded by the var multigenic family are multifunctional macromolecules. *Res Microbiol***,** 152, 141-7.

(36) Bannister, L.; Mitchell, G. (**2003**) The ins, outs and roundabouts of malaria. *Trends Parasitol.***,** 19, 209-213.

(37) Frederich, M.; Dogne, J.M.; Angenot, L.; De Mol, P. (**2002**) New trends in anti-malarial agents. *Curr. Med. Chem.***,** 9, 1435-1456.

(38) Menard, R.; Heussler, V.; Yuda, M.; Nussenzweig, V. (**2008**) Plasmodium pre-erythrocytic stages: what's new? *Trends Parasitol.***,** 24, 564-569.

(39) Frevert, U.; Usynin, I.; Baer, K.; Klotz, C. (**2006**) Nomadic or sessile: can Kupffer cells function as portals for malaria sporozoites to the liver? *Cell Microbiol***,** 8, 1537-1546.

(40) Grobusch, M.P.; Wiese, A.; Teichmann, D. (**2000**) Delayed primary attack of vivax malaria. *Journal of Travel Medicine***,** 7, 104-105.

(41) Oh, S.S.; Chishti, A.H. Host receptors in malaria merozoite invasion. In ***Malaria: Drugs, Disease and Post-Genomic Biology***, **2005**; Vol. 295, pp 203-232.

(42) Hemmer, C.J.; Holst, F.G.E.; Kern, P.; Chiwakata, C.B.; Dietrich, M.; Reisinger, E.C. (**2006**) Stronger host response per parasitized erythrocyte in Plasmodium vivax or ovale than in Plasmodium falciparum malaria. *Trop. Med. Int. Health***,** 11, 817-823.

(43) Dixon, M.W.A.; Thompson, J.; Gardiner, D.L.; Trenholme, K.R. (**2008**) Sex in Plasmodium: a sign of commitment. *Trends Parasitol.***,** 24, 168-175.

(44) Babiker, H.A.; Schneider, P.; Reece, S.E. (**2008**) Gametocytes: insights gained during a decade of molecular monitoring. *Trends Parasitol.***,** 24, 525-530.

(45) Talman, A.M.; Domarle, O.; McKenzie, F.E.; Ariey, F.; Robert, V. (**2004**) Gametocytogenesis: the puberty of *Plasmodium falciparum*. *Malaria Journal***,** 3, Article Number: 24.

(46) Whitten, M.M.A.; Shiao, S.H.; Levashina, E.A. (**2006**) Mosquito midguts and malaria: cell biology, compartmentalization and immunology. *Parasite Immunology***,** 28, 121-130.

(47) Winzeler, E.A. (**2008**) Malaria research in the post-genomic era. *Nature***,** 455, 751-756.

(48) Krugliak, M.; Zhang, J.M.; Ginsburg, H. (**2002**) Intraerythrocytic Plasmodium falciparum utilizes only a fraction of the amino acids derived from the digestion of host cell cytosol for the biosynthesis of its proteins. *Mol. Biochem. Parasit.***,** 119, 249-256.

(49) Goldberg, D.E. Hemoglobin Degradation. In ***Malaria: Drugs, Disease and Post-genomic Biology***, Sullivan, D.J.; Krishna, S., Eds. **2005**; Vol. 295, pp 275-291.

(50) Hempelmann, E.; Motta, C.; Hughes, R.; Ward, S.A.; Bray, P.G. (**2003**) Plasmodium falciparum: sacrificing membrane to grow crystals? *Trends Parasitol.***,** 19, 23-26.

(51) Goldberg, D.E.; Slater, A.F.G. (**1992**) The Pathway of Hemoglobin degradation in Malaria Parasites. *Parasit. Today***,** 8, 280-283.

(52) Klonis, N.; Tan, O.; Jackson, K.; Goldberg, D.; Klemba, M.; Tilley, L. (**2007**) Evaluation of pH during cytostomal endocytosis and vacuolar catabolism of haemoglobin in *Plasmodium falciparum*. *Biochem. J.***,** 407, 343-354.

(53) Saliba, K.J.; Allen, R.J.W.; Zissis, S.; Bray, P.G.; Ward, S.A.; Kirk, K. (**2003**) Acidification of the malaria parasite's digestive vacuole by a H+-ATPase and a H+-pyrophosphatase. *J. Biol. Chem.*, 278, 5605-5612.

(54) Greenwood, B.M.; Fidock, D.A.; Kyle, D.E.; Kappe, S.H.I.; Alonso, P.L.; Collins, F.H.; Duffy, P.E. (**2008**) Malaria: progress, perils, and prospects for eradication. *J. Clin. Invest.*, 118, 1266-1276.

(55) Banerjee, R.; Goldberg, D.E. The Plasmodium food vacuole. In ***Antimalarial Chemotherapy***, PJ, R., Ed. Humana Press Inc.: Totowa, **2001**; pp 43-63.

(56) Olliaro, P.L.; Goldberg, D.E. (**1995**) The *Plasmodium* Digestive Vacuole - Metabolic Headquarters and Choice Drug Target *Parasit. Today*, 11, 294-297.

(57) Fitch, C.D.; Kanjananggulpan, P. (**1987**) The State of Ferriprotoporphyrin-IX in Malaria Pigment. *J. Biol. Chem.*, 262, 15552-15555.

(58) Hamsik, A. (**1936**) Representation of some blood colouring derivatives. *Hoppe-Seylers Zeitschrift Fur Physiologische Chemie*, 241, 156-167.

(59) Hamsik, A. (**1931**) Crystalisation of protoporphyrin. *Hoppe-Seylers Zeitschrift Fur Physiologische Chemie*, 195, A195-A198.

(60) Slater, A.F.G.; Swiggard, W.J.; Orton, B.R.; Flitter, W.D.; Goldberg, D.E.; Cerami, A.; Henderson, G.B. (**1991**) An Iron Carboxilate Bond Links the Heme Units of Malaria Pigment. *Proc. Nat. Acad. Sci. U.S.A.*, 88, 325-329.

(61) Bohle, D.S.; Dinnebier, R.E.; Madsen, S.K.; Stephens, P.W. (**1997**) Characterization of the products of the heme detoxification pathway in malarial late trophozoites by X-ray diffraction. *J. Biol. Chem.*, 272, 713-716.

(62) Malaria: Drugs, Disease and Post-Genomic Biology: Editors: Sullivan, D.; Krishna, S.; Springer-Verlag Berlin Heidelberg: New York, **2005**; Vol. 295, p 439.

(63) Pagola, S.; Stephens, P.W.; Bohle, D.S.; Kosar, A.D.; Madsen, S.K. (**2000**) The structure of malaria pigment beta-haematin. *Nature*, 404, 307-310.

(64) Egan, T.J. (**2002**) Physico-chemical aspects of hemozoin (malaria pigment) structure and formation. *J. Inorg. Biochem.*, 91, 19-26.

(65) Egan, T.J. (**2002**) Haemozoin formation is the pathway of haem disposal in the malaria parasite *Plasmodium falciparum*. *S. Afr. J. Sci.*, 98, 411-412.

(66) Egan, T.J. (**2008**) Haemozoin formation. *Mol. Biochem. Parasit.*, 157, 127-136.

(67) Atamna, H.; Ginsburg, H. (**1993**) Origin of reactive oxygen species in erythrocytes infected with *Plasmodium falciparum*. *Mol. Biochem. Parasit.*, 61, 231-241.

(68) Schmitt, T.H.; Frezzatti, W.A.; Schreier, S. (**1993**) Hemin-Induced Lipid-Membrane Disorder and Increased Permeability - A Molecular-Model for the Mechanism of Cell Lysis. *Archives of Biochemistry and Biophysics*, 307, 96-103.

(69) Stojiljkovic, I.; Evavold, B.D.; Kumar, V. (**2001**) Antimicrobial properties of porphyrins. *Expert Opinion on Investigational Drugs*, 10, 309-320.

(70) de Villiers, K.A.; Kaschula, C.H.; Egan, T.J.; Marques, H.M. (**2007**) Speciation and structure of ferriprotoporphyrin IX in aqueous solution: spectroscopic and diffusion measurements demonstrate dimerization, but not mu-oxo dimer formation. *J Biol Inorg Chem*, 12, 101-117.

(71) Brown, S.B.; Jones, P.; Lantzke, I.R. (**1969**) Infrared Evidence for an oxo-Bridge (Fe-O-Fe) Haemin Dimer. *Nature*, 223, 960-&.

(72) Sullivan, D.J.; Gluzman, I.Y.; Goldberg, D.E. (**1996**) Plasmodium hemozoin formation mediated by histidine-rich proteins. *Science*, 271, 219-222.

(73) Pandey, A.V.; Babbarwal, V.K.; Okoyeh, J.N.; Joshi, R.M.; Puri, S.K.; Singh, R.L.; Chauhan, V.S. (**2003**) Hemozoin formation in malaria: a two-step process involving histidine-rich proteins and lipids. *Biochemical and Biophysical Research Communications*, 308, 736-743.

(74) Ziegler, J.; Chang, R.T.; Wright, D.W. (**1999**) Multiple-antigenic peptides of histidine-rich protein II of Plasmodium falciparum: Dendrimeric biomineralization templates. *J. Am. Chem. Soc.*, 121, 2395-2400.

(75) Noland, G.S.; Briones, N.; Sullivan, D.J. (**2003**) The shape and size of hemozoin crystals distinguishes diverse Plasmodium species. *Mol. Biochem. Parasit.*, 130, 91-99.

(76) Akompong, T.; Kadekoppala, M.; Harrison, T.; Oksman, A.; Goldberg, D.E.; Fujioka, H.; Samuel, B.U.; Sullivan, D.; Haldar, K. (**2002**) trans expression of a Plasmodium falciparum histidine-rich protein II (HRPII) reveals sorting of soluble proteins in the periphery of the host erythrocyte malarial food vacuole. *J. Biol. Chem.*, 277, 28923-28933.

(77) Buller, R.; Peterson, M.L.; Almarsson, O.; Leiserowitz, L. (**2002**) Quinoline binding site on malaria pigment crystal: A rational pathway for antimalarial drug design. *Cryst. Growth Des.*, 2, 553-562.

(78) Jackson, K.E.; Klonis, N.; Ferguson, D.J.P.; Adisa, A.; Dogovski, C.; Tilley, L. (**2004**) Food vacuole-associated lipid bodies and heterogeneous lipid environments in the malaria parasite, Plasmodium falciparum. *Molecular Microbiology*, 54, 109-122.

(79) Pisciotta, J.; Coppens, I.; Tripathi, A.; Scholl, P.; Shuman, J.; Shulaev, V.; Sullivan, D.J. (**2005**) Neutral lipid microspheres in Plasmodium falciparum digestive vacuoles mediate heme crystallization. *Am. J. Trop. Med. Hygien.*, 73, 571.

(80) Coppens, I.; Vielemeyer, O. (**2005**) Insights into unique physiological features of neutral lipids in Apicomplexa: from storage to potential mediation in parasite metabolic activities. *Int. J. Parasito.*, 35, 597-615.

(81) Pisciotta, J.M.; Coppens, I.; Tripathi, A.K.; Scholl, P.F.; Shuman, J.; Bajad, S.; Shulaev, V.; Sullivan, D.J. (**2007**) The role of neutral lipid nanospheres in Plasmodium falciparum haem crystallization. *Biochem. J.*, 402, 197-204.

(82) Egan, T.J.; Tshivhase, M.G. (**2006**) Kinetics of beta-haematin formation from suspensions of haematin in aqueous benzoic acid. *Dalton Transactions*, 5024-5032.

(83) Egan, T.J.; Chen, J.Y.J.; de Villiers, K.A.; Mabotha, T.E.; Naidoo, K.J.; Ncokazi, K.K.; Langford, S.J.; McNaughton, D.; Pandiancherri, S.; Wood, B.R. (**2006**) Haemozoin (beta-haematin) biomineralization occurs by self-assembly near the lipid/water interface. *Febs Lett.*, 580, 5105-5110.

(84) Ehrlich P.; Guttmann P. (**1891**) Ueber die Wirkung des Methylenblau bei Malaria. *Berliner klinische Wochenschrift*, 28, 953-956.

(85) Foley, M.; Tilley, L. (**1998**) Quinoline antimalarials: Mechanisms of action and resistance and prospects for new agents. *Pharmacol. Therap.*, 79, 55-87.

(86) Ridley, R.G.; Hudson, A.T. (**1998**) Quinoline antimalarials. *Expert Opin. Therap. Patents*, **8**, 121-136.

(87) van Agtmael, M.A.; Eggelte, T.A.; van Boxtel, C.J. (**1999**) Artemisinin drugs in the treatment of malaria: from medicinal herb to registered medication. *Trends Pharmacol. Sci*, 20, 199-205.

(88) Wright, C.W. (**2005**) Traditional antimalarials and the development of novel antimalarial drugs. *J. Ethnopharmacol.*, 100, 67-71.

(89) Olliaro, P. (**2001**) Mode of action and mechanisms of resistance for antimalarial drugs. *Pharmacol. Therap.***,** 89, 207-219.

(90) Plowe, C.V.; Kublin, J.G.; Doumbo, O.K. (**1998**) P-falciparum dihydrofolate reductase and dihydropteroate synthase mutations: epidemiology and role in clinical resistance to antifolates. *Drug Resis. Updates***,** 1, 389-396.

(91) Tekwani, B.L.; Walker, L.A. (**2006**) 8-aminoquinolines: future role as antiprotozoal drugs. *Curr Opin Infect Dis***,** 19, 623-631.

(92) Pandey, A.V.; Chauhan, V.S. (**1998**) Heme polymerization by malarial parasite: A potential target for antimalarial drug development. *Curr. Sci.***,** 75, 911-918.

(93) Hyde, J.E. (**2005**) Drug-resistant malaria. *Trends Parasitol.***,** 21, 494-498.

(94) Henry, M.; Alibert, S.; Rogier, C.; Barbe, J.; Pradines, B. (**2008**) Inhibition of efflux of quinolines as new therapeutic strategy in malaria. *Curr. Top. Med. Chem***,** 8, 563-578.

(95) Klayman, D.L. (**1985**) Qinghaosu (Artemisinin) - an Antimalarial Drug from China. *Science***,** 228, 1049-1055.

(96) White, N.J. (**1997**) Assessment of the pharmacodynamic properties of antimalarial drugs in vivo. *Antimicrob. Agents Chemother.***,** 41, 1413-1422.

(97) Noedl, H.; Se, Y.; Schaecher, K.; Smith, B.L.; Socheat, D.; Fukuda, M.M.; Consortium, A.R.C.S. (**2008**) Evidence of Artemisinin-Resistant Malaria in Western Cambodia. *New Eng. J. Med.***,** 359, 2619-2620.

(98) Taylor, S.M.; Juliano, J.J.; Meshnick, S.R. (**2009**) Artemisinin Resistance in Plasmodium falciparum Malaria. *New Eng. J. Med.***,** 361, 1807-1807.

(99) Berman, J. (**2004**) Toxicity of commonly-used antimalarial drugs. *Travel Med. Infect. Dis.***,** 2, 171-184.

(100) Padmanaban, G.; Nagaraj, V.A.; Rangarajan, P.N. (**2007**) Drugs and drug targets. against. malaria. *Curr. Sci.***,** 92, 1545-1555.

(101) Sahu, N.K.; Sahu, S.; Kohli, D.V. (**2008**) Novel molecular targets for antimalarial drug development. *Chemical Biology & Drug Design***,** 71, 287-297.

(102) Biagini, G.A.; O'Neill, P.M.; Nzila, A.; Ward, S.A.; Bray, P.G. (**2003**) Antimalarial chemotherapy: young guns or back to the future? *Trends Parasitol.***,** 19, 479-487.

(103) Leung, D.; Abbenante, G.; Fairlie, D.P. (**2000**) Protease inhibitors: Current status and future prospects. *J. Med. Chem.***,** 43, 305-341.

(104) Martinelli, A.; Moreira, R.; Cravo, P.V.L. (**2008**) Malaria combination therapies: Advantages and shortcomings. *Mini Rev. Med. Chem.***,** 8, 201-212.

(105) Kumar, A.; Katiyar, S.B.; Agarwal, A.; Chauhan, P.M.S. (**2003**) Perspective in antimalarial chemotherapy. *Curr. Med. Chem.***,** 10, 1137-1150.

(106) Choi, S.R.; Mukherjee, P.; Avery, M.A. (**2008**) The fight against drug-resistant malaria: Novel plasmodial targets and antimalarial drugs. *Curr. Med. Chem.***,** 15, 161-171.

(107) Kouznetsov, V.V.; Gomez-Barrio, A. (**2009**) Recent developments in the design and synthesis of hybrid molecules based on aminoquinoline ring and their antiplasmodial evaluation. *Eur. J. Med. Chem.***,** 44, 3091-3113.

(108) Solomonov, I.; Osipova, M.; Feldman, Y.; Baehtz, C.; Kjaer, K.; Robinson, I.K.; Webster, G.T.; McNaughton, D.; Wood, B.R.; Weissbuch, I.; Leiserowitz, L. (**2007**) Crystal nucleation, growth, and morphology of the synthetic malaria pigment beta-hematin and the effect thereon by quinoline additives: The malaria pigment as a target of various antimalarial drugs. *J. Am. Chem. Soc.***,** 129, 2615-2627.

(109) Winter, R.W.; Kelly, J.X.; Smilkstein, M.J.; Dodean, R.; Bagby, G.C.; Rathbun, R.K.; Levin, J.I.; Hinrichs, D.; Riscoe, M.K. (**2006**) Evaluation and lead optimization of anti-malarial acridones. *Exp. Parasit.***,** 114, 47-56.

(110) Kelly, J.X.; Smilkstein, M.J.; Brun, R.; Wittlin, S.; Cooper, R.A.; Lane, K.D.; Janowsky, A.; Johnson, R.A.; Dodean, R.A.; Winter, R.; Hinrichs, D.J.; Riscoe, M.K. (**2009**) Discovery of dual function acridones as a new antimalarial chemotype. *Nature***,** 459, 270-273.

(111) Posner, G.H.; O'Neill, P.M. (**2004**) Knowledge of the proposed chemical mechanism of action and cytochrome P450 metabolism of antimalarial trioxanes like artemisinin allows rational design of new antimalarial peroxides. *Accounts Chem Res***,** 37, 397-404.

(112) O'Neill, P.M.; Posner, G.H. (**2004**) A medicinal chemistry perspective on artemisinin and related endoperoxides. *J. Med. Chem.***,** 47, 2945-2964.

(113) Drew, M.G.B.; Metcalfe, J.; Dascombe, M.J.; Ismail, F.M.D. (**2006**) Reactions of artemisinin and arteether with acid: Implications for stability and mode of antimalarial action. *J. Med. Chem.***,** 49, 6065-6073.

(114) Cui, L.W.; Su, X.Z. (**2009**) Discovery, mechanisms of action and combination therapy of artemisinin. *Expert Review of Anti-Infective Therapy***,** 7, 999-1013.

(115) Kumura, N.; Furukawa, H.; Onyango, A.N.; Izumi, M.; Nakajima, S.; Ito, H.; Hatano, T.; Kim, H.S.; Wataya, Y.; Baba, N. (**2009**) Different behavior of artemisinin and tetraoxane in the oxidative degradation of phospholipid. *Chemistry and Physics of Lipids***,** 160, 114-120.

(116) Greenwood, D. (**1995**) Conflicts-of-Interest - the Genesis of Synthetic Antimalarial Agents in Peace and War. *J. Antimicrob. Chemother.***,** 36, 857-872.

(117) Burckalter, J.H.; Tendick, F.H.; Jones, E.M.; P.A.Jones; Holcomb, W.F.; Rawlins, A.L. (**1948**) Aminoalkylphenols as Antimalarials. II. (Heterocyclic-amino)-α-amino-o-cresol. The Synthesis of Camoquin. *J. Am. Chem. Soc.***,** 70, 1363-1373.

(118) de Dios, A.C.; Tycko, R.; Ursos, L.M.B.; Roepe, P.D. (**2003**) NMR studies of chloroquine-ferriprotoporphyrin IX complex. *J Phys Chem A***,** 107, 5821-5825.

(119) Hawley, S.R.; Bray, P.G.; Mungthin, M.; Atkinson, J.D.; O'Neill, P.M.; Ward, S.A. (**1998**) Relationship between antimalarial drug activity, accumulation, and inhibition of heme polymerization in Plasmodium falciparum in vitro. *Antimicrob. Agents Chemother.***,** 42, 682-686.

(120) Hawley, S.R.; Bray, P.G.; Oneill, P.M.; Park, B.K.; Ward, S.A. (**1996**) The role of drug accumulation in 4-aminoquinoline antimalarial potency - The influence of structural substitution and physicochemical properties. *Biochem. Pharmacol.***,** 52, 723-733.

(121) ONeill, P.M.; Willock, D.J.; Hawley, S.R.; Bray, P.G.; Storr, R.C.; Ward, S.A.; Park, B.K. (**1997**) Synthesis, antimalarial activity, and molecular modeling of tebuquine analogues. *J. Med. Chem.***,** 40, 437-448.

(122) Vippagunta, S.R.; Dorn, A.; Ridley, R.G.; Vennerstrom, J.L. (**2000**) Characterization of chloroquine-hematin mu-oxo dimer binding by isothermal titration calorimetry. *Biochim Biophys Acta***,** 1475, 133-140.

(123) Kaschula, C.H.; Egan, T.J.; Hunter, R.; Basilico, N.; Parapini, S.; Taramelli, D.; Pasini, E.; Monti, D. (**2002**) Structure-activity relationships in 4-aminoquinoline antiplasmodials. The role of the group at the 7-position. *J. Med. Chem.***,** 45, 3531-3539.

(124) Portela, C.; Afonso, C.M.M.; Pinto, M.M.M.; Ramos, M.J. (**2003**) Receptor-drug association studies in the inhibition of the hematin aggregation process of malaria. *Febs Lett.***,** 547, 217-222.

(125) Portela, C.; Afonso, C.M.M.; Pinto, M.M.M.; Ramos, M.J. (**2003**) Computational studies of new potential antimalarial compounds - Stereoelectronic complementarity with the receptor. *Journal of Computer-Aided Molecular Design***,** 17, 583-595.

(126) Portela, C.; Afonso, C.M.M.; Pinta, M.M.M.; Ramos, M.J. (**2004**) Definition of an electronic profile of compounds with inhibitory activity against hematin aggregation in malaria parasite. *Bioorg. Med. Chem.***,** 12, 3313-3321.

(127) Sullivan, D.J.; Gluzman, I.Y.; Russell, D.G.; Goldberg, D.E. (**1996**) On the molecular mechanism of chloroquine's antimalarial action. *Proc. Nat. Acad. Sci. U.S.A.***,** 93, 11865-11870.

(128) Chong, C.R.; Sullivan, D.J. (**2003**) Inhibition of heme crystal growth by antimalarials and other compounds: implications for drug discovery. *Biochem. Pharmacol.***,** 66, 2201-2212.

(129) Bray, P.G.; Ward, S.A.; O'Neill, P.M. (**2005**) Quinolines and artemisinin: Chemistry, biology and history. *Malaria: Drugs, Disease and Post-Genomic Biology***,** 295, 3-38.

(130) Weissbuch, I.; Leiserowitz, L. (**2008**) Interplay Between Malaria, Crystalline Hemozoin Formation, and Antimalarial Drug Action and Design. *Chem. Rev.***,** 108, 4899-4914.

(131) Wellems, T.E.; Plowe, C.V. (**2001**) Chloroquine-resistant malaria. *J. Infec. Disea,***,** 184, 770-776.

(132) Egan, T.J.; Hunter, R.; Kaschula, C.H.; Marques, H.M.; Misplon, A.; Walden, J. (**2000**) Structure-function relationships in aminoquinolines: Effect of amino and chloro groups on quinoline-hematin complex formation, inhibition of beta-hematin formation, and antiplasmodial activity. *J. Med. Chem.***,** 43, 283-291.

(133) Egan, T.J. (**2006**) Interactions of quinoline antimalarials with hematin in solution. *J. Inorg. Biochem.***,** 100, 916-926.

(134) O'Neill, P.M.; Bray, P.G.; Hawley, S.R.; Ward, S.A.; Park, B.K. (**1998**) 4-aminoquinolines - Past, present, and future: A chemical perspective. *Pharmacol. Therap.***,** 77, 29-58.

(135) Stocks, P.A.; Raynes, K.J.; Bray, P.G.; Park, B.K.; O'Neill, P.M.; Ward, S.A. (**2002**) Novel short chain chloroquine analogues retain activity against chloroquine resistant K1 Plasmodium falciparum. *J. Med. Chem.***,** 45, 4975-4983.

(136) De, D.Y.; Krogstad, F.M.; Cogswell, F.B.; Krogstad, D.J. (**1996**) Aminoquinolines that circumvent resistance in Plasmodium falciparum in vitro. *Am. J. Trop. Med. Hygien.***,** 55, 579-583.

(137) Madrid, P.B.; Liou, A.P.; DeRisi, J.L.; Guy, R.K. (**2006**) Incorporation of an intramolecular hydrogen-bonding motif in the side chain of 4-aminoquinolines enhances activity against drug-resistant P-falciparum. *J. Med. Chem.***,** 49, 4535-4543.

(138) Madrid, P.B.; Sherrill, J.; Liou, A.P.; Weisman, J.L.; DeRisi, J.L.; Guy, R.K. (**2005**) Synthesis of ring-substituted 4-aminoquinolines and evaluation of their antimalarial activities. *Bioorg. Med. Chem. Lett.***,** 15, 1015-1018.

(139) Solomon, V.R.; Haq, W.; Srivastava, K.; Puri, S.K.; Katti, S.B. (**2007**) Synthesis and antimalarial activity of side chain modified 4-aminoquinoline derivatives. *J. Med. Chem.***,** 50, 394-398.

(140) Iwaniuk, D.P.; Whetmore, E.D.; Rosa, N.; Ekoue-Kovi, K.; Alumasa, J.; de Dios, A.C.; Roepe, P.D.; Wolf, C. (**2009**) Synthesis and antimalarial activity of new chloroquine analogues carrying a multifunctional linear side chain. *Bioorg. Med. Chem.***,** 17, 6560-6566.

(141) Ekoue-Kovi, K.; Yearick, K.; Iwaniuk, D.P.; Natarajan, J.K.; Alumasa, J.; de Dios, A.C.; Roepe, P.D.; Wolf, C. (**2009**) Synthesis and antimalarial activity of new 4-amino-7-chloroquinolyl amides, sulfonamides, ureas and thioureas. *Bioorg. Med. Chem.***,** 17, 270-283.

(142) Taylor, W.R.J.; White, N.J. (**2004**) Antimalarial drug toxicity - A review. *Drug Safety***,** 27, 25-61.

(143) Churchill, F.C.; Patchen, L.C.; Campbell, C.C.; Schwartz, I.K.; Phuc, N.D.; Dickinson, C.M. (**1985**) Amodiaquine as a Prodrug - Importance of Metabolite(S) in the Antimalarial Effect of Amodiaquine in Humans. *Life Sci.***,** 36, 53-62.

(144) O'Neill, P.M.; Mukhtar, A.; Stocks, P.A.; Randle, L.E.; Hindley, S.; Ward, S.A.; Storr, R.C.; Bickley, J.F.; O'Neil, I.A.; Maggs, J.L.; Hughes, R.H.; Winstanley, P.A.; Bray, P.G.; Park, B.K. (**2003**) Isoquine and related amodiaquine analogues: A new generation of improved 4-aminoquinoline antimalarials. *J. Med. Chem.***,** 46, 4933-4945.

(145) O'Neill, P.M.; Park, B.K.; Shone, A.E.; Maggs, J.L.; Roberts, P.; Stocks, P.A.; Biagini, G.A.; Bray, P.G.; Gibbons, P.; Berry, N.; Winstanley, P.A.; Mukhtar, A.; Bonar-Law, R.; Hindley, S.; Bambal, R.B.; Davis, C.B.; Bates, M.; Hart, T.K.; Gresham, S.L.; Lawrence, R.M.; Brigandi, R.A.; Gomez-Delas-Heras, F.M.; Gargallo, D.V.; Ward, S.A. (**2009**) Candidate Selection and Preclinical Evaluation of N-tert-Butyl Isoquine (GSK369796), An Affordable and Effective 4-Aminoquinoline Antimalarial for the 21st Century. *J. Med. Chem.***,** 52, 1408-1415.

(146) O'Neill, P.M.; Shone, A.E.; Stanford, D.; Nixon, G.; Asadollahy, E.; Park, B.K.; Maggs, J.L.; Roberts, P.; Stocks, P.A.; Biagini, G.; Bray, P.G.; Davies, J.; Berry, N.; Hall, C.; Rimmer, K.; Winstanley, P.A.; Hindley, S.; Bambal, R.B.; Davis, C.B.; Bates, M.; Gresham, S.L.; Brigandi, R.A.; Gomez-de-las-Heras, F.M.; Gargallo, D.V.; Parapini, S.; Vivas, L.; Lander, H.; Taramelli, D.; Ward, S.A. (**2009**) Synthesis, Antimalarial Activity, and Preclinical Pharmacology of a Novel Series of 4 '-Fluoro and 4 '-Chloro Analogues of Amodiaquine. Identification of a Suitable "Back-Up" Compound for N-tert-Butyl Isoquine. *J. Med. Chem.***,** 52, 1828-1844.

(147) Miroshnikova, O.V.; Hudson, T.H.; Gerena, L.; Kyle, D.E.; Lin, A.J. (**2007**) Synthesis and antimalarial activity of new isotebuquine analogues. *J. Med. Chem.***,** 50, 889-896.

(148) Lee, J.; Son, J.; Chung, S.J.; Lee, E.S.; Kim, D.H. (**2004**) In vitro and in vivo metabolism of pyronaridine characterized by low-energy collision-induced dissociation mass spectrometry with electrospray ionization. *J. Mass Spectrom.*, 39, 1036-1043.

(149) Delarue-Cochin, S.; Grellier, P.; Maes, L.; Mouray, E.; Sergheraert, C.; Melnyk, P. (**2008**) Synthesis and antimalarial activity of carbamate and amide derivatives of 4-anilinoquinoline. *Eur. J. Med. Chem.***,** 43, 2045-2055.

(150) Delarue-Cochin, S.; Paunescu, E.; Maes, L.; Mouray, E.; Sergheraert, C.; Grellier, P.; Melnyk, P. (**2008**) Synthesis and antimalarial activity of new analogues of amodiaquine. *Eur. J. Med. Chem.***,** 43, 252-260.

(151) Cowman, A.F.; Deady, L.W.; Deharo, E.; Desneves, J.; Tilley, L. (**1997**) Synthesis and activity of some antimalarial bisquinolinemethanols. *Aust. J. Chem***,** 50, 1091-1096.

(152) Chen, L. (**1991**) Recent Studies on Antimalarial Efficacy of Piperaqunine and Hydroxypiperaqunine. *Chin. Med. J.***,** 104, 161-163.

(153) Ridley, R.G.; Matile, H.; Jaquet, C.; Dorn, A.; Hofheinz, W.; Leupin, W.; Masciadri, R.; Theil, F.P.; Richter, W.F.; Girometta, M.A.; Guenzi, A.; Urwyler, H.; Gocke, E.; Potthast, J.M.; Csato, M.; Thomas, A.; Peters, W. (**1997**) Antimalarial activity of the bisquinoline trans-N-1,N-2-bis (7-chloroquinolin-4-yl)cyclohexane-1,2-diamine: Comparison of two stereoisomers and detailed evaluation of the S,S enantiomer, Ro 47-7737. *Antimicrob. Agents Chemother.***,** 41, 677-686.

(154) Davis, T.M.E.; Hung, T.Y.; Sim, I.K.; Karunajeewa, H.A.; Ilett, K.F. (**2005**) Piperaquine - A resurgent antimalarial drug. *Drugs***,** 65, 75-87.

(155) Blond, P.B. *Drug Resistance in Malaria*; World Health Organization: **2001**; p 27.

(156) Fitch, C.D. (**1970**) Plasmodium Falciparum in Owl Monkeys - Drug Resistance and Chloroquine Binding Capacity. *Science***,** 169, 289-&.

(157) Krogstad, D.J.; Gluzman, I.Y.; Kyle, D.E.; Oduola, A.M.J.; Martin, S.K.; Milhous, W.K.; Schlesinger, P.H. (**1987**) Efflux of Chloroquine from Plasmodium-Falciparum - Mechanism of Chloroquine Resistance. *Science***,** 238, 1283-1285.

(158) Bray, P.G.; Mungthin, M.; Hastings, I.M.; Biagini, G.A.; Saidu, D.K.; Lakshmanan, V.; Johnson, D.J.; Hughes, R.H.; Stocks, P.A.; O'Neill, P.M.; Fidock, D.A.; Warhurst, D.C.; Ward, S.A. (**2006**) PfCRT and the trans-vacuolar proton electrochemical gradient: regulating the access of chloroquine to ferriprotoporphyrin IX. *Molecular Microbiology***,** 62, 238-251.

(159) Spiller, D.G.; Bray, P.G.; Hughes, R.H.; Ward, S.A.; White, M.R.H. (**2002**) The pH of the Plasmodium falciparum digestive vacuole: holy grail or dead-end trail? *Trends Parasitol.***,** 18, 441-444.

(160) Bray, P.G.; Mungthin, M.; Ridley, R.G.; Ward, S.A. (**1998**) Access to hematin: The basis of chloroquine resistance. *Mol. Pharmacol.***,** 54, 170-179.

(161) Bennett, T.N.; Patel, J.; Ferdig, M.T.; Roepe, P.D. (**2007**) Plasmodium falciparum Na+/H+ exchanger activity and quinine resistance. *Mol. Biochem. Parasit.***,** 153, 48-58.

(162) Hayward, R.; Saliba, K.J.; Kirk, K. (**2006**) The pH of the digestive vacuole of Plasmodium falciparum is not associated with chloroquine resistance. *Journal of Cell Science***,** 119, 1016-1025.

(163) White, N.J. (**2004**) Antimalarial drug resistance. *J. Clin. Invest.***,** 113, 1084-1092.

(164) Anderson, T.J.C.; Roper, C. (**2005**) The origins and spread of antimalarial drug resistance: Lessons for policy makers. *Act. Trop.***,** 94, 269-280.

(165) Lanzer, M.; Rohrbach, P. (**2007**) Subcellular pH And Ca^{2+} in *Plasmodium falciparum*: Implications for understanding drug resistance mechanisms. *Curr. Sci.***,** 92, 1561-1570.

(166) Warhurst, D.C. (**2007**) Understanding resistance to antimalarial 4-aminoquinolines, cinchona alkaloids and the highly hydrophobic arylaminoalcohols. *Curr. Sci.***,** 92, 1556-1560.

(167) Mita, T.; Tanabe, K.; Kita, K. (**2009**) Spread and evolution of Plasmodium falciparum drug resistance. *Parasit. Int.***,** 58, 201-209.

(168) Bustamante, C.; Batista, C.N.; Zalis, M. (**2009**) Molecular and Biological Aspects of Antimalarial Resistance in Plasmodium falciparum and Plasmodium vivax. *Curr Drug Targets***,** 10, 279-290.

(169) Fidock, D.A.; Nomura, T.; Talley, A.K.; Cooper, R.A.; Dzekunov, S.M.; Ferdig, M.T.; Ursos, L.M.B.; Sidhu, A.B.S.; Naude, B.; Deitsch, K.W.; Su, X.Z.; Wootton, J.C.; Roepe, P.D.; Wellems, T.E. (**2000**) Mutations in the P-falciparum digestive vacuole transmembrane protein PfCRT and evidence for their role in chloroquine resistance. *Mol. Cell***,** 6, 861-871.

(170) Djimde, A.; Doumbo, O.K.; Cortese, J.F.; Kayentao, K.; Doumbo, S.; Diourte, Y.; Dicko, A.; Su, X.Z.; Nomura, T.; Fidock, D.A.; Wellems, T.E.; Plowe, C.V.; Coulibaly, D. (**2001**) A molecular marker for chloroquine-resistant falciparum malaria. *New Eng. J. Med.***,** 344, 257-263.

(171) Durrand, V.; Berry, A.; Sem, R.; Glaziou, P.; Beaudou, J.; Fandeur, T. (**2004**) Variations in the sequence and expression of the Plasmodium falciparum chloroquine resistance transporter (Pfcrt) and their relationship to chloroquine resistance in vitro. *Mol. Biochem. Parasit.***,** 136, 273-285.

(172) Bodo, A.; Bakos, E.; Szeri, F.; Varadi, A.; Sarkadi, B. (**2003**) The role of multidrug, transporters in drug availability, metabolism and toxicity. *Toxicology Letters*, 140, 133-143.

(173) Klokouzas, A.; Shahi, S.; Hladky, S.B.; Barrand, M.A.; van Veen, H.W. (**2003**) ABC transporters and drug resistance in parasitic protozoa. *Int. J. Antimicrob. Agents*, 22, 301-317.

(174) Saliba, K.J.; Lehane, A.M.; Kirk, K. (**2008**) A polymorphic drug pump in the malaria parasite. *Molecular Microbiology*, 70, 775-779.

(175) Ferdig, M.T.; Cooper, R.A.; Mu, J.B.; Deng, B.B.; Joy, D.A.; Su, X.Z.; Wellems, T.E. (**2004**) Dissecting the loci of low-level quinine resistance in malaria parasites. *Molecular Microbiology*, 52, 985-997.

(176) Bray, P.G.; Hawley, S.R.; Mungthin, M.; Ward, S.A. (**1996**) Physicochemical properties correlated with drug resistance and the reversal of drug resistance in Plasmodium falciparum. *Mol. Pharmacol.*, 50, 1559-1566.

(177) Mu, J.B.; Ferdig, M.T.; Feng, X.R.; Joy, D.A.; Duan, J.H.; Furuya, T.; Subramanian, G.; Aravind, L.; Cooper, R.A.; Wootton, J.C.; Xiong, M.; Su, X.Z. (**2003**) Multiple transporters associated with malaria parasite responses to chloroquine and quinine. *Molecular Microbiology*, 49, 977-989.

(178) Krogstad, D.J.; Gluzman, I.Y.; Martin, S.K.; Oduola, A.M.J.; Kyle, D.E.; Milhous, W.K.; Schlesinger, P.H. (**1987**) Calcium-Channel Blockers and Chloroquine Uptake in Plasmodium-Falciparum. *Clinical Research*, 35, A480-A480.

(179) Martin, S.K.; Oduola, A.M.J.; Milhous, W.K. (**1987**) Reversal of Chloroquine Resistance in Plasmodium-Falciparum by Verapamil. *Science*, 235, 899-901.

(180) Hayward, R.; Saliba, K.J.; Kirk, K. (**2005**) Mutations in pfmdr1 modulate the sensitivity of Plasmodium falciparum to the intrinsic antiplasmodial activity of verapamil. *Antimicrob. Agents Chemother.*, 49, 840-842.

(181) Lakshmanan, V.; Bray, P.G.; Verdier-Pinard, D.; Johnson, D.J.; Horrocks, P.; Muhle, R.A.; Alakpa, G.E.; Hughes, R.H.; Ward, S.A.; Krogstad, D.J.; Sidhu, A.B.S.; Fidock, D.A. (**2005**) A critical role for PfCRT K76T in Plasmodium falciparum verapamil-reversible chloroquine resistance. *Embo Journal*, 24, 2294-2305.

(182) van Schalkwyk, D.A.; Egan, T.J. (**2006**) Quinoline-resistance reversing agents for the malaria parasite Plasmodium falciparum. *Drug Resis. Updates*, 9, 211-226.

(183) Gerena, L.; Bass, G.T.; Kyle, D.E.; Oduola, A.M.J.; Milhous, W.K.; Martin, R.K. (**1992**) Fluoxetine Hydrochloride Enhances Invitro Susceptibility to Chloroquine in Resistant Plasmodium-Falciparum. *Antimicrob. Agents Chemother.*, 36, 2761-2765.

(184) Bhattacharjee, A.K.; Kyle, D.E.; Vennerstrom, J.L.; Milhous, W.K. (**2002**) A 3D QSAR pharmacophore model and quantum chemical structure-activity analysis of chloroquine(CQ)-resistance reversal. *Journal of Chemical Information and Computer Sciences*, 42, 1212-1220.

(185) Alibert, S.; Santelli-Rouvier, C.; Pradines, B.; Houdoin, C.; Parzy, D.; Karolak-Wojciechowska, J.; Barbe, J. (**2002**) Synthesis and effects on chloroquine susceptibility in Plasmodium falciparum of a series of new dihydroanthracene derivatives. *J. Med. Chem.*, 45, 3195-3209.

(186) Rishton, G.M. (**2008**) Natural products as a robust source of new drugs and drug leads: Past successes and present day issues. *Am. J. Cardiol.*, 101, 43D-49D.

(187) Cordier, C.; Morton, D.; Murrison, S.; Nelson, A.; O'Leary-Steele, C. (**2008**) Natural products as an inspiration in the diversity-oriented synthesis of bioactive compound libraries. *Nat. Prod. Rep.*, 25, 719-737.

(188) Kaur, K.; Jain, M.; Kaur, T.; Jain, R. (**2009**) Antimalarials from nature. *Bioorg. Med. Chem.*, 17, 3229-3256.

(189) Krettli, A.U.; Adebayo, J.O.; Krettli, L.G. (**2009**) Testing of Natural Products and Synthetic Molecules Aiming at New Antimalarials. *Curr Drug Targets*, 10, 261-270.

(190) Oliver-Bever, B. *Medicinal Plants in Tropical West Africa*. Editors: University Press: Cambridge, **1986**.

(191) Kerharo, J. *La pharmacopée Sénégalaise traditionnelle, plantes médicinales et toxiques*. Editors: Editions Vigot Frères: **1974**.

(192) Watt, J.M.; Breyer-Brandwijk, M.G. *The medicinal and poisonous plants of Southern and Eastern Africa*. Editors: E. & S. Livingstone Ltd: London, **1962**; p 128.

(193) Bullock, A.A. (**1955**) Notes on African Asclepiadaceae. *Kew Bulletin*, 10, 279-282.

(194) Delvaux, E. (**1931**) Sur la cryptolepine. *J Pharm. Belg.*, 13, 955-976.

(195) Gellert, E.; Raymondhamet; Schlittler, E. (**1951**) Die Konstitution Des Alkaloids Cryptolepin. *Helv. Chim. Acta*, 34, 642-651.

(196) Dwuma-Badu, D.; Ayim, J.S.K.; Fiagbe, N.I.Y.; Knapp, J.E.; Schiff, P.L.; Slatkin, D.J. (**1978**) Constituents of West-African Medicinal-Plants .20. Quindoline from Cryptolepis-Sanguinolenta. *J. Pharm. Sci.*, 67, 433-434.

(197) Paulo, A.; Duarte, A.; Gomes, E.T. (**1994**) In-Vitro Antibacterial Screening of Cryptolepis-Sanguinolenta Alkaloids. *J. Ethnopharmacol.*, 44, 127-130.

(198) Paulo, A.; Gomes, E.T.; Steele, J.; Warhurst, D.C.; Houghton, P.J. (**2000**) Antiplasmodial activity of Cryptolepis sanguinolenta alkaloids from leaves and roots. *Planta Med.*, 66, 30-34.

(199) Crouch, R.C.; Davis, A.O.; Spitzer, T.D.; Martin, G.E.; Sharaf, M.M.H.; Schiff, P.L.; Phoebe, C.H.; Tackie, A.N. (**1995**) Elucidation of the Structure of Quindolinone, a Minor Alkaloid of Cryptolepis-Sanguinolenta - Submilligram H-1-C-13 and H-1-N-15 Heteronuclear Shift Correlation Experiments Using Micro Inverse-Detection. *J. Heterocycl. Chem*, 32, 1077-1080.

(200) Cimanga, K.; DeBruyne, T.; Pieters, L.; Claeys, M.; Vlietinck, A. (**1996**) New alkaloids from Cryptolepis sanguinolenta. *Tetrahedron Lett.*, 37, 1703-1706.

(201) Sharaf, M.H.M.; Schiff, P.L.; Tackie, A.N.; Phoebe, C.H.; Martin, G.E. (**1996**) Two new indoloquinoline alkaloids from Cryptolepis sanguinolenta: Cryptosanguinolentine and cryptotackieine. *J. Heterocycl. Chem*, 33, 239-243.

(202) Pousset, J.L.; Martin, M.T.; Jossang, A.; Bodo, B. (**1995**) Isocryptolepine from Cryptolepis-Sanguinolenta. *Phytochemistry*, 39, 735-736.

(203) Tackie, A.N.; Boye, G.L.; Sharaf, M.H.M.; Schiff, P.L.; Crouch, R.C.; Spitzer, T.D.; Johnson, R.L.; Dunn, J.; Minick, D.; Martin, G.E. (**1993**) Cryptospirolepine, a Unique Spiro-Nonacyclic Alkaloid Isolated from Cryptolepis-Sanguinolenta. *J. Nat. Prod.*, 56, 653-670.

(204) Sharaf, M.H.M.; Schiff, P.L.; Tackie, A.N.; Phoebe, C.H.; Howard, L.; Meyers, C.; Hadden, C.E.; Wrenn, S.K.; Davis, A.O.; Andrews, C.W.; Minick, D.; Johnson, R.L.; Shockcor, J.P.; Crouch, R.C.; Martin, G.E. (**1995**) Submicromole Structure Elucidation - Cryptolepicarboline - a Novel Dimeric Alkaloid from Cryptolepis-Sanguinolenta. *Magn. Reson. Chem*, 33, 767-778.

(205) Gunatilaka, A.A.L.; Sotheeswaran, S.; Balasubramaniam, S.; Chandrasekara, A.I.; Badrasriyani, H.T. (**1980**) Studies on Medicinal-Plants of Sri-Lanka .3. Pharmacologically Important Alkaloids of Some Sida Species. *Planta Med.*, 39, 66-72.

(206) Yang, S.W.; Abdel-Kader, M.; Malone, S.; Werkhoven, M.C.M.; Wisse, J.H.; Bursuker, I.; Neddermann, K.; Fairchild, C.; Raventos-Suarez, C.; Menendez, A.T.; Lane, K.; Kingston, D.G.I. (**1999**) Synthesis and biological evaluation of analogues of cryptolepine, an alkaloid isolated from the Suriname rainforest. *J. Nat. Prod.*, 62, 976-983.

(207) Fichter, F.; Boehringer, R. (**1906**) Ueber Chindolin "Over Quindoline". *Chem. Ber.*, 39, 3932.

(208) Armit, J.W.; Robinson, R.J. (**1922**) Polynuclear Heterocyclic Aromatic Types. Part I. Some Indenoquinoline Derivatives. *J. Chem. Soc., Trans.*, 121, 827.

(209) Holt, S.J.; Petrow, V. (**1947**) Carbazoles, Carbolines, and Related Compounds .1. Quindoline Derivatives. *J. Chem. Soc.*, 607-611.

(210) Wright, C.W.; Addae-Kyereme, J.; Breen, A.G.; Brown, J.E.; Cox, M.F.; Croft, S.L.; Gokcek, Y.; Kendrick, H.; Phillips, R.M.; Pollet, P.L. (**2001**) Synthesis and evaluation of cryptolepine analogues for their potential as new antimalarial agents. *J. Med. Chem.*, 44, 3187-3194.

(211) Cooper, M.M.; Lovell, J.M.; Joule, J.A. (**1996**) Indole-beta-nucleophilic substitution .9. Nitrogen nucleophiles. Syntheses of hydroxycryptolepine, cryptolepine, and quindoline. *Tetrahedron Lett.*, 37, 4283-4286.

(212) Gorlitzer, K.; Ventzke-Neu, K. (**1997**) 10 H-indolo[3,2-b]quinoline-5-oxide (oxyquindoline) and some of its derivatives. *Pharmazie*, 52, 919-926.

(213) Arzel, E.; Rocca, P.; Marsais, F.; Godard, A.; Queguiner, G. (**1998**) First halogen-dance reaction in quinoline series: application to a new synthesis of quindoline. *Tetrahedron Lett.*, 39, 6465-6466.

(214) Arzel, E.; Rocca, P.; Marsais, F.; Godard, A.; Queguiner, G. (**1999**) First total synthesis of cryptomisrine. *Tetrahedron*, 55, 12149-12156.

(215) Timari, G.; Soos, T.; Hajos, G. (**1997**) A convenient synthesis of two new indoloquinoline alkaloids. *Synlett*, 1067-1068.

(216) Radl, S.; Konvicka, P.; Vachal, P. (**2000**) A new approach to the synthesis of benzofuro[3,2-b]quinolines, benzothieno[3,2-b]quinolines and indolo[3,2-b]quinolines. *J. Heterocycl. Chem*, 37, 855-862.

(217) Dhanabal, T.; Sangeetha, R.; Mohan, P.S. (**2006**) Heteroatom directed photoannulation: synthesis of indoloquinoline alkaloids: cryptolepine, cryptotackieine, cryptosanguinolentine, and their methyl derivatives. *Tetrahedron*, 62, 6258-6263.

(218) Peczynska-Czoch, W.; Pognan, F.; Kaczmarek, L.; Boratynski, J. (**1994**) Synthesis and Structure-Activity Relationship of Methyl-Substituted Indole[2,3-B]Quinolines - Novel Cytotoxic, DNA Topoisomerase-Ii Inhibitors. *J. Med. Chem.*, 37, 3503-3510.

(219) Alajarin, M.; Molina, P.; Vidal, A. (**1997**) Formal total synthesis of the alkaloid cryptotackieine (neocryptolepine). *J. Nat. Prod.*, 60, 747-748.

(220) Molina, P.; Fresneda, P.M.; Delgado, S. (**1999**) Iminophosphorane-mediated synthesis of the alkaloid cryptotackieine. *Synthesis-Stuttgart*, 326-329.

(221) Sundaram, G.S.M.; Venkatesh, C.; Kumar, U.K.S.; Ila, H.; Junjappa, H. (**2004**) A concise formal synthesis of alkaloid cryptotackiene and substituted 6H-indolo[2,3-b]quinolines. *J. Org Chem.*, 69, 5760-5762.

(222) Parvatkar, P.T.; Parameswaran, P.S.; Tilve, S.G. (**2007**) Double reductive cyclization: a facile synthesis of the indoloquinoline alkaloid cryptotackieine. *Tetrahedron Lett.*, 48, 7870-7872.

(223) Dubovitskii, S.V.; Radchenko, O.S.; Novikov, Y.L. (**1996**) Synthesis of isocryptolepine, an alkaloid from Cryptolepis sanguinolenta. *Russ. Chem. Bull.*, 45, 2656-2657.

(224) Go, M.L.; Koh, H.L.; Ngiam, T.L.; Phillipson, J.D.; Kirby, G.C.; Oneill, M.J.; Warhurst, D.C. (**1992**) Synthesis and Invitro Antimalarial Activity of Some Indolo[3,2-C]Quinolines. *Eur. J. Med. Chem.*, 27, 391-394.

(225) Molina, P.; Alajarin, M.; Vidal, A. (**1990**) New Methodology for the Preparation of Pyrrole and Indole-Derivatives Via Iminophosphoranes - Synthesis of Pyrrolo[1,2-a]Quinoxalines, Indolo[3,2-C]Quinolines and Indolo[1,2-C]Quinazolines. *Tetrahedron*, 46, 1063-1078.

(226) Murray, P.E.; Mills, K.; Joule, J.A. (**1998**) A synthesis of isocryptolepine. *J. Chem. Research-S*, 377-377.

(227) Jonckers, T.H.; Maes, B.U.W.; Lemiere, G.L.F.; Rombouts, G.; Pieters, L.; Haemers, A.; Dommisse, R.A. (**2003**) Synthesis of isocryptolepine via a Pd-catalyzed 'Amination-Arylation' approach. *Synlett*, 615-618.

(228) Meyers, C.; Rornbouts, G.; Loones, K.T.J.; Coelho, A.; Maes, B.U.W. (**2008**) Auto-tandem catalysis: Synthesis of substituted 11H-indolo [3,2-c]quinolines via palladium-catalyzed intermolecular C-N and intramolecular C-C bond formation. *Adv. Synth. Catal.*, 350, 465-470.

(229) Beauchard, A.; Chabane, H.; Sinbandhit, S.; Guenot, P.; Thiery, V.; Besson, T. (**2006**) Synthesis of original thiazoloindolo[3,2-c]quinoline and novel 8-N-substituted-11H-indolo[3,2-c]quinoline derivatives from benzotriazoles. Part I. *Tetrahedron*, 62, 1895-1903.

(230) Walser, A.; Silverman, G.; Flynn, T.; Fryer, R.I. (**1975**) Nucleophilic Displacement of Aromatic Fluorine .3. Indoloquinolines and Benzofuranoquinolines. *J. Heterocycl. Chem*, 12, 351-358.

(231) Kanaoka, Y.; Nakao, S.; Hatanaka, Y. (**1976**) Stereochemistry of Nonoxidative Photocyclization of Indole-2-Carboxanilides to an Indolo[2,3-C]Quinoline System. *Heterocycles*, 5, 261-266.

(232) Hostyn, S.; Maes, B.U.W.; Pieters, L.; Lemiere, G.L.F.; Matyus, P.; Hajos, G.; Dommisse, R.A. (**2005**) Synthesis of the benzo-beta-carboline isoneocryptolepine: the missing indoloquinoline isomer in the alkaloid series cryptolepine, neocryptolepine and isocryptolepine. *Tetrahedron*, 61, 1571-1577.

(233) Hostyn, S.; Maes, B.U.W.; Van Baelen, G.; Gulevskaya, A.; Meyers, C.; Smits, K. (**2006**) Synthesis of 7H-indolo[2,3-c]quinolines: Study of the Pd-catalyzed intramolecular arylation of 3-(2-bromophenylamino)quinolines under microwave irradiation. *Tetrahedron*, 62, 4676-4684.

(234) Dabaien, S.A.; El-Abadelab, M.M.; Haddad, S.F.; Duddeck, H. (**2007**) Pictet-spengler synthesis of some new indolo[2,3-c]quinolines. *Heterocycles*, 71, 835-846.

(235) Onyeibor, O.; Croft, S.L.; Dodson, H.I.; Feiz-Haddad, M.; Kendrick, H.; Millington, N.J.; Parapini, S.; Phillips, R.M.; Seville, S.; Shnyder, S.D.; Taramelli, D.; Wright, C.W. (**2005**) Synthesis of some cryptolepine analogues, assessment of their antimalarial and cytotoxic activities, and consideration of their antimalarial mode of action. *J. Med. Chem.*, 48, 2701-2709.

(236) Ablordeppey, S.Y.; Fan, P.C.; Clark, A.M.; Nimrod, A. (**1999**) Probing the N-5 region of the indoloquinoline alkaloid, cryptolepine for anticryptococcal activity. *Bioorg. Med. Chem.*, 7, 343-349.

(237) Ablordeppey, S.Y.; Fan, P.C.; Li, S.M.; Clark, A.M.; Hufford, C.D. (**2002**) Substituted indoloquinolines as new antifungal agents. *Bioorg. Med. Chem.*, 10, 1337-1346.

(238) Seville, S.; Phillips, R.M.; Shnyder, S.D.; Wright, C.W. (**2007**) Synthesis of cryptolepine analogues as potential bioreducible anticancer agents. *Bioorg. Med. Chem.*, 15, 6353-6360.

(239) Yamato, M.; Takeuchi, Y.; Chang, M.R.; Hashigaki, K. (**1992**) Synthesis and Antitumor-Activity of Fused Quinoline Derivatives .2. Novel 4-Hydroxyindolo[3,2-B]Quinolines and 7-Hydroxyindolo[3,2-B]Quinolines. *Chem. Pharm. Bull.*, 40, 528-530.

(240) Fan, P.C.; Ablordeppey, S.Y. (**1997**) An alternative synthesis of 10H-indolo[3,2-b]quinoline and its selective N-alkylation. *J. Heterocycl. Chem*, 34, 1789-1794.

(241) Yamato, M.; Takeuchi, Y.; Chang, M.R.; Hashigaki, K.; Tsuruo, T.; Tashiro, T.; Tsukagoshi, S. (**1990**) Synthesis and Antitumor-Activity of Fused Quinoline Derivatives. *Chem. Pharm. Bull.*, 38, 3048-3052.

(242) Chang, M.; Takeuchi, Y.; Hashigaki, K.; Yamato, M. (**1992**) Synthesis of 7-Substituted Indolo[3,2-B]Quinoline Derivatives. *Heterocycles*, 33, 147-152.

(243) Gorlitzer, K.; Stockmann, R.; Walter, R.D. (**1994**) Anti-Malaria Active 10h-Indol[3,2-B]Quinoline-11-Ylamines .1. Phenol-Mannich-Bases of the Amodiaquine and Cycloquine Type. *Pharmazie*, 49, 231-235.

(244) Takeuchi, Y.; Oda, T.; Chang, M.R.; Okamoto, Y.; Ono, J.; Oda, Y.; Harada, K.; Hashigaki, K.; Yamato, M. (**1997**) Synthesis and antitumor activity of fused quinoline derivatives .4. Novel 11-aminoindolo[3,2-b]quinolines. *Chem. Pharm. Bull.*, 45, 406-411.

(245) Takeuchi, Y.; Kitaomo, M.; Chang, M.R.; Shirasaka, S.; Shimamura, C.; Okuno, Y.; Yamato, M.; Harayama, T. (**1997**) Synthesis and antitumor activity of fused quinoline derivatives. V. Methylindolo[3,2-b]quinolines. *Chem. Pharm. Bull.*, 45, 2096-2099.

(246) Jerrum, P.W.; Wright, C.W.; Phillips, R.M.; Gouni, S.R.; Brown, J.E.; Carrington, S. (**2006**) Synthesis and in vitro cytotoxicity evaluation of novel iodocryptolepine analogues. *J. Pharm. Pharmacol.*, 58, A59-A59.

(247) Zhu, X.Y.; Mardenborough, L.G.; Li, S.M.; Khan, A.; Zhang, W.; Fan, P.C.; Jacob, M.; Khan, S.; Walker, L.; Ablordeppey, S.Y. (**2007**) Synthesis and evaluation of isosteres of N-methyl indolo[3,2-b]-quinoline (cryptolepine) as new antfinfective. *Bioorg. Med. Chem.*, 15, 686-695.

(248) Wan, S.B.; Liu, Z.L.; Chen, D.; Dou, Q.P.; Jiang, T. (**2007**) Polyphosphorous acid catalyzed cyclization in the synthesis of cryptolepine derivatives. *Chin. Chem. Lett*, 18, 1179-1181.

(249) Lavrado, J.; Paulo, A.; Gut, J.; Rosenthal, P.J.; Moreira, R. (**2008**) Cryptolepine analogues containing basic aminoalkyl side-chains at C-11: Synthesis, antiplasmodial activity, and cytotoxicity. *Bioorg. Med. Chem. Lett.*, 18, 1378-1381.

(250) Dalton, L.; Humphrey, G.L.; Cooper, M.M.; Joule, J.A. (**1983**) Indole Beta-Nucleophilic Substitution .7. Beta-Halogenation of Indoles - Attempted Intramolecular Beta-Nucleophilic Substitution of Alpha-Arylindoles. *J. Chem. Soc., Perkin Trans. 1*, 2417-2422.

(251) Etukala, J.R.; Kumar, E.; Ablordeppey, S.Y. (**2008**) A short and convenient synthesis and evaluation of the antiinfective properties of indoloquinoline alkaloids: 10H-Indolo[3,2-b]quinoline and 7H-indolo[2,3-c]quinolines. *J. Heterocycl. Chem*, 45, 507-511.

(252) Vaitiekunas, A.; Nord, F.F. (**1953**) Studies on the Chemistry of Heterocyclics .22. Investigations on the Mechanism of Reactions of 2-Thienyl Halides with Sodium Amide and Sodium Acetylide in Liquid Ammonia. *J. Am. Chem. Soc.*, 75, 1764-1768.

(253) Schnurch, M.; Spina, M.; Khan, A.F.; Mihovilovic, M.D.; Stanetty, P. (**2007**) Halogen dance reactions - A review. *Chem. Soc. rev.*, 36, 1046-1057.

(254) Miyaura, N.; Suzuki, A. (**1995**) Palladium-Catalyzed Cross-Coupling Reactions of Organoboron Compounds. *Chem. Rev.*, 95, 2457-2483.

(255) Arzel, E.; Rocca, P.; Grellier, P.; Labaeid, M.; Frappier, F.; Gueritte, F.; Gaspard, C.; Marsais, F.; Godard, A.; Queguiner, G. (**2001**) New synthesis of benzo-delta-carbolines, cryptolepines, and their salts: In vitro cytotoxic, antiplasmodial, and antitrypanosomal activities of delta-caribolines, benzo-delta-carbolines, and cryptolepines. *J. Med. Chem.*, 44, 949-960.

(256) Csanyi, D.; Timari, G.; Hajos, G. (**1999**) An alternative synthesis of quindoline and one of its closely related derivatives. *Synth. Commun.*, 29, 3959-3969.

(257) Ford, A.; Sinn, E.; Woodward, S. (**1997**) Exploitation of differential reactivity of the carbon-chlorine bonds in 1,3-dichloroisoquinoline. Routes to new N,N-chelate ligands and 1,3-disubstituted isoquinolines. *J. Chem. Soc., Perkin Trans. 1*, 927-934.

(258) Schultz, A.G.; Napier, J.J.; Ravichandran, R. (**1983**) Synthetic Applications of Heteroatom-Directed Photoarylation - Benzo[B]Furan Ring Construction. *J. Org Chem.*, 48, 3408-3412.

(259) Dutta, B.; Some, S.; Ray, J.K. (**2006**) Thermal cyclization of 3-arylamino-3-(2-nitrophenyl)-propenal Schiff base hydrochlorides followed by triethyl phosphite mediated deoxygenation: a facile synthesis of quindolines. *Tetrahedron Lett.*, 47, 377-379.

(260) Soderberg, B.C.G. (**2000**) Synthesis of heterocycles via intramolecular annulation of nitrene intermediates. *Curr. Org. Chem.*, 4, 727-764.

(261) Kumar, E.V.K.S.; Etukala, J.R.; Ablordeppey, S.Y. (**2008**) Indolo[3,2-b]quinolines: synthesis, biological evaluation and structure activity-relationships. *Mini Rev Med Chem*, 8, 538-54.

(262) Wright, C.W. (**2007**) Recent developments in naturally derived antimalarials: cryptolepine analogues. *J. Pharm. Pharmacol.*, 59, 899-904.

(263) Cimanga, K.; DeBruyne, T.; Pieters, L.; Vlietinck, A.J. (**1997**) In vitro and in vivo antiplasmodial activity of cryptolepine and related alkaloids from Cryptolepis sanguinolenta. *J. Nat. Prod.*, 60, 688-691.

(264) Kirby, G.C.; Paine, A.; Warhurst, D.C.; Noamese, B.K.; Phillipson, J.D. (**1995**) In-Vitro and in-Vivo Antimalarial Activity of Cryptolepine, a Plant-Derived Indoloquinoline. *Phytother. Res.*, 9, 359-363.

(265) Cimanga, K.; DeBruyne, T.; Lasure, A.; VanPoel, B.; Pieters, L.; Claeys, M.; VandenBerghe, D.; Kambu, K.; Tona, L.; Vlietinck, A.J. (**1996**) In vitro biological activities of alkaloids from Cryptolepis sanguinolenta. *Planta Med.*, 62, 22-27.

(266) Grellier, P.; Ramiaramanana, L.; Millerioux, V.; Deharo, E.; Schrevel, J.; Frappier, F.; Trigalo, F.; Bodo, B.; Pousset, J.L. (**1996**) Antimalarial activity of cryptolepine and isocryptolepine, alkaloids isolated from Cryptolepis sanguinolenta. *Phytother. Res.*, 10, 317-321.

(267) Jonckers, T.H.M.; van Miert, S.; Cimanga, K.; Bailly, C.; Colson, P.; De Pauw-Gillet, M.C.; van den Heuvel, H.; Claeys, M.; Lemiere, F.; Esmans, E.L.; Rozenski, J.; Quirijnen, L.; Maes, L.; Dommisse, R.; Lemiere, G.L.F.; Vlietinck, A.; Pieters, L. (**2002**) Synthesis, cytotoxicity, and antiplasmodial and antitrypanosomal activity of new neocryptolepine derivatives. *J. Med. Chem.*, 45, 3497-3508.

(268) Lavrado, J.; Paulo, A.; Gut, J.; Rosenthal, P.J.; Moreira, R. (**2008**) Cryptolepine analogues containing basic aminoalkyl side-chains at C-11: synthesis, antiplasmodial activity, and cytotoxicity. *Bioorg. Med. Chem. Lett.*, 18, 1378-81.

(269) Van Miert, S.; Hostyn, S.; Maes, B.U.W.; Cimanga, K.; Brun, R.; Kaiser, M.; Matyus, P.; Dommisse, R.; Lemiere, G.; Vlietinck, A.; Pieters, L. (**2005**) Isoneocryptolepine, a synthetic indoloquinoline alkaloid, as an antiplasmodial lead compound. *J. Nat. Prod.*, 68, 674-677.

(270) Van Baelen, G.; Meyers, C.; Lemiere, G.L.F.; Hostyn, S.; Dommisse, R.; Maes, L.; Augustyns, K.; Haemers, A.; Pieters, L.; Maes, B.U.W. (**2008**) Synthesis of 6-methyl-6H-indolo[3,2-c]isoquinoline and 6-methyl-6H-indolo [2,3-c]isoquinoline: two new unnatural isoquinoline isomers of the cryptolepine series. *Tetrahedron*, 64, 11802-11809.

(271) Mardenborough, L.G.; Zhu, X.Y.; Fan, P.C.; Jacob, M.R.; Khan, S.I.; Walker, L.A.; Ablordeppey, S.Y. (**2005**) Identification of bis-quindolines as new antiinfective agents. *Bioorg. Med. Chem.*, 13, 3955-3963.

(272) Van Miert, S.; Jonckers, T.; Cimanga, K.; Maes, L.; Maes, B.; Lemiere, G.; Dommisse, R.; Vlietinck, A.; Pieters, L. (**2004**) In vitro inhibition of beta-haematin formation, DNA interactions, antiplasmodial activity, and cytotoxicity of synthetic neocryptolepine derivatives. *Exp. Parasit.*, 108, 163-168.

(273) Wright, R.G.M.; Wakelin, L.P.G.; Fieldes, A.; Acheson, R.M.; Waring, M.J. (**1980**) Effects of Ring Substituents and Linker Chains on the Bifunctional Intercalation of Diacridines into Deoxyribonucleic-Acid. *Biochemistry***,** 19, 5825-5836.

(274) Bonjean, K.; Pauw-Gillet, M.C.D.; Quetin-Leclercq, J.; Wright, C.W.; L.Angenot; Bassleer, R. (**1996**) Critical evaluation of the DNA-methyl green assay: application to some indole alkaloids. *Phytother. Res.***,** 10, S159-S160.

(275) Dassonneville, L.; Lansiaux, A.; Wattelet, A.; Wattez, N.; Mahieu, C.; Van Miert, S.; Pieters, L.; Bailly, C. (**2000**) Cytotoxicity and cell cycle effects of the plant alkaloids cryptolepine and neocryptolepine: relation to drug-induced apoptosis. *Eur. J. Pharmacol.***,** 409, 9-18.

(276) Ansah, C.; Khan, A.; Gooderham, N.J. (**2005**) In vitro genotoxicity of the West African anti-malarial herbal Cryptolepis sanguinolenta and its major alkaloid cryptolepine. *Toxicology***,** 208, 141-147.

(277) Lisgarten, J.N.; Pous, J.; Coll, M.; Wright, C.W.; Aymami, J. (**2002**) Crystallization and preliminary X-ray analysis of the antimalarial and cytotoxic alkaloid cryptolepine complexed with the DNA fragment d(CCTAGG)(2). *Acta Crystallogr., Sect D: Biol. Crystallogr.***,** 58, 312-313.

(278) Guittat, L.; Alberti, P.; Rosu, F.; Van Miert, S.; Thetiot, E.; Pieters, L.; Gabelica, V.; De Pauw, E.; Ottaviani, A.; Riou, J.F.; Mergny, J.L. (**2003**) Interactions of cryptolepine and neocryptolepine with unusual DNA structures. *Biochimie***,** 85, 535-547.

(279) Olajide, O.A.; Heiss, E.H.; Schachner, D.; Wright, C.W.; Vollmar, A.M.; Dirsch, V.M. (**2007**) Synthetic cryptolepine inhibits DNA binding of NF-kappa B. *Bioorg. Med. Chem.***,** 15, 43-49.

(280) Zhu, J.Z.; Krishnegowda, G.; Gowda, D.C. (**2005**) Induction of proinflammatory responses in macrophages by the Glycosylphosphatidylinositols of Plasmodium falciparum - The requirement of extracellular signal-regulated kinase, p38, c-Jun N-terminal kinase and NF-kappa B pathways for the expression of proinflammatory cytokines and nitric oxide. *J. Biol. Chem.***,** 280, 8617-8627.

(281) Matsui, T.A.; Sowa, Y.; Murata, H.; Takagi, K.; Nakanishi, R.; Aoki, S.; Yoshikawa, M.; Kobayashi, M.; Sakabe, T.; Kubo, T.; Sakai, T. (**2007**) The plant alkaloid cryptolepine induces p21(WAF1/C1P1) and cell cycle arrest in a human osteosarcoma cell line. *Int. J. Oncol.***,** 31, 915-922.

(282) Caprio, V.; Guyen, B.; Opoku-Boahen, Y.; Mann, J.; Gowan, S.M.; Kelland, L.M.; Read, M.A.; Neidle, S. (**2000**) A novel inhibitor of human telomerase derived from 10H-indolo[3,2-b]quinoline. *Bioorg. Med. Chem. Lett.***,** 10, 2063-2066.

(283) Spicer, J.A.; Gamage, S.A.; Atwell, G.J.; Finlay, G.J.; Baguley, B.C.; Denny, W.A. (**1997**) Structure-activity relationships for acridine-substituted analogues of the mixed topoisomerase I/II inhibitor N-[2-(dimethylamino)ethyl]acridine-4-carboxamide. *J. Med. Chem.***,** 40, 1919-1929.

(284) Guyen, B.; Schultes, C.M.; Hazel, P.; Mann, J.; Neidle, S. (**2004**) Synthesis and evaluation of analogues of 10H-indolo[3,2-b]-quinoline as G-quadruplex stabilising ligands and potential inhibitors of the enzyme telomerase. *Org. Biomol. Chem.***,** 2, 981-988.

(285) Chen, J.J.; Deady, L.W.; Desneves, J.; Kaye, A.J.; Finlay, G.J.; Baguley, B.C.; Denny, W.A. (**2000**) Synthesis of substituted indeno[1,2-b]quinoline-6-carboxamides, [1]benzothieno[3,2-b]quinoline-4-carboxamides and 10H-quindoline-4-carboxamides: Evaluation of structure-activity relationships for cytotoxicity. *Bioorg. Med. Chem.***,** 8, 2461-2466.

(286) Chen, J.J.; Deady, L.W.; Kaye, A.J.; Finlay, G.J.; Baguley, B.C.; Denny, W.A. (**2002**) Synthesis and cytotoxic activity of N-(2-diethylamino)ethylcarboxamide and other derivatives of 10H-quindoline. *Bioorg. Med. Chem.***,** 10, 2381-2386.

(287) Le Sann, C.; Huddleston, J.; Mann, J. (**2007**) Synthesis and preliminary evaluation of novel analogues of quindolines as potential stabilisers of telomeric G-quadruplex DNA. *Tetrahedron***,** 63, 12903-12911.

(288) Zhou, J.L.; Lu, Y.J.; Ou, T.M.; Zhou, J.M.; Huang, Z.S.; Zhu, X.F.; Du, C.J.; Bu, X.Z.; Ma, L.; Gu, L.Q.; Li, Y.M.; Chan, A.S.C. (**2005**) Synthesis and evaluation of quindoline derivatives as G-quadruplex inducing and stabilizing ligands and potential inhibitors of telomerase. *J. Med. Chem.*, 48, 7315-7321.

(289) Ou, T.M.; Lu, Y.J.; Zhang, C.; Huang, Z.S.; Wang, X.D.; Tan, J.H.; Chen, Y.; Ma, D.L.; Wong, K.Y.; Tang, J.C.O.; Chan, A.S.C.; Gu, L.Q. (**2007**) Stabilization of G-quadruplex DNA and down-regulation of oncogene c-myc by quindoline derivatives. *J. Med. Chem.*, 50, 1465-1474.

(290) Zhang, C.; Wu, W.B.; Lu, Y.J.; Gu, L.Q.; Huang, Z.S. (**2008**) Molecular modeling studies of interactions between quindoline derivatives and G-quadruplex. *Acta Chim. Sinica*, 66, 953-958.

(291) Lu, Y.J.; Ou, T.M.; Tan, J.H.; Hou, J.Q.; Shao, W.Y.; Peng, D.; Sun, N.; Wang, X.D.; Wu, W.B.; Bu, X.Z.; Huang, Z.S.; Ma, D.L.; Wong, K.Y.; Gu, L.Q. (**2008**) 5-N-Methylated quindoline derivatives as telomeric G-quadruplex stabilizing ligands: effects of 5-N positive charge on quadruplex binding affinity and cell proliferation. *J. Med. Chem.*, 51, 6381-6392.

(292) Noamesi, B.K.; Larsson, B.S.; Laryea, D.L.; Ullberg, S. (**1991**) Whole-Body Autoradiographic Study on the Distribution of H-3 Cryptolepine in Mice. *Archives Internationales De Pharmacodynamie Et De Therapie*, 313, 5-14.

(293) Raymont-Hamet. (**1937**) Sur quelque propriétés physiologiques des alcaloides du *Cryptolepis sanguinolenta* Schlechter. *Compt. Rend. Soc. Biol.*, 126, 768-770.

(294) Ansa-Asamoah, R.; Asante-Frempong, K. In *Preliminary studies on the short term toxicity of cryptolepine in mice*, **First international seminar on cryptolepine**, Faculty of Pharmacy of Kumasi, 1983; Boakye-Yiadom, K.; Bamgbose, S.O., Eds. Faculty of Pharmacy of Kumasi, **1983**; pp 52-56.

(295) Krongauz, E.S.; Rusanov, A.L.; Renard, T.L. (**1970**) Polyphosphoric Acid in Cyclisation and Polycyclisation Reactions *Russ. Chem. Rev.*, 39, 747-765.

(296) Meerwein, H.; Battenberg, E.; Gold, H.; Pfeil, E.; Willfang, G. (**1939**) On tertiary oxonium salts, II. *J Praktische Chemie*, 154, 83-156.

(297) Meerwein, H.; Hinz, G.; Hofmann, P.; Kroning, E.; Pfeil, E. (**1937**) The tertiary oxonium salts, I. *J Praktische Chemie*, 147, 257-285.

(298) Curphey, T.J. (**1988**) Trimethyloxonium Tetrafluoroborate. *Org Synth*, 50-9, 1019-1023.

(299) Mandal, P.K.; McMurray, J.S. (**2007**) Pd-C-induced catalytic transfer hydrogenation with triethylsilane. *J. Org Chem.*, 72, 6599-6601.

(300) Yu, J.Q.; Spencer, J.B. (**1997**) Regioselective hydrometalation of alkenes reveals the amphipolar nature of the Pd-H bond in heterogeneous hydrogenation. *J. Org Chem.*, 62, 8618-8619.

(301) Marciniec, B. (**2005**) Catalysis by transition metal complexes of alkene silylation - recent progress and mechanistic implications. *Coordination Chemistry Reviews*, 249, 2374-2390.

(302) Spitzer, T.D.; Crouch, R.C.; Martin, G.E.; Sharaf, M.H.M.; Schiff, P.L.; Tackie, A.N.; Boye, G.L. (**1991**) Total assignment of the proton and carbon NMR-spectra of the alkaloid quindoline - utilization of HMQC-TOCSY to indirectly establish protonated carbon-protonated carbon connectivities. *J. Heterocycl. Chem*, 28, 2065-2070.

(303) Ablordeppey, S.Y.; Hufford, C.D.; Borne, R.F.; Dwuma-Badu, D. (**1990**) ^{1}H-NMR and ^{13}C-NMR assignments of cryptolepine. A 3,4-benz-δ-carboline derivative isolated from *Cryptolepis sanguinolenta*. *Planta Med*, 56, 416-7.

(304) Silverstein, R.M.; Webster, F.X.; Kiemle, D.J. *Spectrometric Identification of Organic Compounds*. Editors: 7th ed.; John Wiley & Sons, Inc: Hoboken, USA, **2005**; p 502.

(305) Szakacs, Z.; Kraszni, M.; Noszal, B. (**2004**) Determination of microscopic acid-base parameters from NMR-pH titrations. *Anal Bioanal Chem*, 378, 1428-1448.

(306) Clayden, J.; Geeves, N.; Warren, S. Acidity, basicity, and pKa. In ***Organic Chemistry***, Oxford University Press: Oxford, **2001**; pp 181-208.

(307) Grycová, L.; Dommisse, R.; Pieters, L.; Marek, R. (**2009**) NMR determination of pKa values of indoloquinoline alkaloids. *Magn. Reson. Chem*, 47, 977-981.

(308) Box, K.J.; Donkor, R.E.; Jupp, P.A.; Leader, I.P.; Trew, D.F.; Turner, C.H. (**2008**) The chemistry of multi-protic drugs - Part 1: A potentiometric, multi-wavelength UV and NMR pH titrimetric study of the micro-speciation of SKI-606. *Journal of Pharmaceutical and Biomedical Analysis*, 47, 303-311.

(309) Babic, S.; Horvat, A.J.M.; Pavlovic, D.M.; Kastelan-Macan, M. (**2007**) Determination of pK(a) values of active pharmaceutical ingredients. *TrAC, Trends Anal. Chem.*, 26, 1043-1061.

(310) Goldman, J.A.; Meites, L. (**1964**) Theory of Titration Curves .3. Locations of Points at Which Ph-Pka on Potentiometric Acid-Base Titration Curves - End-Point Errors in Titrations to Predetermined Ph Values. *Analytica Chimica Acta*, 30, 28-&.

(311) Benet, L.Z.; Goyan, J.E. (**1967**) Potentiometric Determination of Dissociation Constants. *J. Pharm. Sci.*, 56, 665-&.

(312) Allen, R.I.; Box, K.J.; Comer, J.E.A.; Peake, C.; Tam, K.Y. (**1998**) Multiwavelength spectrophotometric determination of acid dissociation constants of ionizable drugs. *Journal of Pharmaceutical and Biomedical Analysis*, 17, 699-712.

(313) Szakacs, Z.; Hagele, G. (**2004**) Accurate determination of low pK values by H-1 NMR titration. *Talanta*, 62, 819-825.

(314) Gomez-Zaleta, B.; Ramirez-Silva, M.T.; Gutierrez, A.; Gonzalez-Vergara, E.; Guizado-Rodriguez, M.; Rojas-Hernandez, A. (**2006**) UV/vis, H-1, and C-13 NMR spectroscopic studies to determine mangiferin pK(a) values. *Spectrochimica Acta Part a-Molecular and Biomolecular Spectroscopy*, 64, 1002-1009.

(315) Hilal, S.H.; Karickhoff, S.W.; Carreira, L.A. (**1995**) A rigorous test for SPARC's chemical reactivity models: Estimation of more than 4300 ionization pK(a)s. *Quant. Struct.-Act. Relat*, 14, 348-355.

(316) Hilal, S.H.; ElShabrawy, Y.; Carreira, L.A.; Karickhoff, S.W.; Toubar, S.S.; Rizk, M. (**1996**) Estimation of the ionization pK(a) of pharmaceutical substances using the computer program SPARC. *Talanta*, 43, 607-619.

(317) Lee, P.H.; Ayyarnpalayarn, S.N.; Carreira, L.A.; Shalaeva, M.; Bhattachar, S.; Coselmon, R.; Poole, S.; Gifford, E.; Lombardo, F. (**2007**) In silico prediction of ionization constants of drugs. *Mol. Pharmaceut.*, 4, 498-512.

(318) IUPAC. (**1997**) Reference Value Standards and Primary Standards for pH Measurements in D_2O and Aqueous-Organic Solvent mixtures Mixtures: New Accessions and Assessments. *Pure Appl. Chem.*, 69, 1007-1014.

(319) Krezel, A.; Bal, W. (**2004**) A formula for correlating pK(a) values determined in D_2O and H_2O. *J. Inorg. Biochem.*, 98, 161-166.

(320) Holmes, D.L.; Lightner, D.A. (**1995**) Synthesis and acidity constants of 13CO2H-labelled mono and dipyrrole carboxylic acids. pKa from 13C-NMR. *Tetrahedron*, 51, 1607-1622.

(321) Hall, H.K. (**1957**) Correlation of the Base Strengths of Amines. *J. Am. Chem. Soc.*, 79, 5441-5444.

(322) Seybold, P.G. (**2008**) Analysis of the pK(a)s of Aliphatic Amines Using Quantum Chemical Descriptors. *International Journal of Quantum Chemistry*, 108, 2849-2855.

(323) Hall, H.K. (**1957**) Steric Effects on the Base Strengths of Cyclic Amines. *J. Am. Chem. Soc.*, 79, 5444-5447.

(324) Vonhippel, P.H.; Bear, D.G.; Morgan, W.D.; Mcswiggen, J.A. (**1984**) Protein Nucleic-Acid Interactions in Transcription - a Molecular Analysis. *Annu Rev Biochem*, 53, 389-446.

(325) Anderson, C.F.; Record, M.T. (**1982**) Poly-Electrolyte Theories and Their Applications to DNA. *Annual Review of Physical Chemistry*, 33, 191-222.

(326) Mcghee, J.D.; Hippel, P.H.V. (**1974**) Theoretical Aspects of DNA-Protein Interactions - Cooperative and Non-Cooperative Binding of Large Ligands to a One-Dimensional Homogeneous Lattice. *Journal of Molecular Biology*, 86, 469-489.

(327) Al-Soufi, W.; Reija, B.; Felekyan, S.; Seidel, C.A.M.; Novo, M. (**2008**) Dynamics of supramolecular association monitored by fluorescence correlation spectroscopy. *Chemphyschem*, 9, 1819-1827.

(328) Chen, Z.; Weber, S.G. (**2008**) Determination of binding constants by affinity capillary electrophoresis, electrospray ionization mass spectrometry and phase-distribution methods. *TrAC, Trends Anal. Chem.*, 27, 738-748.

(329) Rosu, F.; De Pauw, E.; Gabelica, V. (**2008**) Electrospray mass spectrometry to study drug-nucleic acids interactions. *Biochimie*, 90, 1074-1087.

(330) Jiang, C.X.; Armstrong, D.W. (**2010**) Use of CE for the determination of binding constants. *Electrophoresis*, 31, 17-27.

(331) Raffa, R.B. (**1999**) (Extra)thermodynamics of the drug-receptor interaction. *Life Sci.*, 65, 967-980.

(332) Sideris, E.E.; Georgiou, C.A.; Koupparis, M.A.; Macheras, P.E. (**1994**) Automated Flow-Injection Serial Dynamic Dialysis Technique in the Study of Drug-Binding with Cyclodextrins. *Analytica Chimica Acta*, 289, 87-95.

(333) Masson, M.; Sigurdardottir, B.V.; Matthiasson, K.; Loftsson, T. (**2005**) Investigation of drug-cyclodextrin complexes by a phase-distribution method: Some theoretical and practical considerations. *Chem. Pharm. Bull.*, 53, 958-964.

(334) Archontaki, H.A.; Vertzoni, M.V.; Athanassiou-Malaki, M.H. (**2002**) Study on the inclusion complexes of bromazepam with beta- and beta-hydroxypropyl-cyclodextrins. *Journal of Pharmaceutical and Biomedical Analysis*, 28, 761-769.

(335) Fini, P.; Catucci, L.; Castagnolo, M.; Cosma, P.; Pluchinotta, V.; Agostiano, A. (**2007**) Spectroscopic investigation of Rose Bengal/cyclodextrin interactions in aqueous solution: the case of the hydroxypropyl-cyclodextrins. *J Incl Phenom Macro*, 57, 663-668.

(336) Sheehy, P.A.; Ramstad, T. (**2005**) Determination of the molecular complexation constant between alprostadil and alpha-cyclodextrin by conductometry - Implications for a freeze-dried formulation. *Journal of Pharmaceutical and Biomedical Analysis*, 39, 877-885.

(337) Fielding, L. (**2000**) Determination of association constants (K_a) from solution NMR data. *Tetrahedron*, 56, 6151-6170.

(338) Fox, K.R. Methods in Molecular Biology: *Drug-DNA Interaction Protocols*. Editors: Walker, J.M.; 1st ed.; Humana Press: Totowa NJ, **1997**; Vol. 90, p 288

(339) Job, P. (**1928**) Studies on the formation of complex minerals in solution and on their stability. *Ann Chim France*, 9, 113-203.

(340) Ingham, K.C. (**1975**) Application of Jobs Method of Continuous Variation to Stoichiometry of Protein-Ligand Complexes. *Anal. Biochem.*, 68, 660-663.

(341) Huang, C.Y. (**1982**) Determination of Binding Stoichiometry by the Continuous Variation Method - the Job Plot. *Methods Enzymol.*, 87, 509-525.

(342) Hill, Z.D.; Maccarthy, P. (**1986**) Novel-Approach to Job Method - an Undergraduate Experiment. *J Chem Educ*, 63, 162-167.

(343) Vosburgh, W.C.; Cooper, G.R. (**1941**) Complex Ions. I. The Identification of Complex Ions in Solution by Spectrophotometric Measurements. *J. Am. Chem. Soc.*, 63, 437–442.

(344) Woldbye, F. (**1955**) On the Method of Continuous Variations *Acta. Chem. Scand.*, 9, 299-309.

(345) Dickerson, R.E.; Ng, H.L. (**2001**) DNA structure from A to B. *Proc. Nat. Acad. Sci. U.S.A.*, 98, 6986-6988.

(346) Owczarzy, R.; Gallo, F.J.; Benight, A.S. (**1997**) Global comparison of published nearest-neighbor sequence dependent thermodynamic parameters. *Biophysical Journal*, 72, Th429-Th429.

(347) Vallone, P.M.; Owczarzy, R.; Gallo, F.J.; Benight, A.S. (**1997**) Predicting melting temperatures of short duplex DNA oligomers. *Biophysical Journal*, 72, Th425-Th425.

(348) SantaLucia, J. (**1998**) A unified view of polymer, dumbbell, and oligonucleotide DNA nearest-neighbor thermodynamics. *Proc. Nat. Acad. Sci. U.S.A.*, 95, 1460-1465.

(349) Nakamoto, K.; Tsuboi, M.; Strahan, G.D. *Drug-DNA intercations: Structures and Spectra*. Editors: John Wiley & sons, Inc.: Hoboken, New Jersey, **2008**; p 370.

(350) M.M. Höfliger; A.G. Beck-Sickinger. Receptor-Ligand Interaction. In ***Protein-Ligand Interactions: From Molecular Recognition to Drug Design***, Bohm, H.J.; Scheider, G., Eds. Wiley-VCH: Weinheim, **2003**; Vol. 19, pp 107-136.

(351) Schwarz, G. (**1976**) Some general aspects regarding the interpretation of binding data by means of a Scatchard plot. *Biophysics of Structure and Mechanism*, 2, 1-12.

(352) Lohman, T.M.; Mascotti, D.P. (**1992**) Theromodynamics of Ligand Nucleic-Acid Interactions. *Methods Enzymol.*, 212, 400-424.

(353) Baranovskii, S.F.; Bolotin, P.A.; Evstigneev, M.P.; Chernyshev, D.N. (**2008**) Complexation of heterocyclic ligands with DNA in aqueous solution. *Journal of Applied Spectroscopy*, 75, 251-260.

(354) GraphPadSoftware. Comparing the fits of two models. http://www.curvefit.com/2_models__1_dataset.htm (September 2010).

(355) Z., H.; X., B.; A., E.; M., Z.; Z., Q.; B., S.; L.P.G., W. (**2008**) DNA Threading bis(9-aminoacridine-4-carboxamides): Effects of Piperidine Sidechains on DNA Binding, Cytotoxicity and Cell Cycle Arrest. *Bioorg. Med. Chem.*, 16, 4390-4400.

(356) Corwin, A.H.; Chivvis, A.B.; Poor, R.W.; Whitten, D.G.; Baker, E.W. (**1968**) Interpretation of Porphyrin and Metalloporphyrin Spectra. *J. Am. Chem. Soc.*, 90, 6577-&.

(357) IUPAC. *Compendium of Chemical Terminology*. Editors: McNaught, A.D.; Wilkinson, A.; 2nd ed.; Blackwell Scientific Publications: Oxford, **1997**.

(358) Pandey, A.V.; Bisht, H.; Babbarwal, V.K.; Srivastava, J.; Pandey, K.C.; Chauhan, V.S. (**2001**) Mechanism of malarial haem detoxification inhibition by chloroquine. *Biochem. J.*, 355, 333-338.

(359) Casabianca, L.B.; An, D.; Natarajan, J.K.; Alumasa, J.N.; Roepe, P.D.; Wolf, C.; de Dios, A.C. (**2008**) Quinine and chloroquine differentially perturb heme monomer-dimer equilibrium. *Inorg. Chem.*, 47, 6077-6081.

(360) Egan, T.J.; Mavuso, W.W.; Ross, D.C.; Marques, H.M. (**1997**) Thermodynamic factors controlling the interaction of quinoline antimalarial drugs with ferriprotoporphyrin IX. *J. Inorg. Biochem.*, 68, 137-145.

(361) Kelly, J.X.; Winter, R.; Peyton, D.H.; Hinrichs, D.J.; Riscoe, M. (**2002**) Optimization of xanthones for antimalarial activity: the 3,6-bis-omega-diethylaminoalkoxyxanthone series. *Antimicrob. Agents Chemother.*, 46, 144-150.

(362) Marques, H.M.; Munro, O.Q.; Crawcour, M.L. (**1992**) Coordination of N-Donor Ligands by Hematohemin. *Inorg Chim Acta*, 196, 221-229.

(363) Shelnutt, J.A. (**1983**) Metal Effects on Metalloporphyrins and on Their Pi-Pi Charge-Transfer Complexes with Aromatic Acceptors - Urohemin Complexes. *Inorg. Chem.*, 22, 2535-2544.

(364) Dascombe, M.J.; Drew, M.G.B.; Morris, H.; Wilairat, P.; Auparakkitanon, S.; Moule, W.A.; Alizadeh-Shekalgourabi, S.; Evans, P.G.; Lloyd, M.; Dyas, A.M.; Carr, P.; Ismail, F.M.D. (**2005**) Mapping antimalarial pharmacophores as a useful tool for the rapid discovery of drugs effective in vivo: Design, construction, characterization, and pharmacology of metaquine. *J. Med. Chem.*, 48, 5423-5436.

(365) Auparakkitanon, S.; Chapoomram, S.; Kuaha, K.; Chirachariyavej, T.; Wilairat, P. (**2006**) Targeting of hematin by the antimalarial pyronaridine. *Antimicrob. Agents Chemother.*, 50, 2197-2200.

(366) Auparakkitanon, S.; Chapoomran, S.; Kuaha, K.; Chirachariyavej, T.; Wilairat, P. (**2006**) Antimalarial pyronaridine targets hematin. *Am. J. Trop. Med. Hygien.*, 75, 183.

(367) Moreau, S.; Perly, B.; Chachaty, C.; Deleuze, C. (**1985**) A Nuclear Magnetic-Resonance Study of the Interactions of Antimalarial-Drugs with Porphyrins. *Biochim. Biophys. Acta*, 840, 107-116.

(368) Memic, A.; Spaller, M.R. (**2008**) How Do Halogen Substituents Contribute to Protein-Binding Interactions? A Thermodynamic Study of Peptide Ligands with Diverse Aryl Halides. *Chembiochem*, 9, 2793-2795.

(369) Lu, Y.; Wang, Y.; Zhu, W. (**2010**) Nonbonding interactions of organic halogens in biological systems: implications for drug discovery and biomolecular design. *Phys. Chem. Chem. Phys.*, 12, 4543-51.

(370) Levine, I.N. *Quantum Chemistry*. Editors: 4th ed.; Prentice Hall: New jersey, **1991**.

(371) Bachrach, S.M. Quantum Mechanics for Organic Chemistry. In ***Computational Organic Chemistry***, John Wiley & Sons, Inc.: Hoboken, New Jersey, **2007**; pp 1-37.

(372) DesJarlais, R.L.; Cummings, M.D.; Gibbs, A.C. (**2007**) Virtual Docking: How Are We Doing And How Can We Improve? *Frontiers in Drug Design & Discovery*, 3, 81-103.

(373) Stroud, R.M.; Finer-Moore, J. Computational and Structural Approaches to Drug Discovery: *Ligand–Protein Interactions*. Editors: Neidle, S.; Campbell, S.F.; Clore, D.M.; Lilley, D.M.J.; Royal Society of Chemistry,: Cambridge, UK, **2008**; p 382.

(374) Cramer, C.J. *Essentials of Computational Chemistry*. Editors: 2nd ed.; John Wiley & Sons, Ltd: Chichester, **2004**.

(375) Frisch, M.J.; Trucks, G.W.; Schlegel, H.B.; Scuseria, G.E.; Robb, M.A.; Cheeseman, J.R.; Montgomery, J.A., Jr.; Vreven, T.; Kudin, K.N.; Burant, J.C.; Millam, J.M.; Iyengar, S.S.; Tomasi, J.B., V.; Mennucci, B.; Cossi, M.S., G.; Rega, N.; Petersson, G.A.; Nakatsuji, H.; Hada, M.; Ehara, M.; Toyota, K.; Fukuda, R.; Hasegawa, J.; Ishida, M.; Nakajima, T.; Honda, Y.; Kitao, O.; Nakai, H.; Klene, M.; Li, X.; Knox, J.E.; Hratchian, H.P.; Cross, J.B.; Adamo, C.; Jaramillo, J.; Gomperts, R.; Stratmann, R.E.; Yazyev, O.; Austin, A.J.; Cammi, R.; Pomelli, C.; Ochterski, J.W.; Ayala, P.Y.; Morokuma, K.; Voth, G.A.; Salvador, P.; Dannenberg, J.J.; Zakrzewski, V.G.; Dapprich, S.; Daniels, A.D.; Strain, M.C.; Farkas, O.; Malick, D.K.; Rabuck, A.D.; Raghavachari, K.; Foresman, J.B.; Ortiz, J.V.; Cui, Q.; Baboul, A.G.; Clifford, S.; Cioslowski, J.; Stefanov, B.B.; Liu, G.; Liashenko, A.;

Piskorz, P.; Komaromi, I.; Martin, R.L.; Fox, D.J.; Keith, T.; Al-Laham, M.A.; Peng, C.Y.; Nanayakkara, A.; Challacombe, M.; Gill, P.M.W.; Johnson, B.; Chen, W.; Wong, M.W.; Gonzalez, C.; Pople, J.A. Gaussian 03, Revision C.2. In Gaussian and Inc.: Pittsburgh PA, **2003**.

(376) Foresman, J.B.; Frisch, A. *Exploring chemistry with electronic structure methods*. Editors: 2nd ed.; Gaussian Inc: Pittsburgh, USA, **1996**; p 269.

(377) Lengauer, T.; Rarey, M. (**1996**) Computational methods for biomolecular docking. *Current Opinion in Structural Biology*, 6, 402-406.

(378) Ewing, T.J.A.; Makino, S.; Skillman, A.G.; Kuntz, I.D. (**2001**) DOCK 4.0: Search strategies for automated molecular docking of flexible molecule databases. *Journal of Computer-Aided Molecular Design*, 15, 411-428.

(379) Morris, G.M.; Goodsell, D.S.; Halliday, R.S.; Huey, R.; Hart, W.E.; Belew, R.K.; Olson, A.J. (**1998**) Automated docking using a Lamarckian genetic algorithm and an empirical binding free energy function. *J. Comput. Chem.*, 19, 1639-1662.

(380) Verdonk, M.L.; Cole, J.C.; Hartshorn, M.J.; Murray, C.W.; Taylor, R.D. (**2003**) Improved protein-ligand docking using GOLD. *Proteins-Structure Function and Genetics*, 52, 609-623.

(381) Vilar, S.; Cozza, G.; Moro, S. (**2008**) Medicinal Chemistry and the Molecular Operating Environment (MOE): Application of QSAR and Molecular Docking to Drug Discovery. *Curr. Top. Med. Chem*, 8, 1555-1572.

(382) Dias, R.; de Azevedo, W.F. (**2008**) Molecular Docking Algorithms. *Curr Drug Targets*, 9, 1040-1047.

(383) Pissurlenkara, R.R.S.; Shaikha, M.S.; Iyerb, R.P.; Coutinhoa, E.C. (**2009**) Molecular Mechanics Force Fields and their Applications in Drug Design. *Anti-Infective Agents in Medicinal Chemistry*, 8, 128-150.

(384) Bohm, H.J. (**1998**) Prediction of binding constants of protein ligands: A fast method for the prioritization of hits obtained from de novo design or 3D database search programs. *Journal of Computer-Aided Molecular Design*, 12, 309-323.

(385) Muegge, I. (**2006**) PMF scoring revisited. *J. Med. Chem.*, 49, 5895-5902.

(386) Locatelli, M. (**2000**) Simulated annealing algorithms for continuous global optimization: Convergence conditions. *J Opt. Theo. Applicat.*, 104, 121-133.

(387) Cheatham, T.E.; Kollman, P.A. (**2000**) Molecular dynamics simulation of nucleic acids. *Annual Review of Physical Chemistry*, 51, 435-471.

(388) Orozco, M.; Noy, A.; Perez, A. (**2008**) Recent advances in the study of nucleic acid flexibility by molecular dynamics. *Current Opinion in Structural Biology*, 18, 185-193.

(389) Hashem, Y.; Auffinger, P. (**2009**) A short guide for molecular dynamics simulations of RNA systems. *Methods*, 47, 187-197.

(390) Perdew, J.P. (**1986**) Density-Functional Approximation for the Correlation-Energy of the Inhomogeneous Electron-Gas. *Physical Review B*, 33, 8822-8824.

(391) Lee, C.T.; Yang, W.T.; Parr, R.G. (**1988**) Development of the Colle-Salvetti Correlation-Energy Formula into a Functional of the Electron-Density. *Physical Review B*, 37, 785-789.

(392) Becke, A.D. (**1993**) Density-Functional Thermochemistry .3. the Role of Exact Exchange. *J. Chem. Phys.*, 98, 5648-5652.

(393) Ditchfield, R.; Hehre, W.J.; Pople, J.A. (**1971**) Self-Consistent Molecular-Orbital Methods. IX. An Extended Gaussian-Type Basis for Molecular-Orbital Studies of Organic Molecules *J. Chem. Phys.*, 54, 724-728

(394) Reed, A.E.; Curtiss, L.A.; Weinhold, F. (**1988**) Intermolecular Interactions from a Natural Bond Orbital, Donor-Acceptor Viewpoint. *Chem. Rev.*, 88, 899-926.

(395) Leach, A.R. *Molecular Modelling: Principles and Applications*. Editors: 2nd ed.; Prentice Hall: New York, **2001**; p 720.

(396) *Molecular Operating Environment (MOE, 2005.06)*, 2008.10; Chemical Computing Group Inc.: Montreal, Canada, **2005**.

(397) Wang, J.M.; Cieplak, P.; Kollman, P.A. (**2000**) How well does a restrained electrostatic potential (RESP) model perform in calculating conformational energies of organic and biological molecules? *J. Comput. Chem.*, 21, 1049-1074.

(398) Cornell, W.D.; Cieplak, P.; Bayly, C.I.; Gould, I.R.; Merz, K.M.; Ferguson, D.M.; Spellmeyer, D.C.; Fox, T.; Caldwell, J.W.; Kollman, P.A. (**1995**) A 2nd Generation Force-Field for the Simulation of Proteins, Nucleic-Acids, and Organic-Molecules. *J. Am. Chem. Soc.*, 117, 5179-5197.

(399) Cramer, C.J.; Truhlar, D.G. (**1991**) General Parameterized Scf Model for Free-Energies of Solvation in Aqueous-Solution. *J. Am. Chem. Soc.*, 113, 8305-8311.

(400) Tucker, S.C.; Truhlar, D.G. (**1989**) Generalized Born Fragment Charge Model for Solvation Effects as a Function of Reaction Coordinate. *Chem. Phys. Lett.*, 157, 164-170.

(401) Constanciel, R.; Contreras, R. (**1984**) Self-Consistent Field-Theory of Solvent Effects Representation by Continuum Models - Introduction of Desolvation Contribution. *Theor. Chim. Acta*, 65, 1-11.

(402) Bissantz, C.; Folkers, G.; Rognan, D. (**2000**) Protein-based virtual screening of chemical databases. 1. Evaluation of different docking/scoring combinations. *J. Med. Chem.*, 43, 4759-4767.

(403) Egan, T.J.; Ross, D.C.; Adams, P.A. (**1994**) Quinoline Antimalarial-Drugs Inhibit Spontaneous Formation of Beta-Hematin (Malaria Pigment). *Febs Lett.*, 352, 54-57.

(404) Fidock, D.A.; Eastman, R.T.; Ward, S.A.; Meshnick, S.R. (**2008**) Recent highlights in antimalarial drug resistance and chemotherapy research. *Trends Parasitol.*, 24, 537-544.

(405) Kumar, V.; Mahajan, A.; Chibale, K. (**2009**) Synthetic medicinal chemistry of selected antimalarial natural products. *Bioorg. Med. Chem.*, 17, 2236-2275.

(406) O'Neill, P.M.; Ward, S.A.; Berry, N.G.; Jeyadevan, J.P.; Biagini, G.A.; Asadollaly, E.; Park, B.K.; Bray, P.G. (**2006**) A medicinal chemistry perspective on 4-aminoquinoline antimalarial drugs. *Curr. Top. Med. Chem*, 6, 479-507.

(407) Bray, P.G.; Howells, R.E.; Ward, S.A. (**1992**) Vacuolar Acidification and Chloroquine Sensitivity in Plasmodium-Falciparum. *Biochem. Pharmacol.*, 43, 1219-1227.

(408) Dominguez, J.N.; Leon, C.; Rodrigues, J.; de Dominguez, N.G.; Gut, J.; Rosenthal, P.J. (**2009**) Synthesis of chlorovinyl sulfones as structural analogs of chalcones and their antiplasmodial activities. *Eur. J. Med. Chem.*, 44, 1457-1462.

(409) Semenov, A.; Olson, J.E.; Rosenthal, P.J. (**1998**) Antimalarial synergy of cysteine and aspartic protease inhibitors. *Antimicrob. Agents Chemother.*, 42, 2254-2258.

(410) Wright, C.W.; Addae-Kyereme, J.; Brown, J.E.; Tranter, D.A. (**1997**) Evaluation of cryptolepine and some analogues as leads to selective antimalarial agents. *J. Pharm. Pharmacol.*, 49, 36.

(411) Ridley, R.G.; Hofheinz, W.; Matile, H.; Jaquet, C.; Dorn, A.; Masciadri, R.; Jolidon, S.; Richter, W.F.; Guenzi, A.; Girometta, M.A.; Urwyler, H.; Huber, W.; Thaithong, S.; Peters, W. (**1996**) 4-aminoquinoline analogs of chloroquine with shortened side chains retain activity against chloroquine-resistant Plasmodium falciparum. *Antimicrob. Agents Chemother.*, 40, 1846-1854.

(412) De, D.Y.D.; Krogstad, F.M.; Byers, L.D.; Krogstad, D.J. (**1998**) Structure-activity relationships for antiplasmodial activity among 7-substituted 4-aminoquinolines. *J. Med. Chem.*, 41, 4918-4926.

(413) Prudencio, M.; Rodrigues, C.D.; Ataide, R.; Mota, M.M. (**2008**) Dissecting in vitro host cell infection by Plasmodium sporozoites using flow cytometry. *Cell Microbiol*, 10, 218-224.

(414) Stocks, P.A.; Bray, P.G.; Barton, V.E.; Al-Helal, M.; Jones, M.; Araujo, N.C.; Gibbons, P.; Ward, S.A.; Hughes, R.H.; Biagini, G.A.; Davies, J.; Amewu, R.; Mercer, A.E.; Ellis, G.; O'Neill, P.M. (**2007**) Evidence for a common non-heme chelatable-iron-dependent activation mechanism for semisynthetic and synthetic endoperoxide antimalarial drugs. *Angew. Chem. Int. Ed.*, 46, 6278-6283.

(415) Leed, A.; DuBay, K.; Ursos, L.M.B.; Sears, D.; de Dios, A.C.; Roepe, P.D. (**2002**) Solution structures of antimalarial drug-heme complexes. *Biochemistry*, 41, 10245-10255.

(416) de Dios, A.C.; Casabianca, L.B.; Kosar, A.; Roepe, P.D. (**2004**) Structure of the amodiaquine-FPIX μ-oxo dimer solution complex at atomic resolution. *Inorg. Chem.*, 43, 8078-8084.

(417) Natarajan, J.K.; Alumasa, J.N.; Yearick, K.; Ekoue-Kovi, K.A.; Casabianca, L.B.; de Dios, A.C.; Wolf, C.; Roepe, P.D. (**2008**) 4-N-, 4-S-, and 4-O-chloroquine analogues: Influence of side chain length and quinolyl nitrogen pK(a) on activity vs chloroquine resistant malaria. *J. Med. Chem.*, 51, 3466-3479.

(418) Egan, T.J.; Ncokazi, K.K. (**2004**) Effects of solvent composition and ionic strength on the interaction of quinoline antimalarials with ferriprotoporphyrin IX. *J. Inorg. Biochem.*, 98, 144-152.

(419) Chong, C.R.; Sullivan, D.J. (**2002**) Reversible inhibition of heme crystallization by anti-materials and other compounds: Implications for drug discovery. *Molecular Biology of the Cell*, 13, 402a-403a.

(420) Chambers, J.A.A. Buffers, chelating agents and denaturants. In ***Biochemistry***, Chambers, J.A.A.; Rickwood, D., Eds. Blackwell Scientific Publications: Oxford, **1993**.

(421) Skoog, D.A.; West, D.M.; Holler, F.J.; Crouch, S.R. Propagation of Measurement Uncertainties. In ***Fundamentals of Analytical Chemistry***, Saunders College Publishers: New York, **1996**.

(422) Reed, A.E.; Weinstock, R.B.; Weinhold, F. (**1985**) Natural-Population Analysis. *J. Chem. Phys.*, 83, 735-746.

(423) Reed, A.E.; Weinhold, F. (**1985**) Natural Localized Molecular-Orbitals. *J. Chem. Phys.*, 83, 1736-1740.

(424) Sturgeon, J.B.; Laird, B.B. (**2000**) Symplectic algorithm for constant-pressure molecular dynamics using a Nose-Poincare thermostat. *J. Chem. Phys.*, 112, 3474-3482.

(425) Mendez, P.S.; Guedes, R.C.; dos Santos, D.J.V.A.; Eriksson, L.A. (**2007**) Theoretical prediction of binding modes and hot sequences for allopsoralen-DNA interaction. *Chem. Phys. Lett.*, 450, 127-131.

(426) de Vicente, J.; Lanchares, J.; Hermida, R. (**2003**) Placement by thermodynamic simulated annealing. *Phys. Lett. A*, 317, 415-423.

(427) Cerny, V. (**1985**) Thermodynamical Approach to the Traveling Salesman Problem - an Efficient Simulation Algorithm. *J Opt. Theo. Applicat.*, 45, 41-51.

(428) GoldScore Fitness Function. http://www.ccdc.cam.ac.uk/support/documentation/gold/3_2/doc/portable_html/gold_portable-3-077.html (March 2010).

(429) *Molecular Operating Environment (MOE, 2009.10)*, 2009.10; Chemical Computing Group Inc.: Montreal, Canada, **2009**.

A

Appendices

List of contents

Appendix A. ^{1}H and ^{13}C NMR chemical shifts (ppm) of cryptolepine (1) and derivatives (3) 229
Appendix B. ^{1}H and ^{13}C NMR chemical shifts (ppm) of quindolones (4 and 91a-c) and their derivatives (5, 94 and 95) 233
Appendix C. Fitting of the UV-visible Vs pH experimental data of the cryptolepine derivatives (3) to the Henderson-Hasselbalch equation 236
Appendix D. Acid dissociation constants (pK_a) of cryptolepine and derivatives (3a-y) as well as of quindolones (4, 91a and 91b) and derivatives (5, 94 and 95) predicted by SPARC software (release W4.2.1405-s4.2.1408) 241
Appendix E. UV-Visible Spectrophotometry Determination of Binding Constants to DNA in buffer solutions containing 0.1 M NaCl 243
Appendix F. Spectrophotofluorimetry Determination of Binding Constants to DNA in buffer solutions containing 0.1 M NaCl 245
Appendix G. Spectrophotometric Determination of Binding to DNA in buffer solutions containing 0.01 M or 1.0 M NaCl 250
Appendix H. UV-Visible Spectrophotometry Determination of Binding Constants to FPIX-OH in pH 5.5 HEPES buffer (40 % DMSO) 252
Appendix I. Docking studies with DNA 259
Appendix J. Docking studies with haemozoin dimer 263
Appendix K. Derivation of vacuolar accumulation ratio equation 266
Appendix L. Relevant Publications 268

Appendix A. ^{1}H and ^{13}C NMR chemical shifts (ppm) of cryptolepine (1) and derivatives (3)

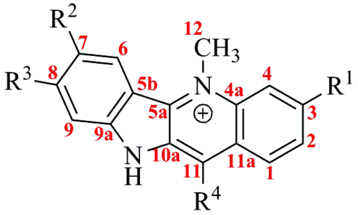

										Aromatic nucleus											Side chain					
Compound	**R^{1}**	**R^{2}**	**R^{3}**	**R^{4}**	**H^{1}**	**H^{2}**	**H^{3}**	**H^{4}**	**CH_3**	**H^{6}**	**H^{7}**	**H^{8}**	**H^{9}**	**^{10}NH**	**H^{11}**	**^{11}NH**	**H^{a}**	**H^{b}**	**H^{c}**	**H^{d}**	**H^{e}**	**H^{f}**	**H^{g}**	**H^{h}**	**NH**	**NH_2**
1	H	H	H	H	8.46	7.83	8.05	8.70	4.92	8.65	7.41	7.83	7.74	12.76	9.17	--	--	--	--	--	--	--	--	--	--	--
3a	H	H	H	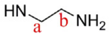	8.84	7.64	7.97	8.31	4.58	8.51	7.32	7.68	8.01	12.29	--	9.24	4.44	3.32	--	--	--	--	--	--	--	8.44
3b	H	H	H	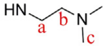	8.71	7.73	8.03	8.28	4.64	8.48	7.40	7.69	7.91	n.d.	--	n.d	4.61	3.72	3.05	--	--	--	--	--	--	--
3c	H	H	H	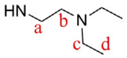	8.82	7.66	7.98	8.30	4.57	8.53	7.34	7.70	7.77	n.d	--	n.d	4.14	2.98	2.71	0.95	--	--	--	--	--	--
3d	H	H	H	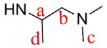	8.69	7.73	8.04	8.30	4.62	8.53	7.42	7.77	7.86	n.d	--	n.d.	5.11	3.81 3.45	2.88	1.44	--	--	--	--	--	--
3e	H	H	H	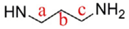	8.90	7.68	8.02	8.36	4.61	8.56	7.37	7.73	8.03	12.28	--	9.27	4.32	2.17	3.01	--	--	--	--	--	--	8.20
3f	H	H	H	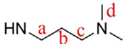	8.65	7.73	8.05	8.30	4.67	8.53	7.44	7.77	7.92	n.d	--	n.d	4.32	2.39	3.37	2.92	--	--	--	--	--	--
3g	H	H	H	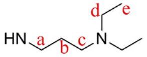	8.62	7.72	8.04	8.25	4.59	8.47	7.41	7.72	7.91	n.d	--	n.d	4.29	2.36	3.38	3.26	1.34	--	--	--	--	--
3h	H	H	H	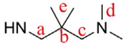	8.20	7.75	8.00	8.33	4.56	8.51	7.32	7.67	7.93	10.75	--	10.75	4.21	--	2.59	2.44	1.13	--	--	--	--	--
3i	H	H	H	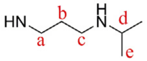	8.67	7.73	8.05	8.30	4.68	8.54	7.44	7.75	7.93	n.d	--	n.d	4.34	2.43	3.27	3.42	1.37	--	--	--	n.d	--
3j	H	H	H	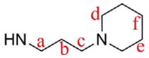	8.87	7.68	8.01	8.34	4.60	8.55	7.36	7.71	8.01	12.31	--	9.21	4.31	2.30	3.23	3.43 2.86	1.78	1.69 1.38	--	--	--	--
3k	H	H	H	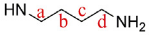	8.89	7.67	8.00	8.34	4.60	8.55	7.36	7.71	7.95	n.d	--	n.d	4.22	1.89	1.75	2.85	--	--	--	--	--	n.d

n.d. – Not determined

Compound	R¹	R²	R³	R⁴	Aromatic Nucleus										Side chain										
					H^1	H^2	H^3	H^4	CH_3	H^6	H^7	H^8	H^9	^{10}NH	^{11}NH	H^a	H^b	H^c	H^d	H^e	H^f	H^g	H^h	NH	OH
3l	H	H	H	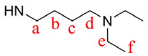	8.89	7.68	8.01	8.33	4.60	8.55	7.38	7.72	7.98	12.36	9.24	4.23	1.89	1.89	3.10	3.10	1.21	--	--	--	--
3m	H	H	H	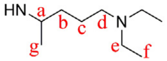	8.85	7.71	8.04	8.37	4.64	8.58	7.39	7.76	7.96	n.d	n.d	4.92	2.05	1.86	3.03	3.03	1.14	1.47	--	--	--
3n	H	H	H	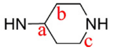	8.29	7.83	8.09	8.56	4.80	8.66	7.44	7.81	7.98	12.16	8.51	3.50	2.29 2.05	4.14 3.86	--	--	--	--	--	n.d.	--
3o	H	H	H	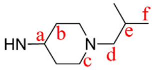	8.64	7.88	8.13	8.46	4.90	8.51	7.50	7.84	7.94	n.d.	n.d	3.92	2.52 2.26	3.70 3.09	2.26	2.16	1.16	--	--	--	--
3p	H	H	H	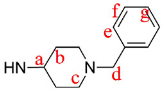	8.47	7.87	8.12	8.50	4.88	8.63	7.48	7.83	7.93	n.d.	n.d.	3.77	2.58 2.28	4.27 3.92	4.44	7.66	7.52	7.56	--	--	--
3q	H	H	H	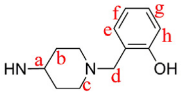	8.30	7.86	8.10	8.58	4.82	8.67	7.46	7.82	7.99	12.18	9.47	3.53	2.46 2.23	4.17 3.85	4.23	7.04	7.28	6.89	7.56	--	--
3r	H	H	H	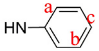	8.49	7.69	8.03	8.34	4.65	8.44	7.35	7.65	7.53	n.d.	n.d.	7.18	7.41	7.28	--	--	--	--	--	--	--
3s	H	H	H	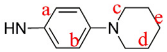	8.65	7.76	8.10	8.42	4.81	8.57	7.43	7.71	7.60	n.d.	n.d.	7.31	7.16	3.37	1.80	1.69	--	--	--	--	--
3t	H	H	H	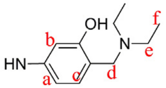	8.60	7.74	8.09	8.58	4.83	8.67	7.43	7.78	7.76	11.84	10.63	6.67	6.95	7.46	4.20	3.13	1.29	--	--	--	10.98
3u	H	H	H	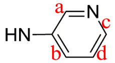	8.79	7.82	8.13	8.64	4.86	8.69	7.44	7.79	7.67	11.64	n.d.	8.63	7.63	8.46	7.51	--	--	--	--	--	--
3v	Cl	H	H	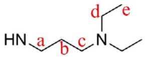	8.91	7.73	--	8.46	4.59	8.55	7.37	7.72	8.00	12.49	9.41	4.32	2.26	3.11	3.30	1.22	--	--	--	--	--
3w	Cl	H	H	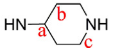	8.28	7.88	--	8.63	4,79	8.66	7.44	7.82	8.03	12.37	n.d	3.54	2.33 2.07	4.18 3.92	--	--	--	--	--	n.d.	--
3x	Cl	H	Cl	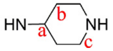	8.35	7.80	--	8.53	4.75	8.55	7.41	--	7.90	n.d	n.d	3.64	2.38 2.15	4.23 3.91	--	--	--	--	--	n.d.	--
3y	H	H	H	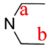	8.45	7.75	8.02	8.41	4.80	8.54	7.39	7.71	7.81	--	--	4.00	1.30	--	--	--	--	--	--	--	--

n.d. – Not determined

		3a	**3b**	**3c**	**3d**	**3e**	**3f**	**3g**	**3h**	**3i**	**3j**	**3k**	**3l**	**3m**
		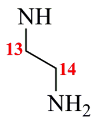	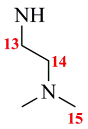	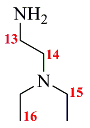	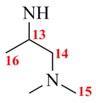	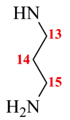	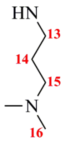	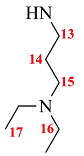	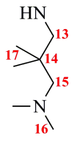	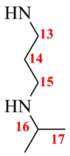	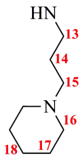	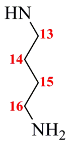	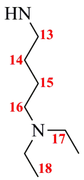	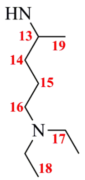
Aromatic nucleus	**C^{1}**	124.63	123.65	124.51	124.82	124.89	123.23	123.39	123.11	123.43	124.44	125.01	124.58	125.73
	C^{2}	123.88	124.51	124.19	125.17	124.39	124.22	124.35	124.83	124.43	123.70	124.26	123.76	124.46
	C^{3}	132.27	132.41	132.52	133.30	132.76	132.22	132.37	132.62	132.43	132.12	132.70	132.23	132.43
	C^{4}	117.24	116.74	117.68	117.76	117.83	116.63	116.70	118.02	116.85	117.15	117.78	117.26	118.04
	C^{4a}	137.02	137.37	137.53	137.49	137.65	137.46	137.46	137.67	137.68	137.02	137.77	137.38	138.04
	C^{5a}	135.65	136.93	135.48	135.73	135.83	136.45	136.35	135.60	135.73	135.16	137.73	135.13	136.08
	C^{5b}	114.32	114.67	115.55	115.01	114.75	114.63	114.63	114.88	114.79	113.58	114.93	114.40	115.25
	C^{6}	124.29	123.78	124.74	125.04	124.74	123.62	123.68	124.56	123.82	124.09	124.69	124.18	124.98
	C^{7}	120.75	121.19	120.83	122.02	121.17	120.93	121.08	120.99	121.16	120.52	121.12	120.63	121.39
	C^{8}	130.52	131.06	130.71	132.04	130.88	130.71	130.81	130.61	130.92	130.20	130.77	130.28	131.09
	C^{9}	113.72	113.35	114.01	114.07	114.18	113.13	113.27	114.18	113.30	114.17	114.18	113.67	114.41
	C^{9a}	143.46	143.73	143.39	143.73	143.21	143.34	143.36	143.08	143.76	142.61	143.13	142.58	143.25
	C^{10a}	115.95	116.85	118.07	130.69	116.59	134.47	116.53	116.63	n.d.	116.06	n.d	132.78	140.36
	C^{11}	142.90	143.16	144.50	143.11	144.01	143.63	143.57	144.59	143.86	143.41	144.20	143.75	144.38
	C^{11a}	115.31	115.78	115.60	116.30	115.68	115.61	115.52	115.58	115.72	115.02	115.67	115.16	116.04
	C^{12}	38.08	37.51	38.24	38.47	38.51	37.22	37.33	38.31	37.43	37.89	38.78	37.95	38.87
Side chain	**C^{13}**	42.41	40.51	44.62	47.64	42.86	42.50	42.84	57.33	42.65	42.93	45.18	44.76	51.01
	C^{14}	38.85	56.55	53.41	60.90	28.05	25.09	24.65	35.51	26.93	23.86	27.12	20.51	34.15
	C^{15}	--	42.68	47.66	44.03	36.75	54.79	49.08	70.03	42.22	53.24	24.75	26.82	20.75
	C^{16}	--	--	11.27	20.56	--	42.08	47.27	48.18	50.86	51.81	38.45	50.27	46.88
	C^{17}	--	--	--	--	--	--	7.87	25.38	17.91	22.12	--	45.97	46.69
	C^{18}	--	--	--	--	--	--	--	--	--	21.28	--	8.34	9.01
	C^{19}	--	--	--	--	--	--	--	--	--	--	--	--	22.55

n.d. – Not determined

		3n	**3o**	**3p**	**3q**	**3r**	**3s**	**3t**	**3u**	**3v**	**3w**	**3x**	**3y**
		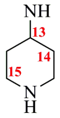 NH 13 14 15 N H	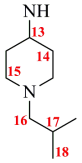 NH 13 14 15 N 16 17 18	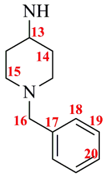 NH 13 14 15 N 16 17 18 19 20	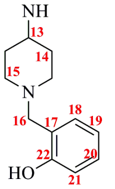 NH 13 14 15 N 16 17 18 19 20 21 22 HO	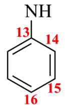 NH 13 14 15 16	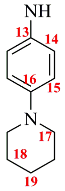 NH 13 14 15 16 N 17 18 19	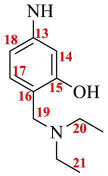 NH 18 13 14 17 16 15 OH 19 N 20 21	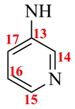 NH 17 13 14 16 N 15	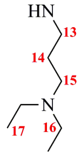 HN 13 14 15 N 17 16	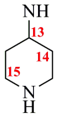 NH 13 14 15 N H	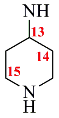 NH 13 14 15 N H	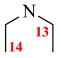
Aromatic nucleus	**C^{1}**	126.54	127.47	126.03	125.97	125.04	125.31	125.61	125.37	127.17	128.75	129.34	125.35
	C^{2}	125.54	126.74	125.32	124.60	126.09	125.95	113.60	125.62	131.01	125.82	126.67	123.26
	C^{3}	132.71	133.83	132.38	132.19	133.65	132.58	132.91	132.83	138.45	138.78	139.18	130.64
	C^{4}	118.63	118.88	117.42	118.24	118.39	118.25	117.94	118.49	116.94	125.59	118.38	115.68
	C^{4a}	138.12	139.80	138.35	137.56	137.94	137.94	137.68	137.42	137.87	137.90	140.16	136.62
	C^{5a}	137.78	139.53	138.06	137.28	137.48	136.79	136.58	137.89	135.95	137.69	139.76	135.73
	C^{5b}	114.71	115.94	114.47	113.67	115.27	113.30	114.94	115.16	114.41	114.63	114.23	113.10
	C^{6}	125.66	126.07	124.61	125.04	125.34	125.21	124.93	125.53	124.56	124.90	127.27	122.90
	C^{7}	121.60	122.55	121.46	121.07	122.32	122.48	120.99	121.95	121.35	121.76	123.55	119.68
	C^{8}	132.46	133.81	132.35	132.21	132.87	132.35	132.32	132.58	124.71	132.52	140.28	130.41
	C^{9}	114.18	114.71	113.27	114.19	114.22	114.45	125.22	113.88	114.79	114.33	114.47	111.49
	C^{9a}	144.42	146.06	144.61	143.94	143.26	141.13	142.71	143.62	143.29	144.48	145.94	142.53
	C^{10a}	125.04	126.81	121.46	131.63	130.98	143.89	144.25	124.55	117.24	119.25	124.91	125.44
	C^{11}	147.20	148.15	146.67	146.54	139.75	139.22	136.19	121.95	144.12	147.35	148.61	145.73
	C^{11a}	120.70	122.92	121.12	121.15	118.18	116.21	118.48	118.69	117.52	118.00	120.84	129.89
	C^{12}	39.61	39.89	38.46	39.27	38.83	39.01	39.32	49.05	38.83	39.49	39.93	36.73
Side chain	**C^{13}**	47.60	56.97	54.92	53.78	138.78	129.48	142.22	137.44	43.60	47.54	49.22	45.78
	C^{14}	30.68	30.22	28.93	28.39	122.76	128.87	111.83	141.60	24.39	30.72	31.62	11.27
	C^{15}	51.13	52.21	50.73	50.74	130.51	118.32	133.43	143.65	48.56	51.38	52.29	--
	C^{16}	--	53.37	48.32	42.04	126.69	152.10	113.36	124.77	46.49	--	--	--
	C^{17}	--	27.66	131.28	155.99	--	51.89	157.28	128.32	8.87\	--	--	--
	C^{18}	--	20.52	129.71	115.44	--	26.85	107.90	--	--	--	--	--
	C^{19}	--	--	129.01	130.34	--	25.23	49.49	--	--	--	--	--
	C^{20}	--	--	129.37	119.04	--	--	46.05	--	--	--	--	--
	C^{21}	--	--	--	131.95	--	--	8.50	--	--	--	--	--
	C^{22}	--	--	--	118.13	--	--	--	--	--	--	--	--

Appendix B. ^{1}H and ^{13}C NMR chemical shifts (ppm) of quindolones (**4** and **91a-c**) and their derivatives (**5**, **94** and **95**)

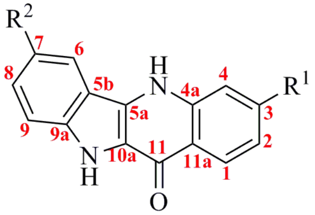

	R^1	**R^2**	**H^1**	**H^2**	**H^3**	**H^4**	**^{5}NH**	**H^6**	**H^7**	**H^8**	**H^9**	**^{10}NH**
4	H	H	8.35	7.28	7.68	7.81	12.80	8.28	7.22	7.48	7.53	11.69
91a	Cl	H	8.35	7.30	--	7.73	12.56	8.15	7.23	7.49	7.51	11.80
91c	Cl	Cl	7.49	7.54	--	8.20	12.57	7.69	--	7.31	8.33	12.02

	R^1	**R^2**	**C^1**	**C^2**	**C^3**	**C^4**	**C^{4a}**	**C^{5a}**	**C^{5b}**	**C^6**	**C^7**	**C^8**	**C^9**	**C^{9a}**	**C^{10a}**	**C^{11}**	**C^{11a}**
4	H	H	125.57	120.87	130.99	118.28	139.64	129.44	116.38	121.63	119.25	127.84	112.98	139.05	123.48	167.77	123.24
91a	Cl	H	127.94	121.31	135.65	117.13	140.02	129.40	116.14	121.15	119.62	128.10	113.17	139.08	123.64	167.30	121.96
91c	Cl	Cl	127.97	114.91	136.04	120.41	140.08	128.52	117.15	117.03	124.51	121.55	128.03	137.54	123.73	167.54	121.91

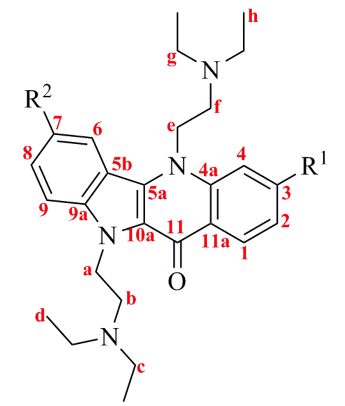

			Aromatic Nucleus								Side chain							
	R^1	**R^2**	**H^1**	**H^2**	**H^3**	**H^4**	**H^5**	**H^6**	**H^7**	**H^8**	**H^a**	**H^b**	**H^c**	**H^d**	**H^e**	**H^f**	**H^g**	**H^h**
5a	H	H	8.69	7.34	7.70	7.70	8.25	7.24	7.54	7.58	5.00	2.92	2.71	1.09	4.84	3.03	2.71	1.09
5b	Cl	H	8.57	7.27	--	7.72	8.18	7.23	7.54	7.59	4.97	3.90	2.69	1.07	4.72	2.90	2.69	1.06
5c	Cl	Cl	8.57	7.30	--	7.72	8.27	--	7.51	7.57	4.97	2.92	2.71	1.13	4.77	3.04	2.71	1.05

			Aromatic Nucleus													Side chain							
	R^1	**R^2**	**C^1**	**C^2**	**C^3**	**C^4**	**C^{4a}**	**C^{5a}**	**C^{5b}**	**C^6**	**C^7**	**C^8**	**C^9**	**C^{9a}**	**C^{10a}**	**C^{11}**	**C^{11a}**	**C^a**	**C^b**	**C^c**	**C^d**	**C^e**	**C^f**	**C^g**	**C^h**
5a	H	H	126.86	120.95	123.73	114.70	139.65	130.62	115.14	122.60	119.52	127.32	110.62	139.70	122.69	169.13	124.89	43.10	53.17	47.69	11.85	47.35	50.87	47.69	11.85
5b	Cl	H	128.43	121.66	137.70	114.33	140.36	130.62	115.05	122.46	119.84	127.56	110.76	139.72	123.26	168.61	122.78	43.08	53.12	47.73	12.03	47.57	51.10	47.67	12.03
5c	Cl	Cl	128.43	121.84	138.04	114.30	140.44	129.74	115.68	121.76	125.38	127.82	111.96	137.96	123.32	168.63	123.18	43.35	53.22	47.78	11.93	47.53	50.91	47.78	11.93

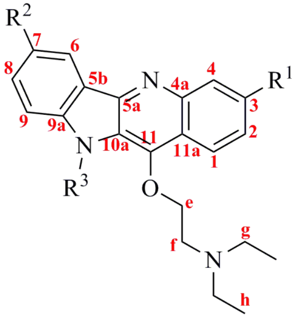

				Aromatic Nucleus									Side chain							
	R^1	**R^2**	R^3	**H^1**	**H^2**	**H^3**	**H^4**	**H^6**	**H^7**	**H^8**	**H^9**	**^{10}NH**	**H^a**	**H^b**	**H^c**	**H^d**	**H^e**	**H^f**	**H^g**	**H^h**
94a	H	H	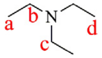	8.40	7.58	7.70	8.33	8.55	7.34	7.66	7.52	--	4.73	2.79	2.62	1.00	4.32	3.10	2.70	1.13
94b	Cl	H	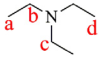	8.39	7.51	--	8.32	8.51	7.35	7.67	7.51	--	4.69	2.80	2.60	0.98	4.28	3.06	2.69	1.12
94c	Cl	Cl	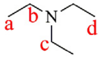	8.37	7.50	--	8.26	8.45	--	7.59	7.42	--	4.69	2.77	2.56	0.93	4.27	3.05	2.69	1.12
95a	H	H	H	8.34	7.54	7.67	8.32	8.56	7.32	7.60	7.46	12.63	--	--	--	--	4.58	3.07	2.90	1.26
95b	Cl	H	H	8.25	7.47	--	8.31	8.51	7.32	7.61	7.49	12.69	--	--	--	--	4.63	3.15	2.97	1.28
95c	Cl	Cl	H	8.24	7.47	--	8.28	8.48	--	7.54	7.39	--	--	--	--	--	4.63	3.15	2.97	1.28

				Aromatic Nucleus															Side chain							
	R^1	**R^2**	R^3	**C^1**	**C^2**	**C^3**	**C^4**	**C^{4a}**	**C^{5a}**	**C^{5b}**	**C^6**	**C^7**	**C^8**	**C^9**	**C^{9a}**	**C^{10a}**	**C^{11}**	**C^{11a}**	**C^a**	**C^b**	**C^c**	**C^d**	**C^e**	**C^f**	**C^g**	**C^h**
94a	H	H	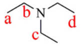	121.27	124.68	126.65	129.31	145.83	148.59	122.23	122.08	119.86	129.69	109.17	144.80	124.87	144.58	122.46	43.51	51.71	47.62	12.06	74.51	52.93	47.62	12.06
94b	Cl	H	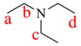	120.68	124.95	132.34	128.00	146.03	149.45	122.23	122.18	120.05	130.02	109.29	144.70	125.54	144.92	122.86	43.60	51.76	47.63	12.10	74.92	53.04	47.71	11.91
94c	Cl	Cl	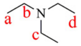	122.91	125.87	132.65	128.04	146.15	148.10	123.33	121.72	125.56	129.86	110.48	143.16	125.36	145.09	120.80	43.88	51.88	47.58	12.07	75.06	53.07	47.69	11.89
95a	H	H	H	128.95	124.23	126.47	120.96	145.54	148.68	122.58	122.20	119.37	129.38	111.04	143.52	123.95	144.65	121.48	--	--	--	--	73.99	55.09	48.51	11.33
95b	Cl	H	H	123.75	125.15	132.16	127.69	145.66	148.60	122.33	122.23	119.62	129.78	111.26	143.71	125.52	n.d	119.73	--	--	--	--				
95c	Cl	Cl	H	122.30	125.36	n.d	127.55	n.d.	n.d.	n.d.	121.63	n.d.	129.63	112.07	n.d.	n.d.	n.d.	n.d.	--	--	--	--	73.19	54.58	48.27	10.74

n.d. – Not determinated

Appendix C. Fitting of the UV-visible Vs pH experimental data of the cryptolepine derivatives (**3**) to the Henderson-Hasselbalch equation

	R^1	R^2	R^3	UV-Visible stacked spectra	UV-Visible date vs. pH fitting
3a	H	H	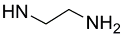	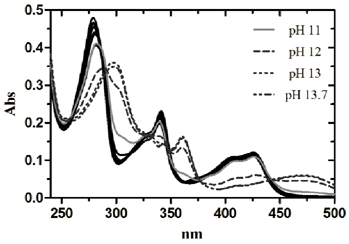	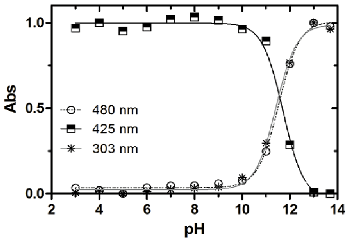
3b	H	H	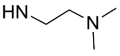	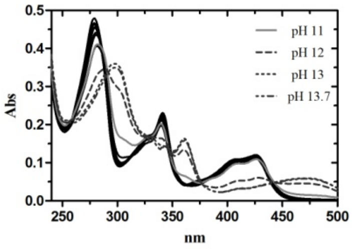	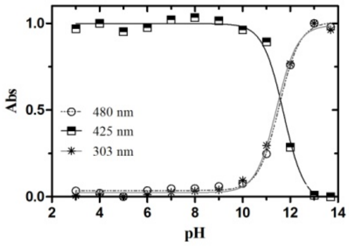
3c	H	H	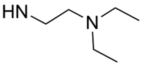	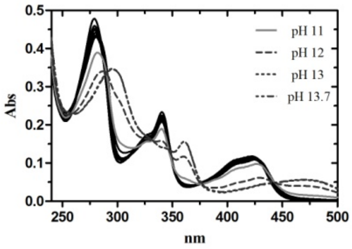	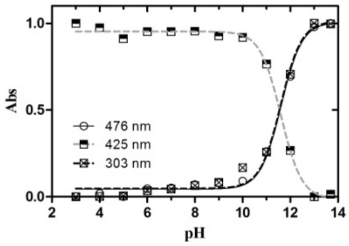
3d	H	H	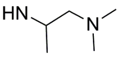	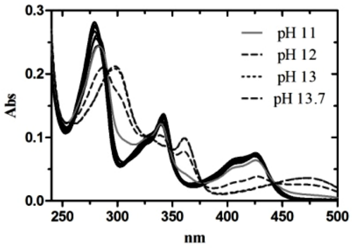	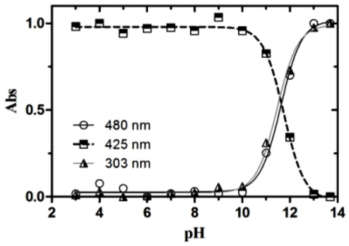
3e	H	H	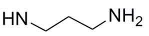	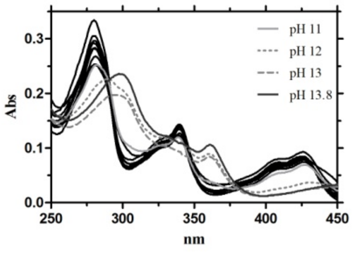	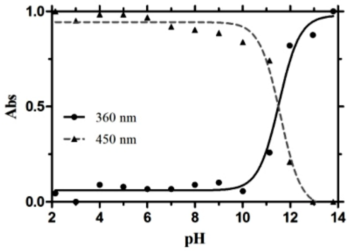

3f	H	H	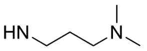	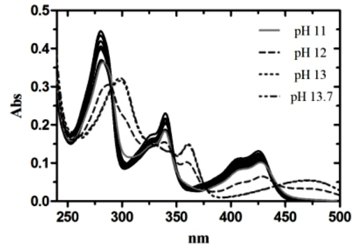	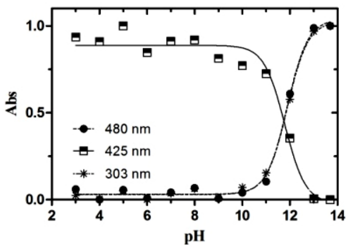
3g	H	H	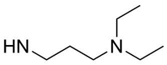	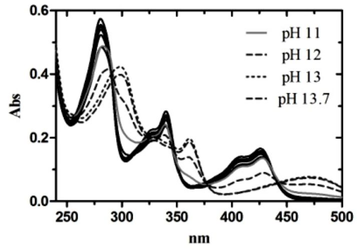	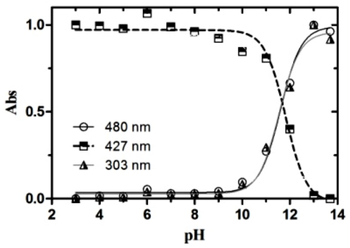
3h	H	H	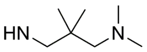	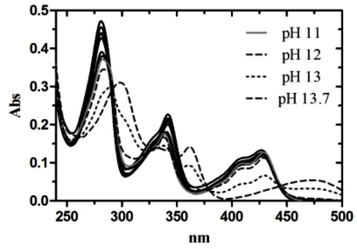	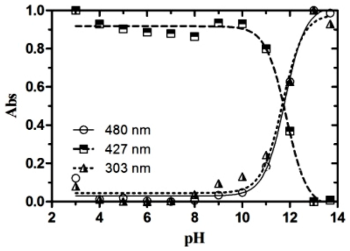
3i	H	H	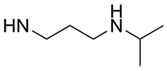	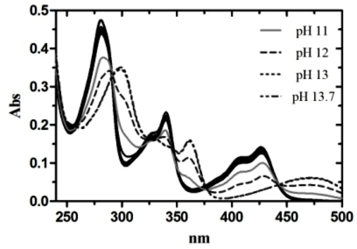	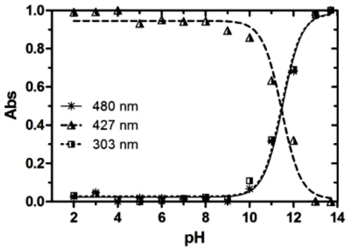
3j	H	H	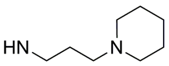	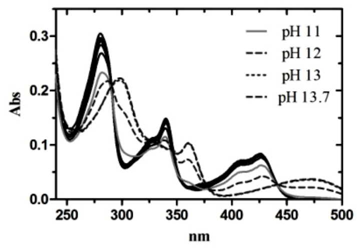	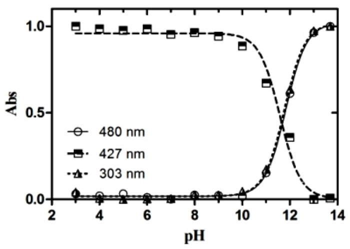
3k	H	H	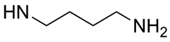	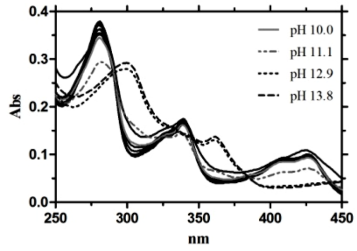	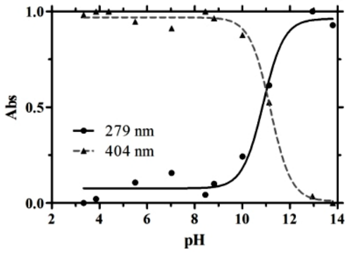

3l	H	H	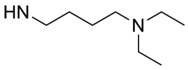	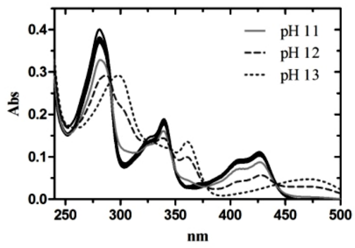	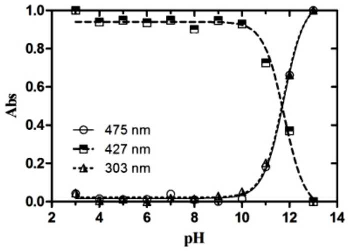
3m	H	H	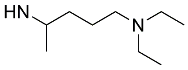	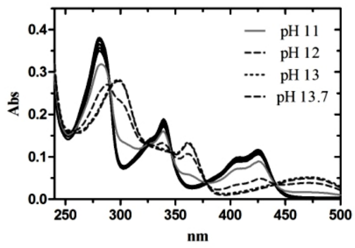	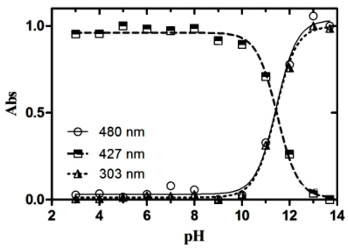
3n	H	H	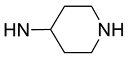	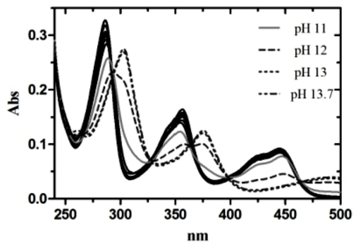	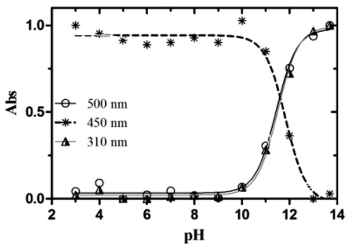
3o	H	H	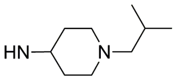	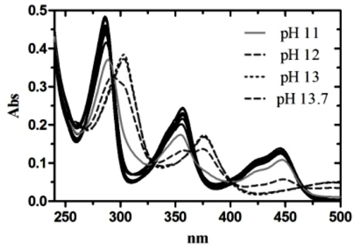	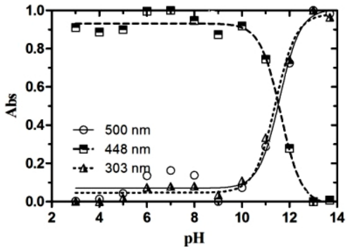
3p	H	H	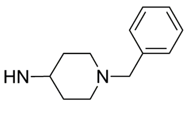	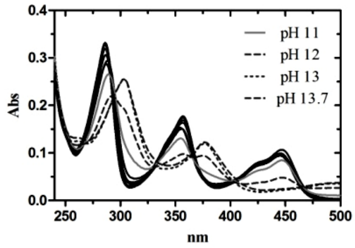	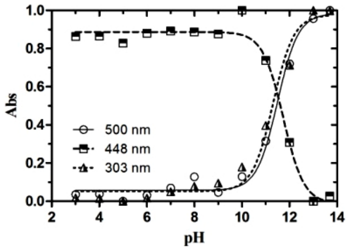
3q	H	H	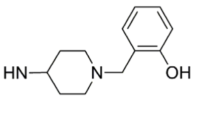	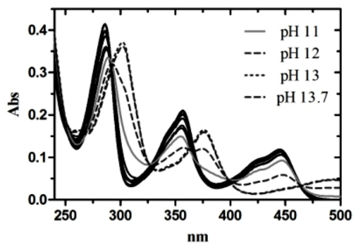	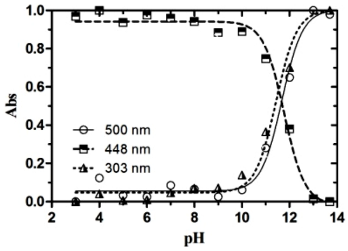

3r H H

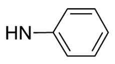

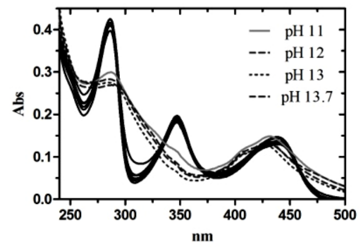

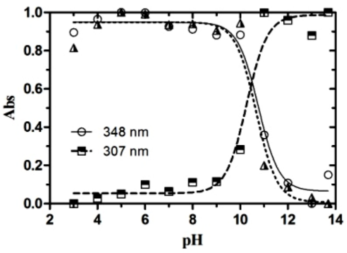

3s H H

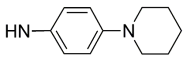

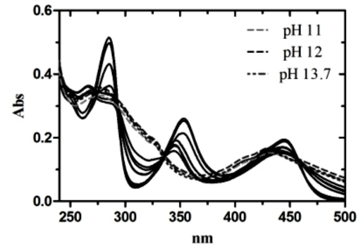

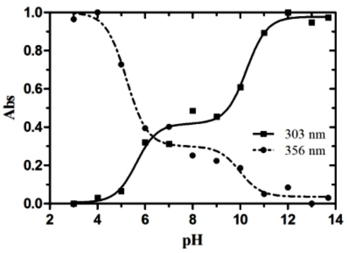

3t H H

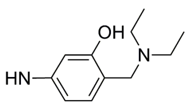

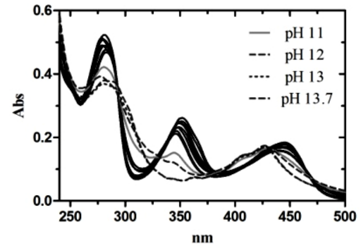

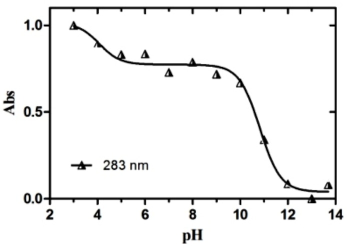

3u H H

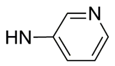

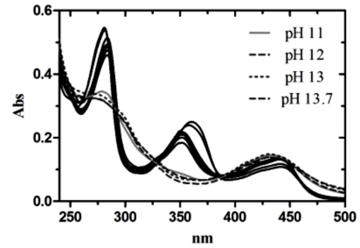

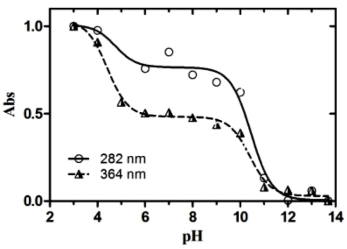

3v Cl H

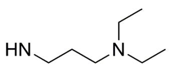

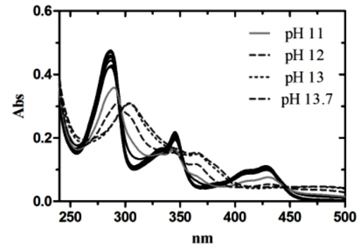

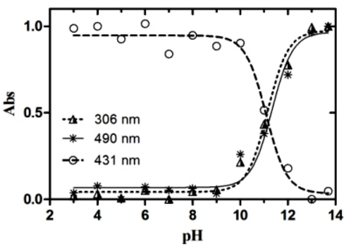

3w Cl H

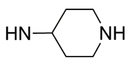

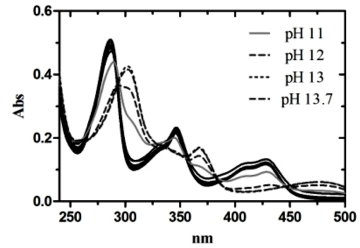

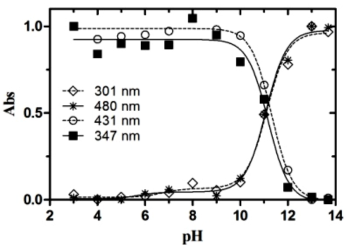

3x	Cl	Cl	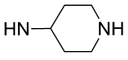HN NH	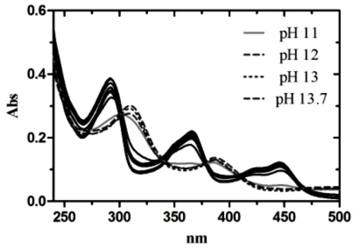Abs nm pH 11 pH 12 pH 13 pH 13.7 0.6 0.4 0.2 0.0 250 300 350 400 450 500	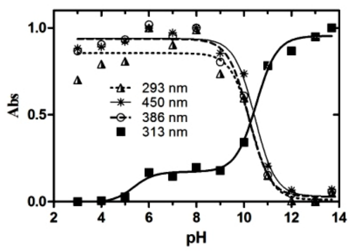Abs pH 293 nm 450 nm 386 nm 313 nm 1.0 0.5 0.0 2 4 6 8 10 12 14
3y	H	H	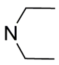N	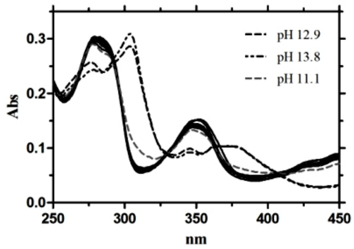Abs nm pH 12.9 pH 13.8 pH 11.1 0.3 0.2 0.1 0.0 250 300 350 400 450	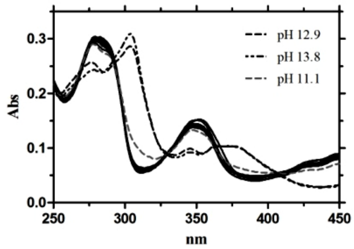Abs nm pH 12.9 pH 13.8 pH 11.1 0.3 0.2 0.1 0.0 250 300 350 400 450

Appendix D. Acid dissociation constants (pK_a) of cryptolepine and derivatives (3a-y) as well as of quindolones (4, 91a and 91b) and derivatives (5, 94 and 95) predicted by SPARC software (release W4.2.1405-s4.2.1408)

Acid dissociation constants for cryptolepine (**1**) and derivatives **3** predicted by SPARC software.

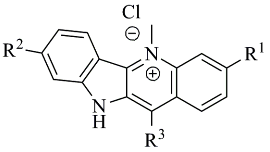

				SPARC[(315-317)]			
	R¹	**R²**	**R³**	**pK_{a1}**	**pK_{a2}**	**pK_{a3}**	**pK_{a4}**
1	H	H	H	15.21	--	--	--
3a	H	H	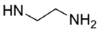	7.49	16.50	16.90	--
3b	H	H	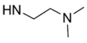	7.37	16.58	18.65	--
3c	H	H	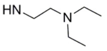	7.37	16.59	18.65	--
3d	H	H	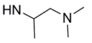	8.30	16.58	18.65	--
3e	H	H	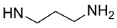	8.57	15.52	17.08	--
3f	H	H	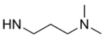	8.30	16.60	18.65	--
3g	H	H	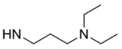	8.30	16.60	18.65	--
3h	H	H	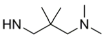	8.30	16.60	18.56	--
3i	H	H	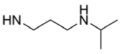	8.83	16.60	18.16	--
3j	H	H	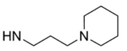	8.39	16.60	18.90	--
3k	H	H	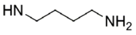	9.56	16.52	17.19	--
3l	H	H	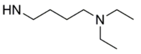	9.34	16.60	19.03	--
3m	H	H	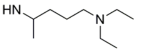	9.40	16.61	18.65	--
3n	H	H	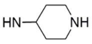	9.25	16.61	18.65	--
3o	H	H	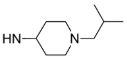	8.50	16.59	18.84	--
3p	H	H	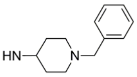	7.61	16.57	18.62	--
3q	H	H	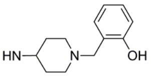	8.86	16.57	18.65	10.28
3r	H	H	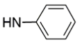	--	15.48	15.51	--
3s	H	H	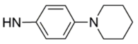	4.46	15.77	16.11	--
3t	H	H	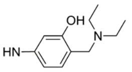	10.47	15.72	15.53	10.15
3u	H	H	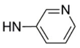	3.00	15.37	14.01	--
3v	Cl	H	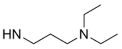	8.42	16.54	18.54	--
3w	Cl	H	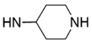	9.23	16.53	18.48	--
3x	Cl	Cl	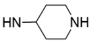	9.23	16.04	18.42	--
3y	H	H		--	15.96	-4.44	--

pK_{a1} – Deprotonation of the terminal nitrogen in the side chain of **3**; pK_{a2} – Ionization of the indolic nitrogen (N^{10}) of **3** ; pK_{a3} – Ionization of the nitrogen attached to C11of **3**; pK_{a4} –Ionization of the hydroxyl function in the side chain of **3q** and **3t**.

The pK_a values for **4**, **91a** and **91b** presented, represent the removal of the hydrogen to give the respective anionic quindolone. Additionally, quindolones have another possible acid dissociation reaction, which correspond to the removal of the hydrogens of the diprotonated quindolone (N^5 and N^{10}). The SPARC predicted pK_a values for these dissociation reactions in N^5 of **4**, **91a** and **91b** range between 3.3 and 4.2. The remain pK_a values presented (**5**, **94** and **94**) represents the deprotonation reaction of the cationic forms of the nitrogen, except the pk_{a3} values of **95** which correspond to removal of the indole nitrogen to give the anionic quindolone.

Acid dissociation constants for quindolones (**4** and **91**) and quindolones derivatives (**5**, **94** and **95**) predicted by SPARC software.

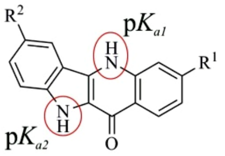

4 or **91**

	R^1	R^2	SPARC pK_{a1}	 pK_{a2}
4	H	H	12.33	16.79
91a	Cl	H	11.85	16.69
91b	Cl	Cl	11.52	16.28

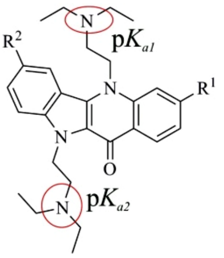

5

	R^1	R^2	SPARC pK_{a1}	 pK_{a2}
5a	H	H	7.90	8.92
5b	Cl	H	7.86	8.92
5c	Cl	Cl	7.84	8.90

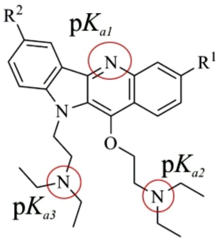

94

	R^1	R^2	SPARC pK_{a1}	 pK_{a2}	 pK_{a3}
94a	H	H	4.21	7.24	8.59
94b	Cl	H	3.62	7.22	8.59
94c	Cl	Cl	3.38	7.21	8.56

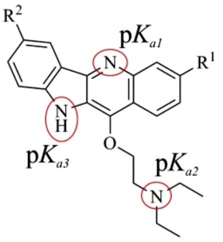

95

	R^1	R^2	SPARC pK_{a1}	 pK_{a1}	 pK_{a3}
95a	H	H	4.23	7.24	17.2
95b	Cl	H	3.63	7.23	17.5
95c	Cl	Cl	3.40	7.21	16.7

Appendix E. UV-Visible Spectrophotometry Determination of Binding Constants to DNA in buffer solutions containing 0.1 M NaCl

Binding to double strand 12-mer oligonucleotide d(GATCCTAGGATC)

UV-visible spectra of the titration of cryptolepine derivatives **3a**, **3e**, **3k**, **3q**, **3r**, and **3y** with the 12-mer oligonucleotide in 0.01 M phosphate buffer, 0.1 M NaCl at 25 ºC and experimental data at 357 and 347 nm, respectively, fitting to binding models. The concentration of cryptolepine derivative were 5 μM.

	R^1	R^2	R^3		
3a	H	H	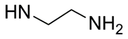	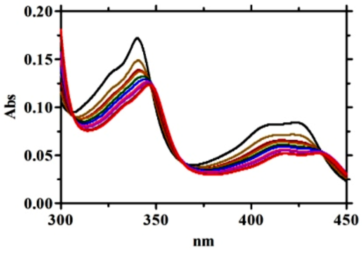	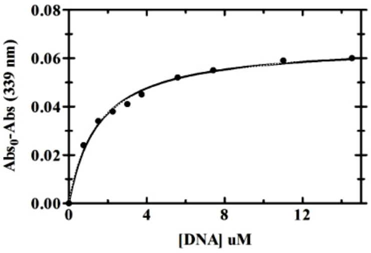
3e	H	H	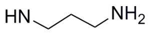	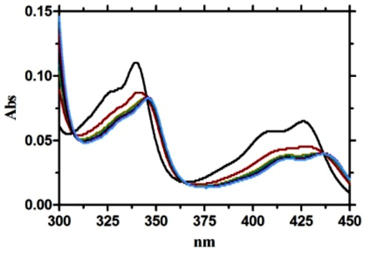	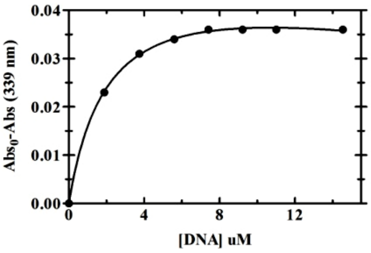
3k	H	H	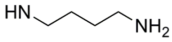	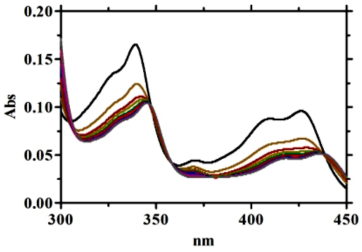	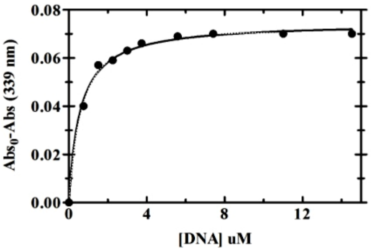
3q	H	H	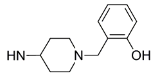	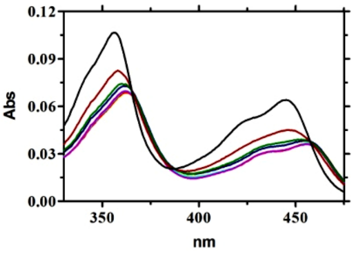	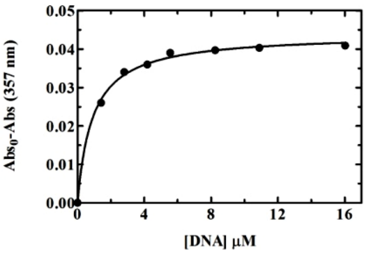
3r	H	H	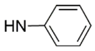	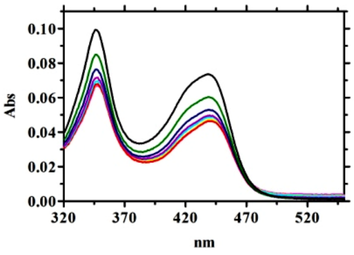	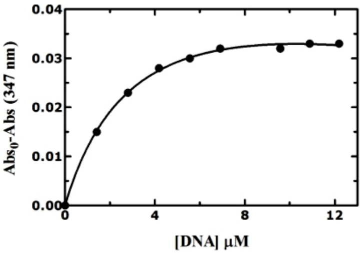

3y	H	H	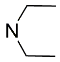	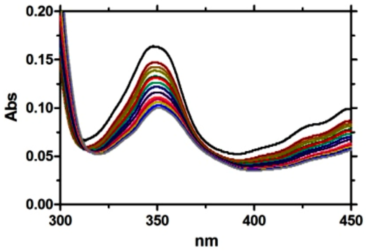	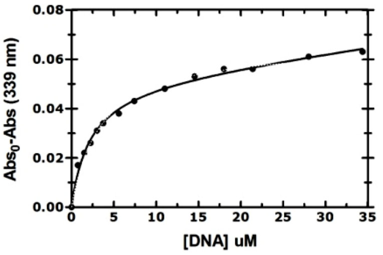

Binding to single strand 16-mer oligonucleotide d(GCCAAACACAGAATCG)

UV-visible spectra of the titration of cryptolepine (**1**) and cryptolepine derivatives **3n** with the 16-mer single strand oligonucleotide in 0.01 M phosphate buffer containing 0.1 M NaCl at 25 ºC and experimental data at 368 and 358 nm, respectively, fitting to binding models. The concentration of cryptolepine and cryptolepine derivative **3n** were 5 μM and the DNA/Ligand ratio increase as follows: 0 (black bold line), 0.25, 0.50, 0.75, 1.00, 1.25, 1.50 and 1.75.

	R^1	**R^2**	**R^3**		
1	H	H	H	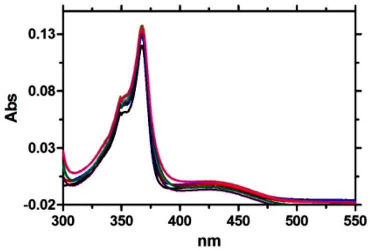	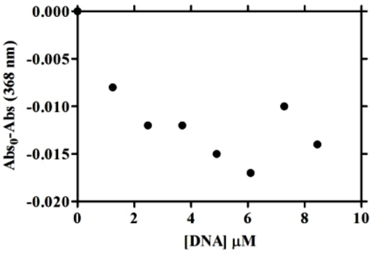
3n	H	H	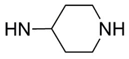	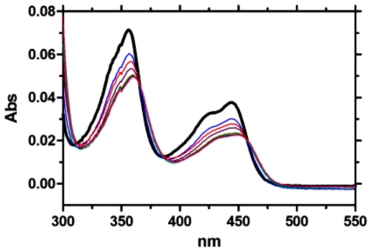	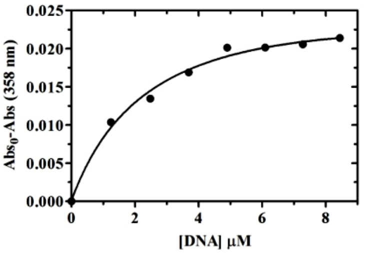

Appendix F. Spectrophotofluorimetry Determination of Binding Constants to DNA in buffer solutions containing 0.1 M NaCl

Binding to double strand 12-mer oligonucleotide d(GATCCTAGGATC)$_2$

Spectrophotofluorimetry titration data of the cryptolepine derivatives **3b-d**, **3f-j,** **3l-q** and **3s-x** (spectrophotofluorimetric data and fitting binding models) with 12-mer double strand oligonucleotide d(GATCCTAGGATC)$_2$

	R^1	R^2	R^3		
3b	H	H	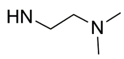	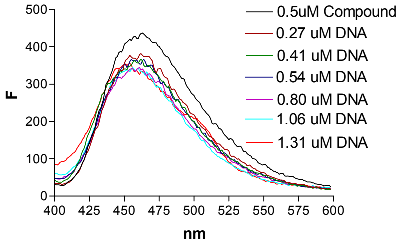	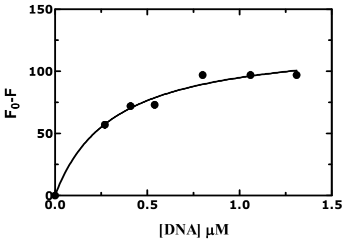
3c	H	H	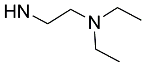	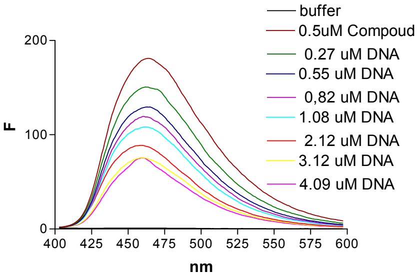	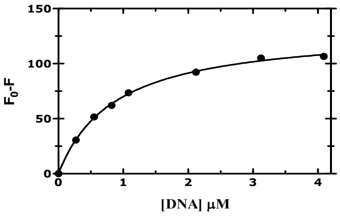
3d	H	H	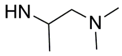	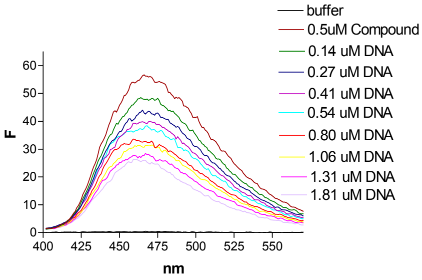	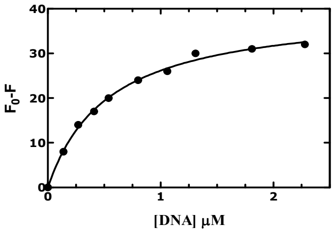
3f	H	H	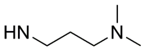	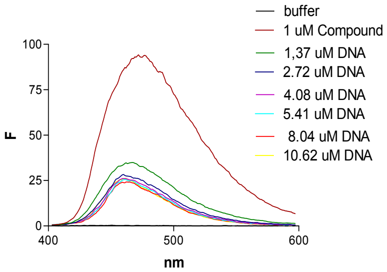	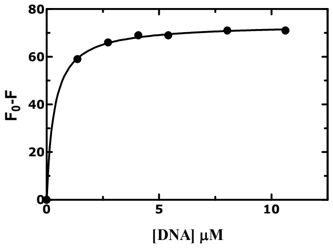

3g H H

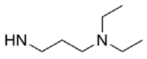

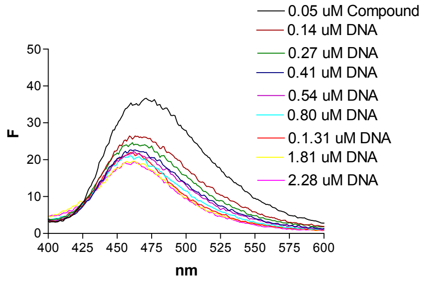

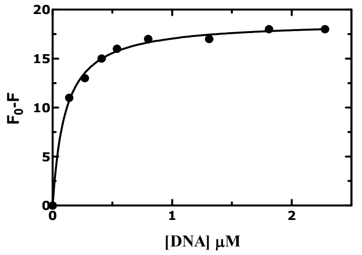

3h H H

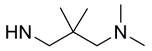

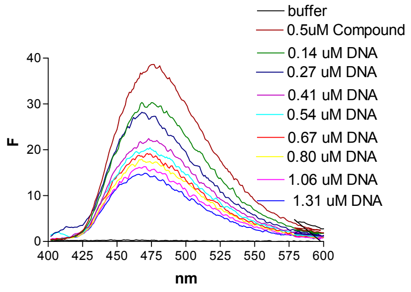

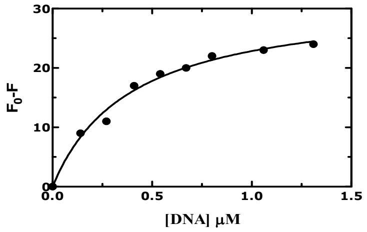

3i H H

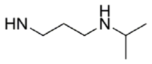

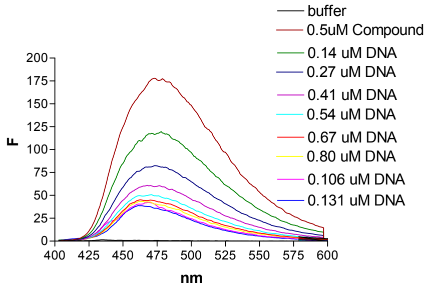

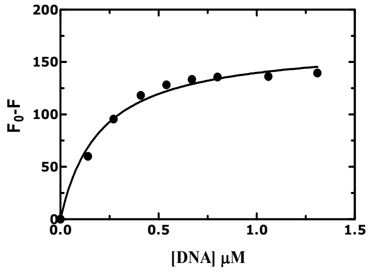

3j H H

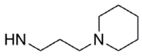

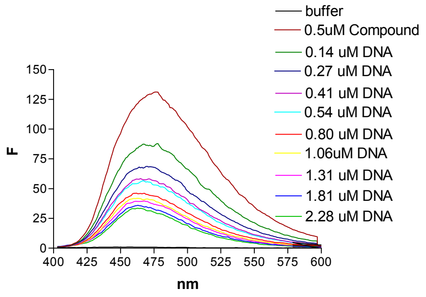

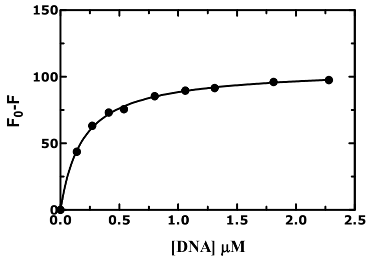

3l H H

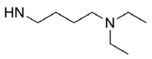

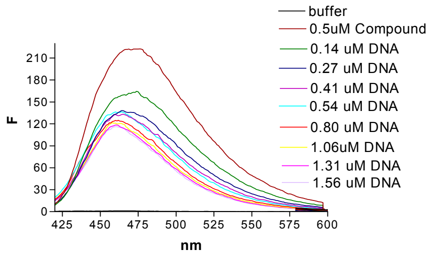

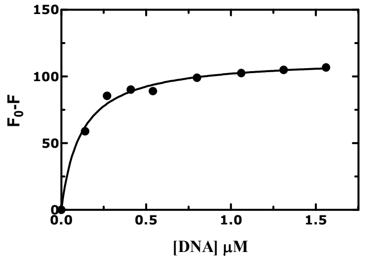

3m	H	H	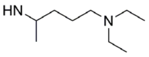	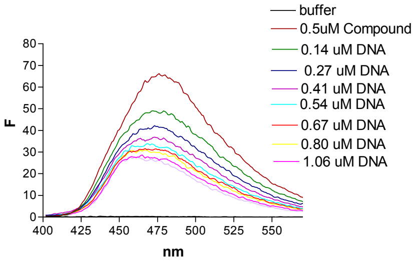	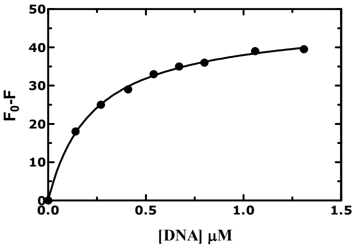
3n	H	H	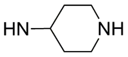	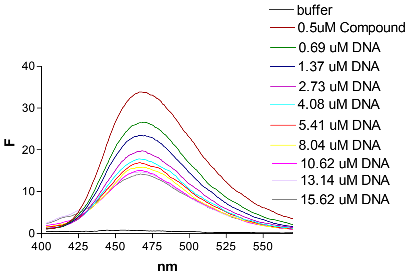	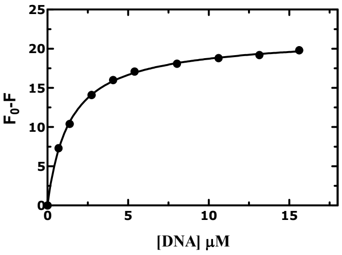
3o	H	H	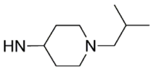	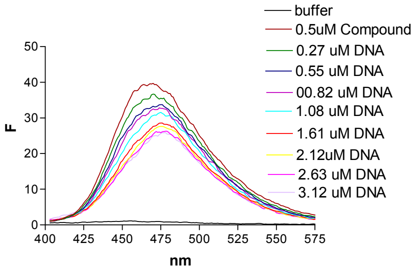	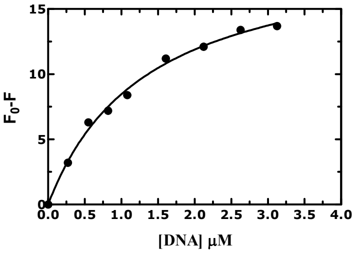
3p	H	H	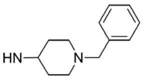	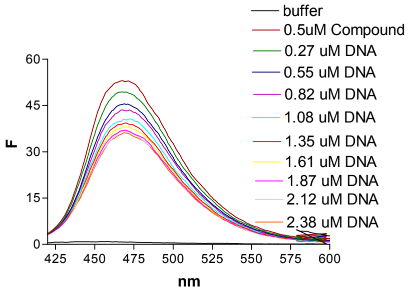	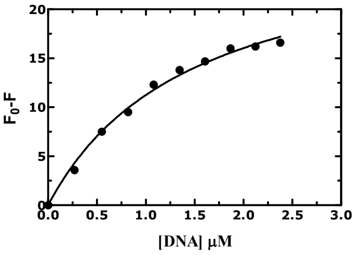
3q	H	H	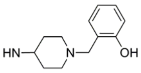	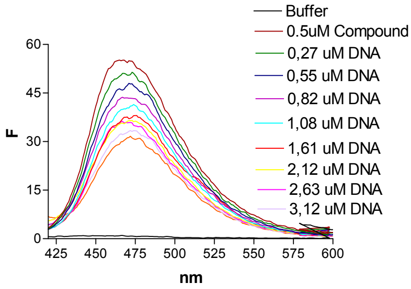	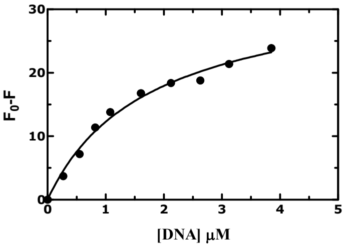

3s H H

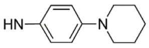

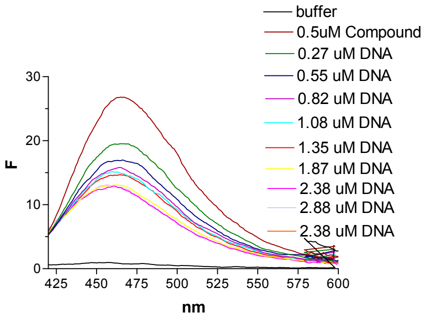

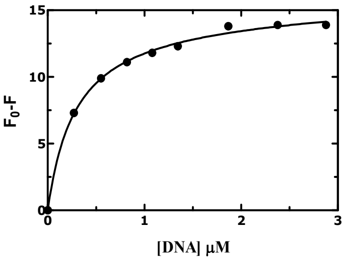

3t H H

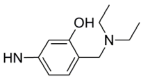

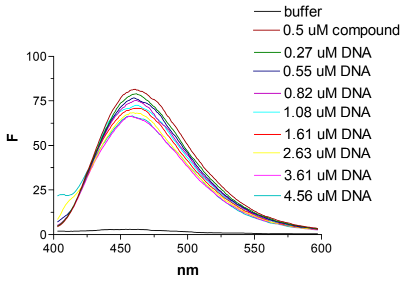

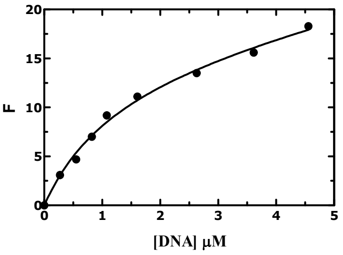

3u H H

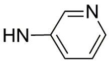

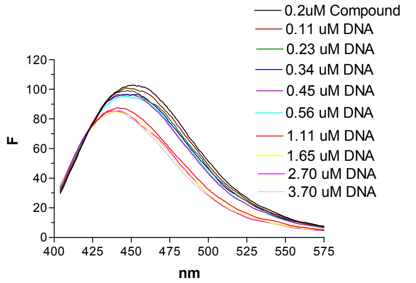

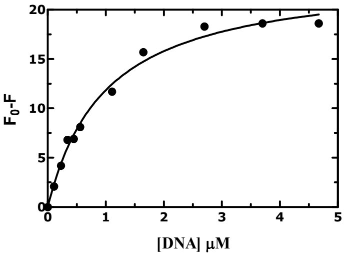

3v Cl H

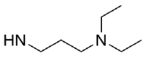

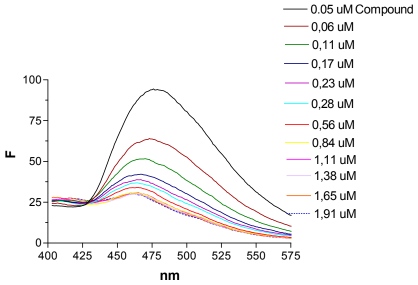

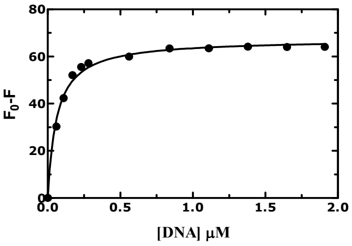

3w Cl H

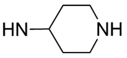

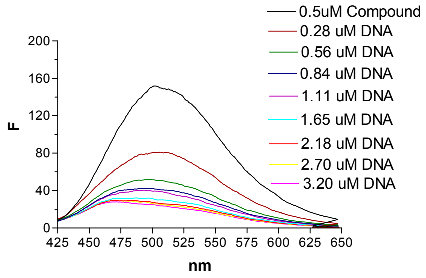

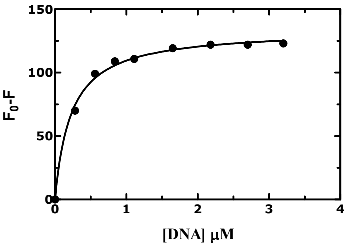

3x	Cl	Cl	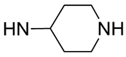	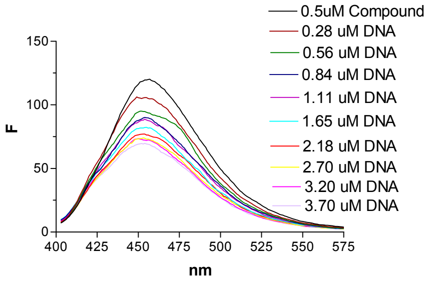0.5uM Compound 0.28 uM DNA 0.56 uM DNA 0.84 uM DNA 1.11 uM DNA 1.65 uM DNA 2.18 uM DNA 2.70 uM DNA 3.20 uM DNA 3.70 uM DNA F 150 100 50 0 400 425 450 475 500 525 550 575 nm	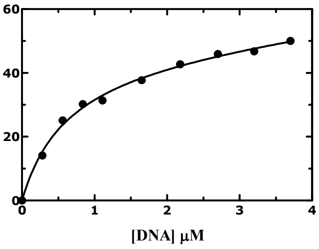60 40 20 0 F_0-F 0 1 2 3 4 [DNA] μM

Appendix G. Spectrophotometric Determination of Binding to DNA in buffer solutions containing 0.01 M or 1.0 M NaCl

Binding to double strand 12-mer oligonucleotide d(GATCCTAGGATC)

UV-visible spectrophotometry titration data of the cryptolepine (**1**) with 12-mer oligonucleotide in 0.01 M phosphate buffer containing 1 M NaCl at 25 ºC. The concentration of **1** was 5 μM and the ligand/DNA ratio increase as follows: 0, 0.3, 0.8, 1.1, 1.4, 1.7, 2.3, 2.8, 3.4, 4,5 and 5.0.

	R^1	R^2	R^3		
1	H	H	H	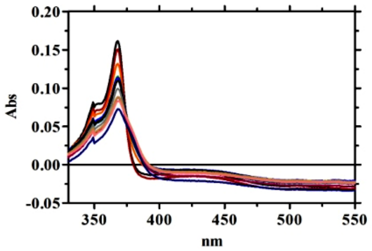	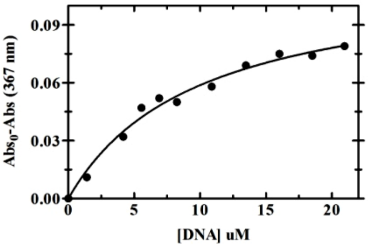

Spectrophotofluorimetry titration data of the cryptolepine analogues **3c** and **3t** with 12-mer double strand oligonucleotide in 0.01 M phosphate buffer at 25 ºC: **3c** 0.01 M NaCl; **3t** 1 M NaCl.

	R^1	R^2	R^3		
3c	H	H	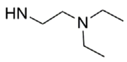	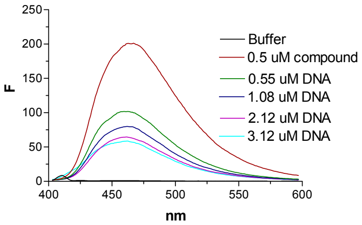	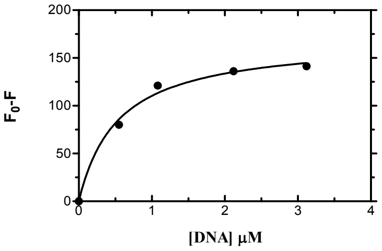
3t	H	H	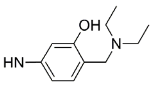	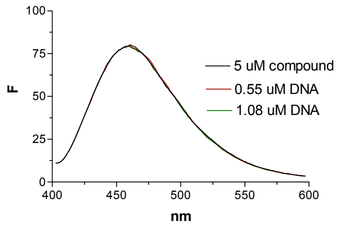	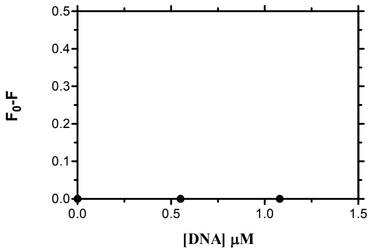

Binding to single strand 16-mer oligonucleotide d(GCCAAACACAGAATCG)

UV-visible spectra of the titration of cryptolepine analogues **3n** with the 16-mer single strand oligonucleotide in 0.01 M phosphate buffer, containing 1 M NaCl at 25 ºC and experimental data at 358 nm. The concentration of cryptolepine analogue **3n** was 5 μM and the DNA/Ligand ratio increase as follows: 0 (black bold line), 0.25, 0.50, 0.75, 1.00, 1.25 and 1.50.

	R^1	R^2	R^3		
3n	H	H	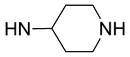	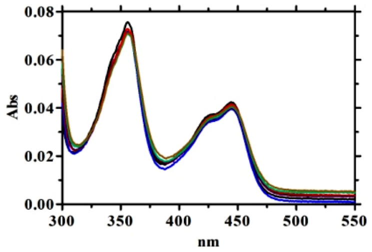	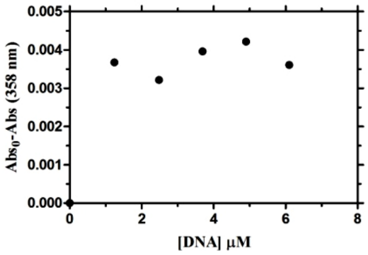

Appendix H. UV-Visible Spectrophotometry Determination of Binding Constants to FPIX-OH in pH 5.5 HEPES buffer (40 % DMSO)

Cryptolepine derivatives

UV-visible spectra λ_{max} changes of FPIX-OH (10 µM) Soret band at 25 ºC, titrated with **3** in buffered pH 5.5, 40 % DMSO , increasing the **3**/FPIX-OH molar ratios sequentially from the top in the region of 401 nm. Soret band wavelength (401 nm) of FPIX-OH (10 µM) titrated with **3**, fitted to the 1:1 (IQ:FPIX-OH) binding equation (model 1).

	R^1	R^2	R^3	UV-visible spectra λ_{max} changes	Fitting to 1:1 binding equation model
3a	H	H	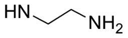	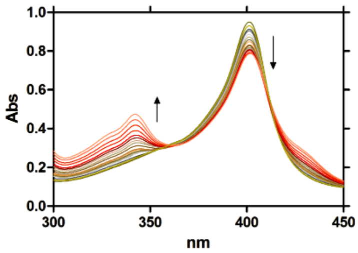	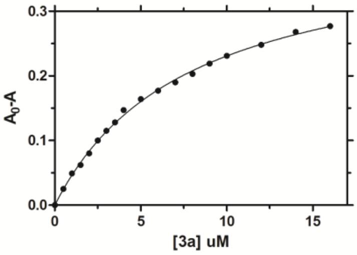
3b	H	H	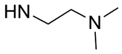	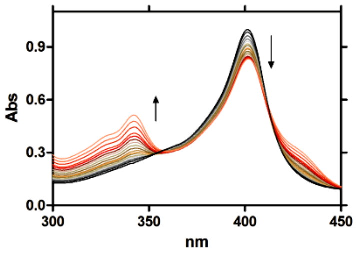	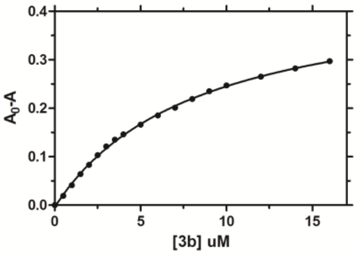
3c	H	H	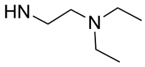	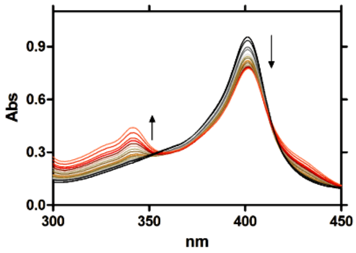	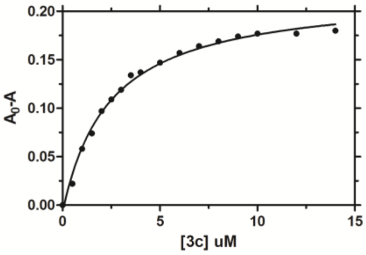
3d	H	H	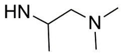	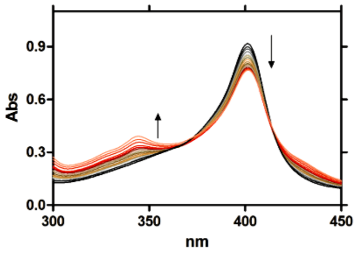	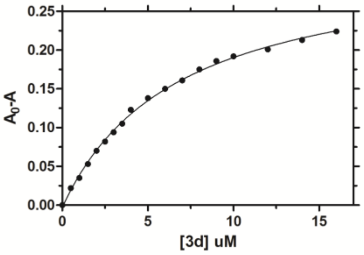

3e	H	H	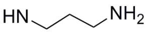	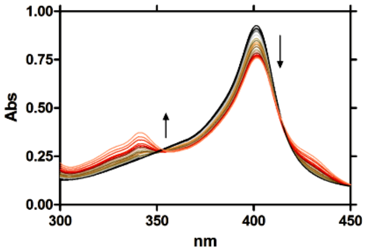	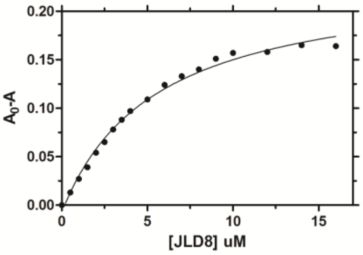
3f	H	H	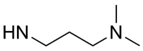	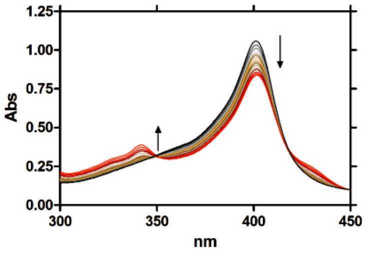	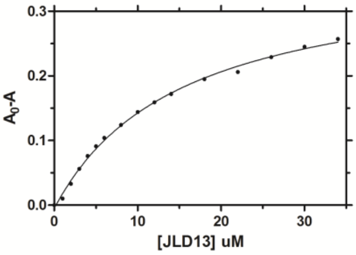
3g	H	H	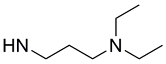	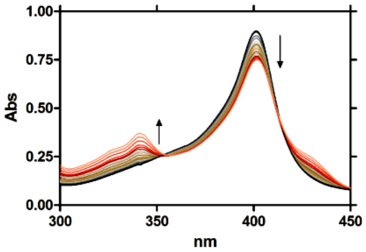	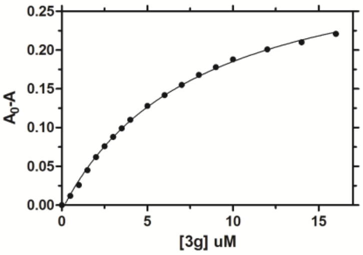
3h	H	H	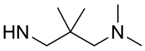	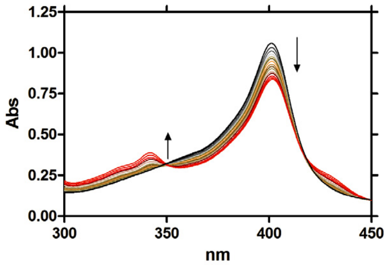	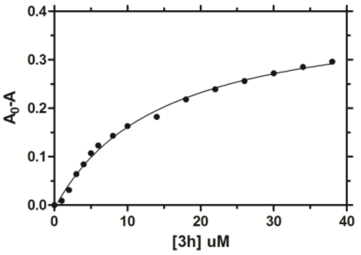
3i	H	H	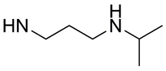	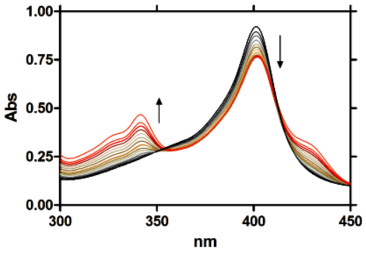	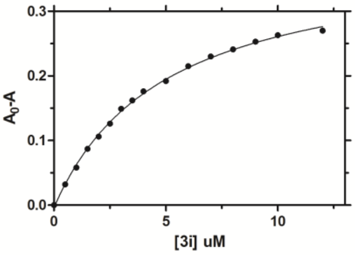
3j	H	H	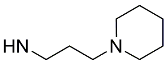	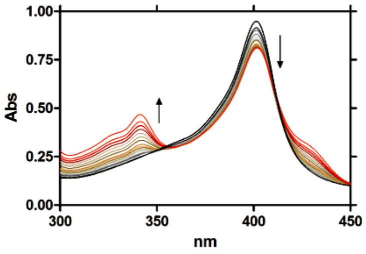	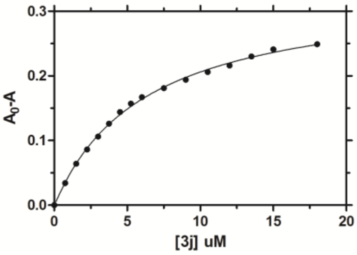

3k	H	H	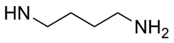	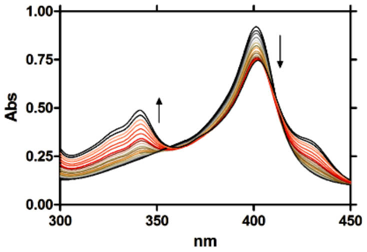	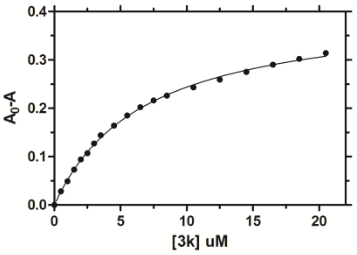
3l	H	H	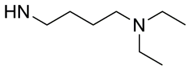	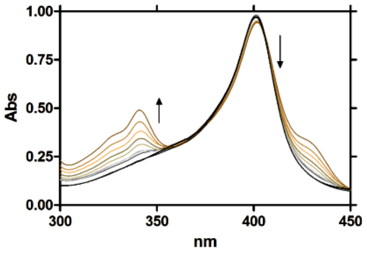	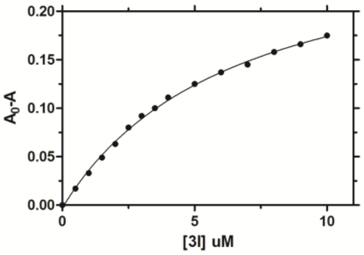
3m	H	H	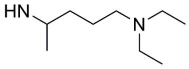	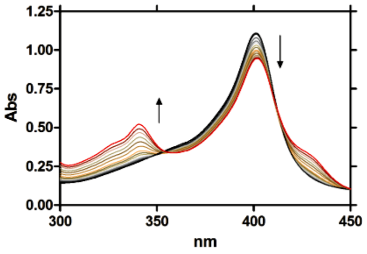	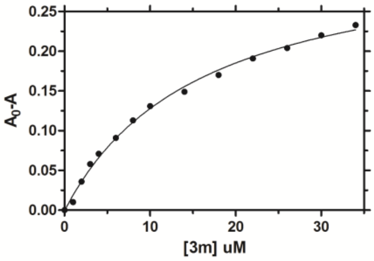
3n	H	H	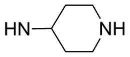	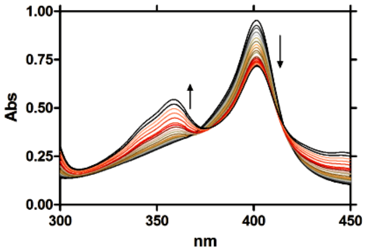	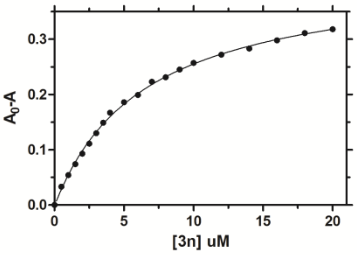
3o	H	H	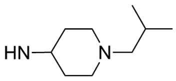	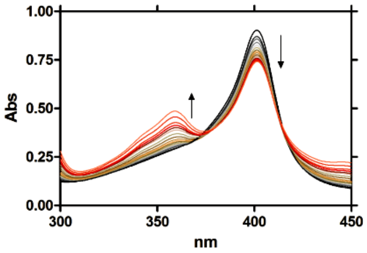	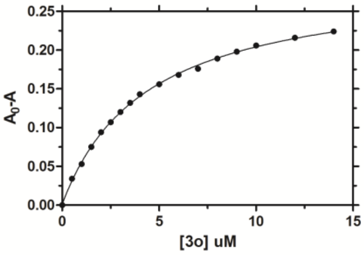
3p	H	H	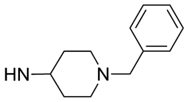	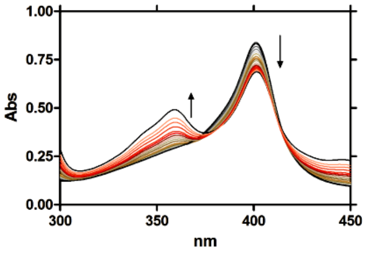	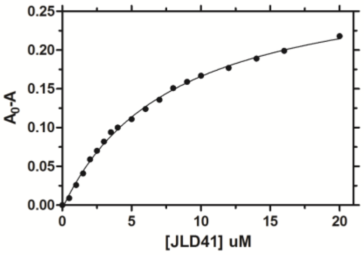

3q	H	H	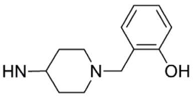	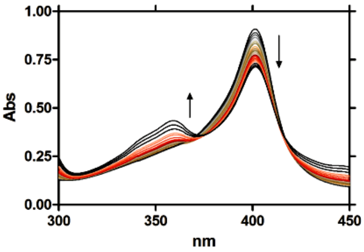	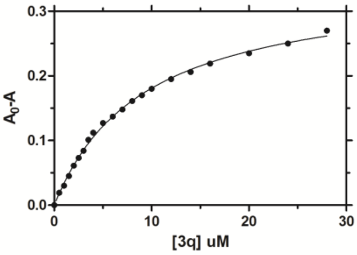
3r	H	H	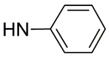	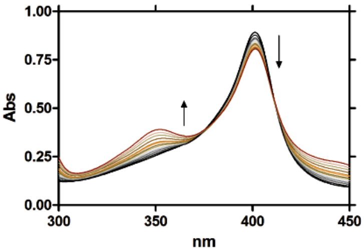	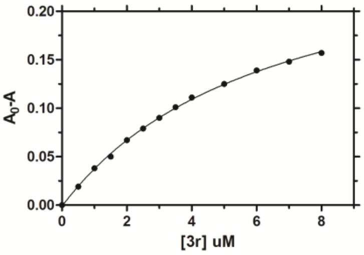
3s	H	H	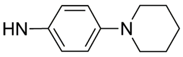	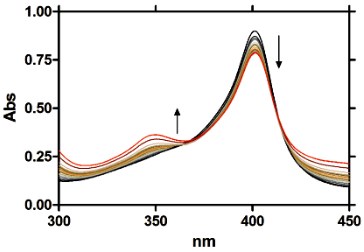	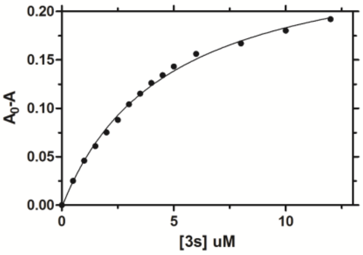
3t	H	H	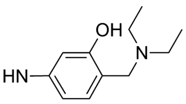	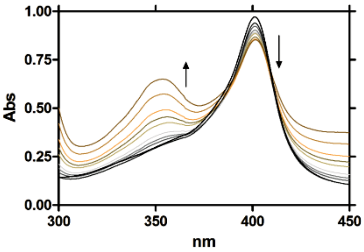	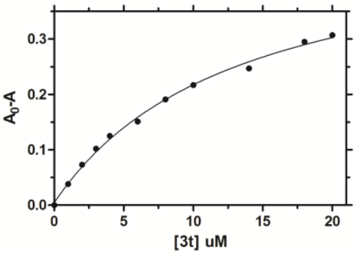
3u	H	H	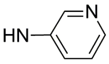	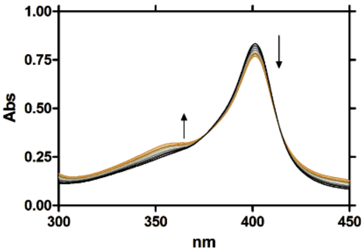	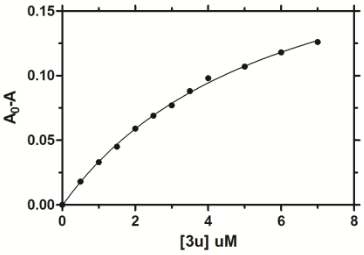
3v	Cl	H	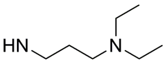	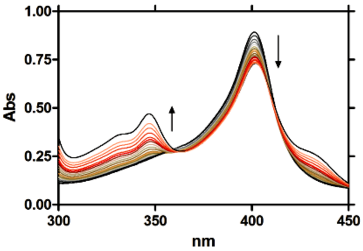	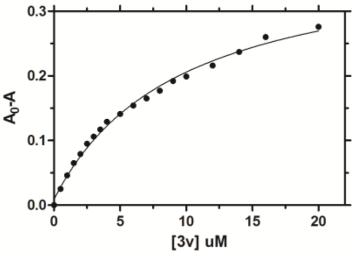

3w	Cl	H	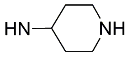	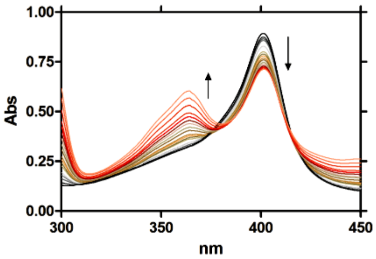	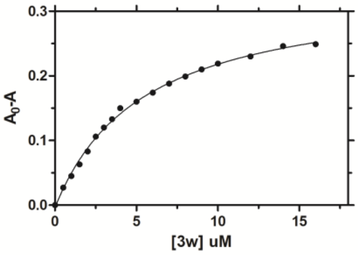
3x	Cl	Cl	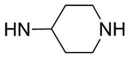	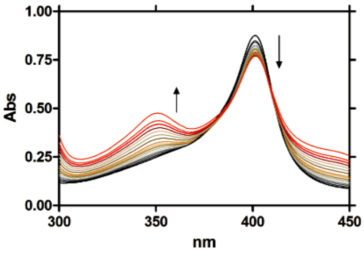	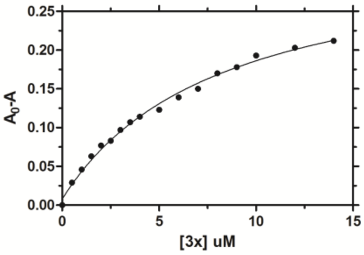
3y	H	H	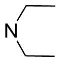	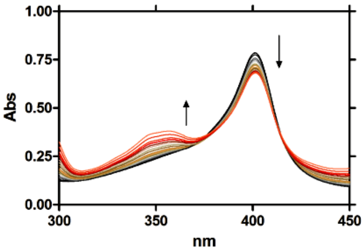	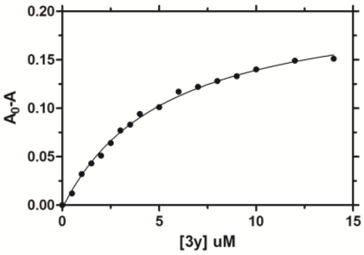

Quindolone derivatives

Soret band wavelength (402 nm) of FPIX-OH (10 µM) titrated with quindolones **4**, **91a** and **91b** and analogues **5**, **94** and **95**, fitted to the 1:1 (IQ:FPIX-OH) binding equation (model 1).

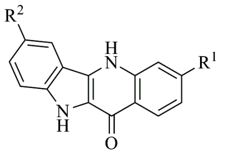

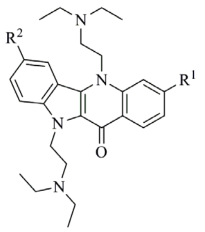

	R^1	R^2			R^1	R^2	
4	H	H	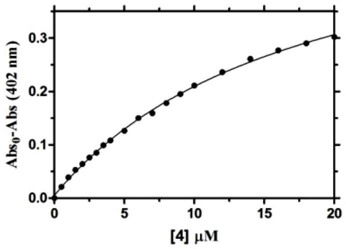	**5a**	H	H	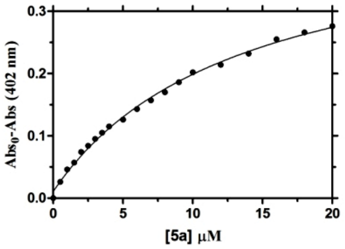
91a	Cl	H	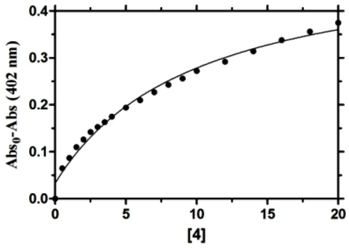	**5b**	Cl	H	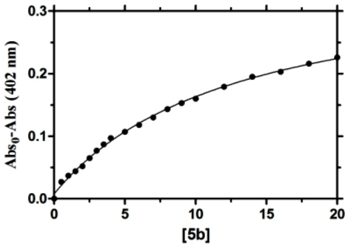
91b	Cl	Cl	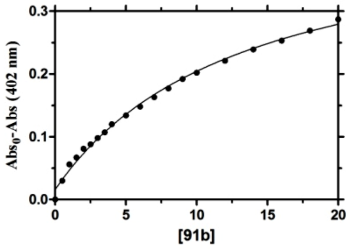	**5c**	Cl	Cl	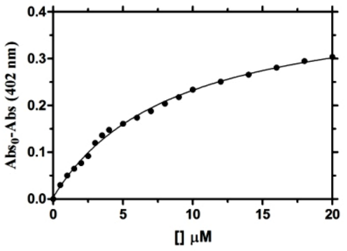

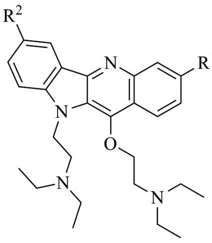

	R^1	**R^2**	
94a	H	H	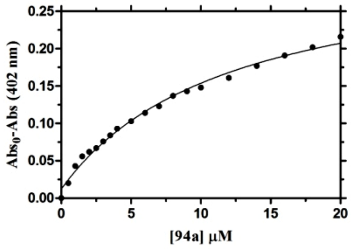
94b	Cl	H	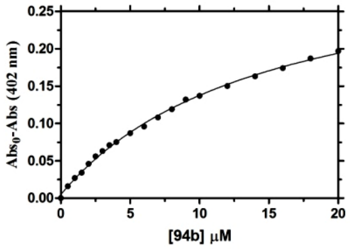
94c	Cl	Cl	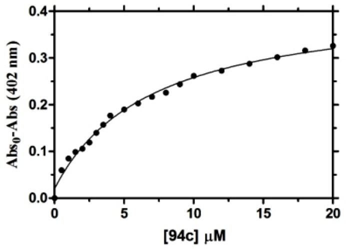

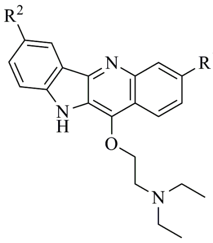

	R^1	**R^2**	
95a	H	H	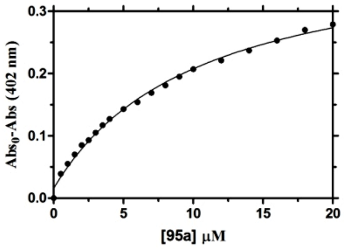
95b	Cl	H	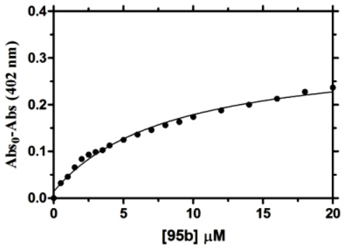
95c	Cl	Cl	--

Appendix I. Docking studies with DNA

a) 3D model of the van der Walls interactions map of cryptolepine and analogues with double-stranded d(GATCCTAGGATC)$_2$ oligonucleotide (blue: mild polar; red: hydrophobic: yellow: H-bonding), shown intercalation pocket only for clarity; **b)** Interactions map of cryptolepine and analogues bind to the double-stranded d(GATCCTAGGATC)$_2$ oligonucleotide (blue circle: receptor exposure; pink circle: polar; blue: ligand exposure; arrow dot green H-bonding with chain; arrow dot ble: H-donding with backbone; dot red: ionic binding; dot purple: proximity contour; values are in Å).

Binding site

3f

a) Minor groove

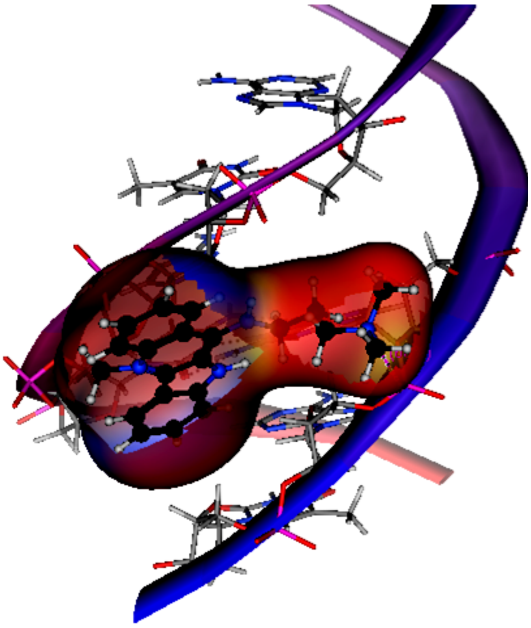

b)

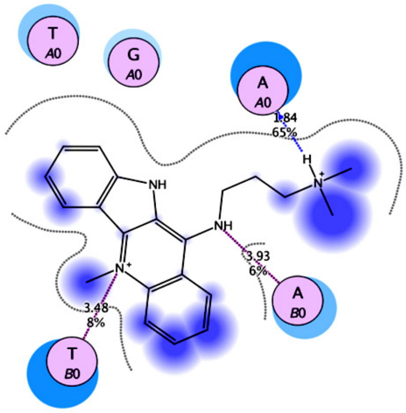
T
A0
G
A0
A
A0
1.84
65%
H
N+
C
B0
NH
NH
N+
3.93
6%
A
B0
3.48
8%
T
B0

3i

a) Minor groove

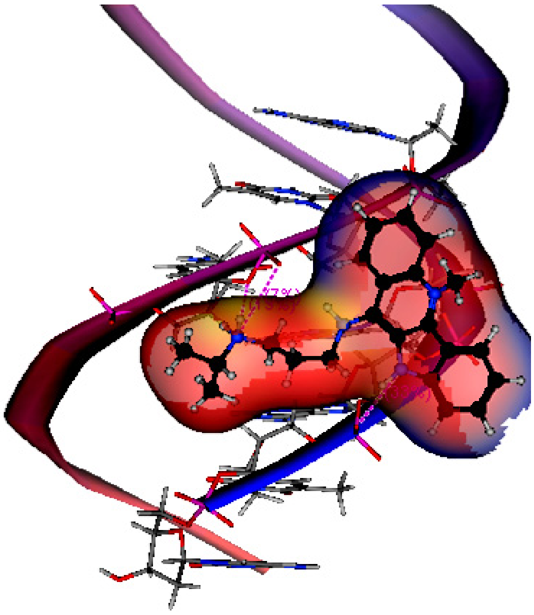

b)

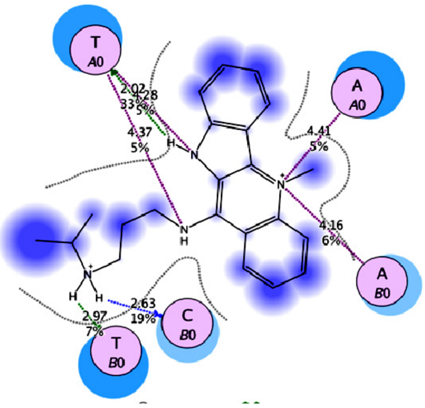
T
A0
2.02
33%
4.28
5%
4.37
5%
H
N
A
A0
4.41
5%
N+
4.16
6%
N
H
N+
H
H
2.63
19%
2.97
7%
A
B0
C
B0
T
B0

3j a) Minor groove

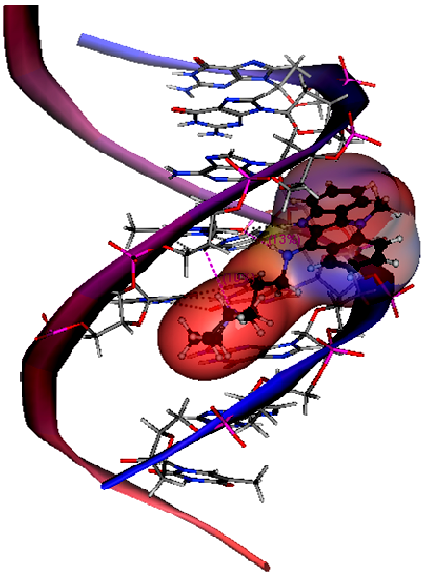

b)

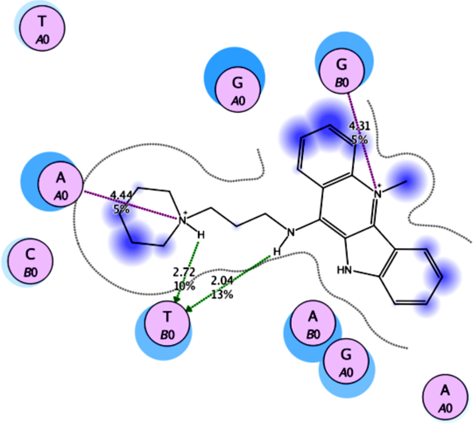
T
A0
G
A0
G
B0
4.31
5%
A
A0
4.44
5%
C
B0
2.72
10%
2.04
13%
T
B0
A
B0
G
A0
A
A0

3n a) Minor groove

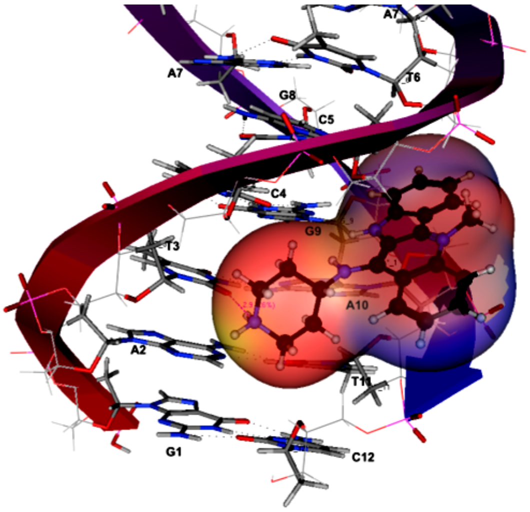
A7
T6
A7
G8
C5
C4
G9
T3
A10
A2
T11
G1
C12

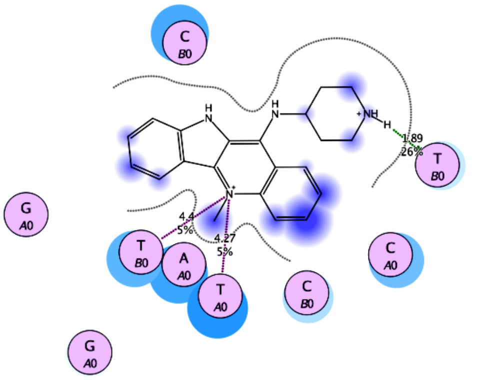
C
B0
1.89
26%
T
B0
G
A0
4.4
5%
4.27
5%
T
B0
A
A0
T
A0
C
B0
C
A0
G
A0

3q a) Minor groove

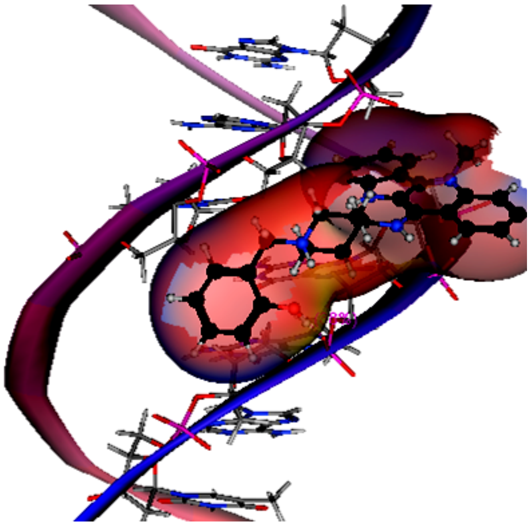

b)

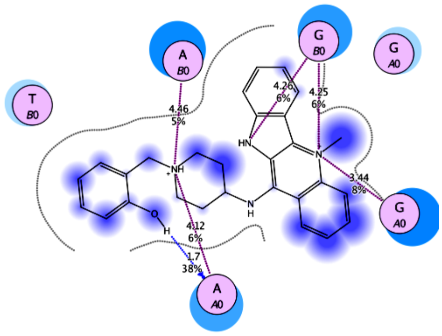
A
B0
G
B0
G
A0
T
B0
4.26
6%
4.25
6%
4.46
5%
3.44
8%
G
A0
4.12
6%
1.7
38%
A
A0

3r

a) Minor groove

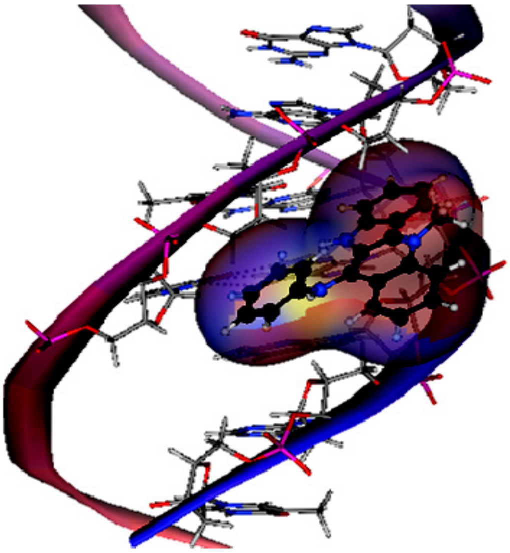

b)

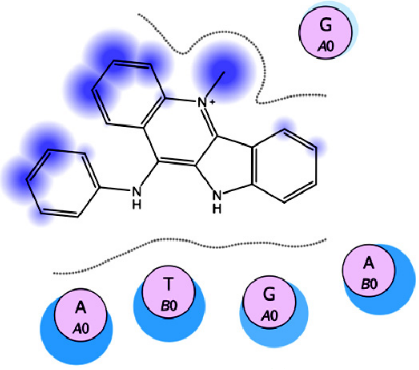
G
A0
N+
N
H
N
H
A
B0
T
B0
G
A0
A
A0

3s

a) Minor groove

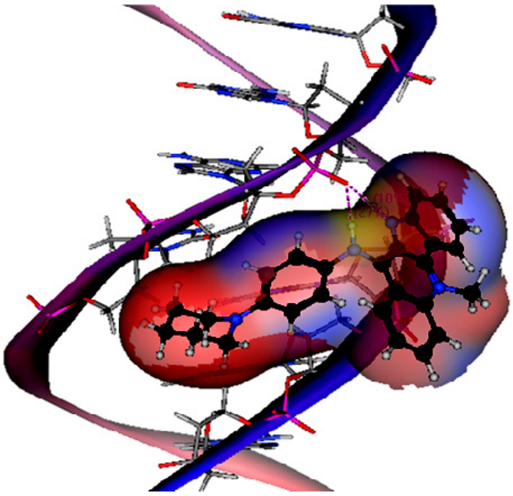

b)

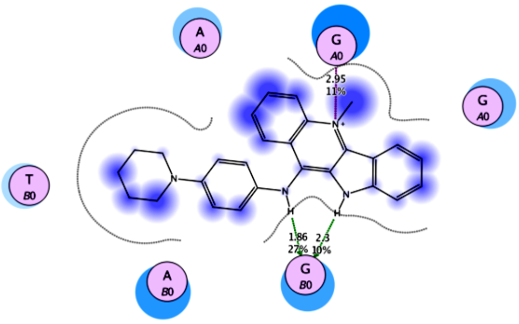
A
A0
G
A0
2.95
11%
G
A0
T
B0
N
N+
N
H
N
H
1.86
27%
2.3
10%
A
B0
G
B0

3v

a) Major groove

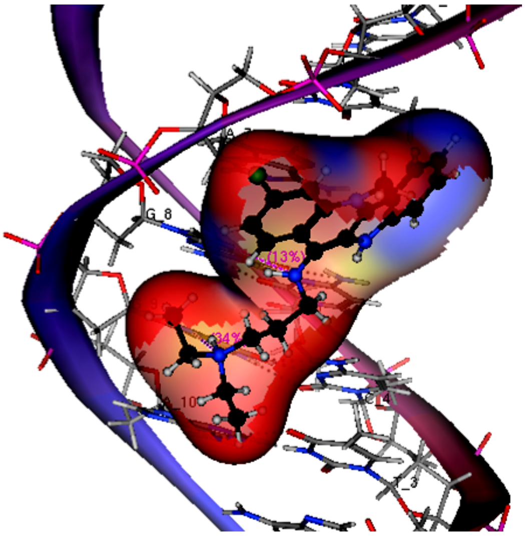

b)

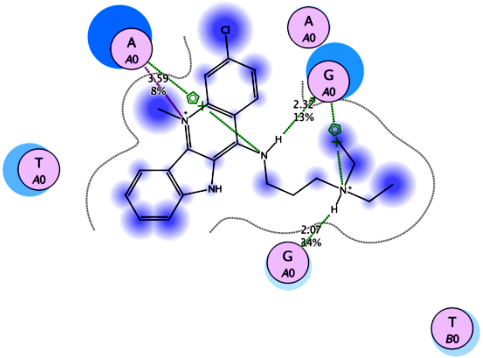
A
A0
Cl
A
A0
3.59
8%
G
A0
2.32
13%
N+
H
N
T
A0
NH
N+
H
2.07
34%
G
A0
T
B0

3w a) Minor groove

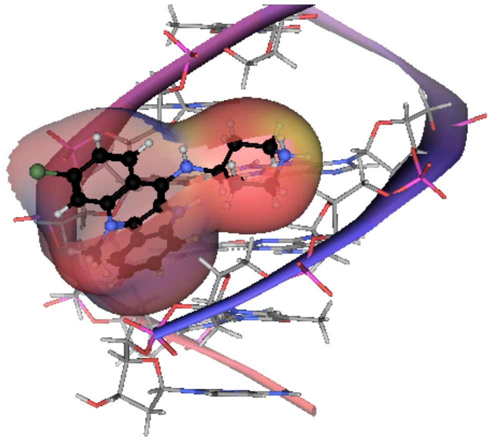

b)

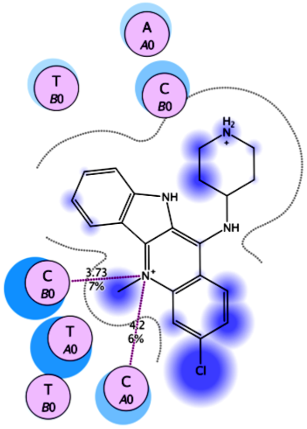
A
A0
T
B0
C
B0
H2
N+
NH
NH
C
B0
3.73
7%
N+
T
A0
4.2
6%
C
A0
T
B0
Cl

3x a) Major groove

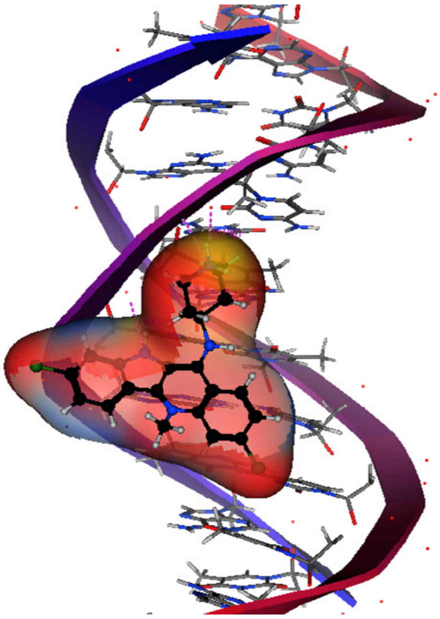

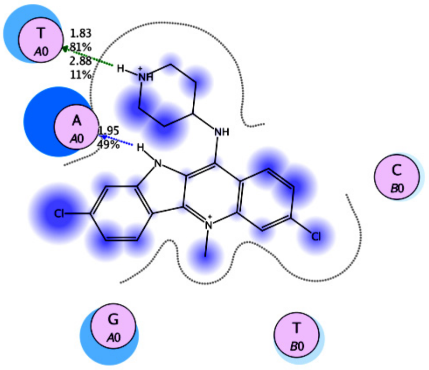
T
A0
1.83
81%
2.88
11%
H
NH
A
A0
1.95
49%
H
NH
N
C
B0
Cl
N+
Cl
G
A0
T
B0

Appendix J. Docking studies with haemozoin dimer

Cryptolepine derivatives

Model of cryptolepine derivatives interacting with haemozoin dimer. (dashed-black: H-bond; solid green: π-π interactions; dashed-red: ionic binding; solid-black: distance; values in Å).

3f

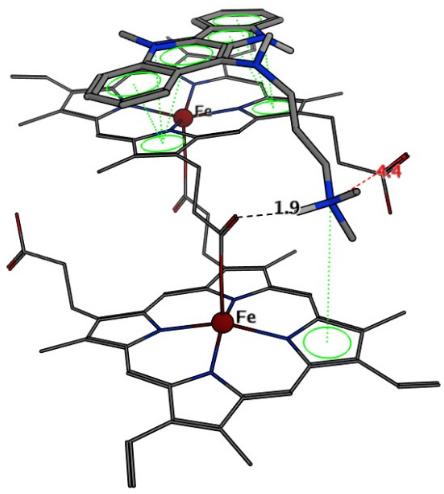

3h

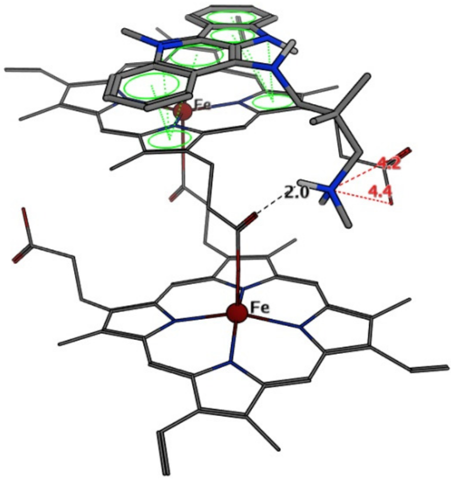
Fe
4.2
2.0
4.4
Fe

3j

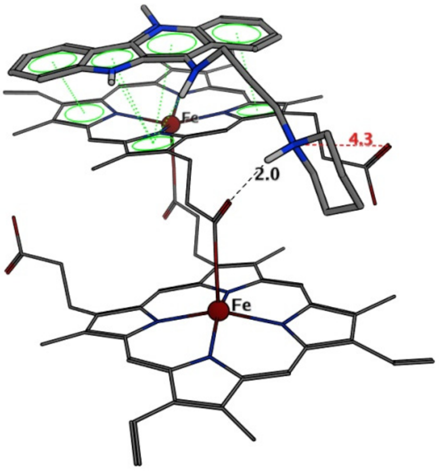

3l

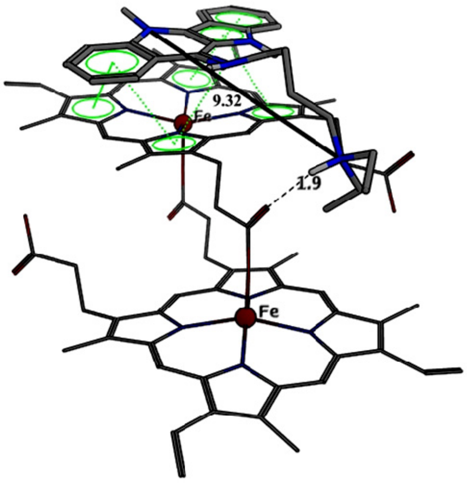

3s

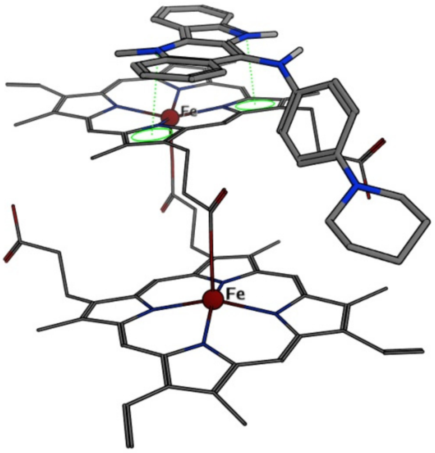

3u

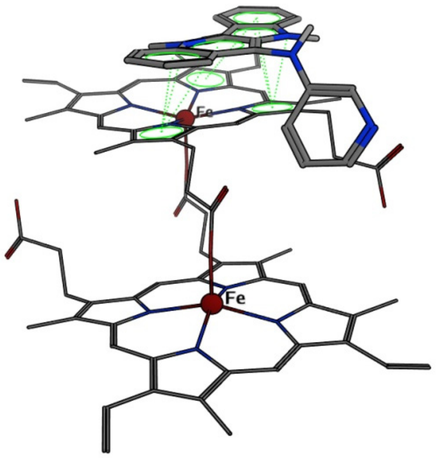

3v **3x**

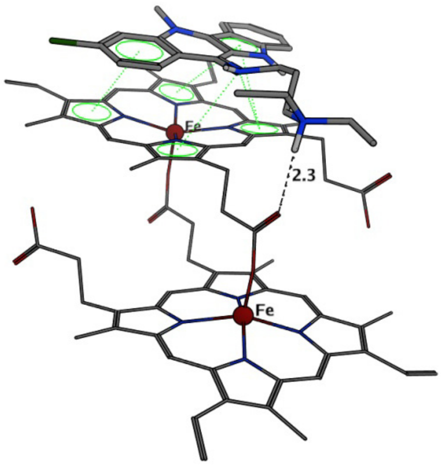

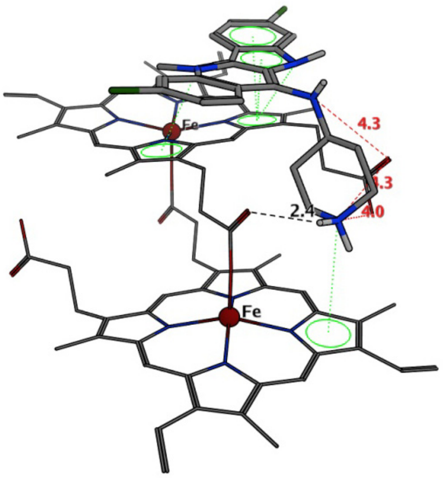
Fe
4.3
3.3
4.0
2.4
Fe

Quindolone derivatives

Model of quindolones and derivatives interacting with haemozoin dimer. (dashed-black: H-bond; solid green: π-π interactions; dashed-red: ionic binding; solid-black: distance; values in Å).

91a **91b**

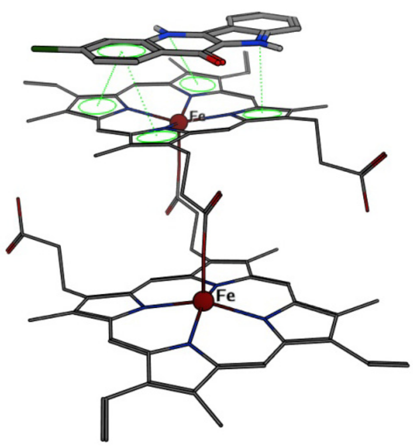

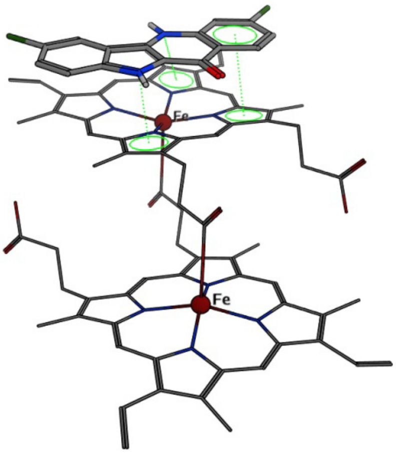

5b **5c**

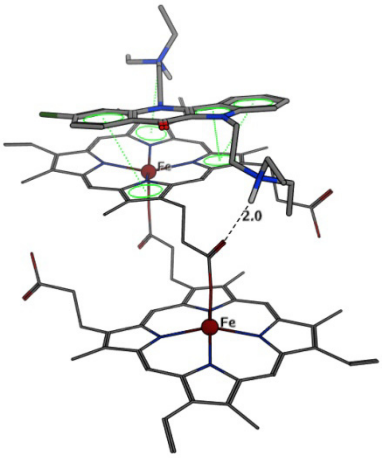

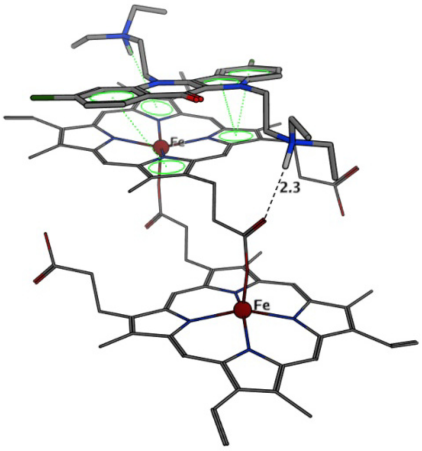

94b **94c**

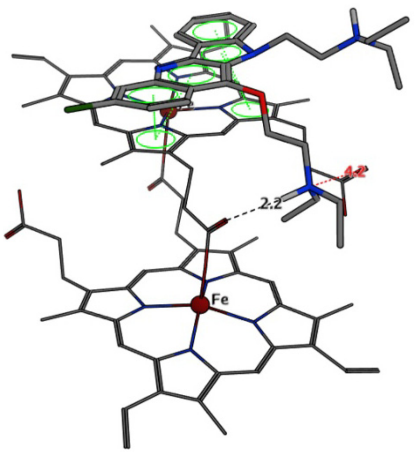

95b

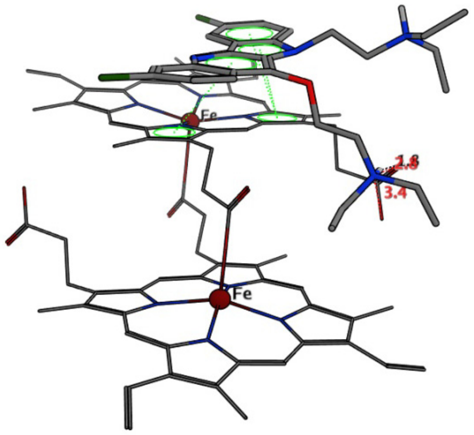

95c

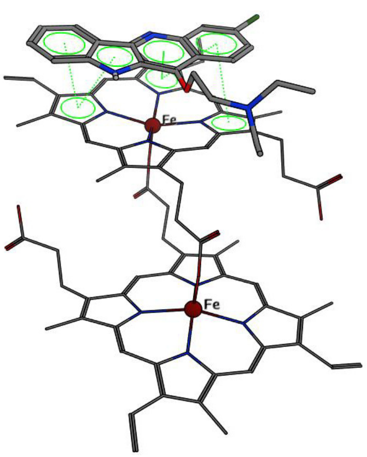

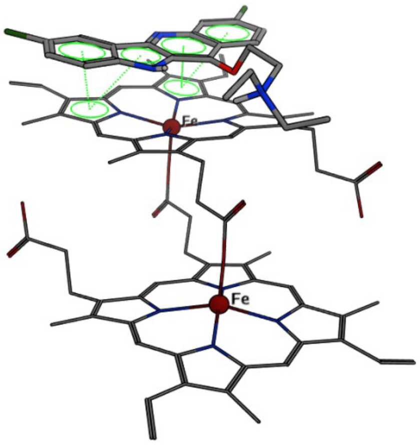

Appendix K. Derivation of vacuolar accumulation ratio equation

Considering an synthesized indolo[3,2-*b*]quinoline (IQ) with three acid dissociation constants:

$$IQH_3^{2+} \xrightleftharpoons{K_{a1}} IQH_2^+ + H^+$$

$$IQH_2^+ \xrightleftharpoons{K_{a2}} IQH + H^+$$

$$IQH \xrightleftharpoons{K_{a3}} IQ^- + H^+$$

The acid-base equilibrium equations will be:

$$K_{a1} = \frac{[IQH_2{}^+]\,[H^+]}{[IQH_3^{2+}]} \qquad K_{a2} = \frac{[IQH]\,[H^+]}{[IQH_2{}^+]} \qquad K_{a3} = \frac{[IQ^-]\,[H^+]}{[IQH]}$$

Solving all equilibrium equations in function of the unprotonated form [IQH], becomes:

$$K_{a1} = \frac{\frac{[IQH]\,[H^+]}{K_{a2}}\,[H^+]}{[IQH_3^+]}$$

$$[IQH_3^+] = \frac{[IQH]\,[H^+]^2}{K_{a1}K_{a2}} \qquad [IQH_2{}^+] = \frac{[IQH]\,[H^+]}{K_{a2}} \qquad [IQ^-] = \frac{K_{a3}[IQH]}{[H^+]}$$

The total concentration of indoloquinoline ($[IQ]_t$) in solution is the sum of the concentrations of all ionizable species in solution, and can be described as.

$$[IQ]_t = [IQH_3^{2+}] + [IQH_2^+] + [IQH] + [IQ^-]$$

Substituting by the equilibrium equations in function of the unprotonated specie [IQH], becomes:

$$[IQ]_t = \frac{[IQH]\,[H^+]^2}{K_{a1}K_{a2}} + \frac{[IQH]\,[H^+]}{K_{a2}} + [IQH] + \frac{K_{a3}[IQH]}{[H^+]}$$

$$[IQ]_t = [IQH]\left\{\frac{[H^+]^2}{K_{a1}K_{a2}} + \frac{[H^+]}{K_{a2}} + 1 + \frac{K_{a3}}{[H^+]}\right\}$$

Considering the vacuolar pH and the external pH, the accumulation ratio between the two pH’s will be:

$$acc.ratio = \frac{[IQ]_v}{[IQ]_e} = \frac{[IQH]_v\left\{\frac{[H^+]_v^2}{K_{a1}K_{a2}} + \frac{[H^+]_v}{K_{a2}} + 1 + \frac{K_{a3}}{[H^+]_v}\right\}}{[IQH]_e\left\{\frac{[H^+]_e^2}{K_{a1}K_{a2}} + \frac{[H^+]_e}{K_{a2}} + 1 + \frac{K_{a3}}{[H^+]_e}\right\}}$$

A fundamental premise of the pH trapping hypothesis is that the non protonated form [IQH] can diffuse across membranes and so the concentration of this species is equal on both sides of the membrane (if equilibrium is reached), and since $[\mathrm{IQH}]_v = [\mathrm{IQH}]_e$ the accumulation ratio equation becomes:

$$acc.ratio = \frac{[\mathrm{IQ}]_v}{[\mathrm{IQ}]_e} = \frac{\left\{\frac{[\mathrm{H}^+]_v^2}{K_{a1}K_{a2}} + \frac{[\mathrm{H}^+]_v}{K_{a2}} + 1 + \frac{K_{a3}}{[\mathrm{H}^+]_v}\right\}}{\left\{\frac{[\mathrm{H}^+]_e^2}{K_{a1}K_{a2}} + \frac{[\mathrm{H}^+]_e}{K_{a2}} + 1 + \frac{K_{a3}}{[\mathrm{H}^+]_e}\right\}} \qquad \text{Eq. 6.2}$$

Appendix L. Relevant Publications

1. Lavrado, J.; Cabal, G.; Prudêncio, M.; Mota, M.M.; Rita C. Guedes, Daniel J.V.A. dos Santos; Gut, J.; Rosenthal, P.J.; Díaz, C.; Bichenkova, E.; Douglas, K.T.; Moreira, R.; Paulo, A. (**Submitted**) Incorporation of Basic Side-Chains into Cryptolepine Scaffold. Structure-Antimalarial Activity Relationships and Mechanistic Studies ***Journal of Medicinal Chemistry***.
2. Lavrado, J.; Gani, K.; Nobre, P.A.; Santos, S.A.; Lopes, D.; Rosário, V.; Gut, J.; Rosenthal, P.J.; Moreira, R.; Paulo, A. (**2010**) Bis-alkylamine quindolone derivatives as new antimalarial leads. ***Bioorganic & Medicinal Chemistry Letters***, 5634-5637.
3. Lavrado, J.; Moreira, R.; Paulo, A. (**2010**) Indoloquinolines as Scaffolds for Drug Discovery. ***Current Medicinal Chemistry*****,** 17, 2348-2370.
4. Lavrado, J.; Paulo, A.; Gut, J.; Rosenthal, P.J.; Moreira, R. (**2008**) Cryptolepine derivatives containing basic aminoalkyl side chains at C11: synthesis, antiplasmodial activity, and cytotoxicity. ***Bioorganic & Medicinal Chemistry Letters*****,** 18, 1378-81.